

Institute for Nerve Medicine

Medical Associates Inc

Aaron G. Filler, MD, PhD, JD, FRCS

- Board Certified: ABNS – American Board of Neurological Surgery
- FRCSN – Fellow of the Intercollegiate Board in Surgical Neurology of England, Ireland, Edinburgh & Glasgow
- Fellow of the Royal College of Surgeons of England
- Member of the Bar of the Court of Appeals for the Federal Circuit
- Member of the Bar of the United States Supreme Court

900 Wilshire Blvd.

Suite 310

Santa Monica, CA 90401

Phone: (310) 314-6410

Fax: (310) 496-0185

INSTITUTE FOR NERVE MEDICINE

CONSULTATION REPORT

MR# 200 100 300

DATE OF EXAMINATION: August 24, 2024

DATE OF REPORT: September 17, 2024

PATIENT NAME: Hon. Pauline Newman

DATE OF BIRTH: 06/20/1927

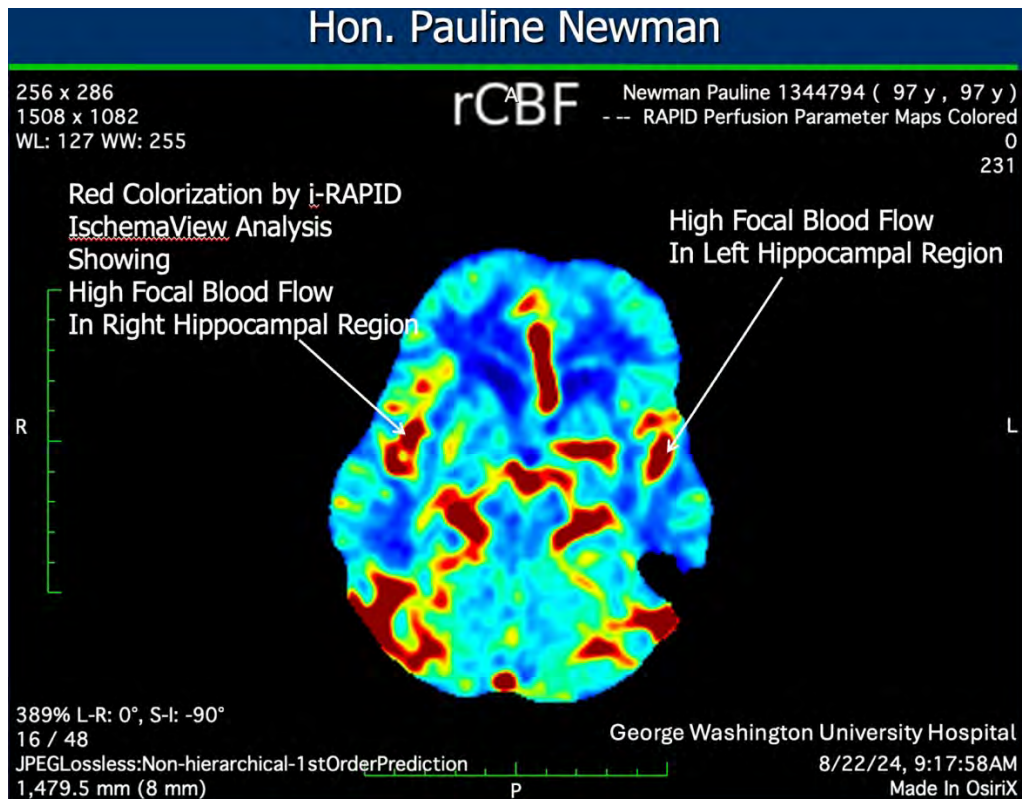


TABLE OF CONTENTS

EXECUTIVE SUMMARY.....	3
<u>I.</u> PREFACE	6
<u>II.</u> STRUCTURE OF THE REPORT	9
<u>III.</u> EXPERT’S BACKGROUND AND QUALIFICATIONS	13
<u>IV.</u> BACKGROUND ON THE UTILIZED PERFUSION CT TECHNOLOGY	14
<u>V.</u> INFORMATION CONSIDERED IN PREPARING THIS REPORT	17
<u>VI.</u> PAST MEDICAL HISTORY	18
<u>VII.</u> PAST MEDICAL RECORDS	18
<u>VIII.</u> EXAMINATION	25
<u>IX.</u> INDICATIONS FOR A PERFUSION CT BRAIN SCAN	26
<u>X.</u> RECENT OPINION WRITING.....	27
<u>XI.</u> DEMEANOR	27
<u>XII.</u> GENERAL PHYSICAL EXAMINATION.....	28
<u>XIII.</u> NEUROLOGIC EXAMINATION	28
<u>XIV.</u> USE OF PERFUSION CT SCANNING FOR COGNITIVE HEALTH ASSESSMENT	31
<u>XV.</u> PARAMETERS IN PERFUSION BRAIN IMAGING:.....	32
<u>XVI.</u> RESULTS AND CONTEXT OF JUDGE NEWMAN’S PERFUSION CT TEST.....	34
<u>XVII.</u> COGNITIVE INTERVIEW FOR TECHNOLOGY AND PATENT LAW	36
<u>XVIII.</u> SUMMARY OF EVALUATION AND TESTING	40
<u>XIX.</u> CONCLUSION: HON. PAULINE NEWMAN IS COGNITIVELY FIT TO RETURN TO ACTIVE DUTY AS A SENIOR JUDGE OF THE FEDERAL CIRCUIT	41

EXECUTIVE SUMMARY

In March of 2023, Chief Judge of the United States Court of Appeals for the Federal Circuit Kimberly A. Moore, acting under the authority of the Judicial Conduct and Disability Act of 1980, 28 U.S.C. §§ 351–364, identified a complaint against her colleague Circuit Judge Pauline Newman alleging, in essence that Judge Newman presents “a concern that [she]... may have a mental or physical disability that renders her unable to discharge the duties of her office.” Special Committee Order of May 16, 2023, at 1, <https://tinyurl.com/yc7c78ap> (“May 16 Order”).¹ A Special Committee (consisting of Chief Judge Moore and Circuit Judges Sharon Prost and Richard G. Taranto) was appointed to investigate the matter. *Id.* The Committee issued a series of orders directing Judge Newman to undergo neurological and neuropsychological testing, and to release her medical records covering the preceding two years to the evaluating physicians. *See id.* at 4-23. Judge Newman declined to undergo the specified examinations, citing, *inter alia*, concerns about objectivity and relevance of the requested examinations. In response, the Judicial Council of the Federal Circuit suspended Judge Newman from hearing cases pending either compliance with the aforementioned orders or when otherwise justified by “changed circumstances.” *See* Special Committee Report & Recommendation of July 24, 2024, at 2, <https://tinyurl.com/28s5hz7u> (“2023 R&R”).

Endeavoring to help resolve the impasse between Judge Newman and the Judicial Council, as well as to address Judge Newman’s concerns about objectivity and reliability of the proposed testing, I volunteered to evaluate her, using modern and objective technology, namely Perfusion Computed Tomography. A significant body of scientific literature confirms that Perfusion CT is highly useful for identifying dementia even prior to clinical signs being present. Specifically, over the preceding decade a spectacular technological advance in our ability to measure blood flow to various areas of the brain has taken place. As a result of these stunning advances in spatial and temporal resolution there is now a widespread medical understanding that Perfusion CT can be used to identify or rule out the presence of dementia or cognitive impairment on a reliable objective basis. Furthermore, unlike a situation where there may be a “defense neuropsychology report” and a “plaintiff neuropsychology report” that disagree completely on nearly every conclusion, there is no “defense CT scan” and “plaintiff CT scan” because the data is completely objective requiring little if any subjective interpretation.

I have significant expertise in neurosurgery, brain injury, cognitive treatment for individuals engaged in intellectually complex professions, and brain imaging. In 1986, I received my MD degree from the University of Chicago and a PhD in Biological Anthropology from Harvard University. I am an editor of the principal textbook in neurosurgery (*Youmans & Winn, Neurological Surgery* (8th ed., Elsevier)) and an author of

¹ All orders of the Special Committee and the Judicial Council of the Federal Circuit are filed under case caption *In re Complaint No. 23-90015* (Judicial Council of the Fed. Cir.).

several chapters including the chapter (Exhibit 3) on Diffusion Tensor Imaging of the brain—a technology I invented and patented. *See* U.S. Pat. No. 5,560,360 (the subject of some 480,000 publications identifiable on Google Scholar). I serve on the Continuing Medical Education Committee of Cedars Sinai Medical Center in Los Angeles. For many years, I have also served on the Joint Guidelines Committee of the American Association of Neurological Surgeons and the Congress of Neurological Surgeons. I have been admitted as an expert in more than a hundred cases in various state and federal courts and my testimony has never been excluded. I also am an attorney (having received my JD degree in 2014) and am a member of the Bar of the United States Court of Appeals of the Federal Circuit and a member of the Federal Circuit Bar Association. Accordingly, I possess unique expertise that permits me to provide an expert opinion on Judge Newman’s state of mental health and her ability “to discharge the duties of her office.”

In addition to the Perfusion CT scan, I conducted a full neurological evaluation as required by the Special Committee’s May 16, 2023, Order. *See* May 16 Order at 22. Furthermore, I conducted an interview with Judge Newman which tested her ability to understand (without any prior preparation) complex technology and to apply complicated patent law doctrines to the same. Finally, I compared Judge Newman’s verbal and analytical abilities during my examination to my prior interactions with her as an attorney who appeared before her on two separate occasions in 2019 and 2022. The examination lasted about three hours *exclusive* of the time necessary to conduct or analyze the Perfusion CT scan.

Prior to conducting my examination, I familiarized myself with evidence compiled by the Special Committee, including affidavits from various Court staff. *See* Exhibits to 2023 R&R. I have also reviewed Judge Newman’s medical history dating back to 2021 as required by the Special Committee. *See* May 16 Order at 6. While the records are described more fully below, nothing in the records shows that Judge Newman has ever suffered a “heart attack” (in the sense of a severe abrupt disabling cardiac event) or had a fainting episode. The records reviewed by me do not “shed light,” *id.* at 5, on Judge Newman’s current condition. Indeed, given that her neurological workup was entirely normal, the records do not appear to be contributory in any way to “the issues of impairment of cognitive and other functioning the Committee is investigating,” *id.* Specifically, although she has received treatment for various hematologic and infectious diagnoses – these related to an infection of unclear source which has now resolved completely.

The Perfusion CT Brain scan conducted at the George Washington University Hospital and evaluated by both myself and a physician of the employ of that hospital was entirely normal. Indeed, Judge Newman’s brain demonstrates a very *high* rate of effective perfusion—a finding consistent with high cognitive ability generally, and Judge Newman’s high capability for integrative thought and memory functioning. Specifically – as explained in detail below – these findings are wholly inconsistent with any dementia or other cognitive deterioration. Her prior Pulmonary Perfusion SPECT scan of 3/4/2022 and

Newman, Pauline
DOB: 6/20/1927
August 24, 2024
Page 5 of 44

Myocardial Perfusion SPECT scan of 2/4/2022 similarly support an assessment of excellent health for her age.

The neurological examination was also normal, save for two minor issues (cataracts and slightly unsteady heel-to-toe walk) which are discussed below, but neither of which raises any concerns with respect to Judge Newman’s cognitive abilities.

My comparison of Judge Newman’s abilities as a jurist (including comparisons to her speech fluency, patterns, diction, and the like) in 2019 and 2022 with those of the present day show no notable changes.

Finally, my evaluation of Judge Newman’s abilities to understand complex technologies and apply, in real time, complicated legal doctrines to the issues raised by these technologies showed that Judge Newman remains fully capable to engage in the work of a judge of the United States Court of Appeals for the Federal Circuit.

In short, in my expert professional opinion, and to a reasonable degree of medical certainty, based on the combined test results there is no evidence that Judge Newman suffers from any cognitive impairment, and she is fully able to discharge the duties of her office. This report should allow the Special Committee and the Judicial Council “to fulfill its assigned task under the Act—namely, making an *informed* assessment ... about whether Judge Newman suffers from a disability.” Judicial Council Order of Sept. 20, 2023, at 68, <https://tinyurl.com/hybufxy2> (emphasis in original) (“Sept. 20 Order”).²

² I have confined this report solely to the issue of Judge Newman’s cognitive state and do not opine on any other matter that the Committee may be investigating. See Special Committee Order of June 20, 2023 at 2-3, <https://tinyurl.com/5n7e3mpp>.

I. PREFACE

As a preface to this report, I provide the following context.

Judge Newman graduated from Vassar College in 1947 with majors in chemistry and philosophy, obtained an M.A. from Columbia University in 1948, and a Ph.D. in chemistry from Yale University in 1952. Thereafter, she worked as a chemist and research scientist with American Cyanamid. She obtained her law degree at NYU in 1958 and worked as patent counsel for FMC Corporation. She served as a science policy specialist for UNESCO, was a member of the State Department Advisory Council for International Intellectual Property between 1974 and 1984, and participated in the creation of the Court of Appeals of the Federal Circuit between 1979 and 1982. She was appointed to the Court on January 30, 1984, by President Ronald Reagan.

The events leading up to the suspension of Judge Newman are thoroughly set forth in a) Special Committee's order of May 16, 2023; b) Special Committee's Report and Recommendation of July 31, 2023; c) Judicial Council's order of September 20, 2023; d) Judge Newman's responses to the above; and e) Defendants' combined memorandum in support of their motion to dismiss in opposition to plaintiff's preliminary injunction motion, in *Newman v. Moore*, No. 23-cv-1334 (D.D.C., Sept. 1, 2023). I have reviewed all of the above documents together with all of the supporting affidavits accompanying the same. *See* Exhibits to 2023 R&R.

At issue in this assessment is a suspicion that the Hon. Pauline Newman, a United States Circuit Judge of the United States Court of Appeals for the Federal Circuit is suffering from a loss of, or deterioration in, her cognitive abilities making her potentially unable to discharge the duties of her office. This suspicion or concern led the Judicial Council of the Federal Circuit to order Judge Newman to undergo neurological and neuropsychological testing. Judge Newman declined to abide by the order to undergo neuropsychological batteries of tests, in large part due to her concerns about objectivity, reliability, and relevance of the ordered tests. This refusal led to an impasse between Judge Newman and her Judicial Council colleagues which ultimately culminated in an order suspending her from the judicial work of the Court for a period of one year. *See* Sept. 20 Order.³ The suspension was recently renewed for another year. *See* Judicial Council Order of Sept. 6, 2024, <https://tinyurl.com/3xxukyac>. Additionally, the dispute between Judge Newman and her colleagues is the subject of an ongoing litigation. *See Newman v. Moore*, No. 1:23-cv-01334-CRC (D.D.C., dismissed on July 9, 2024), *appeal filed* July 10, 2024, (D.C. Cir. No. 24-5173).

³ Judge Newman was suspended from hearing cases as early as March of 2023. The Judicial Council of the Federal Circuit explained that the pre-September 2023 suspension was for reasons unrelated to her refusal to submit to requested testing. *See* Judicial Council Order of June 5, 2023, <https://tinyurl.com/4unuxeyf>.

I am acting *pro bono* and have no financial interest in any of the technologies or methods relied on in this evaluation. Although I am an inventor of a successful technology in brain imaging that saves thousands of lives every year and which is the subject of 480,000 publications identifiable on Google Scholar and nearly 30,000 peer reviewed publications held by the National Library of Medicine, *see Diffusion Tensor Imaging*, US Pat. No. 5,560,360 (Exhibit 2), this technology was not used in the present assessment. I have an extremely busy medical practice booked months in advance, do this medical work eighty to one hundred hours per week, and am in no need of seeking out additional patients through the provision of this report. My only interaction with Judge Newman prior to this contact and evaluation are the wholly routine events attendant on her assignment to the two oral arguments noted above.

Neither Judge Newman nor her attorneys sought out my services. Rather, I contacted Judge Newman's attorneys and offered to provide the evaluation and assessment because, like everyone else involved, I want to see that the resolution of this matter by the relevant courts and administrative bodies benefits from the best possible medical information in support of the ultimate decision.

I have tremendous respect for the entire judicial bench of the Court of Appeals of the Federal Circuit. I believe that this Court makes the world leading patent system of the United States possible. As a member of the Bar of this Court, I have argued before and received a favorable opinion authored by the Hon. Richard Taranto in 2019. I have argued three times before this court: in 2016 (Case No. 15-1687, heard by Circuit Judges Lourie, Dyk, and Hughes); in 2019 (Case No. 18-2363, heard by Circuit Judges Taranto, Newman, and O'Malley); and in 2022 (Case No. 21-1552, heard by Circuit Judges Newman, Reyna, and Wallach).⁴ I have also recently attended the Federal Circuit Judicial Conference held on May 14, 2024, and based on the presentations at the Conference (including the opening presentation by Chief Justice of the United States, the Hon. John G. Roberts)—am highly impressed and appreciative of what Chief Judge Kimberly Moore has done to advance the capabilities and effectiveness of the Court of Appeals for the Federal Circuit.

⁴ My appearances before panels of this Court which included Judge Newman resulted in success once, *see NeuroGrafix v. Brainlab, Inc.*, 787 F. App'x 710 (Fed. Cir. 2019) (opinion by Taranto, J.) (non-precedential) (Exhibit 8), and leaving the ruling below undisturbed once, *see Filler v. United States*, 2022 WL 193199 (Fed. Cir. Jan. 21, 2022) (Rule 36 judgment without opinion). My third (and earliest) argument was not before Judge Newman. *See In Re Filler*, No. 15-1687, 636 F. App'x 802 (Fed. Cir. 2016) (Rule 36 judgment) (affirming a Patent Trial and Appeal Board (Appeal 2014-006569) ruling that reversed 10 but sustained 6 rejections from the original 66 claims where all of the rejections concerned the Magnetic Resonance Neurography claims and did not affect the DTI claims).

This document was not prepared in order to take sides in the dispute between Judge Newman and her colleagues, but to provide objective data to the relevant decision-makers. The utility of the medical opinion that this report sets forth is also detailed below.

Central to this report is an advanced modern Perfusion CT scan obtained at the George Washington University Hospital on August 22, 2024, at my direction and following Judge Newman's consent to proceed with this accurate and objective test. Unlike a situation where there may be a "defense neuropsychology report" and a "plaintiff neuropsychology report" that disagree completely on nearly every conclusion, there is no "defense CT scan" and "plaintiff CT scan" because the data is objective.

Neuropsychology testing is not tethered to neuroanatomy or neurophysiology and is not typically performed by a physician.⁵ In contradistinction, as explained below, technology has advanced, so that measurements such as high cerebral blood volume (CBV), high cerebral blood flow (CBF), absence of any delay in blood transit time (TTmax), and very strong AIF - arterial input function AI calculation for the right and left hippocampal structures of Judge Newman are decisive.

This asserted medical view from my perspective as an expert in this field, is especially decisive when taken together with a) my review of Judge Newman's most recent written opinions, b) the remainder of my examinations, and c) the opinions of Drs. Ted L. Rothstein, MD and Regina M. Carney, MD. On these pillars, I believe that the relevant judicial evaluators should conclude that the components of this report can and do meaningfully and relevantly show that Judge Newman does not suffer from any dementia or detectable decline in intellectual function and that the Judicial Council's request for medical evaluation of the Hon. Pauline Newman has now been sufficiently completed.

Critical Preliminary Fact: Excellent published medical data show that intellectual and/or cognitive decline does not necessarily occur with aging even though it does often occur. The best data is present in Sudlow, *et al.*, *UK Biobank: An Open Access Resource for Identifying the Causes of a Wide Range of Complex Diseases of Middle and Old Age*, 12 PLOS Med. e1001779 (2015). This information was based on assessments of 15,000 individuals. *See also* Powell, *et al.*, *Defining Exceptional Cognition in Older Adults: A Systematic Review of Cognitive Super-Aging*, 38 Int. J. Geriatric Psych. e6034 (2023) (summarizing 44 publications in this field). Given this fact, it is my expert opinion that the demonstration of the absence or presence of cognitive decline as to Judge Newman must be usefully assessed only by an exam on a personal and individual basis pertinent to her to the capabilities expected of her. Therefore, this assessment undertakes to test and document ongoing judicial excellence and capability (or lack thereof) on a particularized and individualized basis with the highest of standards as to her required physiological

⁵ Indeed, the Special Committee ordered that testing be done by a neuropsychologist who does not have medical training and has been in practice for less than a decade. *See* May 16 Order at 19.

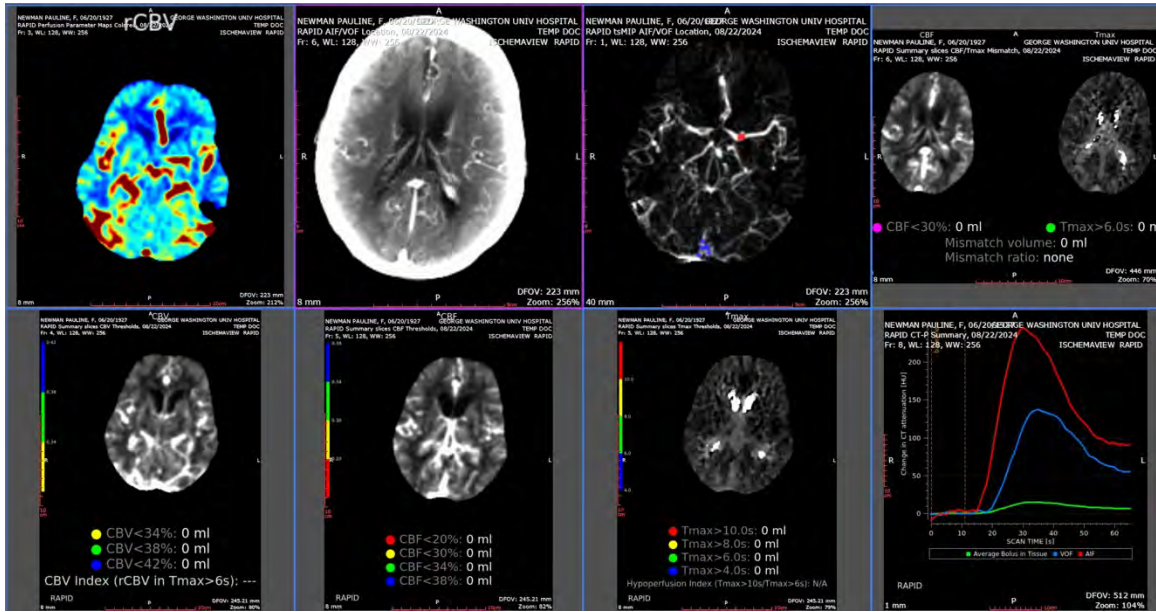
intellectual status and relevant capabilities in technology and patent law and not by assumptions deriving from general population-based expectations.

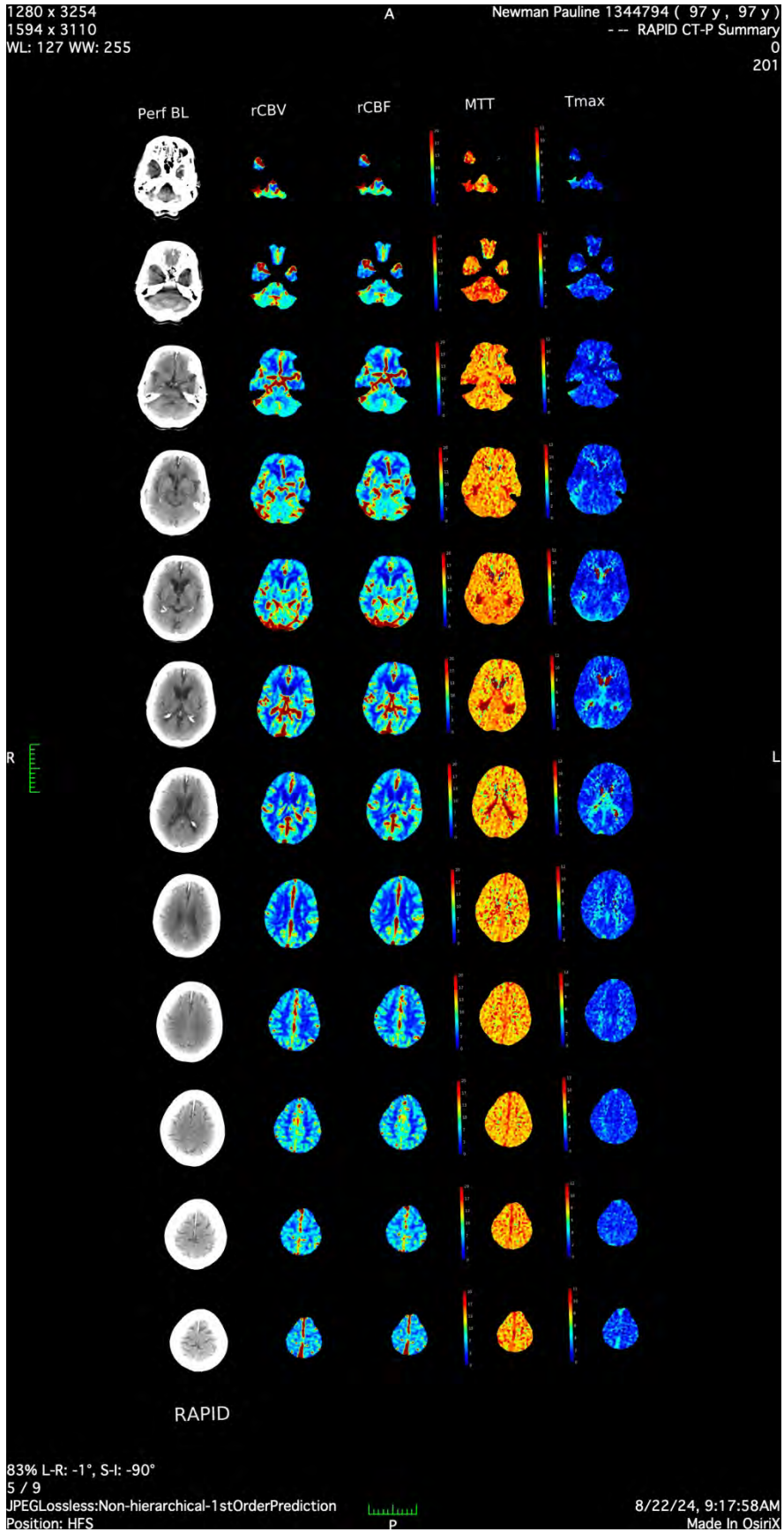
II. STRUCTURE OF THE REPORT

To resolve the essentially medical dispute, *see* Special Committee Report and Recommendation of July 24, 2024 at 21 (“We agree that the proper specialist medical examinations and medical records are crucial to an evaluation of disability.”), as to appropriate and relevant cognitive status testing/evaluation, I have recommended, and I am here reporting three parallel and collectively comprehensive tracks of evaluation I have performed:

1. Detailed Classical Neurological Examination by a cognitive specialist Board Certified neurosurgeon to support inferences as to general neurological status which I conducted. As a neurosurgeon with sub-specialty in this field, I am fully qualified to conduct and have conducted thousands of such examinations.
2. Direct real-time interview, conducted by myself in my capacity as a neurosurgeon, inventor (11 granted patents – *see* attached CV (Exhibit 1)), and author of a book on inventions and patents (Smart Guide series “Smart Guide to Patents” 2012 (Exhibit 11)). This exam component focuses on patenting issues in advanced technology with assessment for immediate rapid fluent verbal generation of patent law analysis. The purpose of this component was to make direct relevant personal experience comparisons relative to two oral arguments in 2019 and 2022 before panels which included Judge Newman, both of which occurred prior to the beginning of the current investigation.
3. Advanced functional testing by brain imaging of Judge Newman, which included a battery of eight separate modern, universally accepted analytical assessments, was conducted on August 22, 2024, at the George Washington University Hospital in Washington, DC as described below.
 - Perfusion CT scan analyzed directly by:
 - Analysis Software: i-RAPID AI CTP Ischemaview
 - (Computed Tomography Perfusion)
 - Scanner: Siemens Somatom Definition Flash
 - Dual Energy 256 Slice CT with Siemens Stellar detectors
 - Rotation Time: 0.28 seconds
 - Isotropic Resolution: 0.33 millimeters
 - Temporal Resolution: 75 milliseconds
 - Scan Speed: 458 mm/s³ with Flash Spiral active

Newman, Pauline
 DOB: 6/20/1927
 August 24, 2024
 Page 10 of 44





Newman, Pauline
DOB: 6/20/1927
August 24, 2024
Page 12 of 44

GWU- George Washington University Hospital
Washington, DC 20037-2342
(202) 715-4000

Patient: NEWMAN, PAULINE

Date of Birth: 6/20/1927

Ordering Physician: Temp MD,Doc 500199

Patient Type: Outpatient

Patient Location: GWU Radiology

Attending Physician: Temp MD,Doc 500199

ATTN: Dr. Aaron Filley, MD
Imaging

PROCEDURE
CT Angio Head w/ Contrst Incl w/o Images

EXAM DATE/TIME
8/22/2024 09:29 EDT

PROCEDURE: CT ANGIO HEAD W/ CONTRAST INCL W/O IMAGES IF PERFO

COMPARISON: None.

TECHNIQUE: Only perfusion scan images are included in this report.

INDICATIONS: Cognitive

FINDINGS:

PERFUSION DATA PROVIDED BY i-RAPID SOFTWARE:

The diagnostic value of the parameters provided below can decrease as a result of different types of artifact including those related to motion.

A = Volume of tissue with CBF <30% relative to contralateral side: 0 ml

B = Volume of tissue with Tmax > 6.0 s relative to contralateral side: 0 ml

Mismatch Volume (B -A): 0 ml

Mismatch Ratio (B / A): N/A

CONCLUSION:

1. Perfusion scan only without accompanying non-con CT or CTA.
2. i-RAPID CT Perfusion analysis documents are available in PACS for review.

I, Dr. M. Reza Taheri, am the attending radiologist, and my electronic signature below attests of the fact that I have personally reviewed the images, and agree with or have edited the findings described above by the resident or fellow, and have personally inserted this statement.

Appendix 1: ASPECT Score

MRN:GWU1344794

FIN:GWU0000146333307

Accession Number: 55-CT-24-030010

Page 1 of 2

Report Request Id: 330589604

The result of these tests—which I have additionally interpreted myself—is that Judge Newman’s Perfusion CT demonstrates no evidence of any identifiable deteriorations that are known to be attendant on age and/or disease. In fact, these scans demonstrate *none* of the various known abnormalities that accompany the various dementias even at their pre-clinical stages. Further, it is my expert opinion that the color map images of regional Cerebral Blood Volume and regional Cerebral Blood Flow—which show that Judge

Newman, Pauline
DOB: 6/20/1927
August 24, 2024
Page 13 of 44

Newman’s brain demonstrates a very high rate of effective perfusion of the hippocampal region bilaterally—are reflective of her high capability for integrative thought, memory and structured creative professional expression.

It is also my expert opinion that this result, taken together with my findings upon neurological examination and the interview with a requirement of immediate response to challenges on complex advanced technology in *biochemistry/molecular biology* and separately, in industrial application of *matter/anti-matter reactions in nuclear physics* as to patent law implications of these technologies, demonstrate excellent cognitive skills sufficient to warrant full return to her judicial duties. It is highly unlikely that any person suffering from even mild cognitive decline could rapidly understand and explain back this level of complex technology in disparate fields and then immediately progress to an on-target analysis of equally complex patent law issues.

III. EXPERT’S BACKGROUND AND QUALIFICATIONS

I am a licensed physician in the District of Columbia, with license number MD600003193, issued on September 9, 2024.⁶ I am also licensed in several other states including, but not limited to Virginia, California, Massachusetts, New York, and Texas.

I have significant expertise in neurosurgery, brain injury, cognitive evaluation and brain imaging. In 1986, I received my MD degree from the University of Chicago and a PhD in Biological Anthropology from Harvard University. I am an editor of the major textbook in neurosurgery (*Youmans & Winn, Neurological Surgery* (8th ed., Elsevier)) and an author of several chapters in that text including the chapter on Diffusion Tensor Imaging of the brain—a technology I invented and patented. *See* U.S. Pat. No. 5,560,360. I serve on the Continuing Medical Education Committee of Cedars Sinai Medical Center in Los Angeles. For many years, I have also served on the Joint Guidelines Committee of the American Association of Neurological Surgeons and the Congress of Neurological Surgeons. I have been admitted as an expert in more than a hundred trials in various state and federal courts and my testimony has never been excluded. My most recent federal court testimony was *Haysbert v. Bloomin’ Brands, Inc.*, No. 20-cv-121 (E.D. Va., Rebecca Beach Smith, J.) regarding a head injury suffered by a 75-year-old university provost.⁷

⁶ At the time of the examination, my practice in the District of Columbia was authorized by D.C. Code §3-1205.02(3A) (authorizing practice by “an individual retained to assess or evaluate a subject and to testify as an expert witness in any court or administrative proceeding, hearing, or trial”) and §3-1205.02(4) (authorizing practice by “a health professional who is authorized to practice a health occupation in any state adjoining the District who treats patients in the District” under certain conditions which I met).

⁷ As in other cases, the Court rejected defendant’s motion to exclude my testimony.

In addition to my medical practice, I am also past president and general counsel for the Society of Brain Mapping and Therapeutics, an organization with several thousand members devoted to advanced technology in the neurological sciences. I have also served as a physician in the United States Army Reserve, reaching the rank of lieutenant colonel and serving as a Commander of the 1466th Med Team Neurosurgery.

I am currently on staff at Cedars-Sinai Medical Center in Los Angeles and St. John's Hospital, Providence, in Santa Monica, California, where my main principal office is located. I also have offices in Houston, Texas, and Dallas, Texas. I have an active practice and most recently (September 6, 2024) performed a complex specialized 12 hour surgery on a patient who traveled from Ontario, Canada. I have extensive experience with evaluating brain function, as set forth most recently in a presentation entitled *Clinical Application of Diffusion Tensor Imaging for Diagnosis and Treatment of Persistent Post-Concussive Symptoms in Individual Traumatic Brain Injury Patients*, delivered on September 10, 2023, at the Walter Washington Convention Center in Washington, DC at the 73rd Annual Meeting of the Congress of Neurological Surgeons.

I am preparing this report to help definitively settle any questions or concerns arising about the cognitive capabilities of Judge Pauline Newman. In doing so, I am relying on my specialty and expertise as a neurosurgeon, as well as my experience as a member of the Bar of the United States Court of Appeals of the Federal Circuit and a member of the Federal Circuit Bar Association. I carry out 10 to 12 similar evaluations per week on a wide variety of individuals, with wide range of occupations and educational backgrounds. Among people I routinely examine are physicians, attorneys, executives of large corporations, and similarly situated patients. From this practice, which includes at least 1,500 individuals evaluated by DTI imaging exam combined with a personal medical examination, in a large clinical report under preparation, I have acquired a focused special expertise, which I am relying on to address to the question of Judge Newman's the neurologic and cognitive capabilities.

IV. BACKGROUND ON THE UTILIZED PERFUSION CT TECHNOLOGY

The first CT scanner was built by Godfrey Hounsfield at Atkinson Morley's Hospital in Wimbledon in 1971—the same institution where I later worked and that funded my research leading to the first Diffusion Tensor Tractogram in 1992. *See* US Pat. No. 5,560,360, Fig. 17; *see also* A.G. Filler, *The History, Development and Impact of Computed Imaging in Neurological Diagnosis and Neurosurgery: CT, MRI and DTI*, 7 *Internet J. Neurosurg.* 1 (2009) (explaining the physics, math and technology of CT scan image generation and showing the first CT scans ever obtained – available online on *ResearchGate* and attached to this report) (Exhibit 4).

In the past, a single X-ray source and oppositely placed detector captured a series of individual image paths as the pair was rotated around the patient.⁸ In contrast, in modern CT technology—such as for the Siemens Definition Flash CT used for this study—effectively 256 rows of “scan and detect” circular sets simultaneously accomplish the complete collection of 256 separate image slices in less than a 100 milliseconds. This process—completing the entire scan of the brain in a fraction of a second—is then repeated over and over again as a single bolus of contrast agent passes through the target structure. The 128 x 2 rows of image collection are each slightly helical so there is no missed “space between slices” as on older CT and MRI scanners. The temporal resolution allows a view into the behavior of blood flow in active tissues that opens up an entirely new realm of understanding and testing in medicine.

The technology involved here is not routine CT scanning. It is Perfusion CT scanning, and Perfusion CT is a modern advance on CT scanning, which is proving more precise and accurate than comparable MRI and nuclear medicine-based approaches. Essentially, these high-count multi-slice scanners, extremely rapid CT scanning with extremely sensitive density assessments have opened a new means of providing important new levels of detail in brain function. An extensive literature has developed showing that a number of analytic paradigms for processing Perfusion CT data are highly relevant to assessment of mild early dementia or even patients showing no symptoms of dementia but having findings that are predictive of the future expectation of dementia.

Perfusion CT additionally differs from routine CT or contrast CT essentially as follows; a timed, mechanically administered precise bolus of contrast agent is injected into the bloodstream and the imaging follows the front wave of this single bolus as it passes through the brain. The data tracks the amount of contrast entering relative to tissue and the rate at which it passes through various parts of the brain and therefore can provide detailed scoring of vascularity and perfusion of numerous particular structures in the brain. This has proven to be highly correlated with disease and disease progression in the field of dementia. It provides a far more accurate and objective basis not only as to the presence or absence of any dementia but of the particular type, subtype, and mechanism.

The scan parameters cited above state that the entire mass of scanning is completed in less than one third of a second. It can then be repeated again and again as the wave front of a single bolus of contrast agent progresses into and through the brain. This allows for very high spatial resolution and detailed studies of the rate and pattern of blood perfusion

⁸ In classical CT scanning a single X-ray source is rotated around the patient taking a series of image beam paths which are reconstructed to generate an image of a “slice” of the patient body through “back projection” mathematical calculations. See Filler (2009), *supra* (offering a detailed explanation). The patient table is then advanced a few millimeters, and another slice image is obtained and so forth until 10 to 20 image slices have been obtained. Originally, the whole process could have taken 20 or 30 minutes to complete an entire brain image.

as the fine patterns of the arrival and passage of the front wave of the bolus of contrast agent passes through the brain.⁹

Twenty years of imaging and neuroscience research show that declines in perfusion pattern correlate strongly with the major categories of mental decline associated with classic dementias. Conversely, excellent flow—such as those demonstrated by Judge Pauline Newman’s Perfusion CT brain scan—provides a reliable basis to exclude/rule out dementia, both on a categorical and individual basis. This is particularly true when the perfusion results correlate with appropriately targeted cognitive assessments which were conducted and are reported on below. There is substantial medical literature that convincingly supports the proposition that high speed perfusion brain imaging supplants the inevitably subjective practice of neuropsychology in the fundamentals of cognitive assessment.

A model based on neuroanatomy, neurochemistry, and neuroimaging can depict impairment on a clear objective basis. As recently as thirty years ago medical imaging was not up to the task. Now it is.

The literature cited in the following paragraphs relates to attempts to improve the technology of the test such as more advanced pulse sequences for more effective Arterial Spin Labeling (ASL is used with MRI for Perfusion scanning but has lower spatial and temporal resolution compared to the most advanced CT scanners) to avoid having to give contrast injections, but really do not provide any dispute as to the fundamental validity that is being shown for these methods. Noting again that the different reports will focus on different disease categories in order to provide homogeneous sets of patients, the underlying result of the validity of these tests is clear.

Togao, et al., Arterial Spin Labeling Based MR Angiography for Cerebrovascular Diseases, Principles, and Clinical Applications, 60 J. Magn. Reason. Imag. 1305 (2023), generally explains the value and clinical uses of brain imaging techniques such as arterial spin labeling.¹⁰

Metting, et al., Cerebral Perfusion and Neuropsychological Followup in Mild Traumatic Brain Injury, Acute Versus Chronic Disturbances, 86 Brain and Cognition 24 (2014) reports, based on a study of 191 patients, that where a variety of neuropsychological batteries are used and then compared to CT results, impairments in executive functioning and emotion perception assessed with neuropsychological tests during *follow-up*, were

⁹ A comparable method in MRI is called arterial spin labelling (ASL), but for this area of imaging, CT exceeds the capabilities of MRI for speed, accuracy and spatial/temporal resolution.

¹⁰ As noted above, *see* n.9, *supra*, Perfusion CT and ASL are comparable technologies, with the former actually exceeding the capabilities of the latter.

related to differences in cerebral perfusion *at admission* in mild traumatic brain injury cases. It further concludes that the focal cerebral perfusion data provides an objective basis for assessing the same functions that the neuropsychological testing such as facial expression of emotional stimuli and tests, the zoom app test for behavioral assessment of dis-executive syndrome, the ADS battery, the trail making test, immediate recall, Rey auditory verbal learning test, and a two-hour battery of various neuropsychological tests.

Dash, *et al.*, *Perfusion CT imaging as a diagnostic and prognostic tool for dementia: prospective case–control study*, 99 *Postgrad. Med. J.* 318 (2022) (Exhibit 6), reports that perfusion CT is a reliable imaging modality for early diagnosis of dementia and differentiating vascular dementia from Alzheimer’s disease. The study shows that perfusion parameters are positively correlated with the results of Montreal Cognitive Assessment (“MOCA”). The study concluded that Perfusion CT can be used as a surrogate marker of cognitive status in the follow-up of patients with dementia.

Hart, *et al.*, *Neuroimaging of Cognitive Dysfunction and Depression in Aging Retired National Football League Players*, 70 *J. Am. Med. Ass’n Neurology* 326 (2013), matches behavioral changes to image findings on the arterial spin labeling,¹¹ thus demonstrating the validity of such image findings.

Streitparth, *et al.*, *Diagnostic Value of Multislice Perfusion CT in Dementia Patients*, 48 *Radiologie* 175 (2008),¹² reports on a study of 55 subjects, and concludes that on an analysis of blood volume, blood flow, and transit time—all parameters of a Perfusion CT scan, while pairing these results with a Mini-Mental Status Examination, cerebral perfusion decreased with an increasing degree of dementia. The study describes Perfusion CT scan as an inexpensive, widely available methodology, which can reveal information about regional differences of cerebral perfusion, which is in turn useful for differentiating severity and types of dementia.

The Perfusion CT performed to scan Judge Newman at George Washington University Hospital on August 22, 2024, is the method at the technological front line of what is available for clinical hospital imaging of brain function as to accuracy and spatial resolution today.

V. INFORMATION CONSIDERED IN PREPARING THIS REPORT

This report makes public selected items of Judge Newman’s medical record (all of the information in my possession) for purposes of providing advanced current medical data and opinion relevant to the Federal Circuit’s Special Committee and Federal Circuit’s

¹¹ *Id.*

¹² This article is written in German, but an English-language abstract is available.

Judicial Council orders, reflecting Judge Newman's colleagues' concerns regarding her cognitive abilities.

VI. PAST MEDICAL HISTORY

I have also been given an opportunity to review¹³ Judge Newman's medical records spanning the last two years in detail and have completed that review. The records reviewed spanned more than 2,000 pages. All of these have been adequately summarized in the notes of Dr. Rothstein and Dr. Carney. Judge Newman's records indicate that she has been (or is being) successfully treated for the various diagnoses identified below. Judge Newman denied having had a heart attack at any point in her life or any fainting episodes, and records do not reveal any such episodes.

The only recent issue of relevance is what appears to be an episode of sub-clinical sepsis leading to acute anemia in late 2023 to early 2024. The problem was diagnosed and once the infection was resolved, she demonstrated a vigorous and rapid resolution of the anemia. In my expert opinion, none of Judge Newman's medical conditions revealed by her records are ultimately contributory or relevant to her current mental state, and none suggest a cognitive decline or neurological deficits.

VII. PAST MEDICAL RECORDS

Prior to preparing this report, I reviewed Judge Newman's medical records dating back to early 2021, wherein Judge Newman provided these to me for review consistent with the Special Committee's orders. *See* May 16 Order at 5-6.

Notes on the Hon. Pauline Newman's Past Medical Records:

Detailed Review of 876-page medical record for George Washington University Hospital (GWUH) and Virginia Hospital Center – (with much internal redundancy)

Detailed Review of 908-page One Medical Group Records (Reston, VA).

Additional Separate Records (with some repetition to the One Medical Group Records) constituting about 90 pages of notes from Jenna Byorek AGNP-BC and John Feigert, MD as to various hematologic concerns were reviewed in parallel.

There were also about 30 pages of LabCorps reports – some of which reported laboratory results that also appeared in the hospital records (VHC and GWUH) and outpatient records from One Medical Group.

¹³ After review, all records were returned to Judge Newman.

- [REDACTED]
- [REDACTED]
- [REDACTED]
- [REDACTED]
- Routine cognitive impairment screening (Mini-Cog Survey) 10/31/2023
 - Normal per neurologist (per One Medical Group records) (form not in records) (unclear if this is a second different test by another neurologist)
- Modified MOCA Cognitive test (Neurologist; Ted L. Rothstein, MD) 6/21/2023
 - Reported as normal
- [REDACTED]
- [REDACTED]
- [REDACTED]
- [REDACTED]
- [REDACTED]
- [REDACTED]
- [REDACTED]
- Myocardial Perfusion Scan 2/4/2022 (Tc99m) (SPECT) (Richard Perrin, MD)
 - Normal
- Depression screening PHQ-2
 - 2/26/2021 – negative
 - 9/2/2022 – negative
 - 4/1/2024 – negative

[REDACTED]

[REDACTED]

[REDACTED]

Primary Care – [REDACTED]

Internal Medicine

- [REDACTED]

Cardiology

- [REDACTED]

Summary Assessment of 2023 to 2024 Medical Events and Treatments

The One Medical Group Records provide a sequential summary of events as additional paragraphs are added to a lead summary, but overall covering the same events

Newman, Pauline
DOB: 6/20/1927
August 24, 2024
Page 24 of 44

demonstrated in the Virginia Hospital Center and George Washington University Hospital Records.

At One Medical, Nurse Practitioners – such as [REDACTED] along with Judge Newman's lead Primary Care physician— [REDACTED]—and their associates/referral/referring medical practitioners ([REDACTED]) manage various routine day to day medical issues, review incoming records from VHC and GWUH and interact with home visit staff.

Entries from 2/8/2024, 3/20/2024, 4/26/2024, 5/1/24, 5/7/2024, 5/9/2024, 5/16/2024, 5/23/2024, 6/10/2024, 7/1/2024, 7/19/2024, and 7/31/2024 were reviewed. Of note, Judge Newman's [REDACTED] now appear to have stabilized in a normal range on a continuing basis.

The overall current assessment of her One Medical Group providers as of 7/31/2024 is: "Able to carry on normal activity; minor signs or symptoms of disease"

Overall – the principal medical events of the previous 12 months appear to be various complications of low-level sepsis – with the underlying causes of the infection being unclear. [REDACTED]

[REDACTED] But ultimately, [REDACTED], the symptoms now appear to be resolved with no lasting consequence. The care record demonstrates an impressive degree of seamless integration among generalist and specialist physicians and nurse practitioners, deploying reasonable testing regimes and timely correct treatments across a wide variety of medical specialties.

Consistent with my evaluation, Judge Newman now appears to be in very good health consistent with the demands and requirements of her usual work – as to her general medical status. She has excellent and promptly responsive physician and nurse practitioner caregivers that appear to seamlessly communicate as to home health, outpatient clinic and hospital-based services. Her recovery from the sepsis [REDACTED] seems complete. The cause is not fully determined but appears to be routine – in that the onset and course could readily have occurred to any individual and does not appear to be age related.

Her medical team clearly makes good use of modern electronic medical record methodology to achieve an excellent level of communication among the various practitioners. The degree of coordinated interactions between the medical providers and Judge Newman is of very high quality, so that despite the number of treatment elements involved, Judge Newman has been able to complete many opinions and clear her previous backlog during 2023, even as some of the earlier of these various medical events were taking place.

VIII. EXAMINATION

On August 24, 2024, I have personally examined Judge Newman, carrying out her evaluation in her chambers at the United States Court of Appeals of the Federal Circuit in Washington, DC.

In addition to the traditional neurologic exam (discussed below) and the aforementioned CT scan, I have reviewed several of Judge Newman's written opinions, including:

- *Commil USA, LLC v. Cisco*, 720 F.3d 1361 (Newman, J., concurring in part and dissenting in part) (Fed. Cir. 2013), *vacated by* 575 U.S. 632 (2015);
- *SAS Inst. v. ComplementSoft, LLC*, 825 F.3d 1341 (Fed. Cir. 2016) (Newman, J., concurring in part and dissenting in part), *rev'd sub nom. by SAS Inst. v. Iancu*, 584 U.S. 357 (2018);
- *Bishay v. United States*, 2022 WL 3754199 (Fed. Cir. Aug. 30, 2022) (Newman, J., dissenting) (non-precedential);
- *Dep't of Transp. v. Eagle Peak Rock and Paving, Inc.*, 69 F.4th 1367 (Fed. Cir. 2023) (Newman, J., dissenting);
- *GSS Holdings (Liberty), Inc. v. United States*, 81 F.4th 1378 (Fed. Cir. 2023) (Newman, J., dissenting);
- *Incept, LLC v. Palette Life SCIS, Inc.*, 77 F.4th 1366 (Fed. Cir. 2023) (Newman, J., concurring in part and dissenting in part);
- *Military-Veterans Advocacy, Inc. v. Secr'y of Vet. Aff.*, 63 F.4th 935 (Fed. Cir. 2023) (opinion by Newman, J.);
- *SAS Inst. v. World Programming LTD*, 64 F.4th 1319 (Fed. Cir. 2023) (Newman, J., dissenting); and
- *Watson v. McDonough*, 2023 WL 7381456 (Fed. Cir. Nov. 8, 2023) (opinion by Newman, J.) (non-precedential).

The review of the above opinions was not legal, but medical. In other words, the purpose of the review was to compare Judge Newman's current written product to that which preceded the allegations of cognitive decline. This review formed part of my assessment of Judge Newman's cognitive status.

Additionally, I drew on my own experience as an attorney appearing before panels which included Judge Newman (case No. 18-2363, argued on August 6, 2019 and case No. 21-1552, argued on January 13, 2022, both in relation to US Pat. No. 5,560,360), to compare Judge Newman's current fluency, attention-span, understanding, affect and the like, to that which she exhibited at the time of the aforementioned oral arguments. Purely from a medical perspective, the participation of Hon. Pauline Newman in the 2019 and 2022 oral arguments in which I participated demonstrated vigorous, thoughtful

participation. This stands out clearly as more than comparable when compared to the audio of the panel which did not include Judge Newman and before which I argued in 2015.

The purpose of this review is limited to my medical and professional assessment of Judge Newman's capabilities. In addition to medical experience and expertise, my legal experience and expertise was brought to bear because the question before me is whether she is mentally and physically fit to fulfill her responsibilities as a United States Circuit Judge for the Court of Appeals for the Federal Circuit. As a litigant, a member of the Bar of the Federal Circuit, and a member of the Federal Circuit Bar Association, I am able to evaluate Judge Newman's medical information as it *specifically* relates to her judicial position.

The evaluation of Judge Newman did not include a DTI image because she was ineligible for MRI scanning due to a pacemaker wherein the current corporate owner of the relevant pacemaker type was not able to provide adequate assurance for MRI imaging.¹⁴

IX. INDICATIONS FOR A PERFUSION CT BRAIN SCAN

Indications are as follows; firstly, of note, I have had a chance to review the evaluations and opinions of Dr. Ted L. Rothstein, Professor of Neurology at George Washington University, who evaluated Judge Newman over the same issues with his report of June 21, 2023, and the report of forensic psychiatrist Dr. Regina M. Carney of her August 25, 2023 evaluation, including the Mini-Mental State Examination carried out by Dr. Carney.

It was my choice to obtain a Perfusion CT because of the ineligibility of Judge Newman for a DTI due to her pacemaker. Nevertheless, it is widely recognized that Perfusion CT scanning and the similar test of MRI-ASL evaluations (see below for further explanation) can, and do, supplant and replace the previously used neuropsychology evaluations, which are subjective and rooted in a testing framework arising in the 16th century.

Current reports indicating the *relevance* of Perfusion CT (and ASL-MRI), and their role in replacing neuropsychology evaluations as a result of the perfusion studies' much higher relevance and accuracy, are set forth in Dash, *supra*; Togao, *supra*; Zhang, *The value of whole-brain CT perfusion imaging and CT angiography using a 320-slice CT scanner in the diagnosis of MCI and AD patients*, 27 *Europ. Radiology* 4756 (2017); Pasternak, *et al.*, *Longitudinal cerebral perfusion in presymptomatic genetic*

¹⁴ Her Pacemaker is a St. Jude Assurity DR 2240, SR#7831442, that was implanted on November 10, 2016 after an episode of bradycardia. The leads are Tendril STC 2088TC of various relevant lengths. Our investigation revealed that when St. Jude was purchased by Abbott, the new owning manufacturer did not file sufficient information with the FDA to allow for any MRI clearances by the new owner. Therefore, she cannot have an MRI scan.

frontotemporal dementia: GENFI results, 20 J Alzheimer's & Dementia 3525 (2024) (Exhibit 7); Latchaw, *et al.*, *Guidelines and recommendations for perfusion imaging in cerebral ischemia: a scientific statement for healthcare professionals by the writing group on perfusion imaging*, 34 Stroke 1084 (2003); and *CT Brain Perfusion Protocol*, Radiopaedia (July 2024).

X. RECENT OPINION WRITING

In our interview in Chambers on August 24, 2024, Judge Newman reported that she recognizes that her rate of production of opinions had slowed somewhat but drew attention to her success in resolving the backlog without compromising the quality of her opinions.

I have reviewed the opinions discussed above and concur with the assessment by Associate Professor Andrew C. Michaels, that the quality of the dissents, as well as other opinions, appears to be completely adequate as would be expected of a skilled, experienced senior Federal Circuit Court Judge. See Andrew Michaels, *Judge Newman's Recent Dissents Show She Is Fit for Service*, Law360 (June 6, 2023).

XI. DEMEANOR

As to demeanor, I found Judge Newman to be gracious, informative and communicative. She demonstrated appropriate personal insight in calmly and evenly describing to me the events leading up to the current impasse with the Federal Circuit Judicial Council. I appreciate that all persons experience episodes of irritability and frustration. I typically assess patients—including attorneys—who are experiencing chronic symptoms of persistent post-concussive syndromes and who complain of difficulty with increased anger and irritability, among other symptoms. It is very corrosive for those it is directed at and is often upsetting for those who are the source (*e.g.*, regret for a person's role in such an episode).

I have reviewed the affidavits of various court staff which report that Judge Newman's episodes have increased in frequency and severity. While I understand that Judge Newman recollects several episodes differently than the affiants, I do not endeavor to resolve which recollection is more accurate, and, for the purposes of my evaluation take affiants' statements at face value. I do note that most of the reports of Judge Newman's outburst concern events that occurred following the launch of the present investigation, and thus may be explained by the stress occasioned by this process. At the same time, if there was any inappropriate behavior towards colleagues or subordinates by Judge Newman, I do not seek to justify or excuse it.

Admittedly, as a physician, I had just a single moment in time at which to evaluate Judge Newman, given her behavior during the evaluation, I cannot make any finding of altered demeanor. In any event, it is my understanding that the episodes recounted in the affidavits have served merely as support for the Special Committee's and Judicial

Council's conclusion that medical testing is necessary to evaluate Judge Newman's cognitive state. This medical testing has now been conducted.

XII. GENERAL PHYSICAL EXAMINATION

Physical exam is as follows; this is a 97-year-old woman who appears generally healthy and active as if 20 or more years younger than her stated age. She engages normally and fluidly in interaction and conversation without any apparent diminishment that might be associated with age in the 10th decade as to other individuals. In this regard she presents as a "Super-Ager" in that she does not demonstrate effects of age on cognition or demeanor comparable to many others at this age (*see Sudlow, supra* and *Powell, supra*). Based on my experience as an attorney and my expertise as a physician, the content of her speech is entirely appropriate for a serving Court of Appeals Judge.

Gait and station are normal. She is observed entering and exiting the vehicle by which we arrived at the Courthouse of the Court of Appeals of the Federal Circuit, and then observed walking to the elevator in the parking garage and from the elevator to her chambers.

Vital signs and general assessment were conducted by myself, using electronic versions of traditional medical assessment devices and technologies.

Blood pressure by automated manometry blood pressure assessment of the radial artery at the wrist was systolic 132 and diastolic 68 by electronic display.

Finger oximetry reveals oxygen saturation of 97%, pulse of 62.

Temperature was assessed with a standard digital LCD infrared temporal artery-based thermometry at the glabella between the eyebrows as recorded as 97.8 Fahrenheit, appropriate for age.

Auscultation with a Littmann CORE 500 EKO electronic stethoscope reveals cardiac rate and rhythm pattern as generally normal as displayed on the screen on the hand-held headpiece of the stethoscope. Depth and airflow of respiration and movement of lungs are also generally normal.

The Littmann stethoscope output was also observed on a linked app in the iPhone and appears normal. No electrocardiographic recording was made. Judge Newman had no complaints of pain or physical disability.

XIII. NEUROLOGIC EXAMINATION

Neurologic examination is as follows; the patient is alert and oriented x4, that is, as to person, place, time, and situation. She is able to cooperate fully in examination. Speech

is fluent and normal and directly comparable to my prior personal experience appearing in front of her as a litigant, without distinction from her diction, flow, rate, and complexity of speech. This was confirmed by a review of the publicly available audio of the oral arguments in *NeuroGrafix v. Brain Lab, Inc.*, No. 18-2363 (Aug. 6, 2019) (transcript provided as Exhibit 9) and *Filler v. United States*, No. 21-1552 (Jan. 13, 2022).

CRANIAL NERVE EXAMINATION:

Cranial Nerve I:

- No olfactory abnormalities reported.

Cranial Nerve II:

- Visual fields are full and intact to confrontation.
- The patient did experience some blurring, looking laterally to the left, and notes that she has had a finding of a small cataract. She finds that this was the basis of her choice not to continue driving herself.
- Retinal Examination, which I carried out with the direct inspection using a Welch Allyn Hillrom, model 11820L, PanOptic ophthalmoscope including blue light and slit lamp, as well as direct inspection demonstrated no retinal abnormalities.

Cranial Nerves III, IV and VI:

- Pupils are equal round and reactive to light.
- Extraocular movements are intact.
- There is no nystagmus or limitation observed upon testing of visual pursuits in six directions (up to right, up center, up to the left, down to left, down center, down to right).
- Convergence distance is normal at four inches – there is no evidence of any internuclear ophthalmoplegia or any other eye movement dysfunction.

Cranial Nerve V:

- Sensation intact and uniform to cotton swab testing.
- Masseter function normal and symmetric.

Cranial Nerve VII:

- Face movement symmetric and intact.

Cranial Nerve VIII:

- Weber and Rinne testing using a 256 Hz tuning fork demonstrated symmetric and intact hearing to bone and air conduction.

- Sensorineural and conductive function are normal.

Cranial Nerves IX and X:

- Uvula and palate elevate midline.

Cranial Nerve XI:

- Head turn, and shoulder shrug are 5/5.

Cranial Nerve XII:

- Tongue protrudes midline and moves left to right without difficulty.
- Speech is normal as to diction and tone and volume.
- No dysarthria is appreciated and is generally indistinguishable from my prior personal experience as a litigant before Judge Newman.¹⁵

CEREBELLAR TESTING:

- Hand Eye Coordination: No evidence of dysmetria on finger-to-nose testing.
- Reflexes are 1+ symmetric to biceps, triceps, brachioradialis, patellar and Achille's tendon by examination with a lightweight Trömner MDF HDP Hammer.
- She is stable on Romberg testing, slightly unsteady on heel-to-toe walking.
- No tremor is observed at rest or with intentional movement.
- Directed movements are fluid and precise with no signs of cogwheel rigidity.

AUTONOMIC:

- There is no evidence of blanching or erythema and no other evidence of dysautonomia.

HEAD, SPINE, AND EXTREMITIES EXAMINATION:

- The patient is normocephalic and atraumatic or NCAT.

¹⁵ Clinical assessment included review and comparison with my verbal interaction with Judge Newman in 2019 and 2022. To refresh my own memory, I reviewed publicly available audio recordings of the oral arguments in cases 18-2363 and in 21-1552 posted on the court's website.

- Negative for tenderness for palpation at the occipito-nuchal line, or over cervical, thoracic, and lumbar spinous processes by percussion.
- Neck flexion and extension, turning and lateral bending are performed without limitation or discomfort.
- Shoulder joint function is normal with her arms at her side, at 90 or 180 degrees, no tenderness to palpation along the glenohumeral joint anteriorly or posteriorly, nor along the biceps or supraspinatus tendons.
- Lumbar flexion and extension, twisting and lateral bending are also performed without apparent difficulty or discomfort.

SENSORY EXAMINATION:

- For upper extremities for light touch, pinprick, temperature and vibration is intact to all dermatomes, all modalities.
- Similar results for lower extremities.

MOTOR EXAMINATION:

- Strength exam for upper extremities for biceps, triceps, wrist flexion, wrist extension, supination, pronation, hand intrinsics, finger abduction, finger adduction, lumbricals, opposition of first and fifth digits all unremarkable.
- Normal strength and movement for shoulder abduction, adduction, protraction, retraction with arm at side at 90 degrees and 180 degrees.
- Lower extremity normal strength for plantarflexion, dorsiflexion, extensor hallucis longus, at the knee for flexion and extension.

PERIPHERAL NERVE EXAMINATION:

- Palpation and percussion for carpal tunnel, Guyon's canal, mid forearm, infraclavicular, scalene region, splenius, semispinalis, all unremarkable.

GAIT AND STATION:

- Normal/unremarkable.

XIV. USE OF PERFUSION CT SCANNING FOR COGNITIVE HEALTH ASSESSMENT

At my direction, Judge Newman underwent a perfusion CT scan at the George Washington University Hospital on August 22, 2024. This study was interpreted by a staff

neuroradiologist, Dr. M. Reza Taheri, MD, PhD,¹⁶ as being completely normal. A more detailed evaluation confirmed his opinion.

There is extensive literature on the use of advanced imaging techniques to replace neuropsychology methods which often date back two and three centuries.

Neuropsychology tests often are designed with little specific connection to neuroanatomy and to modern knowledge of brain localization of function. Localization of functions in the brain is an issue I explained to the Court in my oral argument in the 18-2363 matter.

While the *most* advanced type of structural analysis is my invention—diffusion tensor imaging MRI, because of Judge Newman’s pacemaker, it was not possible to obtain clearance for MRI. Given Judge Newman’s pacemaker and the medical question in need of resolution, a Perfusion CT scan is an adequate substitute for diffusion tensor imaging. This advanced CT scanning test is dynamic as well as structural and is far more accurate and specific than neuropsychological testing.

Advanced Perfusion CT scan is able to uncover tell-tale signs of early-stage dementia in relation to one of several major categories, which might be early Alzheimer’s disease, early signs of senile dementia, vascular dementia, dementia associated with mild traumatic brain injury, dementia associated with cerebral ischemia, dementia associated with genetic frontotemporal dementias, and what is termed a mild cognitive impairment syndrome, and amnesic mild cognitive impairment. The purpose of this test is not so much to assess the *cause* of any asserted dementia, but to assess whether *any* dementia exists. Perfusion CT scan is among a number of more modern and more reliable methods than neuropsychological testing, which is non-medical, not administered by physicians, and which ultimately cannot serve as an objective basis for assessment. *See* Metting, *supra*.

As a preface to these details, I note that the result has been interpreted by the performing physicians as entirely normal in the case of Judge Newman, but it is worthwhile to explain the methodologies involved and the findings. As a further introduction to the relevant literature, much of the literature has to do with determining which of the various possible methodologies in medical imaging are most helpful to look at the same phenomenon which is essentially detailed assessment of blood flow in the brain. Some of the older nuclear medicine-based approach used radioactively labeled tracers to allow the monitoring of the passage of blood through the brain.

XV. PARAMETERS IN PERFUSION BRAIN IMAGING:

¹⁶ Dr. Taheri is a board-certified in Radiology, specializing in neuroradiology, and is a professor at The George Washington University School of Medicine & Health Sciences.

The parameters measured or calculated include are explained below. For further detail, *see* Wong, *et al.*, *A Primer on Computed Tomography Perfusion Imaging for the Emergency Physician*, 58 J. Emerg. Med. 260 (2020).

- (1) Cerebral Blood Volume (CBV) and various regional CBVs in brain structures of interest showing the amount of blood that passes through various measured areas of the brain in a rapid series of fixed amounts of time. These are calculated on a voxel-by-voxel basis.¹⁷
- (2) Cerebral Blood Flow (CBF) which computes the rate at which the blood moves (this speeds up during systole (when the heart is contracting) and slows during diastole (when the heart's outflow valves are closed and the heart is taking in the next amount of blood in preparation for the next pulse contraction).
- (3) Arterial Inflow Function/Venous Outflow Function (AIF/VOF) - Artificial intelligence-based complex analyses of parameters such as arterial inflow function or AIF versus VOF venous outflow curve in spatially identified areas provide subtle insight into the pattern of flow (as the rate of blood flow in a given brain area rises and falls during the course of the result of each heartbeat that drives a bolus of contrast through the brain).
- (4) Voxel level T-max and TTP. The T-Max is the amount of time at which the contrast density is greatest in each voxel relative to the time of bolus administration. The "Time to Peak" (TTP) is a similar measure of the amount of time between bolus injection of the contrast and the time for a particular voxel in the brain to reach its maximum contrast agent density – typically about 6 seconds. The TTP is the basic measurement, while the T-Max is calculated using a deconvolution formula (correcting for imaging noise signal). A longer TTP or T-Max reflects impaired vascularity in a particular part or location in the brain.
- (5) The MTT (Mean Transit Time) assesses and reports the time it takes for a particular voxel to proceed through the entire process of commencing to increase in signal intensity as the front margin of the contrast bolus starts to arrive, through the peak and then completing as the lowest level is reached after the bolus passes. This also is affected in some of the common disorders that cause dementia or other cognitive impairments.
- (6) Subsequent volume calculations – such as penumbra (area of "shadow") that numerically characterizes the bands of severity of abnormality around a focused point of deficient flow (such as would arise in a focal vessel occlusion/stroke).

¹⁷ A voxel is a three-dimensional pixel.

XVI. RESULTS AND CONTEXT OF JUDGE NEWMAN'S PERFUSION CT TEST

Modern investigation of brain blood flow has revealed that various critical regions of the brain are dynamically capable of increasing their blood flow as cognitive work progresses and that loss of this capability is associated with the onset of MCI (mild cognitive impairment) as well as the various dementias. This phenomenon is particularly critical in the hippocampal region of the brain. Decreases in PCT parameters in the hippocampal area constitute the best modern test for the onset of age or disease related cognitive losses. See Kisler, *et al.*, *Cerebral Blood Flow Regulation and Neurovascular Dysfunction in Alzheimer Disease*, 18 *Nature Reviews: Neuroscience* 419 (2017).

An earlier large population-based study showed that diminished CBF velocity precedes cognitive decline and hippocampal atrophy. In addition, individuals exhibiting greater CBF velocity had larger hippocampal and amygdala volumes.

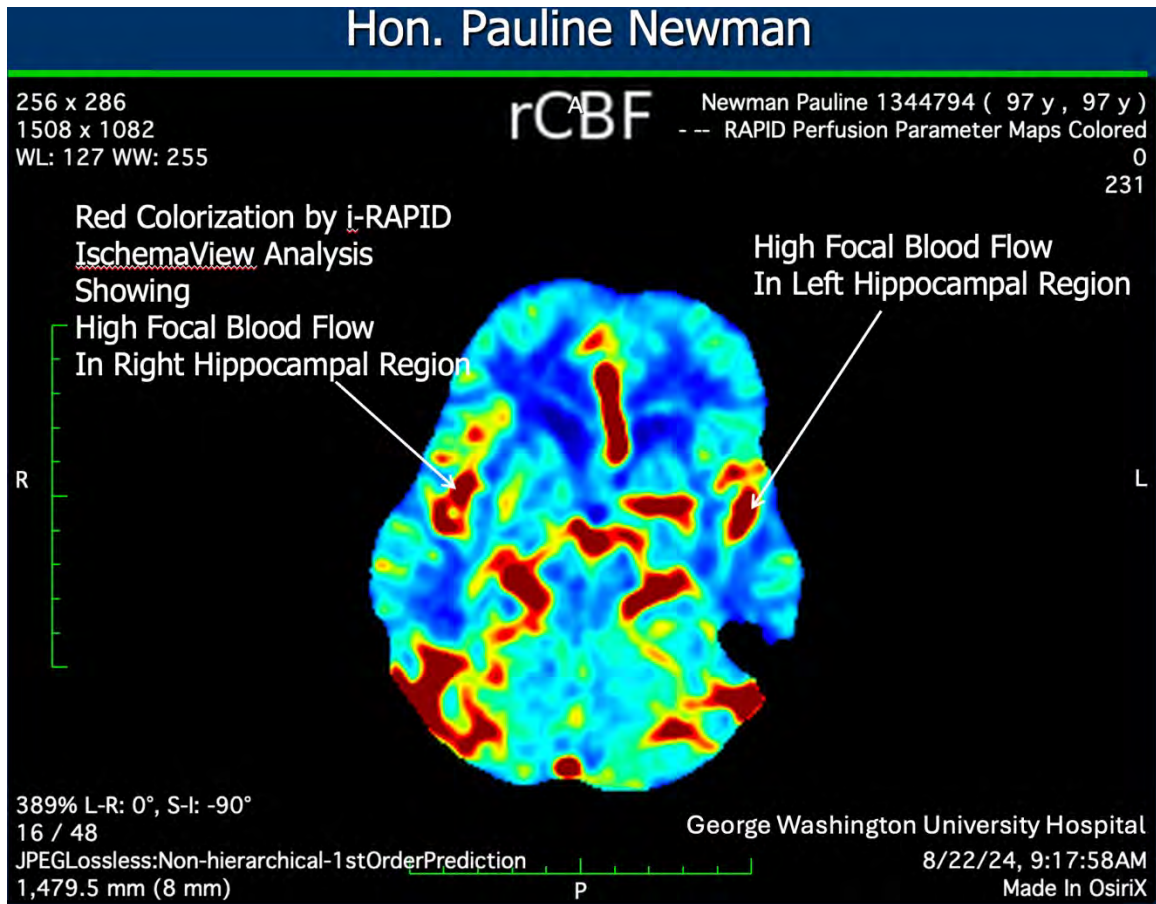
Kisler, *supra* at 430 (citing Ruitenber, *et al.*, *Cerebral Hypoperfusion and Clinical Onset of Dementia: The Rotterdam Study*, 57 *Annals of Neurology* 789 (2005)).

[L]ow CBF velocity contributes to the development of dementia. A decreased delivery of oxygen may lead to hypoxia in vulnerable areas of the brain such as watershed areas or the hippocampus and may negatively affect cognitive function.

Ruitenber, supra at 793.

A recent large study in healthy controls and patients with MCI or AD demonstrated that CBF changes (determined by ASL MRI) and vascular dysregulation are the initial events associated with cognitive decline before changes in classical AD biomarkers, A β and tau, occur.

Kisler, supra at 430.



In Judge Newman's PCT study of August 22, 2024, there are no areas with an abnormally low or high T-max, CBV, CBF, TTP or any other abnormalities of the AIF functions. There are no areas of slowing the flow and the cerebral blood flow, cerebral blood volume, Arterial Inflow Functions all came out completely normal and this is a very sensitive test used in the assessment of large numbers of patients currently around the world. In fact – she had particularly high flow rates in the hippocampus – as seen in the rCBF images at image 16/48 above.¹⁸

The T-max assessments, which look for any focal or regional delays in passage of blood, all demonstrated normal flow throughout. Cerebral blood volume, which demonstrates normal uniform passage of the volume of agent through the brain and most

¹⁸ The software used for the evaluation, which is the i-RAPID AI software, and the iSchemaView methodology, are very widely used throughout the United States.

helpfully, the cerebral blood flow demonstrating high normal symmetric blood flow in the hippocampus.

Hippocampal perfusion is the best direct correlate to most known dementias. For example, this measure has been shown to decline in persons with a known genetic defect that causes early dementia, but to become detectable as a person with the genetic predisposition approaches the typical age of commencement of symptoms, but *before* any clinically detectable symptoms even occur. *See* Kisler, *supra*.

Decreased cerebral blood flow on a focal basis in the hippocampus is responsible for significant problems with memory function and other aspects of dementia. Hippocampus is a critical area in that it plays an important role in attention, concentration, recall, and memory formation, and therefore perfusion problems in this area are highly correlative with dementia. The rCBF test in a high-resolution CT scanner using the iSchemaView I-RAPID perfusion parameter map evaluations is the best test for diagnosing problems with this region of the brain. It is therefore noteworthy that Judge Newman's brain imaging study as seen in frames 14, 15, 16, and 17 in the rCBF dataset shows very good symmetric normal appearing cerebral blood flow in the hippocampus. and this

Judge Newman's Perfusion CT test results obviate any need for a neuropsychology test battery—an outdated methodology, little different in design than their 16th century versions, and administered by non-physicians. Psychologists do not use advanced medical imaging because their discipline is rooted in philosophy rather than objective biology and all medical imaging is outside of their purview. Neuropsychological parameters are not tied to specific brain pathologies or brain anatomy. It may be true that philosophy, psychology and neuropsychology provide a comprehensive scheme of analysis that is in wide use. However, that field has not accommodated the vast advances in neuroscience – including in neuroimaging. *See, e.g.,* Duffy, *The Flexner Report – 100 Years Later*, 84 *Yale J. Biol. Med.* 269 (2011); Howieson, *Current Limitations of Neuropsychological Tests and Assessment Procedures*, 33 *Clinical Neuropsychologist* 200 (2019); Eling, *History of Neuropsychological Assessment*, 44 *Frontiers in Neurology and Neurosci.* 164 (2019). Currently I often receive requests from leading neuropsychologists to carry out Brain DTI imaging to help supplement their classical testing.

XVII. COGNITIVE INTERVIEW FOR TECHNOLOGY AND PATENT LAW

While it is my opinion that Judge Newman's written output does not demonstrate any impairment or decline, because such written output is often dependent on assistance of law clerks and other staff members, it was important to make a direct assessment by a physician in a way where it is clear that the patient was doing the work without aid or assistance.

To accomplish this goal, I compared Judge Newman's current (August 2024) ability at the below-described tasks with my personal experience as an inventor and attorney who appeared before Judge Newman in 2019 and 2022.

As a subsequent set of specialized testing, to be appropriate to the matters at issues, I provided three patent and technology scenarios to Judge Newman.

There was no advance notice to Judge Newman as to the subject matter or type of questions, meaning that she had no opportunity for any preparation. Two of the questions were based on complex inventions that have not sufficiently progressed through the patent office to be widely publicly known, while the third question dealt, with patent history from the 15th century and the difference and historical development of the current “non-obviousness” standard from the old “spark of genius” standard.

The objective of this test was to distinguish her “on the fly” responses, from her written opinions which could take months to prepare, can benefit inputs from clerks, or have other bases for discarding the intellectual output. In contrast, this test approximates how a judge would behave during oral argument when she has to think “on her feet” and may be presented with information that she is not familiar with. In analyzing Judge Newman’s performance, I did not consider my agreement or disagreement with her views on the law, and instead focused on her ability to grasp and analyze complex facts and legal issues in a rapid, yet comprehensive way.

I used two complex patent applications that I had filed, neither of which has yet been widely distributed, one in molecular biology, and one in an area of nuclear physics. The objective was to see whether Judge Newman could rapidly understand the technology explained over three to five minutes, and then address a patent law issue raised by the proposed claiming.

The first scenario related to my published application *Trivalent and Divalent Cations, as Administrable Agents for Increased Processivity and Improved Fidelity of Reverse Transcriptase in Telomerase and in Nucleic Acid Polymerases*, No. U.S. 2020-019-7351-A1 (published June 25, 2020). This involved a discovery that the substitution of a trivalent cation, Scandium 3+, in place of Calcium 2+, improved the efficiency of the reverse polymerase in HIV. The application focused on the medical use of this invention, *viz.*, it having the potential to improve the performance of the human reverse transcriptase (a telomerase enzyme), which in turn can help delay chromosomal senescence.

I provided Judge Newman with the following information:

- The end of each chromosome has a telomere.
- The telomere is gradually consumed with each round of replication, and eventually you reach cellular senescence when replication becomes impossible for many cells in the body.
- This process can be delayed if the telomere can be rebuilt with the human reverse transcriptase, which potentially can serve as an anti-aging method.
- Testing to prove an anti-aging effect could take 30 to 40 years—well beyond the life of a patent.

- A first use in cosmetics was proposed due to the less rigorous standards for efficacy with regard to the time of testing.

After presenting this information, I posed a question about broad claiming analogous to “first medical use” for something as fundamental as an element, which had no prior medical use. Additionally, I asked Judge Newman to analyze whether a cosmetic use with unproven claims on aging could be the basis of a broad claim for first medical use of an element.

The results were as follows. First, Judge Newman was able to describe back the technology that I had previously explained about how the cation improved the efficacy of the reverse transcriptase enzyme and the relevance in aging. Second, she proceeded to extemporaneously explain her views on the first medical use and broad claiming and claiming at the level of an element. Her discussion of the issue was fluid, comprehensive, and well elucidated, indicating that she maintains her abilities to understand both advanced technology and complicated questions of patent law—two key skills for a judge serving on the United States Court of Appeals for the Federal Circuit.

The second scenario presented to Judge Newman was in the area of nuclear physics. It relates to my application for *Positron Systems for Energy Storage Production and Generation*, No. 2016-008-6680-A1.

The following information was presented to Judge Newman:

- The invention relies on the novel issue of incorporating Manganese-52 into the ferrite matrix of dextran coated soluble nanoparticles so that it becomes a pourable liquid anti-matter positron emitter.
- The water-soluble positron emitting particles in the fluid are caused to flow through, for instance, a block of copper in a channel. The Mn^{52} causes matter-antimatter reactions with annihilation of electrons into production of 2 photons within the receiver metal and thereby resulting in a current, so a battery driven by matter-antimatter chemical technology.

The question I posed to her concerned the notoriously difficult area of patent law—patent eligibility under § 101, and limits on claiming “laws of nature” (here, the use of matter/anti-matter reaction to generate electricity). Considering that Judge Newman’s background as a chemist before law, and with the question having to do with limitation on claiming as to laws of nature, it was reasonable to expect that she would be able rapidly demonstrate an understanding of the invention. That expectation was fully met. Judge Newman was also able to quickly grasp the patent issue at hand and to provide an erudite discourse on Section 101 and the claiming of something fundamental about matter/anti-matter reactions in industrial use versus their use in a battery technology, as well as the borderline on the claiming. Again, in my expert opinion, Judge Newman’s performance on this question demonstrates her continued capability to engage with and analyze complex factual, technological and legal issues.

The third question topic related to history of patenting and were drawn mostly from my book on patents in the Smart Guide series, viz., *Smart Guide to Patents* (2012). Judge Newman unsurprisingly had an excellent foundation of knowledge about the history of patents and was able to recall many details. However, I did find that she was unfamiliar with some details of Gutenberg's invention of printing, as set out on page 14 through 16 in my book (see attached excerpt).

I presented the following relevant facts to Judge Newman:

- Gutenberg had organized some investors to help him produce souvenirs for a festival in Aachen Germany, where they were expecting 100,000 visitors.
- His initial idea was using a wine press and making numerous coin-like souvenirs at each compression using coin making/embossing technology that had been around for 2,000 years.
- This well-known method involved having a die poured as the reverse of the intended coin print, driven into the metal disk.
- Due to a plague epidemic the festival was canceled, and Gutenberg was stuck with equipment that he had no use for, while investors were demanding their money back.
- It was in these circumstances that Gutenberg came up with the idea of retooling the wine press to make the imprints positive rather than negative, that is to have the projecting forms of letters in place of space for the metal to rise into in the pressing step. Thus, the first printing-press was born.
- Because in Germany of the 1450s there was no intellectual property regime, Gutenberg had no way to protect his invention, and it became free for everyone to use.

Following the presentation of this history, I asked Judge Newman to discuss and compare the old "spark of genius" inventiveness standard with our current formulation of non-obviousness and how either would have played out in Gutenberg's case. Additionally, I asked Judge Newman to address the societal and policy question of why we need patents given that Gutenberg made his invention, with no expectation of rights and ownership in it, and presumably driven to do so by very different considerations. As with previous topics, Judge Newman was able to fluidly and comprehensively engage with and discuss the history and politics of the origin of the patent system and draw parallels to current issues. In my opinion, spontaneous discussions of these complex subject matters, understanding the subject matter, requiring an extemporaneous response was a reasonable, appropriate and useful test of her abilities to function as a federal judge.

In summary, Judge Newman's discussion of each of the three topics was very on target, comprehensive, and reasonable. It was clear that she showed a rapid ability to uptake and understand complex technology and to apply difficult patent law doctrines and policies to each. She also was able to, without pause, immediately, as one would expect for someone in her position, to take a strong position and make an explanation without assistance or delay with regard to the patenting issues, as well as the history and politics. In short, her

performance on these tasks fully tracks the objective CT data and confirms that she does not suffer from any mental disability that would preclude her from continuing to serve as a judge of the United States Court of Appeals for the Federal Circuit.

XVIII. SUMMARY OF EVALUATION AND TESTING

For all of the above reasons, it is my impression and opinion, to a reasonable degree of medical certainty, that:

- (1) Judge Pauline Newman’s general physical exam and neurologic exam was entirely normal, but for the slight heel-to-toe walking unsteadiness and cataracts as noted, neither of which impacts her ability to continue in judicial office.
- (2) Her Perfusion CT scan which tested multiple different parameters of flow, as well as anatomy, showed an entirely normal blood flow function and anatomy, as assessed objectively by the George Washington University Hospital neuroradiologist reviewing the study. Moreover, there is exceptionally high flow bilaterally in the hippocampus which rules out all of the known causes of MCI (mild cognitive impairment) and any dementias, confirming Dr. Carney’s assessment that Judge Newman is an “unusually cognitively intact 9[7]-year-old woman.”
- (3) Based on the technology and patent law oral examination which I administered on August 24, 2024, my past experience with Judge Newman during my oral arguments in 2019 and 2022, and the comparison between the former and the latter interactions, there is no evidence of any mild cognitive impairment, dementia or other mental deterioration. Instead, Judge Newman’s rapid efficient responses to the difficult questions posed demonstrate an extraordinarily high level of cognitive ability. Therefore, this comprehensive evaluation demonstrates no impediment to her continuing to serve in active capacity as a Circuit Judge of the United States Court of Appeals for the Federal Circuit.
- (4) I am confident in stating (consistent with the opinions rendered by Dr. Ted L. Rothstein and Dr. Regina Carney) that there is no material concern that requires further medical testing. Based on these results, the Special Committee is now able to “able to fulfill its assigned task under the Act— namely, making an *informed* assessment (and recommendation for the Judicial Council) about whether Judge Newman suffers from a disability.” Sept. 20 Order at 68 (emphasis in original).

XIX. CONCLUSION: THE HON. PAULINE NEWMAN IS COGNITIVELY FIT TO RETURN TO ACTIVE DUTY AS A SENIOR JUDGE OF THE FEDERAL CIRCUIT

In summarizing this report, I do particularly want to address the question of testing.

First, from a legitimate medical perspective, and in my position, as a neurosurgical specialist working extensively with patients with various degrees of mental impairment, often very high-functioning patients, Judge Newman is not in need of any medications or other treatments for memory supplementation or for personality change.

Second, as a fundamentally medical issue within my area of specialization, I do not believe any further testing can shed additional light on the issues in dispute. This is particularly true because the Perfusion CT results should be determinative on the principal underlying concerns of the Federal Circuit Judicial Council. The Perfusion CT is the most modern detailed test available for an objective testing assessment and permits the Special Committee and the Judicial Council to “to fulfill its assigned task under the Act—namely, making an informed assessment ... about whether Judge Newman suffers from a disability.”

Ultimately, the central point at issue here is the need for testing. Judge Newman already has the opinion of her senior respected neurologist, Dr. Ted Rothstein, and an extensive formal evaluation with Dr. Regina Carney, a highly experienced forensic psychiatrist which support her continuation in her active judicial role. Utilizing my own special perspective as an expert neurosurgeon, an inventor, and as an attorney practicing before the Court of Appeals for The Federal Circuit (who is in a unique position to compare her current performance with her previous performance in oral argument), I see no signs of deterioration in her functioning as an active judge of the Court of Appeals of the Federal Circuit. Considering the usefulness of a modern Perfusion CT, it is my expert opinion that there is no reason or need for additional testing.

Therefore, it is my expert opinion that there is no medical, neurological, or cognitive basis for requiring additional testing; or, for doubt about Judge Newman’s ability “to discharge the duties of her office.” May 16 Order at 1.

XX. References to Scientific Literature

- Dash S, Agarwal Y, Jain S, Sharma A, Chaudhry N. Perfusion CT imaging as a diagnostic and prognostic tool for dementia: prospective case-control study. *Postgrad Med J*. Jan 19 2022;doi:10.1136/postmj/postgradmedj-2021-141264
- Duffy TP. The Flexner Report--100 years later. *Yale J Biol Med*. Sep 2011;84(3):269-76.
- Eling P. History of Neuropsychological Assessment. *Front Neurol Neurosci*. 2019;44:164-178. doi:10.1159/000494963
- Filler AG, Tsuruda JS, Richards TL, Howe FA, inventors; University of Washington, Seattle, WA, assignee. Image Neurography and Diffusion Anisotropy Imaging. USA patent 5,560,360. 1996.
- Filler AG, *The History, Development and Impact of Computed Imaging in Neurological Diagnosis and Neurosurgery: CT, MRI and DTI*, 7 Internet J. Neurosurg. 1 (2009); <https://www.researchgate.net/publication/275141521>
- Filler AG. Diffusion Tensor Imaging. In: Winn HR, ed. *Youmans & Winn Neurological Surgery 8th Edition*. Eighth Edition ed. Elsevier; 2022:3,822:chap 14.
- Hart J, Jr., Kraut MA, Womack KB, et al. Neuroimaging of cognitive dysfunction and depression in aging retired National Football League players: a cross-sectional study. *JAMA Neurol*. Mar 1 2013;70(3):326-35. doi:10.1001/2013.jamaneurol.340
- Howieson D. Current limitations of neuropsychological tests and assessment procedures. *Clin Neuropsychol*. Feb 2019;33(2):200-208. doi:10.1080/13854046.2018.1552762
- Kisler K, Nelson AR, Montagne A, Zlokovic BV. Cerebral blood flow regulation and neurovascular dysfunction in Alzheimer disease. *Nat Rev Neurosci*. Jul 2017;18(7):419-434. doi:10.1038/nrn.2017.48
- Latchaw RE, Yonas H, Hunter GJ, et al. Guidelines and recommendations for perfusion imaging in cerebral ischemia: A scientific statement for healthcare professionals by the writing group on perfusion imaging, from the Council on Cardiovascular Radiology of the American Heart Association. *Stroke*. Apr 2003;34(4):1084-104. doi:10.1161/01.STR.0000064840.99271.9E

- Metting Z, Spikman JM, Rodiger LA, van der Naalt J. Cerebral perfusion and neuropsychological follow up in mild traumatic brain injury: acute versus chronic disturbances? *Brain Cogn.* Apr 2014;86:24-31. doi:10.1016/j.bandc.2014.01.012
- Pasternak M, Mirza SS, Luciw N, Mutsaerts M, al. e. Longitudinal cerebral perfusion in presymptomatic genetic frontotemporal dementia: GENFI results. *Longitudinal cerebral perfusion in presymptomatic genetic frontotemporal dementia: GENFI results.* Epub 2024 Apr 16 2024;20(5):3525-3542. doi:10.1002/alz.13750
- Powell A, Page ZA, Close JCT, Sachdev PS, Brodaty H. Defining exceptional cognition in older adults: A systematic review of cognitive super-ageing. *Int J Geriatr Psychiatry.* Dec 2023;38(12):e6034. doi:10.1002/gps.6034
- Ruitenbergh A, den Heijer T, Bakker SL, et al. Cerebral hypoperfusion and clinical onset of dementia: the Rotterdam Study. *Ann Neurol.* Jun 2005;57(6):789-94. doi:10.1002/ana.20493
- Streitparth F, Wieners G, Kamena A, et al. [Diagnostic value of multislice perfusion CT in dementia patients]. *Radiologe.* Feb 2008;48(2):175-83. Bedeutung der zerebralen Perfusionsmessung am Mehrzeilenspiral-CT in der Demenzdiagnostik. doi:10.1007/s00117-006-1443-y
- Sudlow C, Gallacher J, Allen N, et al. UK biobank: an open access resource for identifying the causes of a wide range of complex diseases of middle and old age. *PLoS Med.* Mar 2015;12(3):e1001779. doi:10.1371/journal.pmed.1001779
- Togao O, Obara M, Yamashita K, et al. Arterial Spin Labeling-Based MR Angiography for Cerebrovascular Diseases: Principles and Clinical Applications. *J Magn Reson Imaging.* Nov 8 2023;doi:10.1002/jmri.29119
- Wong ML, Flower EN, Edlow JA. A Primer on Computed Tomography Perfusion Imaging for the Emergency Physician. *J Emerg Med.* Feb 2020;58(2):260-268. doi:10.1016/j.jemermed.2019.12.003
- Zhang B, Gu GJ, Jiang H, et al. The value of whole-brain CT perfusion imaging and CT angiography using a 320-slice CT scanner in the diagnosis of MCI and AD patients. *Eur Radiol.* Nov 2017;27(11):4756-4766. doi:10.1007/s00330-017-4865-1

Newman, Pauline
DOB: 6/20/1927
August 24, 2024
Page 44 of 44

I, the undersigned do hereby certify and declare that:


I am over the age of 18, am a resident of the County of Los Angeles and of the State of California. I am an attorney duly licensed to practice law before all Courts in the State of California. I am a member of the Bar of the Court of Appeals for the Federal Circuit. I am a physician licensed to practice medicine in California, Virginia and the District of Columbia.

I declare that the above statements of this 43-page document are true and correct under the pains and penalties of perjury under the laws of the State of California, the laws of the District of Columbia, and under the laws of the United States of America.

Executed on September 17, 2024, at Santa Monica, California.

AARON G. FILLER, MD, PhD, FRCS JD

By:



Aaron Filler, Esq.

Tensor Law PC and
Institute for Nerve Medicine
900 Wilshire Blvd, Ste. 314
Santa Monica, CA 90401
310 450-9689
afiller@tensorlaw.com
Chief of Clinical Services
Institute for Nerve Medicine
Center for Advanced Spinal Neurosurgery
Neurological Injury Specialists
Texas Brain Institute

EXHIBIT 1

Curriculum Vitae

September 9, 2024

Aaron G. Filler, MD, PhD, FRCS, JD

President (2015-16) & General Counsel - Society for Brain Mapping and Therapeutics

Member of the Bar of the United States Supreme Court

Member of the Bar of the Court of Appeal for the Federal Circuit

Member of the Bar of the Court of Federal Claims & all California Courts

Diplomate, American Board of Neurological Surgery

Fellow of the Royal College of Surgeons of England

Fellow of the Intercollegiate Board in Surgical Neurology of England, Ireland,
Edinburgh & Glasgow

Fellowship in Complex Spinal Surgery - UCLA

Fellowship in Peripheral Nerve Surgery - Louisiana State University, New Orleans, LA

Fellowship in Neuroimaging - University of London

Lead Inventor of DTI and Neurography: US Patent 5,560,360 licensed to Siemens, GE
Philips, Hitachi, Toshiba and Medtronic

Medical Director-Institute for Nerve Medicine & Neurography Institute Santa Monica,
CA

Author: "Diffusion Tensor Imaging" Ch. 14, Youmans & Winn Neurological Surgery,
8th edition (2022)

Pioneer in Medicine Award for Role in Invention of Diffusion Tensor Imaging 2016,
Society for Brain Mapping & Therapeutics

Legal Specialist: Patent infringement by sovereign states

Section Editor for Peripheral Nerve,

Youmans & Winn Textbook of Neurological Surgery

Lieutenant Colonel, US Army Reserve, Medical Corps, Retired

Commander, 1466th Med Team, Neurosurgery, United States Army Reserve, Retired

Course founder: Biomechanics & Comparative Primate Anatomy, Harvard University

Medical advisor for: Filler WS - Extracorporeal Shock Wave Lithotripsy Employing
Non-focused Spherical Sector Shock Waves. US Patent #4,890,603 (1990)

Joint Guidelines Committee, American Association of Neurological Surgeons &
Congress of Neurological Surgeons -- AANS & CNS 2015-2020

Spinal Fusion Guidelines Reviewer - American Association of Neurological Surgery &
Congress of Neurological Surgery - Washington Committee (2013)

Course Director - Billing and Coding: Medicine and Law

- American Society for Peripheral Nerve 2013-2014

Course Faculty - Peripheral Nerve Surgical Anatomy and Dissection Course for

Neurosurgery Senior Residents (2014) Neuroscience Research and Education
Fund, AANS, Baltimore, MD

Cedars Sinai Medical Staff, Continuing Medical Education (CME) Committee Member
(2014-18 & 2022 to present)

State Bar of California No. 302956, Managing Partner - Tensor Law, P.C.

Medical Director - Texas Brain Institute, 7205 Fannin St., Houston, TX 77030 &
- 405 State Hwy, 121 Bypass, Bldg. A, Ste 150, Lewisville TX 75067

Office Address

Neurography Institute; Institute for Nerve Medicine; &
Neurological Injury Specialists Medical Associates
900 Wilshire Blvd., Suite 310

Santa Monica, CA 90401

Phone: (310) 314-6410

Fax: (310) 496-0185

E-Mail: afiller@nervemed.com

Web: www.nervemed.com

Web: www.neurography.com

Date of Birth October 21, 1956

Place of Birth Washington, D.C.

Education

High School Walt Whitman H.S., Bethesda, MD (9/71 – 6/74)

BA '77 with honors University of Chicago, Chicago, IL (9/74 – 6/77)
Date of Diploma: June 20, 1977

MA '79 University of Chicago, Chicago, IL (9/77 – 6/79)
Date of Diploma: December 17, 1979

MD '86 University of Chicago, Chicago, IL
(9/77 – 6/79 & 6/84 – 6/86)
Date of Diploma: June 13, 1986

PhD '86 Harvard University, Cambridge, MA (8/79 – 6/86)
Date of Diploma: June 5, 1986

Neurosurgical Residency University of Washington, Seattle, WA(6/86-6/94)

FRCS (SN) '94 Intercollegiate Board in Surgical Neurology
Royal Colleges of Surgeons,
England, Glasgow, Edinburgh, and Ireland

FRCS '07 Fellow of the Royal College of Surgeons of England

JD '14 Concord Law School, Kaplan University (9/10-12/14)
Date of Diploma: January 2, 2015

Post-Graduate Medical Education

- 6/86 – 6/94 Neurosurgical Residency
 Department of Neurological Surgery
 University of Washington, Seattle, WA
 General Surgery Rotating Internship (6/86-6/87)
 Neurosurgical Resident & Chief Resident (7/87-6/94)
 Univ. of Washington Hospitals and Clinics
 Harborview Medical Center, Seattle, WA
 Seattle Veterans Administration Hospital
 Children's Hospital Medical Center, Seattle, WA
 Atkinson Morley's Hospital, London, U.K. &
 St. George's Hospital Med School, London, UK
 Including 18 months MRI Basic Science
 & Research 12/90 to 5/92
- 6/94 – 6/95 Wellcome Trust Clinical Fellow in Magnetic Resonance Nerve
 Imaging, CRC Magnetic Resonance Research Group
 Div. of Biochemistry, St. George's Hosp. Med. School,
 & Departments of Neurosurgery and Neuroradiology
 Atkinson Morley's Hospital, London, U.K.
- 7/95 – 6/96 Spine Fellow
 Professors Ulrich Batzdorf, J. Patrick Johnson, Duncan McBride
 Complex Spine Reconstruction and Syringomyelia
 Division of Neurosurgery
 University of California Los Angeles
 UCLA Medical Center, Los Angeles, CA
- 3/96 – 6/96 Peripheral Nerve Fellow
 Professor David Kline
 Department of Neurosurgery
 Louisiana State University
 New Orleans, LA

Legal Education

- 2/2015 California Bar Exam 2/24/15 - 2/26/15
 - passed at first opportunity

- 9/7/2010 –12/2014 JD - Concord Law School (12/12/14)
Los Angeles, California
Date of Diploma 1/3/15
- 10/2011 FYLSE – State Bar of California (October 25, 2011)
First Year Law Students Examination
– passed exam at first opportunity
- 11/2013 MPRE - Multistate Professional Responsibility Exam
- passed exam at first opportunity
- 11/2013 - present Certified Law Student - California Sate Bar
PTLS - Practical Training of Law Students
California Rules of Court 9.42
Certification #: 34114
- 9/2010 – present California Bar Association
Student File # 403403

Academic and Faculty Positions

- 2019 - 2021 Section Editor - Peripheral Nerve Surgery –
Author – Chapter 11, Diffusion Tensor Imaging
Youman's & Winn Neurological Surgery, 8th Edition
Elsevier (2022). Richard Winn, Editor in Chief
- 2015 - 2017 Section Editor - Peripheral Nerve Surgery - Youman's &
Winn, Neurological Surgery, 7th Edition
Elsevier. (2017). Richard Winn, Editor in Chief
- 2008 - 2009 Section Editor - Peripheral Nerve Surgery - Youman's
Textbook of Neurological Surgery, 6th Edition
Elsevier. (in press). Richard Winn, Editor in Chief
- 2005 - 2008 Director, Peripheral Nerve Surgery Program
Cedars Sinai Medical Center &
Neurosurgical Residency Program
Cedars Sinai Medical Center, Los Angeles, CA

- 2001 - 2005
Director, Peripheral Nerve Surgery Program
Century City Hospital, Los Angeles, CA
- 1996 - 2001
Assistant Professor of Neurosurgery, UCLA
Co-Director, UCLA Peripheral Nerve Surgery Program
Co-Director, UCLA Interventional MRI Program
Director, UCLA Pediatric & Obstetric Brachial Plexus
Injury Program
Associate, Comprehensive Spine Program
Faculty, Neurosurgical Spine Surgery Fellowship Prog.
Division of Neurosurgery
UCLA Medical Center, Los Angeles, CA
- 1995 - 2001
Clinical Assistant Professor
Department of Neurological Surgery
University of Washington, Seattle
- 2000
Faculty, Review Course for Board Certification
American Association of Neurological Surgeons
- 1995 - 1996
Clinical Instructor
Division of Neurosurgery
UCLA Medical Center
- 1994 - 1995
Wellcome Trust Lecturer
Division of Clinical Neuroscience
& Division of Biochemistry
St. George's Hospital Medical School
University of London, London, U.K.
- 1992 - 1994
Acting Instructor in Neurological Surgery
Department of Neurological Surgery
University of Washington, Seattle
- 1991 - 1992
Clinical Lecturer - NeuroImaging
Division of Biochemistry &
Clinical Neuroscience Unit
St. George's Hospital Medical School

- 1990 - 1991 Visiting Research Fellow
 Division of Biochemistry
 Department of Cell & Molecular Science
 St. George's Hospital Medical School
 London, U.K.
- 1980 - 1983 Research Advisor for Undergraduates
 Biological Anthropology
 Harvard University
- 1980 - 1982 Special Lecturer
 - Biomechanics & Comparative Primate Anatomy
 - Laboratory Methods Course
 Biological Anthropology
 Harvard University
- 1979 - 1983 Teaching Fellow
 - General Ed., Biology & Biological Anthropology
 Harvard University
 Cambridge, MA
- 1977 - 1978 Research Fellow,
 Department of Anatomy,
 University of Chicago

Governmental Presentations

- 10/11/2015 G20 World Brain Mapping Initiative:
 The Future of Clinical Neuroscience
 Invention & Innovation in Neuroscience
 1st Brain Mapping Day,
 Australian Parliament,
 Canberra, Australia
- 4/19/2016 Role of the G20+/N20+ Brain Mapping Initiative
 in the Future of Clinical Neuroscience:
 Invention & Innovation in Neuroscience
 Fifth Annual Brain Mapping Day,
 United States Congress
 Washington, DC

- 9/2/1016 N20 World Brain Mapping Initiative:
The Future of Clinical Neuroscience:
Invention & Innovation in Neuroscience
Joint Meeting with Chongqing International
Neuroscience Forum,
通过N20 推进神经科学创新
Chongqing, People's Republic of China
- 8/7/2018 The Invention of DTI (Diffusion Tensor Imaging)
Lessons from a Twenty-Year Process of
Technology Adoption
Brain & Spine Initiative
California State Legislature
Sacramento, California
- 5/10/2019 Brain Mapping Initiative in the Future of Clinical
Neuroscience – Invention and Innovation.
Office of Science and Technology Policy (OSTP),
Executive Office Building
The White House, Washington, D.C.
- 6/26/2019 Diffusion Tensor Imaging & Tractography in the Imaging
Of Hypoxic Brain Injury and in Parkinsonian Disorders
N20 World Brain Mapping Initiative 2019
大阪大学, Osaka, Japan
- 11/16/2020 RGRAS – RNA Genome Reciprocal Amplification System
BARDA – Biomedical Advanced Research &
Development Authority, TechWatch
Department of Health & Human Services
Washington, DC
- Research Support**
- June '77 - August '77 University of Chicago School of Medicine,
Medical Student Research Stipend
Department of Anatomy, University of Chicago
“Morphometric Analysis of Macropodid Skulls”
- Feb. '81 - Feb. '84 NIH PHS Musculo-Skeletal Training Grant
Department of Biology, Harvard University
NIH PHS #5 T32 GM07117-09 0011
“Evolution of the Mammalian Spine”

Feb. '88 - Sept. '88	NIH Neurosurgery Training Grant Dept. of Neurol. Surg., Univ. of Washington Seattle 5T32 NS-07144-09 "Imaging of Axonal Transport & Neural Injury"
Jan. '91 - May '92	Neurosciences Research Foundation Atkinson Morley's Hospital, Harrison Clinical Lectureship Division of Clinical Neuroscience, St. George's Hosp. Med. School, Univ. of London "MR Imaging of Axonal Transport" (\$80,000)
Oct. '91 - May '92	Nycomed Imaging, AS, Oslo, Norway - Academic Investigator Support Div. of Biochemistry, St. George's Hospital Medical School, University of London. Principle Investigator. " Axonal Transport of Ferrite MR Contrast Agents" (\$25,000)
May '94 - June '95	Wellcome Trust Clinical Fellowship Division of Clinical Neuroscience & Division of Biochemistry St. George's Hospital Med. School, Univ. of London "MR Imaging of Neural Tracts" (\$75,000)
July '95 - June '96	UCLA Department of Radiological Sciences Pilot Assessment of MR Neurography for Cervical and Lumbar Spinal Imaging
Sept. '97 - Nov. '97	Nycomed Imaging, AS, Oslo, Norway - Black blood contrast agents for enhancement of Neurography - pilot study. (\$10,000)
Jan. '98 - June '99	U.K. Dept of Trade and Industry - SynGenix LTD, Targeted Drug Delivery to the CNS. (\$100,000)
Jan. '99 - Dec. '01	SynGenix LTD Axonal Transport for Drug Delivery (\$1.3 million)
Sept. '01 - Sept. '03	SynGenix LTD Axonal Transport for Drug Delivery (\$8 million)

Academic Meeting Session Chairman

- 3/20/2010 Filler AG. MRI Imaging. 2nd Chongqing International Clinical Neuroscience Forum & International NeuroDrug Conference, Chongqing, People's Republic of China, 2010重庆国际神经病学论坛
- 6/25/2010 Filler AG. MRI Imaging. NeuroTalk BIT 1st Annual Congress, Singapore. June 25, 2010.
- 3/15/2012 Filler AG. Neuroscience Imaging. International Neuroscience Conference – Omori Medical Center, Toho University, Tokyo, Japan, 東邦大学医療センター大森病院
- 5/14/2013 Filler AG. Multi-modality Imaging. Society for Brain Mapping & Therapeutics, 10th Annual World Congress. Baltimore Convention Center, Baltimore, MD
- 1/11/2014 Filler AG and Malessy MJ. General Scientific Session. American Society for Peripheral Nerve, Maui, Hawaii
- 1/12/2014 Filler AG. Medical and Legal Aspects of Coding and Billing for Peripheral Nerve Surgery. American Society for Peripheral Nerve, Maui, Hawaii
- 3/7/2015 Filler AG. Peripheral Nerve Session I Society for Brain Mapping and Therapeutics, Los Angeles Convention Center, Los Angeles, California
- 4/8/2016 Filler AG. Policy, Ethics and the Law in Neuroscience: Society for Brain Mapping and Therapeutics, Miami Florida.

Medical & Board Certifications

- 1987 Diplomate
 National Board of Medical Examiners of U.S.A.
 NBME # 214994
- 1994 Diplomate
 American Board of Neurological Surgeons,
 Primary Exam for Board Eligibility
- 1994 Diplomate
 Neurological Surgery Residency Training
 Department of Neurological Surgery
 University of Washington, Seattle, WA
- 1994 Diplomate
 Intercollegiate Board in Surgical Neurology
 of the Royal Colleges of Surgeons of
 Edinburgh, Glasgow, England, and Ireland.
 (equivalent to FRCS {SN})
- 1999 Diplomate
 American Board of Neurological Surgeons,
 Oral Exam for Board Certification
 ABNS Cert. #99073, 11/17/99 to 12/31/2009
 Recertification #17043, expiration 12/31/2019
 Recertified 2019 Cert#99073, exp. 12/31/2029

Medical Licensure

- California State
Physician & Surgeon G81778
7/1995 - current
- California State
Fluoroscopy Supervisor and Operator: RHC 145535
11/1998 – current
- District of Columbia
Medical License #: MD600003193
9/9/2024 - Current

Florida State

Medical License #: ME 118548
1/17/14 - current

Indiana State

License #: 01070287A
9/29/2011 to current

Massachusetts State

License #:245500
4/4/2012 to current

Michigan State

Medical Doctor #:4301104352
12/3/2013 to 10/16

New York State

License # - 254556
8/19/2009 to current

Nebraska

License # 26935
8/24/2012 to current

Ohio

License #: 35098599
2/5/2012 to current

Pennsylvania State

Medical Physician & Surgeon MD423086
10/03 – 10/16

Utah State

Medical License 5267292-1205
1/27/2004 to 1/31/2006

Virginia

Medicine & Surgery License #0101252705
9/6/12 to current

Washington State

Physician and Surgeon License #MD00025619
6/30/88 - 10/21/06

State of Texas
Medical License - T1062
4/30/21 - current

U.K. General Medical Council
Medical Practitioner Limited Registration: 89/1233
12/89 - 5/95

U.K. General Medical Council
Medical Practitioner Registration: 4439398
7/97 - current

DEA: BF0683777
6/88 - current

Bar Admissions

State Bar of California
Bar Membership # 302956
May 18, 2015

United States District Court,
Central District of California
June 17, 2015

United States District Court
Northern District of Illinois
August 7, 2018

U.S. Court of Appeals for the Federal Circuit
July 7, 2015

U.S. Court of Appeals for the Ninth Circuit
May 18, 2021

U.S. Court of Federal Claims
January 30, 2019

United States Supreme Court
June 1, 2022

Advanced Cardiac Life Support Certification

3/06 - present	Advanced Cardiovascular Life Support (ACLS)
3/06 - present	Basic Life Support (BLS)
2/13 - present	Pediatric Advanced Life Support (PALS)

Medical Staff Privileges

6/94 – 6/96	University of Washington Medical Center, Seattle, WA
6/94 – 6/96	Harborview Medical Center, Seattle, WA
6/96 – 6/97	Madigan Army Medical Center, Seattle, WA
6/96 – 6/97	Olive View-UCLA Medical Center, Los Angeles, CA
7/96 – 7/09	UCLA Medical Center, Los Angeles, CA
5/01 – 7/05	Century City Hospital, Los Angeles, CA
1/04 – 4/14	Midway/Olympia Hospital Med Center, Los Angeles, CA
7/01 - present	Cedars Sinai Medical Center, Beverly Hills, CA
10/03 – present	St. John’s Health Center, Santa Monica, CA

Membership in Professional Societies

Society for Brain Mapping & Therapeutics

United States Court of Appeals for the Federal Circuit
Bar Association

International Society for Magnetic Resonance in
Medicine

Society for Neuroscience

Los Angeles County Medical Association

California Medical Association

American Medical Association

American Association for the Advancement of Science

North American Spine Society

Congress of Neurological Surgeons

Joint Section for Peripheral Nerve & Spine of the
AANS and CNS

Society of British Neurological Surgeons

Visiting Professorships

University of London

Atkinson Morley's Hospital

St. George's Hospital Medical School

Department of Neurosurgery

London, England, U.K. 10/21/97

Harvard University

Beth Israel/Deaconess Hospital

Harvard Medical School

Department of Anesthesia

Cambridge, Massachusetts 11/2/99 –11/3/99

Academic Honors and Awards

Pioneer in Medicine Award (2016) for invention of
Diffusion Tensor Imaging (DTI)
Society for Brain Mapping & Therapeutics

SMART Award. UK Department of Trade and Industry
Highly competitive national award in UK for
technology in SynGenix LTD (1997)

Wellcome Trust Clinical Fellowship
(5/94) Division of Clinical Neuroscience
& Division of Biochemistry
St. George's Hospital Medical School
University of London

Harrison Clinical Lecturer in Neuroscience
(1/91-5/92) Division of Clinical Neuroscience
St. George's Hospital Medical School
University of London

NIH PHS Musculo-Skeletal Training Grant
(2/81-2/84) Department of Biology,
Harvard University

Faculty Search Committee,
Department of Anthropology,
Harvard University (9/82-9/83)

Bachelors Degree with Honors, (1977)
University of Chicago

Howell Murray Award, (1977)
University of Chicago

Technical Course Certifications

Midas Rex Bone Dissection 4/93 - current

Oratec Intradiscal Electrothermal Therapy 12/98 - current

Academic Symposia

11/98 Fifth Workshop on Obstetric Brachial Plexus Lesions
Atrium MC, Heerlen, Netherlands

Editorial Appointments

7/08 – present Youmans Neurological Surgery
Section Editor – Peripheral Nerve

Peer Scientist Reviewer for Academic Journals

3/95 - present	JMRI, (Journal of Magnetic Resonance Imaging)
9/04 – present	Journal of Human Evolution, Harvard University
10/06 - present	Neuroradiology
4/07 – present	Journal of Neuroimaging
6/09 – preset	NeuroImage
7/09 - present	Clinical Anatomy
4/10 – present	PLOS One
9/10 - present	Journal of Neurological Sciences
11/10 - present	Neurosurgery

University Committees

9/82 - 9/83	Faculty Search Committee, Department of Anthropology, Harvard University
2004	Examiner for Doctoral Thesis School of Medicine University of London

Consultant Appointments

11/97 – 11/98	General Electric Medical Systems IntraOperative MRI Medical Advisory Board
---------------	---

Business Positions

7/15 – present

Managing Partner
Tensor Law, P.C.
2716 Ocean Park Blvd., #3082
Santa Monica, CA 90405
Phone: 310 450-9689
www.tensorlaw.com

11/93 – 3/04

Co-Chief Scientific Officer, Director,
& Co-Founder
SynGenix Ltd. (English Reg. # 2740120)
Babraham Hall
Babraham
Cambridge, CB2 4AT, UK
Phone: (011 44 1223) 496-093
Fax: (011 44 1223) 496-018

1/04 – present

CEO and Co-Founder, Director
Molecular Synthetics Inc.
2716 Ocean Park Blvd., Suite 3082
Santa Monica, CA 90405
Phone 310 314-6410
Fax: 310 314-2414
Babraham, Cambridge, UK Office
Phone: (011 44 1223) 496-121
www.molecularsynthetic.com

12/98 - present

CEO and Co-Founder, Director
NeuroGrafix, Inc.
2716 Ocean Park Blvd., Ste. 3035
Santa Monica, CA 90405
Phone: (310) 664-3944
Fax: (310) 664-3949
www.neurography.com

4/2008 – 10/2008

Host – The Pain Free Hour – CBS Radio/KLSX
with Kerri Kasem and Shirlee Jackson

Event Management

- 9/75 - 6/78 Chairman and Founder: Major Activities Board
University of Chicago
Booking, marketing and staging for concerts
- 9/77 - 4/78 Chairman: Festival of the Arts
University of Chicago
Booking, marketing, scheduling, advertising
- 9/73 - 9/74 International Vice President
United Synagogue Youth
Convention Planning, Budget Planning
- 9/73 - 4/74 Chairman: Conference on American Civilization
National Association of Student Councils
Booking, scheduling, supervision of committee staffs

Non-Technical Writing

- 9/75 - 6/77 *Chicago Maroon* (University of Chicago)
General reporting
- 6/77 - 10/79 *Chicago Reader*
Freelance feature writer

Technical Theater Experience

- 3/74 - 5/74 Stage Manager
Walt Whitman High School Talent Show
- 6/75 - 9/75 Technical Lighting and Construction Assistant
Court Theatre, Chicago
- 9/75 - 6/78 Technical Manager, Stage Manager, Director
University Theatre, University of Chicago
- 1/75 - 6/78 Technical Manager, Stage Manager, Director
Blackfriars, University of Chicago

Athletic Leadership

9/73 - 6/74 Co-Team Captain
Walt Whitman High School Track and Field Team

9/73 - 6/74 Varsity Letterman
Cross Country Team, Walt Whitman High School
Track and Field Team, Walt Whitman High School

11/10 - 6/11 Referee Coordinator
AYSO Pacific Palisades All Stars Soccer

Military Service

7/94 - 2/97 Commander
1466th Med. Detachment, Neurosurgery
and Major, Medical Corps
United States Army Reserve
Fort Lawton, Bldg. S-544
Seattle, WA 98199
Phone: 206 281-3081, Fax: 206 281-3499

3/97 - 08/01 Major, United States Army Reserve, Medical Corps
Independent Ready Reserve

08/01 – 10/02 Lieutenant Colonel, United States Army Reserve, Medical
Corps Independent Ready Reserve

10/02 – present Lieutenant Colonel, United States Army Reserve, Medical
Corps, Retired

Publications

Published Articles

Filler AG, Bell BA. Axonal transport and nerve compression. *Brit. J. Neurosurg.* 6:(4) 293-295 (1992).
(PMID: 1382450)

Howe FA, Filler AG, Bell BA, Griffiths JR. Magnetic resonance neurography. *Magn. Reson. Med.* 28: 328-338 (1992).
(PMID: 1461131)

Filler AG, Howe FA, Hayes CE, Kliot M, Winn HR, Bell BA, Griffiths JR, Tsuruda JS. Magnetic resonance neurography. *Lancet* 341:659-661 (1993).
(PMID: 8095572)

Filler AG. Reverse transcriptase microassay. *Matrix Application Notes, Packard Instrument Company.* PAN0035/MAN-016:1-8 (1993).

Filler AG. Axonal transport and MRI: prospects for contrast agent development. *JMRI* 4:259-267 (1994).
(PMID: 7520308)

Howe FA, Saunders D, Filler AG, McLean MA, Heron C, Brown MM, Griffiths JR. Magnetic resonance neurography of the median nerve. *Brit. J. Radiol.* 67:1169-1172 (1994).
(PMID: 7874414)

Filler AG, Britton JA, Uttley D, Marsh HT. Adult post-repair myelomeningocele & tethered cord syndrome: Good surgical outcome after abrupt neurological decline. *Brit. J. Neurosurg.* 9:659-666 (1995).
(PMID: 8561939)

Britz GW, Dailey AT, West GA, Kuntz C, Grant GA, Filler AG, Tsuruda JS, Goodkin R, Haynor DR, Maravilla K, Kliot M. Magnetic resonance imaging in the evaluation and treatment of peripheral nerve problems. *Perspectives in Neurosurgery* 6:53-66 (1995).

Dailey AT, Tsuruda JS, Goodkin R, Haynor DR, Filler AG, Hayes CE, Kliot M. Magnetic resonance neurography for cervical radiculopathy: a preliminary report. *Neurosurgery* 38:488-492 (1996).
(PMID: 8837800)

- Filler AG, Kliot M, Hayes CE, Howe FA, Saunders DE, Bell BA, Winn HR, Griffiths JR, Tsuruda JS. Application of magnetic resonance neurography in the evaluation of patients with peripheral nerve pathology. *Journal of Neurosurgery* 85:299-309 (1996).
(PMID: 8755760)
- Kuntz C, Blake L, Britz G, Filler A, Goodkin R, Tsuruda J, Hayes C, Maravilla K, Kliot M. Magnetic resonance neurography of peripheral nerve lesions in the lower extremity. *Neurosurgery* 39:750-757 (1996).
(PMID: 8880769)
- Filler AG, Lever AML. Effects of cation substitution on reverse transcriptase and on human immunodeficiency virus production. *AIDS Research and Human Retroviruses* 13:291-299 (1997).
(PMID: 9071428)
- Hayes CE, Tsuruda JS, Mathis CM, Maravilla KR, Kliot M, and Filler AG. Brachial plexus: MR imaging with a dedicated phased array surface coils. *Radiology* 203:286-289 (1997).
(PMID: 9122409)
- Dailey A, Tsuruda JS, Filler AG, Maravilla K, Goodkin R, Kliot M. Magnetic resonance neurography of peripheral nerve degeneration and regeneration. *Lancet* 350: 1221-1222 (1997).
(PMID: 9652565)
- Johnson, JP, Ahn SS, Choi WC, Masciopinto JE, Kim KD, Filler AG, DeSalles AAF. Thoracoscopic sympathectomy: techniques and outcomes. *Neurosurgical Focus* 4 (2): Article4 (1998).
(PMID: 17206769)
- Johnson JP, Filler AG, McBride DC, Batzdorf U. Anterior cervical foraminotomy for unilateral radicular disease. *Spine* 25 (8): 905-909 (2000).
(PMID: 10767800)
- Johnson JP, Filler AG, McBride DC. Endoscopic thoracic discectomy. *Neurosurg. Focus* 9(4): Article 11 (2000).
(PMID: 16833241)
- Filler AG, Maravilla KR, Tsuruda JS. MR Neurography and muscle MR imaging for image diagnosis of disorders affecting the peripheral nerves and musculature. *Neurologic Clinics* 22(3):643-682, (2004).
(PMID: 15207879)

Filler AG, Haynes J, Jordan S, Prager J, Villablanca JP, Farahani K, McBride DQ, Tsuruda JS, Morisoli B, Batzdorf U, Johnson JP. Sciatica of Non-Disk Origin & Piriformis Syndrome: Diagnosis by MR Neurography and Interventional MRI with Outcome Study of Resulting Treatment. *Journal of Neurosurgery – Spine* 2:99-115 (2005).
(PMID: 15739520)

Filler AG. The emergence and optimization of upright posture among hominiform hominoids and the evolutionary pathophysiology of back pain. *Neurosurgical Focus* 23(1):E4 (2007).
(PMID: 17961059)

Filler AG. The first recorded neurosurgical operation – An historical hypothesis: Isis, Osiris, Thoth & the origin of the djed cross spinal symbol. *Neurosurgical Focus* 23(1):E6 (2007).
(PMID: 17961051)

Filler AG. Homeotic evolution in the Mammalia: Diversification of Therian axial seriation and the morphogenetic basis of human origins. *PLOS ONE* 2(10): e1019, (2007).
(PMID: 17925867)

Filler AG. Diagnosis and management of pudendal nerve entrapment syndromes: Impact of MR Neurography and open MR-guided injections. *Neurosurgery Quarterly* 18:1-6 (2008).

Filler AG. Piriformis and related entrapment syndromes: Diagnosis and management. *Neurosurgery Clinics of North America*. 19:609-622, (2008).
(DOI: 10.1016/j.nec.200907.029) (PMID: 19010285)

Filler AG. Diagnosis and treatment of pudendal nerve entrapment syndrome subtypes: imaging, injections, and minimal access surgery. *Neurosurg Focus* 26 (2) E9: (2009).
(PMID: 19323602)

Filler AG. Minimal access nerve surgery and interventional MRI. *Neurosurgery* 65: (4 Suppl), pA212-A221 (2009).
(DOI: 10.1227/01.NEU.0000346253.89837.6C) (PMID: 19927071)

Filler AG. MR Neurography and Diffusion Tensor Imaging: Origins, history, & clinical impact of the first 50,000 cases with an assessment of efficacy and utility in a prospective 5,000 patient study group. *Neurosurgery* 65: (4 Suppl), pA29-A43 (2009).
(DOI: 10.1227/01.NEU.0000351279.78110.00) (PMID: 19927075)

Filler AG. The history, development and impact of computed imaging in neurological diagnosis and neurosurgery: CT, MRI, DTI. *Internet Journal of Neurosurgery*, 7:(1) (2010)

<http://ispub.com/IJNS/7/1/12184>

Filler AG, Lever AML, Bacon M, Munglani R, Abell C, Frederickson M, and Whiteside G. Tri-partite complex for axonal transport drug delivery achieves pharmacological effect. *BMC Neuroscience* 11:8 (2010).

(DOI: 10.1186/1471-2202-11-8) (PMID: 20085661)

Morris K, et al; Neuroscience20 (BRAIN20, SPINE20, and MENTAL20) Health Initiative: A Global Consortium Addressing the Human and Economic Burden of Brain, Spine, and Mental Disorders Through Neurotech Innovations and Policies. *J Alzheimer Disease* 83: 1563-1601 (2021).

(DOI: 10.3233/JAD-215190)

Nami M, et al; A Proposed Brain-, Spine-, and Mental-Health Screening Methodology (NEUROSCREEN) for Healthcare Systems: Position of the Society for Brain Mapping and Therapeutics. *J Alzheimer Disease* 86: 21-42 (2022).

(DOI 10.3233/JAD-215240)

Granted Patents

Filler AG, Tsuruda JS, Richards TL, Howe FA. Image neurography and diffusion anisotropy imaging. PCT - US 93/02036 (filed 3/93), WO 93/18415 (1993). , *European Patent* EP0 630481 B1 issued 6/30/99. Japanese Patent #3457310 issued 8/1/03. *US Patent* #5,560,360 issued 10/1/96.

<http://www.google.com/patents/US5560360>

Filler AG, Lever AML. Nucleic acid amplification using scandium and lanthanum ions. Application: PCT - GB 92/01599 (filed 9/92), WO 93/05714 (1993). *European Patent* EPO 601010 B1 issued 6/14/2000. *US Patent* #5,554,498 issued 9/10/96.

<http://www.google.com/patents/US5554498>

Filler AG, Lever AML. Particulates for antiviral therapy. Application PCT-EP92/00021 (filed 1/4/92), WO 92/11846, priority date 1/91. *European Patent* EPO 566590 B1 issued 3/19/97. *US Patent* #5,614,652 issued 3/25/97.

<http://www.google.com/patents/US5614652>

Filler AG, Howe FA. Focal neurographic MRI system. PCT - US 94/06337 (filed 6/94). *European Patent* EPO 737 319 B1, issued 4/22/98. *US Patent* #5,706,813 issued 1/13/98.

<http://www.google.com/patents/US5706813>

Filler AG. Therapeutic pharmaceuticals for delivery by axonal transport. PCT - EP 91/01780 (filed 9/91), WO 92/04916 (1992). *European Patent* EPO 548157 B1 issued 5/20/1998. *US Patent* #5,948,384 issued 9/7/99.

<http://www.google.com/patents/US5948384>

Filler AG, Lever AML. Compositions comprising a tissue glue and therapeutic agent. Divisional of PCT - EP 91/01780 (filed 1/91), WO 92/04916 (1992), *European Patent* EPO 804153B1, issued 10/1/2003. (filed 12/01) US Patent #6,919,067 issued 7/19/2005. <http://www.google.com/patents/US6919067>

Filler AG, Lever AML. Hydroxide-free ferrites (Ceramic particles and their preparation). Divisional of PCT - GB 92/01703 (filed 9/92), WO 93/05815 (1993). *European Patent* EPO 640350 B1, issued 4/10/2002.

<https://data.epo.org/publication-server/pdf-document?PN=EP0640350%20EP%200640350&iDocId=5279977&iepatch=.pdf>

Filler AG, Lever AML. Synthetic transfection vectors. Divisional of PCT - GB 92/01703. *US Patent* # 6,153,598 issued 11/28/2000.

<http://www.google.com/patents/US6153598>

Filler AG. Drug Delivery via Axonal Transport. Divisional of PCT - EP 91/01780 (filed 9/91), WO 92/04916 (1992). US Patent 6,562,318, issued 5/13/2003.

<http://www.google.com/patents/US6562318>

Filler AG. Joint imaging system utilizing magnetic resonance imaging and associated methods. *US Patent*# 6,560,477 issued 5/6/2003.

<http://www.google.com/patents/US6560477>

Filler AG. Needle Guide. US Provisional Application 60/546,664 filed 2/20/04. US Patent Application Publication 20050187533A1. Filed 11/20/04. US 7,059,368. Issued 6/13/2006. <http://www.google.com/patents/US7059368>

Patent Applications Pending

Filler AG. Positron systems for energy storage, production and generation. USPTO Provisional Application #62/026707 (filed 7/21/2014).

Filler AG and Lever AMLL. Trivalent and Divalent Cations as Administerable Agents for Increased Processivity and Improved Fidelity of Reverse Transcriptase in Telomerase, and in Nucleic Acid Polymerases. USPTO Provisional Application #62/739,347 (filed 10/01/2018).

Filler AG and Lever AMLL. Trivalent Cations for High Speed High Accuracy Home Tests For COVID-19 and Other Viruses by Isothermal RNA Genome Reciprocal Amplification and Individual User Portable Lab System. USPTO Provisional Application #63/113,988 (filed 11/601/2020)

Academic Book Chapters

Filler AG. Evolution of the sacrum in hominoids. In: *Surgical Disorders of the Sacrum*, JR Doty and SS Rengachary eds. Thieme Medical Publishers, New York pp.13-20 (1994).

Filler AG, Principles of MRI and other imaging techniques for studying peripheral nerve and muscle. . Ch. 37: *Neuromuscular Function and Disease: Basic, Clinical, and Electrodiagnostic Aspects*. Brown W., Bolton C., and Aminoff M., eds. W.B. Saunders, Philadelphia; p. 661-674, 2002.

Filler AG. Applications of MRI and other imaging techniques to the study of peripheral nerve and muscle diseases. Ch. 38: *Neuromuscular Function and Disease: Basic, Clinical, and Electrodiagnostic Aspects*. Brown W., Bolton C., and Aminoff M., eds. W.B. Saunders, Philadelphia; p.675-692, 2002.

Filler AG. Imaging of peripheral nerve. In: *Neuromuscular Disorders in Clinical Practice*, Katirji B, Kaminski H, Preston D, Ruff R, and Shapiro B eds. Butterworth Heinemann, Woburn MA, p266-282, 2002.

Filler AG. MR Neurography and Brachial Plexus Neurolysis in the Management of Thoracic Outlet Syndromes. *Advances in Vascular Surgery*. JST Yao & WH Pearce Eds., Precept Press, Chicago, IL p499-523, 2002.

Filler AG, Kline DG. General Principles in Evaluating and Treating Peripheral Nerve Pathology, Injuries, and Entrapments and Their Historical Context. Ch. 229, In: *Youmans Neurological Surgery*, 6th edition. Winn HR editor, Elsevier, Philadelphia, PA; Vol. 3, p2361-2367, 2011.

Campbell W, Filler AG. Peripheral Neuropathies Ch. 233, In: *Youmans Neurological Surgery*, 6th edition. Winn HR editor, Elsevier, Philadelphia, PA; Vol. 3, p2398-2409, 2011.

Filler AG. Imaging for peripheral nerve disorders. Ch. 235, In: *Youmans Neurological Surgery*, 6th edition. Winn HR editor, Elsevier, Philadelphia, PA; Vol. 3, p2413-2426, 2011.

- Filler AG, Gilmer-Hill H. Piriformis syndrome, obturator internus syndrome, pudendal nerve entrapment and other pelvic entrapments. Ch. 238 , In: *Youmans Neurological Surgery*, 6th edition. Winn HR editor, Elsevier, Philadelphia, PA; Vol. 3, p2447-2455, 2011.
- Tiel R, Filler AG. Nerve Injuries of the Lower Extremity Ch. 243, In: *Youmans Neurological Surgery*, 6th edition. Winn HR editor, Elsevier, Philadelphia, PA; Vol. 3, p2504-2517, 2011.
- Filler AG. Imaging of the Peripheral Nerve Disorders. Ch. 196, In. *Schmidek & Sweet's Operative Neurosurgery*, 6th Edition, Elsevier, 2012.
- Filler AG. Non-Extremity Nerve Entrapment Syndromes. In: *Sunderland's Nerves and Nerve Injuries*, Elsevier, 3rd Edition, Ed. Shane Tubbs, Elsevier, (2015).
- Filler AG, Belzberg AJ, Malessy Martijn JA, Chen L. Overview and Controversies Evaluating and Treating Peripheral Nerve Pathology, Injuries, and Entrapments and Their Historical Context., In: *Youmans & Winn Neurological Surgery*, 7th edition. Winn HR editor, Elsevier, Philadelphia, PA; Vol. 3, p1961-1965, 2017.
- Filler AG. Imaging for peripheral nerve disorders. Ch. 248, In: *Youmans & Winn Neurological Surgery*, 7th edition. Winn HR editor, Elsevier, Philadelphia, PA; Vol. 3, p2004-2018, 2017.
- Filler AG. Thoracic Outlet Syndrome and Entrapments of the Brachial Plexus. Ch. 250 , In: *Youmans & Winn Neurological Surgery*, 7th edition. Winn HR editor, Elsevier, Philadelphia, PA; Vol. 3, p2032-2040, 2017.
- Filler AG, Gilmer-Hill H. Piriformis syndrome, obturator internus syndrome, pudendal nerve entrapment and other pelvic entrapments. Ch. 251 , In: *Youmans & Winn Neurological Surgery*, 7th edition. Winn HR editor, Elsevier, Philadelphia, PA; Vol. 3, p2041-2050, 2017.
- Filler AG, Maniker AH & Russell SM. Pain, Complications, and Iatrogenic Injury in Nerve Surgery. Ch. 259 , In: *Youmans & Winn Neurological Surgery*, 7th edition. Winn HR editor, Elsevier, Philadelphia, PA; Vol. 3, p2117-2123, 2017.
- Filler AG. Piriformis Syndrome and Related Nerve Entrapments of the Posterior Pelvis. Neurosurgery Case Series – Peripheral Nerve, Oxford Univ. Press (2018).

Filler AG. Imaging of the Peripheral Nerve Disorders. Ch. 184, In: *Schmidek & Sweet's Operative Neurosurgery*, Karim ReFaey & Alfredo Quiñones-Hinojosa Eds, 7th Edition, Elsevier, 2021.

Filler AG. Diffusion Tensor Imaging. Chapter 14, in: *Youmans & Winn Neurological Surgery*, 8th edition. Winn HR editor, Elsevier, Philadelphia, PA; (2022).

Filler AG, Belzberg AJ, Malessy Martijn JA, Chen L. Overview and Controversies Evaluating and Treating Peripheral Nerve Pathology, Injuries, and Entrapments and Their Historical Context., In: *Youmans & Winn Neurological Surgery*, 8th edition. Winn HR editor, Elsevier, Philadelphia, PA; 2022.

Filler AG. Imaging for peripheral nerve disorders. Ch. 275, In: *Youmans & Winn Neurological Surgery*, 8th edition. Winn HR editor, Elsevier, Philadelphia, PA; 2022.

Filler AG. Thoracic Outlet Syndrome and Entrapments of the Brachial Plexus. Ch. 277, In: *Youmans & Winn Neurological Surgery*, 8th edition. Winn HR editor, Elsevier, Philadelphia, PA; 2022.

Filler AG, Gilmer-Hill H. Piriformis syndrome, obturator internus syndrome, pudendal nerve entrapment and other pelvic entrapments. Ch. 278, In: *Youmans & Winn Neurological Surgery*, 8th edition. Winn HR editor, Elsevier, Philadelphia, PA; 2022.

Filler AG. Nerve Injuries of the Lower Extremities. Ch. 284, In: *Youmans & Winn Neurological Surgery*, 8th edition. Winn HR editor, Elsevier, Philadelphia, PA; 2022.

Filler AG, Maniker AH & Mahan M. Avoiding Iatrogenic Injury Affecting Nerves and Treatment of Consequent Symptoms. Ch. 286, In: *Youmans & Winn Neurological Surgery*, 8th edition. Winn HR editor, Elsevier, Philadelphia, PA; 2022.

Filler AG, Hanna AS. Entrapments of the Pudendal Nerve, Nerve to the Obturator Internus and the Ganglion Impar. Ch. 49, In: *Nerves: Anatomy, Exposures and Techniques*. Hanna, Amgad S. editor, Springer Nature Switzerland AG, Cham Switzerland. 2024.

Academic/Professional Meeting Presentation Abstracts

- Filler AG. Anatomical evidence for the "hylobatian" model of hominoid evolution. Amer. Assoc. Phys. Anthro, 49th Annual Mtg., Niagra Falls, NY; April 17, 1980 *Am. J. Phys. Anthro.* 52:226 (1980).
- Filler AG. Anatomical specializations in the hominoid lumbar region. Amer. Assoc. Phys. Anthro, 50th Annual Mtg., Detroit, MI; April 24, 1981, *Am. J. Phys. Anthro.* 54:218 (1981).
- Kramer M, Deacon T, Sokoloff A, Filler A. Organization of motoneurons innervating epaxial and hypaxial musculature in the frog, rat, and monkey. *Soc. Neurosci. Abs.* 13:526 (1987).
- Filler AG, Britton JA, Uttley D, Marsh HT. Acute paraplegia as an extreme presentation of adult tethered cord syndrome in a post-myelomeningocele patient. Presented 4/91, Society for British Neurological Surgeons. *J. Neurol. Neurosurg. Psych.* 55:81 (1992).
- Filler AG, Winn HR, Howe FA, Griffith JR, Bell BA, Deacon TW. Axonal transport of superparamagnetic metal oxide particles: Potential for magnetic resonance assessments of axoplasmic flow in clinical neuroscience. Published (Aug. 10, 1991). In: Proceedings, Society of Magnetic Resonance in Medicine, 10th Annual Meeting, San Francisco, *Book of Abstracts*, 10:985 (1991).
- Filler AG, Bell BA, Howe FA, Griffiths JR, Flowers M, Sharma H, Winn HR, Deacon TW. Imaging of Axonal Transport: Is the Axoplasmic Flow Clinically Relevant. Presented Sept. 19, 1991, Joint meeting of New England Neurosurgical Society and Society for British Neurological Surgeons. Queens Square National Neurological Hospital. *J. Neurol. Neurosurg. Psych.* 55:515-516 (1992).
- Filler AG, Winn HR, Westrum LE, Sirrotta P, Krohn K, Deacon TW. Intramuscular injection of WGA yields systemic distribution adequate for imaging of axonal transport in intact animals. Presented November 15, 1991 *Soc. Neurosci. Abs.* 17:1480 (1991).
- Howe FA, Filler AG, Bell BA, Griffiths JR. Magnetic resonance neurography: optimizing imaging techniques for peripheral nerve identification. In: Proceedings, Society of Magnetic Resonance in Medicine, 11th Annual Meeting, Berlin, *Book of Abstracts*, 11: 1701 (1992).

Filler AG, Howe FA, Bell BA, Winn HR, Griffiths JR. Image neurography on standard gradient MR imagers, RSNA. *Radiology* 185(P): Suppl.:152 (1992).

Filler AG, Howe FA, Winn HR, Bell BA, Griffiths JR. Design considerations for axonal transport of intraneural MR contrast agents. Joint Section for Peripheral Nerve and Spine, AANS/CNS, 2/93, Tucson, Arizona, (1993).

Filler AG, Howe FA, Golden RN, Tsuruda JS, Winn HR. Magnetic resonance neurography for diagnosis of nerve compression. American Association of Neurological Surgeons 1993 Annual Meeting, 4/93. *J. Neurosurg.* 78:368A (1993).

Filler AG, Kliot M, Hayes CE, Tsuruda J, Howe FA. MR Neurography of peripheral nerve abnormalities. American Society for Neuroradiology, Proceedings of 31st Annual Meeting, 5/93, Vancouver, B.C., Canada; (1993).

Filler AG, Hayes CE, Howe FA, Tsuruda JS, Kliot M. MR Neurography for improved characterization of peripheral nerve pathology. In: Proceedings, Society of Magnetic Resonance in Medicine, 12th Annual Meeting, New York, *Book of Abstracts*, 12: 101 (1993).

Filler AG, Golden RN, Howe FA, Tsuruda JS, Richards TL. High resolution diffusion gradient imaging for neurography in human subjects. In: Proceedings, Society of Magnetic Resonance in Medicine, 12th Annual Meeting, New York, *Book of Abstracts*, 12: 602 (1993).

Howe FA, Saunders DE, McLean MA, Filler AG, Moddares H, Brown MM, Griffiths JR. Neurography of the median nerve. In: Proceedings, Society of Magnetic Resonance in Medicine, 12th Annual Meeting, New York, *Book of Abstracts*, 12: 102 (1993).

Kliot M, Filler A, Hayes CE, Howe FA, Goodkin R, Tsuruda JS. MRI of nerve and muscle in the evaluation and treatment of peripheral nerve problems. Congress of Neurological Surgeons, Vancouver, B.C. 10/93 Meeting (1993).

Filler AG, Tsuruda JS, Hayes CE, Kliot M. Magnetic resonance neurography reveals spin-spin relaxation rate (T2) changes correlated with onset and recovery from symptoms in traumatic & compressive neuropathy. *Soc. Neurosci. Abs.* 19:1486 (611.7) (1993).

Tsuruda JS, Filler AG, Hayes CE, Kliot M. Phased array neurography of peripheral nerve pathology. *Radiology*;189(P)Suppl.328 (1993).

- Peters RJ, Tsuruda JS, Hayes CE, Yuan C, Filler AG, M Kliot, Terry V, Echelard D. MR Neurography: A technologists perspective to nerve imaging. Society of Magnetic Resonance. 4/94
- Blake LC, Tsuruda JS, Filler AG, Kliot M. Phased array MRI Neurography of the sacral plexus, the sciatic nerve, and its major branches. American Society for Neuroradiology, Proceedings of 32nd Annual Meeting, 5/94, Nashville, Tennessee; (1994).
- Filler AG, Howe FA, Hayes CE, Griffiths JR, Bell BA, Tsuruda JS. MR Neurography of cervical roots and brachial plexus. 125th Meeting of the Society of British Neurological Surgeons, 9/94, Dundee, Scotland, U.K., J. Neurol. Neurosurg. Psych. 58:123, (1995).
- Howe FA, Saunders DE, Filler AG, McLean MA, Heron C, Brown MM, Griffiths JR. An evaluation of fat-suppressed fast spin echo imaging of the median nerve in carpal tunnel syndrome. British Institute of Radiology: Progress in Magnetic Resonance. London, 10/94 (1994).
- Kliot M, Filler A, Geil G, Schultz RA, Tsuruda J. Three-dimensional holographic representation of MR neurograms. Congress of Neurological Surgeons. Chicago, IL. 10/94 (1994).
- Filler AG, Bell BA, Britton JA, Tsuruda JS, Kliot M, Hayes CE, Howe FA, Heron C, Foote S, Savy L, Griffiths JR, Clifton A. MR Neurography at 0.5 Tesla and 1.5 Tesla for imaging of cervical roots and brachial plexus. Ninth European Congress of Radiology. Vienna, 3/95. European Radiology 5(S):227, (1995).
- Kliot M, Dailey A, Goodkin R, Filler A, McKhann G, Hayes C, Tsuruda J. MR Neurography for cervical radiculopathy: correlation with clinical and electrodiagnostic findings. Amer. Assoc. Neurol. Surgeons, 4/95, Orlando, Florida (1995).
- Dailey AT, Filler AG, Hayes CE, Goodkin R, Tsuruda J, Kliot M. MR Neurography of degenerating, regenerating and grafted peripheral nerve. Amer. Assoc. Neurol. Surgeons, 4/95, Orlando, Florida (1995).
- Kliot M, Filler A, Dailey A, Kuntz C, Goodkin R, McKhann G, Tsuruda J. Magnetic resonance neurography in evaluating and treating peripheral nerve problems. Amer. Assoc. Neurol. Surgeons, 4/95, Orlando, Florida (1995).

- Howe FA, Saunders DE, Filler AG, McLean MA, Nussey SJ, Griffiths JR. Fat-suppressed fast spin echo imaging in carpal tunnel syndrome: a comparison of diabetic and non-diabetic patients. Society for Magnetic Resonance, 8/95, Nice, France (1995).
- Grant GA, Britz GW, Slimp J, Goodkin R, Haynor DR, Robertson B, Kuntz C, Filler AG, Kliot M. Use of Magnetic Resonance Neurography (MRN) with preoperative and intraoperative electrophysiological monitoring in evaluating peripheral nerve lesions. Congress of Neurological Surgeons, 45th Annual Meeting, San Francisco 10/95 (1995).
- Filler AG, Farahani K, Harris Y, Lufkin RB, Johnson JP. Turbo spin echo for MR neurography. American Roentgen Ray Society, 1996 Annual Meeting, May 5-10, San Diego, CA (1996).
- Farahani K, Filler A, Atkinson D, Johnson JP, Lufkin R. MR Neurography of the lumbar spine: application of 3D turbo spin echo imaging. International Society for Magnetic Resonance in Medicine, 4th Annual Meeting, April 27- May 3, 1996, New York, NY (1996).
- Filler AG, Howe FA, Farahani K, Johnson JP, Griffiths JR, Kennedy A, Lufkin RB, Haynor DR, Maravilla K, Goodkin R, Hayes CE, Tsuruda JS, Kliot M. Diagnosis of brachial plexus pathology by MR Neurography. American Society for Neuroradiology, 34th Annual Meeting, June 21-27, 1996, Seattle, WA (1996).
- Kliot M, Grant G, Kuntz C, Blake L, Hayes C, Goodkin R, Filler A, Tsuruda J, Maravilla K. Magnetic Resonance Neurography in the evaluation and surgical treatment of peripheral nerve tumors. American Society for Neuroradiology, 34th Annual Meeting, June 21-27, 1996, Seattle, WA (1996).
- Filler AG, Johnson JP, Farahani K, Lufkin RB. Neurography of the lumbar and sacral spinal nerves: three dimensional turbo spin echo imaging with phased array coils. North American Spine Society, 11th Annual Meeting, October 23-26, 1996, Vancouver, BC (1996).
- Filler AG, Jabour B, Kliot M, Lufkin RB, Johnson JP. MR Neurography: Imaging Characteristics of the Sciatic Nerve at the Level of the Piriformis Muscle in Patients with Leg Pain. Joint Section on Disorders of the Spine and Peripheral Nerves, AANS/CNS, February 19-22, 1997, Newport Beach, CA, *J. Neurosurg.* 86:416A (1997).

- Dailey AT, Tsuruda JS, Filler AG, Maravilla KR, Goodkin R, Kliot M. Magnetic Resonance Neurography of peripheral nerve degeneration and regeneration: A clinical case presentation. Joint Section on Disorders of the Spine and Peripheral Nerves, AANS/CNS, February 19-22, 1997, Newport Beach, CA, *J. Neurosurg.* 86:416A (1997).
- Johnson JP, Filler AG, Pare LS, McBride DQ, Batzdorf U. Anterior cervical foraminotomy. Joint Section on Disorders of the Spine and Peripheral Nerves, AANS/CNS, February 19-22, 1997, Newport Beach, CA, *J. Neurosurg.* 86:417A (1997).
- Johnson JP, Tabor EN, Filler AG, McBride DQ, Becker DP. Craniovertebral junction stabilization after transoral odontoidectomy. Annual Meeting of the American Association of Neurological Surgeons, April 12-17, 1997 Denver, CO (1997).
- Filler AG, Johnson JP, Machleder H, Jabour BA, Trent J, Kioumehri F, Villablanca P, Lufkin RB, Tsuruda JS, Hayes CE, Maravilla K, Kliot M. Image Findings With MR Neurography in Diagnosis of Thoracic Outlet Syndrome. International Society for Magnetic Resonance in Medicine, 5th Annual Meeting, April 12- 18, Vancouver, B.C. (1997).
- Filler AG, Johnson JP, Machleder H, Trent J, Villablanca P, Lufkin RB, Tsuruda JS, Hayes CE, Maravilla K, Kliot M. MR Neurography in diagnosis of thoracic outlet syndrome. American Neurological Association, 122nd Annual Meeting, September 28 - October 1, San Diego, CA (1997).
- Filler AG, Johnson JP, Machleder H, Villablanca P, Lufkin RB, Hayes CE, Maravilla K, Farahani K, Kliot M. MR Neurographic findings in diagnosis of thoracic outlet syndrome. Congress of Neurological Surgeons Annual Meeting, September 27 - October 2, New Orleans, LA. *Neurosurgery* 41:724 (1997).
- Choi WW, Johnson JP, Filler AG, McBride DQ, Sandhu HS. Simultaneous versus staged anterior and posterior spinal reconstruction: a comparative study. Congress of Neurological Surgeons Annual Meeting, September 27 - October 2, New Orleans, LA. *Neurosurgery* 41:724 (1997).
- Filler AG, Lufkin RB, Villablanca P, Farahani K, Prager J, Johnson JP. MR Neurography & interventional MRI in diagnosis and treatment of sciatica from piriformis syndrome. 2nd Interventional MRI Symposium. European Society for Magnetic Resonance in Medicine and Biology, October 17-18, Düsseldorf, Germany. *European Radiology* 7:1159-60 (1997).

Filler AG, Villablanca P, Lufkin RB, Prager J, Johnson JP. MR Neurography and open MRI in management of piriformis syndrome. 12th Annual Meeting, North American Spine Society. October 22-25, New York, NY. (1997).

Villablanca P, Filler AG, Haynes JA, Tarlo KS. Black blood contrast agents for improved neural selectivity in MR Neurography. American Society for Neuroradiology, 36th Annual Meeting. May 17-21. Philadelphia, PA. (1998).

Johnson JP, Ahn S, Choi W, Masciopinto J, Kim K, Filler A, DeSalles A. Thoracoscopic sympathectomy: techniques and outcomes. Congress of Neurological Surgeons 48th Annual Meeting. October 3-8. Seattle, WA. (1998).

Masciopinto JE, Kim K, Johnson JP, Filler A, Pare L, McBride D, Batzdorf U. Anterior cervical foraminotomy. Congress of Neurological Surgeons 48th Annual Meeting. October 3-8. Seattle, WA. (1998).

Masciopinto JE, Kim KD, Johnson JP, Choi WW, Filler AG, Sandhu HS, McBride DQ, Gelabert H. Simultaneous versus staged anterior and posterior spinal reconstruction: A comparative study. North American Spine Society, 13th Annual Meeting. October 28-31. San Francisco, CA. (1998).

Johnson JP, Ahn SS, Kim KD, Filler AG, DeSalles AAF. Techniques and outcomes of thoracoscopic sympathectomy. American Association of Neurological Surgeons. April 1999.

Johnson JP, Ahn SS, Choi WW, Masciopinto JE, Kim KD, Filler AG, DeSalles AAF. Techniques and outcomes of thoracoscopic sympathectomy. Joint Section for Spine and Peripheral Nerve AANS/CNS. Orlando, Florida, February 1999.

Villablanca JP, Gupta R, Filler A. Experimental neurography in rats at 1.5T – compressive nerve injury model. American Association for Hand Surgery & International Society for Reconstructive and Microsurgery. Los Angeles, California, June 1999.

Johnson JP, Hahn MS, Obasi C, Choi W, Filler A, Sandhu V, McBride DQ, Gelabert H. Simultaneous versus staged anterior and posterior spinal reconstruction: a comparative study. Congress of Neurological Surgeons 43rd Annual Meeting, Boston, MA, November 1999.

- Johnson JP, Hahn MS, Obasi C, Choi W, Filler AG, McBride DQ, Batzdorf U. Anterior cervical foraminotomy for unilateral radicular disease. Congress of Neurological Surgeons 43rd Annual Meeting, Boston, MA, November 1999.
- Obasi C, Johnson JP, Filler A, Park J. Failure of Screw-Plate Fixation in Patients with Osteoporosis and 3-Column Instability. Danek: Spine, Science, Management, New Orleans, LA, November 19, 1999.
- Filler AG, Tarlo KS, Haynes JA, Villablanca JP. Iron oxide black blood contrast agent improves nerve image selectivity in MR Neurography. Int. Society for Magnetic Resonance in Medicine, Annual Meeting, Denver, CO, April 2000.
- Whiteside G, Bacon M, Filler AG, Frederickson M, Abell C, Munglani R, Lever AML. Treatment of neuropathic pain by axonal transport. Society for Neuroscience Annual Meeting, New Orleans, LA, November 7, 2000.
- Filler AG, Haynes J, Villablanca JP, Prager J, McBride D, Batzdorf U, Johnson JP. Sciatica of Non-Disk Origin: Diagnosis by MR Neurography and Interventional MRI with Outcome Study of Resulting Treatment. Congress of Neurological Surgeons, San Diego, CA, October 2, 2001.
- Filler AG, Haynes J. Brachial plexus neurolysis with adhesiolytic agents for neurogenic thoracic outlet syndrome patients diagnosed by MR Neurography: Outcome study results. American Society for Peripheral Nerve. Cancun, Mexico, January 13, 2002.
- Filler AG, Haynes J, Villablanca P, Prager J, McBride D, Farahani, K, Batzdorf U, Johnson, JP. Sciatica of Non-Disk Origin: Diagnosis by MR Neurography and Interventional MRI with Outcome Study of Resulting Treatment. American Society for Peripheral Nerve. Cancun, Mexico, January 13, 2002.
- Filler AG, Whiteside G, Bacon M, Frederickson M, Abell C, Munglani R, & Lever AML. Treatment of neuropathic pain by axonal transport. Joint Section for Disorders of Spine and Peripheral Nerve, AANS/CNS. Orlando, Florida, March 3, 2002.
- Filler AG. Brachial Plexus Neurolysis with Adhesiolytic Agents for Neurogenic Thoracic Outlet Syndrome Diagnosed by MR Neurography: Outcome Study Results. Joint Section for Disorders of Spine and Peripheral Nerve, AANS/CNS. Orlando, Florida, March 2002.

- Filler AG. Minimally Invasive Surgical Approach for Decompression of the Sciatic Nerve at the Piriformis Muscle. Congress of Neurological Surgeons, 52nd Annual Meeting, Philadelphia, Pennsylvania, September 21-25, 2002.
- Filler AG. MRI Demonstration of reinnervation of muscle by sprouting from a severed nerve in a human subject. 32nd Annual Meeting, Society for Neuroscience, Orlando, FL, November 4-7, 2002.
- Tsuruda JS, Filler AG: MR Neurography findings of the bipartite piriformis muscle in the evaluation of sciatica. ASNR 2004.
- Filler AG: The utility of MR Neurography in brachial plexus imaging. Joint Section for Disorders of Spine and Peripheral Nerve, AANS/CNS, 22nd Annual Meeting, Orlando, Florida, March 15, 2006
- Filler AG. MR Neurography of the brachial plexus for identification of surgically responsive neurogenic thoracic outlet syndrome. Congress of Neurological Surgeons, 56th Annual Meeting, Chicago, IL October 7, 2006.
- Filler AG. Real time optical guidance integrated with real time Open MRI for spine and nerve interventions. Congress of Neurological Surgeons, 56th Annual Meeting, Chicago, IL October 7, 2006.
- Filler AG. Open MRI for diagnosis and therapeutic interventional procedures in nerve and spine related pain. Joint Section for Disorders of Spine and Peripheral Nerve, AANS/CNS, 23rd Annual Meeting, Phoenix, Arizona March 8, 2007.
- Filler AG. Diagnosis and management of pudendal neuralgia. American Association of Neurological Surgeons. 75th Annual Meeting. Washington, DC; April 17, 2007.
- Filler AG, Lever AML. Molecular evidence for environmental trigger of mass evolutionary acceleration: An experimental model for the Cambrian explosion. American Association for the Advancement of Science, 88th Annual, Pacific Regional Meeting, Boise, Idaho. June 19, 2007.
- Filler AG. A Humanian Model of Human Evolution: Evidence that habitual upright bipedality is a synapomorphy that defines a hominiform clade of hominoids including humans and all extant apes. American Association of Physical Anthropology, 77th Annual Meeting, Columbus, Ohio April 10, 2008. AJPA 135 (S46): p.96

Filler AG. Impact of Cycle Time in Minimal Access Nerve Surgery and Interventional MRI. International Brain Mapping & Intraoperative Surgical Planning Society – World Congress. 5th Annual Meeting. Los Angeles. August 26, 2008.

Filler AG. The anti-symmetric dyadic tensor model, the arctangent tractographic function and their role in the past & intra-operative future of diffusion tensor imaging. International Brain Mapping & Intraoperative Surgical Planning Society – World Congress. 6th Annual Meeting. Harvard Medical School, Boston, MA. August 29, 2009.

Filler AG. Fractional anisotropy and DTI tractography enhance nerve identification in MR Neurography of the lumbo-sacral plexus. Joint Section for Disorders of Spine and Peripheral Nerve, AANS/CNS, 26th Annual Meeting, Orlando, FL, February 18, 2010.

Filler AG. Fractional anisotropy and DTI tractography enhance nerve identification in MR Neurography of the brachial plexus. 2010 Annual Meeting, American Association of Neurological Surgeons, Philadelphia, PA, May 1-5, 2010.

Filler AG. Integration of High Field DTI Data with Real Time Intraoperative Low Field MRI for Millimeter Scale Guidance – When is High Field DTI Guidance Contra-Indicated? International Brain Mapping & Intraoperative Surgical Planning Society – World Congress. 7th Annual Meeting. Uniformed Services University of the Health Sciences, Bethesda, MD. May 24, 2010.

Filler AG. High Field DTI Data in the Setting of Real Time Intraoperative Low Field MRI for Millimeter Scale Guidance – Effects of Mechanical Tissue Distortion by Surgical Instruments. 8th International Interventional MRI Symposium. Leipzig, Germany, Sept. 24-25, 2010.

Filler AG. Interventional MRI Percutaneous Procedures for Extended Relief and Cure of Thoracic Outlet Syndrome. International Brain Mapping & Intraoperative Surgical Planning Society – World Congress. 8th Annual Meeting. UCSF, San Francisco, CA. June 8-10, 2011.

Filler AG. Interventional MRI Percutaneous Procedures for Extended Relief and Cure of Thoracic Outlet Syndrome. Congress of Neurological Surgeons, Washington Convention Center, Washington, DC October 1-6, 2011.

Filler AG. Real time Open MRI Guidance for Percutaneous Nerve Decompression. Society for Brain Mapping & Therapeutics, 10th Annual World Congress. Baltimore Convention Center, Baltimore, MD. May 12-14, 2013.

Filler AG, Petersen J, Velgos S. Clinical Application of Diffusion Tensor Imaging for Diagnosis and Treatment of Persistent Post-Concussive Symptoms in Individual Traumatic Brain Injury Patients, 2023 Annual Mtg., Congress of Neurological Surgeons, Walter Washington Convention Center, Washington, DC, September 10, 2023.

Presentations and Invited Lectures

Filler AG. Axial Function in Terrestrial Amniotes. The Amniote Seminar. Museum of Comparative Zoology, Romer Library, Harvard University, 10/7/80.

Filler AG. Bipedal Apes Before the Dawn of Man. Presented at the Darwin Festival (on Darwin's Birthday), Dept. of Biology, The Biology Society, Salem State College, Salem, Mass. 2/12/82.

Filler AG. Evolutionary origins of the human upright spine. Presented at 5th annual meeting, Joint Section for Peripheral Nerve and Spine, AANS/CNS, 2/12/89.

Filler AG. Imaging of Axonal Transport. Grand Rounds. Department of Neurological Surgery, University of Washington Medical Center, Seattle, WA, 12/15/89.

Filler AG. Progress in the design of axonally transported intraneural contrast agents for peripheral nerve imaging with MRI. Royal Post-Graduate Medical School, NMR Unit, Hammersmith Hospital, London, UK. 9/24/90.

Filler AG. Mathematical analysis of multiple diffusion gradients for neuronal tract tracing. Resident Research Rounds, Harborview Medical Center, Dept. of Neurol. Surg., University of Washington, Seattle, WA, 8/7/91

Filler AG. Sir Richard Owen, Sir Arthur Keith, and the lost styloid process: Serial homology and the evolution of the human spine. Section of Neurology, Royal Society of Medicine, Registrar's Meeting, London, February 6th, (1992)

Filler AG. Spinel Ferrites and Superparamagnetism in MR Imaging. Division of Biochemistry, Department of Cell & Molecular Biology, St. George's Hospital Medical School, London, 3/15/92.

Magnetism, Spinel, and the Design of Tracers for In Vivo Imaging of Axoplasmic Flow. Neuroscience Seminar, Department of Neurological Surgery, University of Washington, Seattle, 7/25/92.

Filler AG. Diffusion Anisotropy in Magnetic Resonance: Neurography and In Vivo Neural Tract Imaging. Neuroscience Seminar, Department of Neurological Surgery, University of Washington, Seattle, 12/30/92.

Filler AG. Axonal Transport of MR Contrast Agents. Nycomed Imaging, Oslo, Norway, 4/10/93.

Filler AG. MR Neurography in Clinical Medicine. Department of Neurology and Neurosurgery, Columbia University Neurologic Institute, New York, New York, 8/12/93

Filler AG. Evolution of the Axial Skeleton in the Hominoid Apes and Man. Department of Orthopedics, Harborview Medical Center, Seattle, WA, 10/16/93

Filler AG. MR Neurography for Peripheral Nerve Diagnosis. Department of Orthopedics, Harborview Medical Center, Seattle, WA, 1/19/94

Filler AG. Diffusion Anisotropy and Axonal Transport in MR Imaging of Neural Structures. Neurology Study Unit, Seattle, WA, 2/8/94

Filler AG. Diffusion Anisotropy and MR Neurography. Department of Radiology, Addenbrooke's Hospital, Cambridge University, Cambridge, U.K., 11/17/94.

Filler AG. MR Neurography: Clinical Prospects. Presented at meeting of the South of England Neurosciences Association, London, 5/19/95.

Filler AG. Diffusion Anisotropy, Axonal Transport and Endoneurial Fluid in Clinical Magnetic Resonance Neurography. Section of Neurosurgery, Yale University, New Haven, CT, 12/20/95.

Filler AG. New Techniques in MR Imaging: MR Neurography. The role of MRI neurography in imaging of the brachial plexus. Medical Imaging Center of Southern California, Santa Monica, CA, 7/1/96.

Filler AG. Interpretation of MR Neurograms. Long Beach Memorial MRI Center. 11/11/96.

Filler AG. Diffusion Imaging and T2 Neurography in MR Diagnosis of Peripheral Nerve Pathology. UCLA Department of Neurology Outpatient Conference. 11/20/96.

Filler AG, Johnson JP, Farahani K, Lufkin RB. Neurography of the lumbar and sacral spinal nerves. Federation of Spine Associations, American Academy of Orthopaedic Surgeons, February 16, 1997, San Francisco, CA (1997).

Filler AG. Case Presentation: MR Neurography in the Diagnosis of Thoracic Outlet Syndrome in a Patient with Bilateral Hand Pain. Chairman's conference, UCLA Department of Neurology, 3/97.

Filler AG. The Role of Black Blood Contrast Agents and Intraneural Contrast Agents in Magnetic Resonance Neurography. Nycomed Torsten Almen Research Center (TARC), Wayne PA., 6/24/97.

Filler AG. Black Blood Contrast Agents and Intraneural Contrast Agents in Magnetic Resonance Neurography. Nycomed Imaging, Oslo, Norway. 10/14/97.

Filler AG. MR Neurography and Open MRI in the Diagnosis and Management of Extremity Pain. Atkinson Morley's Hospital, London, England, U.K. 10/21/97.

Filler AG. MR Neurography and Interventional MRI in the Diagnosis and Management of Spine and Peripheral Nerve Disorders. General Electric Medical Systems, IntraOperative MRI Medical Advisory Board. Chicago, IL 11/10/97.

Filler AG. MR Neurography for the Evaluation of Nerve Tumors and the Effects of Cancer on Nerves. UCLA Advances in Neurosurgery. 11/15/97.

Filler AG. Progress in the Use of MRI for Management of Peripheral Nerve Disorders. Department of Radiology, UCLA Medical Center. 5/1/98.

Filler AG. Magnetic Resonance Neurography: Application to the Study of Peripheral Nerve Pathology. American Association of Electrodiagnostic Medicine. Orlando, FL. 10/14/98.

Filler AG. MR Neurography and interventional MRI in the diagnosis of sciatica. Department of Surgery Grand Rounds, UCLA Medical Center, 11/18/98.

Filler AG. Imaging of peripheral nerve tumors. Symposium on Peripheral Nerve Tumors. 15th Annual Meeting. Joint Section on Disorders of the Spine and Peripheral Nerves of the AANS/CNS. Orlando, FL 2/11/99.

Filler AG. Open MRI in the management of spine and peripheral nerve pathology. UCLA iMR Program Presentation. Los Angeles, CA 2/17/99.

Filler AG. Imaging of brachial plexus lesions. XIIth Symposium on Brachial Plexus Surgery (A. Narakas Club). Barcelona, Spain 3/14/99.

Filler AG. Magnetic Resonance Neurography for improved preoperative evaluation of brachial plexus disorders. Brachial Plexus Symposium, Obstetrical and Adult. American Association of Hand Surgery & International Society for Reconstructive Microsurgery. Los Angeles, CA 6/22/99.

Filler AG. MR Neurography and open MRI in the management of spine and extremity pain. Grand Rounds, Department of Orthopedics, UCLA Medical Center, Los Angeles, CA 10/9/99.

Filler AG. MR Neurography and Open MRI in the Management of Spine and Extremity Pain. Visiting Professor, Department of Anesthesia, Beth Israel/Deaconess Hospital, Boston, MA 11/3/99.

Filler AG. Diffusion Anisotropy, CNS Tract Tracing and MR Neurography. Research Meeting of Professor John Mazziotta's Brain Mapping Group, December 8, 1999.

Filler AG. Nerve imaging. AANS/CNS Joint Section on Disorders of the Spine and Peripheral Nerves, Annual Meeting, Indian Wells, CA 2/24/00.

Filler AG. Evolution of the human spine. UCLA Comprehensive Spine Program, Joint Spine Conference, Los Angeles, CA 3/00.

Filler AG. MR Neurography & Open MRI for diagnosis and treatment of spine and peripheral nerve pathology. American Association of Neurological Surgeons, Annual Meeting, San Francisco, CA, 4/12/00.

Filler AG. Neurography for peripheral nerve diagnosis. Department of Neurology Grand Rounds, West Los Angeles Veterans Administration Medical Center. Los Angeles, CA 4/21/00.

- Filler AG. MR Neurography, open MRI, and axonally delivered therapy. Millenium Sir Wylie McKissock Neuroscience Lecture. Atkinson Morley's Hospital, Wimbledon, UK. 11/24/2000.
- Filler AG. Outcome study of diagnosis and treatment for sciatic of non-disk origin. UCLA Comprehensive Spine Center, UCLA, Los Angeles, CA 3/5/01.
- Filler AG. Advances in the diagnosis and treatment of nerve disorders. Department of Surgery Grand Rounds, UCLA, Los Angeles, CA. 4/4/01.
- Filler AG. MR Neurography in the diagnosis and treatment of thoracic outlet syndromes. Medical staff grand rounds, Los Robles Regional Medical Center, Thousand Oaks, CA, 5/4/01.
- Filler AG. Advances in the diagnosis and treatment of nerve disorders. Medical Center Grand Rounds, Daniel Freeman Memorial Hospital, Los Angeles, CA 6/4/01.
- Filler AG. Advances in the diagnosis and treatment of nerve disorders. UCLA Department of Surgery Third Year Medical Student Lecture Series, UCLA Medical Center, Los Angeles, CA 6/8/01.
- Filler AG. MR Neurography for diagnosis of spine and peripheral nerve disorders. Institute for Spinal Disorders, Cedars Sinai Medical Center, Los Angeles, CA 8/16/01.
- Filler AG. MR Neurography, Open MRI and Axonal Transport in Advanced Diagnosis and Treatment of Nerve Disorders. Grand Rounds, Department of Neurosurgery, Massachusetts General Hospital, Harvard University, Boston, MA, November 1, 2001.
- Filler AG. Image diagnosis and surgical neurolysis for neurogenic thoracic outlet syndrome. Symposium on Advances in Vascular Surgery, Chicago, IL, December, 2001.
- Filler AG. MR Neurography for the diagnosis of peripheral nerve disorders. Panel Discussion: Innovations in Peripheral Nerve Surgery, American Society for Peripheral Nerve, Cancun, Mexico, January 2002.
- Filler AG. Failed lumbar spine surgery & sciatica of non-disk origin: Diagnosis, treatment & outcomes. Grand Rounds, Los Robles Regional Medical Center, Thousand Oaks, CA, June 21, 2002.

- Filler AG. Image diagnosis and neuroplasty for neurogenic thoracic outlet syndrome. Dept. of Vascular Surgery Grand Rounds, Cedars Sinai Medical Center, Los Angeles, CA July, 2002.
- Filler AG. Chaos and the evolutionary emergence of the human spinal design. Systems Biology Seminar, Santa Monica, CA August, 2002.
- Filler AG. MSD Review of Potential for Neurography in Surgical Image Guidance. Philadelphia, PA, September 24, 2002.
- Filler AG. MR Neurography and Open MRI in the Diagnosis and Treatment of Disorders Affecting the Spine and Nerves. Grand Rounds, Department of Neurosurgery, University of California Irvine, Orange, CA, April 22, 2003.
- Filler AG. Intraneural Drug Delivery via Axonally Transported Molecular Carriers: Novel Pharmaceutical Designs for Intractable Pain Problems. Discovery Research Seminar. Purdue Pharma, Cranbury, New Jersey, September 12, 2003.
- Filler AG. MR Neurography and Open MRI for Diagnosis and Treatment of Spine and Nerve Disorders. CME Spine Conference, Institute for Spinal Disorders, Cedars Sinai Medical Center, Los Angeles, CA, December 3, 2003.
- Filler AG. Thoracic Outlet Syndrome Does Exist. Controversies in Peripheral Nerve. Joint Section on Spine and Peripheral Nerve AANS/CNS, San Diego, CA, March 20, 2004.
- Filler AG. MR Neurography and Open MRI Guided Procedures for Diagnosis and Treatment of Nerve Disorders. Grand Rounds, University of California at San Diego, San Diego, CA, January 13, 2005.
- Filler AG. New Developments in Nerve Imaging. Course 202. American Society for Peripheral Nerve, 14th Annual Meeting, Fajardo, Puerto Rico. January 16, 2005.
- Filler AG. Diagnosis and Treatment of Sciatica from Piriformis Syndrome: The Impact of New Methods on 'Spine-Related' Peripheral Nerve Symptoms. Current Concepts in Spinal Disorders: Clinical Symposia Series, Cedars Sinai Institute for Spinal Disorders, February 9, 2005.

- Filler AG. MR Neurography and Open MRI Guided Procedures for Diagnosis and Treatment of Nerve Disorders. San Diego Neurological Society, San Diego, CA, February 17, 2005.
- Filler AG. Open MR Guided Injections in Spine, Nerve and Neuromuscular Disorders. American Society for Spine Radiology, Isla Verdes, Puerto Rico February 24, 2005.
- Filler AG. MR Neurography and Open MRI Guided Procedures for Diagnosis and Treatment of Nerve Disorders. AANS Section on Peripheral Nerve, Special Symposium, New Orleans, LA 4-19-05 (2005).
- Filler AG. MR Neurography and Open MRI Guided Procedures for Diagnosis and Treatment of Nerve Disorders. San Diego Academy of Neurological Surgery, San Diego, CA 5-25-05. (2005)
- Filler AG. Evolution and Comparative Anatomy of Vertebrae in Reptiles and Mammals and the Emergence of Upright Posture in the Apes and Early Ancestors of Humans. Visiting Professor. Cedars Sinai Medical Center, Los Angeles, CA 6-1-05 (2005)
- Filler AG. MR Neurography, Open MR Injections & Minimal Access Surgery in the Management of Thoracic Outlet Syndrome. Department of Neurosurgery Grand Rounds, University of California at Irvine, Orange, CA 8-3-05 (2005)
- Filler AG. Nerve Imaging Techniques. American Society for Peripheral Nerve, Tucson, Arizona, 1-16-06 (2006)
- Filler AG. New Advanced Imaging Techniques In the Diagnosis of Pain Syndromes – Update Session 402: Sciatica of Non-Disc Origin and Piriformis Syndrome. American Academy of Pain Medicine – Annual Meeting, San Diego, CA 2-25-06 (2006)
- Filler AG. How to read an MR Neurography Image. Joint Section for Disorders of Spine and Peripheral Nerve, AANS/CNS, 22nd Annual Meeting, Orlando, Florida, 3-17-06 (2006)
- Filler AG. Diagnosis and treatment of sciatica of non-disc origin and piriformis syndrome. In: Controversies in Peripheral Nerve Surgery: Piriformis syndrome – Is it real? American Association for Neurological Surgery, Annual Meeting, San Francisco, CA, 4-26-06, (2006)

Filler AG. MR Neurography, Open MR intervention, minimal access operations and physical exam for brachial and lumbo-sacral plexus disorders. Cedars Sinai Medical Center Neurosurgery Residents Lecture. Cedars Sinai Medical Center, Los Angeles, CA 1-26-07 (2007)

Filler AG. Advances in MR Neurography. ABCs of Peripheral Nerve Course, Joint Section for Disorders of Spine and Peripheral Nerve, AANS/CNS, 23rd Annual Meeting, Phoenix, Arizona 3-9-07, (2007)

Filler AG. MR Neurography – Assessment of the first 5,000 cases. The Kline Festschrift – an International Symposium on Nerve. LSU Health Sciences Center, New Orleans, Louisiana. 10-19-07. (2007)

Filler AG. Minimal access surgery for pelvic nerve entrapments and thoracic outlet syndrome. The Kline Festschrift – an International Symposium on Nerve. LSU Health Sciences Center, New Orleans, Louisiana. 10-20-07 (2007)

Filler AG. Diagnostic distinction – lumbo-sacral radiculopathy vs sciatica of non-disc origin: When to consider piriformis syndrome. Cedars Sinai Medical Center, Institute for Spinal Disorders, Clinical Symposium, Los Angeles, CA 2-13-08 (2008)

Filler AG. Piriformis Syndrome: Real or Not – David Cahill Memorial Controversies Session, Joint Section for Spine and Peripheral Nerve of AANS and CNS. Orlando, FL 3-1-08 (2008).

Filler AG. The Humanian Theory of Human Evolution. Evidence fore early homeotic origin of an upright bipedal hominiform lineage. Los Angeles, MENSA Society. Woodland Hills, CA 2-13-09 (2009).

Filler AG. MR Neurography, open MR guided injections, and minimal access surgery in the management of peripheral nerve disorders. Grand Rounds – University of California at Irvine, Department of Neurosurgery. Irvine, CA 10-14-09 (2009)

Filler AG. The Role of MRI in Diagnosis of Traumatic Lesions and Entrapment Syndromes. American Society for Peripheral Nerve. 2010 Annual Meeting, Boca Raton, FL 1-10-10 (2010).

- Filler AG. A historical hypothesis: The first recorded neurosurgical operation: Isis, Osiris, Thoth & the Origin of the Djed Cross. 2nd Chongqing International Clinical Neuroscience Forum & International NeuroDrug Conference, Chongqing, People's Republic of China, 3-20-10, (2010).
- Filler AG. Tri-partite complex for axonal transport drug delivery – Development & demonstration of clinical efficacy. 2nd Chongqing International Clinical Neuroscience Forum & International NeuroDrug Conference, Chongqing, People's Republic of China, 3-20-10, (2010).
- Filler AG. Diffusion tensor imaging (DTI) & Magnetic Resonance Neurography (MRN): Origins, History & Clinical Impact. 2nd Chongqing International Clinical Neuroscience Forum & International NeuroDrug Conference, Chongqing, People's Republic of China, 3-20-10, (2010).
- Filler AG. Diffusion Tensor Imaging (DTI) & Magnetic Resonance Neurography (MRN): Origins, History, Physical Basis & Clinical Impact. NeuroTalk BIT 1st Annual Congress, Singapore. June 25, 2010.
- Filler AG. MRI Neurography, Open MRI Surgery in the Peripheral Nerve Setting & Minimal Access Proximal Plexus Surgery. Association of Extremity Nerve Surgeons. Annual Meeting 2011, Las Vegas Nevada, November 2011
- Filler AG. Neuroimaging – MR Neurography, Diffusion Tensor Imaging, and Open MRI for Nerve and Neural Tract Imaging. American Society for Peripheral Nerve – Annual Meeting 2012, Las Vegas, Nevada, January 2012
- Filler AG. Diffusion Tensor Imaging, MR Neurography and High Resolution Axonal MRI Techniques for Mapping the Human Connectome & Peripheral Nervous System. International Neuroscience Conference – Omori Medical Center, Toho University, Tokyo, Japan, March 2012
- Filler AG. Diffusion Tensor Imaging, MR Neurography and High Resolution Axonal MRI Techniques for Mapping the Human Connectome & Peripheral Nervous System. 周围神经 - 核磁共振成像 - 扩散张量成像技术 International Neuroscience Conference – 2012 Shanghai International Forum on Neuroscience. 8th People's Hospital, Shanghai, Peoples' Republic of China, May 2012

Filler AG. Diffusion Tensor Imaging, MR Neurography and High Resolution Axonal MRI Techniques for Mapping the Human Connectome & Peripheral Nervous System. 周围神经 - 核磁共振成像 - 扩散张量成像技术 International Neuroscience Conference – 3rd Annual World Congress of NeuroTalk, Beijing, People’s Republic of China, May 2012

Filler AG. Advances in Diffusion Anisotropy Imaging – New Mathematical Models: The Anti-symmetric Dyadic Tensor Model. Society for Brain Mapping & Therapeutics, 10th Annual World Congress. Baltimore Convention Center, Baltimore, MD. May 12-14, 2013.

Filler AG. Medical and Legal Aspects of Coding and Billing for Peripheral Nerve Surgery. American Society for Peripheral Nerve, Maui, Hawaii, January 12, 2014

Filler AG. Ultrasound and MRI in Nerve Injury. American Society for Peripheral Nerve, Paradise Island, Bahamas, January 24, 2015.

Filler AG. Open MRI Guided Percutaneous Nerve Treatments. Society for Brain Mapping and Therapeutics, Los Angeles Convention Center, Los Angeles, California, March 7, 2015.

Filler AG. Role of the G20+/N20+ Brain Mapping Initiative in the Future of Clinical Neuroscience – Invention and Innovation. Joint Session, Australian Parliament, Canberra, Australia, October 10, 2015

Filler AG. Welcoming Address Society of Brain Mapping 13th Annual Meeting – The Role of Technological Advance and Multi-Disciplinary Collaboration in the Future of Neuroscience. Miami, Florida, April 8, 2016.

Filler AG. Policy, Ethics and the Law: The Role of Daubert/Frye and Markman Type Evidentiary Hearings in the Application Neuroscience in the Courtroom. Society of Brain Mapping & Therapeutics, Miami, Florida, April 8, 2016.

Filler AG. From the Laboratory to the Technology Start-Up: Invention, Patents, and Entrepreneurship. Society of Brain Mapping & Therapeutics, Miami, Florida, April 9, 2016.

Filler AG. Role of the G20+/N20+ Brain Mapping Initiative in the Future of Clinical Neuroscience – Invention and Innovation. United States Congress, Brain Mapping Day, April 20, 2016.

- Filler AG. Response to Michel Kliot – Diffusion Tensor Methods and Neurography for Imaging in Peripheral Nerve Management. American Association of Neurological Surgeons, Chicago, IL, May 3, 2016.
- Filler AG. Tutorial on Magnetic Resonance Imaging and Diffusion Tensor Imaging Technology as to U.S. Patent 5,560,360 in Support of Plaintiff's Claim Construction Brief. NeuroGrafix Multi-District Litigation (MDL) United States District Court of Massachusetts, Hon. Richard G. Stearns, Presiding. August 18, 2016.
- Filler AG. Role of the Society for Brain Mapping in the Future of Clinical Neuroscience – Invention & Innovation –通过N20 推进神经科学创新 - N20 Joint Meeting with Chongqing International Neuroscience Forum. Chongqing, People's Republic of China, September 3, 2016.
- Filler AG. Diffusion Tensor Imaging & MR Neurography & High Resolution Axonal MRI Techniques for the Evaluation of Peripheral Nerve Entrapments. American Society for Peripheral Nerve, 2017 Annual Meeting, Kona Hawaii, January 13, 2017.
- Filler AG. Methodology for Analysis of DTI Images in the Setting of Brain Injury with Memory Loss. Society for Brain Mapping and Therapeutics, 14th Annual Meeting, Los Angeles, CA; April 20, 2017
- Filler AG. Surgical Treatment of Peripheral Pain: Lower Extremity Nerve Entrapments. Annual Meeting of the AANS/CNS Section on Disorders of the Spine and Peripheral Nerves. Orlando, FL; March 14, 2018.
- Filler AG. Diffusion Tensor Imaging & MR Neurography & High Resolution Axonal MRI Techniques versus Ultrasound for the Evaluation of Peripheral Nerve Entrapments. American Association of Neurological Surgeons, 2018 Annual Meeting, New Orleans, Louisiana; May 1, 2018.
- Filler AG. Methodology for Analysis of DTI Images in the Setting of Brain Injury with Photophobia or Vertigo. Society for Brain Mapping and Therapeutics, 15th Annual Meeting, Los Angeles, CA; April 14, 2018.
- Filler AG. The Invention of DTI (Diffusion Tensor Imaging) Lessons from a Twenty Year Process of Technology Adoption. Brain & Spine Initiative at California State Legislature, Sacramento, CA, August 7, 2018.

- Filler AG. Diffusion Tensor Imaging and Tractography in the Imaging of Hypoxic Brain Injury and in Parkinsonian Disorders. Society for Brain Mapping and Therapeutics (SBMT) 2019 Annual Meeting, Los Angeles, CA, March 16, 2019.
- Filler AG. Brain Mapping Initiative in the Future of Clinical Neuroscience – Invention and Innovation. Office of Science and Technology Policy (OSTP), The White House, Washington, D.C./Executive Office Building, May 10, 2019.
- Filler AG. Diffusion Tensor Imaging and Tractography in the Imaging of Hypoxic Brain Injury and in Parkinsonian Disorders. Society for Brain Mapping and Therapeutics (SBMT) 2019 N20 Meeting, 大阪大学 Osaka, Japan, June 26, 2019.
- Filler AG, Kim C, Straus AR. Tutorial as to Impact of Split Pulse Technology on Claim Step 36(a) of US 5,560,360 NeuroGrafix v. BrainLAB, United States District Court – Northern District of Illinois, Hon. Matthew F. Kennelly, Presiding, September 9, 2020.
- Filler AG and Lever AML. RGRAS – RNA Genome Reciprocal Amplification System: High Speed – High Accuracy Home Testing System for COVID-19 and Other Pathogens. United States Department of Health and Human Services, BARDA – Biological Advanced Research and Development Agency, TechWatch Program – Washington, D.C., (WebEx), November 16, 2020.
- Filler AG, Diffusion Tensor Imaging. Online Lecture Presentation. Link from Youmans & Winn Neurological Surgery, 8th Edition, uploaded May 24, 2021.
- Filler AG. DTI Tractography for Targeted TMS Treatment of TBI Symptoms. Society for Brain Mapping and Therapeutics, 20th Annual Meeting, Los Angeles, CA, March 12, 2022.
- Filler AG. DTI MRI for Medical Proof of Injuries in the Brain. United States District Court, Western District of Washington at Tacoma, in *Torjusen v. Amtrak*, Tacoma, Washington, Hon. Benjamin H. Settle, Presiding, March 21, 2022.
- Filler AG, Petersen J, Velgos S. The Role of DTI Guided TMS in the Management of Symptoms of Mild Traumatic Brain Injury. Society for Brain Mapping and Therapeutics, 20th Annual Meeting, Los Angeles, CA; February 18, 2023.
- Filler AG. Piriformis Syndrome – Differential Diagnosis & Management: a Peripheral Nerve Perspective: Scientific Session 5: Beyond the Foramen: Peripheral Nerve Perplexities; Spine Summit – Joint Section – Disorders of Spine and Peripheral Nerves; American Association of Neurological Surgeons/Congress of Neurological Surgeons, Fountainbleau Hotel, Miami, Florida; March 18, 2023.

Filler AG, Gilmer H, Belzberg A, Ali Z, Jack M, Jacoby S, Smith B, Wilson TJ, Winfree C, Zager E, Moderators: Controversies in Peripheral Nerve Surgery, Congress of Neurological Surgeons 2023 Annual Meeting, Walter Washington Convention Center, Washington, DC; September 13, 2023.

Filler AG, Gilmer H Peripheral Nerve Surgery: Evaluation and Common Surgical Exposure: Congress of Neurological Surgeons 2024 Annual Meeting, Houston Convention Center, Houston, TX; September 28, 2024

Filler AG, Gilmer H, et al: Peripheral Nerve Entrapment versus Radiculopathy: Congress of Neurological Surgeons 2024 Annual Meeting, Houston Convention Center, Houston, TX; September 30, 2024

Books

Filler AG. *Apple Thesaurus* (technical text on Apple II microelectronics, lab interfaces, and machine level programming). Datamost, Chatsworth, California. pp. 893. (1984). For information on the book:

<http://www.amazon.com/Apple-Thesaurus-Aaron-Filler/dp/0881903469>

Filler AG. *Do You Really Need Back Surgery: A Surgeon's Guide to Neck and Back Pain and How to Choose Your Treatment*. Oxford University Press. pp 352.(2004).

<http://www.amazon.com/You-Really-Need-Back-Surgery/dp/019532708X>

Hardcover 1st Edition May 2004

Paperback Edition May 2007

Paperback 2nd Edition January 2013

Filler AG. *The Upright Ape: A New Origin of the Species*. New Page Books, New Jersey, July 2007.

<http://www.amazon.com/Upright-Ape-New-Origin-Species/dp/1564149331>

Filler AG. *Axial Character Seriation in Mammals: An Historical and Morphological Exploration of the Origin, Development, Use, and Current Collapse of the Homology Paradigm*. Brown Walker Press, Boca Raton, FL, April 2007.

<http://www.amazon.com/Axial-Character-Seriation-Mammals-Morphological/dp/1599424177>

Filler AG. Smart Guide to Patents – SmartGuide Publications (September 2012)
<http://www.amazon.com/Smart-Guide-Patents-Aaron-Filler/dp/098344210X>

Theses

Filler, AG. *Brain Size and Social Behavior in East African Bovids: Application of Multivariate Statistics, Eigenvectors and Factor Analysis to Relate Behavioral and Morphometric Data*. (BA, University of Chicago) (1977) (Human Behavior & Institutions)

Filler, AG. *Factor analysis and multivariate statistics for the evaluation of cranial morphometrics in Macropodids*. (Medical Student research project (1978) University of Chicago.

Filler AG. *Functional and Evolutionary Perspectives on Axial Anatomy in Hominoids*. (MA, University of Chicago) (1979).

Filler AG. *Axial Character Seriation in Mammals: An Historical and Morphological Exploration of the Origin, Development, Use, and Current Collapse of the Homology Paradigm*. (PhD, Harvard University) (1986).

Blog Posts

- 1/29/2007 *Oxford University Press Blog*
 Is there an ethical crisis in spinal surgery?
http://blog.oup.com/2007/01/is_there_an_eth/
- 12/15/2007 *Anthropology.net*
 A human ancestor for the apes? – Morotopithecus & Homo sapiens vertebrae
<http://anthropology.net/2007/12/15/a-human-ancestor-for-the-apes/morotopithecus-homo-sapiens-vertebrae/>
- 12/24/2007 *Oxford University Press Blog*
 Redefining the word “Human” – Do some apes have human ancestors?
<http://blog.oup.com/2007/12/human/>
- 8/17/2009 *Research Blogging*
 Diagonal postures & The descent from human to ape
<http://www.researchblogging.org/blogger/home/id/1142>

Major Media Coverage of Academic Work

Print

- 3/16/93 *New York Times* - Magnetic Resonance Gives Better Images of Nerves in the Body. Warren Leary.
- 3/12/93 *LA Times* - Nerve Imaging Could Revolutionize Treatment of Pain. Thomas Maugh.
- 3/12/93 *London Times* - 3D images improve cancer treatment. Nigel Hawkes.
- 3/21/93 *Die Welt* - NMR-Tomographie spürt Nervenstränge auf. Werner Schulz.
- 3/12/93 *Associated Press* - New method lets doctors see nerves more clearly.
- 3/20/93 *Science News* - Seeing the nerves within us
- 9/28/96 *Science News* - Imaging method really shows some nerve
- 7/31/96 *LA Times* - Report touts new nerve imaging technique. Thomas Maugh.
- 9/7/96 *Lancet News* - MRI simplifies diagnosis of peripheral nerve lesions.
- 3/2001 *Discover* - Pulling pain up by the roots. Paul D. Thacker page 11.
- 3/24/01 *The Economist* - Magic bullet for pain-killers. Technology Quarterly, page 20

Internet

- 4/18/1997 *CNN.com*
Enhanced MRI reveals nerves that cause pain
<http://cnn.com/HEALTH/9704/18/nfm/pain/index.html>

- 11/8/2000 *BBC News*
A Step Forward in Killing Pain
http://news.bbc.co.uk/1/hi/english/health/newsid_1011000/1011780.stm
- 11/8/2000 *Web MD*
New Techniques Get at Pain Where It Hurts: Nerves Carry
Pain Medication Directly To Its Target
<http://my.webmd.com/content/article/1728.63588>
- 11/8/2000 *CBS Healthwatch*
New Drug Delivery Method May Target Pain Directly
<http://cbshealthwatch.medscape.com/medscape/p/gcommunity/HNews/hnews.asp?RecID=226860&Channel=0>
- 11/8/2000 *Reuters Health*
Axonal Transport System Targets Drug to Site of Neuropathic
Pain in Rat Model
<http://www.reutershealth.com/archive/2000/11/08/professional/links/20001108scie002.html>
- 11/8/2000 *New Scientist:*
Magic Bullet
<http://www.newscientist.com/dailynews/news.jsp?id=ns9999156>
- 11/8/2000 *Associated Press*
<http://wire.ap.org/APnews/?SITE=JRC&FRONTID=HOME>
- 11/8/2000 *Wired News*
Pain Relief's New Delivery System
<http://www.wirednews.com/news/technology/0,1282,40125,00.html>
- 1/31/2005 *Forbes.com*
New Clues for Sciatica Pain Relief
<http://news.healingwell.com/index.php?p=news1&id=523726>
- 7/15/2007 *Reuters*
Blame that bad back on your ancestors
<http://uk.reuters.com/article/idUKN1427159120070715>
- 10/10/2007 *MSNBC*
Human ancestors walked upright, study claims
<http://www.msnbc.msn.com/id/21223189/wid/11915829/>

- 5/20/2011 *Reuters Legal News*
 Revenge of the Patent Holders
<http://newsandinsight.thomsonreuters.com/Legal/NY/News/ViewNews.aspx?id=16798&terms=%40ReutersTopicCodes+CONTAINS+>
- 10/7/2019 *Bloomberg Law*
 Federal Circuit Reinstates Brainlab MRI Patent Dispute
<https://news.bloomberglaw.com/health-law-and-business/fed-cir-reinstates-brainlab-mri-software-patent-dispute>
- 10/7/2019 *Law 360*
 Federal Circuit Reverses Brainlab MRI Patent Win
<https://www.law360.com/articles/1206835/fed-circ-reverses-brainlab-mri-patent-win>
- 10/24/2019 *Patent Docs*
 NeuroGrafix v. Brainlab, Inc (Fed. Cir. 2019)
<https://www.patentdocs.org/2019/10/neurografix-v-brainlab-inc-fed-cir-2019.html>
- 11/26/2019 *Lexology*
 No Brainer: Summary Judgment Based on Non-Asserted Grounds Procedurally Improper
<https://www.lexology.com/library/detail.aspx?g=0c98741c-f586-43e8-a65f-99bddbfa0589>
- 10/24/2019 *Patent Docs*
 NeuroGrafix v. Brainlab, Inc (Fed. Cir. 2019)
<https://www.patentdocs.org/2019/10/neurografix-v-brainlab-inc-fed-cir-2019.html>

Television

- 3/12/93 *CNN*Headline News
- 11/8/96 *ABC* World News Tonight with Peter Jennings
http://www.aaronfiller.com/Video/AGF_Movie.html
- 4/18/97 *CNN*Headline News
http://www.aaronfiller.com/Video/AGF_Movie.html
- 3/1/05 Fox 11 News

- 7/31/05 Ivanhoe Science Productions
<http://www.ivanhoe.com/science/story/2005/07/31a.html>
- 11/3/2017 *Megyn Kelly - NBC*
 Is Harvey Weinstein About to Be Arrested
<https://www.today.com/video/is-harvey-weinstein-about-to-be-arrested-1091195971711>
- 11/7/2017 *Tucker Carlson - Fox News*
 Will Weinstein Case Go to a Grand Jury
<https://www.youtube.com/watch?v=AB9-xAwOUT4>
 (at 33:20 of 44:14)

Legal Successes in Intellectual Property Litigation

- 6/30/2009 *NeuroGrafix v. Oak Tree Medical* – Dismissal Upon Settlement
 Action for Patent Infringement of US 5,560,360
- 5/17/2011 *NeuroGrafix v. State of California* – State of California, appearing in Los Angeles Superior Court, waives Constitutional 11th Amendment Sovereign Immunity to appear in United States District Court –Central District of California to answer to Claim of Patent Infringement as to US 5,560,360
- 11/22/2011 *NeuroGrafix v. Siemens AG* – Dismissal Upon Settlement
 Action for Patent Infringement of US 5,560,360
- 12/17/2012 *NeuroGrafix v. State of California* – Dismissal Upon Settlement
 Action for Patent Infringement of US 5,560,360
- 2/10/2013 *NeuroGrafix v. General Electric* – Dismissal Upon Settlement
 Action for Patent Infringement of US 5,560,360
- 2/26/2013 *NeuroGrafix v. Medtronic* – Dismissal Upon Settlement
 Action for Patent Infringement of US 5,560,360
- 5/31/2013 Patent Trials & Appeals Board – All substantive claims in US 5,560,360 sustained as patentable in defense of Ex Parte Re-Exam
 (Defense written and argued by Aaron G. Filler)

- 7/31/2014 Patent Trials & Appeals Board – All substantive claims in US 5,560,360 sustained as patentable in defense of Ex Parte Re-Exam on PTAB Appeal (Appeal written and argued by Aaron G. Filler)
- 11/6/2014 *NeuroGrafix v. Philips* – Dismissal Upon Settlement Action for Patent Infringement of US 5,560,360
- 2/8/2016 *Aaron G. Filler v. Solicitor, United States Patent & Trademark Office* - all substantive claims in US 5,560,360 sustained as patentable in defense of Ex Parte Re-Exam on Appeal to Court of Appeals for the Federal Circuit (Appeal written and argued by Aaron G. Filler, Esq.)
- 8/11/2016 *NeuroGrafix v. Hitachi* – Dismissal Upon Settlement Action for Patent Infringement of US 5,560,360
- 5/17/2017 *NeuroGrafix v. Toshiba* – Dismissal Upon Settlement Action for Patent Infringement of US 5,560,360
- 10/7/2019 *NeuroGrafix v. Brainlab*, 787 Fed.Appx. 710 (Fed.Cir., 2019) Reversal & Remand, overturning grant of Motion for Summary of Judgment of No Infringement on Appeal to Court of Appeals for the Federal Circuit (Appeal written and argued by Aaron G. Filler, Esq.)
- 11/1/2020 *NeuroGrafix v. Brainlab*, Dismissal with Prejudice of Counterclaim and Defenses of Invalidity as to US 5,560,360; (Lead Counsel for NeuroGrafix – Aaron G. Filler, Esq.)
- 4/27/2021 *NeuroGrafix v. Brainlab* – Dismissal Upon Settlement Action for Patent Infringement of US 5,560,360

EXHIBIT 2



US005560360A

United States Patent [19]

Filler et al.

[11] **Patent Number:** 5,560,360[45] **Date of Patent:** Oct. 1, 1996[54] **IMAGE NEUROGRAPHY AND DIFFUSION ANISOTROPY IMAGING**

[75] Inventors: **Aaron G. Filler**, Seattle; **Jay S. Tsurda**, Mercer Island; **Todd L. Richards**, Seattle, all of Wash.; **Franklyn A. Howe**, London, England

[73] Assignee: **University of Washington**, Seattle, Wash.

[21] Appl. No.: **28,795**

[22] Filed: **Mar. 8, 1993**

[30] **Foreign Application Priority Data**

Mar. 9, 1992	[GB]	United Kingdom	9205058
Mar. 13, 1992	[GB]	United Kingdom	9205541
Mar. 30, 1992	[GB]	United Kingdom	9207013
May 5, 1992	[GB]	United Kingdom	9209648
May 21, 1992	[GB]	United Kingdom	9210810
Jul. 31, 1992	[GB]	United Kingdom	9216383
Jan. 22, 1993	[GB]	United Kingdom	9301268

[51] **Int. Cl.⁶** **A61B 5/055**

[52] **U.S. Cl.** **128/653.2; 324/307**

[58] **Field of Search** **128/653.1, 653.2, 128/653.3; 324/307, 309**

[56] **References Cited****U.S. PATENT DOCUMENTS**

3,735,247 5/1973 Harker 128/653.1

4,902,973	2/1990	Keren	324/312
5,070,876	12/1991	Wright	128/653.3
5,078,141	1/1992	Suzuki et al.	324/309
5,079,505	1/1992	Deimling et al.	324/309
5,134,372	7/1992	Inoue	324/309
5,151,655	9/1992	Harms et al.	324/309
5,218,964	6/1993	Sepponen	324/309
5,250,899	10/1993	Listerud et al.	324/309
5,261,405	11/1993	Fossel	128/653.2

Primary Examiner—Marvin M. Lateef

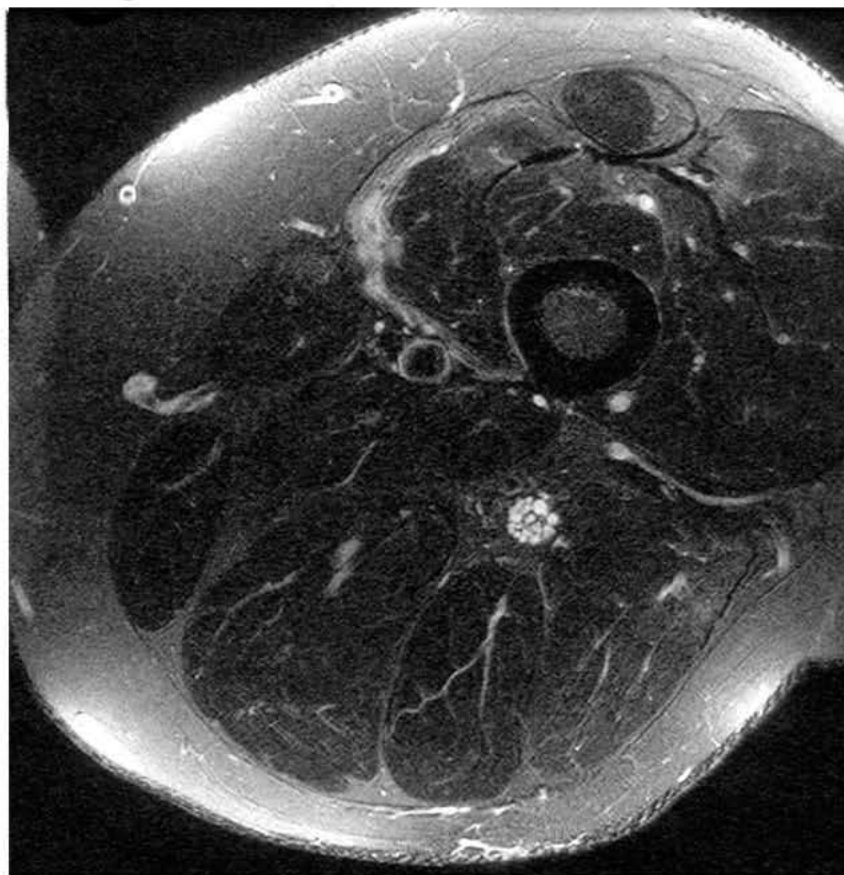
Assistant Examiner—Brian L. Casler

Attorney, Agent, or Firm—Christensen, O'Connor, Johnson & Kindness PLLC

[57] **ABSTRACT**

A neurography system (10) is disclosed for generating diagnostically useful images of neural tissue (i.e., neurograms) employing a modified magnetic resonance imaging system (14). In one embodiment, the neurography system selectively images neural tissue by employing one or more gradients to discriminate diffusion anisotropy in the tissue and further enhances the image by suppressing the contribution of fat to the image. The neurography system is part of a broader medical system (12), which may include an auxiliary data collection system (22), diagnostic system (24), therapeutic system (26), surgical system (28), and training system (30). These various systems are all constructed to take advantage of the information provided by the neurography system regarding neural networks, which information was heretofore unavailable.

66 Claims, 17 Drawing Sheets



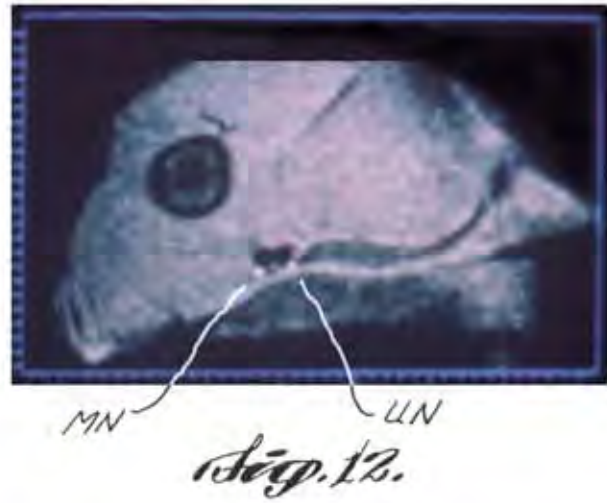
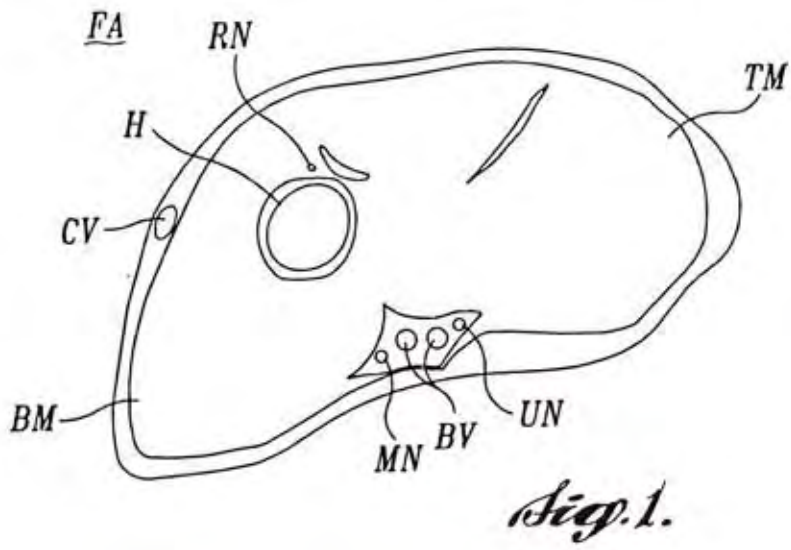




Fig. 3.

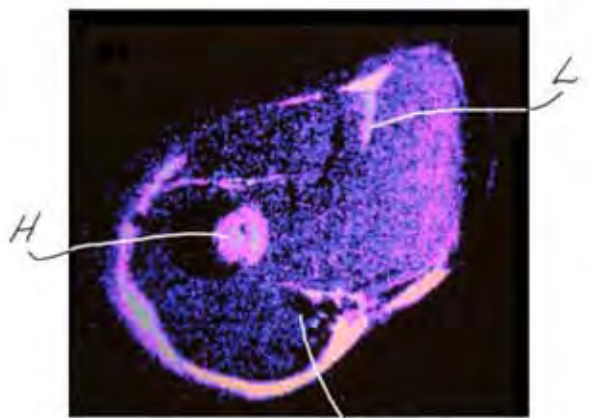


Fig. 2A.

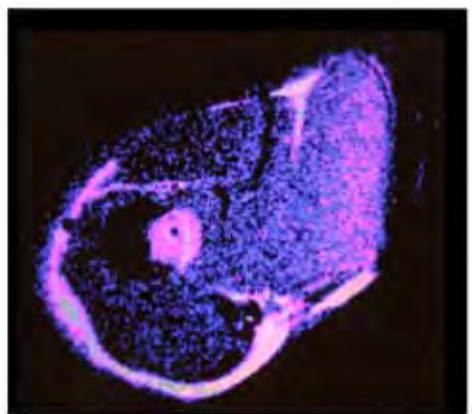


Fig. 2B.

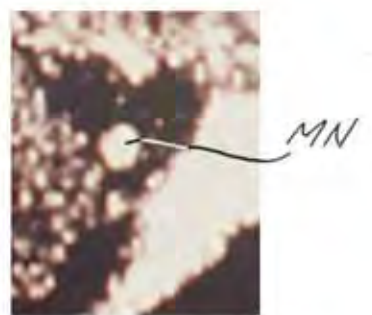


Fig. 4.

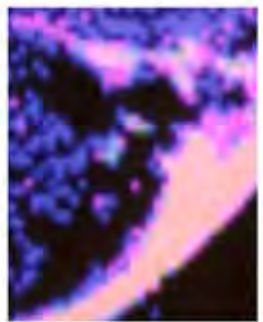


Fig. 5A.



Fig. 5B.

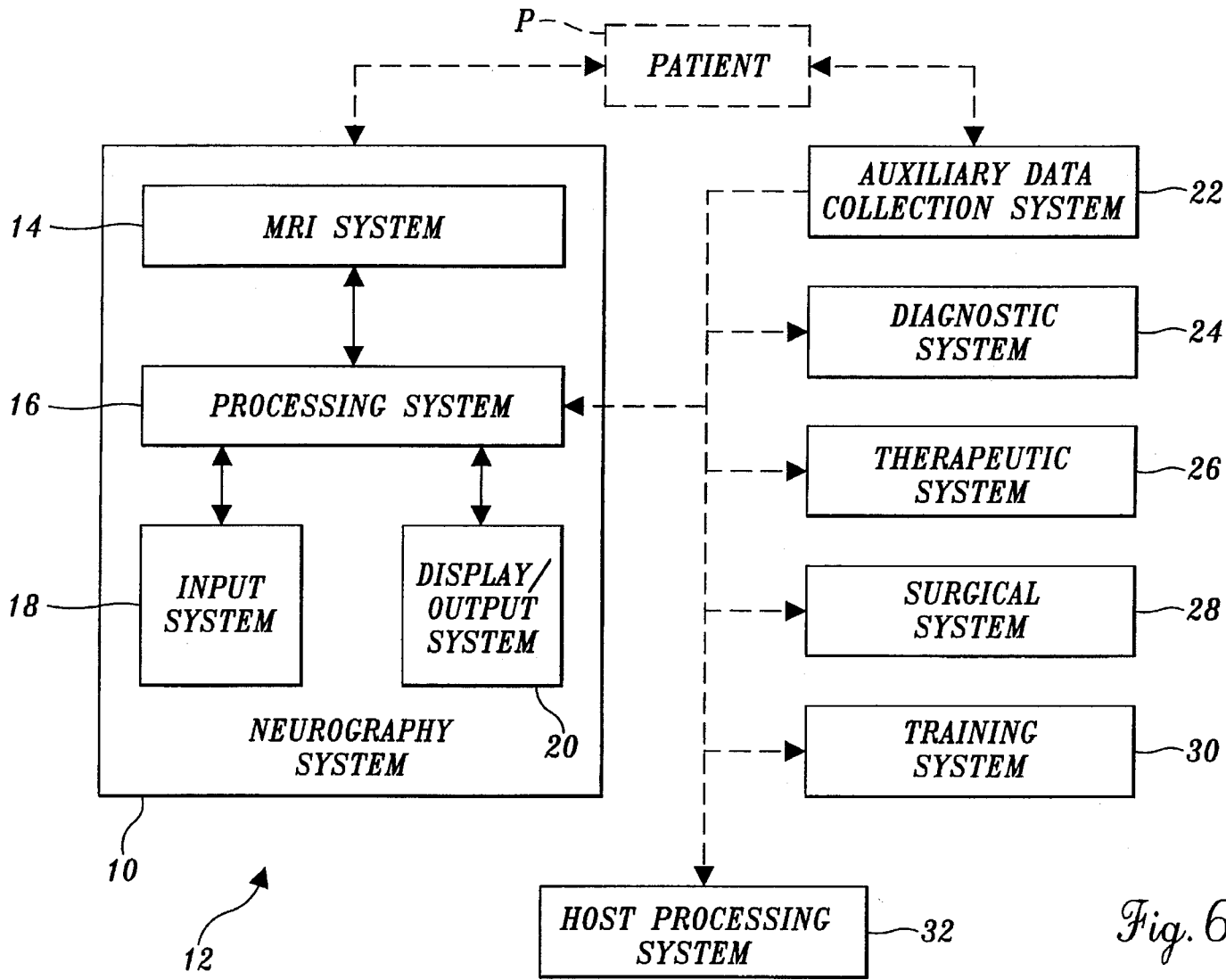


Fig. 6.

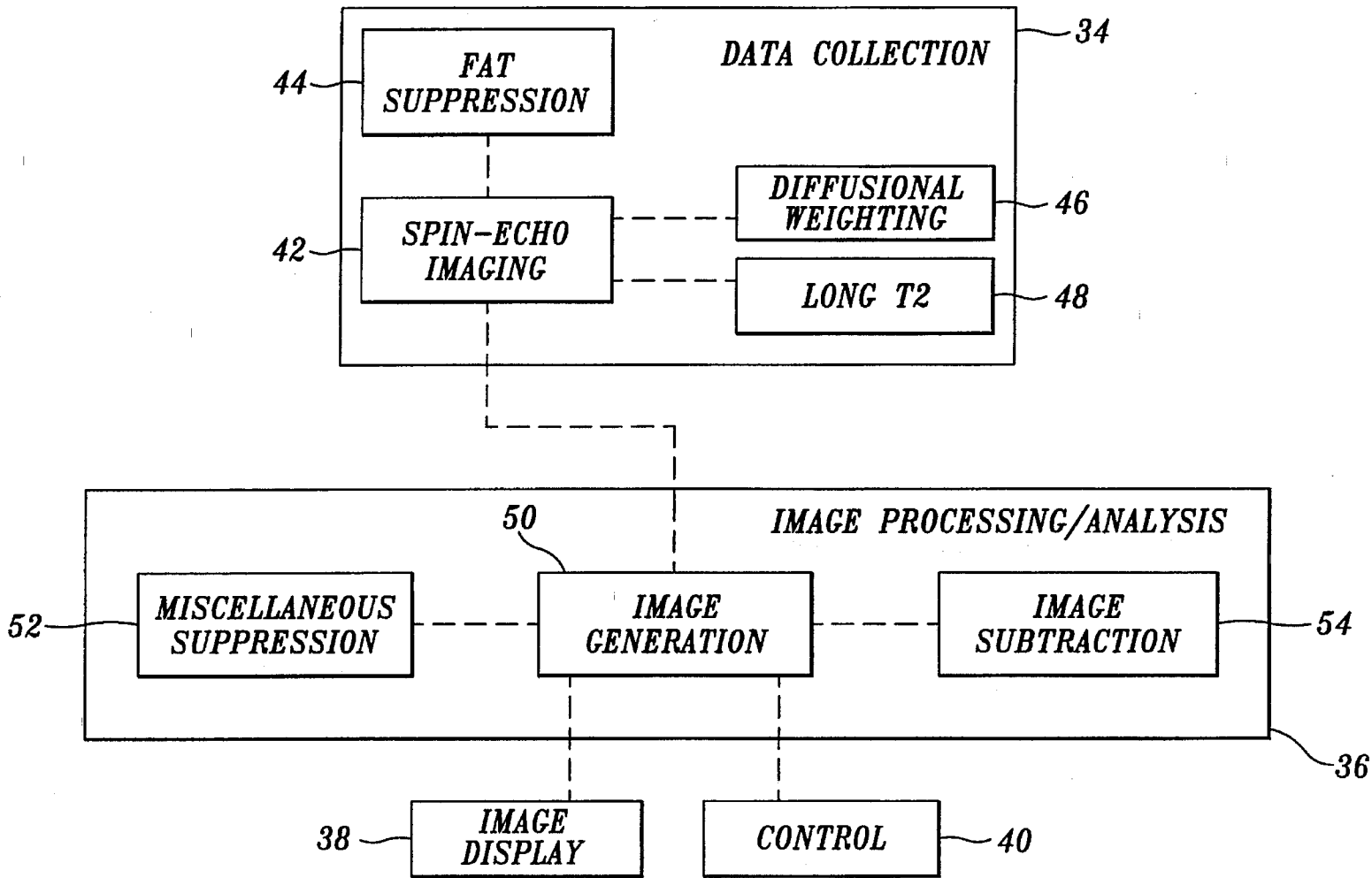
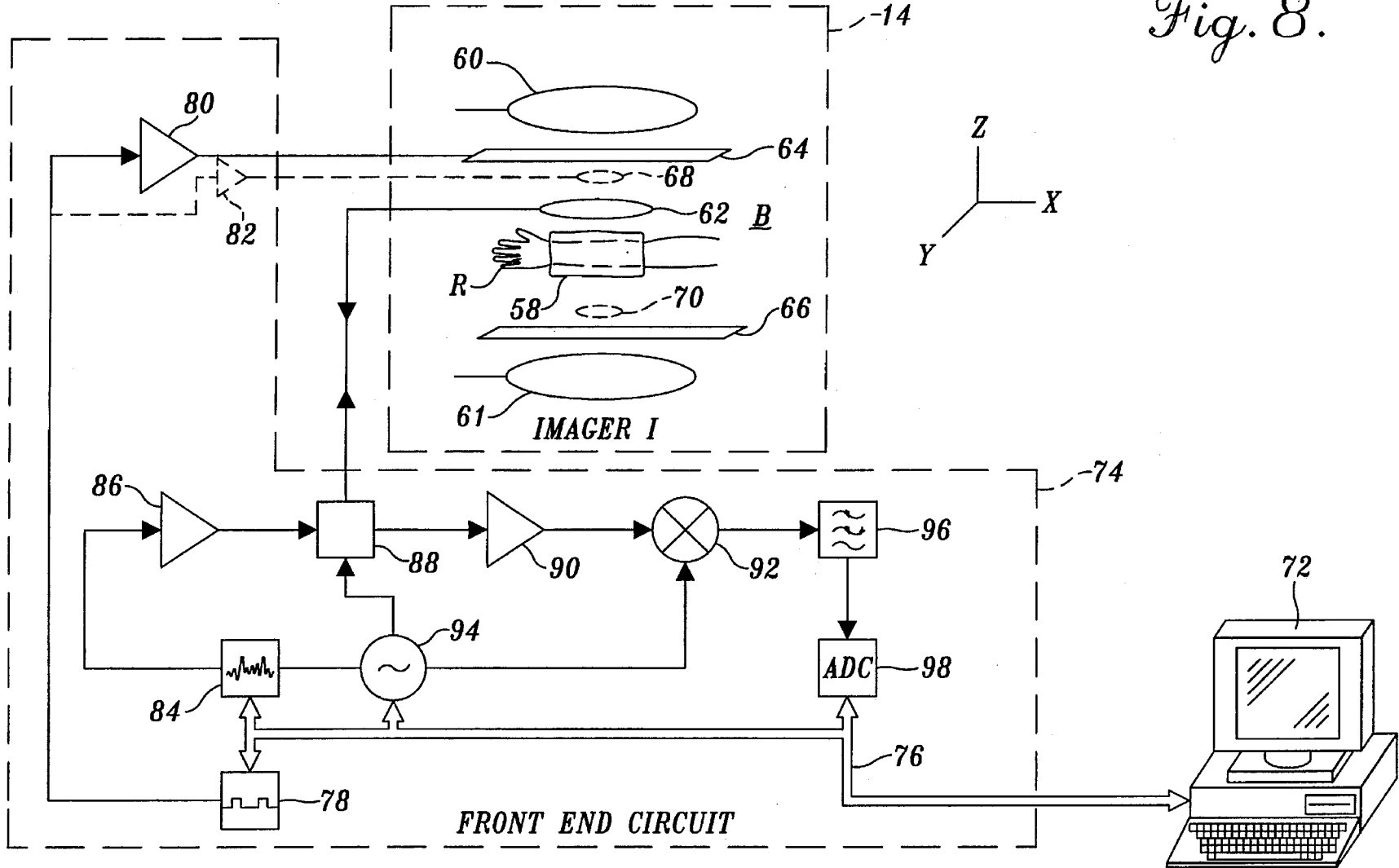


Fig. 7.

Fig. 8.



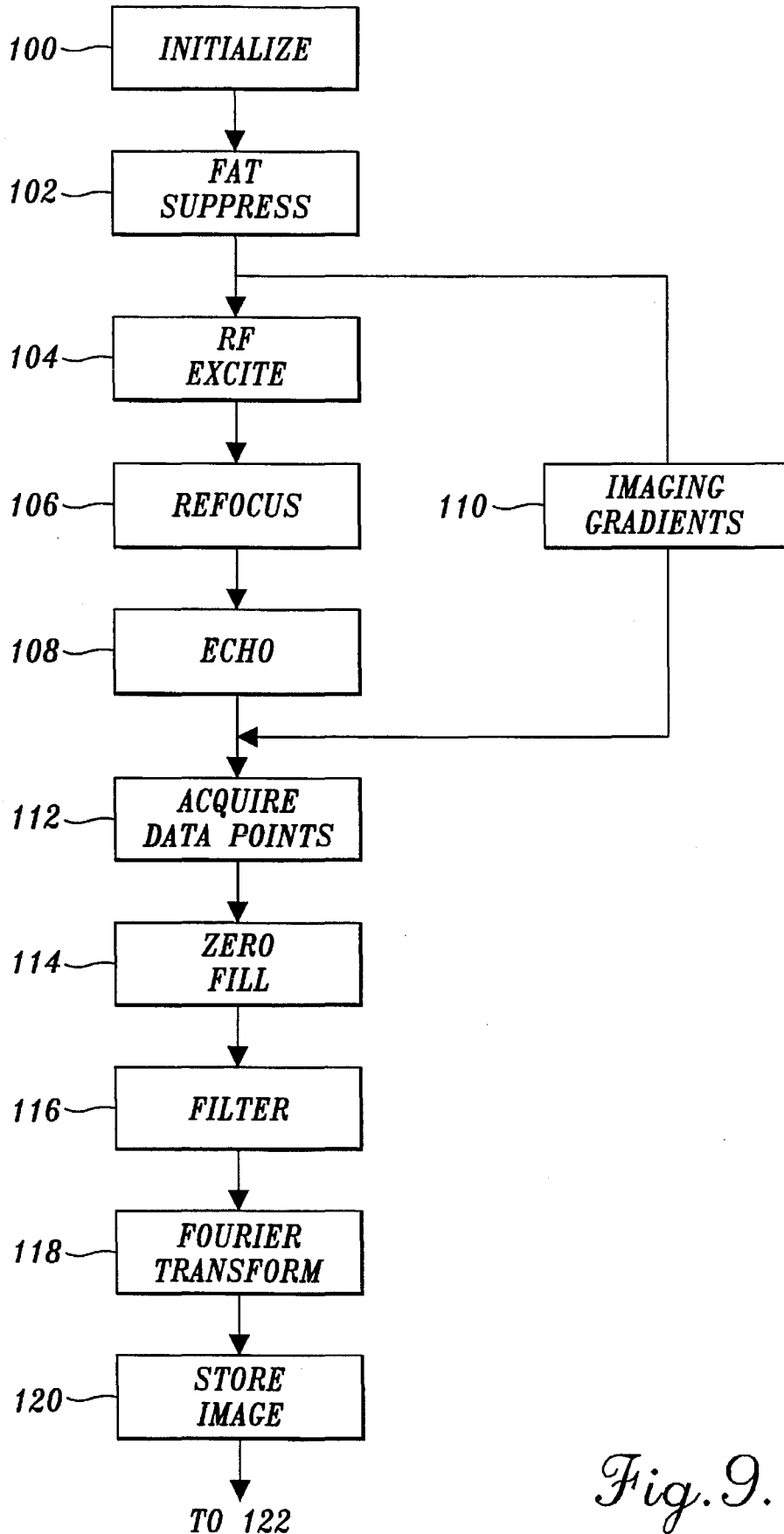


Fig. 9.

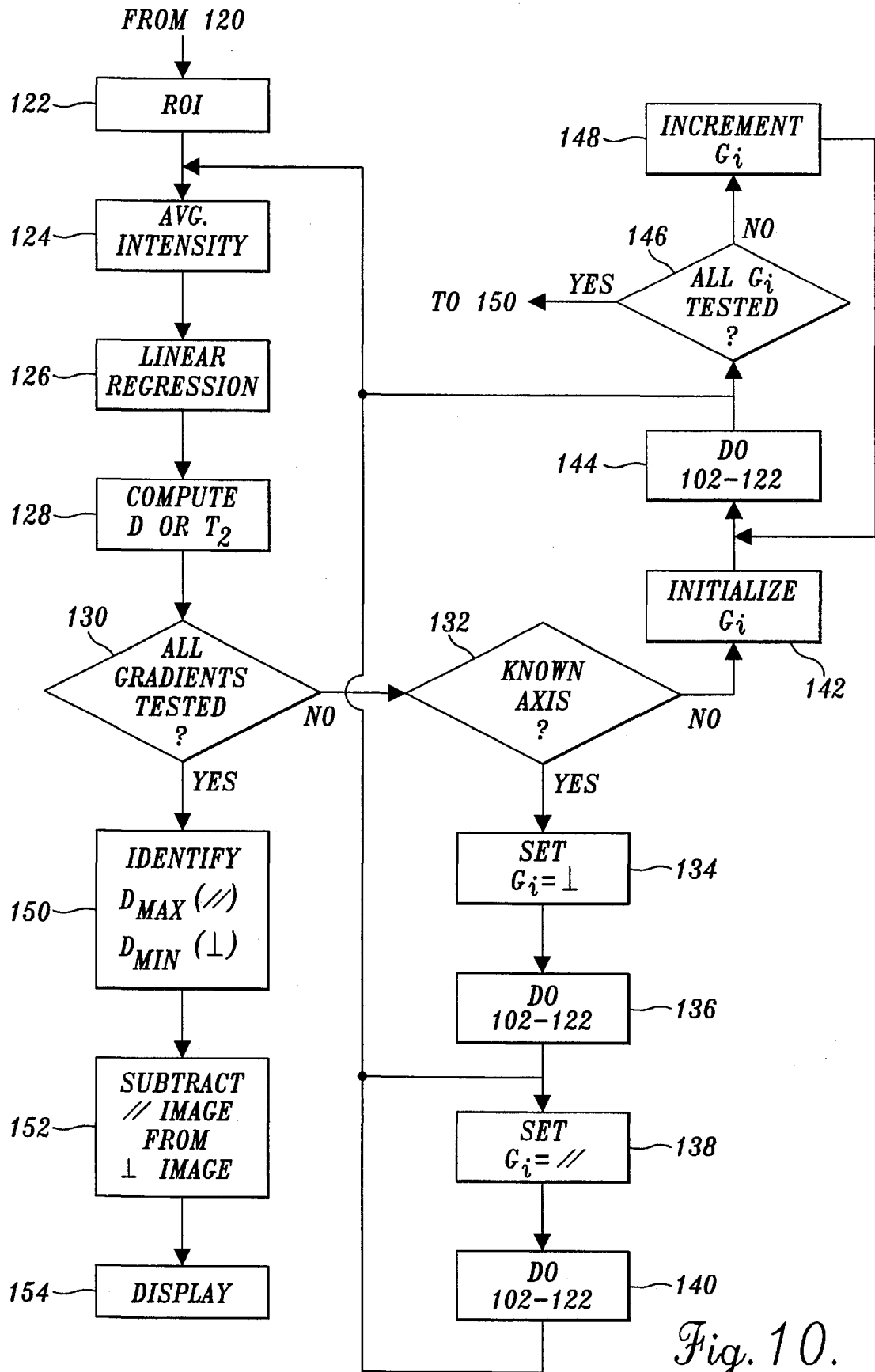
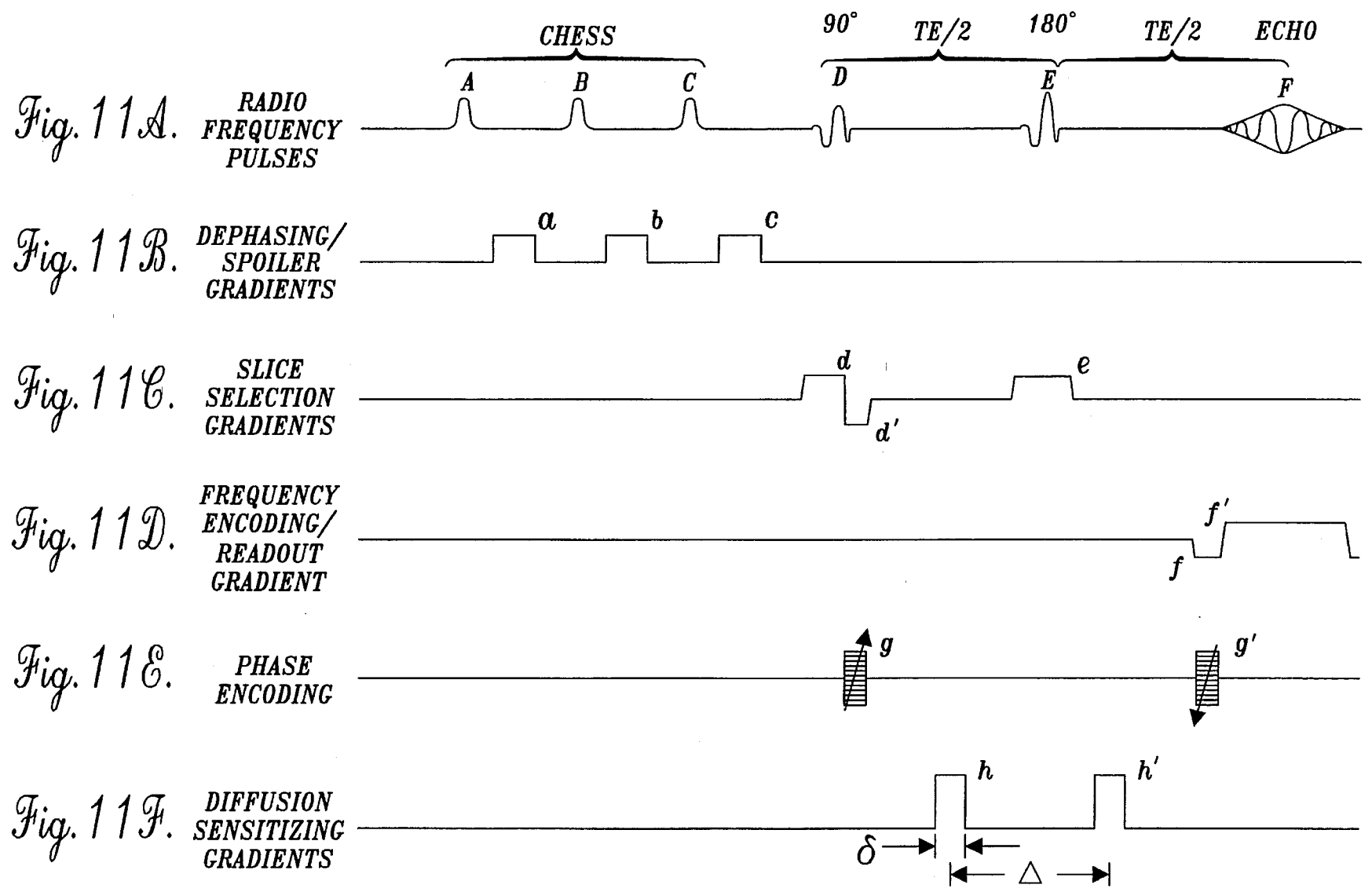


Fig. 10.



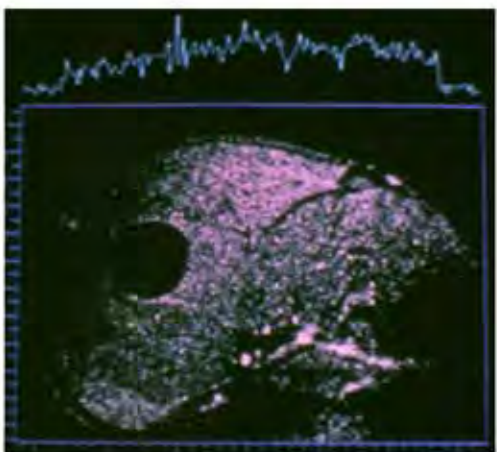


Fig. 11A.

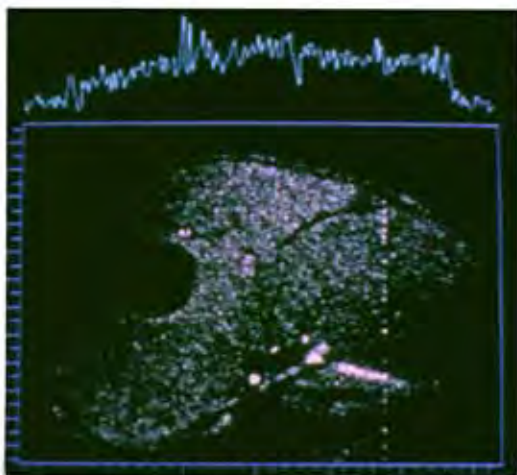


Fig. 11B.

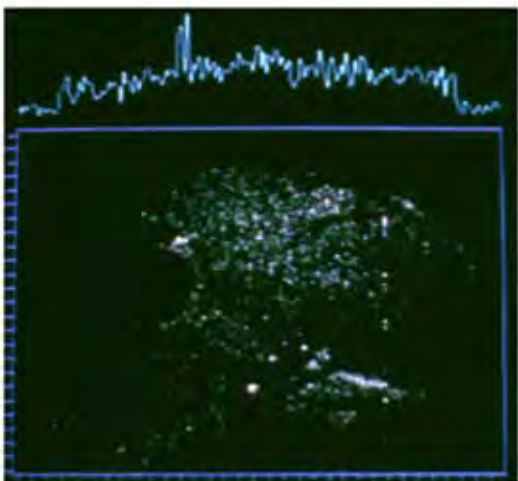


Fig. 11C.

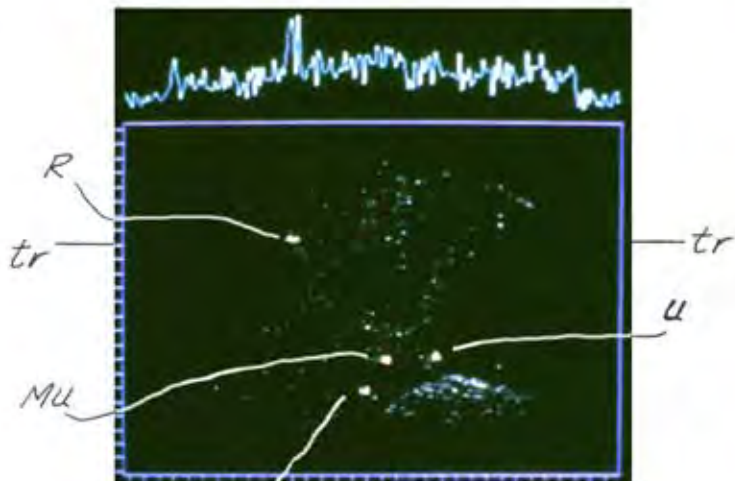


Fig. 11D.

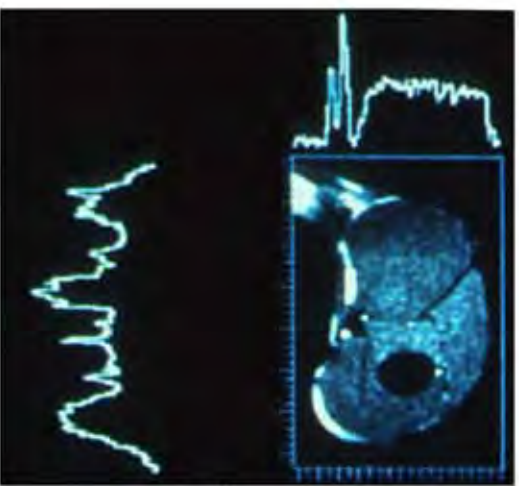


Fig. 15A.

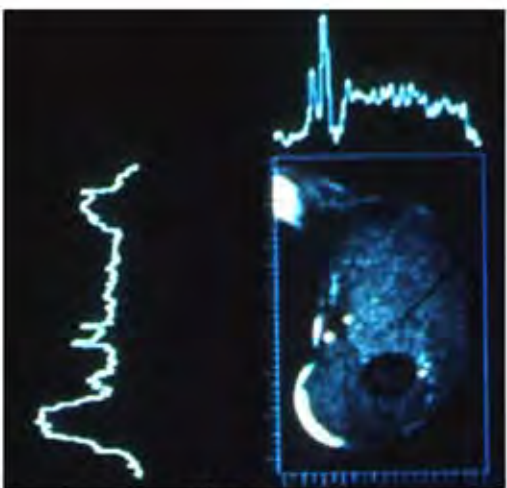


Fig. 15B.

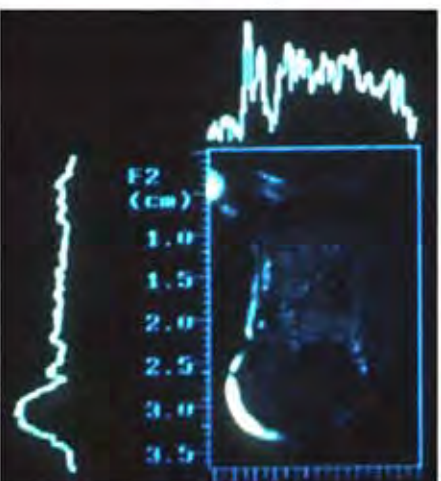


Fig. 15C.

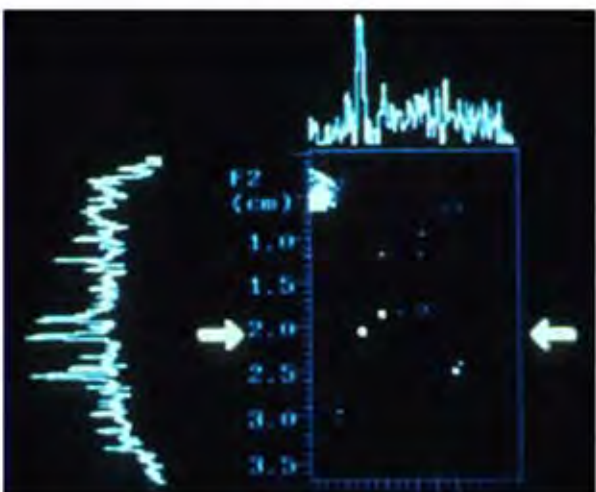


Fig. 15D.

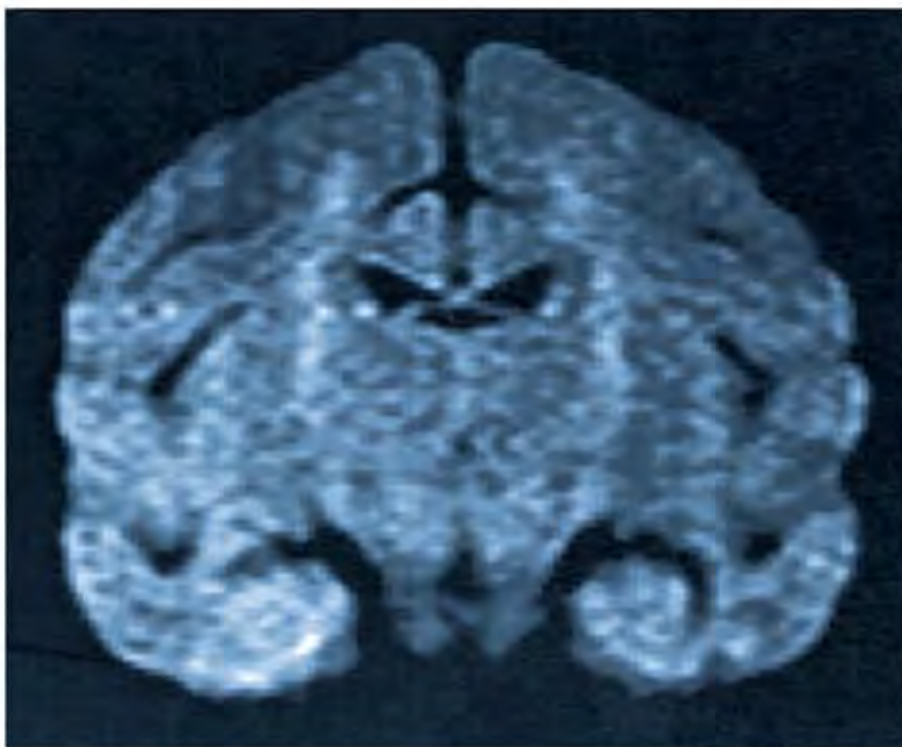


Fig. 16.

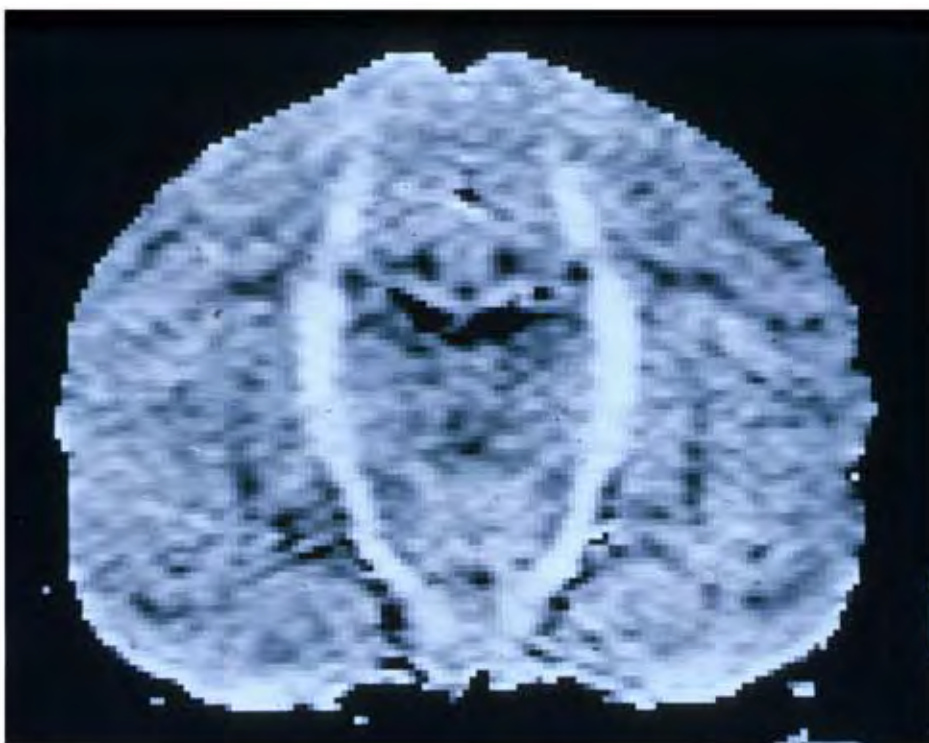


Fig. 17.

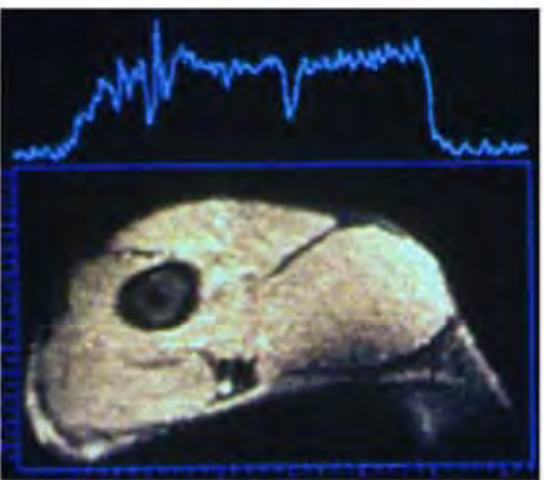


Fig. 10A.

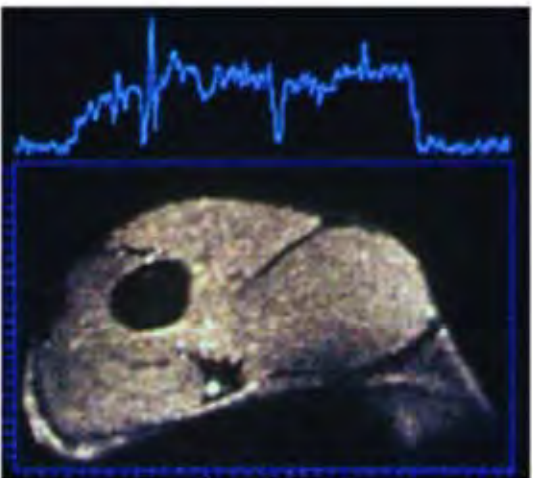


Fig. 10B.

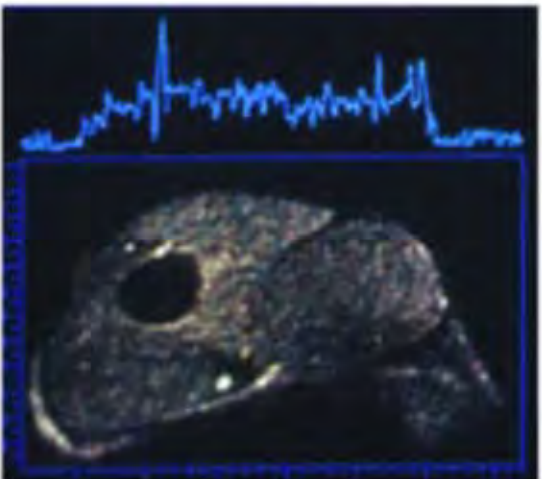


Fig. 10C.

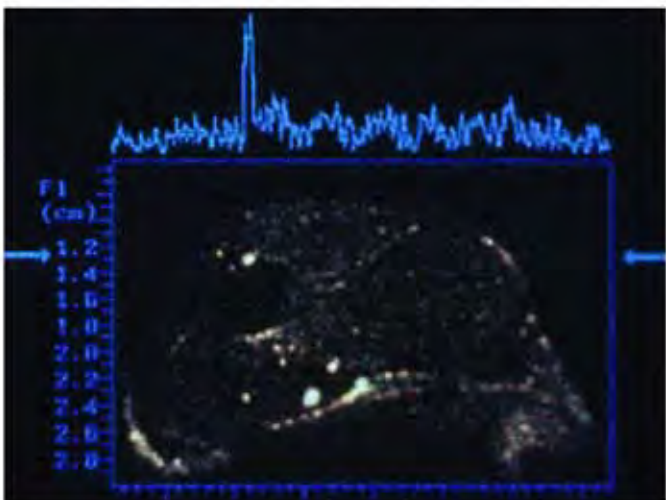


Fig. 10D.

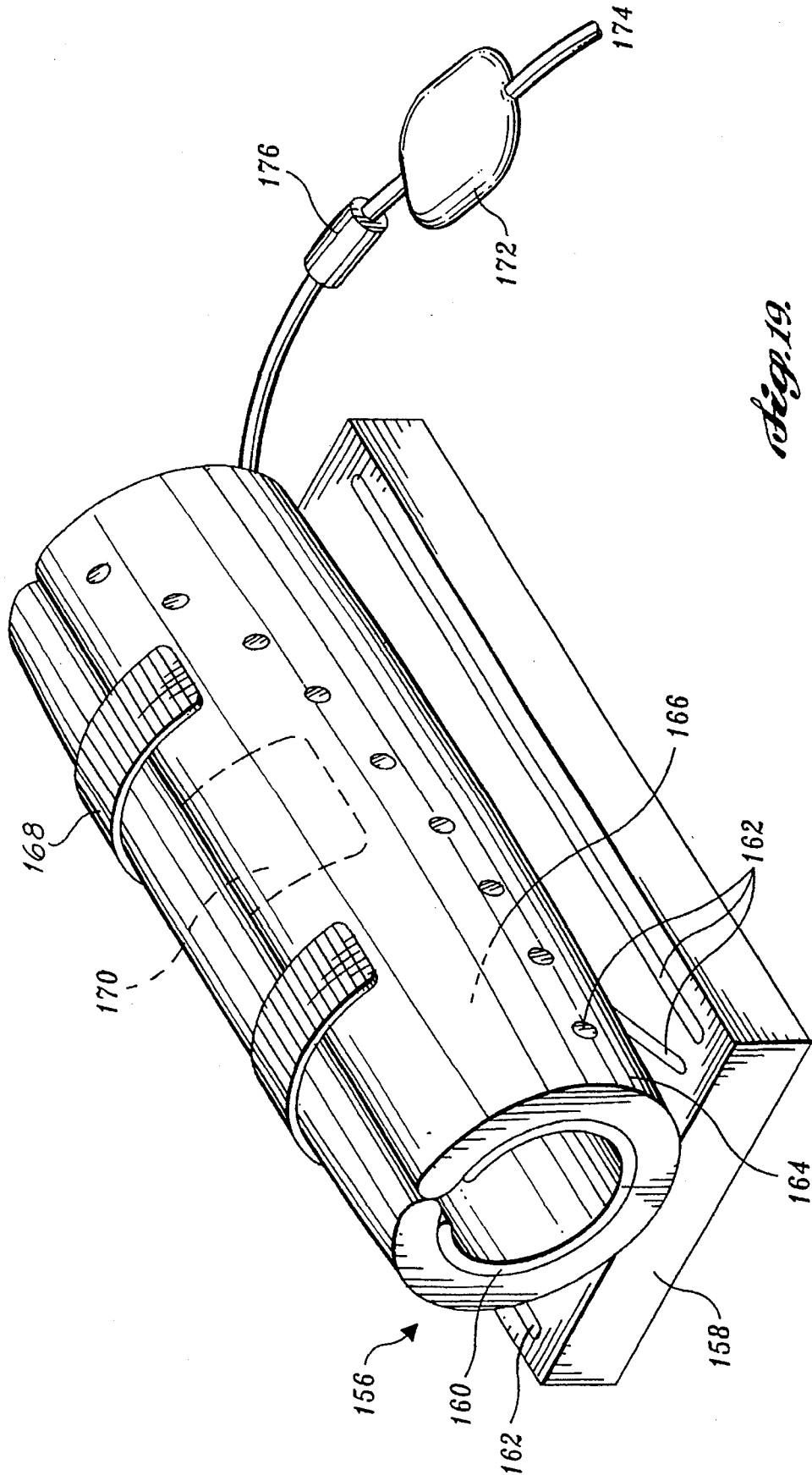


Fig. 19.

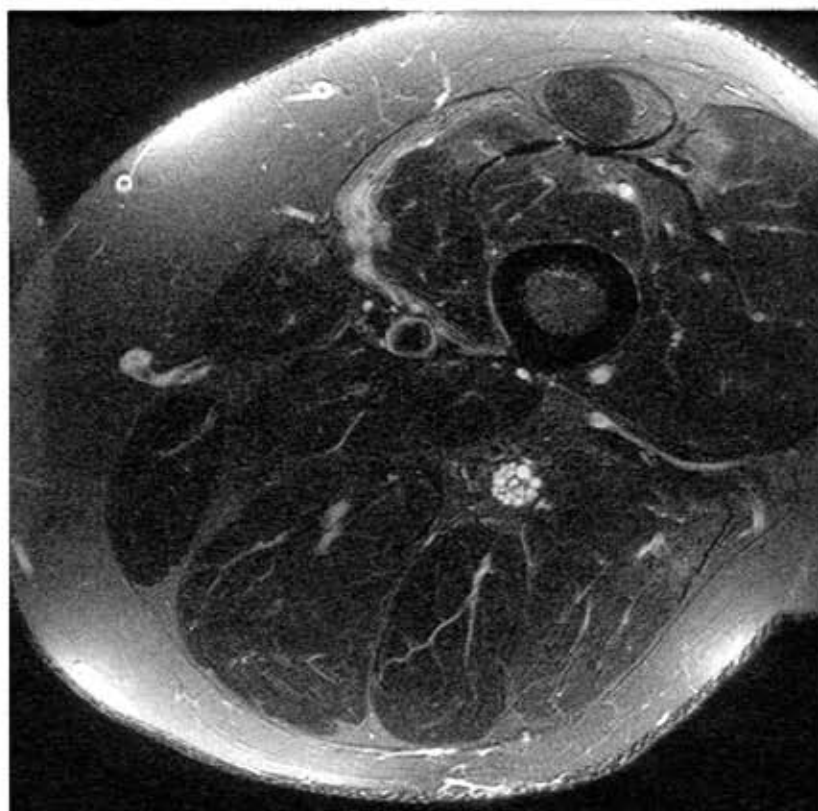


Fig. 20.

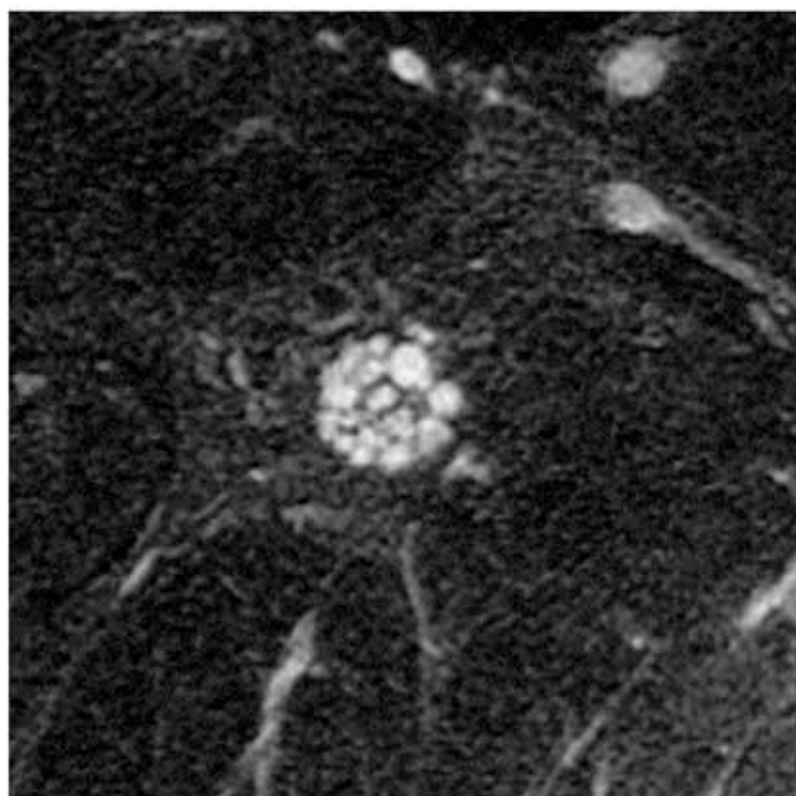


Fig. 21.

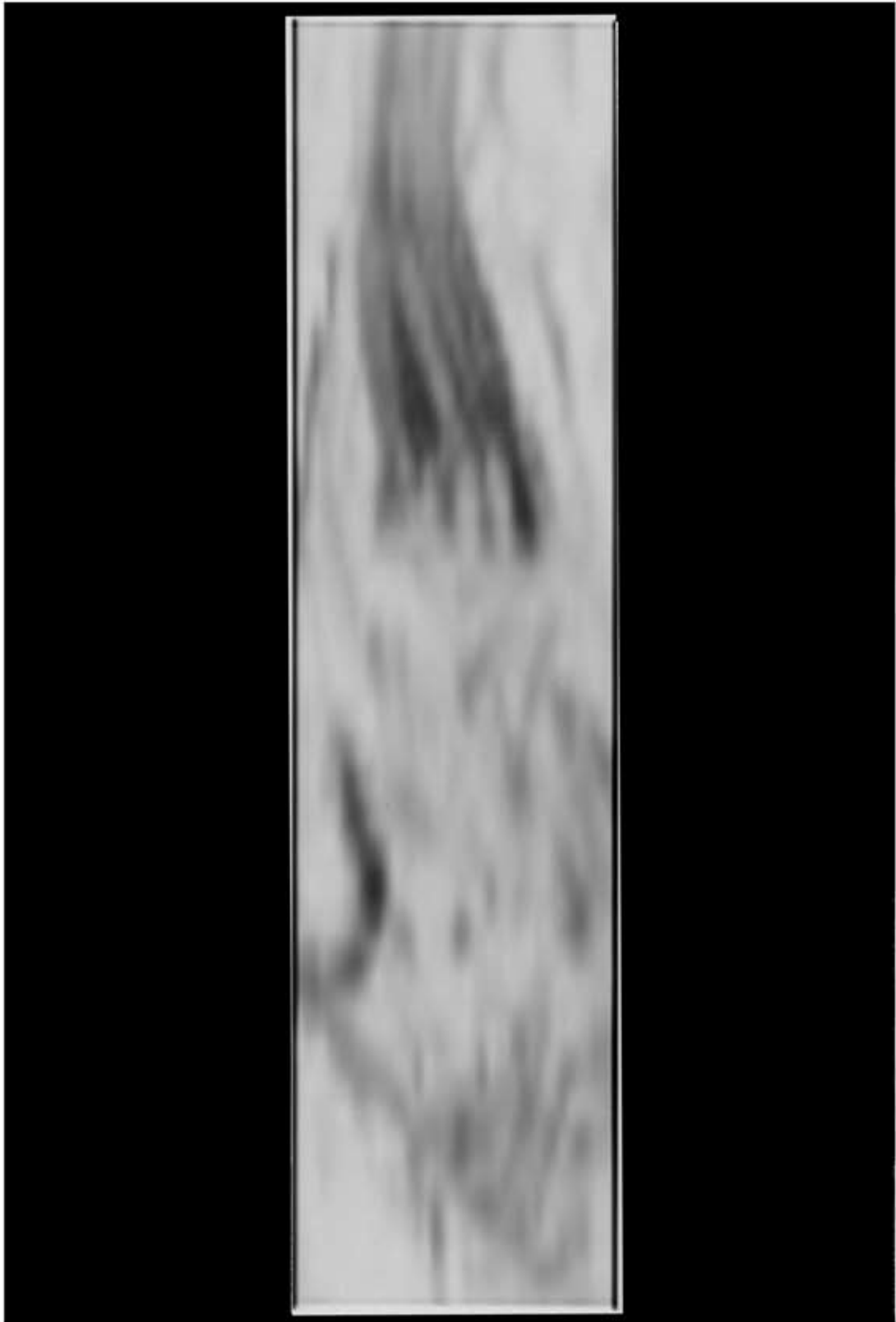


Fig. 22.

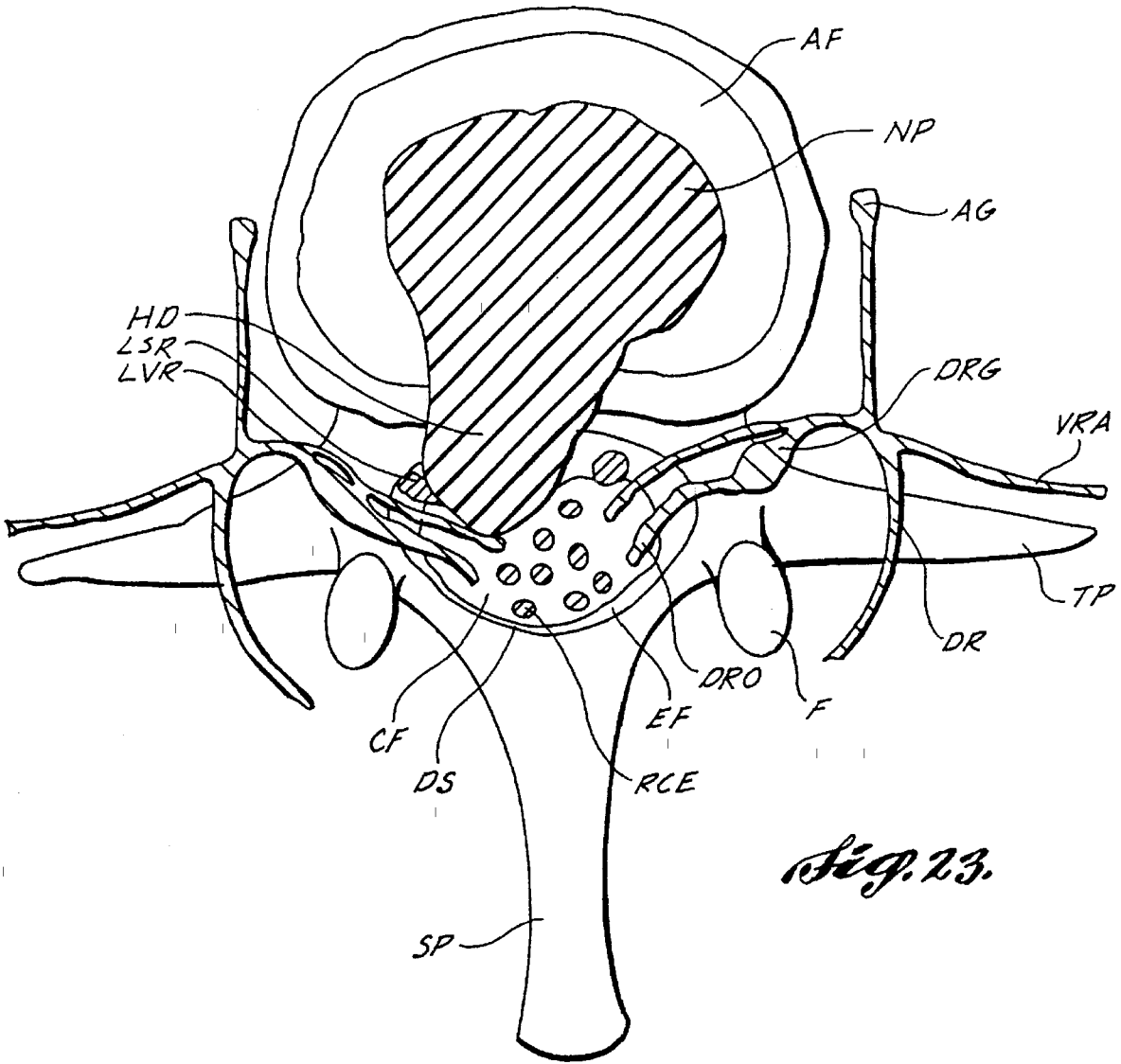


Fig. 23.

Fig. 2A.

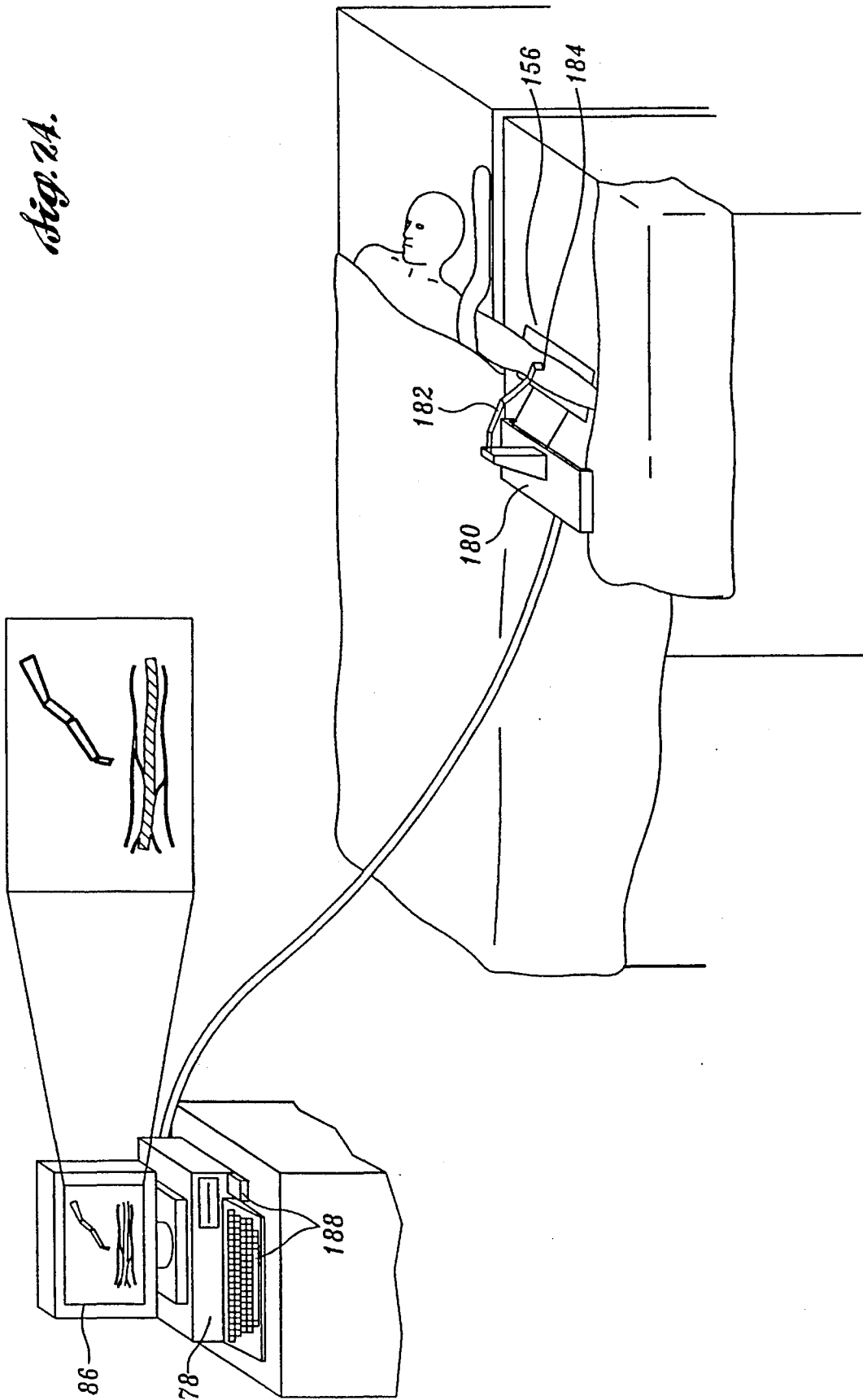


IMAGE NEUROGRAPHY AND DIFFUSION ANISOTROPY IMAGING

This application is based upon an earlier filed U.K. Patent Application No. 9301268.0, filed Jan. 22, 1993, which, in turn, is a continuation-in-part of U.K. Patent Application No. 9216383.1, filed Jul. 31, 1992, which, in turn, is a continuation-in-part of U.K. Patent Application No. 9210810.9, filed May 21, 1992, which, in turn, is a continuation-in-part of U.K. Patent Application No. 9209648.6, filed May 5, 1992, which, in turn, is a continuation-in-part of U.K. Patent Application No. 9207013.5, filed Mar. 30, 1992, which, in turn, is a continuation-in-part of U.K. Patent Application No. 9205541.7, filed Mar. 13, 1992, which, in turn, is a continuation-in-part of parent U.K. Patent Application No. 9205058.2, filed Mar. 9, 1992, the benefit of the filing dates of which is hereby claimed pursuant to 35 U.S.C. §119.

FIELD OF THE INVENTION

The present invention relates generally to the field of imaging and, more particularly, to the imaging of nerve tissue and other diffusional anisotropic structures.

BACKGROUND OF THE INVENTION

Although many techniques have been developed for locating and viewing the brain, spinal cord, and spinal roots within the spinal canal, hitherto there has not been a successful method for viewing the peripheral, autonomic, and cranial nerves. These nerves, collectively referred to herein as peripheral nerves, commonly travel through and along bone, muscle, lymphatics, tendons, ligaments, intermuscular septa, collections of fatty tissues, air and fluid spaces, veins, arteries, joints, skin, mucous membranes and other tissues. The relatively small size of peripheral nerves, as well as their close proximity to other tissue of comparable size and shape, makes them difficult to locate and identify.

The examination of peripheral nerves is further complicated by the complexity of many such neural structures, such as the brachial plexus, lumbar plexus, and sacral plexus. These structures include bundles of nerves that may join together, separate, rejoin, intermix, and segregate, forming intricate three dimensional patterns. A compression or irritation of a small area of nerve within such a plexus (e.g. in the shoulder) can cause pain, numbness, weakness or paralysis at some distant site (e.g. in one finger). Even when a surgeon attempts to expose the plexus for direct inspection, the anatomic complexity can prove overwhelming, rendering diagnosis inconclusive and surgery difficult and dangerous.

Radiologic methods employing, for example, X-rays, have been developed to generate tissue specific images of various physiological structures including bone, blood vessels, lymphatics, the gastrointestinal tract, and the tissues of the central nervous system. Due in part to the neural characteristics noted above, however, these techniques have not been successfully used to generate suitable clinical images of peripheral nerves.

Typically, the position of peripheral nerves in radiologic images has been inferred by reference to more conspicuous, non-neural structures such as tendons, vessels, or bone. For example, by producing an X-ray image of a region of the body through which a nerve of interest passes, non-neural structures can often be readily identified. Then, the locations of peripheral nerves in the region can be inferred from standard reference information about human anatomy. Due

to the variability of nerve position from one individual to another, however, this technique is of limited value.

One approach of particular interest that has been used to image physiological structures is magnetic resonance imaging (MRI). By way of introduction, MRI involves the exposure of tissue to a variety of different magnetic and radio-frequency (rf) electromagnetic fields. The response of the specimen's atomic nuclei to the fields is then processed to produce an image of the specimen.

More particularly, the specimen is initially exposed to a polarizing magnetic field. In the presence of this field, nuclei exhibiting magnetic moments (hereinafter referred to as spins) will seek to align themselves with the field. The nuclei precess about the polarizing field at an angular frequency (hereinafter referred to as the Larmor frequency) whose magnitude depends upon both the field's strength and the magnetogyric constant of the specific nuclear species involved.

Although the magnetic components of the spins cancel each other in a plane perpendicular to the polarizing field, the spins exhibit a net magnetic moment in the direction of the polarizing field. By applying an excitation field perpendicular to the polarizing field and at a frequency near the Larmor frequency, the net magnetic moment can be tilted. The tilted magnetic moment includes a transverse component, in the plane perpendicular to the polarizing field, rotating at the Larmor frequency. The extent to which the magnetic moment is tilted and, hence, the magnitude of the net transverse magnetic moment, depends upon the magnitude and duration of the excitation field.

An external return coil is used to sense the field associated with the transverse magnetic moment, once the excitation field is removed. The return coil, thus, produces a sinusoidal output, whose frequency is the Larmor frequency and whose amplitude is proportional to that of the transverse magnetic moment. With the excitation field removed, the net magnetic moment gradually reorients itself with the polarizing field. As a result, the amplitude of the return coil output decays exponentially with time.

Two factors influencing the rate of decay are known as the spin-lattice relaxation coefficient T_1 and the spin-spin relaxation coefficient T_2 . The spin-spin relaxation coefficient T_2 represents the influence that interactions between spins have on decay, while the spin-lattice relaxation coefficient T_1 represents the influence that interactions between spins and fixed components have on decay. Thus, the rate at which the return coil output decays is dependent upon, and indicative of, the composition of the specimen.

By employing an excitation field that has a narrow frequency band, only a relatively narrow band within a nuclear species will be excited. As a result, the transverse magnetic component and, hence, return coil output, will exhibit a relatively narrow frequency band indicative of that band of the nuclear species. On the other hand, if the excitation field has a broad frequency band, the return coil output may include components associated with the transverse magnetic components of a greater variety of frequencies. A Fourier analysis of the output allows the different frequencies, which can be indicative of different chemical or biological environments, to be distinguished.

In the arrangement described above, the contribution of particular spins to the return coil output is not dependent upon their location within the specimen. As a result, while the frequency and decay of the output can be used to identify components of the specimen, the output does not indicate the location of components in the specimen.

To produce such a spatial image of the specimen, gradients are established in the polarizing field. The direction of the polarizing field remains the same, but its strength varies along the x, y, and z axes oriented with respect to the specimen. By varying the strength of the polarizing field linearly along the x-axis, the Larmor frequency of a particular nuclear species will also vary linearly as a function of its position along the x-axis. Similarly, with magnetic field gradients established along the y-axis and z-axis, the Larmor frequency of a particular species will vary linearly as a function of its position along these axes.

As noted above, by performing a Fourier analysis of the return coil's output, the frequency components of the output can be separated. With a narrow band excitation field applied to excite a select nuclear species, the position of a spin relative to the xyz coordinate system can then be determined by assessing the difference between the coil output frequency and the Larmor frequency for that species. Thus, the MRI system can be constructed to analyze frequency at a given point in time to determine the location of spins relative to the magnetic field gradients and to analyze the decay in frequency to determine the composition of the specimen at a particular point.

The generation and sensing of the fields required for proper operation of an MRI system is achieved in response to the sequential operation of, for example, one or more main polarizing field coils, polarizing gradient field coils, rf excitation field coils, and return field coils. Commonly, the same coil arrangement is used to generate the excitation field and sense the return field. A variety of different sequences have been developed to tailor specific aspects of MRI system operation, as described, for example, in U.S. Pat. No. 4,843,322 (Glover); U.S. Pat. No. 4,868,501 (Conolly); and U.S. Pat. No. 4,901,020 (Ladebeck et al.).

One application of conventional MRI systems is in the production of angiograms, or blood vessel images. Various different pulse sequences and processing techniques have been developed for use in MRI angiography, as described in, for example, U.S. Pat. No. 4,516,582 (Redington); U.S. Pat. No. 4,528,985 (Macovski); U.S. Pat. No. 4,647,857 (Taber); U.S. Pat. No. 4,714,081 (Dumoulin et al.); U.S. Pat. No. 4,777,957 (Wehrli et al.); and U.S. Pat. No. 4,836,209 (Nishimura).

As will be appreciated, blood vessels are readily differentiated from surrounding tissue by the pulsatile flow of blood therethrough. MRI angiography exploits this distinguishing characteristic to generate images of the blood vessels in various ways. For example, if the excitation field is pulsed at systole and diastole, the contribution of blood flow to the return field will differ, while the contribution of static tissue and bone to the return field will be the same. By subtracting one return from the other, the static component cancels, leaving only the contribution from the blood vessel.

Unfortunately, because peripheral nerve does not exhibit the flow-distinctiveness of blood vessels, MRI angiography systems and pulse sequences can not be used to generate suitable images of peripheral nerve. Further, conventional MRI systems and sequences used for general imaging of tissue and bone do not provide acceptable results. Given the poor signal-to-noise (S/N) ratio of the return signals (e.g., on the order of $1 \times$ to $1.5 \times$) and the small size of the nerve, the conspicuity of imaged nerves relative to other tissue is collectively rendered so poor as to be diagnostically useless.

One technique proposed for use in enhancing the utility of MRI systems in imaging neural tissue involves the use of pharmaceutical agents to enhance the contrast of neural

tissue relative to surrounding tissue in the images produced. As described in PCT Patent Application No. PCT EP 91/01780 (Filler et al., WO 92/04916), published on Apr. 2, 1992, a two-part contrast agent, such as wheat germ agglutinin or dextrin-magnetite, is injected so that it is subsequently taken up, and transported, by the nerve of interest. The first part of the agent promotes neural uptake, while the second part of the agent has the desired "imageable" property.

The agent is injected into muscle and undergoes axoplasmic flow in the nerve supplying that muscle, tagging the nerve in subsequently generated images of the specimen. If MRI is used, the second part of the agent is selected to have a magnetically active (e.g., ferrite) component. An agent having a high nuclear density can, however, be used to increase the contrast of the nerve upon X-ray or computed tomography (CT) examination, while a radioactive (e.g. positron emitting) element can be used to enhance visibility during positron emission tomography (PET) scanning.

To illustrate the effectiveness of contrast agents in imaging nerve, reference is had to FIGS. 1-5. In that regard, FIG. 1 is a diagram of a transverse section of the upper forearm FA of a rabbit. The forearm includes the triceps muscle TM, ulnar nerve UN, brachial veins BV, median nerve MN, radial nerve RN, humerus H, cephalic vein CV, and biceps muscle BM.

FIGS. 2A and 2B illustrate spin-echo MR images of such a section, using a ferrite contrast agent, produced by a conventional MRI system at six-hour intervals. Although some of the larger structural elements are readily identified, the location of some objects appears skewed. More particularly, the humerus marrow appears shifted relative to the humerus H, as do ligaments L, and fat F between the biceps or triceps. In addition, smaller neural structures are difficult to distinguish.

Several approaches are available, however, to attempt to identify nerves in the images generated. For example, as shown in FIG. 3, if a short tau inversion recovery (STIR) sequence of the type described in Atlas et al., *STIR MR Imaging of the Orbit*, 151 AM. J. ROENTGEN. 1025-1030 (1988) is used, the humerus marrow disappears from the image as does, more importantly, certain ambiguous, apparently non-neural structures adjacent the median nerve MN. Thus, as shown in the enlarged image of the region including the median nerve MN and ulnar nerve UN, provided in FIG. 4, the median nerve MN is visible.

Similarly, even when the contrast agent images of FIGS. 2A and 2B are enlarged to better illustrate the region including the median nerve MN, as shown in FIGS. 5A and 5B, respectively, the nerves are distinguishable to a highly skilled observer. More particularly, transport of the ferrite contrast agent during the six-hour interval between the generation of images 4A and 4B results in a loss of intensity in the MN relative to the non-neural structure adjacent median nerve MN. Given this observation and the STIR-based assessment, the median nerve MN can, thus, be identified.

The use of contrast agents, while promising, does have certain limitations. For example, there is an increasing preference to avoid the use of invasive technologies in medicine whenever possible. Further, contrast agents generally can be used to image only a single nerve or nerve group. Of perhaps greatest importance, the contrast agents employed typically reduce the intensity of the imaged nerve. Since nerves are already difficult to see in current MRI images, the impact of the contrast agent upon the image can

be difficult to interpret, as illustrated by the discussion of FIGS. 2-5 above.

In another application, MRI has been used, without contrast agents, to map non-peripheral, white matter nerve tracts in the brain. The white matter tracts extend through gray matter tissue in the brain and exhibit relatively high anisotropic diffusion. More particularly, given their physical structure (i.e., axonal pathways surrounded by myelin sheaths), water mobility along the white matter tracts is relatively high, while water mobility perpendicular to the tracts is low. The surrounding gray matter does not, however, exhibit this same anisotropy.

A technique for MRI-based mapping of white matter nerve tracts that exploits this characteristic of neural tissue is described in Douek et al., *Myelin Fiber Orientation Color Mapping*, BOOK OF ABSTRACTS, SOCIETY OF MAGNETIC RESONANCE IN MEDICINE, p. 910 (1991). Basically, in addition to the fields and gradients described above, this process involves the use of a pair of field gradient pulses (hereinafter referred to as diffusion gradients), oriented perpendicular and parallel to the white matter tracts to be imaged. The effect of a pulsed gradient is to change the phase of the received signal from all of the spins. For stationary spins the effect of the two diffusion gradients cancels out. In contrast, spins moving from one spatial position to another in the time between the two diffusion gradients experience changes in the frequency and phase of the spin magnetization with the net effect being a reduction in the received signal. The signal reduction is greatest for those spins that diffuse the greatest distance between the two pulsed gradients.

As noted above, given the anisotropic nature of the tracts, water will diffuse freely along a tract, but is restricted in its motion perpendicular to the tract. When the diffusion gradient is aligned with the tract there is thus a greater reduction in signal than when the diffusion gradient is aligned perpendicular to the tract. Because this phenomenon is not exhibited by the surrounding gray matter tissue, the white matter tracts can be identified.

Anisotropic diffusion is also a recognized characteristic of peripheral nerve, as indicated in Moseley et al., *Anisotropy in Diffusion-Weighted MRI*, 19 MAGNETIC RESONANCE ON MEDICINE 321 (1991). The Douek et al. technology, however, does not distinguish peripheral nerve from muscle and other tissue for a number of previously unrecognized reasons. First, while the size and structure of the white matter tracts ensure that the resultant signals will be sufficiently strong for imaging, peripheral nerve is considerably smaller and more difficult to distinguish. Second, unlike the white matter tracts, peripheral nerve is commonly surrounded by muscle and fat, both of which impair the ability of the Douek et al. system to image nerve.

By way of elaboration, given its fibrous structure, muscle also exhibits diffusional anisotropy, as recognized in Moseley et al., *Acute Effects of Exercise on Echo-Planar T₂ and Diffusion-Weighted MRI of Skeletal Muscle in Volunteers*, BOOK OF ABSTRACTS, SOCIETY OF MAGNETIC RESONANCE IN MEDICINE 108 (1991). As a result, the simple anisotropic analysis of Douek et al. is unable to distinguish peripheral nerve and muscle. While fat is isotropic and, therefore, distinguishable from nerve, it also impairs the imaging of peripheral nerves. Specifically, the relative signal strength of fat returns to neural returns is so high as to render peripheral nerves unidentifiable in images produced.

As will be appreciated from the preceding remarks, it would be desirable to develop a method for rapidly and

non-invasively imaging a single peripheral nerve, or an entire neural network, without resort to contrast agents. The images generated should be sufficiently detailed and accurate to allow the location and condition of individual peripheral nerves to be assessed. It would further be desirable to provide a system that processes neural images to enhance the information content of the images, diagnose neural trauma and disorders, and inform and control the administration of treatments and therapy.

SUMMARY OF THE INVENTION

The present disclosure relates to a new method, which quite remarkably, is capable of generating a three dimensional image of an individual patient's nerves and nerve plexuses. The image can be acquired non-invasively and rapidly by a magnetic resonance scanner. These images are acquired in such a way that some embodiments of the invention are able to make all other structures in the body including bone, fat, skin, muscle, blood, and connective tissues tend to disappear so that only the nerve tree remains to be seen. A plurality of the nerves passing through a given imaged region may be observed simultaneously, thus alleviating any ambiguity of nerve identification which might arise were only a single nerve imaged as with some contrast agent techniques.

The invention is based on the discovery of a method of collecting a data set of signal intensities with spatial coordinates which describes the positions of the nerves within any two dimensional cross section of a living mammal or within any three dimensional data acquisition space. There exist a large number of pulse sequences capable of controlling or operating a magnetic resonance imaging apparatus and each of which accomplishes some preferred image optimization. Previously, however, no simple (single) or complex (double or multiple) pulse sequence has been able to increase the relative signal intensity of nerve so that it is brighter than all other tissues in the body or limb cross section. Surprisingly, the inventors have discovered that there are certain novel ways of assembling complex pulse sequences, wherein even though the simple components of the sequence decrease the signal-to-noise ratio of nerve or decrease the signal strength of nerve relative to other tissues, the fully assembled complex sequence actually results in the nerve signal being more intense than any other tissue. In this fashion, the image conspicuity of nerve is greatly increased.

Thus, a first aspect of the present invention provides a method of selectively imaging neural tissue of a subject without requiring use of intraneural contrast agents, the method comprising subjecting part of the subject anatomy to magnetic resonance imaging fields, detecting magnetic resonance and producing an image of neural tissue from said detected resonance so that a nerve, root, or neural tract of interest in said image can be visually differentiated from surrounding structures.

A second aspect of the present invention provides a method of selectively imaging neural tissue of a subject, the method comprising subjecting part of the subject anatomy to magnetic resonance imaging fields adapted to discriminate anisotropy of water diffusion or other special characteristic of neural tissue, detecting magnetic resonance to produce an electronic signal in accordance with said resonance and producing an image of neural tissue from said electronic signal.

The invention also provides an apparatus for selectively imaging neural tissue of a subject without requiring the use of neural contrast agents, the apparatus comprising means

for subjecting part of the subject anatomy to magnetic resonance fields, means for detecting magnetic resonance to produce an electronic signal in accordance with said resonance, and means for producing an image of neural tissue from said electronic signal so that a nerve, root, or neural tract of interest in said image can be visually differentiated from surrounding structures.

The invention also finds expression as an apparatus for imaging neural tissue of a subject, the apparatus comprising means for subjecting part of the subject anatomy to magnetic resonance fields adapted to discriminate anisotropy of water diffusion, means for detecting magnetic resonance to produce an electronic signal in accordance with said resonance and means for producing a selective image of neural tissue of interest from said electronic signal.

BRIEF DESCRIPTION OF THE DRAWINGS

The foregoing aspects and many of the attendant advantages of this invention will become more readily appreciated as the same becomes better understood by reference to the following detailed description, when taken in conjunction with the accompanying drawings, wherein:

FIG. 1 is a diagram of a transverse section of the upper forearm of a rabbit illustrating various neural and non-neural structures;

FIGS. 2A and 2B are images of the upper forearm of a rabbit, of the type depicted in FIG. 1, produced using an MRI system at two spaced-apart times after the forearm was injected with a ferrite contrast agent;

FIG. 3 is another image of the upper forearm of a rabbit produced using an MRI system employing a short tau inversion recovery (STIR) spin-echo sequence;

FIG. 4 is an enlargement of a portion of the image of FIG. 3 associated with a peripheral nerve of interest;

FIGS. 5A and 5B are enlargements of a portion of the images of FIGS. 2A and 2B, respectively, associated with a peripheral nerve of interest;

FIG. 6 is a block diagram of a neurography system, constructed in accordance with this invention, coupled to a plurality of other systems designed to provide information to the neurography system and to implement, for example, neural diagnoses, therapy, surgery, and training;

FIG. 7 is a functional chart of the operation of the neurography system of FIG. 6;

FIG. 8 is an illustration of the various components included in the neurography system of FIG. 6;

FIGS. 9 and 10 are flow charts depicting one way in which the neurography system of FIG. 8 may be used to generate neurograms;

FIGS. 11A through 11F illustrate one sequence of pulses suitable for use in producing diagnostically suitable images from the neurography system of FIG. 6;

FIG. 12 is another image of the upper forearm of a rabbit produced by an embodiment of the neurography system employing fat suppression;

FIGS. 13A and 13B are additional images of the upper forearm of a rabbit produced by an embodiment of the neurography system employing gradients perpendicular and parallel, respectively, to the anisotropic axis of nerve being imaged;

FIGS. 14A through 14D are images of the upper forearm of a rabbit produced employing gradients of 0, 3, 5, and 7 Gauss/centimeter, respectively;

FIGS. 15A through 15C are images producible by the neurography system with zero, perpendicular, and parallel gradients, while FIG. 15D is an image based upon the images of FIGS. 15B and 15C, referred to herein as a subtraction neurogram

FIG. 16 vector length image of the brain produced using the neurography system of FIG. 8;

FIG. 17 is an arctan image of the brain produced using the neurography system of FIG. 8;

FIGS. 18A through 18D are images of a rabbit forearm produced using the neurography system of FIG. 8, and illustrating the influence of the TE sequence upon the images produced;

FIG. 19 illustrates a splint employed in the neurography and medical systems of the present invention;

FIGS. 20, 21, and 22 are illustrations of images of a human sciatic nerve produced using the neurography system of FIG. 8, with FIGS. 20 and 21 illustrating the ability of the system to image nerve fascicles (in two cross-sectional scales) and FIG. 22 illustrating an axial projection of the nerve;

FIG. 23 is a diagram of a cross-section of a vertebra, illustrating the types of structure present in one neurography application; and

FIG. 24 is a schematic illustration of a surgical system constructed in accordance with this invention for use with the neurography system of FIG. 8.

DETAILED DESCRIPTION OF THE PREFERRED EMBODIMENT

Referring now to FIG. 6, a neurography system 10 is shown as one component of a broader medical system 12. Unlike prior art arrangements, system 10 quickly and non-invasively generates accurate images showing the pattern of individual peripheral nerves, or entire nerve trees, without the use of contrast agents. The system is designed to allow such images, hereinafter referred to as neurograms, to be displayed in two-dimensions, illustrating neural cross sections in the specimen under examination, or in three-dimensions. The images may selectively exclude all other structures within the specimen, or may illustrate the physical relationship of other structures relative to the nerves for reference.

1. Medical System Overview

As shown in FIG. 6, the neurography system 10 included in medical system 12 includes four basic components: MRI system 14, processing system 16, input system 18, and output/display system 20. In the preferred arrangement, the MRI system 14 is a conventional MRI system modified for use in collecting image data of a patient P under examination. The processing system 16 responds to operator inputs applied via input system 18 to control MRI system 14 and process its output to display the resultant neurograms at system 20. As will be described in greater detail below, system 16 employs a variety of different imaging protocols, alone or in combination, to ensure that the images produced are of a quality heretofore unachieved.

The medical system 12 includes a number of components that supplement the imaging information produced by system 10 and/or use that information for a variety of purposes. For example, an auxiliary data collection system 22 may be included to collect image information about non-neural structures, such as blood vessels and bone, in the imaged region of patient P. This information can then be used to

suppress and/or enhance the appearance of those structures in the neurograms produced by system 10.

A diagnostic system 24, included in system 12, may be used to analyze the images produced by system 10. Given the high resolution, detail, and accuracy of neurograms produced by system 10, system 24 can be programmed to analyze neural pathway information to detect discontinuities associated with, for example, neural compressions, injuries, and tumors. System 24 provides outputs indicative of the location of discontinuities and may, by consultation with a database of image information associated with clinically assessed abnormalities, provide an indication of the nature and magnitude of an imaged discontinuity. These outputs can be used for diagnosis, or applied as feedback to system 10 to refine a region of interest (ROI) under examination in patient P.

Medical system 12 may also include a therapeutic system 26 and surgical system 28. Systems 26 and 28 employ information about the patient's neural structure from system 10 to assist in the proper administration of a desired therapeutic or surgical operation. For example, the information may be used to guide a robotic stylus to a damaged neural site for treatment or to allow an operation on non-neural structure to be performed without damage to the patient's peripheral nerves. The systems 26 and 28 may operate independent of physician control or may simply provide the physician with real-time feedback concerning the relationship between an operation being performed and the patient's neural structures.

A training and development system 30 is included in the medical system 12 for a variety of different purposes. For example, the training system 30 may be used to demonstrate the anatomy of various neural structures, along with their positional relationship to non-neural patient structures. This information has great educational value given the extremely limited ability of prior art techniques, including direct examination, to provide detailed anatomical information. Training system 30 may also be designed to analyze the effectiveness of neurography system 10 and provide feedback used to control the pulse sequences and other operational parameters of system 10.

As one final component, medical system 12 may include a host processing system 32 in addition to, or in place of, separate processing systems in the other components of system 12. Although not separately shown in FIG. 6, system 32 includes a central processing unit (CPU) coupled to the remainder of system 12 by input/output circuits. Memory is provided to store software instructions, used to control the operation of the CPU and, hence, the various components of system 12, and to store image and other data collected by system 12. The use of a separate host processing system 32 is particularly desirable where various components of system 12 are to be operated in interactive fashion pursuant to a single set of software instructions.

2. The Neurography System

Turning now to a more detailed discussion of neurography system 10, by way of introduction, some of the more important operational features of system 10 are loosely depicted in the chart of FIG. 7. As will be described in greater detail below, system 10 may be constructed to employ one or more of these features to enhance the imaging ability of conventional MRI sufficiently to provide diagnostically and therapeutically useful information.

As shown, the operation of system 10 can be broken down into the broad steps of data collection 34, image processing and analysis 36, image display 38, and control 40. The data collection process 34 involves, for example, spin-echo imag-

ing 42, which may be supplemented by one or more of the following imaging protocols: fat suppression 44, diffusion weighting 46, and "long T2" processing 48, and other protocols including magnetization transfer. Each of these protocols has been found to enhance the quality of images of peripheral nerve sufficiently to provide heretofore unavailable MRI neurograms.

The data collected by process 34 is subjected to image processing and analysis 36, involving two-dimensional and three-dimensional image generation 50. Image generation 50 may be further enhanced by miscellaneous suppression features 52, responsible for reducing the influence of, for example, blood vessels and patient motion, on the images produced. An image subtraction feature 54 may also be employed to remove all non-neural components from the images.

a. Neurography System Construction

Having briefly summarized the operational aspects of neurography system 10, its construction and operation will now be considered in greater detail. In one embodiment, MRI system 14 includes an imager I of the type sold by GE Medical Systems, under the trademark SIGNA (software release 5.2).

In that regard, as shown in FIG. 8, the region R of the patient to be imaged is placed within the bore B of the MRI system imager I. As will be described in greater detail below, the position of region R relative to the imager may be stabilized by a splint 58. Splint 58 limits motion artifact, provides fiducial markers in a secondary frame of reference, and reduces the system's susceptibility to boundary effects that otherwise might degrade fat suppression near the boundary between skin and air.

MRI system 14 includes polarizing field coils 60 and 61 responsible for exposing region R to the desired polarizing field. The polarizing field has a strength of, for example, 1.5 Tesla and is oriented along a z-axis.

A tuned rf excitation coil 62 is also positioned within bore B over the region R under investigation. Coil 62 is provided with a pulsed rf input, in a manner described below, to generate the field responsible for excitation of nuclear spins in region R. Coil 62 is also responsible for detecting the rf return, or echo, fields generated by the spins, although separate transmit and receive coils may alternatively be used.

The excitation coil 62 may be, for example, a solenoid or surface coil, configured and dimensioned to fit closely over the region R to be imaged (e.g., the patient's arm, leg, shoulder, chest, pelvis, head, neck or back). In a preferred arrangement, however, a phased array coil system is employed to increase the signal-to-noise ratio of the returns, thereby providing an improvement in the spatial resolution of system 14 and allowing information to be retrieved from signals that would otherwise have been too weak to form useful images. For example, where peripheral nerve having a thickness on the order of 1-2 mm is to be sharply resolved, each array includes, for example, 4-6 individual coils, arranged in transverse and longitudinal pairs or linear paired arrays.

Three pairs of gradient coils 64 and 66 are also positioned within the bore B of the imager. These coils superimpose a locational gradient of roughly one Gauss per centimeter upon the polarizing field over the sample region R along each of the x, y, and z-axes. For the sake of simplicity, however, only the z-gradient coils 64 and 66 are shown in FIG. 8.

In the preferred arrangement, the same coil pairs 64 and 66 are used to produce diffusional gradients along the

desired axes, as well as the requisite locational gradients. Alternatively, one or more separate diffusional gradient coil pairs **68** and **70** may be provided within the imager bore **B**. If the separate coil pair **68** and **70** is mounted on a movable track, substantially any desired diffusional gradient orientation can be achieved. The diffusional gradient is relatively strong compared to the locational gradients, e.g., ranging up to 10 Gauss/centimeter or higher.

A computer **72** and front-end circuit **74** form the processing system **16**, input system **18**, and output/display system **20** of neurography system **10** shown in FIG. 6. Computer **72** and circuit **74** cooperatively control and synchronize the operation of MRI system **14**, as well as process and display the acquired data.

The computer **72** is, for example, an IBM-compatible personal computer including a 486 processor, VGA monitor, and keyboard. An interface bus **76**, included in circuit **74**, couples computer **72** to the other components of circuit **74**.

A gradient pulse generator **78** included in circuit **74** produces generally rectangular output pulses used to establish the desired gradients in the polarizing field. The output of generator **78** is applied to x-, y, and z-axis gradient field amplifiers **80**, although only the z-axis amplifier **80** is shown in FIG. 8. As will be appreciated, if separate coils **68** and **70** are employed to establish the diffusional gradients, the output of generator **78** must be applied to those coils via separate amplifiers **82**.

Circuit **74** also includes an rf pulse generator **84**, which produces rf signal pulses used in the establishment of the excitation field. In the preferred arrangement, the pulse generator produces an rf output suitable for use in proton MRI, although frequencies specific to other MRI susceptible nuclei, such as, ¹⁹fluorine, ¹³carbon, ³¹phosphorus, deuterium, or ²³sodium, may be used. The output of generator **84** is amplified by a high-power rf amplifier **86** before being selectively applied to the excitation coil **62** by a duplexer **88**. The duplexer **88** is also controlled to selectively steer the low level MR returns received by the excitation coil **62** to a preamplifier **90**.

A mixer **92** transforms the high frequency output of preamplifier **90** to a low frequency signal by mixing the amplified MR returns with signals from a digitally controlled rf oscillator **94**, which also provides inputs to generator **84**. The analog output of mixer **92** is input to a low pass filter **96** before finally being converted to a digital form by an analog-to-digital converter **98**. The computer **72** processes the resultant digital inputs, which represent the response of the spins to the applied fields, to generate the desired neurograms.

b. Neurography System Operation

Having reviewed the basic construction of the neurography system **10**, its operation to generate the desired two- or three-dimensional neurograms will now be considered. To that end, FIGS. 9 and 10 depict the general sequence of steps performed by system **10** in the production of neurograms. These neurograms exhibit a high nerve conspicuity, which for the purpose of the ensuing discussion will be understood to refer to the contrast (in, for example, intensity or color) between the nerve and the image background. The methods described below may be used to produce neurographic images of substantially any region of the body, including the brain, for example, central nervous system (CNS) neurograms.

As indicated at block **100**, the operation of the system is first initialized to establish certain parameters of the system's operation. In that regard, the operator may input desired parameters via computer **72** in response to queries

generated at start up. Because most aspects of the system's operation are controlled by software resident in the memory of computer **72**, default initialization parameters may also be accessed.

Although the particular parameters to be initialized may vary at the user's discretion, examples include the type of images to be generated (i.e., two-dimensional cross sections or three-dimensional projections), field of view (FOV), thickness of each slice imaged, pulse repetition rate (TR), number of phase encoding steps, the existence of a known axis of diffusional anisotropy, and the strengths and orientations of the diffusional gradients to be used. By way of example, the operator may select a two-dimensional image, a FOV of four cm by four cm, a TR of 1.5 seconds, and 256 phase encoding steps. A discussion of anisotropic axis identification is provided below.

Once initialization has been completed, a series of steps, corresponding to the data collection process **34** discussed in connection with FIG. 7, are performed. This process generally involves the control of pulse sequences used in connection with front end circuit **74**. As will be described in greater detail below, different sets of pulse sequences and combinations of pulse sequences have been devised to unambiguously distinguish small peripheral nerves from neighboring structures of similar shape and location, including the combination of certain existing sequences into new groupings for use in new situations and the design of new sequences that incorporate optimized features for the purpose of neurographic imaging. For illustrative purposes, a graphic illustration of one example of a suitable pulse sequence is provided in FIGS. 11A through 11F.

i. Fat Suppression

As indicated in block **102** of FIG. 9, a first, optional, step performed in the image generation process is fat suppression. Although fat represents a known source of interference in MRI images of bone and tissue, it was not previously recognized as an impediment to effective neural imaging due to the broader perception that neural MR signals were inadequate for imaging regardless of background composition. The value of fat suppression was discovered during the development of the present invention by the fortuitous use of a main field magnet designed for spectroscopy as part of an imaging system.

In that regard, in MR spectroscopy, a relatively strong magnetic field is employed to increase the separation in frequency between signals arising from different chemical species of the same nucleus, thereby allowing these components to be more easily distinguished. MRI also uses a frequency distribution (created by applying a field gradient) over a sample to locate spins and create an image. The signals from fat and water are at slightly different frequencies and therefore appear shifted relative to each other in an image.

The fat/water shift is relatively small when a low field, clinical MRI system is used. Fortuitously, a much stronger spectroscopic field magnet was used during initial efforts at imaging nerve, introducing a much greater displacement of fat in the image produced. With the high intensity fat signal shifted away from the nerve, an enhancement of the nerve's conspicuity was observed. The recognition of this enhancement led to the realization that effective neural imaging could, in fact, be achieved through the inclusion of fat suppression in system **14**.

Fat suppression apparently enhances the use of conventional MRI systems for neurography in several ways. First, the removal of extraneous components reduces the number of imaged structures to be distinguished. Second, in a fat

suppressed image a peripheral nerve exhibits a relatively high intensity and will stand out sharply against the low intensity space left behind by the suppressed fat. As will be described in greater detail below, fat suppression also synergistically increases the apparent magnitude of diffusion anisotropy and magnetization transfer effect.

One suitable fat suppression technique involves the use of a chemical shift selective (CHESS) pulse sequence, described in detail, for example, in Haase et al. *NMR Chemical Shift Selective Imaging*, 30 *PHYS. MED. BIOL.* 341-344 (1985).

As shown in FIG. 11A, CHESS involves the application of a sequence of narrow band rf pulses A, B and C to the excitation coil 62 to selectively excite the nuclear spins of fat molecules within the region R of the patient being imaged. By way of example, three millisecond Gaussian pulses having a minus three dB bandwidth of 600 Hertz may be employed. A sequence of gradient pulses a, b, and c is then applied to the three sets of gradient coils 64 and 66 to dephase the excited spins, thereby minimizing the contribution of the fat signals to the final image. The gradient pulses a, b, and c applied to the orthogonal gradient coil pairs produce, for example, gradients of five Gauss per centimeter for three milliseconds along the x, y, and z-axis, respectively.

FIG. 12 illustrates the effect of fat suppression on neurograms produced with the MRI system 14. The image provided in FIG. 12 is of the forearm of a rabbit and corresponds to the images of FIGS. 1-5 described above. The darker portions of the image represent greater image intensity. As shown in FIG. 12, the ulnar nerve UN and median nerve MN are readily identified.

As an alternative to the use of CHESS for fat suppression, the desired suppression may be effected by selective water stimulation. Other suitable alternatives include the Dixon technique for fat suppression described in, for example, Dixon et al., *Simple Proton Spectroscopic Imaging*, 153 *RADIOLOGY* 189-194 (1984) and also STIR (short tau inversion recovery) described in *Improved Fat Suppression in STIR MR Imaging: Selecting Inversion Time through Spectral Display*, 178 *RADIOLOGY* 885-887 (1991).

Although in the preferred embodiment fat suppression is combined with other techniques such as diffusional weighting and long T_2 processing, fat suppression by itself enhances conventional MRI processing sufficiently to generate clinically useful neurograms. Similarly, as will be described in greater detail below, other techniques employed by system 10 can be used without fat suppression to generate suitable neurograms.

ii. Spin-Echo Sequence (Without Diffusional Weighting)

Having discussed the optional introductory portion of the illustrative pulse sequence depicted in FIG. 11, the next phase of the neurography system's operation will now be considered.

In that regard, an rf excitation pulse D, shown in FIG. 11A, is applied to coil 62 to tilt the net magnetic moment of the spins by ninety degrees relative to the polarizing field, into the transverse plane. The resultant maximum transverse magnetization then decays to zero as the spins dephase. A second pulse E, having twice the intensity of pulse D, is applied to coil 62 after a delay of one-half the return or echo time (TE). This pulse rotates the spins a further 180 degrees and causes a spin-echo to form as the spins rephase. The spin echo has a maximum amplitude after a further delay of TE/2. A spin-echo signal F is, thus, generated in coil 62 at time TE in response to the combined influence of excitation pulse D and refocusing pulse E. These steps are depicted in blocks 104, 106, and 108 of FIG. 9.

At the same time, the imaging gradients are produced by the orthogonal coil pairs 64 and 66 to encode the echo signal F in the usual manner, allowing an MR image to be constructed, as indicated in block 110. With the sample oriented along the z-axis, the "slice select" pulses d, d', and e shown in FIG. 11C are applied to the z-axis coil pair 64 and 66, to excite and refocus the z-axis slice of interest. The "readout gradient" pulses f and f', shown in FIG. 11D, are applied to, for example, the x-axis coil pair 64-66 to achieve the desired output that is to be Fourier transformed. The "phase encoding" pulses g and g', shown in FIG. 11E, are applied to the y-axis coil pair 64 and 66, to control the number of echoes (e.g., 256) to be received. The sequence may be used to generate images from contiguous slices or regions of the patient.

As will be appreciated, if the operator indicates (at block 100) that diffusional weighting is not required for the generation of a particular image by neurography system 10, the pulses shown in FIGS. 11A-11E define substantially the entire spin-echo sequence. Even if diffusional weighting is to be employed, in the preferred embodiment an initial image is generated using only fat suppression for enhancement and, as a result, diffusional weighting is not used during the first performance of the spin-echo sequence (blocks 104-110) for a particular slice.

Although spin-echo imaging is employed in the preceding embodiment of neurography system 10, other techniques can be employed. Suitable alternative techniques include, for example, stimulated echo imaging and gradient-recalled echo imaging, e.g., echo planar imaging (EPI). Such alternative techniques are described in Parikh, *MAGNETIC RESONANCE IMAGING TECHNIQUES* (1992).

iii. Echo Processing

In the imaging sequence depicted in FIG. 11, a series of echo signals F are acquired to create a two-dimensional image. For example, at block 112 in FIG. 9, 256 echoes with 256 different phase encoding gradient amplitudes are used to construct a 256-by-256 pixel image. The data set is then enlarged at block 114 by zero filling to produce a 1024-by-1024 matrix of data. As a result, the apparent resolution of the final image is increased, making the image clearer.

Next, the enlarged data set is processed using a 2D Gaussian filter at block 116. The filter smoothes the image by attenuating the high frequency components in the image and, thus, clarifies the delineation of small details without altering the relative average pixel intensities over a region of interest. At block 118, the two-dimensional matrix of data then undergoes a two-dimensional Fourier transform, which yields an image to be stored. If desired, the image may also be displayed on the computer monitor, although in the preferred arrangement this image is but one component used in a more extensive analysis performed to generate a select, enhanced image.

Once an initial image has been generated, the analysis of the image is initiated, as shown in FIG. 10. At block 122, one or more regions of interest (ROI) within the image can be identified. Each ROI may be a single pixel or voxel, or a larger region. ROI selection can be performed manually using, for example, a keyboard or mouse to move a cursor over the ROI on the displayed image. Alternatively, ROI selection may be accomplished automatically via a sequential selection of all pixels or via an external input regarding a particular region from, for example, diagnostic system 24.

Next, the average image or pixel intensity within each ROI is computed at block 124. This average image intensity S can be represented by the following expression:

$$S = A_0 [\exp(-TE/T_2)] [\exp(-bD)] \quad (1)$$

where A_0 is the absolute signal intensity for a particular pixel and b is the gradient factor, determined in accordance with the expression:

$$b = \gamma^2 (G_i^2) (\delta^2) (\Delta - \delta/3) \quad (2)$$

where γ is the gyromagnetic ratio, G_i is the polarizing field strength, δ is the length of a diffusional weighting gradient pulse, and Δ is the interval between diffusional weighting gradient pulses. As will be appreciated, in the first iteration before diffusional weighting is employed, the final term of equation (1) is, thus, unity.

To make use of the expressions in equations (1) and (2), the preceding data acquisition process is repeated for different values of echo time TE. On the other hand, if diffusional weighting is employed, as described in greater detail below, the data acquisition process is repeated for different gradient strengths (controlled by adjusting gradient magnitude and/or duration) or gradient orientations. For example, TEs of 30, 60, 90, and 110 milliseconds, or gradient magnitudes of 0, 3, 5, and 7 Gauss/centimeter, may be employed. The image intensity S for a particular pixel of these multiple images of the same transverse slice for particular values of TE (or b , if diffusional weighting is employed) is available and a linear regression analysis of the logarithmic relationship is performed at block 126.

Finally, the value of the apparent T_2 relaxation time (or the apparent diffusion coefficient D , if diffusional weighting is employed) is computed for a particular ROI at block 128. These computations provide quantitative assessments of the various ROI in the image that are useful in subsequent image processing by other components of the medical system 12. Gradient Orientation for Diffusion Weighting

In the preferred arrangement, after the initial fat suppressed image has been collected and its ROI characterized, a diffusional weighting analysis is initiated to further enhance the neurograms generated by evaluating the diffusional anisotropy exhibited by nerve and other tissue. The first aspect of this analysis is the selection of the diffusional gradients to be used.

By way of introduction, in one currently preferred embodiment, the analysis involves the application of pulsed magnetic field gradients to the polarizing field in two or more directions to produce images in which the peripheral nerve is enhanced or suppressed, depending upon the "diffusion weighting" resulting from the particular pulsed gradient axis chosen. Discrimination of water diffusion anisotropy is then achieved by subtracting the suppressed image from the enhanced image, in the manner described in greater detail below, producing an image depicting only the peripheral nerve.

Most preferably, the magnetic field gradients are applied in mutually substantially orthogonal directions. For example, with gradients approximately perpendicular and parallel to the axis of the peripheral nerve at the particular point being imaged, the parallel gradient image can be subtracted from the perpendicular gradient image to produce the desired "nerve only" image.

As will be appreciated, if the axis of the nerve is generally known to the operator and its relationship to the referential frame of the MRI system 14 has been indicated at initialization block 100, the direction of the desired orthogonal diffusional weighting gradients can be readily determined. On the other hand, if the axis of the peripheral nerve is not known, or if many nerves having different axes are being imaged, the neurography system 10 must employ a system of gradient orientations suitable for imaging nerve having substantially any axial alignment. For example, as will be

described in greater detail below, a full three-dimensional vector analysis can be used to characterize the diffusion coefficient and provide a nerve image by construction based upon a fixed arrangement of diffusion weighting gradients.

In anatomical regions, such as the upper arm or wrist, it is also possible to achieve adequate enhanced isolation of the nerve image by applying only a single diffusion gradient perpendicular to the axis of the nerve at the site of interest. As a result, no subtraction need be carried out to produce the neurogram. The fat suppressed, orthogonally diffusion weighted image can either be processed directly, or it can be subject to threshold processing to remove signals of lower intensity associated with non-neural tissue, or nerves with different axes and directions of travel at the imaging location.

As will be appreciated, for quicker and more efficient data collection and processing, the establishment of diffusion gradients in the polarizing field should be responsive to the particular one of the foregoing scenarios that applies to the imaging problem at hand. Depending upon the inputs provided at block 100, the system may have been advised that (a) only one gradient of known orientation is required, (b) two orthogonal gradients of known orientation are required, or (c) two or more gradients of unknown orientation are required.

As indicated in block 130 of FIG. 10, upon completion of the analysis of an image, the system considers whether all of the desired diffusional gradients have been applied to the polarizing field during subsequent data acquisition by, for example, spin-echo processing, or fast spin-echo processing. Because no diffusional gradient was used in the initial fat suppression processing, the answer is initially NO and operation proceeds to block 132.

There, the computer determines whether the operator initially indicated that the axis of diffusional anisotropy is known. If the axis is known, a perpendicular diffusional gradient is employed, as indicated at block 134. Then, as indicated at block 136, a diffusion-weighted spin-echo sequence is performed (modified by the inclusion of the diffusional gradient in the manner described in greater detail below) and image generated, pursuant to blocks 102-122, before quantification of the image data occurs at blocks 124-128 to compute D or T_2 . If the operator indicated at initialization that orthogonal diffusion gradients are required for the particular imaging problem at hand, this process is then repeated at blocks 138 and 140 for a parallel diffusional gradient.

If the inquiry performed at block 132 determines that the axis of diffusional anisotropy is unknown, operation proceeds to block 142. There an initial diffusional gradient is arbitrarily selected, to be followed by a sequence of alternative gradients selected for use by the operator when the anisotropic axis is unknown.

At block 144, using the initial diffusional gradient, a spin-echo sequence is performed (modified by the inclusion of the diffusional gradient in the manner described in greater detail below) and image generated, pursuant to blocks 102-122, before quantification of the imaged data occurs at blocks 124-128. Then, at block 146, a test is performed to determine whether the desired number of different diffusional gradients (e.g., three gradients, along the x-, y-, and z-axes) have been used. If not, the next diffusional gradient is selected at block 148 and the spin-echo sequence, imaging and processing operations are performed, as indicated at block 144. This process is then repeated until the desired number of alternative diffusional gradients have been employed.

As will be appreciated, additional gradient coils may be provided where gradients are desired along axes other than those provided by the locational gradient coils. To that end, diffusional gradient coils may be mounted on a magnetically compatible, adjustable track within the bore of the imager to allow gradients to be repositioned and applied over a substantially continuous range of orientations. Similarly, the region to be imaged may be movably supported relative to a fixed set of gradient coils to introduce the desired variability in gradient direction. As another option, a plurality of different gradient coils may be employed and activated in various combinations to effect the desired gradient variations. Alternatively, the results obtained from a limited number of gradient directions can be processed using a vector analysis to estimate the results obtainable with a gradients other than those directly available, as described in greater detail below.

v. Spin-Echo Sequence For Diffusional Weighting

As noted briefly above, for each of the different diffusional gradients employed, the spin-echo sequence is repeated, followed by the generation of image data and the processing of that data to, for example, quantify the relaxation time T_2 or diffusion coefficient D . In the preferred arrangement, the use of diffusion gradients influences a number of aspects of the spin-echo sequence.

As shown in FIG. 11F, two pulses h and h' , applied to the desired pair of gradient coils are used to establish a particular diffusional gradient in the polarizing field. For an echo time (TE) of 50 milliseconds, the duration (δ) of each pulse is, for example, 10 milliseconds and their separation (Δ) is 20 milliseconds. In the presence of the diffusional gradient, the echo signal F , and therefore the pixel or voxel intensity in the image ultimately produced, is made sensitive to the spatial diffusion of water molecules in the imaged region R .

In that regard, as indicated above, with the diffusional gradient oriented substantially perpendicular to the diffusional anisotropic nerve, the nerve image is enhanced and generally exhibits the highest intensity of various features imaged. This phenomena is depicted in FIG. 13A, which is an image of the forearm of a rabbit, corresponding to the diagram provided in FIG. 1. The ulnar nerve UN and median nerve MN are both relatively dark (high intensity) and are easily seen. Alternatively, with the diffusional gradient oriented substantially parallel to the diffusional anisotropic nerve, the nerve image is suppressed and generally exhibits a lower intensity than other features imaged, as illustrated in FIG. 13B. These images can be combined, via a subtraction process described in greater detail below, to produce an image of the nerve isolated from all other structure.

To reduce the effect of cross-terms between the imaging gradients and the diffusion weighting gradients, the spin-echo sequence illustrated in FIG. 11 is a modified version of conventional sequences. More particularly, the readout gradient rephasing pulse f shown in FIG. 11D, is placed directly before the acquisition of echo F in FIG. 11A, instead of after the slice-selective excitation pulse d , shown in FIG. 11C. However, a consequence of this change was the appearance of artifacts in the non-diffusion-weighted images due to an unwanted echo, presumably formed from imperfections in the slice-selection pulses d , d' , and e , shown in FIG. 11C. To overcome this problem, a second modification of the pulse sequence was made. Specifically, the phase-encoding gradient was split into two sections g and g' , and two or four transients (depending upon S/N) were acquired with phase cycling. As a result, the remaining cross terms contribute less than three percent to the diffusion weighting factor.

Although fat suppression is not required to take advantage of the image enhancements available through diffusional

weighting gradients, in the preferred arrangement, the fat suppression sequence shown in FIGS. 11A and 11B is employed prior to the initiation of the diffusion-weighted spin-echo sequence. As will be described in greater detail below, the combination of these techniques generally provides an image quality that exceeds that available from either technique individually.

The echo F produced using the diffusion weighted pulse echo sequence is processed in the manner described above in connection with blocks 112 through 128 of FIGS. 9 and 10. With diffusion weighting, the computation of the diffusional coefficient D at block 128 is preferably based upon the analysis of data collected for different gradient magnitudes. For example, the computation may be based upon gradients of 0, 3, 5, and 7 Gauss/centimeter, resulting in the production of image data as represented in FIGS. 14A through 14D, respectively. While fat, bone, marrow, skin and vessels are generally absent even at the lower gradients, muscle and ligaments drop out at the higher gradients. As suggested previously, the increasingly stronger gradients may be achieved by increasing gradient duration, rather than magnitude. Alternatively, the iterative data collection process may be performed using different gradient directions.

vi. Image Selection/Production

Once computer 72 determines, at block 130, that images have been collected for all of the desired diffusional gradients, operation proceeds to block 150. If the axis of anisotropy is unknown, the various diffusional coefficients D computed for each ROI using different gradient orientations are compared at block 150 to identify the maximum and minimum values. These coefficients provide a measure, associated with each pixel or voxel, of the magnitude of diffusional anisotropy at that point, while the anisotropic direction is indicated by the gradient orientation.

(a) Subtraction Neurography

In the preferred arrangement, the images associated with the maximum and minimum values of the diffusional coefficients for a particular ROI are then used in a subtraction process, as indicated at block 152. The image associated with the larger coefficient is produced by a gradient that is more nearly perpendicular to the neural axis, enhancing the nerve image, while the image associated with the smaller coefficient is produced by a gradient that is more nearly parallel to the axis, selectively destroying the nerve signal. When these two penultimate images are then mathematically (or photographically or optically) subtracted from one another, a subtraction neurogram is produced.

By way of illustration, FIG. 15A is an image produced without diffusion weighting. FIGS. 15B and 15C then illustrate images produced using parallel and perpendicular gradients, respectively. Finally, the subtraction neurogram produced when the image of FIG. 15C is subtracted from that of FIG. 15B is shown in FIG. 15D.

This "ideal" neurogram is somewhat analogous to a subtraction angiogram (an image showing only blood vessels), but sharply highlights a nerve rather than a vessel. Such an image is particularly useful for confirming the identification of nerves in a given imaging plane or space as well as for locating nerve injuries and nerve compressions. Despite the well known existence of angiograms showing the entire vascular pattern in an anatomic region, and despite the existence of MRI techniques that could have been applied to the problem of neural imaging techniques, and despite the great need for the visualization of nerves, particularly, in isolation, there has not previously been any way of creating such neurograms.

Although image subtraction is employed in the preferred arrangement, it is not necessary. For example, in some

applications of known anisotropy, subtraction is unnecessary and can be foregone in favor of a threshold analysis. Also, the subtraction process can be further supplemented, if desired. For example, the output of the subtraction process can be divided by the signal information from a fat suppressed, T₂-weighted spin echo sequence (e.g. using the aforementioned CHESSE technique).

One potential problem to be addressed by the use of the subtraction process is image registration. As will be appreciated, provided that non-neural tissue is identically located in both images subjected to the subtraction process, the non-neural component will cancel out of the resultant image. On the other hand, if some shift or other discrepancy in the apparent position of non-neural tissue is introduced into an image due, for example, to movement of the subject, cancellation may not occur and the nerve may actually be more difficult to identify in the resultant image.

In one embodiment, acceptable image registration is evaluated prior to initiation of the subtraction process. More particularly, the intensities of pixels in one image are compared to the intensities of corresponding pixels in the second image. Pixels of neural tissue are disqualified on the basis of their high diffusional anisotropy, assessed via their diffusion coefficients. Unless the intensities of the remaining, non-neural pixels fall within a certain range of each other, indicating acceptable image registration, subtraction will be inhibited.

(b) Vector Processing and Three-Dimensional Image Generation

Up to this point, the output produced is generally in the form of a single two-dimensional image, or a series of two-dimensional images that can be related to form a three-dimensional image. In a simple form of three-dimensional image generation, described in greater detail below, the high S/N ratio of the two-dimensional neurograms produced by system 14 readily allows the imaged nerve cross-sections to be identified and then linked together to form a three-dimensional projection of the neural structure.

As will be appreciated, however, depending upon the neural pattern involved and the spatial resolution required, this simplified approach may introduce undesired discontinuities into the three-dimensional projection. A more sophisticated processing scheme employs information about the anisotropic direction of the nerve in each two-dimensional image to further enhance the accuracy of three-dimensional image projections. The availability of information regarding anisotropic direction is also useful in establishing the optimal directions for the gradients used in the diffusional weighting analysis described above to produce a two-dimensional image.

In that regard, the anisotropic axis of the peripheral nerve being imaged is sometimes known to the operator, allowing the operator to input the directional information at block 100 and select the best diffusional gradients for imaging. More commonly, however, nerves and CNS neural tracts follow relatively complex paths and the direction in which the diffusion anisotropy coefficient of the nerve or tract is greatest gradually shifts from one plane or axis to another as the nerve or tract curves or turns. As a result, one or two arbitrarily oriented, standard gradients may be inadequate to provide the desired images.

Changes in neural direction can be monitored by moving the patient relative to a fixed set of gradient coils or employing movable diffusional gradient coils mounted, on a track with a non-magnetic drive system, within the bore of the imager to adjustably control the orientation of the diffusional gradients applied to the region of interest. By

monitoring changes in the ratio of D_{pl}/D_{pr} obtained for a given pixel using alternative gradient alignments, or for sequential pixels using the same gradient alignments, changes in neural direction can be estimated and suitable gradient directions selected. Alternatively, gradient coils oriented in three planes can be simultaneously activated in various combinations to achieve the effect of an infinite variety of differently oriented gradients.

One advantage of attempting to track changes in neural direction is that parallel and perpendicular gradient information can then be collected and used to produce a subtraction neurogram of the type described above. If, however, the optimal gradient directions for a given pixel are determined using feedback from images generated with repetitively adjusted gradients, processing speed may be significantly impaired.

In many cases the well known anatomy of a nerve will permit the use of a particular axis orientation in advance. Initial imaging information will provide a description of the gross course of the nerve. A subsequent "informed" approximation can optimize the orientation in each slice. This can be useful to insure excellent homogeneity of nerve image intensity or to measure the coefficient of anisotropy along the course of the nerve.

As a preferred alternative, requiring less mechanical complexity and faster processing speed, a technique has been developed for observing diffusional anisotropy, independent of its degree of alignment with any individual gradient axes. This process involves the combination of information from anisotropy measurements obtained along three standard orthogonal axes or using information from multiple fixed axes. For example, in the preferred embodiment, a vector analysis is used to produce interpolated images and directional information from the three orthogonal diffusion-weighted images described above.

In that regard, image information is collected from, for example, four "multi-slice" sets using a zero diffusion gradient B₀ and diffusion gradients B_x, B_y, B_z in the x-, y-, and z-orthogonal directions, respectively. For each pixel in the image to be produced, information concerning the corresponding pixels in the four diffusion gradients images is combined to produce a diffusion vector, representative of water molecule movement along the nerve fiber in either direction. This vector has a magnitude representative of the image intensity of the pixel and a direction representative of an "effective" diffusion gradient associated with the pixel.

More particularly, the image intensity S_n of a given pixel in the new image is calculated using the following vector equation:

$$S_n = \text{vector length} = [(S_x^2 + S_y^2 + S_z^2) S_0^2]^{1/2} \quad (3)$$

where S_x, S_y, and S_z are the image intensities of the corresponding pixels in the images produced by the B_x, B_y, and B_z gradients. S₀ is the image intensity of the corresponding pixel in the image produced by the B₀ gradient and is included in equation (3) to normalize the resultant image intensity S_n. The direction of the effective gradient associated with this pixel image includes components θ_{xy}, θ_{xz}, and θ_{yz}, computed in the following manner:

$$\theta_{xy} = \text{diffusion vector angle between } B_x \text{ and } B_y = \text{arc tan } (S_y/S_x) \quad (4)$$

$$\theta_{xz} = \text{diffusion vector angle between } B_x \text{ and } B_z = \text{arc tan } (S_z/S_x) \quad (5)$$

$$\theta_{yz} = \text{diffusion vector angle between } B_y \text{ and } B_z = \text{arc tan } (S_y/S_z) \quad (6)$$

The parameters computed in equations (3), (4), (5), and (6) can be used to generate images in a variety of different

ways. For example, the intensities of the pixels can be displayed as a "vector length" image. An illustration of a vector length CNS image, in which the intensity of the image is proportional to the magnitude of S_n , is shown in FIG. 16.

The image of FIG. 16 is a brain scan of a monkey (*macaca fascicularis*) weighing 2–2.5 kg, performed using diffusion imaging (spin-echo) on a General Electric CSI II imager/spectrometer (2 Tesla, equipped with actively shielded gradients). The acquisition parameters were: TR=1000 ms, TE=80 ms, diffusion gradients=5 Gauss/cm, diffusion gradient duration=20 ms, diffusion gradient separation=40 ms. Four slices of thickness 4 mm were imaged. T_2 -weighted images were used to reproducibly select the diffusion images.

As an alternative to the use of vector length images, arctan images can be employed. These images are obtained by establishing the intensity of a pixel in direct proportion to the angular output of one of equations (4), (5), or (6). An illustration of an arctan image is provided in FIG. 17. As shown in this example of a CNS neurogram, a select neural tract of interest can be effectively traced and made to stand out in isolation from other neural tracts.

When used to evaluate lesions in CNS images of the type shown in FIGS. 16 and 17, vector length images will be more sensitive to water diffusion changes where all three orthogonal images change in the same way, while the vector angle images will be sensitive to changes in anisotropy between two orthogonal directions. A CNS lesion caused by experimental allergic encephalomyelitis induced by myelin basic protein is demonstrated by its departure from the diffusional anisotropy, which appears as vector length decreases and image intensity changes accentuated in particular vector angle images.

Alternative forms of vector analysis can also be applied, for example, as described in Basser et al., *Fiber Orientation Mapping in an Anisotropic Medium with NMR Diffusion Spectroscopy*, SMRM BOOK OF ABSTRACTS 1221 (1992). Similarly, tensor analyses employing tensors of various ranks, as described in Basser et al., *Diagonal and Off Diagonal Components of the Self-Diffusion Tensor: Their Relation to an Estimation from the NMR Spin-Echo Signal*, SMRM BOOK OF ABSTRACTS 1222 (1992), can be used to treat, or transform the coordinates of, MR diffusional anisotropy data. Suitable alternative processing techniques have been developed for use in the evaluation of magnetic, thermal, and structural anisotropy data.

Unlike prior art systems, because the non-neural components of the neurograms produced by system 14 exhibit a relatively low intensity, or indeed disappear entirely from the images, the computer 72 is readily able to identify nerve locations in the anatomical structure and to correctly trace the course of the nerves between two-dimensional image planes or through a three-dimensional acquisition volume. For example, the location of nerves in a given image plane can be detected by comparing pixel intensity to some threshold level. A three-dimensional image can then be formed by linking or projecting the results of these two-dimensional analyses over the desired volume.

As an alternative, the vector information obtained above can be used to track continuous serial changes in the direction of maximum anisotropy of a nerve or neural tract as the nerve or tract travels along its natural course. In that regard, the direction of maximum anisotropy for each voxel associated with a nerve is determined and a voxel connection routine, of the type described in Saloner et al., *Application of a Connected-Voxel Algorithm to MR Angiographic*

Data, 1 JOURNAL OF MAGNETIC RESONANCE IMAGING 423–430 (1991), is then used to link up voxels of maximum anisotropy. The resultant plot of the nerve or neural tract provides enhanced spatial resolution and less discontinuity from one image plane to the next.

As an alternative to the two-dimensional imaging sequences described above, it is also possible to carry out the signal acquisition using a "three dimensional" imaging sequence of the type described in Frahm et al., *Rapid Three-Dimensional MR Imaging Using the FLASH Technique*, 10 JOURNAL OF COMPUTER ASSISTED TOMOGRAPHY 363–368 (1986). The output of this sequence is then processed using a three-dimensional Fourier transform to extract the returns from nuclei over the volume being imaged. The resultant processing used to compute D for a given voxel and to generate, for example, a subtraction angiogram is substantially the same as described above.

Regardless of the routine employed to project the neural structure in three-dimensions, the system 10 may be further programmed to implement the projection by referring to known characteristics of the structure. More particularly, once a given nerve has been identified in a given two-dimensional image, an "expert" system 10 is able to predict the occurrence of certain branches and mergers in this structure, albeit at unknown locations. This information can then be used to test the plausibility of the projection being generated, refining it where necessary.

vii. Results of Combined Fat Suppression and Diffusion Weighting

As previously noted, both muscle and nerve exhibit diffusional anisotropy. In view of the relatively low signal strength of neural components, diffusional analyses were not expected to provide clinically useful neurograms. The combined use of fat suppression and diffusional weighting has, however, been found to be extremely effective in providing the desired nerve image enhancement.

By way of illustration, for a gradient strength of 7 G/cm and an echo time of 50 ms, an nerve image signal intensity (S_n) of 17 and a muscle image signal intensity (S_m) of 7 were calculated, based upon the difference between signal intensities with pulsed gradients oriented perpendicular and parallel to the nerve. A nerve-to-muscle contrast parameter R of 2.43 was then computed as the ratio S_n/S_m . Similarly, a comparison of the apparent diffusion coefficients for diffusional gradients perpendicular (D_{pr}) and parallel (D_{pl}) to nerve and muscle are as follows:

Apparent Diffusion Coefficients (10^{-5} cm ² /sec)		
	Muscle	Nerve
D_{pr}	1.17	0.65
D_{pl}	2.18	2.00
D_{pl}/D_{pr}	1.9	3.1

These results clearly illustrate that the neural components exhibit a far larger relative change in intensity than muscle components when subjected to diffusion anisotropy analysis.

An unexpected and apparently synergistic benefit of fat suppression, when used in combination with diffusional weighting, is that an actual increase in neural signal anisotropy is experienced, with the conspicuity of the neural component of the image increasing by roughly 250 percent when the fat component is removed. The combined increase in nerve conspicuity and reduction in fat interference significantly enhances the effectiveness of neural imaging.

Although not entirely understood, there are several potential explanations for the synergistic relationship between fat

suppression and diffusional weighting. First, it appears that fat suppression may increase the apparent diffusional anisotropy of nerve, enhancing the utility of diffusional weighting gradients in the detection of neural tissue. By way of illustration, an indicated in the following test data, obtained with the signal from fat and "short T_2 " water removed, the intensity of the remaining image signal was due largely to anisotropically diffusing water.

Nerve Imaged	CHESS Applied Gradient Direction			CHESS Not Applied Gradient Direction		
	pr	pl	Ratio	pr	pl	Ratio
Ulnar Nerve	29	<8	>3.6	62	49	1.3
Median Nerve	30	<8	>3.8	46	22	2.1
Muscle	14	8	1.8	18	12	1.5

The synergistic role of fat suppression can also be viewed as a demonstration of a magnetization transfer effect. More particularly, the irradiation of protons on e.g., myelin lipids surrounding the nerve by the saturation pulse of the fat suppression sequence may allow transfer of the saturation pulse to water molecules in close association with the lipid, allowing for very efficient transfer. Subsequently, these molecules can exchange into the anisotropically diffusing mobile water pool.

vii. Long TE/TR/ T_2 Processing

As an alternative to the use of diffusional gradients described above, in some regions of interest, it is possible to achieve adequate enhanced isolation of the nerve image by use of a spin echo fat suppression technique with a relatively long TE (echo time) or TR (repetition time) to achieve a T_2 -weighted image. In that regard, after fat suppression, the dominant component remaining in the echo F is returned from muscle. Because the T_2 of peripheral nerve has been measured by the inventors to be roughly twice as long as the T_2 of muscles, the use of a relatively long TE or TR in the spin echo sequence allows the muscular return to be removed.

The basic operation of a neurography system 14 employing this feature remains the same as that shown in FIGS. 9 and 10 except that the initialized value for TE is extended. In that regard, the operator may be called upon to initially consider whether the desired imaging is likely (e.g., neural imaging in a patient's limbs) or unlikely (e.g., CNS imaging) to be disrupted by the presence of muscle. If muscular interference is likely, a relatively long TE of between 50 and 100 milliseconds or even longer is initialized at block 100. The particular TE or TR selected depends upon the degree of T_2 weighting desired. Alternatively, the system 14 may be programmed to compare the imaging data separately collected using long TE processing and diffusional weighting to assess which provides the best results.

Illustrations of the results available with long TE imaging are provided in FIGS. 18A through 18D, for TE equal to 30, 40, 60, and 100 milliseconds, respectively. In the image of the forearm of a rabbit, provided in FIG. 18D, produced with a field strength of 4.7 Tesla, nerves are brighter than any other structure in the image. The extent of the increased nerve conspicuity is on the order of ten-fold, rendering the images clearly susceptible for use in constructing neurograms. As will be appreciated, lesser conspicuities on the order of 1.1 may also be useful.

The use of extended TE processing had previously been considered unfeasible. In that regard, as described in Moseley et al., *Anisotropy in Diffusion-Weighted MRI*, 19 MAGNETIC RESONANCE IN MEDICINE 321, 325 (1991),

nerve was believed to exhibit a relatively short T_2 time. Surprisingly, however, measurements have been conducted indicating that the T_2 of muscle is approximately 27 milliseconds, while the T_2 of peripheral nerve is approximately 55 milliseconds, providing a factor of two difference between the two types of tissue.

ix. Additional Enhancements for Neural Imaging

(a) Vessel Suppression

In addition to the fat suppression and muscle suppression techniques described above, vessel suppression may be employed to improve the neurographic selectivity of the images generated by system 14. Due to the brightness of slowly moving blood in some otherwise useful sequences, vessel suppression has particular value when used in connection with long TE sequence neurograms.

A variety of alternative approaches can be employed to achieve the desired blood vessel suppression. For example, in a first embodiment, the blood vessels are separately imaged to produce a flow-based MR angiogram, employing phase contrast or time-of-flight information. The angiogram may be produced using the MRI system 14, under separate program instructions, or the auxiliary data collection system 22 described below. The angiogram is then subtracted from the neural image to provide a neurogram in which blood vessels content is completely suppressed.

As previously noted in connection with the discussion of image subtraction, a registration problem occurs when the information to be removed from one image is not identically represented with the same intensity and location in the subtrahend image. With vessel image information obtained using an angiography pulse-echo sequence (or other techniques described below) and neural image information obtained using the neural pulse-echo sequence described above, some difference in vessel intensity in the two images is to be expected. One way of avoiding registration error in this situation is to normalize the angiogram to the corresponding neural image (i.e., equalize angiogram intensity based upon comparative measurements at a vessel pixel identified on the angiogram).

A second technique used for vessel suppression is to employ a short TE sequence to produce a first image in which blood vessels are relatively bright and nerves are relatively dim. This image is then subtracted from a second image obtained using a long TE and exhibiting bright nerves and dim vessels.

A third blood vessel suppression technique involves the administration of an intravenous "black blood" contrast agent to the vessels. The agent is preferably (but not necessarily) of the "blood pool" type including dysprosium-DOTA poly lysine or iron oxide type contrast agent. The blood vessels are thereby blacked out by the pharmaceutical agent so there is no need for a subtraction step to produce the desired vessel-suppressed neurogram.

Finally, carefully adjusted water suppression techniques can be used to limit the contribution of the blood vessels and cerebro-spinal fluid (CSF) to the neural image generated by system 14. One such technique is fluid-attenuated, inversion recovery (FLAIR), described in, for example, Bydde et al., *Comparison of FLAIR Pulse Sequences with Heavily T_2 Weighted SE Sequences in MR Imaging of the Brain*, 185 RADIOLOGY SUPP. 151 (1992).

(b) Motion Suppression

Some of the image processing techniques described above, including, for example, the use of diffusion weighting, may be adversely influenced by motion of the region being imaged. To limit the introduction of ambiguous or erroneous content into the images produced (i.e., motion

artifact), several different hardware and software features may be employed by the neurography system 14.

As shown in FIG. 19, the acquisition of image information can be electively carried out with the region of the patient under examination immobilized by a splint 156. The splint 156 includes a rigid base 158, made of plastic or some other non-ferro-magnetic material. Base 158 is included to provide a fixed frame of reference for the region under examination and is designed to be optionally rigidly secured within the bore of the imager I. As will be described in greater detail below, once the neurography system 10 has imaged the region, the reference frame provided by base 158 allows another system, like surgical system 28, to operate within that reference frame in a known relationship to the imaged nerves. A non-rigid system, described below, employs fiduciary markers applied to the skin surface within the splint.

A rigid frame 160, made of plastic or some other non-ferromagnetic material, is attached to base 158 and provides structural support for the splint 156. One or more fiduciary markers 162, e.g. water-filled beads or linear marker strips, are provided on the frame 160 and/or base 158 to allow the relationship of frame 160 and base 158 relative to the imaged region to be determined from the images generated. In the preferred arrangement, each marker 162 extends the length of splint 156, so that it is visible in each cross sectional image generated. At least one of the markers or strips 162 is aligned at a non-zero angle to the x, y, and z axes of the image plane, ensuring that its particular location in the image provides a positional reference to the splint.

A sleeve 164, made of a thin film plastic and filled with a conformable substance 166, such as water containing gel, silicone, foam, or cobalt-chloride doped water, is formed around the frame 160 and includes straps 168 for use in attaching the splint to the patient. As shown, the frame 160 and sleeve 164 include a number of open regions 170, providing access to select areas of the region under examination by, for example, surgical system 28. Alternatively, the base 158 may be used with two sleeves. A first such sleeve provides complete and continuous skin contact for imaging, while a second sleeve secures the arm but generally allows access by a surgical device.

A pump 172 is included to allow the fluid to be introduced into sleeve 164 from a reservoir 174 under pressure, forcing the sleeve against the patient's skin and immobilizing the region under examination. A release valve 176, allows the fluid within the sleeve 164 to return to the reservoir 174, relieving pressure within sleeve 164.

In addition to reducing motion artifacts, the splint 156 performs several other functions. First, as suggested above, the splint 156 provides a reference frame that can be used by other components of medical system 12 to ensure that actions are taken in proper relationship to an imaged neural network. Second, the splint 156 may be required to keep the region under examination immobilized for the successful administration of therapy or performance of surgery by system 12.

A third function of splint 156 is the reduction of edge effects that might otherwise be experienced using fat suppression. In that regard, the surface of a region under examination (i.e. the patient's skin) presents an abrupt transition in the nature of the material being imaged. The field inhomogeneity caused by this tissue-to-air interface causes the fat signals in the patient's surface adipose tissue to spread out and/or shift in frequency relative to deeper lying fat surrounding the nerve. The desired effect of fat suppression is, however, to suppress the signal from the

underlying tissue adjacent the neural tissue to be imaged. By employing thin flexible polyethylene or other plastic for sleeve 164 and paramagnetically doped water for substance 166, these edge effects introduced at the surface of the region under examination are reduced on the order of 1.5 to 5 for nerve tissues.

Additionally, the splint can be specially designed to move a particular body region during an imaging series to introduce serial stepped repositionings of the limb. The movement can be controlled externally by a hydraulic system with fiber optic feedbacks to assess repositioning. In this fashion, it is possible to collect a series of images with the limb in a controlled series of positions. These can be later assembled to provide a kinematic view of stress or impingements upon a nerve during motion as for the ulnar nerve at the elbow.

Motion artifact can also be addressed by the software used to control neurography system 10. In that regard, to ensure adequate echo amplitude for MRI, the net magnetic moment generated by one pulse sequence typically must be allowed to return near its equilibrium value before the next pulse sequence is initiated. This factor, in combination with the sheer number of sequences typically required for imaging, typically causes data collection to occur over a relatively long period of time (e.g., on the order of 1 to 20 minutes or longer). As will be appreciated, the likelihood that significant patient motion will be experienced during the data collection process increases in direct proportion to the time required for data collection.

The software controlling the data collection processed is optimized to reduce at least some of the delays contributing to motion artifact sensitivity. In the arrangement described above, information from a number of different images may be used to selectively produce a final image. For example, the subtraction neurogram is typically generated on a pixel-by-pixel (or voxel-by-voxel) basis using information from two images obtained with orthogonal diffusion gradients. By interleaving the image sequence so that data for a given pixel is collected for each diffusional gradient before collecting data for any other pixel, the susceptibility of the subtraction process to motion artifact is reduced. Similarly, where multiple images are collected at different gradient strengths to compute the diffusion coefficient D for a given pixel or voxel, as part of the gradient selection process, the susceptibility of the computation to motion artifact can be reduced by collecting data for all gradient strengths at one pixel before data for other pixels is collected. Thus, despite the relatively simple data collection process depicted in FIGS. 9 and 10, in the preferred arrangement, data collection is interleaved by collecting data in several planes at each acquisition rather than completely collecting all repetitions for a given plane before proceeding to the next.

Another technique used to provide the desired motion suppression is based upon the anticipation of certain periodic sources of motion that can be monitored by, for example, the auxiliary data collection system 22. For example, depending upon the region of the patient under examination, the patient's heartbeat and respiration may introduce some motion that is not suppressed by the splint 156. With information regarding the periodicity of these sources available from system 22, computer 72 may then adjust the data collection sequence so that the excitation and echo pulses occur at consistent times relative to the motion introduced by the sources.

One technique for reducing respiratory motion artifact in MRI is disclosed in U.S. Pat. No. 4,930,508 (Shimoni et al.). In contrast, the neurography system 10 can be used with a variety of techniques including mass-spectrometer monitor-

ing of carbon dioxide output, fiber-optic observation at chest wall movement, or auditory monitoring by long tube stethoscope with automated sound analysis.

(c) Fascicle Identification and Nerve Enhancement

Another feature of the neurography system **10** is its ability to image individual nerve fascicles. For example, when a phased array coil **62**, or other high resolution MRI system is used with a long TE sequence, individual nerve fascicles appear much brighter than the perineural and epineural tissue within the nerve and between the fascicles, and the nerve takes on the appearance of a multifascicled structure.

By way of illustration, neural images depicting fascicles in the nerve of a patient having a nerve graft are provided in FIGS. **20**, **21**, and **22**. These images were obtained using a 1.5 Tesla MRI system (Signa System 5.2 software release, sold by GE Medical Systems) with standard 1 Gauss/cm gradients and a phased array RF coil system of the type described above. A "fast" spin-echo sequence with a TR of 5000 ms, TE of 102 ms, and 8 echo train was used with fat suppression and spatial RF pulses for vessel suppression.

Two axial series of images were produced using a two dimensional Fourier transformation. The first series consisted of 24, five mm thick sections, a 512x512 matrix, one mm skip, and one nex (number of excitations). The second series consisted of 41, three mm thick axial sections, a 256x256 matrix, zero mm skip, and two nex. The field of view was 18 cm and acquisition time was 10.6 minutes for both series.

Images from the second series were post-processed by selecting (manually) an elliptical region of interest, approximately two cm in diameter, around the sciatic nerve in each of the sections. This region of interest was selected to exclude blood vessels, without requiring the use of the more analytically complex vessel suppression features described above.

Projectional images were obtained using a maximum intensity projection (MIP) algorithm, available as part of System 5.1 (IVI) provided by GE Medical Systems. The resultant neurograms show the interface between the tibial component of the sciatic nerve and the surgically placed sural nerve graft, with FIGS. **20** and **21** illustrating the nerve in progressively larger scale and FIG. **22** illustrating an axial projection of the nerve including graft g. As an additional benefit, this imaging protocol depresses the signal from tissues within the nerve, between and among the fascicles, so that the individual fascicles (f) of the nerve stand out in sharp profile.

The ability of the neurography system **10** to image fascicles is important for several reasons. First, fascicle imaging enhances the diagnostic usefulness of the neurogram because it makes it possible to observe and analyze the internal structure of the nerve for evidence of disease. As will be appreciated, this observation and analysis may be performed visually by the operator or automatically, as part of the operation of the diagnostic system **24** described in greater detail below.

Second, this unique internal organization can be used to provide neural selectivity and enhancement in the imaging process, even when the conspicuity or signal intensity of a particular nerve does not permit identification. More particularly, blood vessels, lymphatics, lymph nodes and collections of adipose tissue, are often similar to nerve in shape, location, and intensity in the cross-sectional images. None of these features, however, exhibit the internal fascicular structure of nerve.

By way of illustration, fascicle identification and nerve confirmation may be used to distinguish nerve from other

structures in an ambiguous image in the following manner. First, a thresholding process is used to identify relatively bright regions of the image potentially representative of nerve. With the boundaries of these regions established, the intensity of the pixels associated with each region is evaluated and average image intensities for the regions are computed.

If the intensity of a given pixel within a region is more than some predetermined amount below the average intensity, the structure associated with that pixel is a potential fascicle. A positive fascicle identification is, however, only made if one or more of a plurality of predetermined sequences of such pixel groups representative of fascicular structure are identified. For example, a group of at least 3 such pixels must be found which are adjacent each other and bounded on at least one side by pixels not satisfying this criteria.

The results of this analysis can be used to distinguish bright regions associated with nerve from those associated with, for example, blood vessels or lymphatics. The image intensity of regions not satisfying the fascicular identification parameters may then be adjusted to zero, effectively eliminating these ambiguous structures from the image. Alternatively, a neuroradiologist or other specialist may use this information to select a volume of interest which the neurography system can then render into a projection neurogram.

(d) Miscellaneous Nerve Enhancement Techniques

The various embodiments and features of the neurography system **10** described above can be modified to incorporate alternative approaches to nerve identification and enhancement.

For example, a magnetization transfer pulse sequence can be employed after the fat suppression sequence to enhance neural imaging. Magnetization transfer involves the excitation of chemically shifted protons with an "off resonance" pulse. These protons in a short T₂ isotropically diffusing water compartment then exchange into a long T₂ anisotropically diffusing compartment. In doing so, they carry the high intensity magnetization signal with them, thus inducing a transfer of magnetization to surrounding neural tissue to increase its conspicuity in the image. Nerve may exhibit efficient exchange between the off-resonance, relatively stationary protons in the myelin sheath and the resonant, mobile protons of axoplasmic water. On the other hand, muscle does not exhibit exchange with a large off-resonant proton pool to a comparable degree. The magnetization transfer pulse sequence is designed to exploit this differential sensitivity between nerve and muscle by using stimulation methods similar to fat suppression to synergistically improve the neurographic selectivity of the image in two ways simultaneously.

Other alternative pulse sequences can also be used. For example, a version of steady state free precession (SSFP), as described in Patz et al., *The Application of Steady-State Free Precession to the Study of Very Slow Fluid Flow*, 3 MAG. RES. MED. 140-145 (1986), can be used. The SSFP is, however, modified to be included in an imaging protocol to achieve fat suppression. Similarly, a magnetization prepared rapid gradient echo (MP-RAGE) sequence, as described in Mugler et al., *Three Dimensional Magnetization Prepared Rapid Gradient-Echo Imaging (3D MP RAGE)*, 15 MAG. RES. MED. 152-157 (1990) can be used if modified to improve T₂ contrast. In addition, neural selectivity can be achieved by employing proton fast exchange rates or T₁ relaxation rates.

Further alternative techniques for generating neurograms employ sequences optimized to be sensitive to the slow

coherent flow of the endoneurial fluid. These sequences provides a unique signal because of the proximal to distal direction of flow and because of the slow flow rate which can be monitored by techniques originally developed to distinguish diffusion from perfusion. Such techniques include, for example, velocity compensation by gradient moment nulling as described in Ehman et al., *Flow Artifact Reduction in MRI: A Review of the Roles of Gradient Moment Nulling and Spatial Pre-saturation*, 14 MAG. RES. MED. 293-307 (1990) and Moran, *A Flow Velocity Zeumatographic Interface for NMR Imaging*, 1 MAG. RES. IM. 197-203 (1982).

3. Medical System Construction and Operation

As noted previously, the neurography system 10 is one component of a broader medical system 12. The remaining components of system 12 are described in greater detail in the following sections. These components provide information to, and process information from, neurography system 10 in accordance with software instructions executed by, for example, a host processing system 32 or the processing systems of individual components of the system 12 to achieve a variety of functions beyond the imaging of peripheral nerve.

a. Auxiliary Data Collection System

The auxiliary data collection system 22 may take any one of a variety of different forms. For example, as suggested above, system 22 may be designed to collect supplemental information regarding structure present within the images produced by system 10. Examples of such systems include a secondary MRI system, employing conventional pulse-echo sequences suitable for use in angiography or STIR sequences to show areas of high muscle signal due to denervations or functional loss of the muscle; an X-ray imaging system suitable for use in generating image data of bone and/or tissue, a PET scanning system for showing the progress of an axionally transported pharmaceutical agent; or a CT system for collecting contrast agent lymphography data. The splint 156 is also formed with fiduciary markers visible using CT and MRI (e.g., iodine contrast material in water), allowing the information from systems 10 and 22 to be integrated.

The supplemental information may be used to suppress structural content in the image and provide greater neural selectivity. For example, an angiogram may be used to remove vessel image content from the neurogram or to distinguish nerve and vessels on the basis of color. Alternatively, because non-neural structure is generally absent in the image anyway, the additional information may be employed to add specific structures, such as blood vessels, back into the neurogram unambiguously. This process allows alternative structure to be readily differentiated using different colors to display information from different sources. As will be appreciated, the addition of structure into a MR image viewed to assess neural structure was virtually unthinkable with prior art systems due to the low signal content of neural return components.

An alternative type of data collection system 22 is employed to collect information about the patient for use in controlling the operation of the neurography system 10, rather than modifying its output. Examples of such systems include conventional heart rate and respiration monitors, used to time the data collection sequencing of system 10 relative to the heart rate and respiration of the patient.

A final type of data collection system 22 of interest is one designed to collect supplemental information about the neural network. For example, system 22 may be constructed to produce an output indicative of nerve conduction velocity

(NCV), including the approximate location of a change in NCV or the NCV response to magnetic stimulation. Information from evoked potential electrodes or magnetic SQUID detectors might also be collected and integrated for a multi-input display.

b. Diagnostic System

The diagnostic system 24 is selected to process the image neurograms and other information (such as D and T₂) provided by neurography system 10 to provide an attending physician with, for example, diagnoses of neural anomalies. Alternatively, system 24 may assist the physician in making a diagnosis, or assessing the need for, or likely success of, surgery. In one embodiment, system 24 may be employed simply to confirm or question the physician's diagnoses.

By way of illustration, one region in which problematic neural disorders commonly occur but are difficult to diagnose is the spinal canal. As shown in the cross sectional view of one vertebra provided in FIG. 23, the region of interest exhibits a relatively high physiological complexity. The illustrated structures include a herniated disc (HD), compressed left spinal root (LSR), spinous process (SP), annulus fibrosus (AF), nucleus pulposus (NP), autonomic ganglion (AG), left ventral root (LVR), ventral ramus (VRA), transverse process (TP), dorsal ramus (DRA), dorsal root ganglion (DRG), facet (F), dorsal root (DRO), extradural fat (EF), root in cauda equina (RCE), dural sac (DS), and cerebrospinal fluid (CF).

In this diagram, the two features of primary interest are the left spinal root (LSR) and the left ventral root (LVR), which are both in risk of compression from the herniating disc (HD). Both nerves are traveling through extradural fat (EF) but are surrounded by bone, which could impair observation by an X-ray based technique. Both nerves are also near the strong water signal of the disc (HD), cerebrospinal fluid (CF) in the dural sac (DS), and other inflamed tissue (which often diminishes image resolution and quality in generally used magnetic resonance techniques).

The left spinal root (LSR) and left ventral root (LVR) of diagnostic interest are small relative to the numerous large anatomic structures nearby. Also, these roots are nearly perpendicular to each other. This common imaging problem can be addressed by the use of a neurography system 10 programmed to employ fat suppression, followed by pulsed diffusion gradients oriented to enhance either the left spinal root (LSR) or left ventral root (LVR), so that each can be clearly seen in a given image. If either root is compressed, its image will demonstrate physical distortion or an imprint due to the compression, which may manifest itself as a change in structure or signal intensity between the two sides of a compression.

As will be appreciated, due to the selectivity and resolution of the neurograms produced by system 10, they can be evaluated by a physician to diagnose any neural abnormalities present. In addition, the image produced by system 10 can be analyzed by diagnostic system 24 to detect, for example, evidence of compression or inflammation and provide the appropriate diagnosis.

The operation of system 24 depends, in part, upon the condition to be evaluated. In one embodiment, the operator initially views a two- or three-dimensional image generated on a cathode-ray tube (CRT) display, included with system 24 and uses a cursor to identify a particular imaged nerve to be evaluated. The operator may also input the particular types of anomalies to be detected.

The system 24 then determines the boundaries of the imaged nerve in each of the two dimensional images available, using a thresholding process. These boundaries can

then be compared from one image to the next to look for discontinuities or changes in shape associated with a particular anomaly of interest. For example, if this analysis were used with a nerve severed in an accident, the nerve might disappear entirely from certain images in which it would otherwise be expected to appear. The system 24 is able to readily identify such regions and provide the physician with precise locational information regarding the anomaly.

Similarly, the physician may be interested in conditions associated with less pronounced changes in nerve boundary or intensity. The system 24 is readily able to provide outputs indicative of the average intensity of a bounded neural area, as well as the size and shape of the bounded area on an image-by-image basis. This information can then be used to detect anomalies such as compressions.

In one arrangement, a cursor can be used to initialize a reference boundary of interest on the CRT (e.g., associated with a "normal" neural cross section) for use by system 24. System 24 then compares the actual boundary of the nerve in subsequent images to the reference boundary to locate and quantify the extent of neural compressions. This quantification of an anomaly then allows the physician to monitor the recovery of the nerve and assess the effectiveness of any therapy being provided.

Another approach that may be employed by system 24, is based upon the apparent increase in T_2 exhibited by injured nerve. More particularly, an initial "long T_2 " analysis or diffusion weighted image can be performed to image all neural structures. Then T_2 can be extended to roughly 100 milliseconds to image only those nerves that are injured.

An additional approach for use in the manual evaluation of, for example, bone fractures and injuries to joints, involves the analysis of an image in which the fat component is selectively demonstrated and remaining tissues suppressed. This approach emphasizes the appearance of skin, adipose collections, and of bone (in many locations) due to the presence of marrow. When such an image is collected and assigned a color other than that used to display nerve, the two images can be shown transparently in the same three dimensional construction. As a result, the physician is provided with useful information regarding the physical relationship between nerves and bones. This information is most important in the evaluation and treatment of bone fractures and joint injuries.

In some applications, a contrast agent may be used to synergistically highlight the anomaly of interest. Alternatively, because nerves appear bright and isolated in an image, it may be more informative to selectively black out one of the nerves by means of administering an intraneural pharmaceutical contrast agent.

In addition to analyzing the output of neurography system 10, the diagnostic system 24 may also provide feedback to system 10 to control the pulse sequences used and the type of information produced. For example, where sites of nerve compression, section, laceration, or fibrosis are imaged, the alteration in endoneurial fluid flow and in axoplasmic flow are readily detected by monitoring the increase in signal intensity when T_2 -based, or other, neurographic sequences are used.

Although not described in detail herein, a variety of different diagnostic applications are contemplated including:

1. The demonstration of a patient's peripheral, cranial, and autonomic nerve and nerve plexus anatomy.
2. The demonstration of a patient's spinal root anatomy, particularly the cervical, thoracic and lumbar spinal roots and nerves where they pass through fat at the foramina through which they exit the spinal canal.

3. The demonstration of a patient's spinal root anatomy within the lumbar canal where the roots pass through quantities of extradural fat.

4. The examination of a patient's cranial nerves for compressions by vessels or other structures which could cause trigeminal neuralgia (Vth nerve), hemifacial spasm or Bell's palsy (VIIth nerve), essential hypertension (Xth nerve) or other cranial nerve syndromes.

5. The demonstration of nerve, plexus or root compressions or injuries in a patient, where abnormal changes in the direction, position, or other diffusional properties are caused by an injurious process, such as nerve transection, demyelinating diseases, neuritis, multiple sclerosis, peripheral neuropathies and crush injuries, as well as the monitoring of the regrowth of nerves.

6. The determination of the location of tumors or other masses within the spinal cord where it is useful to know the position of cortico-spinal motor tracts or other functional white matter long tracts relative to some abnormality.

7. Demonstrating the anatomy of the optic nerve, an extension of the brain, where it passes through the peri-orbital fat or other fat on its route to the retina.

8. Tract tracing within the brain to provide useful images for study by radiologists, surgeons or physicians and, in particular, for identification of the location of areas of 'eloquent cortex' such as the motor strip, or speech-related areas. This method involves the spatial identification of relevant areas of the thalamus or internal capsule and then following projecting tracts to the area of interest on the cortical surface, or identifying regions of interest by reference to their connections with other areas on the cortical surface. For example, speech cortex projection tracts can be followed from areas known to be involved in speech production to (and through) other areas where an injury or stroke may have blocked proper nerve function.

9. Tracing of nerves as they pass through tumors of low diffusional anisotropy, such as the passage of the VIIIth nerve through an acoustic neuroma to permit a surgeon to know the location of the nerve in or near the tumor and so to have the ability to avoid the nerve during surgery on the tumor.

10. Application of diffusion anisotropy imaging for the evaluation of diffuse axonal injury, as may occur in head injury.

11. The evaluation of bone fractures and joint dislocations or dislocation/fractures in which surgical planning, management and fixation would benefit from knowing the course of the nerve in the region of the abnormal anatomy.

c. Therapeutic System

As noted previously, a therapeutic system 26 is also employed to process information from neurography system 10 or other components of medical system 12 to better effect the administration of therapy to the patient. For example, system 26 may be a drug-delivery system or a current-stimulation system that employs feedback from neurography system 10 to regulate its operation. In this fashion, more precise nerve conduction velocity (NCV) or evoked potential tests can be done using neurographic data to place stimulating or recording electrodes. For therapy, tract information could aid in the placement of transplant tissue or for lesions of areas of abnormal activity that might cause tremor in the thalamus.

d. Surgical System

The surgical system **28** employs neurographic information from system **10** to influence any one of a variety of surgical operations that may be performed. The information obtained may be used to avoid neural paths during surgery or to confirm the location and nature of neural surgery required. The operation of surgical system **28** may be automatically controlled in response to feedback from system **10** or may manually controlled by a surgeon based upon his or her review of the information provided.

In one embodiment, the region of the patient that is to undergo surgery is placed in the splint **156** described above. The open regions **170** of splint **156** need to be designed and positioned to ensure that splint **156** will not interfere with the surgical system **28** during the performance of an operation. With the splint **156** applied, image data is then collected via the neurography system **10**. As noted previously, the processing system **16** of neurography system **10** provides numerical coordinates, in three dimensions, describing the position of the nerves along their courses with reference to the splint base **158** and fiduciary markers **162**.

Depending upon the nature of the operation to be performed, outputs from the auxiliary data collection system **22** may also be required. For example, if system **28** is employed to operate on bone within the region imaged, system **22** may be called upon to generate a fat selective image of the bone, or the patient may be brought to a C-T scanner for preparation of a bone image. The MRI splint **156** will be worn while this additional information is collected, but additional markers (e.g., chalk or iodine solution for CT X-rays) are required to extract locational information from the secondary image and, hence, provide the requisite registration between the two images generated.

The image information is loaded into the memory of a surgical system processor **178**, shown in FIG. **24**. As will be described in greater detail below, in the preferred arrangement, processor **178** is programmed to guide surgical operations performed in a coordinate system that is referenced to the image coordinate system. The base **158** of splint **156** is secured to a platform **180** included in surgical system **28** to provide a fixed relationship between the coordinate systems used in the image and by system **28**. The coordinate systems are then linked by processor **178** using a computer model of three-dimensional space. Confirmatory X-rays may be taken conveniently during the procedure to assure correct positioning of the markers.

An articulated surgical arm **182** is coupled to the platform **180** and has a stylus **184** (e.g., a surgical apparatus, such as a focused laser beam or a drill) provided at its free end. The arm **182** can be moved electrically or pneumatically to any select point, or along any select path, defined relative to the operating environment in response to outputs from processor **178**. The position of the arm **182** can, thus, be tracked via the control outputs applied by the processor **178**. As will be appreciated, a separate coordinate-based or laser-based positioning system may be employed if desired.

In the preferred embodiment, the position of the stylus relative to the imaged neural and other networks is illustrated on a system display **186** during the course of a surgical operation. The surgeon may manually guide the stylus **184** during the operation via, for example, a joystick, electronic glove, or other input device **188**, visually monitoring the position of the stylus relative to anatomical structure. This visual feedback may be based simply upon a comparison of the known positional relationship of the stylus to the previously collected image.

Alternatively, it is possible to obtain visual confirmation using imaging feedback data collected in real time. For

instance, with the use of high-speed MRI data collection sequences, such as echo planar imaging described in Worthington et al., *The Clinical Applications of Echo Planar Imaging in Neuroradiology*, 32 NEURORADIOLOGY 367-370 (1990), it is possible to rapidly update images. When the resulting images are displayed, the surgeon may observe the progression of an appropriately labeled, non-magnetic probe into the body in real time. If a slower image collection process is employed, the probe or device is advanced in steps as a series of images are taken. In either case, the neurographic image provides the surgeon with apparent vision of sensitive neural tissue inside opaque, solid body structures, in much the same manner as fluoroscopy, but while also providing information regarding neural paths.

As an alternative to requiring the surgeon to control the operation of system **28** during surgery, a computer-guided, stereotaxic, or fiduciary system may be employed. In that regard, the surgeon may provide processor **178** with input identifying the nature of the operation to be performed, including the stylus path and operation appropriate for the surgery to be performed. These steps can be performed with the arm **182** disengaged, allowing the surgeon to simulate the operation and view the stylus path on the image, before the surgical procedure is confirmed. Once confirmed, the processor **178** can then be instructed to automatically guide the arm **182** over the desired path during the actual surgical operation.

The use of surgical system **28** has a number of important advantages over the "neurally blind" surgical methods currently employed. For example, because nerves are readily imaged, the surgeon is better able to assess any neural conditions that might require treatment or alter the surgical plan. In addition, because the position of the stylus **182** relative to nerve is readily imaged and can be confirmed before an operation is performed, accidental intrusion of the stylus upon neural paths is avoided.

Although a splint **156** is employed in the embodiment described above to provide a link between the referential frames of the neurogram and surgical system **28**, it is not mandatory. For example, particularly in regions that are relatively unsusceptible to motion artifact, fiduciary markers can be applied directly to the body (e.g., on the head or face when nerves of facial sensation or movement are involved, or adjacent the iliac crests and lumbar vertebral spinous processes when lumbar nerve roots are involved).

The use of a computer-guided surgical system **28** employing such fiduciary markers is believed to be of particular importance in cervical, thoracic or lumbar spine surgery. In that regard, system **28** will eliminate the problem of doing a "good" operation but at the wrong level, e.g., inadvertently decompressing the lumbar 3/4 root when the symptomatic compression to be relieved was actually at the lumbar 4/5 root. For spine work, the original image can be collected with a strip of fiduciary markers taped to the patient's back and independently marked in a manner that can be sensed by system **28** to allow location of the stylus **182** during surgery.

As will be appreciated, the various components of the surgical system **28** can be altered in a variety of manners. For example, the stylus **182** may include a surface detector of electrical fields or a magnetic detector of nerve activity, constructed to detect the activity of nerves. Examples of such devices include a somatosensory evoked potential or magneto-encephalography system. As a result, the detection of nerves offered by embodiment of the stylus **182** allows the position of the stylus relative to nerve determined by reference to the neurogram to be confirmed.

One application for surgical system **28** that is of particular importance is in surgery of the neck. Surgery of this type includes, for example, a carotid endarterectomy to remove stroke producing plaque from the internal carotid artery, an anterior cervical discectomy to relieve a cervical root compression, or an operation for cancer in the neck. One of the most common complications of such surgery is the accidental crushing or transection of the recurrent laryngeal nerve, possibly resulting in permanent paralysis of one or both sets of vocal cords. Optimally, a preoperative neurographic image is used to demonstrate the course of the recurrent laryngeal nerve, allowing the surgeon to more effectively avoid it or at least identify and protect it during surgery.

Neurographic guidance can be also used for percutaneous needle biopsy of lesions, or for the placement of more elaborate percutaneous systems such as ultrasonic or other mechanical devices used to remove tissues. By way of illustration, such operations include discectomies, the introduction of laser/suction systems, the placement of RF lesioning devices used in procedures such as gangliolysis of the fifth cranial nerve, the placement of probes to carry out deep tissue localized drug administration, diathermy, cryotherapy, or other physical or mechanical techniques. Neurographic guidance may also be used to control the passage of rigid endoscopes through solid tissues or to guide the placement of directable flexible endoscopes.

Yet another important application of surgical system **28** is in the use of CNS neurograms to guide stereotactic surgery in the brain. Currently, tissue structures visible by virtue of their T_1 or T_2 MRI are used to guide stereotactic surgery. In contrast, CNS neurograms provide information concerning the connections or relation of specific tracts of interest, which may travel in or among other tracts from which they cannot be differentiated by means of conventional tissue-based images.

e. Training and Development System

The training and development system **30** may take any one of a variety of forms designed to process information collected from the neurography system **10**. In one embodiment, neurographic images are collected from a plurality of patients to produce an anatomical atlas of normal and abnormal neural paths for reference by surgeons and others. Images obtained from a patient can be compared to the clinically known population in the atlas to rapidly identify anomalous nerve courses in a patient set to undergo surgery for some condition. As a result, the surgeon may be able to modify his or her technique to reduce the risk of injury to nerves which happen to be in the field of surgery. Similarly, a neurographic map of an individual patient's skin and cutaneous nerves can be used to help the surgeon plan incisions that avoid the very common complication of accidental transection of cutaneous nerves in the course of routine surgical incision to reach structures below the skin.

In another embodiment, the training and development system **30** may be designed to assess the effectiveness of the programming employed by neurography system **10** and may provide feedback to system **10** to regulate its operation and enhance the quality of the neurograms generated. More particularly, once a sequence able to positively identify nerve has been employed, alternative sequences can be employed and their results compared to the confirmed method. As a result, a collection of techniques can be established and programmed into neurography system, along with the conditions under which each sequence offers the best performance.

Another alternative training and development system **30** may be employed to assess the effectiveness of intraneural,

pharmaceutical contrast agents designed to help in the diagnosis of nerve compressions. More particularly, such a training system **30** is used to quantify the image contrast produced using different contrast agents to image known neural anomalies. As a result, system **30** is able to identify those agents providing the best results for particular neural imaging problems.

Yet another embodiment of training and development system **30** allows information from neurograms to be used in the design of any of a variety of products. For example, the neurograms produced by system **10** provide information that is of great advantage to designers of ergonomic furniture, high gravity air or space craft seats, specialized body suits, boots, and various kinds of electronic or electric medical equipment, which can be best used when the positions of nerves can be precisely located in advance. The system **30** incorporates information regarding neural paths from system **10** into the computational processes involved in designing such equipment to provide enhanced product performance.

As one illustration, in the ergonomic design of a chair, system **30** would be programmed to ensure that the primary support provided by the chair does not coincide with a neural path in the relevant customer population. This can be done by superimposing the neural network of a sitting person upon a mathematical model of the chair, identifying the primary points of support, and generating flags on the display for any support points that are within some predetermined distance of a nerve. As a result, the chair design can be manipulated to avoid neural compressions.

In another application, the system **30** can be used to control electronic prosthesis. More particularly, the information from system **10** can be used to locate electronic detectors adjacent, for example, a severed nerve to detect neural activity associated with the limb replaced by the prosthesis. The detected activity of the nerve is then used to control the prosthesis.

4. Non-neural Imaging Applications

In principle, selective imaging of any other object or subject may be effected using the MRI techniques described above, if that subject or object exhibits characteristics corresponding to the neural characteristics described above. For example, objects exhibiting diffusion anisotropy in any part thereof can be imaged using diffusional weighting. Thus, in medicine, for example, the cardiovascular system could also be imaged in this fashion and the technique can also be employed to examine, for example, rock strata and plants, if they exhibit diffusion anisotropy.

5. Conclusion

The lack of a suitable method for creating a distinct image of the nerves has been a great hindrance to physicians, surgeons, athletic trainers, and pain treatment specialists. Although, previously, it has sometimes been possible to make a nerve stand out from immediately surrounding structures, the unique ability of system **10** to make the nerve stand out from all other structures represents a significant advance. The sensitivity of the system **10** allows even the smallest nerves to be accurately identified and linked to form three-dimensional projections of a neural network. The neurographic information can be collected rapidly, without requiring contrast agents.

While the preferred embodiment of the invention has been illustrated and described, it will be appreciated that various changes can be made therein without departing from the spirit and scope of the invention.

The embodiments of the invention in which an exclusive property or privilege is claimed are defined as follows:

1. A method of utilizing magnetic resonance to determine the shape and position of mammal tissue, said method including the steps of:

- (a) exposing an in vivo region of a subject to a magnetic polarizing field, the in vivo region including non-neural tissue and a nerve, the nerve being a member of the group consisting of peripheral nerves, cranial nerves numbers three through twelve, and autonomic nerves;
- (b) exposing the in vivo region to an electromagnetic excitation field;
- (c) sensing a resonant response of the in vivo region to the polarizing and excitation fields and producing an output indicative of the resonant response;
- (d) controlling the performance of the steps (a), (b), and (c) to enhance, in the output produced, the selectivity of said nerve, while the nerve is living in the in vivo region of the subject; and
- (e) processing the output to generate a data set describing the shape and position of said nerve, said data set distinguishing said nerve from non-neural tissue, in the in vivo region to provide a conspicuity of the nerve that is at least 1.1 times that of the non-neural tissue, without the use of neural contrast agents, said processing including the step of analyzing said output for information representative of fascicles found in peripheral nerves, cranial nerves numbers three through twelve, and autonomic nerves.

2. The method of claim 1, wherein the step of processing further includes using the results of said step of analyzing the output for information representative of fascicles to suppress from said data set tissue that is not fascicular.

3. A method of utilizing magnetic resonance to determine the shape and position of mammal tissue, said method including the steps of:

- (a) exposing an in vivo region of a subject to a magnetic polarizing field, the in vivo region including non-neural tissue and a nerve, the nerve being a member of the group consisting of peripheral nerves, cranial nerves numbers three through twelve, and autonomic nerves;
- (b) exposing the in vivo region to an electromagnetic excitation field;
- (c) sensing a resonant response of the in vivo region to the polarizing and excitation fields and producing an output indicative of the resonant response;
- (d) controlling the performance of the steps (a), (b), and (c) to enhance, in the output produced, the selectivity of said nerve, while the nerve is living in the in vivo region of the subject, said step of controlling the performance of steps (a), (b), and (c) including selecting a combination of echo time and repetition time that exploits a characteristic spin-spin relaxation coefficient of peripheral nerves, cranial nerves numbers three through twelve, and autonomic nerves, wherein said spin-spin relaxation coefficient is substantially longer than that of other surrounding tissue; and
- (e) processing the output to generate a data set describing the shape and position of said nerve, said data set distinguishing said nerve from non-neural tissue, in the in vivo region to provide a conspicuity of the nerve that is at least 1.1 times that of the non-neural tissue, without the use of neural contrast agents.

4. The method of claim 3, wherein the step of selecting said combination of echo time and repetition time includes selection of an echo time that is greater than 60 milliseconds to enhance the distinction of said nerve from non-neural tissue in the in vivo region.

5. The method of claim 4, further comprising the step of repeating said step of exposing the in vivo region to an excitation field after a repetition time that is greater than one second to enhance the distinction of said nerve from the non-neural tissue in the in vivo region.

6. The method of claim 4, wherein the non-neural tissue includes fat and said method further comprises exposing the in vivo region to electromagnetic fields that suppress the contribution of the fat in said output prior to producing an output at step (c).

7. A method of utilizing magnetic resonance to determine the shape and position of mammal tissue, said method including the steps of:

- (a) exposing an in vivo region of a subject to a magnetic polarizing field, the in vivo region including non-neural tissue and a nerve, the nerve being a member of the group consisting of peripheral nerves, cranial nerves numbers three through twelve, and autonomic nerves, said magnetic polarizing field including a first diffusion-weighted gradient that is substantially parallel to the nerve and a second diffusion-weighted gradient that is substantially perpendicular to the nerve;
- (b) exposing the in vivo region to an electromagnetic excitation field;
- (c) sensing a resonant response of the in vivo region to the polarizing and excitation fields and producing a first output indicative of the resonant response to said first diffusion-weighted gradient and a second output indicative of the response to said second diffusion-weighted gradient;
- (d) controlling the performance of the steps (a), (b), and (c) to enhance, in the output produced, the selectivity of said nerve, while the nerve is living in the in vivo region of the subject; and
- (e) subtracting said first output from said second output to generate a data set describing the shape and position of said nerve, said data set distinguishing said nerve from non-neural tissue, in the in vivo region to provide a conspicuity of the nerve that is at least 1.1 times that of the non-neural tissue, without the use of neural contrast agents.

8. The method of claim 7, wherein the step of subtracting further includes the step of determining a registration between the first output and the second output.

9. The method of claim 8, wherein said method includes the step of inhibiting the step of subtracting unless a threshold level of registration is exhibited between the first and second outputs.

10. The method of claim 7, wherein the non-neural tissue includes fat, and wherein the method includes the step of exposing the in vivo region to electromagnetic fields that suppress the contribution of the fat in said first and second outputs prior to the steps exposing the in vivo region to said first and second gradients.

11. A method of utilizing magnetic resonance to determine the shape and position of mammal tissue, said method including the steps of:

- (a) exposing an in vivo region of a subject to a magnetic polarizing field that includes a predetermined arrangement of diffusion-weighted gradients, the in vivo region including non-neural tissue and a nerve, the nerve being a member of the group consisting of peripheral nerves, cranial nerves numbers three through twelve, and autonomic nerves;
- (b) exposing the in vivo region to an electromagnetic excitation field;

- (c) sensing a resonant response of the in vivo region to the polarizing and excitation fields and producing an output indicative of the resonant response, said producing an output indicative of the resonant response including the step of producing a separate output for each diffusion-weighted gradient of said predetermined arrangement of diffusion-weighted gradients;
- (d) controlling the performance of the steps (a), (b), and (c) to enhance, in the output produced, the selectivity of said nerve, while the nerve is living in the in vivo region of the subject;
- (e) processing the output to generate a data set describing the shape and position of said nerve, said data set distinguishing said nerve from non-neural tissue, in the in vivo region to provide a conspicuity of the nerve that is at least 1.1 times that of the non-neural tissue, without the use of neural contrast agents, said processing the output including the step of vector processing the separate outputs for each said diffusion-weighted gradient of said predetermined arrangement of diffusion-weighted gradients to generate data representative of anisotropic diffusion exhibited by the nerve, and processing said data representative of said anisotropic diffusion to generate said data set describing the shape and position of the nerve.
- 12.** A method of utilizing magnetic resonance to determine the shape and position of mammal tissue, said method including the steps of:
- (a) exposing an in vivo region of a subject to a magnetic polarizing field, the in vivo region including non-neural tissue that includes fat and a nerve, the nerve being a member of the group consisting of peripheral nerves, cranial nerves numbers three through twelve, and autonomic nerves;
- (b) exposing the in vivo region to an electromagnetic excitation field;
- (c) sensing a resonant response of the in vivo region to the polarizing and excitation fields and producing an output indicative of the resonant response;
- (d) controlling the performance of the steps (a), (b), and (c) to enhance, in the output produced, the selectivity of said nerve, while the nerve is living in the in vivo region of the subject; and
- (e) processing the output to generate a data set describing the shape and position of said nerve, said data set distinguishing said nerve from non-neural tissue, in the in vivo region to provide a conspicuity of the nerve that is at least 1.1 times that of the non-neural tissue, without the use of neural contrast agents; and said steps of exposing the in vivo region to an excitation field and producing an output being designed to suppress the contribution of fat in the output, said step of processing the output to generate the data set including the step of analyzing the output for information representative of fascicles found in peripheral nerves, cranial nerves numbers three through twelve and autonomic nerves.
- 13.** The system of claim 12, wherein the contribution of fat is suppressed by employing a chemical shift selective sequence.
- 14.** The method of claim 12, wherein the step of processing further includes using the results of said step of analyzing the output for information representative of fascicles to suppress from said data set tissue that is not fascicular.
- 15.** A method of utilizing magnetic resonance to determine the shape and position of mammal tissue, said method including the steps of:

- (a) exposing an in vivo region of a subject to a magnetic polarizing field, the in vivo region including non-neural tissue that includes blood vessels and a nerve, the nerve being a member of the group consisting of peripheral nerves, cranial nerves numbers three through twelve, and autonomic nerves;
- (b) exposing the in vivo region to an electromagnetic excitation field;
- (c) sensing a resonant response of the in vivo region to the polarizing and excitation fields and producing an output indicative of the resonant response;
- (d) performing the steps (a), (b), and (c) to produce a second output in which the conspicuity of blood vessels is enhanced; and
- (e) processing said output indicative of the resonant response and said second output to generate a data set in which conspicuity of the blood vessels is suppressed, said data set describing the shape and position of said nerve and distinguishing said nerve from non-neural tissue, in the in vivo region to provide a conspicuity of the nerve that is at least 1.1 times that of the non-neural tissue, without the use of neural contrast agents.
- 16.** A method of utilizing magnetic resonance to determine the shape and position of mammal tissue, said method including the steps of:
- (a) exposing an in vivo region of a subject to a magnetic polarizing field, the in vivo region including non-neural tissue and a nerve, the nerve being a member of the group consisting of peripheral nerves, cranial nerves numbers three through twelve, and autonomic nerves;
- (b) exposing the in vivo region to an electromagnetic excitation field;
- (c) sensing a resonant response of the in vivo region to the polarizing and excitation fields and producing an output indicative of the resonant response;
- (d) controlling the performance of the steps (a), (b), and (c) to enhance, in the output produced, the selectivity of said nerve, while the nerve is living in the in vivo region of the subject; and
- (e) processing the output to generate a data set describing the shape and position of said nerve, said data set distinguishing said nerve from non-neural tissue, in the in vivo region to provide a conspicuity of the nerve that is at least 1.1 times that of the non-neural tissue, without the use of neural contrast agents;
- wherein said steps (a) through (c) include the step of exposing the in vivo region to a readout gradient rephasing pulse and a slice-selective excitation pulse, said readout gradient rephasing pulse being generated directly before said output pulse is produced instead of directly after the generation of the slice-selective excitation pulse, so as to reduce the appearance of undesirable cross-terms in said data set.
- 17.** The method of claim 16, wherein said steps (a) through (c) further include the step of exposing the in vivo region to a two-part phase encoding gradient, so as to further reduce the appearance of undesirable cross-terms in said data set.
- 18.** A method of utilizing magnetic resonance to determine the shape and position of mammal tissue, said method including the steps of:
- (a) exposing an in vivo region of a subject to a magnetic polarizing field, the in vivo region including non-neural tissue and a nerve, the nerve including epineurium and perineurium and being a member of the group consist-

ing of peripheral nerves, cranial nerves numbers three through twelve, and autonomic nerves;

- (b) exposing the in vivo region to an electromagnetic excitation field;
- (c) sensing a resonant response of the in vivo region to the polarizing and excitation fields and producing an output indicative of the resonant response;
- (d) controlling the performance of the steps (a), (b), and (c) to enhance, in the output produced, the selectivity of said nerve, while the nerve is living in the in vivo region of the subject; and
- (e) processing the output to generate a data set describing the shape and position of said nerve, said data set distinguishing said nerve from non-neural tissue, in the in vivo region to provide a conspicuity of the nerve that is at least 1.1 times that of any adjacent non-neural tissue, without the use of neural contrast agents.

19. The method of claim 18, wherein said data set distinguishes said nerve from non-neural tissue in the in vivo region so that said data set describes the nerve at an intensity at least 5 times that of the non-neural tissue.

20. The method of claim 18, wherein the step of exposing the in vivo region to a polarizing field includes the step of exposing the in vivo region to a polarizing field including at least one diffusion-weighted gradient.

21. The method of claim 20, wherein the at least one diffusion-weighted gradient includes a first gradient substantially parallel to the nerve and a second gradient substantially perpendicular to the nerve, and the step of producing an output includes the steps of producing a first output when the first gradient is employed and a second output when the second gradient is employed, and the step of processing the output includes the step of subtracting the first output from the second output.

22. The method of claim 20, wherein the at least one diffusion-weighted gradient includes a predetermined arrangement of gradients, the step of producing an output includes the step of producing a separate output associated with each gradient, and the step of processing the output includes the steps of vector processing the separate outputs to generate data representative of anisotropic diffusion exhibited by the nerve, and processing said data representative of anisotropic diffusion to generate said data set describing the shape and position of the nerve.

23. The method of claim 18, wherein the non-neural tissue includes fat, and the steps of exposing the in vivo region to an excitation field and producing an output involve the excitation of any fat in the in vivo region in a manner designed to suppress the contribution of the fat to the output.

24. The method of claim 23, wherein the step of processing further includes the step of analyzing the output for information representative of fascicles found in peripheral nerves, cranial nerves numbers three through twelve, and autonomic nerves.

25. The method of claim 18, wherein step (d) includes the step of selecting a combination of echo time and repetition time that exploits a characteristic spin-spin relaxation coefficient of peripheral nerves, cranial nerves numbers three through twelve, and autonomic nerves, said spin-spin relaxation coefficient of these nerves being substantially longer than that of other surrounding tissue.

26. The method of claim 18, wherein step (d) includes the step of controlling said step (b) to expose the in vivo region to an excitation field that induces a magnetization transfer from non-anisotropically diffusing water in the in vivo region to anisotropically diffusing water in said nerve, to more readily distinguish the nerve from non-neural tissue.

27. The method of claim 26, wherein the non-neural tissue includes fat and said method further comprises exposing the in vivo region to electromagnetic fields that suppress the contribution of the fat in said output prior to producing an output at step (c).

28. The method of claim 18, wherein the in vivo region includes blood vessels and said step (d) suppresses the blood vessels from said data set.

29. The method of claim 28, wherein the conspicuity of nerve is enhanced in said output and said steps (a), (b), and (c) are performed a second time to produce a second output in which the conspicuity of blood vessels is enhanced and wherein said step (e) of processing the output includes the step of processing said output and said second output to suppress the blood vessels from said data set.

30. The method of claim 18, wherein if the non-neural tissue in said in vivo region includes blood vessels and cerebrospinal fluid, said step (d) includes the step of selecting the polarizing field of step (a) and the excitation field of step (b) to suppress the blood vessels and the cerebrospinal fluid from said data set.

31. The method of claim 18, wherein said step (c) includes the step of processing said output on an interleaved pixel-by-pixel basis to suppress the influence of motion of the in vivo region on said data set.

32. The method of claim 18, wherein said method further includes the step of immobilizing the in vivo region in a splint to reduce motion artifact in said data set.

33. The method of claim 18, wherein the in vivo region includes a plurality of peripheral nerves, cranial nerves numbers three through twelve, or autonomic nerves, and said method further includes the step of administering a contrast agent to a selected one of the plurality of peripheral nerves, cranial nerves numbers three through twelve, or autonomic nerves to remove said selected one nerve from said data set.

34. The method of claim 18, wherein the intensity of said nerve in said data set is at least 10 times that of non-neural tissue in the in vivo region.

35. The method of claim 18, wherein said method further includes the step of processing said data set to generate an image displaying the shape and position of said nerve.

36. A method of utilizing magnetic resonance to determine the shape and position of a structure, said method including the steps of:

- (a) exposing a region to a magnetic polarizing field including a predetermined arrangement of diffusion-weighted gradients, the region including a selected structure that exhibits diffusion anisotropy and other structures that do not exhibit diffusion anisotropy;
- (b) exposing the region to an electromagnetic excitation field;
- (c) for each of said diffusion-weighted gradients, sensing a resonant response of the region to the excitation field and the polarizing field including the diffusion-weighted gradient and producing an output indicative of the resonant response; and
- (d) vector processing said outputs to generate data representative of anisotropic diffusion exhibited by said selected structure in the region, regardless of the alignment of said diffusion-weighted gradients with respect to the orientation of said selected structure; and
- (e) processing said data representative of anisotropic diffusion to generate a data set describing the shape and position of said selected structure in the region, said data set distinguishing said selected structure from

other structures in the region that do not exhibit diffusion anisotropy.

37. The method of claim 36, wherein said selected structure is neural tissue in a mammal and said other structures are non-neural tissue in the mammal.

38. The method of claim 37, wherein said step of processing said data representative of anisotropic diffusion includes the steps of:

analyzing said data representative of anisotropic diffusion to determine an effective direction of the anisotropic diffusion exhibited by said neural tissue, so as to determine an optimal orientation for diffusion-weighted gradients;

exposing the region to two additional diffusion-weighted gradients respectively substantially parallel to and substantially perpendicular to said effective direction;

producing two additional outputs indicative of the region's resonant responses respectively to said two additional diffusion-weighted gradients; and

calculating a difference between said two additional outputs to generate said data set describing the shape and position of said neural tissue.

39. The method of claim 37, wherein said data set describing the shape and position of said neural tissue describes the shape and position of a selected cross section of said neural tissue, and the steps used to generate said data set are repeated to generate additional data sets describing different cross sections of said neural tissue, and a further data set that describes the three dimensional shape and position of a segment of said neural tissue is generated by steps including:

analyzing the data representative of anisotropic diffusion to determine how to relate said data set and said additional data sets describing the shape and position of cross sections of said neural tissue; and

based upon the results of said step of analyzing the data representative of anisotropic diffusion, combining said data set and said additional data sets to generate said further data set that describes the three dimensional shape and position of the segment of said neural tissue, thereby enabling the three dimensional shape and position of curved neural tissue to be described.

40. The method of claim 39, wherein said step of analyzing the data representative of anisotropic diffusion includes determining an effective direction of the anisotropic diffusion exhibited by said neural tissue in each of said selected and different cross sections.

41. The method of claim 37, wherein said predetermined arrangement of gradients includes first, second, and third orthogonal gradients, and said data representative of anisotropic diffusion include a description of an effective vector representative of the anisotropic diffusion exhibited by said neural tissue.

42. The method of claim 41, wherein said data set describing the shape and position of said neural tissue is based upon the length of said effective vector.

43. The method of claim 42, wherein the step of exposing the region to a magnetic polarizing field includes the step of exposing the region to a zero diffusion gradient polarizing field that does not include a diffusion-weighted gradient, the step of producing an output includes the step of producing a zero diffusion gradient output indicative of the region's resonant response to said zero diffusion gradient polarizing field, and the length of said effective vector is normalized by a magnitude of said zero diffusion gradient output.

44. The method of claim 41, wherein said data set describing the shape and position of said neural tissue is

based upon an angle describing in part the direction of said effective vector.

45. The method of claim 41, wherein said step of processing said data representative of anisotropic diffusion includes the steps of:

exposing the region to two additional diffusion-weighted gradients respectively substantially parallel to and substantially perpendicular to the direction of said effective vector representative of the anisotropic diffusion exhibited by said neural tissue;

producing two additional outputs indicative of the region's resonant responses respectively to said two additional diffusion-weighted gradients; and

calculating a difference between said two additional outputs to generate said data set describing the shape and position of said neural tissue.

46. The method of claim 41, wherein said data set describes the shape and position of a selected cross section of said neural tissue, and the steps used to generate said data set are repeated to generate additional data sets describing different cross sections of said neural tissue, and a further data set that describes the three dimensional shape and position of a segment of said neural tissue is generated by steps including:

analyzing the data representative of anisotropic diffusion to determine how to relate said data set and said additional data sets describing the shape and position of cross sections of said neural tissue; and

based upon the results of said step of analyzing the data representative of anisotropic diffusion, combining said data set and said additional data sets to generate said further data set that describes the three dimensional shape and position of the segment of said neural tissue, thereby allowing the three dimensional shape and position of curved neural tissue to be described.

47. The method of claim 46, wherein said step of analyzing the data representative of anisotropic diffusion includes the step of analyzing the direction of the effective vector representative of the anisotropic diffusion exhibited by said neural tissue in each of said cross sections.

48. The method of claim 46, wherein said step of processing said data representative of anisotropic diffusion includes the steps of:

analyzing said data representative of anisotropic diffusion to determine an effective direction of the anisotropic diffusion exhibited by said selected structure, so as to determine an optimal orientation for diffusion-weighted gradients;

exposing the region to two additional diffusion-weighted gradients respectively substantially parallel to and substantially perpendicular to said effective direction;

producing two additional outputs indicative of the region's resonant responses respectively to said two additional diffusion-weighted gradients; and

calculating a difference between said two additional outputs to generate said data set describing the shape and position of said selected structure.

49. The method of claim 36, wherein said data set describing the shape and position of said selected structure describes the shape and position of a selected cross section of said selected structure, and the steps used to generate said data set are repeated to generate additional data sets describing different cross sections of said selected structure, and a further data set that describes the three dimensional shape and position of a segment of said selected structure is generated by steps including:

analyzing the data representative of anisotropic diffusion to determine how to relate said data set and said additional data sets describing the shape and position of cross sections of said selected structure; and

based upon the results of said step of analyzing the data representative of anisotropic diffusion, combining said data set and said additional data sets to generate said further data set that describes a three dimensional shape and position of the segment of said selected structure, thereby allowing the three dimensional shape and position of a curved structure exhibiting anisotropic diffusion to be described.

50. The method of claim **36**, wherein said predetermined arrangement of gradients includes first, second, and third orthogonal gradients, and said data representative of anisotropic diffusion include a description of an effective vector representative of the anisotropic diffusion exhibited by said selected structure.

51. A method of utilizing magnetic resonance to determine data representative of diffusion anisotropy exhibited by a structure, said method including the steps of:

- (a) exposing a region to a suppression sequence of electromagnetic fields that suppresses the electromagnetic responsiveness of structures in the region that do not exhibit diffusion anisotropy, so as to increase the apparent diffusion anisotropy of structures in the region that exhibit diffusion anisotropy, said suppression sequence of electromagnetic fields not including diffusion-weighted magnetic gradients;
- (b) exposing the region to a predetermined arrangement of diffusion-weighted magnetic gradients, said predetermined arrangement of diffusion-weighted magnetic gradients chosen to:
 - i) emphasize a selected structure in the region exhibiting diffusion anisotropy in a particular direction; and
 - ii) suppress other structures in the region exhibiting diffusion anisotropy in directions different from said particular direction;
- (c) for each of said diffusion-weighted gradients, sensing a resonant response of the region to the diffusion-weighted gradient and producing an output indicative of the resonant response; and
- (d) processing said outputs to generate data representative of the diffusion anisotropy of the selected structure.

52. The method of claim **51**, wherein said data representative of the diffusion anisotropy of the selected structure is processed to produce a data set that describes the shape and position of the selected structure.

53. The method of claim **52**, wherein the selected diffusion anisotropic structure is neural tissue in vivo and living.

54. A magnetic resonance apparatus for determining data representative of the diffusion anisotropy exhibited by a structure, said apparatus including:

- (a) excitation and output arrangement means for exposing a region to a suppression sequence of electromagnetic fields that suppresses the electromagnetic responsiveness of structures in the region that do not exhibit diffusion anisotropy, so as to increase the apparent diffusion anisotropy of structures in the region that exhibit diffusion anisotropy, said suppression sequence of electromagnetic fields not including diffusion-weighted magnetic gradients;
- (b) polarizing field source means positioned near said excitation and output arrangement means for exposing the region to a predetermined arrangement of diffusion-weighted magnetic gradients chosen to:

i) emphasize a selected structure in the region exhibiting diffusion anisotropy in a particular direction; and

ii) suppress other structures in the region exhibiting diffusion anisotropy in directions different from said particular direction, said excitation and output arrangement means further for sensing a resonant response of the region to the diffusion-weighted gradient and producing an output indicative of the resonant response, for each of said diffusion-weighted gradients; and

(c) processor means coupled to said excitation and output arrangement means for processing said outputs to generate data representative of the diffusion anisotropy of the selected structure.

55. A magnetic resonance apparatus for determining the shape and position of a structure, said apparatus including:

(a) polarizing field source means for exposing a region to a magnetic polarizing field including a predetermined arrangement of diffusion-weighted gradients, the region including a selected structure that exhibits diffusion anisotropy and other structures that do not exhibit diffusion anisotropy;

(b) excitation and output arrangement means positioned near said polarizing field source means for:

i) exposing the region to an electromagnetic excitation field; and

ii) for each of said diffusion-weighted gradients, sensing a resonant response of the region to the excitation field and the polarizing field including the diffusion-weighted gradient and producing an output indicative of the resonant response; and

(c) processor means coupled to said excitation and output arrangement means for:

i) vector processing said outputs to generate data representative of anisotropic diffusion exhibited by the selected structure in the region, regardless of the alignment of said diffusion-weighted gradients with respect to the orientation of said selected structure; and

ii) processing said data representative of anisotropic diffusion to generate a data set describing the shape and position of said selected structure in the region, said data set distinguishing said selected structure from other structures in the region that do not exhibit diffusion anisotropy.

56. The apparatus of claim **55**, wherein said selected structure is neural tissue in a mammal and said other structures are non-neural tissue in the mammal.

57. The apparatus of claim **56**, wherein:

said processor means is further for analyzing said data representative of anisotropic diffusion to determine an effective direction of the anisotropic diffusion exhibited by said neural tissue, so as to determine an optimal orientation for diffusion-weighted gradients;

said polarizing field source means is further for exposing the region to two additional diffusion-weighted gradients respectively substantially parallel to and substantially perpendicular to said effective direction;

said excitation and output arrangement means is further for producing two additional outputs indicative of the region's resonant responses respectively to said two additional diffusion-weighted gradients; and

said processor means is further for determining the difference between said two additional outputs to generate said data set describing the shape and position of said neural tissue.

58. The apparatus of claim 56, wherein said data set describing the shape and position of said neural tissue describes the shape and position of a selected cross section of said neural tissue, and said apparatus is further for generating additional data sets describing different cross sections of said neural tissue, and said processor means is further for calculating a further data set that describes the three dimensional shape and position of a segment of said neural tissue by:

analyzing the data representative of anisotropic diffusion to determine how to relate said data set and said additional data sets describing the shape and position of cross sections of said neural tissue; and

based upon the results of said analyzing the data representative of anisotropic diffusion, combining said data set and said additional data sets to generate said further data set that describes the three dimensional shape and position of the segment of said neural tissue, thereby allowing a three dimensional shape and position of curved neural tissue to be described.

59. The apparatus of claim 56, wherein said predetermined arrangement of gradients includes first, second, and third orthogonal gradients, and said data representative of anisotropic diffusion include a description of an effective vector representative of the anisotropic diffusion exhibited by said neural tissue.

60. The apparatus of claim 55, wherein:

said processor means is further for analyzing said data representative of anisotropic diffusion to determine an effective direction of the anisotropic diffusion exhibited by said selected structure, so as to determine an optimal orientation for diffusion-weighted gradients;

said polarizing field source means is further for exposing the region to two additional diffusion-weighted gradients respectively substantially parallel to and substantially perpendicular to said effective direction;

said excitation and output arrangement means is further for producing two additional outputs indicative of the region's resonant responses respectively to said two additional diffusion-weighted gradients; and

said processor means is further for determining a difference between said two additional outputs to generate said data set describing the shape and position of said selected structure.

61. The apparatus of claim 55, wherein said data set describing the shape and position of said selected structure describes the shape and position of a selected cross section of said selected structure, and said apparatus is further for generating additional data sets describing different cross sections of said selected structure, and said processor means is further for determining a further data set that describes the three dimensional shape and position of a segment of said selected structure by:

analyzing the data representative of anisotropic diffusion to determine how to relate said data set and said additional data sets describing the shape and position of cross sections of said selected structure; and

based upon the results of said analyzing the data representative of anisotropic diffusion, combining said data set and said additional data sets to generate said further data set that describes the three dimensional shape and position of the segment of said selected structure, thereby enabling a three dimensional shape and position of curved structure exhibiting anisotropic diffusion to be described.

62. The apparatus of claim 55, wherein said predetermined arrangement of gradients includes first, second, and third orthogonal gradients, and said data representative of anisotropic diffusion include a description of an effective vector representative of the anisotropic diffusion exhibited by said selected structure.

63. The method of claim 61, wherein the selected diffusion anisotropic structure is a member of the group consisting of peripheral nerves, cranial nerves numbers three through twelve, and autonomic nerves, and is living.

64. The apparatus of claim 61, wherein said processor means is further for processing said data representative of the diffusion anisotropy of the selected structure to produce a data set that describes the shape and position of the selected structure.

65. The apparatus of claim 64, wherein the selected diffusion anisotropic structure is neural tissue and is living.

66. The apparatus of claim 64, wherein the selected diffusion anisotropic structure is a member of the group consisting of peripheral nerves, cranial nerves numbers three through twelve, and autonomic nerves, and is living.


* * * * *

EXHIBIT 3

- Editor in Chief: H. Richard Winn, MD
- Hardcover ISBN: 9780323661928
- eBook ISBN: 9780323674997

14: Diffusion Tensor Imaging

Aaron G. Filler

This chapter includes an accompanying lecture presentation that has been prepared by the author:  Video 14.1.

Key Concepts

- The ability of diffusion tensor imaging (DTI) tractography to depict eloquent white matter structures such as the pyramidal tract, arcuate fasciculus, and optic radiation (geniculocalcarine tract) has reduced surgical morbidity and supported improved extent of resection for brain tumors.
- Longitudinal studies have shown that the accumulation of successive head injuries by athletes correlates with losses in DTI fractional anisotropy (FA) that match with functional impairments in postconcussive individuals. For athletes commencing impact sports, a preinjury DTI scan greatly improves the diagnostic value of subsequent DTI imaging. FA is generally subject to statistical analysis regarding the presence or absence of injuries to specific tracts by right-left comparison and by comparison to data on control subjects.
- The Human Connectome Project has resulted in dramatic further advancements in the complexity and detail of tractography, while generally abandoning the tensor model in favor of newer mathematical models such as constrained spherical deconvolution (CSD).
- Specific injuries identifiable with DTI—such as a damage to the fornix—can be identified to explain specific functional deficits such as impairment of new memory formation or damage to the angular gyrus resulting in problems with word finding after head injury.
- Tractographic imaging provides an increased access to critical targets for functional neurosurgery both for lesioning and for stimulation.
- DTI is based on special MRI pulse sequences that allow pulsed magnetic field diffusion gradients to be applied in multiple directions without disrupting the x , y , and z gradients that make imaging possible. The resulting data are then processed with tensor or advanced vector mathematics to calculate the direction or directions of axons in each image voxel.

Introduction

The advent of imaging methods that measure and depict directional diffusion in neural tissue have revolutionized neuroscience and continue to have a progressively transformative impact in several subdisciplines of neurosurgery. Tractography based on diffusion anisotropy imaging has become critical to surgical planning for surgical treatments for brain tumors, epilepsy, and trauma, as well as for functional treatments that require highly targeted lesioning or deep brain stimulation targeting (Fig. 14.1). Applications in evaluating spinal cord pathology and peripheral nerve disorders are advancing as well. Early localization of areas of ischemia and occult stroke has also emerged as an important new application of this technology and has the potential to enable better understanding of recovery or progression after an initial ischemic event.¹

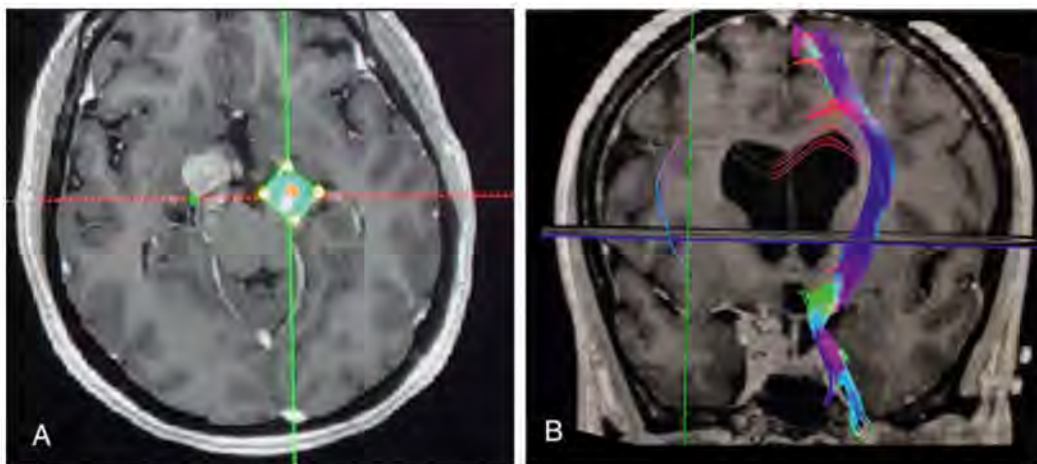


FIGURE 14.1 Using specialized diffusion tensor imaging (DTI) tractography software (Nordic Neurolabs BrainEx), a user can select a region of interest as shown in (A) incorporating the cerebral peduncle on the left, opposite to a tumor affecting the right side. (B) The deterministic tractography then generates a three-dimensional tractographic representation of the pyramidal tract running both cranially and caudally through the image volume.

Diffusion tensor imaging (DTI) tractography is now increasingly deployed for complex surgical planning tasks in aneurysm surgery,² approaches to arteriovenous malformations,³ and for assessment of effects of vasospasm in subarachnoid hemorrhage.⁴ Developing procedural treatments for psychiatric disorders⁵ and planning for neuroendoscopy^{6,7} are other areas that reach beyond the longstanding role of DTI tractography in neuro-oncology.

In tumor surgery, the potential to have a detailed view of the pyramidal tract, the arcuate fasciculus and the optic radiations and other critical white matter pathways as they traverse the centrum semiovale has greatly increased the safety of many surgeries. In 2007 Wu et al.⁸ reported from a randomized controlled prospective study of 260 glioma operations that the use of tractography led to a 43% decrease in surgically related mortality and a 62% decrease in surgical morbidities such as unnecessary paralysis, muteness, and blindness.

The field continues to advance rapidly with the advent of remarkably high resolution from new 7-Tesla imagers⁹ and similar advances based on technologic advances applied in advanced 3-T systems.¹⁰ Advances in analytic methodology also continue at a rapid pace.^{11,12}

The introduction of this technology arose from a single key breakthrough invention, which, once accomplished, led rapidly to the production of the first tractogram over a matter of weeks. The initial published report of the critical advance in MRI physics that makes the entire field possible was the September 1992 publication¹³ by Franklyn Howe (an MR physicist with a doctorate from Oxford) and Aaron Filler (a neurosurgery resident at the University of Washington who commenced the research during his doctoral work at Harvard), which revealed that they had solved the problem of how to direct an off-angle diffusion gradient through the location gradients required for MRI without causing the destructive cross-term interactions that had stymied all other researchers in this field. A number of groups were racing to find a way to make the first diffusion anisotropy image, and by 1991 all had identified the seemingly insoluble problem of destructive cross terms destroying the image.^{14,15} After this first fundamental discovery, the subsequent steps that led to the production of the first tractogram in early 1992 occurred over a matter of just a few weeks.

The discovery was in the field of MRI pulse sequence technology. Spin echo MRI uses a method called a 180-degree inversion pulse to eliminate noise and refocus the image signal of spinning protons (Fig. 14.2). Howe and Filler showed that the same inversion pulse could be used to untangle the chaos that resulted when a powerful diffusion gradient magnetic field was directed through the delicate magnetic field array of the x , y , and z direction gradients required by all MRI. If the location gradient that was activated closest in time to the diffusion gradient was split into two oppositely directed pulses equally timed in opposite directions a few milliseconds before and a few milliseconds after the inversion pulse, then the destructive cross terms would disappear. When this critical innovation was tested and proven to work, the first diffusion image from an off-angle diffusion gradient was thus obtained, and this was reported in the 1992 publication along with the pulse sequence (Fig. 14.3). This fundamental method, which also appeared in the Filler et al. patent application that led to US patent number 5,560,360¹⁶ (initial filing in March 1992), is used to this day in every DTI, Q-Ball, high angular resolution diffusion imaging (HARDI), or other diffusion anisotropy image. The method is also called a "single-shot" method because the destructive cross terms are applied and then cancelled in a few milliseconds within a single pulse sequence acquisition.¹⁷

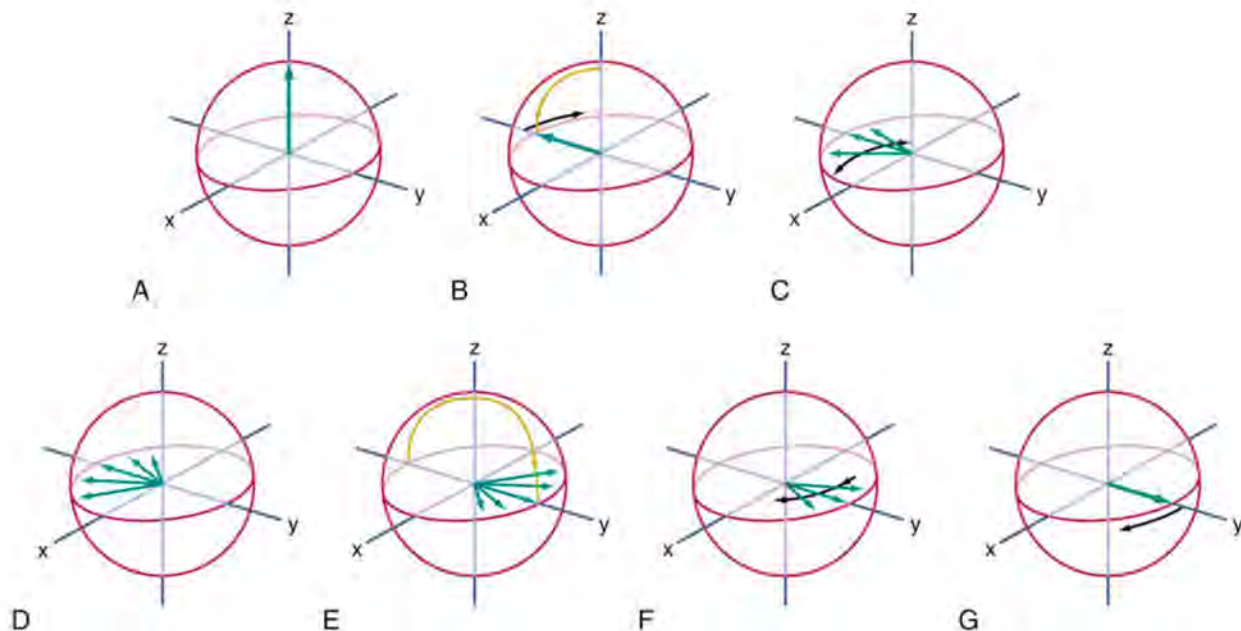


FIGURE 14.2 The spin echo inversion pulse. (A) The vertical green arrow is the average magnetic moment of a group of protons. All are vertical in the main field and spinning on their long axis. (B) A 90-degree pulse (yellow arrow) has been applied that flips the arrow into the horizontal (x - y) plane. The black arrow shows the precession of the net magnetic moment. (C and D) Owing to T_2^* effects, as the net moment precesses, some protons slow down because of lower local field strength (and so begin to progressively trail behind) while some speed up because of higher field strength and start getting ahead of the others. This makes the signal broaden progressively, dephasing and decaying. (E) A 180-degree pulse is then applied (yellow arrow) so that the slower protons lead ahead of the main moment and the fast ones trail behind. (F) Progressively, the fast moments catch up with the main moment and the slow moments drift back toward the main moment. (G) Complete refocusing has occurred, and at this time an accurate T_2 echo can be measured with all T_2^* effects removed. Quite separately, return of the green arrow toward the vertical (not shown) would reflect the T_1 relaxation.¹⁹

Illustration by AG Filler. © GDFL 1.3/CCASA 3.0, image. http://en.wikipedia.org/wiki/File:Spin_Echo_Diagram.jpg.

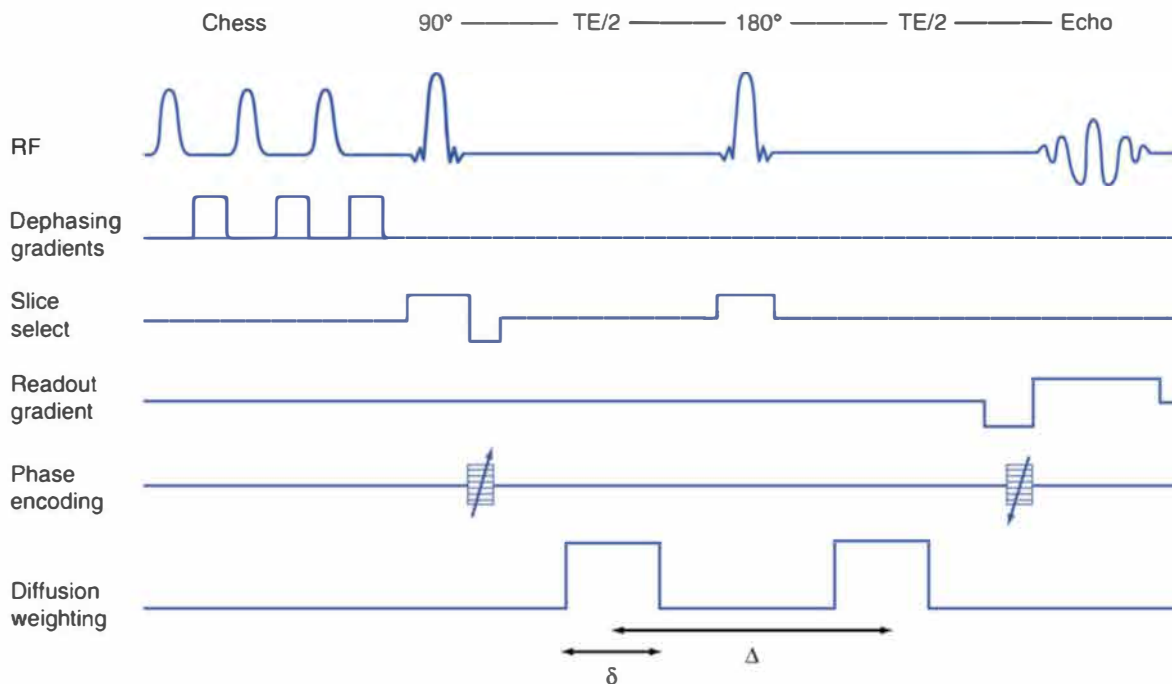


FIGURE 14.3 Radiofrequency (RF) and gradient pulse timing of the spin echo sequence modified to incorporate fat suppression and diffusion weighting. Note the position of the readout dephasing gradient, which is placed toward the end of the sequence to minimize the effects of coupling between the imaging and diffusion-weighting gradients.¹³ The two split parts of the phase-encoding gradient are oppositely polarized and placed symmetrically around the time of the 180-degree inversion RF pulse. This arrangement nearly eliminates cross terms and allows high-resolution imaging no matter the angle of the diffusion gradient relative to the x , y , and z location gradients. This is the key inventive advance that made all subsequent diffusion tensor and vector anisotropy methods possible. The authors produced the first pyramidal tract tractogram within a few weeks of the discovery.

From Howe FA, Filler AG, Bell BA, Griffiths JR. *Magnetic resonance neurography*. *Magn Reson Med*. 1992;28(2):328–338.

The next step in the development of DTI was to show that diffusion-related MRI could in fact detect directional structure in brain tissue as the inventors had anticipated when multiple directions of off-angle diffusion gradients were used and a mathematical calculation of a vector or tensor direction was made in each voxel—a method developed with regard to vectors by Todd Richards (one of the US patent number 5,560,360 co-inventors from the University of Washington) and extended to tensors by Filler.

The final step was to apply the connected voxel algorithms that had been used for MR angiography to the directional information in each voxel so that selected white matter tracts could be visualized by starting at a seed location and using the orientation data to march along from voxel to voxel with a result that shows the actual white matter tracts in the brain in a way that could be captured in a medical image. This was developed by Jay Tsuruda (a neuroradiologist who is a coauthor of Moseley's seminal 1990 paper¹⁵), the fourth of the University of Washington US patent number 5,560,360 inventors in further work with Filler. These original discoveries that underlie the technology were made 30 years ago. There are now more than 20,000 peer-reviewed publications in this field, and the pace of research and optimization continues to progress.

History of the Invention of Diffusion Tensor Imaging

This work emerged from two groups working in this area during 1991 and 1992 on the fundamental method of data acquisition for DTI—one team led by neurosurgical resident Aaron Filler and colleagues at the University of Washington (Todd Richards and Jay Tsuruda) and University of London (Franklyn Howe)^{18,19} and, separately, a second team led by Peter Basser²⁰ and Dennis Le Bihan²¹ at the National Institutes of Health (NIH). In 1994 Peter Basser, an engineer, and Denis Le Bihan, a physician with training in neurosurgery and radiology, along with James Mattiello, a medical physicist, published a critical foundational paper in this field setting forth the mathematical basis for the design of the imaging method.²² The first pyramidal tract tractogram image from the Filler group was published in 1996²³ (filed in 1993) and the first from the Basser group, with Carlo Pierpaoli, appeared in 2000.^{24–26}

Both Filler and Basser were involved in strain gauge mathematics at Harvard University in the early 1980s—Basser as an undergraduate and Filler as a graduate student. This was one of two areas in which tensor mathematics was applied at Harvard's Museum of Comparative Zoology (Functional Morphology group) and Department of Anthropology.^{27,28} The application of the tensor method in structural and functional biology was taught by Filler and others as part of Harvard's Biology 21 course. Filler also worked with Terrence Deacon doing axonal transport tracer studies to study the anatomy of the arcuate fasciculus in primates²⁹ and for peripheral nerve imaging.³⁰ Filler had been applying multivariate mathematics for analysis of brain anatomy dating back to a bachelor's thesis at the University of Chicago in 1977.

In 1990 Lisa Tauxe,^{27,28,31} working with David Pilbeam's team at the Department of Anthropology at Harvard, published an application of tensor mathematics for use in the field of magnetic stratigraphy—the use of changes in the direction of the earth's magnetic field to identify stratigraphic layers. This was to support efforts to provide dates for hominoid fossils from the Miocene era (12 million years ago) in the Siwalik mountains of Pakistan. In the method, magnetometer data were collected from six different directions for each rock sample, so that a tensor could be determined that showed the orientation of the magnetic field in each sample. Numerous samples were collected, their orientation was noted when they were collected, and then each was subjected to tensor analysis from multiple directions so that magnetic flux stratigraphic lines in the mountainside could be determined.

Filler was a graduate student and lecturer in this research group (1979–1984), but later applied this exact mathematical paradigm to axonal directions to determine tracts in the brain, along with colleagues Todd Richards, an MR physicist who created software to determine the vector array for the brain; Franklyn Howe, who designed MRI pulse sequences capable of acquiring the data; and Jay Tsuruda, a neuroradiologist who showed how to postprocess the image data to depict the tracts. Both Tsuruda and Richards had trained under Michael Moseley, who introduced diffusion-weighted imaging (DWI) to brain imaging in 1990.^{15,32-34}

Filler, who in 1990 was a fourth-year resident in neurosurgery at the University of Washington under H. Richard Winn, filed a National Research Service Award (NRSA) grant application for a new method of MRI with off-angle gradients for anisotropic diffusion imaging in May 1991. This was rejected by NIH in October 1991 on the grounds that (1) the project was just about developing a method and had not focused on any one specific neurological hypothesis and (2) Filler had been unable to identify any experienced supervisor in this field (a field that had not yet come into existence).

Filler was seconded to London to work as a neurosurgery registrar at Atkinson Morley's Hospital in Wimbledon—the site where Hounsfield invented and built the first CT scanner.¹⁹ In light of the NIH grant rejection, the consultant neurosurgery staff of Atkinson Morley's Hospital—David Uttley, Anthony Bell, Henry Marsh, and Anne Moore—decided to put up funds from the hospital research foundation to support the project. When the project succeeded, Filler gave the first report of the new advance in imaging axonal flow by MRI at a joint meeting of the Society of British Neurological Surgeons and the New England Neurosurgical Society at a September 19, 1991 conference at the National Hospital for Neurology and Neurosurgery at Queen Square in London.

Peter Basser came to NIH in 1991 as an engineer working on strain gauges and magnetic stimulation of nerves, with no involvement or background in medical imaging. In September 1991, he came across a poster from another NIH scientist, Denis Le Bihan, showing early work in MRI of diffusion anisotropy. Basser realized that the tensor formalism he had learned as a student at Harvard could be applied to solve part of the imaging problem that Le Bihan was struggling with. On November 11, 1991, he wrote a confidential letter to several colleagues proposing the mathematical tensor solution to determining the orientation of diffusion in a voxel in MRI,²⁰ essentially applying the same mathematics in which both Filler and he had been trained by the same sources at Harvard.

Filler, Howe, Richards, and Tsuruda—the four inventors on the Seattle/London patent—had poster presentations at the International Society for Magnetic Resonance in Medicine meeting in Berlin in August 1992; Basser, Le Bihan, and Mattiello had their poster in the same hall at the same meeting. Michael Moseley, one of the leading diffusion MRI scientists, saw the posters from Filler, Howe, Richards, and Tsuruda in Berlin, obtained copies of their images from them, and presented the work as part of a plenary session for the annual meeting of the Society for Magnetic Resonance Imaging in San Francisco in March 1993 in front of hundreds of MRI scientists. Denis Le Bihan was the moderator of the San Francisco session. The Seattle/London patent²³ was filed in March 1993 as well, and subsequently Basser, Le Bihan, and Mattiello filed their patent²⁵ in August 1993.

However, despite filing a patent, neither Basser nor Le Bihan knew how to collect the off-angle diffusion data necessary to actually make the image. Filler and Howe solved this problem and generated the first image data.

Richards wrote a program in Fortran on a Mac computer that took the diffusion data and then performed the voxel-by-voxel calculation on an actual brain MRI image data set to determine a mathematical summary of neural direction in each voxel of a brain image. Tsuruda showed how to generate a pyramidal tract tractogram from Todd Richard's data by mathematically marching from voxel to voxel, and the result of the work by the four inventors is **Figure 17** in US patent number 5,560,360—a patent with initial filings in the United Kingdom in March 1992 and completed filing in the United States in March 1993²³ (**Fig. 14.4**).

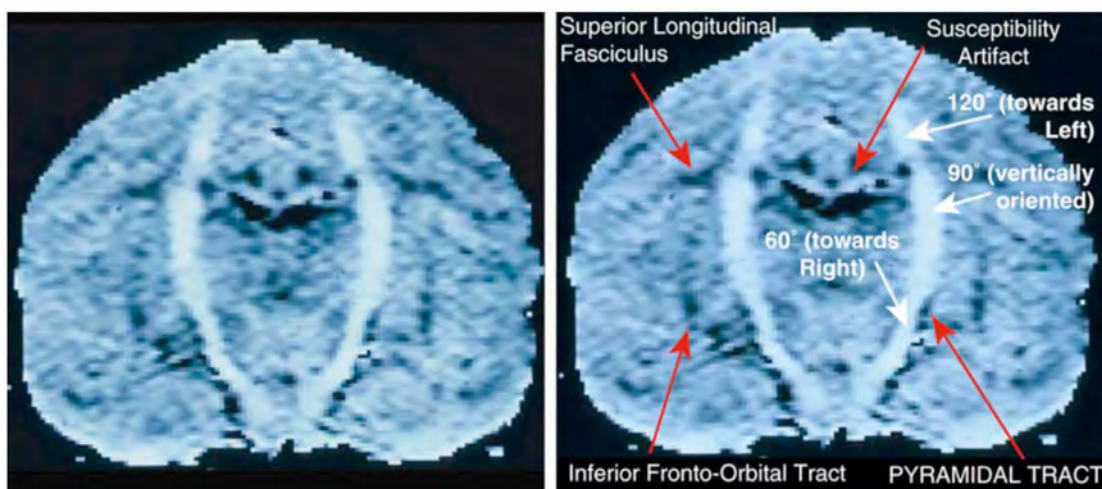


FIGURE 14.4 The image on the *left* is the first tractogram explaining in the patent that an infinite number of gradient directions could be applied and then calculated by tensor and vector analysis methods. This image was made by applying a seed-based connectivity algorithm from an MR angiography application but using the criteria of adjacency and similarity of arctangent orientation to select and extend voxel inclusion. The result was a curving tractogram on each side, selectively showing the pyramidal tract bilaterally.

From Filler AG, Howe FA, Richards TR, Tsuruda JS. Image neurography and diffusion anisotropy imaging, US Patent 5,560,360,¹⁶ filed March 8 1993 with priority to March 9, 1992. **Figure 17**.

Basser, Mattiello, and Le Bihan filed their patent in August 1993,³⁵ but it covered only a proposed method for collecting DTI data at a voxel level, with no means of performing the voxel-by-voxel calculations in an image array, and no method for tractography. They could not create a recognizable first brain image, but only rotated a pork loin in an MRI scanner to show that the fibers would change intensity when the muscle tissue was reoriented.

The key difference in the two images—a set of two-dimensional gray patches versus a pyramidal tract tractogram—was due to a discovery by Filler and Howe, which they reported in 1992¹³ but which Basser and Le Bihan and others failed to notice in the literature. Many researchers at the time knew that a tensor method needed to be developed. Both Filler and Basser were familiar with the tensor mathematics. However, none of the other scientists solved a difficult issue in MRI physics that was blocking the way forward.

There is an interference that arises, called a *cross term*, in which the magnetic field from a diffusion gradient shot in at an off angle disrupts the magnetic field from the location gradients that are along the *x*-, *y*-, and *z*-axes of the scanner, which are necessary for MR imaging. Multiple researchers at the time knew that this was the unsolved problem (see Moseley et al.,¹⁵ Mori and van Zijl,¹⁷ Le Bihan et al.,¹⁴ and Conturo et al.³⁶). Indeed, Basser reported in his history that when he told Le Bihan they just needed to measure the diffusion signal in six different directions, he was crestfallen when Le Bihan said he knew this was necessary, but no one knew how to do it.²⁰

This was the problem that Filler and Howe solved in February 1992³²—developing a process of refocusing the location gradients in order to virtually eliminate the destructive cross terms. Mori and van Zijl published a nearly identical strategy to reduce the interference in their 1995 paper,¹⁷ but this was not sufficient by itself to make DTI possible. As pointed out by the Filler group, with this solution set forth in detail in their patent, diffusion gradient application directed from an essentially infinite number of different directions is possible.²³

The Basis of Diffusion Anisotropy Imaging Physics Underlying the Image Signal in Nuclear Magnetic Resonance

The physical basis of the DTI technique is that water tends to diffuse more rapidly along the long axis of an axon as opposed to diffusing transversely through the walls of the axon. At a theoretical level, water should be able to diffuse transversely through axon membranes and myelin sheaths, but the directionality of water diffusion in neural tissue is well proven. When water diffuses uniformly in all directions in a material or tissue, that pattern is described as isotropic, or equal in all directions. When there is a preferred direction of diffusion, then the behavior of water in that tissue is termed anisotropic.

Fundamentally, MRI scanning is based on measurement of nuclear spins of water protons. A proton in a given compound (such as the hydrogen proton in a water molecule) spins around its axis at a rate that is related to a surrounding magnetic field based on the Larmor equation. Stated simply, for example, if the applied magnetic field is at 4.7 T, the water protons will have an intrinsic spin rate of exactly 200 MHz (200 million times around per second). If radiofrequency (RF) energy is pumped into the volume of water in the 4.7-T field at a frequency of 200 MHz, then that will be introducing energy at exactly the resonant frequency of those protons, and they will commence absorbing the energy.

At the start, all of the protons can be thought of as standing vertically, each spinning on its axis and all aligned with the direction of the main magnetic field of the scanner. The absorbed energy cannot make the proton spin any faster; however, like a top, the proton's magnetic axis may be pushed off of vertical so that the protons begin to precess, all coherently with one another, in response to the incoming wave of the applied RF signal. In MR, a pulse of RF is applied at the exact necessary frequency and then the RF is turned off and an antenna is brought into use to detect an RF signal coming back from the spinning protons as they coherently precess en masse, giving off their excess energy as the "spinning tops" return toward vertical. With elapsing time—a few microseconds—the excess energy will gradually be transmitted out of the coherently spinning protons, and the signal from the protons will decay away as their vertical axis of spin returns to alignment with the main magnetic field.

In T1 or T2 MR paradigms, the rate of decay provides the image contrast, with some tissues having faster or slower rates of decay. T1 decay relates to interactions between the spinning protons and magnetically active components in surrounding tissue components, whereas T2 contrast is related to decay interactions with other spinning protons.

Use of Location Gradients to Create a Magnetic Resonance Image

The difference between nuclear magnetic resonance (NMR)—a laboratory technique going back to the 1950s—and MRI is the application of "locational" magnetic gradients that establish a three-dimensional Cartesian grid in MRI.¹⁹ A gradient is an addition to the main magnetic field such that, for instance, for voxels on the left side of the imaging volume the field strength is at 4.72 T and for voxels on the right side of the volume the field strength is at 4.68 T. The spin frequency for protons in the voxels on the left will be higher (e.g., 200.1 MHz), and the resonant frequency for protons in the voxels on the right side will be lower (e.g., 199.8 MHz).

The gradient is turned on briefly by running an electrical current through a loop of wire that results in generation of a magnetic field. The field is strongest near the loop and lowest at a distance, so there is a gradient from weak to strong along one direction. A first gradient is applied from head to foot (axial or *z*-axis—"slice select"), a second gradient is applied from back to front (anteroposterior or *y*-axis—"phase encode"), and a third gradient is applied right to left (transverse or *x*-gradient—"frequency encode"). When all three gradients are used, each voxel in the three-dimensional volume will have a unique and different field strength, so each will have a unique and distinct resonant frequency and phase. The system can learn about signal strength in each voxel and know exactly where in the three-dimensional grid each of the voxel signal return sources is located.

With this—the invention of MRI (by Paul Lauterbur and by Raymond Damadian¹⁹)—it became possible to individually and separately address different voxels in an image. If one wanted to test a voxel in the lower left part of the volume in the back, one would use a lower precise frequency to stimulate and the antenna to learn the decay rate in that voxel, and so on. In this fashion the decay rate could be individually measured in each separate voxel in the imaged volume, such as the brain. Operationally, all the different frequencies are pumped in at the same time (often slice by slice). The receiving antenna receives a complex cacophony of thousands of signals at the full array of frequency and uses the mathematics of Fourier transforms to sort the data into an ordered array of data measurements. The measurements are repeated a number of times over—for example, a second—and some voxels will begin to decay in strength faster. For a T2 image, voxels with cerebrospinal fluid (CSF) will decay slowly and will still have a bright strong signal at the end of the second, whereas voxels with denser brain tissue will have return resonance signals that decay more rapidly and so can be shown as a darker voxel (three dimensional) or a darker pixel (two dimensional) on an image on the screen.

Diffusion-Weighted Magnetic Resonance Imaging

Diffusion MRI is based on the addition of an additional magnetic field gradient during the image acquisition. In this case the gradient is used to make a measurement of the diffusion of water. When the diffusion gradient is applied there will be (as for the imaging gradients), for example, a higher field strength on the left side of the voxel and a lower strength on the right side of the voxel. If water molecules with their protons diffuse (physically move or spread owing to brownian forces of energy such as heat) equally in all directions, then the diffusion is isotropic or equal in all directions.

At the initial instant of the imaging experiment, all the water molecules in the voxel are set to precessing coherently, all spinning at their resonant frequency for the applied field strength (e.g., 4.7 T, so 200 MHz). However, as some of the water molecules wander, by diffusion, into an area of the voxel where the applied diffusion gradient is stronger, they will speed up. Others will diffuse or spread into areas of the voxel where the applied main magnetic field is weaker and will slow down by a small amount. Very soon the various water protons in the voxel will each have their own distinct spin rate frequencies. The coherence of the signal will have decayed owing to their diffusion or physical movement in the voxel.

In a voxel with isotropic diffusion (e.g., CSF), this decay of the coherent signal due to diffusion movements will happen at exactly the same rate whether the diffusion gradient is applied from right to left or from head to toe, and so on. However, in axons, diffusion is anisotropic. Water molecules diffuse preferentially up and down the length of an axon. If, for instance, a peripheral nerve is to be imaged as to diffusion, we can consider what happens when a gradient is applied perpendicular to the nerve direction. The entire length of the nerve will travel along at one level of the gradient strength. The water diffusion preferentially up and down the length of the axon will not experience decay from diffusion, because as the molecules diffuse up and down along the axon, they remain at the same gradient strength. However, if the gradient is then turned so that it is applied down the length of the nerve—higher strength proximally, lower strength distally—then as the water diffuses the molecules will move rapidly into higher or lower magnetic field strengths at a rapid rate and there will be accelerated decay from diffusion.

In isotropic tissue, the gradual decay rate caused by the diffusion gradient is the same no matter which way the gradient is oriented. However, for an anisotropic tissue such as a nerve axon, the rate of diffusion decay is highly dependent on the orientation of the applied diffusion gradient. Because of this difference, a given voxel will remain brightest when the gradient is applied perpendicular to the long axis of an axon passing through it; will be intermediate in decay rate if it contains isotropic tissue; and will decay rapidly, becoming dark in intensity, if it contains an axon and the gradient is applied parallel to the direction of the axon. Because of this, we can learn about the direction in which an axon is oriented by the way its image signal strength responds to the orientation of a particular applied diffusion gradient.

Diffusion MRI was first introduced into clinical use because of its capability to detect stroke in an MRI scan. There is a characteristic pattern of image intensities in a brain MRI image slice when diffusion gradients are applied. However, in the setting of stroke, axons start to lose their apparent diffusion when they suffer infarction. Therefore the image characteristics of a diffusion-weighted MR image will start to change in an area affected by stroke. The affected area of neural tissue will begin to act as if it were restricted or decreased rather than unrestricted. For diffusion-weighted MRI, there is no need to know the precise direction of diffusion.

One additional technical aspect of diffusion MRI is that the diffusion gradient is pulsed on twice during each acquisition to actually detect the effect. In essence, it is turned on briefly to “label” the protons by giving them a particular coherent spin at their location at the beginning of the acquisition and then it is pulsed on a second time a few milliseconds later with the two pulses symmetrically placed on either side of the 180-degree inversion pulse. The difference in physical position in the gradient between the two pulses will sharply and precisely delineate the effects of diffusion. This is called a Stejskal-Tanner pulse after its two developers.^{19,37}

Diffusion Anisotropy Imaging: Tensor and Vector Techniques

As described earlier, when the orientation of a nerve is simple and linear and known in advance (such as the median nerve in the upper arm), diffusion-weighted gradients can be applied parallel or perpendicular to the nerve to show the anisotropy, or health, of the nerve. However, as in many locations for peripheral nerves and for most locations in the brain, neural tracts will curve and turn as they progress, so there is no simple method of planning a perpendicular or parallel diffusion gradient. In DTI or in vector versions (e.g., HARDI, Q-Ball imaging), a larger number of gradient directions are applied and mathematical methods are then used to calculate neural direction on a voxel-by-voxel basis.

Note, however, that the diffusion gradients have to be set to about 10 times the strength of the location gradients in order to work. Without diffusion gradients, there is an ordered array of magnetic field strengths voxel by voxel in a cube generated by the x , y , and z gradients. With the addition of a far more powerful gradient from some off angle, the ordered array of field strengths set up by the location gradients, particularly the “phase encode” or y gradient, turns to chaos. These interactions are called cross terms, and they made it impossible to actually get a useful image when off-angle gradients were applied to generate tensor data.

For standard diffusion-weighted MRI, a single diffusion gradient could be applied parallel to one of the location gradients. The cross terms could be managed in this situation by using a balanced opposing pair of gradients—for example, one pointing along the x -axis and a second one pointing in the same orientation but from the opposite direction.³⁸ However, to calculate a tensor, it was necessary to send in diffusion gradients from multiple different angles. As Mori pointed out,¹⁷ the two balanced pulses Neeman³⁸ had proposed have to arrive at substantially different times, so diffusion is progressing between the two arrival times and therefore full correction is not possible. With the added the complexity of a gradient that is not parallel to the location gradient, the geometry of correction becomes inordinately complex. The cross terms get far more complicated. There is then the additional issue that multiple images, at least seven, will be obtained with different gradient orientations, so failures of compensation will be different from one gradient direction to the next, even as the water molecules are diffusing in complex, anatomically determined pathways that do not follow a Cartesian grid.

The fundamental invention that created the field of DTI—which is wholly attributable to the Filler group in their US patent number 5,560,360—was a method for allowing a non-Cartesian gradient (a gradient not directed along the x -, y -, or z -axis) to be applied without destroying the locational gradients (x , y , and z). Unlike in other scientific fields (such as the use of tensor analysis to determine the direction of magnetization in anisotropic rocks by the Harvard group where Filler trained [Tauxe²⁷ and colleagues]) the same physical process (precisely oriented magnetic field gradients) is used to create the image in MRI and to apply the method for disruption to assess diffusion direction and anisotropy.

Filler identified the problem in 1991 and tasked Franklyn Howe, an MRI physicist, with finding a refocusing method that would work intrinsically with each gradient orientation (no balanced pair). Howe developed two different methods of refocusing the location gradients immediately after each application of a diffusion gradient so that diffusion could be measured in any direction without disrupting the image being created simultaneously by the image gradients. This

discovery was published in 1992¹³ showing detailed high-resolution imaging despite application of an off-angle diffusion gradient. With this problem solved, there was no limit to how many diffusion gradient directions could be obtained without the image being significantly affected by cross terms.

In addition, based on work by co-inventor Todd Richards, the group showed that the image could be constructed in an entirely novel way. In radiography, CT, MRI, and DWI, the result of imaging is that each voxel in the image is ultimately assigned a single image intensity number (a scalar quantity). These various shades of black, gray, and white make up the image, whether as exposed silver grains on a film or as pixel intensities on a computer monitor screen.

In the diffusion anisotropy techniques (e.g., DTI, HARDI, Q-Ball), each voxel becomes the subject of a mathematical calculation, with the result that it contains one or more vectors and not a single scalar quantity. The direction(s) of the vector will show the orientation of axons in the voxel, and the length of the vector will show the health or relative degree of anisotropy in that voxel. For simple DTI methods, each voxel can contain only one vector. For the vector methods HARDI and Q-Ball, for instance, there can be multiple vectors in the voxel, illustrating the fact that there may be crossing, joining, or splitting brain tracts captured within a single voxel. Richards et al.^{38a} published this methodology for mathematically combining the several different diffusion direction image acquisitions into a single image whose voxels contained the directional information in 1992 as well.

For all of these diffusion anisotropy methods, the fundamental paradigm is to collect the image by using multiple diffusion gradients (each as a Stejskal-Tanner paired pulse^{19,37}). The gradients for a tensor method must be applied in a minimum of six different directions; modern DTI/DVI (diffusion vector imaging) scanning is typically done with about 30 directions of diffusion, but there may be as many as 256 directions of diffusion gradients applied for super-high resolution analysis. The MRI unit may still have the original design of just three gradient coils used for the three imaging gradients (*x*, *y*, and *z* directions). However, by turning two or all three of them on together in multiple varying strengths, the scanner can generate an infinite number of diffusion gradient orientations. The gradient refocusing is carried out in the course of each gradient acquisition.

Prior to this advance, in papers such as the Moseley work on anisotropy, the researcher would publish a grid of four images, one routine with no diffusion, one showing how the slice appeared with an *x*-direction gradient, one with the *y*-direction appearance, and one with the *z*-direction appearance. Using Todd Richards's method, it was possible to do a calculation for each voxel that incorporated all of the image results for that voxel and produced an invariant result. The data in the voxel would show the calculated orientation in space of an effective vector (either truly a vector or as the summary primary axis of a tensor). In addition, it would encode in the length of the vector—just how relatively isotropic or anisotropic the tissue was within that particular voxel.

The word *tensor* is involved for two entirely separate reasons. In physics the phenomenon of diffusion is called a tensor quantity. In anisotropic diffusion in various materials (rocks, polymer liquid crystal solutions, and so on) there is no single pure direction of movement, but rather the result is a sort of oriented ovoid or ellipsoid. It cannot be accurately and fully described by a single vector, but rather forms a sort of ovoid cloud of movement, with a long axis and two short axes. This is described as the tensor quantity phenomenon. One therefore can speak of the diffusion tensor as the quantity to be measured, although in clinical brain MRI we are interested in the orientation of axons and have no clinical interest in describing the niceties of "the diffusion tensor" of axonal tissue as a general physical phenomenon.

Separately, there is a type of mathematical analysis developed by Einstein called tensor analysis,^{19,38b,38c} which he applied to the study of space and time and also to the "Brownian motion" of diffusion. This mathematics is one of a number of mathematical techniques that can take an input of multiple vector measurements and convert them into a result that reveals the orientation and length of the principal axis of the ellipsoid and the orientation and length of the two short axes (Fig. 14.5). This will show whether the ellipsoid is nearly spherical (as occurs in tissues with isotropic diffusion) or whether it is thin and elongated (as occurs in tissues with anisotropic diffusion), as well as determining the precise orientation in space of the principal or long axis of the ellipsoid. Typically in DTI of the brain, we are mostly interested in the long axis—its direction and how long is it (relative to the short axes). These are individually calculated for each voxel in the brain.

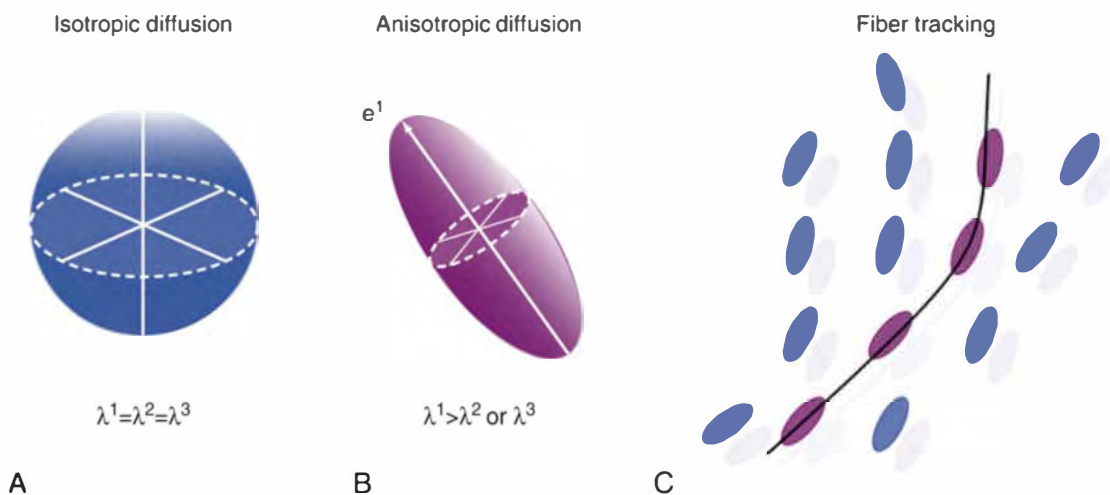
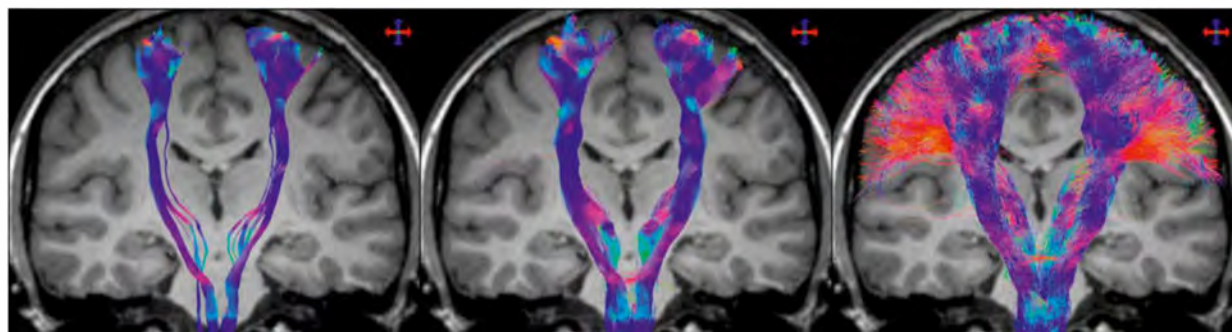


FIGURE 14.5 The principal eigenvector is termed λ_1 . This long axis of the ovoid representation of a symmetrical tensor volume is used as an effective vector to guide the tractography (fiber-tracking) process.¹⁵⁹
 From Lerner A, Mogensen MA, Kim PE, Shiroishi MS, Hwang DH, Law M. Clinical applications of diffusion tensor imaging. *World Neurosurg.* 2014;82[1–2]:96–109.

By contrast, in a vector mathematical analysis, multiple crossing, joining, or splitting tracts can be identified. A typical vector concept is based on treating each voxel as a multitessellated icosidodecahedron (polyhedron with 60 sides), like an elaborate buckminsterfullerene. We then simply ask if there are any faces of the polyhedron that are particularly bright on image acquisition. These will be potential multiple different axonal orientations within the single imaged voxel. There are

also statistical spherical deconvolution methods (Fig. 14.6) that can find multiple maxima for image directional intensity within the data space of each single vector. For certain regions of the brain, such as the optic radiation, the ability to follow multiple tracts and to follow tracts through sharp turns is critical for patient safety when tractograms are used to guide glioma surgery.



DTI + Deterministic algorithm

DTI + Probabilistic algorithm

CSD + Probabilistic algorithm

FIGURE 14.6 Fiber-tracking results in a healthy human subject obtained using a seed region in the brainstem and target region in the sensorimotor cortices. Coronal T1-weighted images overlaid with tractography results for diffusion tensor imaging (DTI) combined with a deterministic algorithm (left); DTI combined with a probabilistic algorithm (middle); and constrained spherical deconvolution (CSD) combined with a probabilistic algorithm (right). Data were acquired using 60 diffusion-weighted directions with $b = 3000 \text{ s/mm}^2$. The color-coding indicates the fiber orientation.
 Modified from Farquharson S, Tournier JD, Calamante F, et al. White matter fiber tractography: why we need to move beyond DTI. *J Neurosurg.* Jun 2013;118(6):1367–77.

The Method of Tractography

As a fourth aspect of the invention, Jay Tsuruda, a neuroradiologist, introduced the use of the connected voxel algorithm. This was a method under development at the time to improve carotid artery MR angiography. Tsuruda reprocessed brain image data produced by Richards to show that the algorithm could progress from voxel to voxel in a stepwise fashion. He also applied whole-volume ray projection (maximum intensity projection), but that method is not well suited to sorting out individual tracts. This led to the discovery that it was actually possible to produce images of brain tracts based on postprocessing of the voxel by voxel diffusion direction anisotropy data. The first DTI tractogram of the pyramidal tract appeared as Figure 17 in US patent number 5,560,360 (see Fig. 14.4).

The Bases of Fractional Anisotropy and Tractography in Brain Evaluation

Analyzing the Structure of the Voxel

Given that some data acquisition and data processing methods have filled the voxels of the brain image with an elaborate array of calculated effective vectors, the next step for many neurosurgical analyses is to proceed to further process the data into a clinically useful form. There are two major categories of final analysis. The first of these is to generate fractional anisotropy (FA) data. This is a simple further transformation that can abandon the directional information of the vectors and just ask whether or not the voxel is highly anisotropic. This is particularly helpful in evaluating closed head injuries.

Several different summary numbers can be obtained for each voxel, but FA is the most widely used. This is simply a matter of treating a completely isotropic voxel (e.g., the CSF in a ventricle) as having an FA of zero and of treating a highly aligned anisotropic voxel (e.g., the splenium of the corpus callosum) as having an FA of nearly 1.0. In fact, the highest FA in the brain is usually the splenium measurement, which is typically between 0.75 and 0.85. This measure can be used as a baseline for comparison with other individuals or for comparison with FA measures in other white matter tracts in the brain.

The gray matter of the brain has very low FA and cannot be evaluated with tractography. This is because there is no uniform coherent direction of diffusion in a voxel of gray matter. The mass of neuron cell components of axon and dendrite branches and hillocks is not susceptible to determination in currently available MRI scanners. There is no theoretical limit to the spatial resolution of MRI, but practically speaking, even with the most advanced experimental 7-T MRI scanners, the voxels size is about 100 microns on a side.^{38d} DTI FA analysis is therefore currently primarily a white matter technique.

The Tensor model produces what is often described as an ellipsoid. The details of the ellipsoid include its orientation in space, but also the measures of the three primary axes of the ellipsoid, termed (lambda) λ_1 , λ_2 , and λ_3 . If all three are equal, the result will be a sphere. Working with these three measures, several different summary results can be determined that have clinical significance (see Fig. 14.5).

$$\begin{aligned} \lambda_1 &= \text{longitudinal (axial) diffusivity (AD)} \\ (\lambda_2 + \lambda_3)/2 &= \text{radial diffusivity (RD)} \\ (\lambda_1 + \lambda_2 + \lambda_3)/3 &= \text{mean diffusivity (MD)} \\ \frac{\sqrt{\frac{1}{2} \sqrt{(\lambda_1 - \lambda_2)^2 + (\lambda_1 - \lambda_3)^2 + (\lambda_2 - \lambda_3)^2}}}{\sqrt{(\lambda_1^2 + \lambda_2^2 + \lambda_3^2)}} &= \text{fractional anisotropy (FA)} \end{aligned}$$

The most commonly used of these is FA based on the formula above, which forces the FA result number down toward zero when the three measures λ_1 , λ_2 , and

λ_3 are nearly equal—as in the sphere demonstrating an isotropic voxel in Fig. 14.5—and also magnifies the numerical effect of a “flattened” ellipsoid. This varies from 1 to 0, with a typical highest value in the splenium of the corpus callosum of as high as 0.85. This states how anisotropic or isotropic a given voxel is found to be. It is well established that with injury this number will generally be reduced. The axial diffusivity is similar but does not really balance with the two shorter axes. Radial diffusivity is an expression of the degree of isotropy. What has proven to be more interesting as the capability of MRI scanners has improved is the mean diffusivity. This is similar to the trace, which is 3 times the mean diffusivity. This measure is applicable to DTI studies of gray matter as well as white matter.³⁹⁻⁴²

Yet another measure of increasing clinical interest is kurtosis.⁴³ This is assessed with at least 15 directions of diffusion analyzed with a vector model. In a tensor model, all of the data gets forced into the one resulting ellipsoid oriented within the voxel. However, for vector models the voxel is filled with multiple vectors, some longer than others. The pattern of the set of vectors may reveal internal structure. This kurtosis measure of the uniformity or nonuniformity of the array of vectors has proven to be helpful for distinguishing some clinical conditions.

Carrying Out the Tractography

Tractography is clearly the most surprising and dramatic advance to emerge from the development of diffusion anisotropy imaging. Tractography involves a process in which the voxels are filled with vectors (or an effective vector summarizing the primary direction, or eigenvector, of the tensor ellipsoid) and then an algorithm is used to step from voxel to follow an axonal tract. This is a mathematical reinvention of retrograde axonal transport techniques that were used to map out the tracts of the brain starting in the 1950s. In those methods an axonal tracer stain compound would be injected into a location of interest in the brain of an experimental animal. The tracer would be carried along a tract by the natural phenomenon of axonal transport for a few days, after which the animal would be killed and the brain preserved, removed, sliced, and stained, and thereby the route of the tracer compound through the brain would be identified. Virtually all tracts of the brain had been mapped in this fashion, in tremendous detail, but obviously none of this could be used to evaluate human subjects.

DTI tractography works by having an operator select a seed location and then allowing an algorithm to check neighboring voxels to see if a neighbor has similar orientation. The algorithm then draws a tract from one voxel to the next and then looks for another neighbor that continues the direction without too sharp a turn and that has sufficient FA to have reliable directional data. Alternately, all the tracts of the brain are mapped at the outset and the user then selects a subset by placing a seed “ROI” (region of interest).

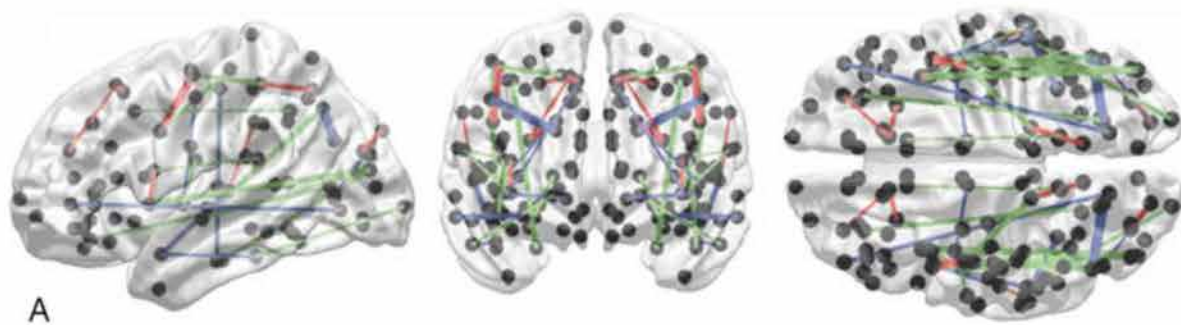
Tractography differs from general imaging because, like angiography, it is tissue selective—it only images white matter tracts. In addition, like, for example, angiography of the middle cerebral artery, it is often used to image one single tract of interest, leaving all others dark. An example is the situation in which a surgeon wants to achieve maximal resection of a glioma near the pyramidal tract (pyramidal tract = superior portion of combined corticospinal and corticobulbar tracts). A functional MRI (fMRI) paradigm may be useful—for instance, having the patient open and close the hand repeatedly during the acquisition of a blood oxygen level-dependent (BOLD) imaging acquisition will cause the hand motor cortex to be identifiable. The operator then selects that gyrus as one seed and then makes an anatomic selection of the crus cerebri (cerebral peduncle), and this will result in an image with just the hand portion of the corticospinal (pyramidal) tract. This can be projected into a routine detailed brain image. Then the surgeon is able to examine a detailed routine MR image of the brain and tumor, but with the critical hand corticospinal tract lit up in color, revealing its exact relation to the tumor, even if it has been distorted in its course and pushed out of the way by the tumor. This can also be projected into a heads-up display or into the visual field of a surgical microscope that has been integrated into an image guidance system so that the surgeon can see the tracts superimposed on white matter in view during operation (most accurate if the data are updated by means of intraoperative MRI after the skull is opened and as the dissection progresses).

The fiber assignment by continuous tracking (FACT) algorithm developed by Susumu Mori^{44,45} is widely used for tractography in systems such as Brainlab FiberTracking. However, the FACT method is a deterministic method that works effectively when only a single vector is present in a voxel. Some centers such as University of California at San Francisco (UCSF) have shown that probabilistic methods used with HARDI or Q-Ball data can be safer and more reliable for surgical guidance.⁴⁶ This is because a FACT algorithm brain tract originating at a seed (e.g., in the brainstem) will come to a halt and leave out two following tracts that split from each other. Probabilistic methods also allow for visualization of more than one direction in a voxel, such as occurs where two tracts join or where one tract passes through another tract. For these reasons, probabilistic tractography has been strongly preferred in many centers. These are sometimes called model-free methods because the mathematics involve various types of vector analysis as opposed to tensor analysis.

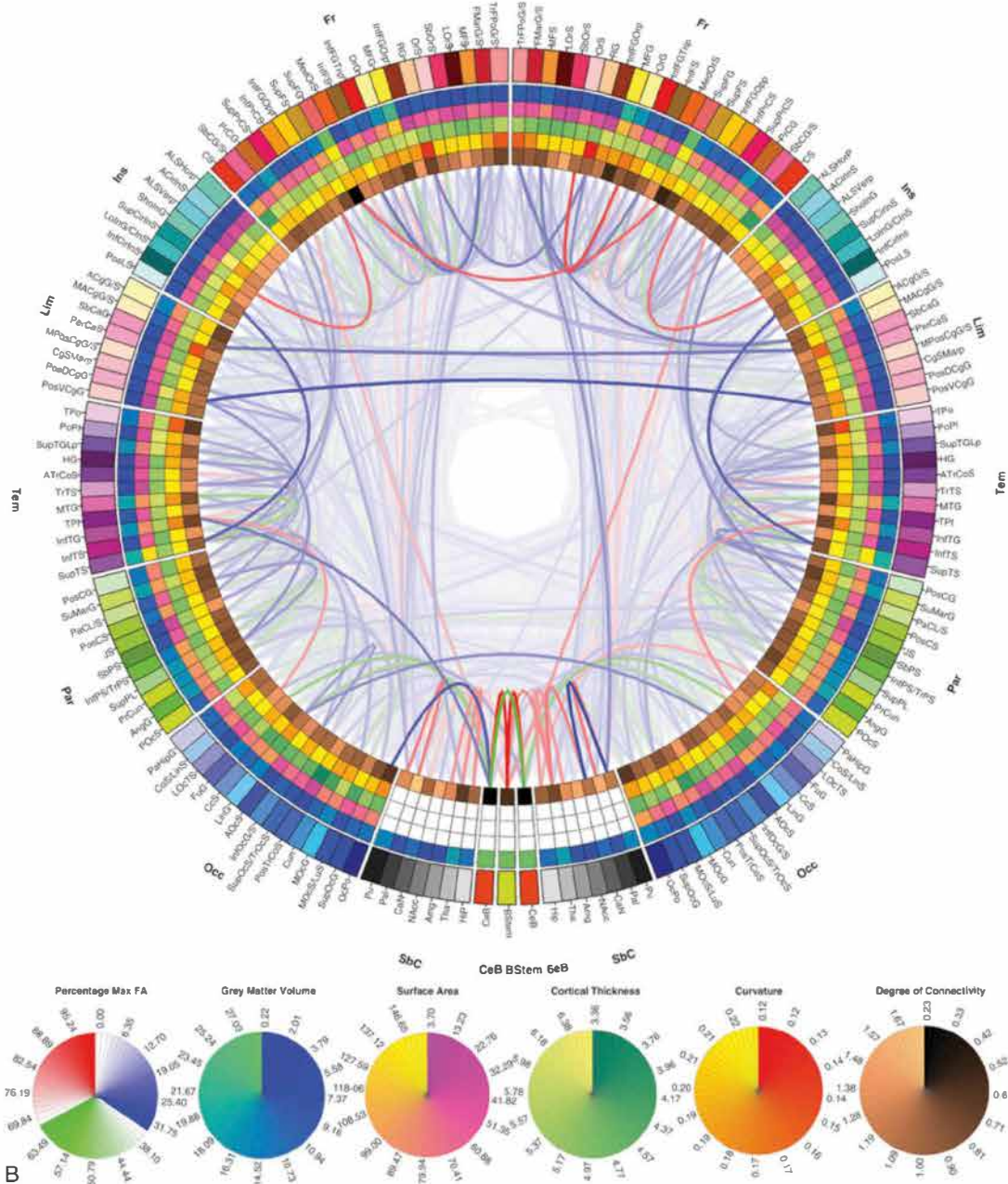
To some extent, simple transition to progressively higher spatial resolution, together with a few tweaks to the tractographic algorithm, can substantially improve the accuracy and safety of surgical guidance tractography. Although nontensor algorithms with probabilistic tractography have been viewed as more accurate and reliable in general, newer constrained spherical deconvolution methods (discussed later in the chapter) are now allowing the speed of deterministic tractography to be employed with accuracy that matches or exceeds the clinical accuracy of older probabilistic methods.

Connectomics and Constrained Spherical Deconvolution Mapping the Human Connectome

Inspired by and paralleling the Human Genome Project, the NIH launched the Human Connectome Project in 2009, with the result now exceeding 4000 peer-reviewed publications and a detailed map of the human connectome (Fig. 14.7).⁴⁷⁻⁴⁹ The fundamental methodology of the project was to reassess the classical parcellation of the cortical surface by authors such as Brodmann, who identified 52 areas based on histology in his famous 1909^{50,51} work, into finer detail such as 165 parcels by Irimia and colleagues⁵² or larger numbers such as 360 nodes of identified locations.⁵³ Currently this is accomplished by relying on fMRI, histology, anatomy, and even neurochemistry,⁵⁴ then determining the standard connections between and among the locations via high-resolution tractography (Fig. 14.8).



A



B

FIGURE 14.7 Graphical representation of the human brain connectivity scaffold. Standard three-dimensional (3D) graphs (A) and a connectogram (B) are used to visualize white matter connections whose removal leads to significant changes in network integration and segregation. Only connections with this property are represented, and the strength of the link associated with each of them is indicated by the F statistic of the test. Link transparency varies such that most transparent links are those associated with the smallest F -values, and the most opaque ones are associated with the largest F -values (see section “Statistical Significance of Edge Removals” in Irimia et al.⁵² for details). To facilitate visibility of the most prominent core connections, the significance threshold used for 3D graphs ($\alpha/m = 7.4 \times 10^{-9}$ where $\alpha = 0.0001$ is the statistical significance level, $m = G \times (G - 1)/2$ is the number of comparisons, and $G = 165$ is the number of parcels) is more stringent than for the connectogram ($\alpha/m = 3.7 \times 10^{-6}$ where $\alpha = 0.05$). The significance threshold used for 3D graphs (A) is more stringent than for the connectogram (B) in order to facilitate visibility of the most prominent core connections (A), as opposed to all the connections whose removal leads to statistically significant changes in network integration and segregation (B). Regions whose connectogram wedges are highlighted in *red* correspond to rich club nodes as identified by Van Den Heuvel and Sporns¹⁶⁴; the number of core scaffold connections and the complexity of their pattern compared with rich club interlinks both suggest considerable differences between the rich club network and the core scaffold (see discussion). For a connectogram in which network metrics rather than morphometric variables are encoded in each concentric circle, see Van Horn et al.¹⁶⁵

From Van Horn JD, Irimia A, Torgerson CM, Chambers MC, Kikinis R, Toga AW. Mapping connectivity damage in the case of Phineas Gage. *PLoS One*. 2012;7[5]:e37454; and Irimia A, Van Horn JD. Systematic network lesioning reveals the core white matter scaffold of the human brain. *Front Hum Neurosci* 2014;8:51.

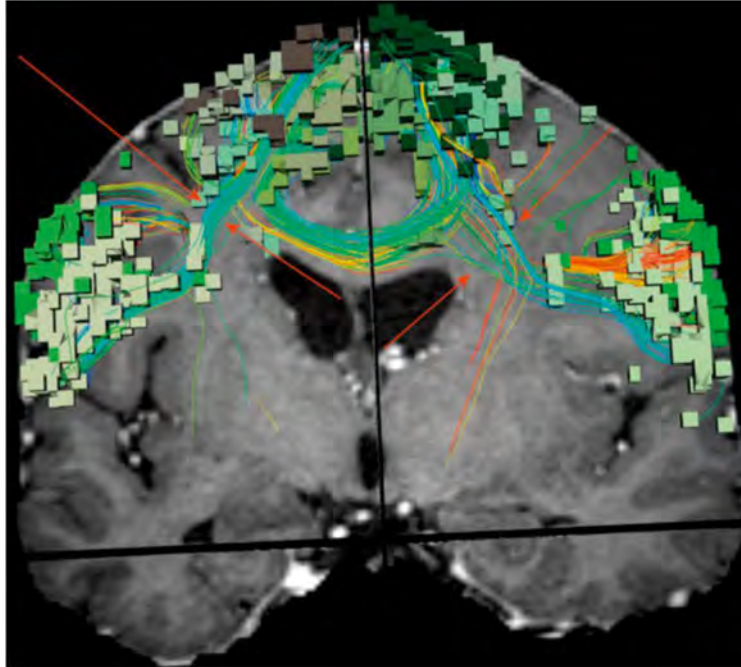


FIGURE 14.8 Tracts identified by connectomic analysis with origins in functional parcellation map. Note the splaying of tracts on the left side that link the area of the inferior frontal gyrus to the superior frontal gyrus (red arrows).

DTI cannot be used reliably for detailed connectomics because it obliterates many tracts that have crossing, joining, or splitting portions⁵⁵⁻⁵⁷ (see Fig. 14.6). Although a variety of nontensor methods have been developed, the bulk of the connectomics work was ultimately carried out using constrained spherical deconvolution (CSD),⁵⁸ a refinement of HARDI; these techniques are broadly classified as spherical vector methods as opposed to tensor methods.⁵⁹

With the dramatically improved efficiency of tract identification when CSD is used instead of DTI, it becomes difficult to use probabilistic methodology because of the vastly increased number of possible trajectories. Fortunately, deterministic tractography used with CSD produces highly useful anatomic data, so the combined use of these two methods has become an effective standard for many types of tractographic analysis.^{60,61}

However, a further problem arises in head injury analysis wherein measures of FA are essential. Voxels that have multiple directions of diffusion due to splitting, crossing, or joining fibers may incorrectly reveal low FA because of the absence of a single coherent direction of diffusion; an emerging solution for this issue is to supplement FA data with tract density measures summarized under the term *neurite orientation dispersion and density imaging* (NODDI).^{61a,61b} An effective solution is to use deterministic CSD or probabilistic CSD to map the tracts and thus avoid false termination points that make important tracts disappear, but then to perform a posttractographic sorting so that only those voxels with a single direction are queried as to FA.⁶²

Clinical Applications

Tractographic Guidance for Intracranial Resective Surgery

The capability for tractographic depiction of eloquent or functionally significant tracts greatly improves both safety and efficacy of glioma surgery and, in addition, plays an increasingly significant role in functional surgery.

For tumor resections, efforts to achieve the maximal safe resection are aided by tractographic information.^{8,63} For tumor resection, tractography is commonly used to develop depictions of the pyramidal tract for the reduction of risk of paresis and paralysis for tumors near the motor strip. To avoid fluent aphasias from injury to the arcuate fasciculus, surgeons may select seed points by obtaining fMRI identification of the Broca area in the inferior frontal gyrus and of Wernicke area in the superior temporal gyrus (Fig. 14.9).^{63a}

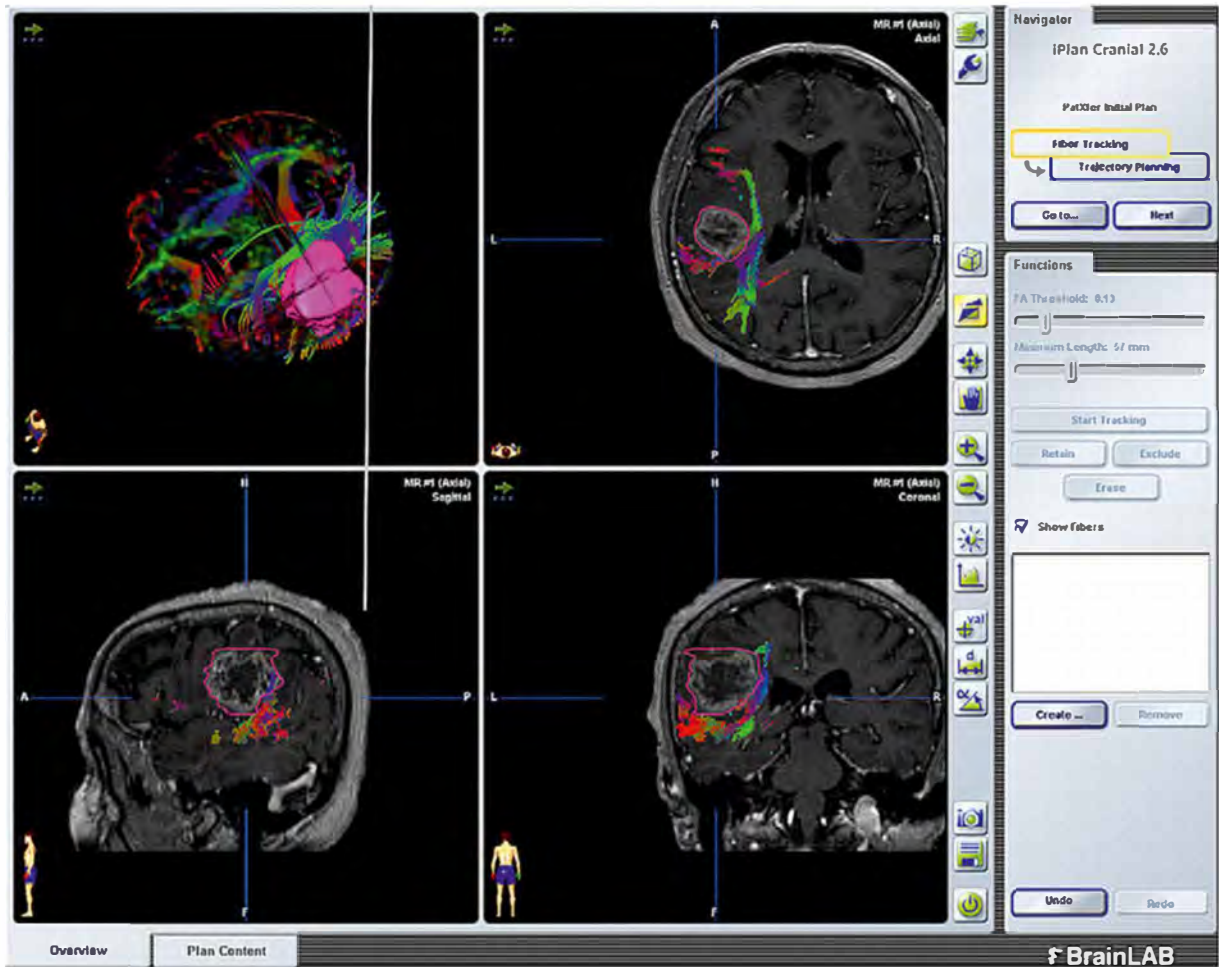


FIGURE 14.9 Tractography seeded from fMR imaging activated voxels in Broca's and Wernicke's areas: screensave from BrainLAB neuronavigational software (clockwise from top left: tractography in three dimensions, and overlaid on axial, coronal, and sagittal contrast T1-weighted images).fMR imaging and DT imaging data show segmented tumor in left parietal lobe (right side of image is left side of patient) causing medial displacement of the arcuate fasciculus fibers.
Image courtesy Nicole Brennan, The New School for Social Research, New York, NY.

There have been repeated attempts to accurately assess the impact of intraoperative tractography on extent of resection.⁶⁴⁻⁷⁴ These studies have tried to balance advances in tractographic technology with other aspects of technical advances in glioma resection.⁷⁵ The leading edge of this field at present is around efforts to pull multimodality data about function, various assessments of edema, tumor penetration of tracts, and advanced methodologies to accurately determine the true functional contours of tracts to directly guide surgery.⁷⁶⁻⁷⁸

The optic radiation is often put at risk because a contralateral upper quadrantanopia can develop, affecting visual input from both eyes when an injury to the Meyer loop occurs during a temporal lobe resection for tumor or for treatment of epilepsy.⁷⁹ A tractographic depiction can be obtained from the anatomic landmark of the lateral geniculate body following tracts that reach from there to the occipital cortex arrayed around the calcarine fissure. The risk occurs because the Meyer loop portion of the optic radiation proceeds anteriorly into the temporal lobe before turning 180 degrees to reach the occipital cortex. This area of anatomy is a particular weak point for deterministic tractography based on diffusion tensor paradigm imaging but is generally well handled by probabilistic tractography with vector (HARDI or Q-Ball) data.⁸⁰⁻⁸⁵

Improved Access to Functional Stimulation and Lesion Sites

Another important impact of tractography is to greatly expand the range of accessible functional targets for stimulation and lesioning in functional neurosurgery.⁸⁶⁻⁹¹ This is particularly the case when an important treatment goal requires access to a small nucleus with many adjacent nuclei where injury must be avoided. Reaching the target with an electrode may be rendered unfeasible by the necessity of avoiding damage to other nuclei. An alternative in some situations is to select the target nucleus and then generate a tractogram showing the course of a projection that may be more readily and safely accessed for stimulation or lesioning. The tracts from adjacent nuclei can be mapped separately to ensure that they will be avoided.^{92,93} In addition, the area around the intended lesion or stimulation site on a projecting tract can be used as a seed to learn whether any other eloquent tracts are too close.

In addition to the experience with tractographic assistance for the placement of stimulation targets and surgical lesioning, tractography is now playing an increasingly important role in incisionless functional procedures such as focused ultrasound, which takes place entirely in the setting of the scanner performing the tractography.^{94,95}

Evaluation of Closed Head Injury

Studies of FA and tractographic interruptions play an increasingly crucial role in evaluation of closed head injuries. A number of deficits seen after concussion can now be matched to specific tract injuries. This is important because a small area of injury affecting a critical tract can cause a very significant deficit. Further, sequential objective FA measurements reveal whether a patient is likely to develop dementia, chronic traumatic encephalopathy (CTE), or other progressive disorders. Longitudinal studies have shown that FA losses and mean diffusivity changes are correlated with development of cognitive deficits in patients who sustain head injury and sports-related concussion.^{96,98}

Overall, it is compellingly clear that traumatic brain injuries that do not result in acute abnormalities on routine CT or MRI often do result in characteristic abnormalities detectable with DTI scanning.^{98,99} Furthermore, there is mounting evidence that specialized DTI studies can be used to make early predictions about which head-injured patients are more likely to have persisting symptoms, contributing to the 10% to 20% of patients who do not follow the normal arc of improvement after injury.¹⁰⁰ There is also considerable methodologic variability; many radiologists who are not equipped with advanced software for processing and analyzing DTI studies have relied on simple one-point assessments of FA levels in the corpus callosum¹⁰¹ or temporo-occipital white matter.¹⁰² Increasingly, evaluations of patients with closed head injuries involves extensive analysis of numerous locations for statistical assessment of FA changes, methods that have shown high reliability and reproducibility (Fig. 14.10).¹⁰³⁻¹⁰⁵

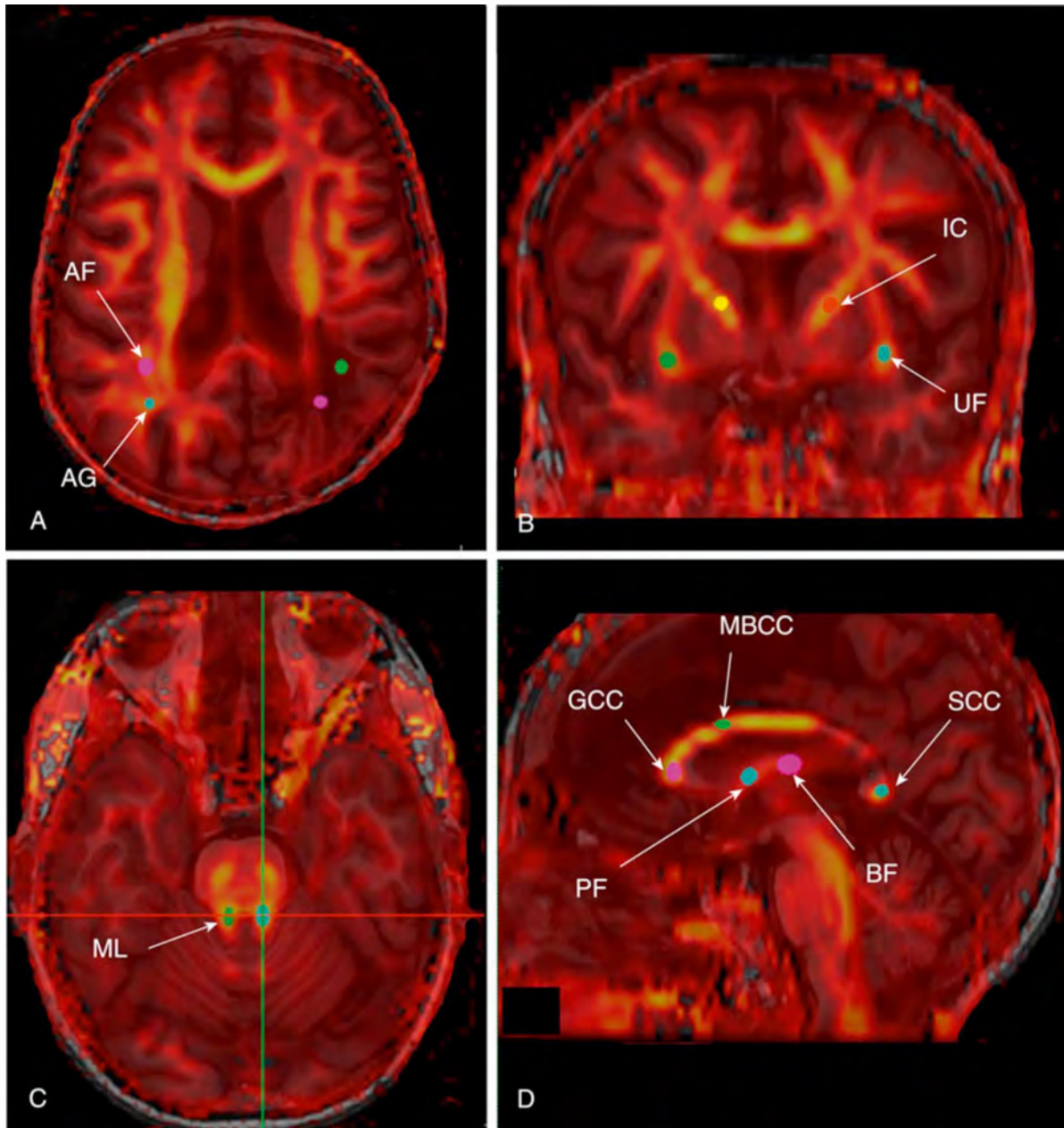


FIGURE 14.10 Small tract-centric volume of interest (VOI) selections can be made using specialized software such as Nordic BrainEx (Nordic NeuroLabs). The mean fractional anisotropy and standard deviation, along with other statistics, are reported by the software. This allows the right and left side to be compared to demonstrate any statistically significant difference and allows for comparison with normal standards. This patient with a prior history of left parietal tumor resection, radiation, chemotherapy, and bacterial meningitis, then sustained a head injury with new onset of focal symptoms. The analytic framework of VOI-based fractional anisotropy analysis allows for identification of the different sources of neurological impairment. Axial view at the level of the genu of the corpus callosum (A), coronal view at level of the genu of the internal capsule (B), axial view at the level of the pons (C), and sagittal midline view (D). *AF*, Arcuate fasciculus; *AG*, angular gyrus, right side; *BF*, body of fornix; *GCC*, genu of corpus callosum; *IC*, internal capsule; *MBCC*, mid-body of corpus callosum; *ML*, medial lemniscus; *PF*, pillars of fornix; *SCC*, splenium of corpus callosum; *UF*, uncinata fasciculus.

Clinical analysis of an FA data set requires comparisons that establish statistically significant difference from a standard set of normal FA values. The data appearing in Table 14.1 are derived from the normal control subjects in the 11 studies cited in the table footnote, drawing data from 546 individuals established as normal control subjects in institutional review board (IRB)-approved studies, published in peer-reviewed journals. Data in Cancelliere et al.¹⁰⁶ show that there is little or no age-associated change in FA in children older than 5 years through the 18 years of age end point in that study.

TABLE 14.1

Summary Data on Tract Central Region of Interest (ROI) Measures of Normal Control Subjects for Fractional Anisotropy (FA) *

General	No. of Subjects	Ages	Mean	b	1000	Tesla	Scanner	Pons/MCP	MidBr/CP	IC-Ant	IC-Genu	IC-Post	CorRad	ACoRad	CentSemi	CC Genu	CC Corp	CCSpLen	Fornix	FF-ST	AntUnc	UF	ForMin	IFOF	SLF-AF	ILF	Cing	SubNigra	GenCalc	Tapetum	MedLim	
Bisdas	12	31-45	38	y	3 T	Philips	0.63		0.66	0.72	0.74					0.79		0.83														
							Intera	7.56		7.92	8.64	8.88			9.48		9.96															
Brander	40	19-61	38	y	3 T/1.5 T	Siemens	0.65	0.79			0.77	0.53			0.55	0.85	0.66	0.87														
						Trio/Avanto	26	31.6			30.8	21.2		22	34	26.4	34.8															
Hakulinen	30	18-60	38	y	3 T	Siemens	0.65	0.85			0.73	0.5	0.55	0.51	0.83	0.74	0.86				0.54	0.54										
						Trio	19.5	25.5			21.9	15	16.5	15.3	24.9	22.2	25.8							16.2	16.2							
Cancelliere	200	0-18		y	1.5 T	GE			0.57		0.66					0.72	0.74	0.79														
						Horizon LX			114		132			144	148	158																
Sadeghi	61	4-22	14	y	1.5 T	Siemens	0.76	0.72	0.54	0.67	0.67					0.87	0.63	0.87							0.63		0.6		0.56		0.57	
							46.36	43.92	32.94	40.87	40.87				53.07	38.43	53.07										38.43		36.6		34.16	
Wilde	36		21	y	3 T	Philips																		0.46		0.43						
																											16.56		15.48			
Shakeel	36	12-25	19	y	3 T	GE																		0.52								
						Discover/750																						18.72				
Vaillancourt	14		58	y	3 T	Phillips																						0.53				
																															7.42	
Du	16		57	y	3 T	Siemens																						0.5				
						Trio																										8
Dillon	52	18-64	34	y	3 T	Siemens			0.6							0.67							0.52					0.55				
						Trio			31.2						34.84												27.04				28.6	
Kristensen	49	18-40	24	y	3 T	Philips								0.5						0.56	0.59				0.55			0.67	0.63			
																		24.5						27.44	28.91			26.95			32.83	30.87
Prefim totals	546							99.42	101.02	186.06	49.51	234.45	36.2	41	37.3	300.29	235.03	281.63	27.44	28.91	16.2	27.04	16.2	35.28	65.38	15.48	69.2	15.42	34.16	32.83	65.64	
Total cases								143	131	325	73	343	70	79	70	395	331	343	49	49	30	52	30	72	110	36	113	30	61	49	110	
Result								0.70	0.77	0.57	0.68	0.68	0.52	0.52	0.53	0.76	0.71	0.82	0.56	0.59	0.54	0.52	0.54	0.49	0.59	0.43	0.58	0.51	0.56	0.67	0.60	

Ant, Anterior; b 1000, b = gradient strength in seconds/square millimeter; CC, corpus callosum; CentSemi, centrum semiovale; Cing, cingulate tract; Corp, corpus; CorRad, corona radiata; FF-ST, fimbria fovea-stria terminalis; ForMin, fornix minor; GenCalc, geniculocalcarine tract; IC, internal capsule; IFOF, inferior fronto-occipital fasciculus; ILF, inferior longitudinal fasciculus; MCP, middle cerebellar peduncle; MedLim, medial lemniscus; MidBr/CP, midbrain cerebellar peduncle; Post, posterior; SLF-AF, superior longitudinal fasciculus-arcuate fasciculus; Spler, splenium; SubNigra, substantia nigra; UF, uncinate fasciculus; y, yes.

Data from Bisdas et al.,¹⁰¹ Brander et al.,¹⁰² Hakulinen et al.,¹⁰³ Cancelliere et al.,¹⁰⁶ Sadeghi et al.,¹⁰⁴ Wilde et al.,¹⁰⁵ Shakeel et al.,¹⁰⁷ Vaillancourt et al.,¹⁰⁸ Dillon et al.,¹⁰⁹ Du et al.,¹¹⁰ Kristensen et al.¹¹¹

The normal control values of measured FA are dependent on the methodology used. One method well suited to analysis of DTI in head injury is validated in Brander,¹⁰³ wherein a knowledgeable user selects small regions of interest (ROIs) in the central portion of various identified tracts with data provided on interrater and intrarater variability (Fig. 14.10). Brander also found no substantive differences between the use of a 1.5-T or a 3.0-T MRI scanner. However, an important proviso is that FA measured with a 4.7-T¹⁰⁷ scanner does not appear to be consistent with the data obtained at 3.0 T.

The data in also show no differences between GE, Philips, and Siemens scanners. Review of reports of FA with gradient strengths of lower than $b = 1000 \text{ s/mm}^2$, however, were not consistent with data from lower gradient strengths such as the $b = 700 \text{ s/mm}^2$ used by Mielke et al.,¹⁰⁸ and also not consistent with data from Alho et al.¹⁰⁹ using gradients at $b = 3000 \text{ s/mm}^2$. For the aforementioned reasons, the data in Table 14.1 are reliably relevant only when assessing the abnormality of FA measured with a 3-T scanner using gradients at $b = 1000 \text{ s/mm}^2$ and are apparently applicable for 1.5-T scanners at $b = 1000 \text{ s/mm}^2$ as well.

The major alternative method for FA evaluation is an automated approach.¹¹⁰ In these methods an algorithm marches through the known anatomy and attempts to segment (e.g., the entire arcuate fasciculus) and then produces an average FA for the entire selected volume.^{111,112} To determine the edge of the tract the algorithm has to be provided with a threshold to determine when it is at the gray-white border, or the algorithm may instead segment regions by means of automated mapping of the patient's brain onto a presegmented electronic brain atlas database.

Automated whole-tract FA is always lower than a selected central sample FA of a tract because the whole tract will include a wider range of variation than a given small central tract sample. Whole-tract automated FA data therefore are likely to be more applicable to medical disorders affecting larger brain regions or diffuse processes such as diffuse axonal injury, whereas central tract selected ROI FA will be more relevant to evaluation of small focal injuries. The physician evaluating the head injury with a central tract method identifies an area of apparent losses in a central tract location in an FA map image, applies a measurement ROI, and then compares the FA measure to the contralateral side and to published standards derived from central sampling.

Aside from the growing literature developing from sports-related¹¹³ or motor vehicle head injury, there is also a sizable literature related to blast injuries from military settings.^{114,115}

Nonetheless, some have contended that abnormalities appreciated on DTI imaging cannot be used to prove the veracity of head injury (e.g., if a patient complains of cognitive, emotional, or functional impairments and the DTI image shows correlated FA losses or tractographic dropout, is the existence of the injury proven?). These positions rest on the scientifically uncommon proposition that most traumatic brain injury (TBI) research focuses on groups of patients but there are not many studies with just one patient, so there is alleged to be limited predictive value.¹¹⁶⁻¹¹⁸ The head injury research community has responded by organizing large multicenter longitudinal studies.^{114,119-124} These show that, for example, when high school or college football players are provided with annual DTI imaging, the changes match the number and severity of head impacts and correlate with functional impairments reported as a collection of individual longitudinal data sets. Data are also emerging regarding whether a history of concussions increases the severity of injury from additional head impacts.¹²⁵

General Cognitive Losses

Cognitive losses can be expected in injuries that cause FA losses in the frontal lobe. These are particularly identified as losses in ability for multistep planning and map-based activities. Another important location is the superior longitudinal fasciculus because of its role in integrative processing requiring interactions between frontal and parietal subcircuits.

Memory Function Deterioration

Memory disturbances after closed head injury can be categorized generally into effects on long-term memory, effects on memory formation, and effects on immediate memory. Among the most critical circuits for memory formation are the fornix pathway and the stria terminalis of the hippocampus (Fig. 14.11).^{126,127} Injuries that affect immediate memory—such as verbal working memory—may be assessed from measures of the thalamo-prefrontal tracts.^{127a} These are readily assessed as to FA and by tractography (see Fig. 14.10).

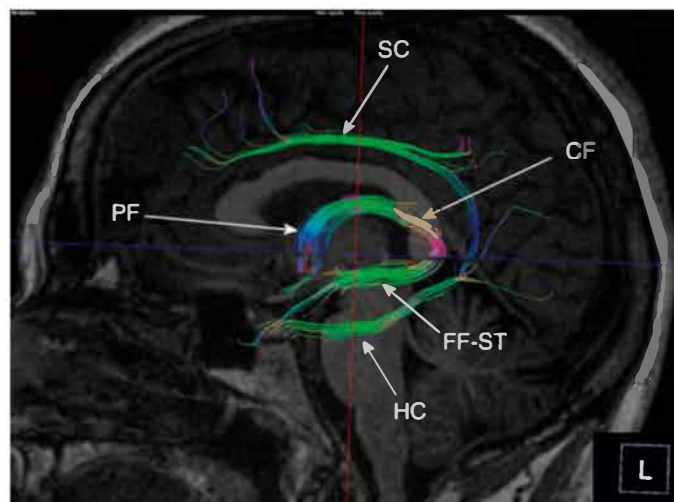


FIGURE 14.11 Left lateral view of a limbic system tractogram. The lowest tract is the hippocampal cingulum (*HC*) which can be inspected for tract losses indicating problems with attention and concentration. This arcs up to the supracallosal cingulum (*SC*) above the corpus callosum, where anterior injury observed by inspection will indicate a basis for increased anxiety and depression. The second strip from the bottom is the fimbria fornix and stria terminalis (*FF-ST*) which arch upward through the crus of the fornix (*CF*) and reach the midline descending pillars of the fornix anteriorly (*PF*). Injuries in the fornix will result in impairment in new memory formation capabilities. At the inferior margin of the anterior pillars of the fornix there is a split to an anterior portion projecting to the anterior septal nucleus, reaching above the anterior commissure and a posteriorly directed portion. After a head injury, the neurosurgeon may inspect the various tracts of the brain in conjunction with an examination and interview in order to assess possible locations of injury.

Emotional Behavioral Dysfunction

Many patients develop problems with emotional control and release after frontal lobe trauma. This is typified by uncontrolled and inappropriate rage and inexplicable anger. In contrast, depending on the mechanics of the head injury impact, some patient will experience flat affect and loss of emotional drive. This tends to implicate an injury to the uncinate fasciculus, which normally conducts emotional tone from the amygdala to the frontal lobe. Evaluation of tractographic losses or FA decreases in this setting can explain the behavioral paradox.¹²⁸ Injuries in the anterior portions of the supracallosal cingulum may be associated with increased anxiety and depression.¹²⁹

Visual Disturbances

Common complaints after closed head injury include photophobia and problems with accommodation. A typical site for evaluation in this setting is the medial lemniscus. This is a general sensory pathway in the midbrain, but focal unilateral abnormalities in this structure can be used as a marker for midbrain abnormalities that can be perceived as photophobia, as well as diplopias, and complaints of problems with visual accommodation and convergence.

Central Vertigo

Another common complaint after closed head injury is vertigo or other balance problems. In many cases these symptoms will be due to middle ear abnormalities or injuries, but the neurosurgeon may be faced with a patient who complains of abrupt triggers of vertigo or oscillopsia but in whom an ear, nose, and throat evaluation reveals no vestibular abnormalities. In some of these cases, DTI tractography may reveal injuries to the middle cerebellar peduncle. This should be considered particularly in any diagnosis of central vertigo, balance dysfunction, or problems with eye movements.

Tremor

FA analysis of the substantia nigra, just deep to the crus cerebri in the cerebral peduncle, can provide a marker for early onset of posttraumatic parkinsonian tremor.¹³⁰⁻¹³³

Chronic Traumatic Encephalopathy

CTE, a severe progressive deterioration associated with recurrent head injury, is still poorly understood. There is some expectation that DTI will play a role in tracking patients with recurrent head injury to identify early signs of progressive deterioration.^{134,135}

Spinal Cord Diffusion Tensor Imaging

Although technically challenging, DTI can be used for the assessment of spinal cord injury and to follow recovery. The small volumes to be imaged and motion sensitivity due to respiratory movements require excellent signal-to-noise performance of the scanner and often require respiratory gating to eliminate respiratory movements that affect the position of the spinal cord.¹³⁶⁻¹³⁸

Aside from application for spinal cord injury, the use of DTI to assess cervical spondylotic myelopathy is an important application,¹³⁹⁻¹⁴² and FA measurements can also identify severity of cervical spinal root impingement.¹⁴³ This is particularly the case when a patient with cervical spinal canal stenosis is being followed during a period of conservative management. It can provide objective data on whether or not there is any progressive change that would warrant proceeding with decompression.

Peripheral Nerve Diffusion Tensor Imaging

DTI and tractographic analysis of peripheral nerve can also provide a sensitive method for identifying a location of injury along a peripheral nerve.¹⁴⁴⁻¹⁴⁷ It is also helpful for defining the relationship between nerve and tumor for surgical planning.¹⁴⁸ A tractographic depiction of the brachial plexus, for instance, can be very helpful in following the elements of the plexus through various image planes.^{131,149-154} DTI can also provide a method for assessing the severity of conditions such as carpal tunnel syndrome in which the degree of tractographic or FA losses^{155,156} may be determinative for the decision to shift from conservative to surgical management. DTI is also helpful for locating and characterizing cranial nerve impingements and disorders.^{157,158}

Suggested Readings

- Basser P.J, Mattiello J, LeBihan D. MR diffusion tensor spectroscopy and imaging. *Biophys J* . 1994;66(1):259-267.
- Becker D, Scherer M, Neher P, et al. Going Beyond diffusion tensor imaging tractography in eloquent glioma surgery-high-resolution fiber tractography: Q-Ball or constrained spherical deconvolution? *World Neurosurg* . 2020;134:e596-e609. doi: 10.1016/j.wneu.2019.10.138.
- Brander A, Kataja A, Saastamoinen A, et al. Diffusion tensor imaging of the brain in a healthy adult population: normative values and measurement reproducibility at 3 T and 1.5 T. *Acta Radiol* . 2010;51(7):800-807.
- Ellingson B.M, Salamon N, Hardy A.J, Holly L.T. Prediction of neurological impairment in cervical spondylotic myelopathy using a combination of diffusion MRI and proton MR spectroscopy. *PLoS One* . 2015;10(10):e0139451.
- Essayed W.I, Zhang F, Unadkat P, Cosgrove G.R, Golby A.J, O'Donnell L.J. White matter tractography for neurosurgical planning: a topography-based review of the current state of the art. *Neuroimage Clin* . 2017;15:659-672.
- Feigl G.C, Hiergeist W, Fellner C, et al. Magnetic resonance imaging diffusion tensor tractography: evaluation of anatomic accuracy of different fiber tracking software packages. *World Neurosurg* . 2014;81(1):144-150.
- Filler A.G. MR neurography and diffusion tensor imaging: origins, history & clinical Impact of the first 50,000 cases with an assessment of efficacy and utility in a prospective 5,000 patient study group. *Neurosurgery* . 2009;65(suppl 4):29-43.
- Filler A.G. The history, development and impact of computed imaging in neurological diagnosis and neurosurgery: CT, MRI, DTI. *Int J Neurosurg* . 2010;7(1):1-37.
- Henderson F, Abdullah K.G, Verma R, Brem S. Tractography and the connectome in neurosurgical treatment of gliomas: the premise, the progress, and the potential. *Neurosurg Focus* . 2020;48(2):E6.
- Irimia A, Van Horn J.D. Systematic network lesioning reveals the core white matter scaffold of the human brain. *Front Hum Neurosci* . 2014;8:51. doi: 10.3389/fnhum.2014.00051.
- Niogi S.N, Luther N, Kutner K, et al. Increased sensitivity to traumatic axonal injury on postconcussion diffusion tensor imaging scans in National Football League players by using pre-morbid baseline scans. *J Neurosurg* . 2019:1-9.
- Oudeman J, Verhamme C, Engbersen M.P, et al. Diffusion tensor MRI of the healthy brachial plexus. *PLoS One* . 2018;13(5):e0196975.
- Poplawski M.M, Alizadeh M, Oleson C.V, et al. Application of diffusion tensor imaging in forecasting neurological injury and recovery after human cervical spinal cord injury. *J Neurotrauma* . 2019;36(21):3051-3061.
- Salminen L.E, Conturo T.E, Laidlaw D.H, et al. Regional age differences in gray matter diffusivity among healthy older adults. *Brain Imaging Behav* . 2016;10(1):203-211.

- Sarwar T, Ramamohanarao K, Zalesky A. Mapping connectomes with diffusion MRI: deterministic or probabilistic tractography? *Magn Reson Med*. Feb. 2019;81(2):1368–1384. doi: [10.1002/mrm.27471](https://doi.org/10.1002/mrm.27471).
- Tian Q, Wintermark M, Jeffrey Elias W, et al. Diffusion MRI tractography for improved transcranial MRI-guided focused ultrasound thalamotomy targeting for essential tremor. *Neuroimage Clin*. 2018;19:572–580.
- Vassal F, Dilly D, Boutet C, Bertholon F, Charier D, Pommier B. White matter tracts involved by deep brain stimulation of the subthalamic nucleus in Parkinson's disease: a connectivity study based on preoperative diffusion tensor imaging tractography. *Br J Neurosurg*. 2020;34(2):187–195.
- Wintermark M, Sanelli P.C, Anzai Y, Tsiouris A.J, Whitlow C.T, Institute ACoRHL. Imaging evidence and recommendations for traumatic brain injury: advanced neuro- and neurovascular imaging techniques. *AJNR Am J Neuroradiol*. 2015;36(2):E1–E11.
- Wu J.S, Zhou L.F, Tang W.J, et al. Clinical evaluation and follow-up outcome of diffusion tensor imaging-based functional neuronavigation: a prospective, controlled study in patients with gliomas involving pyramidal tracts. *Neurosurgery*. 2007;61(5):935–948 discussion 948–939.
- Wu M, Qiu J, Jiang X, et al. Diffusion tensor imaging reveals microstructural alteration of the trigeminal nerve root in classical trigeminal neuralgia without neurovascular compression and correlation with outcome after internal neurolysis. *Magn Reson Imaging*. 2020;71:37–44.
- Wu Y.C, Harezlak J, Elsaid N.M.H, et al. Longitudinal white-matter abnormalities in sports-related concussion: a diffusion MRI study. *Neurology*. 2020.
- Yuh E.L, Cooper S.R, Mukherjee P, et al. Diffusion tensor imaging for outcome prediction in mild traumatic brain injury: a TRACK-TBI study. *J Neurotrauma*. 2014;31(17):1457–1477.
- Zheng Z, Shemmassian S, Wijekoon C, Kim W, Bookheimer S.Y, Pouratian N. DTI correlates of distinct cognitive impairments in Parkinson's disease. *Hum Brain Mapp*. 2014;35(4):1325–1333.

References

- Soulard J, Huber C, Baillieux S, et al. Motor tract integrity predicts walking recovery: a diffusion MRI study in subacute stroke. *Neurology*. 2020;94(6):e583–e593. doi: [10.1212/WNL.00000000000008755](https://doi.org/10.1212/WNL.00000000000008755).
- O'Connor K.P, Strickland A.E, Bohnstedt B.N. A contralateral transventricular approach for microsurgical clip ligation of a ruptured intrathalamic aneurysm. *J Clin Neurosci*. 2019;68:329–332. doi: [10.1016/j.jocn.2019.07.028](https://doi.org/10.1016/j.jocn.2019.07.028).
- Germanò A, Raffa G, Conti A, et al. Modern treatment of brain arteriovenous malformations using preoperative planning based on navigated transcranial magnetic stimulation: a revisitation of the concept of eloquence. *World Neurosurg*. 2019;131:371–384. doi: [10.1016/j.wneu.2019.06.119](https://doi.org/10.1016/j.wneu.2019.06.119).
- Cho M.K, Jang S.H. Diffusion tensor imaging studies on spontaneous subarachnoid hemorrhage-related brain injury: a mini-review. *Front Neurol*. 2020;11:283. doi: [10.3389/fneur.2020.00283](https://doi.org/10.3389/fneur.2020.00283).
- Versace A, Graur S, Greenberg T, et al. Reduced focal fiber collinearity in the cingulum bundle in adults with obsessive-compulsive disorder. *Neuropsychopharmacology*. 2019;44(7):1182–1188. doi: [10.1038/s41386-019-0353-4](https://doi.org/10.1038/s41386-019-0353-4).
- García-García S, Kakaizada S, Oleaga L, Benet A, Rincon-Toroella J, González-Sánchez J.J. Presurgical simulation for neuroendoscopic procedures: virtual study of the integrity of neurological pathways using diffusion tensor imaging tractography. *Neurol India*. 2019;67(3):763–769. doi: [10.4103/0028-3886.263199](https://doi.org/10.4103/0028-3886.263199).
- Ozgural O, Al-Beyati E.S.M, Kahilogullari G. MR navigation and tractography-assisted transcranial neuroendoscopic aspiration of pediatric thalamic abscess. *Pediatr Neurosurg*. 2019;54(5):354–358. doi: [10.1159/000501914](https://doi.org/10.1159/000501914).
- Wu J.S, Zhou L.F, Tang W.J, et al. Clinical evaluation and follow-up outcome of diffusion tensor imaging-based functional neuronavigation: a prospective, controlled study in patients with gliomas involving pyramidal tracts. *Neurosurgery*. 2007;61(5):935–948 discussion 948–9.
- Edlow B.L, Mareyam A, Horn A, et al. 7 Tesla MRI of the ex vivo human brain at 100 micron resolution. *Sci Data*. 2019;6(1):244. doi: [10.1038/s41597-019-0254-8](https://doi.org/10.1038/s41597-019-0254-8).
- Holdsworth S.J, O'Halloran R, Setsompop K. The quest for high spatial resolution diffusion-weighted imaging of the human brain in vivo. *NMR Biomed*. 2019;32(4):e4056. doi: [10.1002/nbm.4056](https://doi.org/10.1002/nbm.4056).
- Jelescu I.O, Budde M.D. Design and validation of diffusion MRI models of white matter. *Front Phys*. 2017;11:28. doi: [10.3389/fphy.2017.00061](https://doi.org/10.3389/fphy.2017.00061).
- Schilling K.G, Daducci A, Maier-Hein K, et al. Challenges in diffusion MRI tractography - lessons learned from international benchmark competitions. *Magn Reson Imaging*. 2019;57:194–209. doi: [10.1016/j.mri.2018.11.014](https://doi.org/10.1016/j.mri.2018.11.014).
- Howe F.A, Filler A.G, Bell B.A, Griffiths J.R. Magnetic resonance neurography. *Magn Reson Med*. 1992;28(2):328–338.
- Le Bihan D, Turner R, Moonen C.T, Pekar J. Imaging of diffusion and microcirculation with gradient sensitization: design, strategy, and significance. *J Magn Reson Imaging*. 1991;1(1):7–28.
- Moseley M.E, Cohen Y, Kucharczyk J, et al. Diffusion-weighted MR imaging of anisotropic water diffusion in cat central nervous system. *Radiology*. 1990;176(2):439–445.
- Filler A.G, Tsuruda J.S, Richards T.L, Howe F.A. *Image Neurography and Diffusion Anisotropy Imaging*. Unites States Patent Office; 1996.
- Mori S, van Zijl P.C. Diffusion weighting by the trace of the diffusion tensor within a single scan. *Magn Reson Med*. 1995;33(1):41–52.
- Filler A.G. MR Neurography and diffusion tensor imaging: origins, history & clinical impact of the first 50,000 cases with an assessment of efficacy and utility in a prospective 5,000 patient study group. *Neurosurgery*. 2009;65(suppl 4):29–43.
- Filler A.G. The history, development and impact of computed imaging in neurological diagnosis and neurosurgery: CT, MRI, DTI. *Int J Neurosurg*. 2010;7(1):1–37.
- Basser P.J. Invention and Development of Diffusion Tensor MRI (DT-MRI or DTI) at the NIH. In: Jones D.K, ed. *Diffusion MRI: Theory, Methods, and Applications*. Oxford University Press; 2010:730–740 (chap 47).
- Le Bihan D, Le Bihan D, Denis. Diffusion MRI: a historical account. In: Grant D.M, Harris R.K, eds. *Encyclopedia of Magnetic Resonance*. John Wiley; 2010:1–4.
- Basser P.J, Mattiello J, LeBihan D. MR diffusion tensor spectroscopy and imaging. *Biophys J*. 1994;66(1):259–267.
- Filler A.G, Tsuruda J.S, Richards T.L, Howe F.A, inventors; University of Washington, assignee. Image neurography and diffusion anisotropy imaging (ref copy2). *US Patent*. 1996 5560360.
- Basser P.J. New histological and physiological stains derived from diffusion-tensor MR images. *Ann N Y Acad Sci*. 1997;820:123–138.
- PJ B., Fiber-Tractography via Diffusion Tensor MRI (DT-MRI). presented at: *International Society for Magnetic Resonance in Medicine 6th Annual Meeting*. Sydney, Australia; 1998
- Basser PJ, Pajevic S, Pierpaoli C, Duda J, Aldroubi A. In vivo fiber tractography using DT-MRI data. *Magn Reson Med*. 2000;44(4):625–632. [https://doi.org/10.1002/1522-2594\(200010\)44:4<625::aid-mrm17>3.0.co;2-o](https://doi.org/10.1002/1522-2594(200010)44:4<625::aid-mrm17>3.0.co;2-o)
- Tauxe L, Constable C, Stokking L, Badgley C. Use of anisotropy to determine the origin of characteristic remanence in the Siwalik red beds of Northern Pakistan. *J Geophys Res*. 1990;95(B4):4391–4404.
- Constable C, Tauxe L. The bootstrap for magnetic susceptibility tensors. *J Geophys Res*. 1990;95:8383–8395.
- Deacon T.W. Cortical connections of the inferior arcuate sulcus cortex in the macaque brain. *Brain Res*. 1992;573(1):8–26.

30. Kramer M, Deacon T.W, Sokoloff A, Filler A. Organization of motoneurons innervating epaxial and hypaxial musculature in the frog, rat, and monkey. *Soc Neurosci Abs* . 1987;13:526.
31. Tauxe L, Behrensmeyer A.K. Paleomagnetic stratigraphy. In: Pilbeam D, Behrensmeyer A.K, Barry J.C, Shah I, eds. *Postilla: Miocene Sediments and Faunas of Pakistan* . Yale University; 1979:11–16.
32. Moseley M.E, Kucharczyk J, Mintorovitch J, et al. Diffusion-weighted MR imaging of acute stroke: correlation with T2-weighted and magnetic susceptibility-enhanced MR imaging in cats. *AJNR Am J Neuroradiol* . 1990;11(3):423–429.
33. Moseley M.E, Mintorovitch J, Cohen Y, et al. Early detection of ischemic injury: comparison of spectroscopy, diffusion-, T2-, and magnetic susceptibility-weighted MRI in cats. *Acta Neurochir Suppl (Wien)* . 1990;51:207–209.
34. Moseley M.E, Kucharczyk J, Asgari H.S, Norman D. Anisotropy in diffusion-weighted MRI. *Magn Reson Med* . 1991;19(2):321–326.
35. Basser P.J, Mattiello J.H, LeBihan D. *Method and System for Measuring the Diffusion Tensor and for Diffusion Tensor Imaging* . United States Patent Office; 1996.
36. Conturo T.E, McKinsty R.C, Aronovitz J.A, Neil J.J. Diffusion MRI: precision, accuracy and flow effects. *NMR Biomed* . 1995;8(7-8):307–332. doi: [10.1002/nbm.1940080706](https://doi.org/10.1002/nbm.1940080706).
37. Stejskal E.O. Use of spin echoes in a pulsed magnetic-field gradient to study anisotropic, restricted diffusion and flow. *J Chem Phys* . 1965;43(10):3597–3603.
38. Neeman M, Freyer J.P, Sillerud L.O. A simple method for obtaining cross-term-free images for diffusion anisotropy studies in NMR microimaging. *Magn Reson Med* . 1991;21(1):138–143. doi: [10.1002/mrm.1910210117](https://doi.org/10.1002/mrm.1910210117).
9850. a. Richards T.L, Heide A.C, Tsuruda J.S, Alvord E.C. *Vector Analysis of Diffusion Images in Experimental Allergic Encephalomyelitis. Book of Abstracts* . Berlin: Society of Magnetic Resonance in Medicine; 1992:412.
9851. b. Einstein A. Zur Theorie der Brownschen Bewegung [on the theory of Brownian Motion]. *Annalen der Physik* . 1906;19:371–381.
9852. c. Einstein A. Die Grundlage der allgemeinen relativitätstheorie. *Annalen der Physik* . 1916;49(7):769–822.
9853. d. Lohmann G, Bohn S, Müller K, Trampel R, Turner R. Image restoration and spatial resolution in 7-tesla magnetic resonance imaging. *Magn Res Med* . 2010;64:15–22.
39. Kamagata K, Andica C, Hatano T, et al. Advanced diffusion magnetic resonance imaging in patients with Alzheimer's and Parkinson's diseases. *Neural Regen Res* . 2020;15(9):1590–1600. doi: [10.4103/1673-5374.276326](https://doi.org/10.4103/1673-5374.276326).
40. Kumar M, Duda J.T, Yoon S.Y, et al. Diffusion tensor imaging for assessing brain gray and white matter abnormalities in a feline model of α -mannosidosis. *J Neuropathol Exp Neurol* . 2016;75(1):35–43. doi: [10.1093/jnen/nlv007](https://doi.org/10.1093/jnen/nlv007).
41. Salminen L.E, Conturo T.E, Laidlaw D.H, et al. Regional age differences in gray matter diffusivity among healthy older adults. *Brain Imaging Behav* . 2016;10(1):203–211. doi: [10.1007/s11682-015-9383-7](https://doi.org/10.1007/s11682-015-9383-7).
42. Taylor K.I, Sambataro F, Boess F, Bertolino A, Dukart J. Progressive decline in gray and white matter integrity in. *Front Aging Neurosci* . 2018;10:318. doi: [10.3389/fnagi.2018.00318](https://doi.org/10.3389/fnagi.2018.00318).
43. Revuelta G, McGill C, Jensen J.H, Bonilha L. Characterizing thalamo-cortical structural connectivity in essential tremor with diffusional kurtosis imaging tractography. *Tremor Other Hyperkinet Mov (N Y)* . 2019;9. doi: [10.7916/tohm.v0.690](https://doi.org/10.7916/tohm.v0.690).
44. Mori S, Crain B.J, Chacko V.P, van Zijl P.C. Three-dimensional tracking of axonal projections in the brain by magnetic resonance imaging. *Ann Neurol* . 1999;45(2):265–269.
45. Mori S. Method of fiber reconstruction employing data acquired by magnetic resonance imaging. *United States Patent Office* . 2003.
46. Feigl G.C, Hiergeist W, Fellner C, et al. Magnetic resonance imaging diffusion tensor tractography: evaluation of anatomic accuracy of different fiber tracking software packages. *World Neurosurg* . 2014;81(1):144–150. doi: [10.1016/j.wneu.2013.01.004](https://doi.org/10.1016/j.wneu.2013.01.004).
47. Yeh F.C, Tang P.F, Tseng W.Y. Diffusion MRI connectometry automatically reveals affected fiber pathways in individuals with chronic stroke. *Neuroimage Clin* . 2013;2:912–921. doi: [10.1016/j.nicl.2013.06.014](https://doi.org/10.1016/j.nicl.2013.06.014).
48. Fan Q, Witzel T, Nummenmaa A, et al. MGH-USC human connectome project datasets with ultra-high b-value diffusion MRI. *Neuroimage* . 2016;124(Pt B):1108–1114. doi: [10.1016/j.neuroimage.2015.08.075](https://doi.org/10.1016/j.neuroimage.2015.08.075).
49. Jolly A.E, Scott G.T, Sharp D.J, Hampshire A.H. Distinct patterns of structural damage underlie working memory and reasoning deficits after traumatic brain injury. *Brain* . 2020;143(4):1158–1176. doi: [10.1093/brain/awaa067](https://doi.org/10.1093/brain/awaa067).
50. Brodmann K. Vergleichende Lokalisationslehre der Grosshirnrinde in ihren Prinzipien dargestellt auf Grund des Zellenbaues. *Barth* . 1909:324 x.
51. Brodmann K, Garey L. *Brodmann's Localisation in the Cerebral Cortex*. Imperial College Press; Distributed by World Scientific Pub.; 1999:xviii, 300.
52. Irimia A, Van Horn J.D. Systematic network lesioning reveals the core white matter scaffold of the human brain. *Front Hum Neurosci* . 2014;8:51. doi: [10.3389/fnhum.2014.00051](https://doi.org/10.3389/fnhum.2014.00051).
53. Paquola C, Seidlitz J, Benkarim O, et al. A multi-scale cortical wiring space links cellular architecture and functional dynamics in the human brain. *PLoS Biol* . 2020;18(11):e3000979. doi: [10.1371/journal.pbio.3000979](https://doi.org/10.1371/journal.pbio.3000979).
54. James G.M, Gryglewski G, Vanicek T, et al. Parcellation of the human cerebral cortex based on molecular targets in the serotonin system quantified by positron emission tomography in vivo. *Cereb Cortex* . 2019;29(1):372–382. doi: [10.1093/cercor/bhy249](https://doi.org/10.1093/cercor/bhy249).
55. Farquharson S, Tournier J.D, Calamante F, et al. White matter fiber tractography: why we need to move beyond DTI. *J Neurosurg* . 2013;118(6):1367–1377. doi: [10.3171/2013.2.JNS121294](https://doi.org/10.3171/2013.2.JNS121294).
56. Calamante F. The Seven deadly sins of measuring brain structural connectivity using diffusion MRI Streamlines Fibre-Tracking. *Diagnostics (Basel)* . 2019;9(3) doi: [10.3390/diagnostics9030115](https://doi.org/10.3390/diagnostics9030115).
57. Dell'Acqua F, Tournier J.D. Modelling white matter with spherical deconvolution: how and why? *NMR Biomed* . 2019;32(4):e3945. doi: [10.1002/nbm.3945](https://doi.org/10.1002/nbm.3945).
58. Jeurissen B, Tournier J.D, Dhollander T, Connelly A, Sijbers J. Multi-tissue constrained spherical deconvolution for improved analysis of multi-shell diffusion MRI data. *Neuroimage* . 2014;103:411–426. doi: [10.1016/j.neuroimage.2014.07.061](https://doi.org/10.1016/j.neuroimage.2014.07.061).
59. Becker D, Scherer M, Neher P, et al. Going beyond diffusion tensor imaging tractography in eloquent glioma surgery-high-resolution fiber tractography: Q-Ball or constrained spherical deconvolution? *World Neurosurg* . 2020;134:e596–e609. doi: [10.1016/j.wneu.2019.10.138](https://doi.org/10.1016/j.wneu.2019.10.138).
60. Sarwar T, Ramamohanarao K, Zalesky A. Mapping connectomes with diffusion MRI: deterministic or probabilistic tractography? *Magn Reson Med* . 2019;81(2):1368–1384. doi: [10.1002/mrm.27471](https://doi.org/10.1002/mrm.27471).
61. Nabulsi L, McPhilemy G, Kilmartin L, et al. Bipolar disorder and gender are associated with frontolimbic and basal ganglia dysconnectivity: a study of topological variance using network analysis. *Brain Connect* . 2019;9(10):745–759. doi: [10.1089/brain.2019.0667](https://doi.org/10.1089/brain.2019.0667).
- 61a. Oehr L.E, Yang J.Y.-M, Chen J, et al. Investigating white matter tract microstructural changes at six-twelve weeks following mild traumatic brain injury: a combined diffusion tensor imaging and neurite orientation dispersion density imaging study. *J Neuro Trauma* . 2021 doi: [10.1089/neu.2020.7310](https://doi.org/10.1089/neu.2020.7310).
- 61b. Wright D.K, Johnston L.A, Kershaw J, Ordridge R, O'Brien T.J, Shultz S.R. Changes in apparent fiber density and track-weighted imaging metrics in white matter following experimental traumatic brain injury. *J Neurotrauma* . 2017;43:2109–2118.

62. Mohammadian M, Roine T, Hirvonen J, et al. High angular resolution diffusion-weighted imaging in mild traumatic brain injury. *Neuroimage Clin* . 2017;13:174–180. doi: [10.1016/j.nicl.2016.11.016](https://doi.org/10.1016/j.nicl.2016.11.016).
63. Berman J.I, Berger M.S, Chung S.W, Nagarajan S.S, Henry R.G. Accuracy of diffusion tensor magnetic resonance imaging tractography assessed using intraoperative subcortical stimulation mapping and magnetic source imaging. *J Neurosurg* . 2007;107(3):488–494. doi: [10.3171/JNS-07/09/0488](https://doi.org/10.3171/JNS-07/09/0488).
- 63a. Gupta A, Shah A, Young R.J, Holodny A.I. Imaging of brain tumors: functional magnetic resonance imaging and diffusion tensor imaging. *Neuroimaging Clin N Am* . 2010;20:379–400.
64. Becker D, Scherer M, Neher P, et al. Going Beyond diffusion tensor imaging tractography in eloquent glioma surgery-high-resolution fiber tractography: Q-ball or constrained spherical deconvolution? *World Neurosurg* . 2020;134:e596–e609. doi: [10.1016/j.wneu.2019.10.138](https://doi.org/10.1016/j.wneu.2019.10.138).
65. Castellano A, Bello L, Michelozzi C, et al. Role of diffusion tensor magnetic resonance tractography in predicting the extent of resection in glioma surgery. *Neuro Oncol* . 2012;14(2):192–202. doi: [10.1093/neuonc/nor188](https://doi.org/10.1093/neuonc/nor188).
66. Conti Nibali M, Rossi M, Sciortino T, et al. Preoperative surgical planning of glioma: limitations and reliability of fMRI and DTI tractography. *J Neurosurg Sci* . 2019;63(2):127–134. doi: [10.23736/S0390-5616.18.04597-6](https://doi.org/10.23736/S0390-5616.18.04597-6).
67. Essayed W.I, Zhang F, Unadkat P, Cosgrove G.R, Golby A.J, O'Donnell L.J. White matter tractography for neurosurgical planning: a topography-based review of the current state of the art. *Neuroimage Clin* . 2017;15:659–672. doi: [10.1016/j.nicl.2017.06.011](https://doi.org/10.1016/j.nicl.2017.06.011).
68. Henderson F, Abdullah K.G, Verma R, Brem S. Tractography and the connectome in neurosurgical treatment of gliomas: the premise, the progress, and the potential. *Neurosurg Focus* . 2020;48(2):E6. doi: [10.3171/2019.11.FOCUS19785](https://doi.org/10.3171/2019.11.FOCUS19785).
69. Krivosheya D, Prabhu S.S. Combining functional studies with intraoperative mri in glioma surgery. *Neurosurg Clin N Am* . 2017;28(4):487–497. doi: [10.1016/j.nec.2017.05.004](https://doi.org/10.1016/j.nec.2017.05.004).
70. Panesar S.S, Abhinav K, Yeh F.C, Jacquesson T, Collins M, Fernandez-Miranda J. Tractography for surgical neuro-oncology planning: towards a gold standard. *Neurotherapeutics* . 2019;16(1):36–51. doi: [10.1007/s13311-018-00697-x](https://doi.org/10.1007/s13311-018-00697-x).
71. Potgieser A.R, Wagemakers M, van Hulzen A.L, de Jong B.M, Hoving E.W, Groen R.J. The role of diffusion tensor imaging in brain tumor surgery: a review of the literature. *Clin Neurol Neurosurg* . 2014;124:51–58. doi: [10.1016/j.clineuro.2014.06.009](https://doi.org/10.1016/j.clineuro.2014.06.009).
72. Sanai N, Berger M.S. Surgical oncology for gliomas: the state of the art. *Nat Rev Clin Oncol* . 2018;15(2):112–125. doi: [10.1038/nrclinonc.2017.171](https://doi.org/10.1038/nrclinonc.2017.171).
73. Verburg N, de Witt Hamer P.C. State-of-the-art imaging for glioma surgery. *Neurosurg Rev* . 2020 doi: [10.1007/s10143-020-01337-9](https://doi.org/10.1007/s10143-020-01337-9).
74. Kleiser R, Staempfli P, Valavanis A, Boesiger P, Kollias S. Impact of fMRI-guided advanced DTI fiber tracking techniques on their clinical applications in patients with brain tumors. *Neuroradiology* . 2010;52(1):37–46. doi: [10.1007/s00234-009-0539-2](https://doi.org/10.1007/s00234-009-0539-2).
75. Barbosa B.J., Mariano E.D., Batista C.M., et al. Intraoperative assistive technologies and extent of resection in glioma surgery: a systematic review of prospective controlled studies. *Neurosurg Rev* . 2015;38(2):217–226; discussion 226–227. <https://doi.org/10.1007/s10143-014-0592-0>
76. Zhang F, Noh T, Juvekar P, et al. SlicerDMRI: diffusion MRI and tractography research software for brain cancer surgery planning and visualization. *JCO Clin Cancer Inform* . 2020;4:299–309. doi: [10.1200/CCI.19.00141](https://doi.org/10.1200/CCI.19.00141).
77. Javadi S.A, Nabavi A, Giordano M, Faghihzadeh E, Samii A. Evaluation of diffusion tensor imaging-based tractography of the corticospinal tract: a correlative study with intraoperative magnetic resonance imaging and direct electrical subcortical stimulation. *Neurosurgery* . 2017;80(2):287–299. doi: [10.1227/NEU.0000000000001347](https://doi.org/10.1227/NEU.0000000000001347).
78. Vassal F, Schneider F, Nuti C. Intraoperative use of diffusion tensor imaging-based tractography for resection of gliomas located near the pyramidal tract: comparison with subcortical stimulation mapping and contribution to surgical outcomes. *Br J Neurosurg* . 2013;27(5):668–675. doi: [10.3109/02688697.2013.771730](https://doi.org/10.3109/02688697.2013.771730).
79. Bopp M.H, Pietruk P.M, Nimsky C, Carl B. Fiber tractography of the optic radiations: impact of diffusion model, voxel shape and orientation. *J Neurosurg Sci* . 2019 doi: [10.23736/S0390-5616.19.04622-8](https://doi.org/10.23736/S0390-5616.19.04622-8).
80. Hess C.P, Mukherjee P. Visualizing white matter pathways in the living human brain: diffusion tensor imaging and beyond. *Neuroimaging Clin N Am* . 2007;17(4):407–426. vii. doi: [10.1016/j.nic.2007.07.002](https://doi.org/10.1016/j.nic.2007.07.002).
81. Mukherjee P, Chung S.W, Berman J.I, Hess C.P, Henry R.G. Diffusion tensor MR imaging and fiber tractography: technical considerations. *AJNR Am J Neuroradiol* . 2008;29(5):843–852. doi: [10.3174/ajnr.A1052](https://doi.org/10.3174/ajnr.A1052).
82. Mukherjee P, Berman J.I, Chung S.W, Hess C.P, Henry R.G. Diffusion tensor MR imaging and fiber tractography: theoretic underpinnings. *AJNR Am J Neuroradiol* . 2008;29(4):632–641. doi: [10.3174/ajnr.A1051](https://doi.org/10.3174/ajnr.A1051).
83. Jeurissen B, Descoteaux M, Mori S, Leemans A. Diffusion MRI fiber tractography of the brain. *NMR Biomed* . 2019;32(4):e3785. doi: [10.1002/nbm.3785](https://doi.org/10.1002/nbm.3785).
84. Fekonja L, Wang Z, Bährend I, et al. Manual for clinical language tractography. *Acta Neurochir (Wien)* . 2019;161(6):1125–1137. doi: [10.1007/s00701-019-03899-0](https://doi.org/10.1007/s00701-019-03899-0).
85. Sagar S, Rick J, Chandra A, Yagnik G, Aghi M.K. Functional brain mapping: overview of techniques and their application to neurosurgery. *Neurosurg Rev* . 2019;42(3):639–647. doi: [10.1007/s10143-018-1007-4](https://doi.org/10.1007/s10143-018-1007-4).
86. Vassal F, Dilly D, Boutet C, Bertholon F, Charier D, Pommier B. White matter tracts involved by deep brain stimulation of the subthalamic nucleus in Parkinson's disease: a connectivity study based on preoperative diffusion tensor imaging tractography. *Br J Neurosurg* . 2020;34(2):187–195. doi: [10.1080/02688697.2019.1701630](https://doi.org/10.1080/02688697.2019.1701630).
87. Coenen V.A, Schlaepfer T.E, Reinacher P.C, Mast H, Urbach H, Reisert M. Machine learning-aided personalized DTI tractographic planning for deep brain stimulation of the superolateral medial forebrain bundle using HAMLET. *Acta Neurochir (Wien)* . 2019;161(8):1559–1569. doi: [10.1007/s00701-019-03947-9](https://doi.org/10.1007/s00701-019-03947-9).
88. Paek S.H. The role of ultra-high field magnetic resonance imaging for track density imaging: application in neuromodulation of the brain. *World Neurosurg* . 2015;83(1):4–6. doi: [10.1016/j.wneu.2013.09.033](https://doi.org/10.1016/j.wneu.2013.09.033).
89. Panther P, Kuehne M, Voges J, et al. Electric stimulation of the medial forebrain bundle influences sensorimotor gaiting in humans. *BMC Neurosci* . 2019;20(1):20. doi: [10.1186/s12868-019-0503-y](https://doi.org/10.1186/s12868-019-0503-y).
90. Polanski W.H, Zolal A, Klein J, et al. Somatosensory functional MRI tractography for individualized targeting of deep brain stimulation in patients with chronic pain after brachial plexus injury. *Acta Neurochir (Wien)* . 2019;161(12):2485–2490. doi: [10.1007/s00701-019-04065-2](https://doi.org/10.1007/s00701-019-04065-2).
91. See A.A.Q, King N.K.K. Improving surgical outcome using diffusion tensor imaging techniques in deep brain stimulation. *Front Surg* . 2017;4:54. doi: [10.3389/fsurg.2017.00054](https://doi.org/10.3389/fsurg.2017.00054).
92. Su J.H, Thomas F.T, Kasoff W.S, et al. Thalamus Optimized Multi Atlas Segmentation (THOMAS): fast, fully automated segmentation of thalamic nuclei from structural MRI. *Neuroimage* . 2019;194:272–282. doi: [10.1016/j.neuroimage.2019.03.021](https://doi.org/10.1016/j.neuroimage.2019.03.021).
93. Tohyama S, Walker M.R, Sammartino F, Krishna V, Hodaie M. The utility of diffusion tensor imaging in neuromodulation: moving beyond conventional magnetic resonance imaging. *Neuromodulation* . 2020;23(4):427–435. doi: [10.1111/ner.13107](https://doi.org/10.1111/ner.13107).
94. Sammartino F, Yeh F.C, Krishna V. Longitudinal analysis of structural changes following unilateral focused ultrasound thalamotomy. *Neuroimage Clin* . 2019;22:101754. doi: [10.1016/j.nicl.2019.101754](https://doi.org/10.1016/j.nicl.2019.101754).
95. Tian Q, Wintermark M, Jeffrey Elias W, et al. Diffusion MRI tractography for improved transcranial MRI-guided focused ultrasound thalamotomy targeting for essential tremor. *Neuroimage Clin* . 2018;19:572–580. doi: [10.1016/j.nicl.2018.05.010](https://doi.org/10.1016/j.nicl.2018.05.010).

96. Visser M.M, Yassi N, Campbell B.C.V, et al. White matter degeneration after ischemic stroke: a longitudinal diffusion tensor imaging study. *J Neuroimaging* . 2019;29(1):111–118. doi: [10.1111/jon.12556](https://doi.org/10.1111/jon.12556).
97. Yu X, Jiaerken Y, Wang S, et al. Changes in the corticospinal tract beyond the ischemic lesion following acute hemispheric stroke: a diffusion kurtosis imaging study. *J Magn Reson Imaging* . 2020;52(2):512–519. doi: [10.1002/jmri.27066](https://doi.org/10.1002/jmri.27066).
98. Barber Foss K.D, Yuan W, Diekfuss J.A, et al. Relative head impact exposure and brain white matter alterations after a single season of competitive football: a pilot comparison of youth versus high school football. *Clin J Sport Med* . 2019;29(6):442–450. doi: [10.1097/JSM.0000000000000753](https://doi.org/10.1097/JSM.0000000000000753).
99. Borja M.J, Chung S, Lui Y.W. Diffusion MR imaging in mild traumatic brain injury. *Neuroimaging Clin N Am* . 2018;28(1):117–126. doi: [10.1016/j.nic.2017.09.009](https://doi.org/10.1016/j.nic.2017.09.009).
100. Gozt A, Licari M, Halstrom A, et al. Towards the development of an integrative, evidence-based suite of indicators for the prediction of outcome following mild traumatic brain injury: results from a pilot study. *Brain Sci* . 2020;10(1) doi: [10.3390/brainsci10010023](https://doi.org/10.3390/brainsci10010023).
101. Jang S.H, Kwon Y.H. A review of traumatic axonal injury following whiplash injury as demonstrated by diffusion tensor tractography. *Front Neurol* . 2018;9:57. doi: [10.3389/fneur.2018.00057](https://doi.org/10.3389/fneur.2018.00057).
102. Lipton M.L, Kim N, Zimmerman M.E, et al. Soccer heading is associated with white matter microstructural and cognitive abnormalities. *Radiology* . 2013;268(3):850–857. doi: [10.1148/radiol.13130545](https://doi.org/10.1148/radiol.13130545).
103. Brander A, Kataja A, Saastamoinen A, et al. Diffusion tensor imaging of the brain in a healthy adult population: Normative values and measurement reproducibility at 3 T and 1.5 T. *Acta Radiol* . 2010;51(7):800–807. doi: [10.3109/02841851.2010.495351](https://doi.org/10.3109/02841851.2010.495351).
104. Bisdas S, Bohning D.E, Besenski N, Nicholas J.S, Rumboldt Z. Reproducibility, interrater agreement, and age-related changes of fractional anisotropy measures at 3T in healthy subjects: effect of the applied b-value. *AJNR Am J Neuroradiol* . 2008;29(6):1128–1133. doi: [10.3174/ajnr.A1044](https://doi.org/10.3174/ajnr.A1044).
105. Magnotta V.A, Matsui J.T, Liu D, et al. Multicenter reliability of diffusion tensor imaging. *Brain Connect* . 2012;2(6):345–355. doi: [10.1089/brain.2012.0112](https://doi.org/10.1089/brain.2012.0112).
106. Cancelliere A, Mangano F.T, Air E.L, et al. DTI values in key white matter tracts from infancy through adolescence. *AJNR Am J Neuroradiol* . 2013;34(7):1443–1449. doi: [10.3174/ajnr.A3350](https://doi.org/10.3174/ajnr.A3350).
107. Valdes Cabrera D, Stobbe R, Smyth P, Giuliani F, Emery D, Beaulieu C. Diffusion tensor imaging tractography reveals altered fornix in all diagnostic subtypes of multiple sclerosis. *Brain Behav* . 2020;10(1):e01514. doi: [10.1002/brb3.1514](https://doi.org/10.1002/brb3.1514).
108. Mielke M.M, Kozauer N.A, Chan K.C, et al. Regionally-specific diffusion tensor imaging in mild cognitive impairment and Alzheimer’s disease. *Neuroimage* . 2009;46(1):47–55. doi: [10.1016/j.neuroimage.2009.01.054](https://doi.org/10.1016/j.neuroimage.2009.01.054).
109. Alho A, Hamani C, Alho E.J.L, et al. Magnetic resonance diffusion tensor imaging for the pedunculopontine nucleus: proof of concept and histological correlation. *Brain Struct Funct* . 2017;222(6):2547–2558. doi: [10.1007/s00429-016-1356-0](https://doi.org/10.1007/s00429-016-1356-0).
110. Hakulinen U, Brander A, Ryymin P, et al. Repeatability and variation of region-of-interest methods using quantitative diffusion tensor MR imaging of the brain. *BMC Med Imaging* . 2012;12:30. doi: [10.1186/1471-2342-12-30](https://doi.org/10.1186/1471-2342-12-30).
111. Tang X, Yoshida S, Hsu J, et al. Multi-contrast multi-atlas parcellation of diffusion tensor imaging of the human brain. *PLoS One* . 2014;9(5):e96985. doi: [10.1371/journal.pone.0096985](https://doi.org/10.1371/journal.pone.0096985).
112. O’Phelan K.H, Otoshi C.K, Ernst T, Chang L. Common patterns of regional brain injury detectable by diffusion tensor imaging in otherwise normal-appearing white matter in patients with early moderate to severe traumatic brain injury. *J Neurotrauma* . 2018;35(5):739–749. doi: [10.1089/neu.2016.4944](https://doi.org/10.1089/neu.2016.4944).
113. Suri A.K, Lipton M.L. Neuroimaging of brain trauma in sports. *Handb Clin Neurol* . 2018;158:205–216. doi: [10.1016/B978-0-444-63954-7.00021-5](https://doi.org/10.1016/B978-0-444-63954-7.00021-5).
114. Mac Donald C.L, Barber J, Andre J, Panks C, Zalewski K, Temkin N. Longitudinal neuroimaging following combat concussion: sub-acute, 1 year and 5 years post-injury. *Brain Commun* . 2019;1(1) doi: [10.1093/braincomms/fcz031](https://doi.org/10.1093/braincomms/fcz031) fcz031.
115. Morey R.A, Haswell C.C, Selgrade E.S, et al. Effects of chronic mild traumatic brain injury on white matter integrity in Iraq and Afghanistan war veterans. *Hum Brain Mapp* . 2013;34(11):2986–2999. doi: [10.1002/hbm.22117](https://doi.org/10.1002/hbm.22117).
116. Douglas D.B, Muldermans J.L, Wintermark M. Neuroimaging of brain trauma. *Curr Opin Neurol* . 2018;31(4):362–370. doi: [10.1097/WCO.0000000000000567](https://doi.org/10.1097/WCO.0000000000000567).
117. Douglas D.B, Ro T, Toffoli T, et al. Neuroimaging of Traumatic Brain Injury. *Med Sci (Basel)* . 2018;7(1) doi: [10.3390/medsci7010002](https://doi.org/10.3390/medsci7010002).
118. Wintermark M, Sanelli P.C, Anzai Y, Tsiouris A.J, Whitlow C.T, Institute ACoRHI, . Imaging evidence and recommendations for traumatic brain injury: advanced neuro- and neurovascular imaging techniques. *AJNR Am J Neuroradiol* . 2015;36(2):E1–E11. doi: [10.3174/ajnr.A4181](https://doi.org/10.3174/ajnr.A4181).
119. Yuh E.L, Cooper S.R, Mukherjee P, et al. Diffusion tensor imaging for outcome prediction in mild traumatic brain injury: a TRACK-TBI study. *J Neurotrauma* . 2014;31(17):1457–1477. doi: [10.1089/neu.2013.3171](https://doi.org/10.1089/neu.2013.3171).
120. Wu Y.C, Harezlak J, Elsaid N.M.H, et al. Longitudinal white-matter abnormalities in sports-related concussion: a diffusion MRI study. *Neurology* . 2020 doi: [10.1212/WNL.00000000000009930](https://doi.org/10.1212/WNL.00000000000009930).
121. Wallace E.J, Mathias J.L, Ward L. Diffusion tensor imaging changes following mild, moderate and severe adult traumatic brain injury: a meta-analysis. *Brain Imaging Behav* . 2018;12(6):1607–1621. doi: [10.1007/s11682-018-9823-2](https://doi.org/10.1007/s11682-018-9823-2).
122. Wallace E.J, Mathias J.L, Ward L. The relationship between diffusion tensor imaging findings and cognitive outcomes following adult traumatic brain injury: a meta-analysis. *Neurosci Biobehav Rev* . 2018;92:93–103. doi: [10.1016/j.neubiorev.2018.05.023](https://doi.org/10.1016/j.neubiorev.2018.05.023).
123. Mac Donald C.L, Barber J, Wright J, et al. Longitudinal clinical and neuroimaging evaluation of symptomatic concussion in 10- to 14-year-old youth athletes. *J Neurotrauma* . 2019;36(2):264–274. doi: [10.1089/neu.2018.5629](https://doi.org/10.1089/neu.2018.5629).
124. Mustafi S.M, Harezlak J, Koch K.M, et al. Acute white-matter abnormalities in sports-related concussion: a diffusion tensor imaging study from the NCAA-DoD care consortium. *J Neurotrauma* . 2018;35(22):2653–2664. doi: [10.1089/neu.2017.5158](https://doi.org/10.1089/neu.2017.5158).
125. Niogi S.N, Luther N, Kutner K, et al. Increased sensitivity to traumatic axonal injury on postconcussion diffusion tensor imaging scans in National Football League players by using premorbid baseline scans. *J Neurosurg* . 2019;1–9. doi: [10.3171/2019.3.JNS181864](https://doi.org/10.3171/2019.3.JNS181864).
126. Raslau F.D, Augustinack J.C, Klein A.P, Ulmer J.L, Mathews V.P, Mark L.P. Memory part 3: the role of the fornix and clinical cases. *AJNR Am J Neuroradiol* . 2015;36(9):1604–1608. doi: [10.3174/ajnr.A4371](https://doi.org/10.3174/ajnr.A4371).
127. Zheng Z, Shemmassian S, Wijekoon C, Kim W, Bookheimer S.Y, Pouratian N. DTI correlates of distinct cognitive impairments in Parkinson’s disease. *Hum Brain Mapp* . 2014;35(4):1325–1333. doi: [10.1002/hbm.22256](https://doi.org/10.1002/hbm.22256).
9880. a. Guberman G.I, Houde J.-C, Ptito I, Descoteaux M. Structural abnormalities in thalamo-prefrontal tracks revealed by high angular resolution diffusion imaging predict working memory scores in concussed children. *Brain Struct Funct* . 2020;225:441–459.
128. Dillon D.G, Gonenc A, Belleau E, Pizzagalli D.A. Depression is associated with dimensional and categorical effects on white matter pathways. *Depress Anxiety* . 2018;35(5):440–447. doi: [10.1002/da.22734](https://doi.org/10.1002/da.22734).
129. Madonna D, Delvecchio G, Soares J.C, Brambilla P. Structural and functional neuroimaging studies in generalized anxiety disorder: a systematic review. *Braz J Psychiatry* . 2019;41(4):336–362. doi: [10.1590/1516-4446-2018-0108](https://doi.org/10.1590/1516-4446-2018-0108).
130. Atkinson-Clement C, Pinto S, Eusebio A, Coulon O. Diffusion tensor imaging in Parkinson’s disease: review and meta-analysis. *Neuroimage Clin* . 2017;16:98–110. doi: [10.1016/j.nicl.2017.07.011](https://doi.org/10.1016/j.nicl.2017.07.011).

131. Chan L.L., Rumpel H, Yap K, et al. Case control study of diffusion tensor imaging in Parkinson's disease. *J Neurol Neurosurg Psychiatry* . 2007;78(12):1383–1386. doi: [10.1136/jnnp.2007.121525](https://doi.org/10.1136/jnnp.2007.121525).
132. Vaillancourt DE, Spraker MB, Prodoehl J, et al. High-resolution diffusion tensor imaging in the substantia nigra of de novo Parkinson disease. *Neurology*. 2009;72(16):1378–1384. <https://doi.org/10.1000340982.01727.6e> [pii]
133. Du G, Lewis M.M, Styner M, et al. Combined R2* and diffusion tensor imaging changes in the substantia nigra in Parkinson's disease. *Mov Disord* . 2011;26(9):1627–1632. doi: [10.1002/mds.23643](https://doi.org/10.1002/mds.23643).
134. Singla A, Leineweber B, Monteith S, Oskouian R.J, Tubbs R.S. The anatomy of concussion and chronic traumatic encephalopathy: a comprehensive review. *Clin Anat* . 2019;32(3):310–318. doi: [10.1002/ca.23313](https://doi.org/10.1002/ca.23313).
135. Gandy S, Ikonovic M.D, Mitsis E, et al. Chronic traumatic encephalopathy: clinical-biomarker correlations and current concepts in pathogenesis. *Mol Neurodegener* . 2014;9:37. doi: [10.1186/1750-1326-9-37](https://doi.org/10.1186/1750-1326-9-37).
136. Hendrix P, Griessenauer C.J, Cohen-Adad J, et al. Spinal diffusion tensor imaging: a comprehensive review with emphasis on spinal cord anatomy and clinical applications. *Clin Anat* . 2015;28(1):88–95. doi: [10.1002/ca.22349](https://doi.org/10.1002/ca.22349).
137. Poplawski M.M, Alizadeh M, Oleson C.V, et al. Application of diffusion tensor imaging in forecasting neurological injury and recovery after human cervical spinal cord injury. *J Neurotrauma* . 2019;36(21):3051–3061. doi: [10.1089/neu.2018.6092](https://doi.org/10.1089/neu.2018.6092).
138. Talbot J.F, Huie J.R, Ferguson A.R, Bresnahan J.C, Beattie M.S, Dhall S.S. MR imaging for assessing injury severity and prognosis in acute traumatic spinal cord injury. *Radiol Clin North Am* . 2019;57(2):319–339. doi: [10.1016/j.rcl.2018.09.004](https://doi.org/10.1016/j.rcl.2018.09.004).
139. Ellingson B.M, Salamon N, Hardy A.J, Holly L.T. Prediction of neurological impairment in cervical spondylotic myelopathy using a combination of diffusion MRI and Proton MR Spectroscopy. *PLoS One* . 2015;10(10):e0139451. doi: [10.1371/journal.pone.0139451](https://doi.org/10.1371/journal.pone.0139451).
140. d'Avanzo S, Ciavarrò M, Pavone L, et al. The functional relevance of diffusion tensor imaging in patients with degenerative cervical myelopathy. *J Clin Med* . 2020;9(6) doi: [10.3390/jcm9061828](https://doi.org/10.3390/jcm9061828).
141. Shabani S, Kaushal M, Budde M.D, Wang M.C, Kurpad S.N. Diffusion tensor imaging in cervical spondylotic myelopathy: a review. *J Neurosurg Spine* . 2020:1–8. doi: [10.3171/2019.12.SPINE191158](https://doi.org/10.3171/2019.12.SPINE191158).
142. Wu W, Yang Z, Zhnag T, et al. Microstructural changes in compressed cervical spinal cord are consistent with clinical symptoms and symptom duration. *Spine* . 2020;45(16):E999–E1005.
143. Liang K.N, Feng P.Y, Feng X.R, Cheng H. Diffusion tensor imaging and fiber tractography reveal significant microstructural changes of cervical nerve roots in patients with cervical spondylotic radiculopathy. *World Neurosurg* . 2019;126:e57–e64. doi: [10.1016/j.wneu.2019.01.154](https://doi.org/10.1016/j.wneu.2019.01.154).
144. Simon N.G, Lagopoulos J, Gallagher T, Kliot M, Kiernan M.C. Peripheral nerve diffusion tensor imaging is reliable and reproducible. *J Magn Reson Imaging* . 2016;43(4):962–969. doi: [10.1002/jmri.25056](https://doi.org/10.1002/jmri.25056).
145. Jeon T, Fung M.M, Koch K.M, Tan E.T, Sneag D.B. Peripheral nerve diffusion tensor imaging: overview, pitfalls, and future directions. *J Magn Reson Imaging* . 2018;47(5):1171–1189. doi: [10.1002/jmri.25876](https://doi.org/10.1002/jmri.25876).
146. Marquez Neto O.R, Leite M.S, Freitas T, Mendelovitz P, Villela E.A, Kessler I.M. The role of magnetic resonance imaging in the evaluation of peripheral nerves following traumatic lesion: where do we stand? *Acta Neurochir (Wien)* . 2017;159(2):281–290. doi: [10.1007/s00701-016-3055-2](https://doi.org/10.1007/s00701-016-3055-2).
147. Martin Noguero T, Barousse R, Gomez Cabrera M, Socolovsky M, Bencardino J.T, Luna A. Functional mr neurography in evaluation of peripheral nerve trauma and postsurgical assessment. *Radiographics* . 2019;39(2):427–446. doi: [10.1148/rg.2019180112](https://doi.org/10.1148/rg.2019180112).
148. Gersing A.S, Cervantes B, Knebel C, et al. Diffusion tensor imaging and tractography for preoperative assessment of benign peripheral nerve sheath tumors. *Eur J Radiol* . 2020;129:109110. doi: [10.1016/j.ejrad.2020.109110](https://doi.org/10.1016/j.ejrad.2020.109110).
149. Acer N, Turgut M. Evaluation of brachial plexus using combined stereological techniques of diffusion tensor imaging and fiber tracking. *J Brachial Plex Peripher Nerve Inj* . 2019;14(1):e16–e23. doi: [10.1055/s-0039-1687913](https://doi.org/10.1055/s-0039-1687913).
150. Gallagher T.A, Simon N.G, Kliot M. Visualizing nerve fibers surrounding a brachial plexus tumor using MR diffusion tensor imaging. *Neurology* . 2016;86(6):582–583. doi: [10.1212/WNL.0000000000002360](https://doi.org/10.1212/WNL.0000000000002360).
151. Magill S.T, Brus-Ramer M, Weinstein P.R, Chin C.T, Jacques L. Neurogenic thoracic outlet syndrome: current diagnostic criteria and advances in MRI diagnostics. *Neurosurg Focus* . 2015;39(3):E7. doi: [10.3171/2015.6.FOCUS15219](https://doi.org/10.3171/2015.6.FOCUS15219).
152. Oudeman J, Verhamme C, Engbersen M.P, et al. Diffusion tensor MRI of the healthy brachial plexus. *PLoS One* . 2018;13(5):e0196975. doi: [10.1371/journal.pone.0196975](https://doi.org/10.1371/journal.pone.0196975).
153. Wade R.G, Tanner S.F, Teh I, et al. Diffusion tensor imaging for diagnosing root avulsions in traumatic adult brachial plexus injuries: a proof-of-concept study. *Front Surg* . 2020;7:19. doi: [10.3389/fsurg.2020.00019](https://doi.org/10.3389/fsurg.2020.00019).
154. Wade R.G, Blich E.R, Nar K, et al. The Geometry of the roots of the Brachial Plexus. *J Anat* . 2020 doi: [10.1111/joa.13270](https://doi.org/10.1111/joa.13270).
155. Andreisek G, White L.M, Kassner A, Sussman M.S. Evaluation of diffusion tensor imaging and fiber tractography of the median nerve: preliminary results on intrasubject variability and precision of measurements. *AJR Am J Roentgenol* . 2010;194(1):W65–W72. doi: [10.2214/AJR.09.2517](https://doi.org/10.2214/AJR.09.2517).
156. Kabakci N, Gurses B, Firat Z, et al. Diffusion tensor imaging and tractography of median nerve: normative diffusion values. *AJR Am J Roentgenol* . 2007;189(4):923–927. doi: [10.2214/AJR.07.2423](https://doi.org/10.2214/AJR.07.2423).
157. Wu M, Qiu J, Jiang X, et al. Diffusion tensor imaging reveals microstructural alteration of the trigeminal nerve root in classical trigeminal neuralgia without neurovascular compression and correlation with outcome after internal neurolysis. *Magn Reson Imaging* . 2020;71:37–44. doi: [10.1016/j.mri.2020.05.006](https://doi.org/10.1016/j.mri.2020.05.006).
158. Nowinski W.L, Chua B.C. Three-dimensional interactive atlas of cranial nerve-related disorders. *Neuroradiol J* . 2013;26(3):263–275. doi: [10.1177/197140091302600303](https://doi.org/10.1177/197140091302600303).
159. Lerner A, Mogensen M.A, Kim P.E, Shiroishi M.S, Hwang D.H, Law M. Clinical applications of diffusion tensor imaging. *World Neurosurg* . 2014;82(1-2):96–109. doi: [10.1016/j.wneu.2013.07.083](https://doi.org/10.1016/j.wneu.2013.07.083).
160. Sadeghi N, Nayak A, Walker L, et al. Analysis of the contribution of experimental bias, experimental noise, and inter-subject biological variability on the assessment of developmental trajectories in diffusion MRI studies of the brain. *Neuroimage* . 2015;109:480–492. doi: [10.1016/j.neuroimage.2014.12.084](https://doi.org/10.1016/j.neuroimage.2014.12.084).
161. Wilde E.A, Ware A.L, Li X, et al. Orthopedic injured versus uninjured comparison groups for neuroimaging research in mild traumatic brain injury. *J Neurotrauma* . 2019;36(2):239–249. doi: [10.1089/neu.2017.5513](https://doi.org/10.1089/neu.2017.5513).
162. Shakeel M.K, MacQueen G, Addington J, et al. White matter connectivity in youth at risk for serious mental illness: a longitudinal analysis. *Psychiatry Res Neuroimaging* . 2020;302:111106. doi: [10.1016/j.psychres.2020.111106](https://doi.org/10.1016/j.psychres.2020.111106).
163. Kristensen T.D, Mandl R.C.W, Raghava J.M, et al. Widespread higher fractional anisotropy associates to better cognitive functions in individuals at ultra-high risk for psychosis. *Hum Brain Mapp* . 2019;40(18):5185–5201. doi: [10.1002/hbm.24765](https://doi.org/10.1002/hbm.24765).
164. Van Den Heuvel M.P, Sporns O. Rich-club organization of the human connectome. *J Neurosci* . 2011;31(44):15775–15786.
165. Van Horn J.D, Irimia A, Torgerson C.M, Chambers M.C, Kikinis R, Toga A.W. Mapping connectivity damage in the case of Phineas Gage. *PLoS One* . 2012;7(5):e37454.

EXHIBIT 4

The History, Development and Impact of Computed Imaging in Neurological Diagnosis and Neurosurgery: CT, MRI, and DTI

A Filler

Citation

A Filler. *The History, Development and Impact of Computed Imaging in Neurological Diagnosis and Neurosurgery: CT, MRI, and DTI*. The Internet Journal of Neurosurgery. 2009 Volume 7 Number 1.

Abstract

A steady series of advances in physics, mathematics, computers and clinical imaging science have progressively transformed diagnosis and treatment of neurological and neurosurgical disorders in the 115 years between the discovery of the X-ray and the advent of high resolution diffusion based functional MRI. The story of the progress in human terms, with its battles for priorities, forgotten advances, competing claims, public battles for Nobel Prizes, and patent priority litigations bring alive the human drama of this remarkable collective achievement in computed medical imaging.

BACKGROUND

Atkinson Morley's Hospital is a small Victorian era hospital building standing high on a hill top in Wimbledon, about 8 miles southwest of the original St. George's Hospital building site in central London. On October 1, 1971 Godfrey Hounsfield and Jamie Ambrose positioned a patient inside a new machine in the basement of the hospital turned a switch and launched the era of modern neurosurgery and neuroimaging.

Henceforth, there was a saying at Atkinson Morley's that "one CT scan is worth a room full of neurologists." Indeed, neurological medicine and neurological surgery would never be the same. Everything that neurosurgeons had learned about diagnosis and surgical planning before that first scan was totally transformed by that event.

What came together on that remarkable fall day, was a confluence of mathematics, science, invention, clinical medicine, and industrial resources that all arrived at that one time and place in a dramatic and powerful way. From a number of points of view, that first scan was no surprise to those who made it. Like Damadian's first MR image in 1977, Ogawa's first fMRI image in 1990[1], the first DTI image in 1991[2], or the first neurography image in 1992[3-5], Hounsfield's first scan was simultaneously expected yet astonishing[6-9]. The participants knew generally what they hoped to see, but in each case the result both met and exceeded the dream. The scientist was rewarded by the

shimmering appearance on a computer screen of a view of the human body that no one else had seen before.

Because of the complexity of computed imaging techniques, their history has remarkable depth and breadth. The mathematical basis of MRI relies on the work of Fourier - which he started in Cairo while serving as a scientific participant in Napoleon's invasion of Egypt in 1801. Diffusion Tensor Imaging relies on tensor math that was developed in part by Albert Einstein in his efforts to summarize the transformations of space and time in his general theory of relativity. The physics involves matter-antimatter reactions, nuclear spins, and superconducting magnets. What we can see ranges from the large tumors of the first CT images to the subtle patterning of fMRI that reveals the elements of self and consciousness in the human mind.[10] Medical imaging is starting to press upon the edge of philosophy itself.

Another reflection of the complexity of these technologies is that each major advance has a variety of facets - many different competing inventors and scientists therefore seem to see primarily their own reflection when looking at the same resulting gem. Lenard fought bitterly with Rontgen over the discovery of the X-ray, continuing to vigorously attack him and his work for decades after Rontgen had died. A dozen inventors of tomography fought each other for priority until their shared technology was abruptly superseded by CT scanning so that all of their works faded

into irrelevance before the dust of the internecine battles could even begin to settle. Efforts by Oldendorf and by Cormack to develop computed tomography were totally outrun by Hounsfield because his employer EMI (Electrical and Musical Industries, LTD) was buoyed by a vast cash geyser from John Lennon and Ringo Starr - the competitors couldn't beat an engineering genius funded by sales of Beatles records in the late 1960s. Damadian pled his rage to the world in full page ads in the New York Times when the Nobel prize committee discarded his contribution in favor of his longtime rival Paul Lauterbur and for Mansfield who he regarded as totally insignificant.

In fMRI, one group from Harvard's Massachusetts General Hospital grabbed the scientific imagination with Belliveau's dramatic cover illustration in Science,[11] but eventually lost out to the rightness of Seiji Ogawa's model of fMRI using BOLD (blood oxygen level dependent) MRI[12] that did not require injection of contrast agents and which was published a year earlier. Filler, Richards, and Howe published the first DTI images in 1992,[2, 13] but Basser and Le Bihan at NIH who hold a competing claim to the invention of DTI never referenced the work by the Filler group even once after more than 17 years.

The Basser and LeBihan story is most illuminating as a number of historians have marveled at how in the 1930's and perhaps as late as the 1960's, major early workers in a given field of imaging research could progress over years without being aware of each other's work.[14, 15] The apparent lack of awareness has appeared to be due to barriers to information flow in the 19th and earlier 20th centuries such as difficulties for English speaking scientists in accessing work done outside the major Western centers of science. The prime example of this is Tetel-Baum's early work in CT scanning[16-18] done in Soviet era Kiev in the 1950's and published only in Russian - which had to be "discovered" many years later. The DTI story shows that the causes of apparent unawareness may have more to do with anthropology and psychology than with limitations of academic communication per se.

The story of computed imaging therefore provides both a fascinating opportunity to understand the progress of a science that underlies much of what neurologists and neurosurgeons do today, as well as providing a riveting view into competition and victory in the arena of scientific accolades, clinical impact, patent litigation, and the media, as well as the ultimate judgment of the eyes of history.

X-RAYS AND TOMOGRAPHY

Discovery of an unexpected natural phenomenon coupled with the eery ability to see the skeleton in a living person captured the world's imagination on an almost explosive basis when Wilhelm Rontgen (Figure 1) showed his first images. He had been working with apparatus developed by Lenard that was used to generate "cathode rays." These are electrons generated in a glass vacuum tube when a voltage is applied between a cathode and an anode. When the electrons strike the glass, they cause it to glow - and this can be seen in a darkened room. Rontgen had sealed up a tube to be sure no light would be emitted from the glass so that he could see if the cathode ray would penetrate the glass to strike a piece of cardboard next to the tube that had been painted with a flourescent substance - barium platinocyanide. However when he tested the device to make sure it was completely light sealed, he noticed a glow from a table at some distance away - a distance far too great to be reached with cathode rays. On the table was a sheet of cardboard painted with the barium platinocyanide. He turned off the current to his tube and the glow from the distant table stopped abruptly. He turned on the current to the tube, and distant cardboard immediately began to glow again.

Figure 1

Figure 1 - Wilhelm Roentgen (1845-1923) and Philipp Lenard (1862-1947) - Rontgen was awarded the first Nobel prize for Physics in 1901 for his discovery of X-rays. He was working with Philip Lenard on cathode ray properties when he saw and appreciated the surprise finding of a high energy emission capable of passing through materials that were opaque to light. Lenard was awarded the Nobel Prize in 1905 for his work on cathode rays, but bitterly denounced Rontgen for stealing the X-ray invention from him - later pursuing his academic biases as a high level Nazi official.



Wilhelm Roentgen

Philipp Lenard

He discovered this on November 8th 1895, but told no one,

working feverishly in secret for seven weeks to fully explore his discovery of "X"rays. Finally he submitted a publication that showed a photograph of a skeletal hand. The report published on December 28, 1895 and although the first few newspapers he approached declined to report about it initially, the editor of an Austrian paper did run the story and the news was then rapidly picked up and reported in newspapers around the world.[14, 15]

We now understand the X-rays to be electromagnetic radiation emitted by electrons that have much higher energy and far shorter wavelength than photons of light. Formerly, there was a distinction made between X-rays and gamma rays based on the even higher energy and even shorter wavelength of gamma rays. There is now thought to be so much overlap in the spectra that the two are distinguished by source - gamma rays originate in the nucleus. Although Rontgen really had no idea at all what his "X-rays" were, he was the first winner of the Nobel Prize in physics which was awarded in 1901.

Philipp Lenard, however, was furious that he did not get the prize and the recognition since the apparatus and basic experimental set up were his. He also insisted that he had seen the same phenomenon of distant fluorescence and was doing a more reasoned and formal investigation of the physics before Rontgen rushed out with the dramatic photographs of the skeletal fingers. Although Lenard was awarded the Nobel prize himself in 1905 for his work in cathode rays, he continued to bitterly criticize Rontgen. Philipp Lenard later attacked Einstein for differing from him over the behavior of cathode rays. Still later, Lenard became the Chief of Physics under Hitler - in which position he attacked Einstein's physics as a fraud which no doubt allowed the Germans to fall far behind the allies in the development of the atomic bomb.

PLANAR TOMOGRAPHY

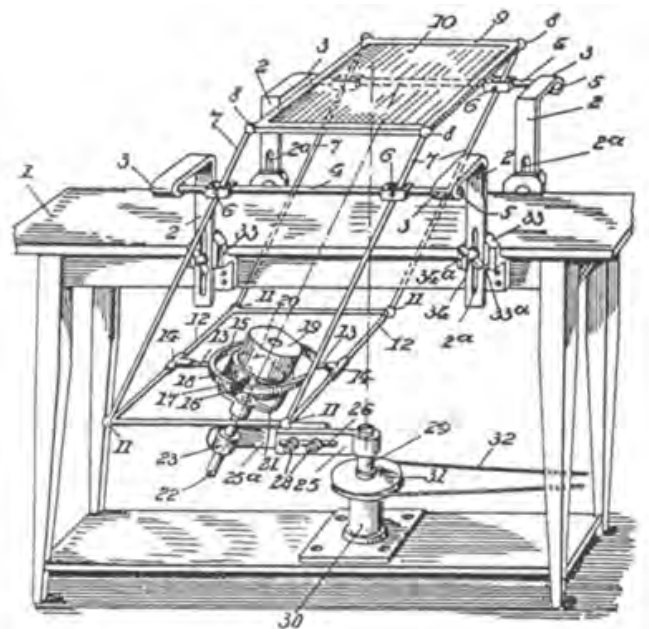
Against the drama of the discovery of X-rays and its truly electrifying effect on the world at large, the history of tomography presents a very pale shadow. The driving idea here was to get a better look inside the chest so that the heart, lungs, and any tuberculosis or tumors could be better seen with out the interference of the rib cage in front and behind. The fact that radiologists today still rely primarily on non-tomographic chest X-rays speaks volumes about the clinical impact of the whole endeavor. Essentially, the idea is to move the X-ray source to the left while the image plate is moved to the right. The axis of rotation of a line from the

source to the plate must be on a plane of interest inside the body. The result will be that structures in the middle of the patient (along the plane of the axis of rotation) will remain relatively clear while those in back and front will be blurred.

The various patents and theories of accomplishing this varied in regards to details such as whether the source and plate would be linked rigidly as by a pendulum (the plate goes through an arc) or alternately, whether the plate would remain parallel to the imaged plane in the patient, and so on (see Figure 2). Each different method had a different name - stratigraphy, planigraphy, sterigraphy, laminography, etc. The patents were often competing and overlapping, but filed in different countries. The machines were generally mechanical devices with hinges, and levers and pendulums. The patents were typically pure mechanical devices without any obvious proof that the images produced were better or worse than those from any other method if any images were produced at all. There was no serious mathematical or physical analysis of the designs.

Figure 2

Figure 2 - Tomographic device. A typically complex mechanical drawing from a patent granted to Ernst Pohl in 1930.[154] This type of tomography was called planigraphy in part because the X-ray plate remained parallel to the subject and the X-ray tube changed angle as the field was covered.



With the elapse of time, the tomographic systems became more complex without becoming any better or more useful. The movements of the source and plate could be quite

complex involving circles and spirals. Systems were provided for advancing the plane of imaging so a series of tomograms could be made.

In 1937, William Watson[19] filed a patent application (granted in 1939) for the first important system that made a series of axial tomographic images slices. The patient sat on a stool that was rotated through a full circle as the image was being made, while the X-ray plate was moved as well. The seat of the stool was mounted on a telescoping column that could be raised or lowered to get axial sections at various locations in the body. This device actually achieved considerable commercial success.

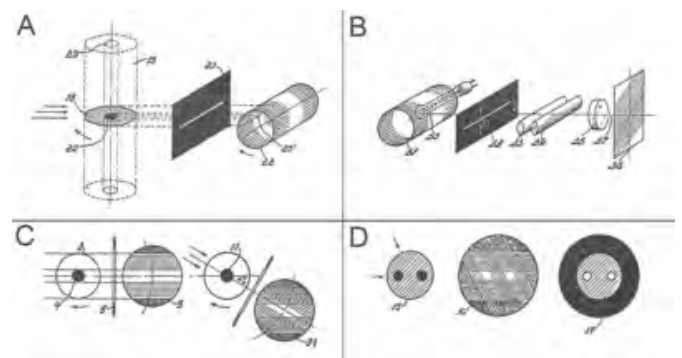
A number of inventors developed devices that rotated the patient. Among the most interesting aspects of these later developments conceptually was the emergence of the idea of 'non-blurring' tomography that could produce an axial cross section of the patient in which the tissue outside the plane of interest was not even exposed. Although these worked, they involved a truly enormous amount of X-ray exposure.

FROM AXIAL TOMOGRAPHY TO COMPUTED AXIAL TOMOGRAPHY

The next important advance was a non-computed axial tomographic device that employed the novel idea of "back-projection." This is also one of the fundamental aspects of Hounsfield's computed tomography and of Paul Lauterbur's initial MRI design. It is certainly the single most important technical advance to emerge from the sixty year history of non-computed tomography. Gabriel Frank filed a patent in 1940 that fully worked out the methodology for this approach to imaging[14, 20] (see figure 3).

Figure 3

Figure 3 - Gabriel Frank's back projection design. These drawings from the patent granted in 1940[20] explain the back projection image collection and reconstruction mechanism - essentially what is accomplished by a CT scanner today using a computer. (A) A cross sectional image is being collected at (18) in a subject structure with a solid dense dowel standing vertically in a low density cylinder. X-rays approach from the left and are collimated so they strike and expose a single line on a drum. The subject is then rotated on its long axis a few degrees, and the drum is rotated on its long axis a few degrees, and another line is recorded - and so on. (B) Image reconstruction - with a light source in the center of the drum, each line is then projected through a collimating plate, then strikes a film. As the drum is rotated on its long axis, the film can be rotated on an axis linking the center of the film to the center point of the drum line or the mirror wheel (35,37) is rotated to change the angle of projection. (C) How the reconstructions assemble on the film, line by line, to accomplish the back projection process that constructs the image. The intervening step of recording on the drum and projecting out through the projection collimator has been collapsed to give a clearer impression of the connection between the subject and its back projection (D) A progressing back projection of a different subject with two dense areas, again with the system collapsed for diagrammatic purpose.



In back-projection, an emitter shines an x-ray through a subject to a "receiver" that transduces the incoming X-ray light to produce a linear trace on a rotating drum. Gradually, the X-ray source and the collimated entry filter of the receiver are swept from the one edge of the subject to the other. If the subject is a phantom cylindrical column made of perspex with a dense dowel at its core, then the receiver will show a high intensity linear trace as the beam progresses steadily across the perspex, then drops off abruptly when the beam line crosses the dowel and then comes back up again once the dowel is passed.

We now have a linear trace that describes the position of the dowel as an area of decreased exposure along one portion of

the detection line. We then rotate the subject a few degrees and do the same thing again producing a new trace and continue to do so again and again until traces are obtained from a large number of directions (for instance 360 views if the subject is on a turntable that is turned by one degree just before each complete edge to edge trace is carried out).

At this point we have a drum with a record of the series of linear exposures - much like an archaic gramophone cylinder. We can now use the lines recorded on the cylinder to drive an exposure light to create a film image of what has been recorded. Note that the data collection step is now completely separated from the film exposure step.

We lay a sheet of unexposed film flat on a turntable. We have a light source that shines a narrow beam across the film. When the beam is on, it exposes a line of light onto the film. When the beam is off, no exposure takes place. We shine a focused line of light from the source from one edge of the film to the other edge, controlling the intensity of the exposing light by the intensity recorded on our trace. As the source moves across from one edge towards the other it remains dark, but when it encounters the blip where the dowel blocked the x-ray, it turns on the beam and a line of light is exposed onto the film at that point. The turntable is then rotated and the next line played out. Eventually, a thin line of light will be projected across the film from one point during each of the 360 differently angle exposure traverses. Importantly, all of the 360 lines will cross at just one point on the film. This point will have by far the greatest exposure and this point will expose as bright white exactly where the dowel was in our perspex model.

This is the fundamental idea of back-projection. The idea of positron emission tomography, computed axial tomography, and Paul Lauterbur's MRI is to do what the mechanical back projection system has done, but to do it quickly relying on electronics, computer reconstruction techniques, and more advanced physics.

INVENTION AND REDUCTION TO PRACTICE OF CT SCANNING

We know the most about four entirely independent researchers who saw the opportunity to take advantage of recent advances in computers in the 1960's to develop a computer based, back projection, axial tomography system. These workers published and filed patents as they progressed. Hounsfield was the fifth worker. He was not an academic. He did not publish. He only filed patents very late

in the process so that most of the work was done before the patents were published. He was funded internally at EMI so there were no grant proposals. He had an unmatched budget to do his work. He made a series of well executed stepwise advances that allowed him to continue to work in secrecy while renewing his financial support within the corporation.

Oldendorf at UCLA developed a model that differed from the non-computed axial tomogram in that the subject moved along a line as it rotated.[14, 15] A computer then sorted out the motions to carry out the back projections and display the results on a computer screen. He presented it to an imaging manufacturer and was patiently told that there was no use for his machine - so he abandoned the effort. A group in Kiev built a working model, but published in Russian and never progressed the work.[16, 17] At Massachusetts General Hospital, Brownell[21] and Chesler[22] used positron emissions in a computed back projection system and then later developed a system in which a gamma ray source was used to carry out a transmission computed tomographic image experiment.

Allan Cormack was a South African physicist who joined the faculty at Tufts University in Boston in 1957 and later published (in 1963 and 1964) a solution of the problem of "line integrals"[23, 24] a mathematical technique that is used in most modern CT scan computation - although Hounsfield did not use this mathematical approach. Cormack was awarded the Nobel Prize in 1979 for the invention of CT scanning along with Hounsfield. It was later appreciated that several decades earlier, Johann Radon (an Austrian mathematician) had solved and published[25] much of what Cormack had done. It was also appreciated later that further advances on the mathematics had also been published previously - in Russian - by the Kiev group[18]. Hounsfield cites Cormack's papers in his 1968 patent submission (granted in 1973)[26] but dismisses Cormack's math as not usable for practical applications. None of the others (Cormack, Kuhl, Oldendorf) knew of Hounsfield's secret work.

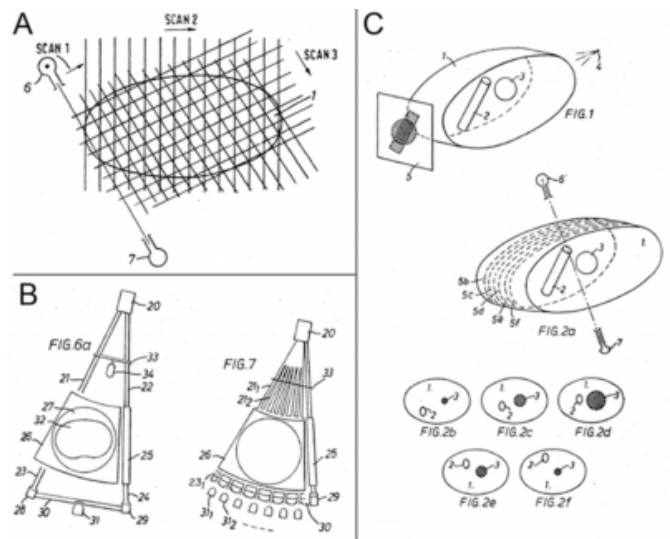
Hounsfield's biggest setback came when the moment arrived to travel to the National Neurological Hospital at Queen's Square in London to meet with the chief of neuroradiology. He explained what he had accomplished and proposed the construction of the first tomographic scanner in order to make computed tomographic images to show slices of brain structure in patients. The neuroradiologist patiently

explained to Hounsfield that with pneumoencephalography, plane tomography, and angiography, there was no existing brain lesion that could not be diagnosed by imaging already. There was no obvious clinical used for a computed tomogram machine as tomograms in general weren't really all that useful. He was sent packing. It is told apocryphally at Atkinson Morley's Hospital (AMH) that as soon as Hounsfield had left, the radiologist at Queen's Square took the time to pick up the phone to call the official at the ministry of health who had sent Hounsfield to see him - the official was warned in no uncertain terms never again to waste the radiologists time with crackpot inventors peddling ridiculous contraption ideas such as this.

Hounsfield, of course, figuratively picked himself up, dusted himself off, and managed to solicit a referral to the chief of neuroradiology at the number two neurological hospital in London - Jamie Ambrose at Atkinson Morley's Hospital in Wimbledon - the initial meeting took place in 1967. Ambrose had an interest in using ultrasound to image inside the skull and was familiar with the axial tomography concept. He liked Hounsfield's proposal, and others at AMH thought it sounded sufficiently eccentric and interesting as to be worth a try (see figure 4).

Figure 4

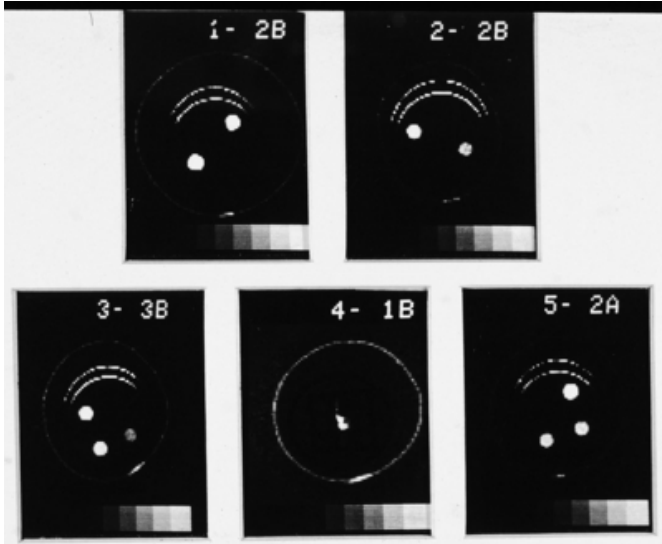
Figure 4 - Explanatory drawings from Hounsfield's patent granted in 1973. (A) Demonstration of the basic back-projection tomography principle of taking a series of linear parallel intensity transmission measurements 6 - source, 7 - detector. The orientation of the acquisition is then rotated. (B) The structure on the left takes a single intensity transmission measurement with 28 as the primary detection site, with the signal intensity reflected into the detector at 31. At 29 there is a second pathway provides a simultaneous standard measurement with no tissue. The apparatus is then rotated as a series of linear measurements are made, then repositioned for another set. The more complex apparatus on the right takes all the measurements for one view at once, then the whole unit is rotated. It still uses one X-ray source, but has multiple detectors 31-1, 31-2, etc. (C) Because serial axial sections were novel, this drawing was provided to explain how objects would appear on multiple sections.



The entire staff of the hospital was sworn to secrecy during the duration of the construction and testing. Atkinson Morley's is fairly secluded and surrounded by woodlands on three sides so secrecy was easily achieved. The machine was built along a plan for commercial production. The first test resulted in the images shown as figure 5.

Figure 5

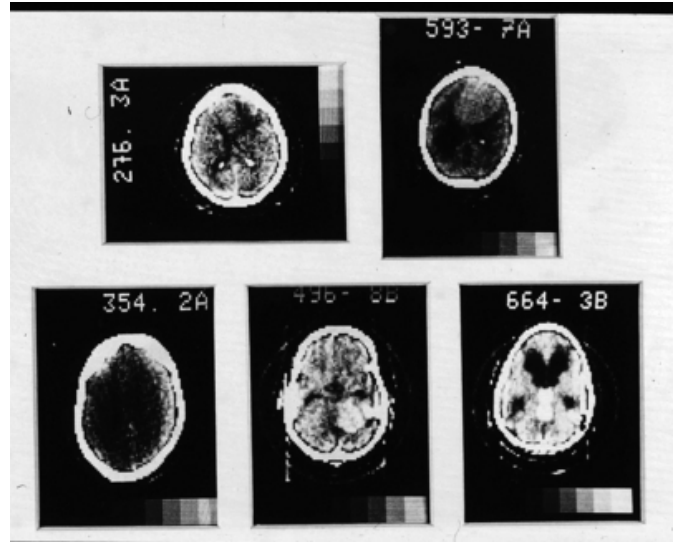
Figure 5 - Initial test images after installation of the first commercial CT scanner at Atkinson Morley's Hospital in 1971 (Photograph courtesy of St. George's, University of London).



It was time for the first patient - the data tape was collected and then sent across London for analysis, computed back projection and image reconstruction. The new image tape was rushed back to AMH where the result was viewed by Jamie Ambrose. It was immediately apparent to the assembled neuroradiologists, neurologists and neurosurgeons of AMH that something of truly spectacular clinical utility had emerged. Several more patients were scanned - each with complex pathology, each producing a crude but riveting set of image scans.

Figure 6

Figure 6 - First clinical images from the original CT scanner. These images were posted on the wall of the neuroradiology department at Atkinson Morley's Hospital until the hospital moved to the main St. George's site in 2003. (Photograph courtesy of St. George's, University of London).



Photographs of the first five patient scans hung on the wall of the radiology department of AMH until the service was moved out to an "Atkinson Morley Wing" of the new St. George's Hospital in Southwest London in 2003. Figure 6 is a photograph taken of the wall in the radiology reading room at AMH and figure 7 shows Hounsfield holding a data tape, talking with one of the first CT technologists.

Figure 7

Figure 7 - Godfrey Hounsfield and one of the first CT radiographers (technologists) near one of the operating consoles at Atkinson Morley's Hospital in Wimbledon. Hounsfield is holding a computer tape (Photograph courtesy of St. George's, University of London).



The result was announced to the world and received enormous media and clinical attention. Hundreds of radiologists, neurologists and neurosurgeons from around the world headed for Wimbledon to see the new machine at AMH. Orders poured in to EMI despite the then astonishing \$300,000 price tag.

As one might imagine ongoing worldwide sales of working clinical units (EMI scanners as they were called) abruptly put an end to all other attempts to learn how to do computed axial tomography, but simultaneously launched an intensive, high powered battle to achieve commercially valuable improvements of the device which continue to this day. For nearly ten years, EMI deployed its patents to try to hold off potential competitors in court. It used a strategy of filing patent infringement litigation then offering settlements with

sealed documents. In this way, each company that they sued had to start from scratch to try to assess the strength of the EMI patents, but EMI avoided the huge expense and unpredictability of full jury trials to assess its patent rights. Since back projection itself was not an invention and no unique algorithms were used at first, much of the patent was based on Hounsfield's findings that the X-ray beam itself could sensitively distinguish tissues when properly deployed at low intensity.

EMI rapidly advanced through four generations of scanners, steadily reducing scan time, reducing computing time and improving spatial resolution. It also started development of an MRI scanner project. However, in the early 1980's the scanner unit succumbed to the pressure of competition and litigation becoming a money losing activity - upon which it was sold off to the British company GEC (General Electric Company, plc). It's corporate remnants were later assembled with products from an American company called Picker and from Elscint - also scanner manufactures - to result in a division at GEC called Picker International which was later renamed Marconi. This unit was sold to Philips in 2001.

Continuing advances in CT scanning include dramatic advances in the speed of scanning and the use of simultaneous acquisition of as many as 128 image slices, all of which have improved CT's capabilities to stop motion like a fast camera. Together with advanced intravenous contrast agents, the detail and quality of CT angiography for coronary and cerebral vessels continues to advance. At a different extreme, small light mobile "O-arm" units have been developed that allow for real time CT scanning in the operating room.

THE PHYSICAL BASIS OF NUCLEAR MAGNETIC RESONANCE

The history of MRI can be considered in three phases - the discovery of the fundamental physics and biological properties of nuclear magnetic resonance, the emergence of designs to accomplish imaging with MRI, and finally the emergence of neurologically optimized methods such as diffusion tensor tractography and functional MRI.

From a number of points of view, the very possibility of MRI at its outset and the most exciting destination of the technology in modern fMRI are embodied by its true grandfather Wolfgang Pauli (see figure 8), an extraordinarily talented and extraordinarily troubled Viennese physicist. He differs in many ways from the other scientists and inventors

covered in this article but in no way more strikingly, than in the fact that he was utterly unconcerned with establishing priority for his work. He generally did not even bother to publish but just sent out his ideas in letters to his prominent friends and colleagues such as Werner Heisenberg and Neils Bohr. Despite the carelessness of documentation, we know more about him than about nearly any other scientist because - following a nervous breakdown after a divorce at age 31 in 1931 (no doubt precipitated in part by his intensive work leading to his discovery of the neutrino), he became a patient of Carl Jung who later published descriptions of more than 400 of Pauli's dreams.

Figure 8

Figure 8 - Leading scientific contributors to the development of Nuclear Magnetic Resonance. Jean Baptiste Joseph Fourier (1768-1830) a French mathematician and physicist developed the mathematical methods for converting data between the time domain and the frequency domain - a method now used in a critical step in utilizing NMR and MRI data (image source: <http://en.wikipedia.org/wiki/File:Fourier2.jpg>). Wolfgang Pauli (1900-1958) initially proposed the existence of the physical basis of magnetic resonance. Isidor Rabi (1898-1988) did the first experiment that proved the existence of magnetic resonance. Felix Bloch (1905-1983) and Edward Purcell (1912-1997) independently demonstrated the presence of nuclear magnetic resonance in solids (photo of Felix Bloch courtesy of Stanford News Service). Erwin Hahn (born 1921) conceived of the refocusing pulse/spin echo concept that greatly improves the utility of measurement of T2 relaxation in most biological situations (photo courtesy of Lawrence Berkeley National Laboratory).



Pauli's first publication was an article evaluating Einstein's theory of general relativity that he published at age 18. In fact Pauli's analyses of relativity were so well received that it was Albert Einstein himself who nominated Pauli for the Nobel prize he received in 1945. Pauli discovered many remarkable things about nature, its particles and their quantum behavior. Most importantly for MRI, noticing some irregularities in some spectra he was evaluating, he made the suggestion - in 1924 - that atomic nuclei should have magnetically related spins. He was correct in this and this is the physical basis of magnetic resonance upon which everything else in this field is established.

A number of physicists set out to test Pauli's ideas on nuclear magnetism deploying a variety of experimental devices and systems. Most important in this period of time was the success of Isidor Rabi in 1938 (see figure 8). Rabi - who won the Nobel Prize in 1944 - beat out numerous brilliant competitors by realizing how to design an experiment to detect and measure the magnetic spin of atomic nuclei.[27] In an arrangement used by other nuclear physicists, a gaseous beam of nuclei of a given element was sent past a magnet which deflected the beam before it hit a detector. Rabi added an additional electromagnet whose field strength could be rapidly oscillated. In an inverse of how this is typically done today, the he was able to vary the strength of magnet. At a particular combination of field strength and frequency of the magnetic oscillator, the beam would abruptly begin to bend to a new deflection point. Rabi was using a tuned resonant frequency to pump electromagnetic energy into the protons. The particular mix of field strength and frequency varied from one element to another. He had proven the existence of magnetic spin, showed how to identify the "gyromagnetic ratio" of every element, and demonstrated the phenomenon of using varying fields to manipulate magnetic resonance.

An interesting historical note about another famous contest that Rabi won concerns the first atomic bomb explosion - the Trinity test at Los Alamos in July of 1945. Bets from the various physicists at site about the potential force that would result from the fission chain reaction ranged from dud to annihilation of the universe. Rabi predicted 18 kilotons of TNT coming very close to the measured 20 kiloton force that was actually recorded.

With the end of World War II later that year, physicists returned to peaceful pursuits and the first great result for MR came independently from Purcell[28] at Stanford and Bloch[29] at Harvard in 1946 (see figure 8). Each published their finding that the magnetic resonance effect that Rabi[27] had observed in gases could also be detected in solid materials. Bloch filed a patent for the first NMR spectrometer in December of 1946 (granted in 1951).[30] This opened the era of nuclear magnetic resonance study of a wide array of materials including biological specimens. Further work in Nuclear Magnetic Resonance by Hermann Carr - along with Purcell [31] together with modifications by Saul Meiboom and Gill[32] led to the development of pulse sequences of radiofrequency and magnetic energy (CPMG sequences - for Carr, Purcell, Meiboom, Gill) that could

identify different rates of magnetic field decay in a given type of element situated in various different chemical and physical surroundings.

An example of the kind of tasks that can be accomplished this way is the "spin echo" - a term that applies to what is done in the vast majority of modern MRI scans. This was conceived of, measured and proven by Erwin Hahn (see figure 8).[33] When a radiofrequency pulse of the correct frequency is applied to a sample in a magnet, the selected protons will spin in phase with each other because they are all being driven by the same stimulating oscillating wave form. We then turn off the stimulating signal and listen to the emitted oscillating signal from the stimulated protons. As they all spin around together, they generate a signal that is strong as the tipped magnetic poles swing towards our antenna and weak as they spin away. This emission oscillates at the same resonant frequency at which the protons were stimulated. However, with the elapse of time, the signal decays away as the added energy from our stimulating pulse is dissipated. The signal - oscillating and steadily decaying away is called the FID (free induction delay).

Hahn had an ingenious idea to alter the way in which the spinning protons dissipate their introduced spin energy. Thinking of the spinning protons as spinning tops, imagine knocking them with the RF energy in such a way that instead of their axis of spin being vertical, it is actually horizontal with the foot of the spinning top resting on a vertical wire axis. In addition to spinning around its now horizontal axis, the top also "precesses" around the vertical wire.

As long as the axis of the spinning proton is horizontal it emits a strong signal. With dissipation of the pulsed-in energy, the angle of the axis slowly returns towards vertical. We can call the magnetic output of the proton when it is vertical the "longitudinal" magnetization and when it is horizontal we say there is also a "transverse magnetization." As the orientation of the spinning proton returns to vertical - which is parallel with the main magnetic field of the magnet - the signal generated by the spinning transverse magnetization fades away - this is the T1 relaxation process.

Another aspect of the way in which the RF pulse tips the spin axes is that in addition to being horizontal, they are precessing around the wire coherently in phase with all the other surrounding protons. Because they are all in phase with each other as they precess around and as they spin, they join

together to produce a strong coherent oscillating radiofrequency signal that we “hear/analyze” with our antenna once the stimulating pulse is turned off.

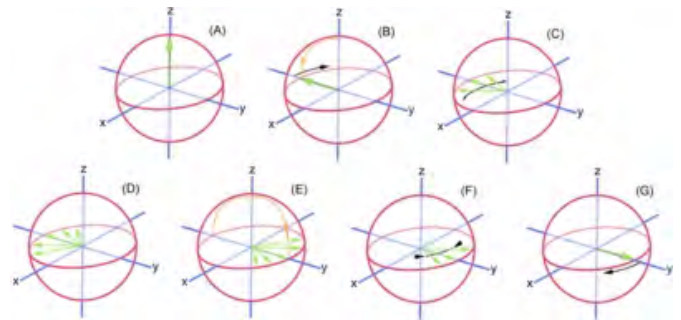
However, two other types of signal decay come into play as we consider this situation. Firstly, the precessing protons will interact with each others' magnetic fields and will disrupt each others' spin rates so that the spins gradually dephase from each other and the signal fades away. These are called “spin-spin” interactions and this type of signal decay is called the T2 relaxation decay. These random interactions will differ in quality from one tissue to another depending on how freely mobile the water protons are - fast in protein laden solutions, slow in water where the protons tumble freely.

In addition, there may be non-uniform aspects of the general environment. For instance, a blood vessel nearby will have some iron in deoxyhemoglobin and this will uniformly affect spins nearby causing more rapid loss of phase coherence and therefore signal loss. This is called T2* decay. In some types of imaging such as BOLD for functional MRI, we want to emphasize these effects. In most other types of imaging we want to suppress T2* effects as they may be irrelevant to the aspects of tissue anatomy we are interested in.

Erwin Hahn's idea - further updated by Carr and Purcell[31] - was that there was a way to “refocus” the precessing protons to eliminate T2* effects (see figure 9). First, we deliver the RF pulse that flips the protons into horizontal configuration. This is called the 90 degree pulse. Then after a selected echo time interval, we apply a second 180 degree pulse that flips the axis into the opposite horizontal position.

Figure 9

Figure 9 - The spin echo concept. (A) - The vertical green arrow is the average magnetic moment of a group of protons. All are vertical in the main field and spinning on their long axis. (B) A 90 degree pulse (orange arrow) has been applied that flips the arrow into the horizontal (x-y) plane. The black arrow shows the precession of the net magnetic moment. (C) & (D) Due to T2* effects, as the net moment precesses, some protons slow down due to lower local field strength (and so begin to progressively trail behind) while some speed up due to higher field strength and start getting ahead of the others. This makes the signal broaden progressively, dephasing and decaying. (E) A 180 degree pulse is now applied (orange arrow) so now the slower protons lead ahead of the main moment and the fast ones trail behind. (F) Progressively, the fast moments catch up with the main moment and the slow moments drift back toward the main moment. (G) Complete refocusing has occurred and at this time, an accurate T2 echo can be measured with all T2* effects removed.



Quite separately, return of the green arrow towards the vertical (not shown) would reflect the T1 relaxation (drawing by AG Filler - copyright: GDFL 1.3/CCASA 3.0, image source: http://en.wikipedia.org/wiki/File:Spin_Echo_Diagram.jpg).

In the initial 90 degree position, we can think of a single thick vector line representing the combined output from the all the vectors spinning at identical speed and phase representing the effects from all the stimulated protons in a sample. As these spins slowly lose coherence - some going a little faster, some a little slower - the single thick vector spreads out. Some component protons slow their precession and some actually speed up - all in response to the local magnetic environment - these T2* effects make the T2 decay occur rapidly. Strangely enough, with the 180 degree refocusing pulse, the spreading effect reverses itself. The spins that were spreading apart in their phases, begin slowly drifting back into phase with each other. We typically measure the T2 signal intensity at the point at which the refocusing is complete. This places the refocusing pulse

exactly half way between the time of the 90 degree stimulating pulse and the echo time (TE). The TE is the point at which the frequency and phase gradients are deployed to read out the resulting signal strength. The removal of the T2* effects allows for the T2 decay itself to be observed over far longer decay times and so provides far more complex and subtle T2 contrast between and among various tissues.

INVENTION OF MAGNETIC RESONANCE IMAGING

With all of these pieces in place, the stage was set for the great drama of the invention of magnetic resonance imaging itself.

DAMADIAN'S CONTRIBUTION

Throughout the 1950's and 1960's, NMR was used to test and evaluate a wide variety of substances and tissues. In a typical NMR machine, there is a small tube in the midst of the magnet and the material or tissue to be studied is placed in the test tube. In 1970 Raymond Damadian (see figure 10) - a research physician at the State University of New York (SUNY) Brooklyn campus, thought to measure T1 and T2 relaxation time on various tumors in comparison with related tissues. Damadian found that the T2 was longer in the tumors he studied by comparison with normal tissue. This finding, published in Science in 1971[34] electrified the magnetic resonance community because it suggested that there could be an important medical use for NMR in testing tissues for the presence of cancer.

Figure 10

Figure 10 - Inventors of MRI. Paul C. Lauterbur (1929-2007) proposed the use of three orthogonal gradients that is the basis of most modern MRI systems. Raymond V. Damadian (born 1936) in the early days conducting MRI experiments - he showed that cancerous cells should be distinguishable from normal cells by NMR and invented the first systems capable of collecting localized NMR data from various parts of the intact body in living humans (photo courtesy of Fonar Corporation).



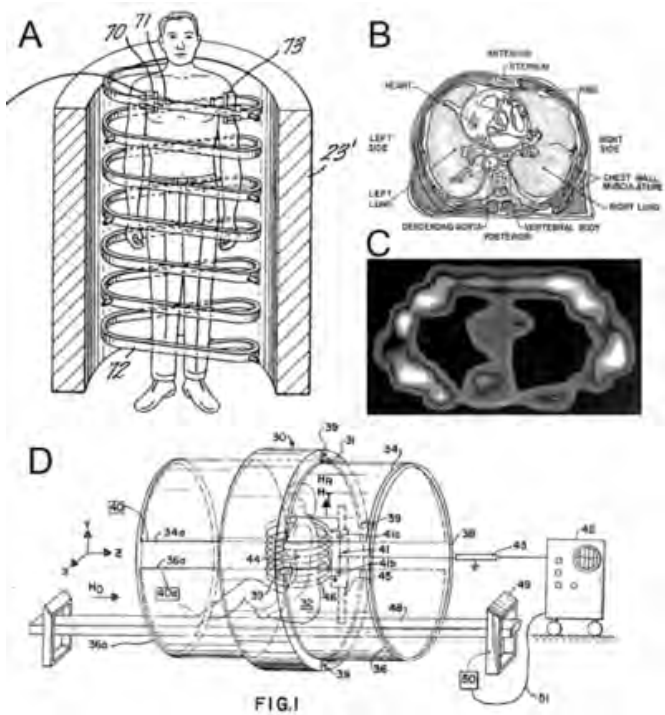
Paul Lauterbur

Raymond Damadian

As is well known today, the T2 decay rate of most cancers does not follow the behavior that Damadian observed - but nonetheless “a thousand ships were launched.” Damadian himself decided that his next step would be an enormous advance. He would progress directly from his measurement of a piece of excised tissue in a test tube to a project to immediately construct an NMR machine that was truly enormous by the test tube standards of that era - big enough for a living person to stand and move around inside the machine (see figure 11). This is what is described in his 1972 patent filing (granted in 1974)[35].

Figure 11

Figure 11 - Damadian's designs and results. (A) The human size NMR spectrometer with spiral carriage for the RF apparatus submitted in his original 1972 patent application 1972 (granted 1974).[35] Images from Damadian's later application submitted in 1978 (granted in 1982): (B) Drawing of human thoracic cross section, (C) the first image from 1977, (D) a design from this patent equipped with a system (49 & 50) for moving the patient within the device.[155]



He conceived of a means to do NMR tissue measurements in a vertical column of uniform magnetic field (a few centimeters in diameter) in the center of the magnet. The radiofrequency emitter and detector would then spiral their way down, measuring again and again as they progressed from the top of the head to the foot. Only the vertical column at the very center of the person would have just the right homogeneous magnetic field strength for the magnetic resonance testing to occur. Then, the person would move a little bit so that the central magnetic field would pass through a different vertical column of the body and the spiral process would be repeated. In this way, measurements would be taken of all parts of the body that would allow the machine to detect an anomalous T2 signal that could indicate cancer and would allow the physician to know approximately where in the body to look for it.

There were many problems with this device. First and foremost, it was not actually capable of making an image.

Secondly, the T2 phenomenon would only identify a small fraction of all the possible tumor types, the rest remaining undetected. The transmit and receive device he postulated would not provide a “beam” of RF energy as he proposed since the radiowaves are broadcast and then received from the antenna along a wide area. This machine did not work and was never used. It also differed from the step by step magnificent precise and triumphant theoretical experimental physics of earlier workers - instead it was large crude, hypothetical, irrational in many ways and took a giant leap without working through the necessary steps along the way.

NOBEL PRIZE CONTROVERSY

When the Nobel Prize for invention of MRI scanning was announced in 2003, Damadian was snubbed and the award went to two more traditional scientists, Paul Lauterbur and Peter Mansfield. Damadian is a creationist so he accepts magical and divine intervention in biology. That has made him an intellectual martyr for the creation science crowd. Nonetheless, his omission from the Nobel Prize is a Rohrsach test meaning different things to different observers. The Prize committee, despite an intensive effort by Damadian and a wide array of supporters - held to their position. In a reverse answer to a question Damadian asked in one of his newspaper ads - they believed that MRI would have been developed by Lauterbur with or without Damadian's contribution and that Lauterbur would have accomplished it no sooner and no later. They did not accept the possibility that the reverse of this premise might in fact be correct.

DAMADIAN'S PATENT LITIGATION

Damadian was ultimately able to enforce one of the later patents from his company, Fonar, that covered oblique angle imaging. However, his original patent faced many difficulties, - when a jury awarded Damadian a 2.2 million dollar settlement for patent infringement against a subsidiary of Johnson and Johnson, the judge threw out the verdict. When a jury awarded him more than \$100 million in his patent infringement lawsuit against GE for both MRI and for oblique angle imaging, Judge Wexler threw out the entire award leading to a complex appeal process.

Damadian won the appeal and was ultimately able to collect damages for patent infringement from GE and from all the other MRI manufacturers for the oblique angle software feature. This result has sometimes been misstated as an action by the US Supreme Court that vindicates his claim to

invention of MRI scanning. In fact, the US Supreme Court did decline to review Damadian's success in the appeal that reinstated the jury verdict against GE however the details of the decision (by the United States Court of Appeals for the Federal Circuit 96-1075,-1106,-1091 under judges Lourie, Skelton, and Rader) warrant a close reading.

In the successful appeal, the court did deal with Damadian's original patent and found infringement because the GE scanner also distinguished the T2 decay time of cancerous tissue not because of the issue of imaging. In addition, the appeal judge ruled that the grey scale images that the GE scanner produced were equivalent to numerical comparisons of the T2 values of selected tissues that were produced by the Damadian machine. However, there is no support in the judicial decision for the assertion that the Damadian machine produced an image. For these reasons, Damadian has a valid enforceable patent that is infringed by all MRI scanners, but his assertion that the US Supreme Court decided that he invented MR imaging is not correct.

LAUTERBUR AND THE TECHNICAL BASIS OF MR IMAGING

So what is it that Lauterbur and Mansfield did that led to sharing the Nobel Prize for the invention of MRI? It is really Paul Lauterbur who had the transforming idea that makes magnetic resonance into a viable imaging method.

Like Damadian, Lauterbur (see figure 10) was a professor at the State University of New York (SUNY) but at its northern Long Island location at Stonybrook. In addition he was the CEO of a small company - NMR Specialties - that manufactured and operated NMR equipment. Partly as a result of Damadian's publication about the increased T2 time of tumors[34], Lauterbur had been forced to run NMR analyses of pieces of rats that he had to put into test tubes. Damadian was a physician but Lauterbur was a physicist who was generally sickened by the specimens that were starting to arrive. After one grisly day, he sat at a hamburger restaurant (a Big Boy to be precise) trying to get his appetite back, and searching through his mind for any possible ways he could think of that would let him measure the NMR data on intact animals. He needed a way to focus the experiment on a single location inside the animal. An answer occurred to him and almost immediately he realized that his method would allow individual locatable measurements of any point in the animal and that these could be reconstructed into images like tomograms. He jotted it all down on a napkin, then rushed out to buy a notebook where he could write out

the idea in more detail to get it dated and witnessed (September 2, 1971) for a patent filing.

Lauterbur filed a preliminary patent disclosure but as the 12 month point arrived when he would need to spend money to file the actual patent, he received advice from all sides that magnetic resonance imaging had no imaginable commercial use. He allowed the deadline to pass without filing, publishing the method in *Nature* (after successfully appealing an initial rejection by an editor who felt this would be of limited specialist interest only).[36]

Lauterbur's idea was to use magnetic gradients to assign a different magnetic field strength to each point in a subject volume. This idea was based on the gyromagnetic ratios that Isidor Rabi had first measured more than thirty years earlier. Essentially, for protons for example, at 4.7 Tesla, the resonant frequency for the protons (hydrogen atoms) in water is 200 megahertz. If you apply a magnetic field gradient across a specimen then (using approximate illustrative numbers) on the left the field strength will be 4.701 Tesla and on the right it will be 4.699 Tesla. The proton resonant frequency on the left will now be 200.01 MHz and the frequency on the right will be 199.99 MHz.

In this fashion, and by applying gradients in three different directions (X, Y and Z) you can assign a unique field strength to each location (voxel) in the sample volume so that each location in the object being imaged produces a signal at its own unique identifiable radio frequency. You can adjust your radio dial for the receiving antenna and for each frequency you select you can check on a T1 or T2 measurement experiment in just that voxel. By running the experiment hundreds of times, once for each voxel, you can determine the T1 or T2 for each voxel, know all the locations, and generate an image showing the T1 and T2 intensities as grey scale pixels in an image.

For Lauterbur's initial design he read out a line of the volume to produce an output very much like the mechanical back projection data described earlier in this paper for Gabriel Frank's non-computed axial tomogram. Once Lauterbur's device had collected data for all the lines for an image slice, he could run them through a computed back projection algorithm and voila - an MRI axial tomographic image emerged.

ERNST AND EDELSTEIN COMPLETE THE PARADIGM

A few years later, in 1975, Richard Ernst filed a patent (granted in 1978)[37] showing how a group of voxel data sets could be collected simultaneously as a complex mix of frequency spectra. Then a Fourier transform could be applied to extract the different frequency component information elements. This is really the fundamental completion of our modern magnetic resonance imaging paradigm - a complex array of magnetic field gradients to spatially encode each voxel in an image by its unique frequency and then a Fourier transform to sort it all out into a series of signal strengths (each depicted as a relative brightness on a grey scale) to generate an image based on the voxel signal data.

Fourier transforms had been used for a hundred years in the study of radiowave data and had been deployed in the evaluation of NMR spectra since the 1950's.[33] This is a mathematical approach that dates to work by Jean Baptiste Joseph Fourier in the early 1880's that can be used to convert a "time domain" oscillating signal into a "frequency domain" description of the content of the signal. It was Ernst's insight to use this classical method from NMR analysis in order to resolve the complex information arising from an MR image data set.

Another improvement came from Bill Edelstein in 1980[38] who showed that a pulsed gradient he called a "spin warp" could be applied that would result in an array of positional encoding by the phase that was far more efficient and usable than the frequency encoding system that Richard Ernst had described. Essentially, with the gradient applied briefly, spins on one side that had a higher magnetic field strength would speed up and the ones on the other side would slow down. When the gradient is turned off, they all resume the same speed. However, the spins that had sped up are out of phase with the ones that slowed down. If you listen/analyze for the early phase info, you will be getting information from one side of the subject, if you listen/analyze for late phase info, it will be coming from the other side.

In practice, the three types of gradients are used as follows. The X-gradient along the length of the magnet (head to toe in a cylindrical magnet) is turned on and we provide "slice selection" by doing the RF stimulation with a range of frequencies that work at just one region of the gradient at a time. To move towards the closer end of the magnet with the higher field strength we stimulate with a higher frequency, to move towards the far end we stimulate with a lower frequency. The stimulation frequency activates spins in a

slab that is the image slice. By using a very narrow band of frequencies we get a thin slice, while a wider range of frequencies results in a wider slice. Areas of the subject outside of the selected slice will not be stimulated.

Now, to get the two-dimensional information out of the slice, we use the Y-axis and the Z-axis gradients. For the Y-axis (frequency encoding) we apply the gradient from right to left across the magnet. The entire slab has already been stimulated by the X-direction slice select gradient, so we now want to manipulate those spins to get the data from each location in the slab. The Y-gradient is applied and kept on so that frequencies will be higher on the left, lower on the right. This allows us to distinguish data coming from a tall column of the subject's left side, distinct from a series of neighboring columns. The column with the lowest frequency will be on the right.

Then, we apply the Z-gradient briefly to get each column labeled top to bottom by the phase differences mentioned earlier. Now we have a unique access to each voxel of the subject. The X-gradient selected the slice/slab by activating it, the Y-gradient applied frequency encoding information identifying the positional source of the signal within the slab from left to right. The Z-gradient applied phase encoding top to bottom. Edelstein's improvement was to use various strengths of gradient in a fixed time as opposed to Ernst's method of applying a gradient of uniform strength for various lengths of time. Edelstein's spin warp was much easier to accommodate in a pulse sequence.

Finally, we turn the antenna on and make a recording of the complex mix of signals coming from our slab. This data is run through a two dimensional Fourier transform and the output is an image slice. If we split the frequency codes into 128 separate bins and the phase codes into 128 bins, we have an image with 128 x 128 voxels. In each voxel, the image intensity will be determined by the impact of the pulse sequence applied during the image session and the results of various decay effects (T1, T2, or others) that cause some voxels to lose signal faster than others. In a T2 weighted image, for instance, voxels in the middle of a brain ventricle will have strong bright signal because of the freely tumbling water molecules of CSF. Voxels in the skull will have little signal at all because the water (proton) content is lower and there is very little movement.

If we want to collect all the information from an entire slab there are two approaches. One is to use the slice select

gradient to activate the slab and then use the Y-direction frequency gradient to leave only one column of the slab in an appropriate field strength to remain activated by the pulse. We then use the phase encode gradient to read out the signal from the various different vertically distributed locations along the column. We then repeat this 128 times, gradually working our way across the slab from left to right. If each event of RF stimulation, spatial encoding and readout of a column takes 100 milliseconds, we will have all the data for the slice collected after 12.8 seconds. If the slices are 4 mm thick with a 1mm blank space between them, we can get through a 15 centimeter volume with 30 slices. This will take about six and half minutes.

Peter Mansfield pointed out that it would be possible to rapidly switch the gradients so that the entire slab volume could be sampled with a single acquisition. This is called “echo planar” imaging (EPI). In this fashion the entire slice is imaged in 100 milliseconds and the whole scan is completed after three seconds. This sort of very fast imaging is critical for “stop motion” studies such as cardiac imaging. It is also very important for studies such as “diffusion tensor imaging” (discussed below) in which each image is really composed out of at least 7 and up to 256 or more image repetitions to be complete. One can readily see that 100 repetitions at six minutes each is completely outside the range of feasibility, but 100 repetitions at 3 seconds each is going to be just 5 minutes - the same general length as a non-EPI standard scan.

DIFFUSION TENSOR IMAGING (DTI) AND DIFFUSION ANISOTROPY IMAGING (DAI)

The broader field of Diffusion Anisotropy Imaging includes what is widely known a Diffusion Tensor Imaging (DTI), tractography based on this (diffusion tensor tractography or DTT) as well as other advanced methods for following neural tracts such as Q-ball and HARDI (High Angular Resolution Diffusion Imaging) which do not deploy the classic tensor mathematical model. It also incorporates lower order non-tensor methods in which three gradient axes are sampled to minimize anisotropic effects where they occur in relatively isotropic tissue such as gray matter of brain and spinal cord.

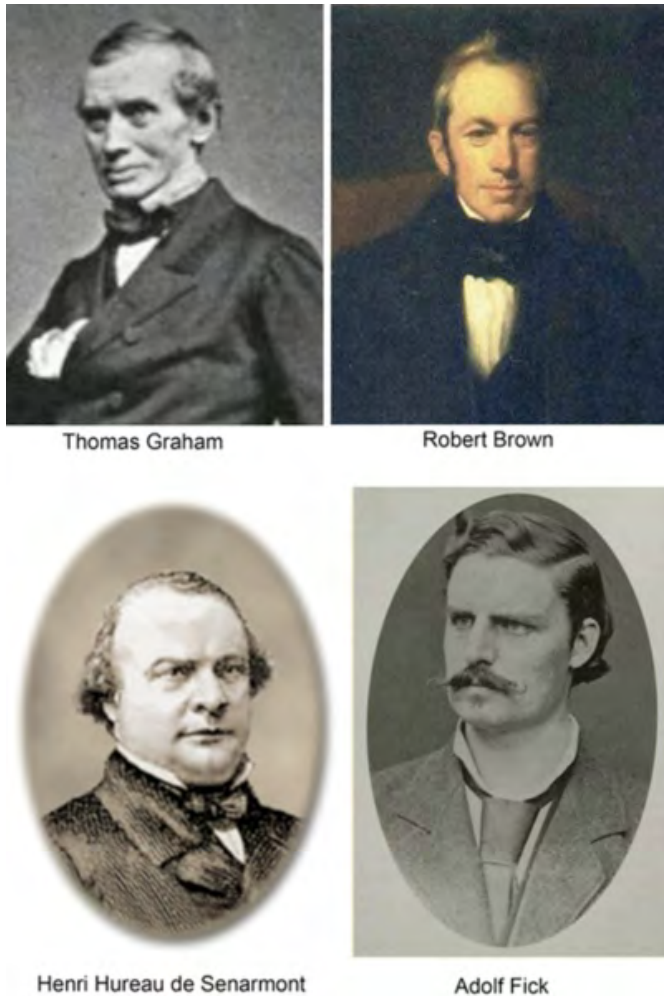
DIFFUSION NMR

Understanding how to assess diffusion in solids and liquids has a long history extending back into the 1700's. Among the most fundamental investigations of the process of diffusion

are the studies by Thomas Graham (see figure 12) in the early 1800's. He initiated the quantitative analysis of diffusive processes through his work with intermingling gases and with salts in solution carried out at what is now Strathclyde University in Glasgow in the late 1820's and early 1830's. Another important element of understanding came from the botanist Robert Brown who was the first to fully describe and name the cell nucleus. In 1827,[39] he reported observations in his microscope that very small (6 micron) granules derived from pollen grains from a wildflower - *Clarkia pulchella* from the American Pacific Northwest - displayed random motion as he observed them in liquid suspension - the first observation of “Brownian motion” that underlies the process of diffusion.

Figure 12

Figure 12 - Leading figures in the development of diffusion science. Thomas Graham (1805-1869) did the first systematic quantitative measurements of diffusion. Robert Brown (1773-1858) discovered the “Brownian” motion that underlies diffusion. Henri Hureau de Sénarmont (1808-1862) did experimental work demonstrating that anisotropic diffusion could be represented by an ellipsoid. Adolf Eugen Fick (1828-1901) organized the mathematical basis of diffusion and showed its relation to studies of heat.



A fascinating experiment that introduced the concept of using ellipsoids to describe diffusion was published by French mineralogist and physician Henri Hureau de Sénarmont in 1848 (see figure 12).[40] He applied wax to the cut polished surface of a crystalline material. He then applied heat to the center of the structure with a heated piece of metal. The heat diffused through the crystal and melted the wax around a progressively expanding front moving centripetally away from the heat source. In materials in which there was uniform diffusion in all directions (isotropic) - the melting edge would spread as a circle. If the

crystal structure contained preferred axes of mobility - the heat would spread more quickly along some directions than others. The result was a growing ellipse on the wax coated surface.

A few years later in 1855, Adolf Eugen Fick published his insights that provided a mathematical basis for describing diffusion.[41] Most importantly, he showed that much of the mathematics that had been developed by Joseph Fourier and other to describe thermal processes could be readily applied to diffusion.

The origin of tensor mathematics was a sudden event that occurred on the evening of October 16, 1843 as Sir William Rowan Hamilton (see figure 13) was walking with his wife near the Broom Bridge on the Royal Canal in Dublin. He was trying to imagine ways of describing complex numbers above the level of two dimensions. He abruptly realized a method to accomplish a description in four dimensions. Fearing he would forget and having no pen and paper, he drew a pen-knife from his pocket and carved the fundamental equation into the stone of the bridge. Hamilton's math is called “quaternions”[42] and he explicitly imagined it as dealing with the three dimensions of space and the fourth dimension of time. The notation and concepts an proponents of quaternions then came into conflict with proponents of vector math and its notations among mathematicians and scientists. Gradually, vector math came to dominate in many areas, but the mathematical descendants of the quaternion have remained important as well.

Figure 13

Figure 13 - Mathematicians & physicists responsible for tensors. Sir William Rowan Hamilton (1805-1865) conceived of quaternions - the initial mathematical basis of tensors. (photo by permission of the Royal Irish Academy Â© RIA). Gregorio Ricci-Curbastro (1853-1925) together with his student Tullio Levi-Civita (1873-1941) developed differential calculus and established the modern form of tensors. Albert Einstein (1879-1955) contributed to and transformed many areas of mathematics and physics including diffusion studies and tensor mathematics.



More than fifty years later, in the closing years of the 19th century, Woldemar Voigt expanded Hamilton's usage of the word "tensor" into its modern sense by applying it in his studies of the physics of crystals.[43] Gregorio Ricci-Curbastro,[44] (see figure 13) in the process of developing differential calculus with his student Tullio Levi-Civita[45] used the term "tensor" to describe an updated version of Hamilton's quaternions, and developed a fully worked tensor calculus. Their work was read by Albert Einstein who then began to consider diffusion[46] and tensor mathematics. Albert Einstein significantly advanced the mathematical development of tensors in his work on general relativity,

using tensors to describe transformations in space and time.[47]

In the early 1950's, Erwin Hahn[33] as well as Herman Carr & Edward Purcell[31] pointed out that it was possible to consider an additional form of NMR signal decay - other than T1 and T2 - based on diffusion. The idea was to turn on a magnetic field gradient during the measurement process. Recall that at this time, long before MR imaging was invented, there were no field gradients used for position. It was Lauterbur who borrowed from the idea of diffusion gradients to conceive of the positional gradients now used for MR imaging. Herman Carr points out that in his 1952 Harvard PhD thesis, he was the first to report the idea of using the diffusion gradient to encode spatial information - at least along a single axis.[48]

Initially, diffusion was thought of as an artifact that could cause signal decay that was not truly due to T1 or T2 effects as well as a phenomenon of interest in its own right. If there was relatively little diffusion of the molecules that held the protons being measured, then the protons would remain in the area of strong uniform magnetic field strength. However, if the molecules tended to diffuse isotropically in all directions, then they would move to positions of different magnetic field strength and would rapidly dephase and lose signal. Hahn used his idea of the spin echo generated from a refocusing second RF pulse in order to remove the effects of diffusion from the T2 signal. Carr and Purcell more explicitly pointed out not only how to perfect the refocusing pulse, but also how to make quantitative measurements of diffusion.[31] Hence, NMR could measure rates of diffusion under various conditions and with various elements and molecules.

Donald Woessner[49] - then a chemist working at Mobil - was the first to extensively consider and investigate the use of NMR in a setting of restricted diffusion. He pointed out in an article published in June of 1963 that if there were barriers to the free diffusion of molecules, then the apparent diffusion coefficient would be decreased due to the physical barriers. The parameters of the measurement could be adjusted based on the typical space between barriers to bring out the effect. This method showed some promise for measuring the free diffusion space inside some porous structures. Woessner appreciated that the existing gradient diffusion method was clumsy to use at small scale and introduced the idea of using two pulsed diffusion gradients - set at different time intervals - to determine the size of the

compartment in which the diffusion was taking place.[50, 51]

Edward Stejskal (see figure 14) was a 30 year old assistant professor in the Department of Chemistry at the University of Wisconsin in Madison when John Tanner joined his group as a graduate student in 1962. Tanner, who was actually two years older than his professor, had been working at a small technology firm in Madison after finishing his Masters degree in 1954. Although Stejskal's focus was NMR, it was Tanner that introduced the diffusion issue to the lab. He had been working on fluid viscosity in gels at the technology firm and had the idea of doing a PhD focused on trying to use NMR diffusion methods to clarify the behavior of fluids in this situation. Stejskal was aware of the use of diffusion in NMR and decided to green light Tanner's project. However, after 18 months, Tanner was making very little progress - and not for lack of trying.

Figure 14

Figure 14 - Scientific leaders in the development of diffusion NMR and MRI. Edward Stejskal together with John Tanner conceived of the symmetrical, refocused pulsed gradient that is employed by virtually all MRI and NMR work that measures diffusion (photo by Cynthia Wertz, reproduced by permission of Edward Stejskal). Michael Moseley initiated the use of diffusion in MRI and discovered that it could identify early signs of stroke (photo by permission of Michael Moseley).



The diffusion gradient methods Tanner started with dated back to early observations by Hahn[33] and by Carr & Purcell[31]. The problem Tanner was having is that the water in gels diffuses slowly and it was requiring progressively larger gradient to try to detect an effect. The gradients required were at the limit of what was possible and there were effects of the gradients that were swamping out the diffusion information.

Stejskal tried to imagine theoretical approaches to solve the problem. Then, for reasons he cannot explain, shortly before midnight on May 1st of 1963, he suddenly conceived the solution - two pulsed gradients rather than continuous application of a single gradient. He jotted the idea down on the margin of an equipment logbook, left a note for Tanner and left the lab around 1am. The next day, Tanner abandoned the approaches he had been trying and set to work immediately to try to get the apparatus to generate the pulses to run the experiment. This succeeded and led to their very widely cited 1965 publication[52]. The Stejskal-Tanner method is still the workhorse of all diffusion imaging 45 years later.

At the time there wasn't much interest in this. Both Stejskal and Tanner moved on to other areas. Stejskal also points out that standard NMR equipment didn't handle the pulses well. Years later, as the equipment capabilities in NMR caught up, interest resumed. The introduction of their method into MR imaging by Michael Moseley in 1984[53, 54] laid the ground work for the explosion of interest in diffusion imaging caused by Moseley's subsequent finding of diffusion MRI's utility in early detection of ischemic stroke in 1990.[55-58]

The idea of using two gradient pulses is a transformation of the ideas that Hahn[33] and Carr & Purcell[31] had applied to RF pulses. The Stejskal & Tanner[52] idea was to pulse the diffusion magnetic field gradient on for only a brief period and then to do this a second time after a carefully selected interval. The two pulses are placed symmetrically before and after the 180 degree refocusing spin echo pulse. This has the effect of amplifying the diffusion sensitivity since it removes the T2* effects of the gradient pulses, leaving just the impact of physical repositioning of the protons due to diffusion. Effectively, the first pulsed gradient causes dephasing, then, after the 180 degree pulse, the second pulsed gradient reverses and eliminates the dephasing - but only does so for those protons still at the same position in the gradient.

The time interval between the two pulses also sets the rate of diffusion that is being sampled - if the two are fired very close together, only fast diffusing molecules will be affected. When the time between them is relatively large, then even slowly diffusing molecules will be affected.

Stejskal apparently was not aware of Woessner's work at the time of his initial idea in May of 1963. However, the

Stejskal solution was more effective because it placed the two pulsed gradients on either side of a refocusing pulse - just as Hahn had done with the spin echo.

Even more importantly for future applications, Stejskal fully considered the implications of this advance for exploring diffusion in all its aspects. Prophetically, Stejskal appreciated the basic features of applying pulsed gradients to study diffusion in anisotropic media using the tensor ellipsoid model.[59] Drawing upon the classical work of Carslaw & Jaeger[60] in heat diffusion, he pointed out in a second paper published in 1965 that NMR measurements of anisotropic diffusion should be oriented along the principal axis of a tensor ellipsoid. This is almost the exact idea that Peter Basser & Dennis LeBihan believed they had discovered at the time of their patent filing nearly 30 years later.[61, 62] In the file history of their patent examination, they incorrectly - but successfully - asserted that no one had ever measured this diffusion tensor for the translational (bulk random-walk movement) self-diffusion of water and that was the basis upon which their patent was granted.

In the 1970's other researchers such as Blinc[63] pointed out that by rotating an anisotropic specimen relative to the direction of measurement, a number of different values for the translational diffusion coefficient could be obtained and that these could be used to accurately fill in the diagonal and off-diagonal elements of the diffusion tensor. This step had the practical use of making it possible to determine the orientation of the true parallel and true perpendicular orientations for accurately measuring the relative amount and direction of anisotropy within a sample.

By this point, it was clear that various NMR scientists had considered what would happen if the structure they were measuring had a strong axis of anisotropy. If they placed the structure so that its axis of anisotropy was perpendicular to the direction of the gradient, relatively little decay took place because the diffusing components tended to stay in an area of similar signal strength as they diffused. Similarly there was an increased rate of decay if the axis of anisotropy was parallel to the direction of the gradient. With this theoretical basis in hand, several groups began exploring the detailed behavior of water diffusion in muscle cells in order to show that cell shape could be measured by its effect on water diffusion.[64, 65]

DIFFUSION WEIGHTED IMAGING

In 1984, Michael Moseley (see figure 14) initiated the field of diffusion imaging by inserting the Stejskal-Tanner pulsed gradient into an imaging sequence to assess the diffusion coefficient in structures seen in an MR image.[53, 54] Two years later, Le Bihan[66] reported diffusion coefficients from various normal and pathologic tissues following Moseley's method. The most important clinical discovery in diffusion weighted imaging was Moseley's finding published in 1990 that diffusion weighted imaging could detect the effect of acute stroke.[55] Prior to this time, both CT and MRI were relatively ineffective for determining if a patient had an ischemic stroke. The impact of Moseley's finding was analogous to Damadian's discovery 20 years earlier[34] that tumors could have different T2 relaxation properties when compared to their parent normal tissues. Moseley's finding caused an explosion of interest in diffusion MRI so that in short order, diffusion weighted imaging was being applied in tens of thousands of clinical images throughout the world.

Michael Eugene Moseley started his academic career in the Department of Physical Chemistry at the University of Uppsala. He worked with Peter Stilbs - then just two years out from completing his own PhD. Moseley published his first papers on NMR spectroscopy with Nitrogen in 1978.[67] His University of Uppsala PhD Thesis, submitted in 1980[68] covered solvent and polymer dynamics in polystyrene solutions, so he will have encountered NMR diffusion problems similar to the one that John Tanner was struggling with when Tanner joined Stejskal's lab fifteen years earlier. After leaving Sweden, Moseley did a post-doc at the Weizmann Institute in Rehovot, Israel (where Saul Mieboom had done the work leading to the CPMG pulse paradigm many years earlier[32]). Moseley's project as a post-doc involved the use of the Stejskal-Tanner pulse sequence[52] to study the anisotropic diffusion of methane and chloroform in smectic liquid crystals.[69]

From there, Moseley moved to California, joining the Department of Radiology at UCSF in 1982. At this point he shifted focus from inorganic chemistry and ultimately applied his classical training in NMR with his recent experience in anisotropic diffusion in crystals to the new field of MR imaging.[53-55, 70, 71] He went on to revolutionize the field with his insights and discoveries in the application and use of NMR diffusion methods to solve important clinical problems in medical imaging. He has recently served as the President of the International Society

for Magnetic Resonance in Medicine - the leading academic research society focused on MR, a group that has tens of thousands of member from the MR research and clinical community.

ORIGINS OF DIFFUSION TENSOR IMAGING

The initial diffusion weighed imaging studies quickly revealed that there was a troubling aspect of the use of diffusion for image contrast - Moseley reported at a 1989 meeting of the Society for Magnetic Resonance in Medicine (SMRM) that the image intensity of white matter areas varied in their diffusion contrast appearance depending upon the relative angle between the diffusion gradient and the long axis of the fiber tract[72]. Further details of his findings were presented at a workshop in Bethesda, Maryland in June of 1990. This complicated the utility of diffusion MRI for identifying stroke in white matter regions, but Moseley also appreciated that there was an unanticipated potential new opportunity for MRI in this as well. Both Moseley's group at UCSF[70] and a group at the Hammersmith Hospital in London[73] published papers later that year showing that by taking images with one gradient parallel and one gradient perpendicular to known tracts, that a significant difference in intensity could be observed. Radiologists thrive on the discovery of new forms of tissue contrast, and this finding of contrast from diffusion anisotropy generated tremendous interest and anticipation.

One solution to the imaging problem of producing a single valid image that correctly depicted the anisotropy in each voxel came from studies of plant tissues. Paul Callaghan and his associates[74] carried out NMR imaging of a thin cross section of a wheat grain. They rotated the sample, collecting images at each 2 degrees of rotation and then carried out a filtered back projection algorithm - like Gabriel Frank, and Godfrey Hounsfield had done - to generate a cross sectional image.

However in a July 1992 patent filing,[2] Filler and his associates revealed a series of critical aspects of diffusion anisotropy imaging that preceded other groups by several years and which became the basis for modern diffusion tensor imaging. The key elements were initially made public in an abstract at the August 1992 SMRM (Society for Magnetic Resonance in Medicine) meeting in Berlin.[13] However, the field of diffusion tensor imaging and tractography were truly launched when Michael Moseley again presented the findings, methods and images from the Filler group to a packed plenary session of more than 700

MR scientists at the SMRI meeting in March of 1993.[75] As Moseley wrote to Filler later "...your slides were of course an instant hit..." It was an electrifying scientific moment - numerous projects in the development of tractography were launched that day.(personal communication: Michael E. Moseley, April 8, 1993, <http://www.neurography.com/neurography-1993moseleyletter.pdf>, by permission of Michael Moseley).

The most important idea is that instead of each voxel having an image intensity for a 2D image, each voxel should instead contain an arrow with a specific length and direction in the three dimensional space of the voxel. From the length of the arrow we can learn about the anisotropic diffusion coefficient for the voxel. From the direction in space, we can learn about the dominant direction of neural fiber tracts within the volume.

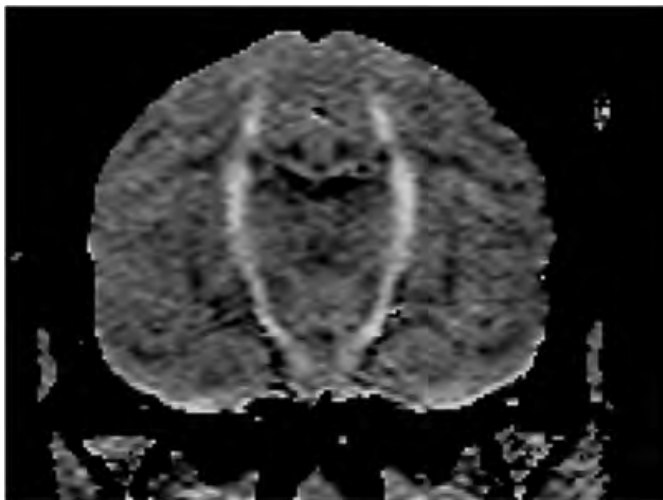
The patient being imaged does not need to be rotated, rather, the diffusion gradients can be applied from many different directions by mixing inputs from the standard three gradients. Several different images are acquired, but these are then combined via vector or tensor math, to result in a single image that is "rotationally invariant" - the image intensities - based on the anisotropic diffusion coefficient is a single true value instead of being different in each of a series of images obtained from various angles.

The use of a tensor formalism in NMR of diffusion had been well known for decades, but this concept of generating a single calculated image made up of complexly data-laden voxels capable of generating neural tract traces was entirely new. Instead of being flattened into a pixel of data with a gray scale of 1 to 256, each voxel would be a "container" that could hold complex spatial information that could be used in various computational methods to demonstrate various aspects of the physiology and pathology of a tissue. Voxels could be associated with each other across three dimensional space based on similarity of axonal orientation.

The Filler[76] patent presents both a simple geometric method using arctangents with input from three gradient directions and also points out that with diffusion gradients activated in more than three directions, a diffusion tensor may be calculated. It then goes on to show various ways to generate tractographic images (see figure 15).

Figure 15

Figure 15 - The first diffusion anisotropy tractographic image. This is a coronal image in a macaque monkey imaged in an experimental MRI system at the University of Washington in Seattle. This image uses the arctangent of the relationship among diffusion gradient axes. Because of the multiple gradients - the vector length images are "rotationally invariant" - the intensities will be the same no matter how the gradients are oriented. In this arctangent image, the precise spatial orientation of the tract components are calculated on a voxel by voxel basis to generate the underlying data and to establish the criteria for image intensity in the tract image.[2]



It should be noted that patent went well beyond simply demonstrating voxel orientations in an image slice. The idea was selective, progressive tract tracing. The radiologist could select a seed and destination, then learn what tracts progressed from the start point to the end point - an MRI version of classical tract tracing techniques.

Among the most important clinical findings reported in the 1992 patent filing, was the discovery that in an encephalitis model, there were some pathologies that were best detected by alterations in the tractographic data. This meant that DTI could detect white matter pathology that could not be seen with any other MRI method. This finding was analogous to Damadian's finding on tumor T2's[34] or Moseley's discovery that diffusion coefficients changed in stroke[55]. It is the basis for the current vast literature in which DTI is used for early detection of Alzheimer's,[77, 78] Parkinsons,[79, 80] diffuse axonal injury in head trauma[81] and in numerous other clinical applications.[82] It would be nearly five years before any other group reported the use of vector or tensor methods to assess pathologies in the living brain that could only be detected with this technique.

In the vector/arctangent model, if diffusion data were collected in three different orthogonal directions, then a vector could be calculated. The length of the vector calculated from data on the three main axes would show a close estimate of the real diffusion coefficient for an anisotropic voxel, independent of the orientation of the gradients relative to the direction of anisotropy. This type of measurement is similar to what is now called the diffusion trace or "Fractional anisotropy" or FA .

This approach of using vector length rather than a single axis diffusion acquisition is one of several similar methods for calculating a composite result for the diffusion coefficient of a voxel so that the result is independent of the angle of the gradients.[62, 76] This strategy now also dominates standard diffusion weighted MRI for stroke.[83, 84] This is because grey matter is not truly "isotropic" and strokes involve both grey and white matter. By collecting gradient information in three axes and using vector or tensor math to calculate the true - directionally independent - measure of diffusion, the artifacts that arise from single direction information can be eliminated. In some sequences with short echo times (reduced T2 weighting), all three gradients can be activated simultaneously so that no calculation is required.[85] This is also the approach now being used to apply diffusion imaging to functional MRI (see below).[86, 87]

The diffusion tensor concept had been very well worked out in other fields several decades earlier. One of the most important applications of diffusion tensor theory in magnetic resonance before 1992 was in the analysis of spinel crystals such as those being developed as ferrite-type magnetic resonance contrast agents.[88-90] The diffusion tensor theoretically requires data from at least six different directions although in practice, the three major or diagonal elements of the 3x3 matrix that describes the tensor will provide most of the needed information. It is clear that at the time LeBihan wrote his 1991 review of diffusion imaging[91] as well as other papers that year,[92, 93] that the major thrust is to obtain just the x, y and z directions as independent data elements. In the 1991 review paper,[91] LeBihan cites the 1960 edition of Jost's textbook on diffusion[94] in which the mathematics of the diffusion tensor and the ellipsoid model are discussed in context of the 110 years of work in these fields (1848 to 1960). Nonetheless, - aside from the information in the Filler et al 1992 patent filing,[2] no MR researcher actually reported having calculated such a true anisotropic diffusion

coefficient in a brain imaging situation until several years later.[95]

In August of 1993, Peter Basser and Denis LeBihan (see figure 16) filed a patent application[62] based on applying the ellipsoid model of diffusion - with a filing date one year after their presentations at the SMRM meeting in Berlin in 1992.[96, 97] Denis LeBihan had been involved in pioneering work in diffusion MRI for a number of years at that point and had filed a patent to do with the study of intravoxel incoherent motion of water.[98] Peter Basser was filing patents about strain gauges in which the mathematics of the strain tensor was employed.[99] Basser learned of Le Bihan's work when he wandered in to a poster presentation in a tent in a parking lot at NIH in the fall of 1991. He immediately became very excited about the potential for deploying tensor math to solve the problem of the need to have a rotationally invariant method of processing the data. Although the two signed a "disclosure document" at that time with an eye towards a future patent filing, Basser reports that he became dejected when Denis Le Bihan pointed out that although this was a nice idea, neither of them knew how to actually measure the tensor.

Figure 16

Figure 16 - Scientific innovators in diffusion tensor imaging. Denis Le Bihan pioneered and developed many areas of diffusion imaging including the use of tensors and the application of diffusion MR to functional studies (photo by permission of Dennis Le Bihan). Susumu Mori developed a set of rules and algorithms that are widely used to accomplish tractography (photo by permission of Susumu Mori). Aaron Filler showed how a set of techniques could be deployed to tract trace throughout the CNS and peripheral nervous system. (photo by Mikel Healey; copyright GFDL 1.3/ CCASA 3.0; image source: http://en.wikipedia.org/wiki/File:Aaron_G_Filler.jpg).



Denis Le Bihan



Susumu Mori



Aaron Filler

However, with the impending deadline of the abstract submission date on March 6, 1992, for the August SMRM meeting in Berlin, and working with James Mattiello, they worked out the concepts. Somewhat ignominiously, they obtained a pork loin which they rotated around in an MRI scanner as they collected diffusion image data. The numbers apparently were fed into software such as MathTensor that had recently become available to run with Steven Wolfram's Mathematica 2.0 software. The results showed that as they rotated the pork loin, the ellipse constructed in the software

rotated in the reference frame. This is what they published in the 1992 abstract.

In 1994, Basser and LeBihan published an initial summary article on their ellipsoid tensor model[61] and it is this paper that is mostly widely cited as the original paper on diffusion tensor imaging. This is indeed a fundamental paper that provides a rigorous mathematical basis for tensor based diffusion anisotropy imaging. In 1995, Basser[100] pointed out the potential to calculate the fractional anisotropy number and the following year the first actual data of this sort was published by Pierpaoli et al,[95] four years after the Filler et al patent filing[2] and the meeting abstract by Todd Richards[13] - one of the co-inventors on the Filler et al patent.

CONFLICT BETWEEN DTI INVENTOR GROUPS

For various unclear historical reasons, the publications by the group of inventors in the Filler patent[101] as well as the reports at the principal magnetic resonance research meeting[13] went unheeded by virtually all other researchers in the field for several years. In part, this appears to have occurred because of Peter Basser and Denis LeBihan at NIH held the attention of the MR community through their vigorous program of publication and reporting on the development of the technique. Basser and LeBihan published steadily in this field reporting increasingly complex math without showing experimental results.[61, 100] Eventually, as Basser told an interviewer[102] he became concerned at how few MR scientists were entering this field and decided he must “dumb down” diffusion MR if he expected any other group to follow.

Many academics are unfamiliar with the process of patent submission and evaluation so some explanation helps clarify what happened with these two patents - US 5,560,360 from the Filler group and US 5,539,310 from the Basser group. The laws have changed over time and they differed significantly at that time for inventors working in Europe versus those working in the United States. In Europe, once a discovery or invention has been publicly disclosed - even verbally at a meeting presentation - it can no longer be patented. However, in the U.S. an inventor was allowed one full year from the date of disclosure before having to file a patent application. In the U.S., if there is a dispute over the priority of two patents - who invented first - then one can look to signed and witnessed notes to find a date of conception - however the US Patent Office will not recognize any such documents if they are not prepared in the

geographical United States.

Once the initial applications are filed, the inventors are allowed one year to update or add to or change the contents before the final application with all legal “claims” attached must be submitted. This document is then usually published by the World Intellectual Property Organization (WIPO) as a “Patent Cooperation Treaty” or PCT document within 18 months of the original earliest filing date. This PCT version gets an initial search of the literature for competing published prior art that might invalidate it. The inventors are required to turn in any prior art they are aware of. The inventors then send the PCT document out to different jurisdictions (e.g. United States, Japan, Europe, Australia, Canada) with appropriate translations where each goes about its own process of patent examination for non-obviousness, validity and novelty. Various objections and rejections are raised by the examiners, the applicants reply, and if there is agreement, an amended version of the patent is accepted and published by each of the jurisdictions as it finishes its process. Patent examination can take 1 to 12 years - or longer!

In the case of these two patents, Filler et al started to file in March of 1992 and had a series of “priority documents” up to July 31 of 1992 containing the inventive material - including a discussion of tensors and numerous orientations of the gradients - and then filed the final application in March of 1993 upon which it was published as a PCT in September of 1993. Like the Filler group, the Basser group presented papers at the August, 1992 Berlin meeting of the Society for Magnetic Resonance in Medicine, emphasizing the mathematics but not including any actual images.[96, 97] The Basser group then filed their initial application 12 months later in August of 1993,[62] filed their final draft in August of 1994 and had their PCT publication in February of 1994. Both patents were granted and published in the United States in 1996, apparently without the relevant examiners being aware of each others work.

When Michael Moseley requested the images from Filler and Richards and re-presented them in the plenary session at the 11th Annual Meeting of the SMRI (Society for Magnetic Resonance Imaging) in San Francisco on March 28, of 1993 - the session was moderated by Denis Le Bihan.[75] This was five months before Le Bihan filed his patent for diffusion tensor imaging.

The patent by Filler et al[76, 101] was granted in the US and

some of the initial reports were published in the Lancet and reported in the New York Times, CNN and ABC news. Nonetheless, Bassler and LeBihan apparently remained unaware or at least unwilling to acknowledge by reference. Even after the Filler patent was cited 32 times in an exchange between the US Patent Office and Peter Bassler in 1999 (see below), Bassler and LeBihan both continued in never referencing any of that work in numerous publications to the present day - despite submitting more than 150 clinical and historical publications and book chapters on the subject since that time.

The Bassler, Mattiello, and LeBihan patent[62] is very narrowly focused on using an NMR or MRI system to fill the six matrix components of a diffusion tensor ellipsoid model. The biggest problem it faced in the patent examination was a series of comparisons to a patent issued in 1984 to Wilfried Bergmann.[103] In that patent, Bergmann proposed an MRI scanner in which the transmit and receive coils were superconducting. He argued that this would increase the precision of the system for measuring T1, T2, and the diffusion tensor. He also provided superconducting coils for generating “three dimensional pulsed field gradients” to measure the diffusion tensor.

The patent examiner initially rejected all of the claims by Bassler saying that Bergmann had already invented a method of using MRI to measure the diffusion tensor. Bassler replies by arguing that Bergmann must be talking about the tensor of magnetic spins. The examiner again rejects all the claims saying, no - it is unmistakable that Bergmann is talking about using pulsed gradients to measure the diffusion tensor. Bassler replies that this must then be the rotational diffusion tensor (a means of using NMR to study the rotations of molecules) rather than water displacement. To support this, Bassler points out that when Bergmann gives a reference to a textbook by Farrar and Becker[104] to support the methodology for measuring the tensor, that the text only covers rotational diffusion. The examiner, Raymond Mah, again rejects all the claims because the textbook actually does describe how to measure both the rotational and the translational diffusion with NMR. The Supervisory Examiner then confirms final rejection of the patent in July of 1995.

However, Bassler et al finally get a Christmas present - on December 26, 1995, their attorney David Rossi makes a phone call to Raymond Mah and convinces him that no one has ever measured the diffusion tensor of water with an

NMR system. Mah sends out a note on December 27th allowing all 35 claims of the patent. Rossi appears to have been completely wrong on this, but the patent was then granted without further discussion. The Bergmann patent really does not provide methodology for measuring the diffusion tensor and the primary references that Bergmann cited do not describe it. The Tanner [105] reference in the Farrar book does describe measuring the translational diffusion tensor, but the examiner did not check these further references.

So when did Peter Bassler become aware of the Richards report and the Filler patent if he missed the 1992 Berlin abstract, the patent publication and the 1993 plenary session about diffusion MRI in San Francisco and never heard about this from Denis Le Bihan? This definitely took place in 1999.

In a conflict with the US Patent Office in examination of a later US Patent 5,969,524 from Pierpaoli and Bassler,[106] the examiner cited the Filler patent[76] numerous times in rejecting claims filed by the NIH scientists regarding similar subject matter Bassler was submitting in this 1997 application. The supervisory US patent examiner Leo Boudreau wrote: “Regarding the above claims, Filler et al teaches a method for assessing diffusion anisotropy in an object; obtaining information signals representing a diffusion tensor for each of a plurality of localized regions in said object (note col. 20 lines 35-67); Information is being obtained to represent a diffusion vector”. Pierpaoli and Bassler responded only by incorrectly trying to assert that the Filler patent did not include more than two axes of diffusion - directly in conflict with both the Filler patent[76] and Richards 1992 publication[13] . The Filler patent actually states:

“gradient coils oriented in three planes can be simultaneously activated in various combinations to achieve the effect of an infinite variety of differently oriented gradients a technique has been developed for observing diffusional anisotropy, independent of its degree of alignment with any individual gradient axes. This process involves the combination of information from anisotropy measurements obtained along three standard orthogonal axes or using information from multiple fixed axes.”[76]

In the July 31, 1992 priority document by Filler et al (p.21) the utilization for tensor treatment is explicit as is the relationship to known tensor analysis methods for magnetic

data[107] which they state:

“The use of vector analysis algorithms of this sort, or involving the treatment or coordinate transformation of MR diffusional anisotropy data with tensors of various rank can improve the generality and flexibility of neurographic imaging. The example described above demonstrates that by the application of tensor and/or vector analysis methods such as algorithms similar to those developed for the evaluation of e.g, magnetic, thermal, or structural anisotropy data, it is possible to greatly improve the flexibility and generality of image techniques for neurological diagnosis.”[2]

Further, Rossi argues on behalf of Pierpaoli and Basser that even if the Filler patent does mention using the tensor for tractography that none of the four inventors on the Filler patent would have known how to use it for that purpose. This assertion did not impress the examiner.

Pierpaoli and Basser were forced to amend the new patent[106] and narrowly limit the claims that were subsequently granted to cover only a theoretical lattice concept that has not proven to have any utility.

Aside from the dispute, the fact that Filler's patent is one of only three documents cited and that it is referenced 32 times in the correspondence makes it quite impossible that Peter Basser was unaware of the Filler patent or its contents as he continued to publish numerous topical and historical articles about the field without referencing that patent or related publications or any of the authors over the following 10 years. His patent was then licensed to GE, Philips and Siemens apparently without these companies being alerted to the competing patent.

DIFFUSION ANISOTROPY AND TRACTOGRAPHY

The special problems in this task arise because of two ways in which the MRI diffusion tractography problem differs from other diffusion measurement systems. Dating back to the non-computed axial tomogram, continuing on through CT scanning and all MRI work to that point - researchers were concerned with determining how best to determine contrast between one pixel and an adjacent pixel in a two dimensional or tomographic representation. Tractography calls for shifting fully into a three dimensional realm where the structure being determined extends beyond the plane of imaging.

In diffusion MRI, we can tell that diffusion anisotropy in a

neural tract is causing water molecules to move preferentially perpendicular to a gradient, but we can't tell which direction along the tract the water molecules are traveling - towards us or away from us. The image intensity is identical for the measurement of diffusion along any axis whether the water is moving in either direction along the tract because it does move in both directions in the neural tract. In general diffusion work this is never a problem. In fact if we are calculating fractional anisotropy (FA) values that essentially give the length of the resultant vector, the answer always comes out the same whether or not we know the true sign (positive or negative) of the direction of the neural tract relative to each axis.

However, for tractography, we have to know the true direction of the tensor relative to the shared Cartesian frame of reference. Filler[82] has outlined elsewhere an anti-symmetric dyadic tensor model that best explains how the additional gradient axis information solves this problem. Basser and LeBihan in their 1993 patent filing (granted in 1996)[62] failed to suggest any method for achieving tractography. Basser has stated in an interview that as of 1994, tractography seemed like science fiction to him.[102] Basser and LeBihan were not able to discover a method to do tractography.

In the 1993 patent application, the Basser group did not propose any means to describe or utilize the angular orientation of the tensor in Cartesian space. Like a number of authors before and after their filing[92, 108, 109] they proposed the use of color maps[110] so that each independent axis of data collection could be assigned a color and the colors then mixed to provide a general view of the directional quality of the data. Even this approach is fairly unproductive if the data is not multiplied by FA information.

Basser has stated that he sought to accomplish tractography by developing a mathematical tensor field model[102] based on the physics of streamlining that would extend his ellipsoid diffusion tensor model to the tractographic level. However he never succeeded in this task. It seems as though this approach could not work since neural tract directions are determined by evolutionary history and neural function and not by any laws of physics.

It is helpful to keep in mind that in the voxel you can imagine a three dimensional set of axes (x, y, and z) but that the center of this Cartesian system is at the center of the voxel rather than any arbitrary corner of the voxel. Now

imagine what happens when you have a diffusion measurement of 1 along the X-axis. You will see 0.5 on the -x side and 0.5 on the +x side of the center of the grid. Now suppose you have a measurement of 1 along the Y-axis also - again there will be 0.5 on the negative side and 0.5 on the positive side. We can keep this simpler by coming back with a very low value on our Z- measurement - nearly 0. Even now though, you can imagine four different vectors pointing out from the origin. One midway between the +x and the +y arms, one midway between the +x and the -y arms, and so on - four different vectors organized into two anti-symmetric pairs. How do you decide which is correct? You need to collect data from an additional plane between the axes to learn which is a ghost dyad and which one represents the real Cartesian direction.[82]

In the 1992 patent application Filler et al[2] provided both a simple vector model and tensor model for tractography and actually produced and published the first tractographic brain images. In the final patent they suggest selecting seed points in two remote axial slices and then using an algorithm to tract trace between the regions of interest based on the directional anisotropy data.

In 1999, Susumu Mori (see figure 16)[111, 112] reported success with tractography, in part by retracing the steps outlined in the Filler patent, but also providing further details of the algorithm. He filed a patent that year that was subsequently granted in 2003.[113] In both the Filler et al 1992[2] and the Mori et al 1999 method,[113, 114] one critical aspect is to select two areas demonstrating a high level of anisotropy and then to allow the algorithm to follow the principal main direction of each voxel to travel from a seed or source point to reach a target point.

There are two methods for tractography that are explained in the Filler application.[2] The first is based on the arctangent function (also applicable using an algorithm called “arctan2” in the version of FORTRAN used for the original work). This function results in the angle of the main vector relative to the selected Cartesian axes. This allowed images analogous to more modern tractography in which an angle parameter was set to determine image intensity. Anisotropic voxels sharing that angle were bright, others were dark, this resulted in a tractographic image that followed long tracts through the brain. Richards[13] also reported that in some pathologies, there seemed to be more disturbance of the angular data than the vector length data.

The second method used true tensor data in a connected voxel algorithm.[115] This type of algorithm - which is a three dimensional elaboration on older “connected pixel” algorithms[116], provides for a threshold for eliminating voxels of low signal strength under the conditions assessed as well as for decision making about adjacent tracts. It is a seed based method that generates both linear and surface regions based on the input data. In Filler[2] it was applied to the vector length/arctan angular data that describe the orientation of the primary diffusion vector in the voxel to assess connectedness to adjacent voxels. In addition Filler[2] described the use of multiple gradient acquisition hardware that allowed mathematical assembly of an infinite number of differently oriented diffusion gradients run in echo planar sequences to obtain multidimensional tensor data of various ranks.

Jay Tsuruda, a neuroradiologist who was a co-author on Moseley's original 1990 report of anisotropic diffusion[70] and a co-inventor on the Filler patent, joined Richards, Filler and Howe in 1992 after the initial tensor and arctan tractographic work had been done, and started investigating additional issues in tractographic processing. Filler and Tsuruda (along with Grant Hieshima - a neuroradiologist who made several of the major inventions in the directable catheters of interventional radiology) formed a company called NeuroGrafix to develop the technology. In his capacity as chief scientific officer of the company, Tsuruda participated with other scientists in a series of further developments that help refine the tractographic method.[117-120] Members of the inventor group also reported extensively on the development and clinical evaluation of the peripheral nerve tractographic (= neurographic) methodology.[3, 5, 82, 121-126]

One continuing problem with tractographic methods has been that the ellipsoid tensor model of Basser and LeBihan cannot accommodate the biological situation of two neural tracts crossing through each other. This is because in the ellipsoid model there can be only one principal eigenvector or main longitudinal axis in a voxel. We can look at the short axes but these are always orthogonal to the main axis and cannot accept any different direction.

In the anti-symmetric dyad model, we can have multiple different dyads arise from multiple measures. If there is one dominant measure in a voxel then any differences or “wobble” between the dyads will reflect the equivalent of the “radial diffusion” from the ellipsoid model - this assesses

the degree of isotropy or noise in a voxel. However, if there are two different tracts in the voxel, then strong enough gradients and sufficiently numerous gradient acquisitions in various directions can result in dyadic tensors that group into two different directions reflecting the two different tracts. The HARDI (high angular resolution diffusion imaging)[127] and q-ball[128] methods work in this fashion by abandoning Basser and LeBihan's application of the classical diffusion ellipsoid model. David Tuch and Van Wedeen at the Massachusetts General Hospital were granted a patent for this method in 2006.[129]

THE ORIGINS OF THE DIFFUSION ANISOTROPY IMAGING PATENT

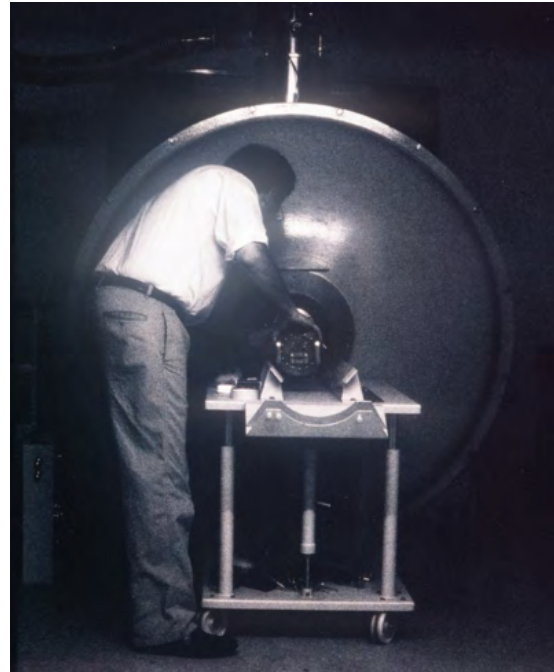
The Neurography and Diffusion Anisotropy Imaging patent[76] was an important step forward for the general problem of treating neural structures in their linear form like bones or blood vessels and accomplished advances in this area on many fronts.

Aaron Filler first proposed an MRI nerve tract imaging project in 1988 at the University of Washington where he was a second year neurosurgery resident and the project went forward under one of the radiology faculty, Jim Nelson. Todd Richards was the lead physicist of the research group. The project envisioned the use of MR contrast agents for delivery by axonal transport with the intention of using a contrast agent to generate linear images of nerves and tracts that would be analogous to the axonal tracers he had used for anatomical studies as a graduate student at Harvard ten years earlier.

In 1990, Filler was working on that project at St. George's Hospital in London using a 4.7 Tesla imager with high slew rate 70 milliTesla/meter gradients (see figure 17) - note that at this time, most clinical imagers had only 10 milliTesla/meter gradients at best and these typically had much lower slew rates than the St. George's research system. A grant application for the MR tract imaging work was rejected by the MR imaging section at NIH but the project was funded by the Neurosciences Research Foundation of Atkinson Morley's Hospital (where Filler worked as a neurosurgical registrar) - the same facility that supported Hounsfield's project to deploy the first CT scanner.

Figure 17

Figure 17 - Aaron Filler loads test samples into the 4.7 Tesla experimental MRI system at St. George's Hospital in 1991 in the course of experiments that led to the development of diffusion tensor imaging (photograph by Franklyn Howe, copyright: GDFL/CCASA 3.0, image source:http://en.wikipedia.org/wiki/File:UK_lab_MRI_Aaron_Filler.jpg).



Filler learned of Moseley's report on anisotropy in white matter when Filler gave a visiting presentation of his progress at the Hammersmith Hospital in the early fall of 1990. He then started formulating a plan to try to apply diffusion MRI to the nerve imaging problem. Working with Franklyn Howe, an Oxford trained MR physicist, he noticed that the chemical shift artifact at the very high field had separated the small nerves into two neighboring structures. When diffusion weighting was applied, his finding was similar to the minimal effect in peripheral nerve noticed by Moseley. However, in order to fully distinguish among the water and fat nerve images that partially overlapped in the forearm of a rabbit under anesthesia in the high field high gradient magnet, he added chemical shift selection fat suppression to the diffusion sequence and this yielded a remarkably large increase in apparent anisotropy in the water images of the nerve - quite aside from removing the fat signals from the image. This revealed that the nerve water included both isotropic (or slow diffusing) and anisotropic (or fast diffusing) components, but that the chemical shift selective pulse removed most of the isotropic water from the image because the isotropic water had a shorter T2.

The result was a pure nerve image with no use of contrast agents. He traced a series of images onto acetates and when

the nerves in the series of slices were stacked up, they clearly revealed the three dimensional branching pattern of the major nerves of the forearm. The problem was that the nerve images would only be bright when the nerves were directly parallel to the gradient so image intensities dropped out and even disappeared as the nerves curved out of plane. Filler and Howe quickly discarded a three axis solution because of the bipolarity of diffusion and identified the solution as requiring a multiple gradient acquisition with tensor analysis. This was a solution that was apparent because Filler's work at that point included chemical work on manipulating the spinel crystal anisotropy of mixed ferrites he was working with for contrast agents. This was another example - as with Michael Moseley's background in smectic liquid crystals - where a background in the anisotropic diffusion science of crystals resulted in insights into water diffusion in images of neural tracts.

Yet another interesting cross pollination arose from Filler's PhD research in biological anthropology at Harvard. His 1986 PhD thesis dealt with the evolution of Miocene hominoids.[130-133] In particular there was great interest in accurately dating a Miocene vertebra from the Moroto site in Uganda. A key aspect of dating the site utilized studies of paleomagnetism. A similar issue arose with Miocene hominoid fossils from the Siwaliks in Pakistan.[134] Filler's thesis adviser was David Pilbeam - who later served as Dean of Harvard College - and Pilbeam had played an important role in fostering the development of methodology in paleomagnetism. Paleomagnetic structure is assessed by making six differently oriented magnetic remanence measurements around a sample and then using a tensor ellipsoid calculation to determine the eigenvalues and eigenvectors[135-138] - almost exactly the method for diffusion tensor MRI. A 1990 summary article by two of Pilbeam's associates provides full details of the method and the mathematics.[107] A significant portion of the initial theoretical work in paleomagnetism was done by Jelinek[135] who concludes his article by stating: "We expect that this method will also be useful in other fields in which symmetric tensors of the 2nd order are employed." Other more general works on the relevant tensor methodology are also available.[139, 140]

There is nonetheless an interesting intellectual, scientific and technological mystery about the whole series of events of the development of diffusion tensor imaging that seems to go to the heart of the way that humans advance their technologies.

What is striking is that although many brilliant researchers discussed the diffusion tensor in NMR and MRI, it is clear that it was not really being calculated before 1992, even though there were many sources available to explain exactly how to go about it. In part, this appears to have occurred because the tensor is being used as a symbolic concept that states more or less that we all know the appropriate formalism to apply. However, in nearly all situations in NMR, all that we need to know is the orientation of the principal axis of the tensor since that will allow the measurement of the anisotropic diffusion coefficient. If you can find the orientation by manually rotating the sample on a turntable until you see the maximum output, then why bother going through elaborate data collection and calculation steps that once challenged Albert Einstein?

From a philosophical point of view, the history of diffusion tensor imaging shows that in the process of invention, in response to a perception of an unmet technological need, we must disrupt our symbolic understanding[141] of the elements of a problem in order to see its components in their fundamental state then reassemble the elements into novel and unpredicted new relationships and outputs.

FUNCTIONAL MRI (FMRI)

Earlier in this paper, the use of the spin echo to eliminate the "T2*" effects of local magnetic field inhomogeneities was discussed. Functional MRI (fMRI) is based on trying to enhance the impact of T2* effects that result from local bloodflow. Louis Sokoloff had shown that in the neuroscience lab, radiolabeled (carbon 14) deoxyglucose (FDG) could be used to track how much brain metabolism was taking place in various regions. With the tracer in blood, an experimental animal's brain would draw glucose into those regions with higher energy consumption. The synthetic glucose analog molecule would block the normal glucose breakdown and accumulate inside the cell - accumulating larger amounts in more active cells. Then when the animal was sacrificed and the brain was sectioned, the radiolabel would cause increased exposure of X-ray film at the locations with the most retained tracer.[142]

Sokoloff and his colleagues then made FDG with fluorine-18 - a positron emitter. David Kuhl - who had worked on both radio-isotope scanning and an early CT scanner design - together with Michael Phelps (all at the University of Pennsylvania) had made good progress with a positron emission tomography scanner. Working together, Sokoloff, Kuhl, Phelps and colleagues then used 18-FDG and an early

PET scanner to observe changes in regional metabolism in the living human brain[143].

Raichle and colleagues[144] had been using simple detector arrays to monitor regional cerebral blood flow in humans with oxygen-15 (positron emitting) labeled water. This group also progressed to the use of PET scanning, deploying a variety of tracers including Carbon-11 labelled glucose (to try to see a more normal glucose metabolism relative to flourodeoxyglucose).[145] A tremendous amount was learned about the physiology of cerebral metabolism by deploying these various techniques. However, they all required an intravenous injection of a powerful radiation source - something that seems appropriate for assessing the potential growth rate of a patient's brain tumor, but not for routine psychology experiments. Further, the spatial resolution of PET limited the degree of detail possible for these functional studies.

Belliveau and associates at Massachusettes General Hospital showed that MRI contrast agents would distribute differentially based on blood flow and that - at the time scale of MRI - it was possible to show relative increase in contrast agent flow in areas of the brain that were most active.[11] The initial clinical excitement was for the possibility of having a patient engage in a physical movement and using these functional images to help identify the motor strip of the brain's cortex.

However, unknown to Belliveau and the awestruck reviewers at Science, Seiji Ogawa (see figure 18) at AT&T's Bell Labs had already achieved a far more subtle and powerful solution[12]. The effects of de-oxygenated blood are different from the effects of oxygenated blood. Oxygenated hemoglobin is diamagnetic - no external magnetic field, but deoxygenated blood is paramagnetic - it does have an external magnetic field effect. The process of deoxygenation - if it occurred in an area of increased brain activity - could mark that location by causing increased T2* effects. The general class of imaging techniques used are called BOLD for "blood oxygen level dependent" imaging.

Figure 18

Figure 18 - Leading scientific contributors to fMRI. Seiji Ogawa demonstrated that BOLD (blood oxygen level dependent) imaging could reveal functional activation in the brain (photo by permission of Seiji Ogawa). Debra Gusnard showed how fMRI baseline measures could be used to explore the biological basis of "self" as a background for understanding mental function (photo by permission of Debra Gusnard).



Brain activity does increase blood flow to a brain region, but the level of control is not very fine in scale. If one small area has increased activity and increased demand, then a region that may be ten to fifty times larger may see the increased flow. However, although the active area will deoxygenate the blood more rapidly than the less active areas the blood flow response overcompensates.

Gusnard and Raichle[146] pointed out that background oxygen extraction fraction (OEF) rather than oxygen consumption per se would be the best measure because it is relatively uniform across the brain at rest. Because of the overcompensation of flow in response to activity, the OEF actually decreases in areas of increased activity. With this information in hand and with appropriate pulse sequences selected, even very fine scale patterns of brain activation could be reliably monitored. An extra bonus was the finding that time scale of the changes was shorter when assessed in this way.

These changes have led fMRI researchers to deploy very high resolution systems that can differentiate progressively more precise patterns and locations of activity. The analysis of these activations has progressed both toward the particular - identifying precise regions of function along a cortical gyrus, and also toward the level of organization of higher

level patterns - assessing patterns of coactivation between limbic, temporal, frontal and parietal functional centers.

Debra Gusnard (see figure 18), a neuroradiologist trained at the University of Chicago and University of Pennsylvania after studying at the Sorbonne (University of Paris) chose to do a second residency in psychiatry while doing fMRI research at the Mallinckrodt Institute of Washington University in St. Louis. Double boarding in neuroradiology and psychiatry would have been difficult to predict a few years ago, but Gusnard's work has shown how compelling this may prove to be in the future. Working with Marcus Raichle, she authored or co-authored several widely cited major papers reporting important advances in the understanding of the baseline functioning of the human brain as well as establishing the OEF (oxygen extraction factor) as a key paradigm for quantitation and analysis of fMRI data.[147-151]

In addition however, Gusnard has helped launch a fascinating new field in which fMRI is deployed to gain biological insight into elements of thought, perception and consciousness. She has pointed out that although traditional neuropsychology has generally considered the concept of "self" as non-biological, the baseline function concept of fMRI provides an alternative explanation. By monitoring the degree of function in coordinated regions of brain when the individual has no external stimuli, the functional properties and components of "self" become subject to study.[10, 147] Gusnard also points out that other fundamental aspects of consciousness - such as attention, self reflection, motivation, and the temporal sequencing of thought are becoming increasingly susceptible to study on a biological basis. This helps provide a substantive methodological basis to the widely anticipated possibility that not only the functioning of the mind but the pathological variations from normal function will be progressively unraveled by future progress in fMRI.

Although tremendous strides have been made in fMRI using the BOLD technique, the field of fMRI has started to undergo another revolutionizing transformation due to methodological improvements in diffusion imaging. In 2001, Le Bihan and colleagues[85] noticed that the isotropic diffusion measurement in grey matter increased with functional activation. Recently advances in signal to noise performance of scanners have led to the finding that diffusion methods can be used to measure functional activation. This measure is entirely different from the

oxygen consumption model that dates back to the laboratory autoradiography studies. It appears to be due to swelling of cells associated with their neural activation. The diffusion effect (DfMRI) starts abruptly within 1 second and then resolves before the BOLD changes even start to appear. Onset and resolution is 2-3 seconds for DfMRI and about 9-10 seconds for BOLD studies, so the time resolution is much better using diffusion. In addition, the spatial resolution of the changes appears to be more precise.

Diffusion methods detect a fast diffusing phase and a slow diffusing phase. The relative amount of water in the slow diffusing phase (restricted diffusion) increases with brain activation. The actual cellular and biophysical basis for this remains unclear. It is also unclear whether the already low anisotropy of the grey matter changes as well. [85-87, 152] A similar cellular swelling phenomenon seems to affect the axons of activated neurons as well - this change is proving to be observable with a DTI paradigm that may be termed fDTI.[153]

SUMMARY

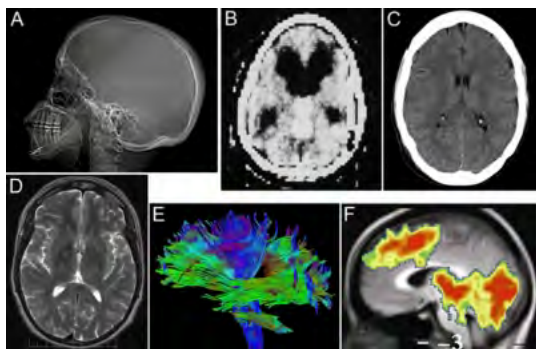
Overall, the competitive arenas of the academic, intellectual property, and corporate aspects of these historical developments appear to have acted to spur on the advance of technology. It is certainly clear in this area that patents must be considered along with academic publications if we want to clearly understand the historical sequence of ideas and innovations.

Medical imaging continues to be an exciting focus that draws in the most complex aspects of physics, mathematics, computers and neuroscience. Neurosurgeons must remain closely engaged with this process - recognizing where critical clinical needs are not being met by existing technology while striving to find insight into potential solutions. In this way, further rounds of advancement and insight will best serve the practitioners.

Ultimately, a medical image is an extension of the physical exam, allowing the surgeon to probe and examine the patient. As imaging methodology draws more subtle and complex functional capability into the diagnostic arena, the range of problems that will be available for neurosurgeons to try to treat will certainly continue to grow larger as well (see figure 19).

Figure 19

Figure 19 - Image history series. (A) Skull X-ray - only hard tissues can be observed and all features are overlaid upon each other, (B) one of the first CT scans from AMH in 1971 - starting point for the cross sectional image paradigm, (C) recently obtained CT scan showing higher resolution and better tissue contrast, (D) T2 weighted brain MRI showing subtle contrast differences with small thalamic abnormalities - extending the cross sectional paradigm (E) DTI tractographic image with selective depiction of white matter anatomical structures deployed in three dimensions, (F) fMRI study with individual looking at pictures, making judgments and button-press responses with resultant activation in visual cortex, and prefrontal + SMA (supplementary motor) area. Credits: A, C, D, E: image credit Aaron Filler, copyright: GDFL 1.3/CCASA 3.0; image source A: http://en.wikipedia.org/wiki/File:Skull_X-ray_lateral_view.jpg; C: http://en.wikipedia.org/wiki/File:Brain_CT_scan.jpg; D: http://en.wikipedia.org/wiki/File:MRI_T2_Brain_axial_image.jpg; E: http://en.wikipedia.org/wiki/File:DTI_Brain_Tractogram_lateral_view.jpg; B:courtesy of St. George's Hospital, Univ. London; F: courtesy of D. Gusnard, Mallinckrodt Institute of Radiology, Washington University, St. Louis.



ACKNOWLEDGEMENTS

I thank H. Richard Winn, B. Anthony Bell, John R. Griffiths, Franklyn A. Howe, Todd L. Richards, Terrence W. Deacon, Jodean Peterson, and Shirlee B. Jackson for their assistance, contributions, and inspiration in the course of this effort. The original introduction and guidance for the tractographic concept as it arose in axonal transport work was through two great innovators and teachers, Walle J. H. Nauta and Richard L. Sidman.

References

- Ogawa S, Lee TM, Nayak AS, Glynn P: Oxygenation-sensitive contrast in magnetic resonance image of rodent brain at high magnetic fields. *Magn Reson Med* 1990, 14(1):68-78.
- Filler AG, Tsuruda JS, Richards TL, Howe FA: Images, apparatus, algorithms and methods - July 31, 1992. GB 9216383: (<http://www.neurography.com/neurography-GB9216383A.pdf>) UK Patent Office; 1992.
- Howe FA, Filler AG, Bell BA, Griffiths JR: Magnetic resonance neurography. *Magn Reson Med* 1992, 28(2):328-338.
- Howe FA, Filler AG, Bell BA, Griffiths JR: Magnetic resonance neurography: optimizing imaging techniques for peripheral nerve identification. In *Society for Magnetic Resonance in Medicine, 11th Annual Meeting*: 1992; Berlin, Germany; 1992:1701.
- Filler AG, Howe FA, Hayes CE, Kliot M, Winn HR, Bell BA, Griffiths JR, Tsuruda JS: Magnetic resonance

- neurography. *Lancet* 1993, 341(8846):659-661.
- Ambrose J: Computerized transverse axial scanning (tomography). 2. Clinical application. *The British journal of radiology* 1973, 46(552):1023-1047.
 - Ambrose J: Computerized transverse axial scanning of the brain. *Proc R Soc Med* 1973, 66(8):833-834.
 - Ambrose J, Hounsfield G: Computerized transverse axial tomography. *The British journal of radiology* 1973, 46(542):148-149.
 - Ambrose JA: Computerized transverse axial tomography. *The British journal of radiology* 1973, 46(545):401.
 - Gusnard DA: Being a self: considerations from functional imaging. *Conscious Cogn* 2005, 14(4):679-697.
 - Belliveau JW, Kennedy DN, Jr., McKinstry RC, Buchbinder BR, Weisskoff RM, Cohen MS, Vevea JM, Brady TJ, Rosen BR: Functional mapping of the human visual cortex by magnetic resonance imaging. *Science* 1991, 254(5032):716-719.
 - Ogawa S, Lee TM, Kay AR, Tank DW: Brain magnetic resonance imaging with contrast dependent on blood oxygenation. *Proc Natl Acad Sci U S A* 1990, 87(24):9868-9872.
 - Richards TL, Heide AC, Tsuruda JS, Alvord EC: Vector analysis of diffusion images in experimental allergic encephalomyelitis. In *Society for Magnetic Resonance in Medicine*: 1992; Berlin; 1992:412.
 - Webb S: *From the watching of shadows : the origins of radiological tomography*. Bristol ; New York: A. Hilger; 1990.
 - Kevles B: *Naked to the bone : medical imaging in the twentieth century*. New Brunswick, N.J.: Rutgers University Press; 1997.
 - Tetel'Baum SI: About the problem of improvement of images obtained with the help of optical and analogue instruments. *Bull Kiev Polytech Inst* 1956, 21.
 - Tetel'Baum SI: About a method of obtaining volume images with the help of X-rays. *Bull Kiev Polytech Inst* 1957, 22:154-160.
 - Korenblum BI, Tetel'Baum SI, Tyutin AA: About one scheme of tomography. *Izv Vyssh Uchebn Zaved, Radiofiz* 1958, 1:151-157.
 - Watson W: Improvements in or relating to X-ray apparatus. GB 508381: UK Patent Office; 1939.
 - Frank G: Verfahren zur Herstellung von Korperschichtbildern mittels Röntgenstrahlen (Method of and apparatus for obtaining cross-sections of bodies by means of x-rays). DE 693,374: German patent office; 1940.
 - Brownell G, Burnham C, Hoop BJ, Kazemi H: Positron scintigraphy with short-lived cyclotron-produced radiopharmaceuticals and a multicrystal positron camera. In *Medical Radioisotope Scintigraphy, Proceedings, Symposium, October, 1972, Monte Carlo International Atomic Energy Agency, Vienna: October 1972*; 1972:313-330.
 - Chesler D: Three-dimensional activity distribution from multiple positron scintigraphs. *Journal of Nuclear Medicine* 1971, 12:347-348.
 - Cormack A: Representation of a Function by Its Line Integrals, with Some Radiological Applications. *Journal of Applied Physics* 1963, 34(9):2722-2727.
 - Cormack A: Representation of a Function by Its Line Integrals, with Some Radiological Applications. II. *Journal of Applied Physics* 1964, 35(10):2908-2913.

25. Radon J: Über die Bestimmung von Functionen durch ihre Integralwerte längs gewisser Mannigfaltigkeiten (On the determination of functions from the integrals along certain manifolds)
Ber Verhbandl Sächs Akad Wiss Leipzig, Math-Phys Kl 1917, 69:262-277.
26. Hounsfield GN: Method and apparatus for measuring X- or gamma-radiation absorption or transmission at plural angles and analyzing the data. US 3,778,614: United States Patent Office; 1973.
27. Rabi I: A new method of measuring nuclear magnetic moment.
Phys Rev 1938, 53:318.
28. Purcell EM, Torrey HC, Pound RV: Resonance absorption by nuclear magnetic moments in a solid.
Phys Rev 1945, 69(1-2):37-38.
29. Bloch F: Nuclear Induction.
Physical Review 1946, 70:460-474.
30. Bloch F, Hansen WW: Methods and means for chemical analysis by nuclear inductions. US 2,561,489: United States Patent Office; 1951.
31. Carr HY, Purcell EM: Effects of diffusion on free precession in nuclear magnetic resonance experiments.
Phys Rev 1954, 94:630-638.
32. Meiboom S, Gill D: Modified spin-echo method for measuring nuclear relaxation times.
Review of Scientific Instruments 1958, 29(8):688-691.
33. Hahn EL: Spin Echoes.
Physical Review 1950, 80(4):580-594.
34. Damadian R: Tumor detection by nuclear magnetic resonance.
Science 1971, 171(976):1151-1153.
35. Damadian R: Apparatus and method for detecting cancer in tissue. US 3,789,832: United States Patent Office; 1974.
36. Lauterbur PC: Image formation by induced local interactions: Examples employing nuclear magnetic resonance.
Nature 1973, 242:190-191.
37. Ernst R: Gyromagnetic resonance fourier transform zeugmatography. US 4,070,611: United States Patent Office; 1978.
38. Edelstein WA, Hutchison JM, Johnson G, Redpath T: Spin warp NMR imaging and applications to human whole-body imaging.
Phys Med Biol 1980, 25(4):751-756.
39. Brown R: A brief account of microscopical observations in the months June, July and August 1827 on the particles contained in pollen.
Edin New Phil J 1827, 5:358-371.
40. de Sénarmont HH: Mémoire sur la conductibilité des substances cristallisées pour la chaleur.
Comptes Rendu Hebdomadaires des Séances de L'Académie des Science, Paris 1848, 25:459-461.
41. Fick A: Ueber Diffusion [On Diffusion].
Poggendorff's Annalen der Physik 1855, 94:59-86.
42. Hamilton WR: On some extensions of Quaternions.
The London, Edinburgh and Dublin Phil Mag & J Sci 1854, 7-9:492-499, 125-137, 261-269, 446-451, 280-290.
43. Voigt W: Die Fundamentalen Physikalischen Eigenschafen der Krystalle in Elementarer Darstellung.
Leipzig: Verlag von Veit & Co; 1898.
44. Ricci Curbastro G, Levi-Civita T: Méthodes de calcul différentiel absolu et leurs applications. Paris: A. Blanchard; 1923.
45. Levi-Civita T, Persico E: The absolute differential calculus (calculus of tensors). London.; Blackie; 1927.
46. Einstein A: Zur Theorie der Brownschen Bewegung [On the theory of Brownian Motion].
Annalen der Physik 1906, 19:371-381.
47. Einstein A: Die Grundlage der allgemeinen Relativitätstheorie
Annalen der Physik 1916, 49(7):769-822.
48. Carr HY: Sharper images of MRI's origins.
Physics Today 1993, 46(1):93-96.
49. Woessner D: NMR Spin-echo self diffusion measurements on fluids undergoing restricted diffusion.
J Chem Phys 1963, 67:1365-1367.
50. Woessner D: Field gradient measurement of self-diffusion constant. US 3,109,986: United States Patent Office; 1963.
51. Woessner D: NMR Measurement of Container Dimensions. US 3,213,355: United States Patent Office; 1965.
52. Stejskal EO, Tanner JE: Spin diffusion measurements: Spin echoes in the presence of a time-dependent field gradient.
Journal of Chemical Physics 1965, 142:288-292.
53. Wesbey GE, Moseley ME, Ehman RL: Translational molecular self-diffusion in magnetic resonance imaging. I. Effects on observed spin-spin relaxation.
Investigative radiology 1984, 19(6):484-490.
54. Wesbey GE, Moseley ME, Ehman RL: Translational molecular self-diffusion in magnetic resonance imaging. II. Measurement of the self-diffusion coefficient.
Investigative radiology 1984, 19(6):491-498.
55. Moseley ME, Kucharczyk J, Mintorovitch J, Cohen Y, Kurhanewicz J, Derugin N, Asgari H, Norman D: Diffusion-weighted MR imaging of acute stroke: correlation with T2-weighted and magnetic susceptibility-enhanced MR imaging in cats.
Ajnr 1990, 11(3):423-429.
56. Sevick RJ, Kucharczyk J, Mintorovitch J, Moseley ME, Derugin N, Norman D: Diffusion-weighted MR imaging and T2-weighted MR imaging in acute cerebral ischaemia: comparison and correlation with histopathology.
Acta Neurochir Suppl (Wien) 1990, 51:210-212.
57. Moseley ME, Mintorovitch J, Cohen Y, Asgari HS, Derugin N, Norman D, Kucharczyk J: Early detection of ischemic injury: comparison of spectroscopy, diffusion-, T2-, and magnetic susceptibility-weighted MRI in cats.
Acta Neurochir Suppl (Wien) 1990, 51:207-209.
58. Moseley ME, Cohen Y, Mintorovitch J, Chileuitt L, Shimizu H, Kucharczyk J, Wendland MF, Weinstein PR: Early detection of regional cerebral ischemia in cats: comparison of diffusion- and T2-weighted MRI and spectroscopy.
Magn Reson Med 1990, 14(2):330-346.
59. Stejskal EO: Use of spin echoes in a pulsed magnetic-field gradient to study anisotropic, restricted diffusion and flow.
J Chem Phys 1965, 43(10):3597-3603.
60. Carslaw HS, Jaeger JC: Conduction of Heat in Solids. 2nd edition edition. Oxford: Oxford University Press; 1959.
61. Basser PJ, Mattiello J, LeBihan D: MR diffusion tensor spectroscopy and imaging.
Biophysical journal 1994, 66(1):259-267.
62. Basser PJ, Mattiello JH, LeBihan D: Method and system for measuring the diffusion tensor and for diffusion tensor imaging. US 5,539,310: United States Patent Office; 1996.
63. Blinc R, Burgar M, Luzar M, Pirs J, Zupancic I, Zumer S: Anisotropy of self diffusion in the smectic-A and smectic-C phases.
Phys Rev Lett 1974, 33(20):1192-1195.
64. Hazelwood C, Chang D, Nichols B, Woessner D:

- Nuclear magnetic resonance transverse relaxation times of water protons in skeletal muscle. *Biophysical journal* 1974, 14:583-606.
65. Brownstein K, Tarr C: Importance of classical diffusion in NMR studies of water in biological cells. *Phys Rev A* 1979, 19(6):2446-2453.
66. Le Bihan D, Breton E, Lallemand D, Grenier P, Cabanis E, Laval-Jeantet M: MR imaging of intravoxel incoherent motions: application to diffusion and perfusion in neurologic disorders. *Radiology* 1986, 161(2):401-407.
67. Moseley ME, Stilbs P: A study of ¹⁴N relaxation and nitrogen-proton spin coupling in nucleoside, indole, and epsilon-caprolactam systems through Fourier transform measurement of NH proton spin-lattice relaxation in the rotating frame. *Can J Chem* 1978, 56:1302-1305.
68. Moseley ME: Nuclear magnetic resonance studies of solvent and polymer dynamics in polystyrene solutions. PhD Thesis. Uppsala: University of Uppsala; 1980.
69. Moseley ME, Loewenstein A: Anisotropic translational diffusion of methane and chloroform in thermotropic nematic and smectic liquid crystals. *Molecular Crystals and Liquid Crystals* 1982, 90(1):117-144.
70. Moseley ME, Cohen Y, Kucharczyk J, Mintorovitch J, Asgari HS, Wendland MF, Tsuruda J, Norman D: Diffusion-weighted MR imaging of anisotropic water diffusion in cat central nervous system. *Radiology* 1990, 176(2):439-445.
71. Moseley ME, Kucharczyk J, Asgari HS, Norman D: Anisotropy in diffusion-weighted MRI. *Magn Reson Med* 1991, 19(2):321-326.
72. Moseley ME: Evidence of anisotropic self-diffusion in cat brain (abst). In *Society of Magnetic Resonance in Medicine*: 1989; 1989:136.
73. Doran M, Hajnal JV, Van Bruggen N, King MD, Young IR, Bydder GM: Normal and abnormal white matter tracts shown by MR imaging using directional diffusion weighted sequences. *J Comput Assist Tomogr* 1990, 14(6):865-873.
74. Eccles C, Callaghan P, Jenner C: Measurement of the self-diffusion coefficient of water as a function of position in wheat grain using nuclear magnetic resonance imaging. *Biophysical journal* 1988, 53:77-81.
75. Moseley ME: Diffusion. *JMRI* 1993, 3 (S1):24-25.
76. Filler AG, Tsuruda JS, Richards TL, Howe FA: Image Neurography and Diffusion Anisotropy Imaging. US 5,560,360: Unites States Patent Office; 1996.
77. Parente DB, Gasparetto EL, da Cruz LC, Jr., Domingues RC, Baptista AC, Carvalho AC: Potential role of diffusion tensor MRI in the differential diagnosis of mild cognitive impairment and Alzheimer's disease. *AJR Am J Roentgenol* 2008, 190(5):1369-1374.
78. Ringman JM, O'Neill J, Geschwind D, Medina L, Apostolova LG, Rodriguez Y, Schaffer B, Varpetian A, Tseng B, Ortiz F et al: Diffusion tensor imaging in preclinical and presymptomatic carriers of familial Alzheimer's disease mutations. *Brain* 2007, 130(Pt 7):1767-1776.
79. Gattellaro G, Minati L, Grisoli M, Mariani C, Carella F, Osio M, Ciceri E, Albanese A, Bruzzone MG: White Matter Involvement in Idiopathic Parkinson Disease: A Diffusion Tensor Imaging Study. *AJNR Am J Neuroradiol* 2009.
80. Vaillancourt DE, Spraker MB, Prodoehl J, Abraham I, Corcos DM, Zhou XJ, Comella CL, Little DM: High-resolution diffusion tensor imaging in the substantia nigra of de novo Parkinson disease. *Neurology* 2009, 72(16):1378-1384.
81. Sidaros A, Engberg AW, Sidaros K, Liptrot MG, Herning M, Petersen P, Paulson OB, Jernigan TL, Rostrup E: Diffusion tensor imaging during recovery from severe traumatic brain injury and relation to clinical outcome: a longitudinal study. *Brain* 2008, 131(Pt 2):559-572.
82. Filler AG: MR Neurography and Diffusion Tensor Imaging: Origins, history & clinical Impact of the first 50,000 cases with an assessment of efficacy and utility in a prospective 5,000 patient study group. *Neurosurgery in press*.
83. Wong EC, Cox RW, Song AW: Optimized isotropic diffusion weighting. *Magn Reson Med* 1995, 34(2):139-143.
84. Mori S, van Zijl PC: Diffusion weighting by the trace of the diffusion tensor within a single scan. *Magn Reson Med* 1995, 33(1):41-52.
85. Darquie A, Poline JB, Poupon C, Saint-Jalmes H, Le Bihan D: Transient decrease in water diffusion observed in human occipital cortex during visual stimulation. *Proceedings of the National Academy of Sciences of the United States of America* 2001, 98(16):9391-9395.
86. Le Bihan D, Urayama S, Aso T, Hanakawa T, Fukuyama H: Direct and fast detection of neuronal activation in the human brain with diffusion MRI. *Proceedings of the National Academy of Sciences of the United States of America* 2006, 103(21):8263-8268.
87. Kohno S, Sawamoto N, Urayama SI, Aso T, Aso K, Seiyama A, Fukuyama H, Le Bihan D: Water-diffusion slowdown in the human visual cortex on visual stimulation precedes vascular responses. *J Cereb Blood Flow Metab* 2009.
88. Filler AG, Winn HR, Howe FA, Griffiths JR, Bell BA, Deacon TW: Axonal transport of superparamagnetic metal oxide particles: Potential for magnetic resonance assessments of axoplasmic flow in clinical neuroscience. In *Society for Magnetic Resonance in Medicine, 10th Annual Meeting*: 1991; San Francisco; 1991:985.
89. Filler AG, Bell BA: Axonal transport, imaging, and the diagnosis of nerve compression. *British journal of neurosurgery* 1992, 6(4):293-295.
90. Putnis A: Introduction to mineral sciences. Cambridge [England] ; New York: Cambridge University Press; 1992.
91. Le Bihan D: Molecular diffusion nuclear magnetic resonance imaging. *Magnetic Resonance Quarterly* 1991, 7:1-30.
92. Douek P, Turner R, Pekar J, Patronas N, Le Bihan D: MR color mapping of myelin fiber orientation. *Journal of computer assisted tomography* 1991, 15(6):923-929.
93. Le Bihan D, Turner R, Moonen CT, Pekar J: Imaging of diffusion and microcirculation with gradient sensitization: design, strategy, and significance. *J Magn Reson Imaging* 1991, 1(1):7-28.
94. Jost W: Diffusion in solids, liquids, gases. 3d print., with addendum. edition. New York: Academic Press; 1960.
95. Pierpaoli C, Jezzard P, Basser PJ, Barnett A, Di Chiro G: Diffusion tensor MR imaging of the human brain. *Radiology* 1996, 201(3):637-648.
96. Basser PJ, LeBihan D: Fiber orientation mapping in an anisotropic medium with NMR diffusion spectroscopy. In *Society for Magnetic Resonance in Medicine 11th Annual Meeting*: 1992; Berlin, Germany; 1992:1221.

97. Basser PJ, Mattiello J, LeBihan D: Diagonal and off-diagonal components of the self-diffusion tensor: their relation to and estimation from the NMR spin-echo signal. In Society for Magnetic Resonance in Medicine, 11th Annual Meeting: 1992; Berlin, Germany; 1992:1222.
98. Le Bihan D: Method for the imaging of intra-voxel movements by NMR in a body. US 5,092,335: United States Patent Office; 1992.
99. Basser P: Pressure sensor element and method to measure contact stress. US 5,125,408: United States Patent Office; 1992.
100. Basser PJ: Inferring microstructural features and the physiological state of tissues from diffusion-weighted images. *NMR Biomed* 1995, 8(7-8):333-344.
101. Filler AG, Howe FA, Richards TL, Tsuruda JS: Image Neurography and Diffusion Anisotropy Imaging. PCT/US93/02036: World Intellectual Property Organization, International Bureau; 1993.
102. Wassmann C: The development of diffusion tensor imaging and tractography at NIH: Interview with Dr. Peter Basser. http://history.nih.gov/01docs/historical/documents/PeterBasser_edited_001pdf 2005.
103. Bergmann W: Method and means for the non-invasive, local, in-vivo examination of endogenous tissue, organs, bones, nerves and circulating blood on account of spin-echo techniques. US 4,442,404: United States Patent Office; 1984.
104. Farrar T, Becker E: Pulse and Fourier Transform NMR: Introduction to Theory and Methods. New York: Academic Press; 1971.
105. Tanner J, Stejskal EO: Restricted self-diffusion of protons in a colloidal systems by the pulsed-gradient, spin-echo method. *J Chem Phys* 1968, 49(4):1768-1777.
106. Pierpaoli CM, Basser PJ: Method to significantly reduce bias and variance of diffusion anisotropy measurements. US 5,969,524: United States Patent Office; 1999.
107. Tauxe L, Constable C, Stokking L, Badgley C: Use of anisotropy to determine the origin of characteristic remanence in the Siwalik red beds of Northern Pakistan. *J Geophys Res* 1990, 95(B4):4391-4404.
108. Coremans J, Luypaert R, Verhelle F, Stadnik T, Osteaux M: A method for myelin fiber orientation mapping using diffusion-weighted MR images. *Magnetic resonance imaging* 1994, 12(3):443-454.
109. Nakada T, Matsuzawa H: Three-dimensional anisotropy contrast magnetic resonance imaging of the rat nervous system: MR axonography. *Neurosci Res* 1995, 22(4):389-398.
110. Mori S, Barker PB: Diffusion magnetic resonance imaging: its principle and applications. *The Anatomical record* 1999, 257(3):102-109.
111. Xue R, van Zijl PC, Crain BJ, Solaiyappan M, Mori S: In vivo three-dimensional reconstruction of rat brain axonal projections by diffusion tensor imaging. *Magn Reson Med* 1999, 42(6):1123-1127.
112. Mori S, Crain BJ, Chacko VP, van Zijl PC: Three-dimensional tracking of axonal projections in the brain by magnetic resonance imaging. *Ann Neurol* 1999, 45(2):265-269.
113. Mori S: Method of fiber reconstruction employing data acquired by magnetic resonance imaging. US 6,526,305: United States Patent Office; 2003.
114. Mori S: Introduction to Diffusion Tensor Imaging. New York: Elsevier; 2007.
115. Saloner D, Hanson WA, Tsuruda JS, van Tyen R, Anderson CM, Lee RE: Application of a connected-voxel algorithm to MR angiographic data. *JMRI* 1991, 1:423-430.
116. Cline HE, Holik AS, Lorensen WE: Computer aided surface reconstruction for interference countours. *Applied Optics* 1982, 21(24):4481-4488.
117. Alexander AL, Tsuruda JS, Parker DL: Elimination of eddy current artifacts in diffusion-weighted echo-planar images: the use of bipolar gradients. *Magn Reson Med* 1997, 38(6):1016-1021.
118. Alexander AL, Hasan K, Kindlmann G, Parker DL, Tsuruda JS: A geometric analysis of diffusion tensor measurements of the human brain. *Magn Reson Med* 2000, 44(2):283-291.
119. Alexander AL, Hasan KM, Lazar M, Tsuruda JS, Parker DL: Analysis of partial volume effects in diffusion-tensor MRI. *Magn Reson Med* 2001, 45(5):770-780.
120. Lazar M, Weinstein DM, Tsuruda JS, Hasan KM, Arfanakis K, Meyerand ME, Badie B, Rowley HA, Haughton V, Field A et al: White matter tractography using diffusion tensor deflection. *Hum Brain Mapp* 2003, 18(4):306-321.
121. Filler AG, Kliot M, Howe FA, Hayes CE, Saunders DE, Goodkin R, Bell BA, Winn HR, Griffiths JR, Tsuruda JS: Application of magnetic resonance neurography in the evaluation of patients with peripheral nerve pathology. *Journal of neurosurgery* 1996, 85(2):299-309.
122. Dailey AT, Tsuruda JS, Filler AG, Maravilla KR, Goodkin R, Kliot M: Magnetic resonance neurography of peripheral nerve degeneration and regeneration. *Lancet* 1997, 350(9086):1221-1222.
123. Hayes CE, Tsuruda JS, Mathis CM, Maravilla KR, Kliot M, Filler AG: Brachial plexus: MR imaging with a dedicated phased array of surface coils. *Radiology* 1997, 203(1):286-289.
124. Filler AG: Principles of MRI and other imaging techniques for studying peripheral nerve and muscle. In *Clinical Neurophysiology and Neuromuscular Diseases*. Edited by Brown W, Bolton C, Aminoff M. Philadelphia: W.B. Saunders; 2002:661-674.
125. Filler AG, Maravilla KR, Tsuruda JS: MR neurography and muscle MR imaging for image diagnosis of disorders affecting the peripheral nerves and musculature. *Neurologic clinics* 2004, 22(3):643-682, vi-vii.
126. Filler AG, Haynes J, Jordan SE, Prager J, Villablanca JP, Farahani K, McBride DQ, Tsuruda JS, Morisoli B, Batzdorf U et al: Sciatica of nondisc origin and piriformis syndrome: diagnosis by magnetic resonance neurography and interventional magnetic resonance imaging with outcome study of resulting treatment. *Journal of neurosurgery* 2005, 2 (Spine)(2):99-115.
127. Tuch DS, Reese TG, Wiegell MR, Makris N, Belliveau JW, Wedeen VJ: High angular resolution diffusion imaging reveals intravoxel white matter fiber heterogeneity. *Magn Reson Med* 2002, 48(4):577-582.
128. Tuch DS: Q-ball imaging. *Magn Reson Med* 2004, 52(6):1358-1372.
129. Tuch DS, Van Wedeen VJ: Diffusion MRI Using Spherical Shell Sampling. US 7,034,531: United States Patent Office; 2006.
130. Filler AG: Axial Character Seriation in Mammals: An Historical and Morphological Exploration of the Origin, Development, Use and Current Collapse of the Homology Paradigm - PhD Thesis. Cambridge, Massachusetts: Harvard

University; 1986.

131. Filler AG: The Upright Ape: A New Origin of the Species. Franklin Lakes, NJ: New Page Books; 2007.
132. Filler AG: The emergence and optimization of upright posture among hominiform hominoids and the evolutionary pathophysiology of back pain. *Neurosurgical Focus* 2007, 23(1):E4:1-6.
133. Filler AG: Homeotic evolution in the mammalia: diversification of therian axial seriation and the morphogenetic basis of human origins. *PLoS ONE* 2007, 2(10):e1019.
134. Pilbeam D, Meyer GE, Badgley C, Rose MD, Pickford MH, Behrensmeyer AK, Shah SM: New hominoid primates from the Siwaliks of Pakistan and their bearing on hominoid evolution. *Nature* 1977, 270(5639):689-695.
135. Jelinek V: Statistical processing of anisotropy of magnetic susceptibility measured on groups of specimens. *Studia Geoph et Geod* 1978, 2:50-62.
136. Tauxe L, Behrensmeyer AK: Paleomagnetic stratigraphy. In *Postilla: Miocene Sediments and Faunas of Pakistan*. Volume 179. Edited by Pilbeam D, Behrensmeyer AK, Barry JC, Shah I. New Haven: Yale University; 1979:11-16.
137. Tauxe L, Kent D, Opdyke N: Magnetic components contributing to the NRM of Middle Siwalik red beds. *Earth and Planetary Science Letters* 1980, 47:279-284.
138. Constable C, Tauxe L: The bootstrap for magnetic susceptibility tensors. *J Geophys Res* 1990, 95:8383-8395.
139. Ortnier B: On the selection of measurement directions in second-rank tensor (e.g. elastic strain) determination of single crystals. *J Appl Cryst* 1989, 22:216-221.
140. Nye F: *Physical Properties of Crystals*. New York: Oxford University Press; 1957.
141. Deacon TW: *The Symbolic Species :The Co-evolution of Language and the Brain*. 1st edition. New York: W.W. Norton; 1997.
142. Sokoloff L, Reivich M, Kennedy C, Des Rosiers MH, Patlak CS, Pettigrew KD, Sakurada O, Shinohara M: The [¹⁴C]deoxyglucose method for the measurement of local cerebral glucose utilization: theory, procedure, and normal values in the conscious and anesthetized albino rat. *Journal of neurochemistry* 1977, 28(5):897-916.
143. Reivich M, Kuhl D, Wolf A, Greenberg J, Phelps M, Ido T, Casella V, Fowler J, Hoffman E, Alavi A et al: The [¹⁸F]fluorodeoxyglucose method for the measurement of local cerebral glucose utilization in man. *Circ Res* 1979, 44(1):127-137.
144. Raichle ME, Grubb RL, Jr., Gado MH, Eichling JO, Ter-Pogossian MM: Correlation between regional cerebral blood flow and oxidative metabolism. In vivo studies in man. *Archives of neurology* 1976, 33(8):523-526.
145. Raichle ME, Welch MJ, Grubb RL, Jr., Higgins CS, Ter-Pogossian MM, Larson KB: Measurement of regional substrate utilization rates by emission tomography. *Science* 1978, 199(4332):986-987.
146. Gusnard DA, Raichle ME: Searching for a baseline: functional imaging and the resting human brain. *Nat Rev Neurosci* 2001, 2(10):685-694.
147. Gusnard DA, Akbudak E, Shulman GL, Raichle ME: Medial prefrontal cortex and self-referential mental activity: relation to a default mode of brain function. *Proceedings of the National Academy of Sciences of the United States of America* 2001, 98(7):4259-4264.
148. Raichle ME, MacLeod AM, Snyder AZ, Powers WJ, Gusnard DA, Shulman GL: A default mode of brain function. *Proceedings of the National Academy of Sciences of the United States of America* 2001, 98(2):676-682.
149. Raichle ME, Gusnard DA: Appraising the brain's energy budget. *Proceedings of the National Academy of Sciences of the United States of America* 2002, 99(16):10237-10239.
150. Gusnard DA, Ollinger JM, Shulman GL, Cloninger CR, Price JL, Van Essen DC, Raichle ME: Persistence and brain circuitry. *Proceedings of the National Academy of Sciences of the United States of America* 2003, 100(6):3479-3484.
151. Raichle ME, Gusnard DA: Intrinsic brain activity sets the stage for expression of motivated behavior. *The Journal of comparative neurology* 2005, 493(1):167-176.
152. Song AW, Harshbarger T, Li T, Kim KH, Ugurbil K, Mori S, Kim DS: Functional activation using apparent diffusion coefficient-dependent contrast allows better spatial localization to the neuronal activity: evidence using diffusion tensor imaging and fiber tracking. *Neuroimage* 2003, 20(2):955-961.
153. Mandl R, Schnack H, Zwiers M, van der Schaaf A, Kahn R, Hulshoff-Pol H: Functional diffusion tensor imaging: Measuring task-related fractional anisotropy changes in the human brain along white matter tracts. *PLoS ONE* 2008, 3(11):e3631:3631-3610.
154. Pohl E: Improvements in and relating to the radioscopic and radiographic reproduction of a section through a body. GB 369,662: UK Patent Office; 1930.
155. Damadian R: Apparatus and method for nuclear magnetic resonance scanning and mapping. US 4,354,499: United States Patent Office; 1982.

Author Information

Aaron G. Filler, MD, PhD, FRCS

Institute for Nerve Medicine

EXHIBIT 5

MAGNETIC RESONANCE NEUROGRAPHY AND DIFFUSION TENSOR IMAGING: ORIGINS, HISTORY, AND CLINICAL IMPACT OF THE FIRST 50 000 CASES WITH AN ASSESSMENT OF EFFICACY AND UTILITY IN A PROSPECTIVE 5000-PATIENT STUDY GROUP

Aaron Filler, M.D., Ph.D.

Institute for Nerve Medicine,
Santa Monica, California

Reprint requests:

Aaron G. Filler, M.D., Ph.D.,
Institute for Nerve Medicine,
2716 Ocean Park Boulevard #3082,
Santa Monica, CA 90405.
Email: afiller@nervemed.com

Received, April 30, 2008.

Accepted, April 21, 2009.

Copyright © 2009 by the
Congress of Neurological Surgeons

OBJECTIVE: Methods were invented that made it possible to image peripheral nerves in the body and to image neural tracts in the brain. The history, physical basis, and dyadic tensor concept underlying the methods are reviewed. Over a 15-year period, these techniques—magnetic resonance neurography (MRN) and diffusion tensor imaging—were deployed in the clinical and research community in more than 2500 published research reports and applied to approximately 50 000 patients. Within this group, approximately 5000 patients having MRN were carefully tracked on a prospective basis.

METHODS: A uniform Neurography imaging methodology was applied in the study group, and all images were reviewed and registered by referral source, clinical indication, efficacy of imaging, and quality. Various classes of image findings were identified and subjected to a variety of small targeted prospective outcome studies. Those findings demonstrated to be clinically significant were then tracked in the larger clinical volume data set.

RESULTS: MRN demonstrates mechanical distortion of nerves, hyperintensity consistent with nerve irritation, nerve swelling, discontinuity, relations of nerves to masses, and image features revealing distortion of nerves at entrapment points. These findings are often clinically relevant and warrant full consideration in the diagnostic process. They result in specific pathological diagnoses that are comparable to electrodiagnostic testing in clinical efficacy. A review of clinical outcome studies with diffusion tensor imaging also shows convincing utility.

CONCLUSION: MRN and diffusion tensor imaging neural tract imaging have been validated as indispensable clinical diagnostic methods that provide reliable anatomic pathological information. There is no alternative diagnostic method in many situations. With the elapsing of 15 years, tens of thousands of imaging studies, and thousands of publications, these methods should no longer be considered experimental.

KEY WORDS: Brachial plexus, Brain, Diffusion tensor imaging, Magnetic resonance imaging, Nerve, Piriformis, Thoracic outlet

Neurosurgery 65:A29–A43, 2009

DOI: 10.1227/01.NEU.0000351279.78110.00

www.neurosurgery-online.com

The discovery of a series of magnetic resonance pulse sequence strategies for tissue-specific imaging of nerve and nerve tracts in 1991 and 1992 opened a new diagnostic world in which a wide variety of pathological condi-

ABBREVIATIONS: ADC, apparent diffusion coefficient; CNS, central nervous system; DTI, diffusion tensor imaging; DWI, diffusion-weighted imaging; FA, fractional anisotropy; MRI, magnetic resonance imaging; MRN, magnetic resonance neurography; 3-D, 3-dimensional

tions involving nerves and neural tracts can be visualized directly (5, 7, 22, 29, 32, 38, 39, 59); these techniques are grouped under the terms *magnetic resonance neurography* (MRN) for peripheral nerves and *diffusion tensor imaging* (DTI) or *tractography* for the central nervous system (CNS). Many specialists in these 2 fields are not aware that they have a common origin in a shared set of fundamental imaging strategies and algorithms that grew out of a unitary development project.

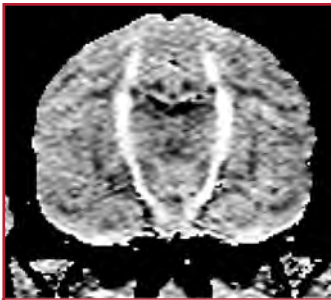


FIGURE 1. First diffusion tractographic imaging case. This image is primarily the work of Todd Richards and shows the use of spatial diffusion information to highlight a neural tract curving through brain. This is the brain of a long-tailed macaque monkey (*Macaca fascicularis*) imaged as part of an effort to improve the sensitivity of magnetic resonance imaging for the early detection of encephalomyelitis. (From Filler AG, Tsuruda JS, Richards TL, Howe FA, inventors; University of Washington, assignee. Images, apparatus, algorithms and methods. UK patent GB920016383. July 31, 1992 [29]; and Filler AG, Tsuruda JS, Richards TL, Howe FA, inventors; University of Washington, assignee. Image neurography and diffusion anisotropy imaging. US patent 5,560,360. March 8, 1993 [30]).

The first tractographic image using multidimensional directional information to show curved neural tracts traversing the brain (Fig. 1) and the first neurography images were submitted in a series of United Kingdom patent descriptions by Filler et al. (24, 29) between March and July of 1992 and were published by the World Intellectual Property Organization in 1993 (26, 30). Related images were published in the proceedings of the Society for Magnetic Resonance in Medicine annual meeting in Berlin in August 1992 (39, 59).

Before these developments in 1992, it had been generally assumed among radiologists that the peripheral nerves simply could not be imaged reliably. The potential to use diffusion magnetic resonance imaging (MRI) to tract trace through the brain was also not really anticipated in the clinical community. The strategy of using diffusion-based MRI sequences to help pro-

duce linear neural images was first discussed by Filler et al. in 1991 (32) and emerged as a workable technique through discoveries by Filler, Howe, and Richards (in London and Seattle) in late 1991 and by LeBihan and Basser (in Bethesda) in early 1992.

As a historical note, it is worth mentioning that the original work on DTI and Neurography in London was funded by the Neuroscience Research Foundation of Atkinson Morley's Hospital—the site where Hounsfield built the first experimental computed tomographic scanner in 1971 and also the site of the first clinical computed tomographic scan in 1973 (3, 37).

Treatment of each image voxel as a mathematical entity for vector and tensor math analysis represented a fundamental rethinking of neurological imaging data. This constituted a very significant transformation of the legacy of cross-sectional imaging from computed tomographic scanning—with its conceptual origins in X-ray beams and film exposures.

Vector and tensor representation of the internal structure of voxel image data also represented a shift in the conceptual basis of MRI from “slab”-based neuroanatomy into the realm of tract tracing that had dominated neuroanatomic research in the 1970s and 1980s. Interest in tract tracing for evolutionary studies of uniquely human neuroanatomic structures in the brain related to speech (12, 13) and in the periphery related to

the lumbar reorganization in hominoids (15, 17–19, 22, 33, 49) provided the original impetus for development of imageable tractographic methods for the CNS and nerves (16, 31).

Previously, the methodology of MRI had been focused on identifying methods to assign contrasting image intensities to various voxels (3-dimensional [3-D] pixels) in an MRI slice. This was accomplished by a wide array of pulse sequences that manipulated aspects of the T1 and T2 relaxation time of protons. Positional information for the voxels was obtained by using magnetic gradients to assign unique magnetic field strengths to each location in the volume to be imaged and then using Fourier transforms to extract signal strength data from each voxel at various echo times after a simple or complex radiofrequency pulse. Diffusion nuclear magnetic resonance per se had also known for decades; it acted as yet another source for obtaining contrast on the voxels by assessing relaxation rates (signal decays) that related to the degree to which nerve fibers tended to have water diffuse anisotropically (in a primary direction) rather than isotropically (in all directions) (52, 53). This is the basis for the diffusion-weighted imaging (DWI) that has been used to detect strokes for many years (43, 51, 56).

In magnetic resonance angiography, we typically produce a series of image slices in which blood vessel voxels are bright and then reconstruct the vessel tree from a stack of slices with vessels shown prominently in each cross section. DTI works very differently. The critical insight was a modification in the fundamental data acquisition process of the MRI scanning system so that each voxel would yield not only image intensity data but also directional data showing the tensor (3-D complex vector) direction in 3-D space.

Each voxel could be represented by a small arrow pointed in the direction of the principal nerve orientation in that volume. Instead of producing a cross section with dots, we produce an array of directional arrows along neural tracts, and these can be strung together by various standard 3-D graphics techniques to produce linear images of nerve tracts. In addition, pulse sequence modifications could be applied that made these data discoverable in the peripheral nerve as well. The resulting neurograms then served as a model for discovering additional non-diffusion tractographic methods for peripheral nerves.

By 1993, there were several major publications in these fields (25, 30, 36). In the subsequent 15 years, more than 100 academic publications have reported on various aspects of this new imaging modality in peripheral nerves, including several large-scale formal outcome assessment trials (23, 41, 42). Nonetheless, most textbooks of radiology or neuroradiology do not devote any pages to nerve imaging (4), as if nerves were not a clinically significant part of the body. Most practicing physicians still do not realize that high-quality diagnostically efficacious nerve imaging is available.

More than 2000 studies that explore DTI tractography in the CNS have been published (55), with most of these appearing in the past 3 years. The clinical impact of DTI is still difficult to predict. However, it encodes a great deal of information that is usually discarded in the course of CNS imaging. Therefore, it has shown great promise for detecting subtle derangements of

brain architecture that are difficult to recognize with cross-sectional imaging.

Formal outcome studies on the use of DTI for evaluation of traumatic brain injury (60), for predicting outcome after intracerebral hemorrhage (63), and for surgical guidance to optimize glioma resection (62) have appeared along with numerous preliminary studies for a wide variety of clinical uses in neuroscience, such as in the evaluation of dementia in Alzheimer's disease (10) and in identifying subtle lesions involved in the etiology of epilepsy (14). Recent diffusion image presentation algorithms have also been used to further advance earlier work on the use of DTI for peripheral nerves (38, 46, 61).

In the smaller but more clinical peripheral nerve imaging arena, MRN has proven to be more efficacious than electrodiagnostic studies for identifying nerve compressions that will improve with surgical treatment. This efficacy is seen both in diagnoses that are typically evaluated by electrodiagnostic studies such as carpal tunnel syndrome (41, 42) and in diagnoses in which electrodiagnostic studies have proven difficult such as piriformis syndrome and related sciatic nerve entrapments (20, 23).

The utility of MRN has now been established in the evaluation of entrapment syndromes (1, 2, 23, 27, 50), in the evaluation of nerve injury/repair (11), in nerve tumor assessment (8, 34, 35), and in the setting of neuritis and a variety of neuropathies (28). It is also effective for evaluating nerve disorders affecting young pediatric patients such as obstetrical brachial plexus palsy.

Over the 15 years since MRN was initially brought into clinical use, approximately 25 000 peripheral nerve imaging studies have been conducted. DTI in conjunction with brain MRI scans has been performed in tens of thousands of patients, mostly in the past 2 years. This report assesses the use and diagnostic range for MRN in a prospective group of more than 5000 patients for whom standardized protocols were applied, research consent obtained, and clinical data collected and organized.

For both T2 MRN and DTI, the clinical results can be used to help verify hypotheses about the physical basis of the underlying biophysical phenomena that result in the observed image effects in both normal and pathological situations. In addition, by identifying the most effective parameters to optimize, the clinical results can best identify the way forward for future developments.

PATIENTS AND METHODS

All patients had a physical examination to identify specific suspect nerve pathological conditions. Images were ordered through St. George's Hospital Medical School (1992–1996); University of Washington Department of Radiology (1993–1995); University of California, Los Angeles or OliveView/ University of California, Los Angeles Department of Radiology (1996–2001); or the Neurography Institute (2000–2007). Image protocols included matched T1 (anatomic) and neurographic image pulse sequences in multiple planes including at least one "nerve perpendicular" plane for fascicle assessment. Echo times were greater than 40 milliseconds (usually 70–100 milliseconds) for all MRN studies to assure that no magic angle effects could occur (8). Referral

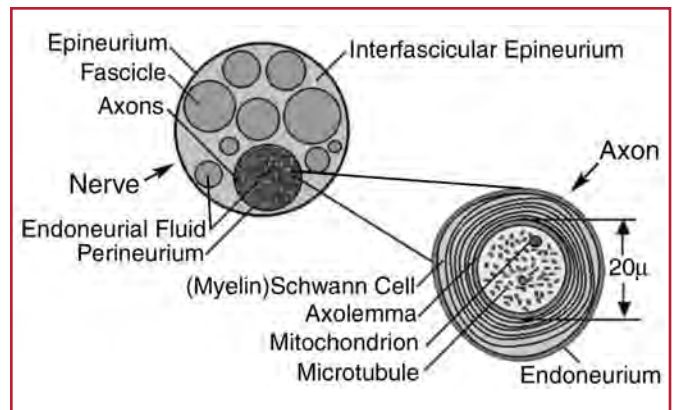


FIGURE 2. Nerve water compartments. Magnetic resonance pulse sequences can be optimized to detect a water signal arising in one of several compartments. Important nerve water components with unique characteristics for magnetic resonance imaging include the endoneurial fluid, axoplasmic water, organelle water, and myelin-associated water.

biases toward these specialty centers because of their widely recognized expertise in this area was an unavoidable aspect of the data.

RESULTS

T2-based MRN

Physical Basis

The clinical pathological data in T2-based MRN seem to derive from alterations in endoneurial fluid content in nerves. This fluid seems to be the sole candidate for the class of water to which the image parameters should apply. It is a low-protein fluid (long T2), confined to the endoneurium of nerve fascicles (Fig. 2), that physiologically participates in a bulk proximal to distal flow (54, 57, 58). Compressions or irritative processes seem to be capable of increasing the amount of this fluid relative to the other cellular components of the fascicle in a variety of pathological conditions (40).

Usage by Type of Pathological Condition

The dominant class of pathological conditions for which MRN studies were ordered in this group were for nerve entrapment. Usage in tumors (Figs. 3 and 4), trauma (Fig. 5), and neuropathy represented only a very small percentage of the studies. However, this usage also reflects the relative incidence of these conditions. Nerve entrapment/degenerative problems such as carpal tunnel syndrome, piriformis syndrome, thoracic outlet syndrome, and radicular spinal syndromes are far more prevalent. When correction for incidence of the major classes of disorders is considered, the usage pattern seems to be similar for degenerative/pain/entrapment, neoplastic, and traumatic nerve pathological conditions. Our study participants represented approximately 0.01% of the total incidence for the time period for these types of cases. Usage for the evaluation of neuropathy is very low.

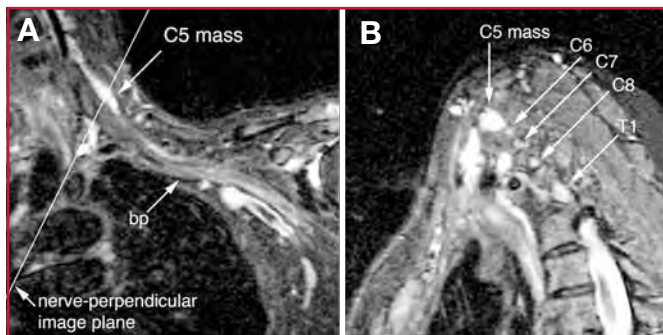


FIGURE 3. Relations of a small C5 mass to brachial plexus (bp) elements. In many patients, by collecting images in planes that are perpendicular to the main longitudinal axis of the nerve elements of interest, it is possible to obtain extremely specific information about the location of a mass within the brachial plexus. **A**, multiplanar reformat oriented parallel to the main longitudinal orientation of the brachial plexus. **B**, oblique acquisition perpendicular to the orientation of the main longitudinal direction of the brachial plexus.



FIGURE 4. Relations of brachial plexus (bp) elements to an axillary mass. Although a schwannoma (sc) can be detected by various techniques, it is extremely valuable for the surgeon to have a method of determining the position of the nerve elements relative to the position of the mass.

Usage by Body Region/Nerve

Use of MRN is heavily concentrated in the evaluation of large proximal nerves that are difficult to assess accurately by routine electrodiagnostic techniques and physical examination. Studies of the lumbosacral plexus, proximal sciatic nerve, and other pelvic nerves (ilioinguinal, pudendal, femoral, and obturator) constituted approximately 42% of cases. Brachial plexus imaging accounted for an additional 18% of cases and lumbar spinal nerve studies accounted for 5%. The remaining 35% were studies of knee/peroneal nerve, elbow/ulnar nerve, wrist/median

nerve, ankle/tibial nerve, upper neck/occipital nerves, and thigh/distal sciatic, calf, foot, upper arm, abdominal wall, face, intercostal spaces, and various individual study types.

Usage by Practitioner Category

Most MRN studies were ordered by neurosurgeons (43%), and this ordering seemed to represent a combined influence of diagnostics and surgical planning. Surgical planning as a reason for ordering was inferred when the study was ordered by a surgeon and the diagnosis was already established. Neurologists ordered an additional 21% of the studies, whereas pain specialists (12%), physiatrists (8%), orthopedic surgeons (6%), and various others ordered the remaining studies. Only a very

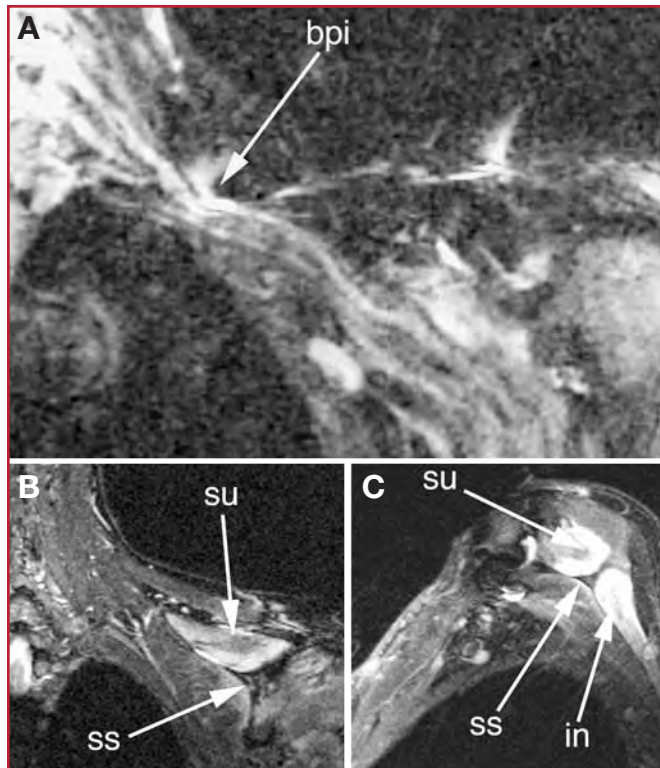


FIGURE 5. Upper trunk brachial plexus injury (bpi) with denervation of C5 muscles. **A**, apparent discontinuity of the C5 component of the upper trunk. The C6 component is swollen upstream of the injury and sharply narrowed and hyperintense. Coronal view (**B**) and nerve perpendicular view (**C**) showing severe denervation changes in supraspinatus (su) and infraspinatus (in) muscles. ss, scapular spine.

small number were ordered for pediatric patients, and these generally were not ordered by pediatricians.

Diagnostic Efficacy and Ordering

MRN had a high diagnostic efficacy. More than 96% of studies resulted in either specific findings involving the nerve of interest or in a definitive statement that the nerve or nerves in question were entirely normal in appearance. The remaining 4% of studies were nondiagnostic because of movement, artifact from implants, body habitus or pain limiting appropriate positioning in the scanner, or ordering errors. Ordering errors arose because many practitioners were not experienced in ordering nerve imaging. For example, a neurologist or neurosurgeon (or staff member) seeking to evaluate sciatica due to piriformis syndrome would order a lumbar MRN instead of the necessary pelvic MRN because of the habit of using lumbar MRI for sciatica.

Contrast Agent Use

Intravenous gadolinium contrast material was used in approximately 0.4% of cases. When tumor was part of an initial

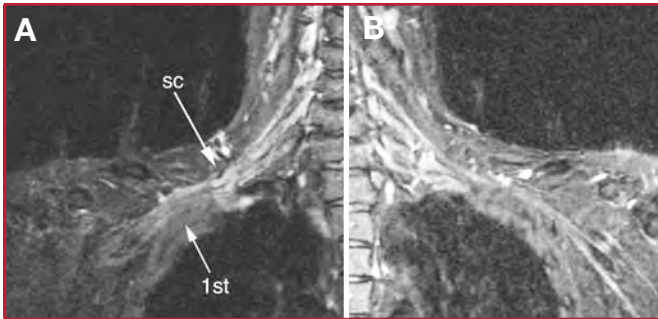


FIGURE 6. Right and left side comparison of a patient suffering from right-sided thoracic outlet syndrome. The image demonstrates several types of abnormalities detectable by magnetic resonance neurography relative to the normal side. There is increased caliber and image intensity of nerve elements on the left and 2 sites of impingement. A sharp focal downward distortion at the lateral border of the scalene triangle (sc) and then a gently sloped upward distortion over the first rib (1st).

differential diagnosis but not proven, contrast material was not used. Only patients with known tumors underwent intravenous contrast studies.

Follow-up Imaging Studies

Approximately 1% of the studies were part of a repetitive set. These were generally done in patients who had diagnostic MRN and were then referred for repeat imaging when symptoms recurred after treatment, when an extended time elapsed between initial imaging and treatment, when recurrent tumor was suspected, or when new symptoms arose in the same body region. Generally, the use of repetitive imaging was lower than what has been reported for lumbar or cervical MRI.

Geographic Distribution

The highest usage of MRN was in Southern California, accounting for approximately 82% of patients imaged. Usage was lower in other regions with the only other significant concentration being in Northern California and the remainder coming from nearly all states in the United States, England, Spain, France, Japan, Mexico, and China.

Classes of Image Findings

Image findings in MRN studies include the presence of regions of nerve hyperintensity, distortions of normal nerve course, abnormal contours, and alterations of nerve caliber (Figs. 6 and 7), any of which can be classed by the degree or severity of the abnormality. These findings seem most reliable for the larger named nerves (>3 mm in diameter), although there is no technical limit on the imageable size of a nerve. In trauma, assessments of nerve continuity (Fig. 5) and/or location of severed nerve endings are feasible, although edema at a site of injury limits the utility of MRN in acute injury settings, but this becomes less of an issue after the elapse of 2 to 4 weeks. In chronic trauma or late evaluation of the effects of trauma, the development of fibrosis does not hinder nerve imaging because most classes of fibrosis have very different

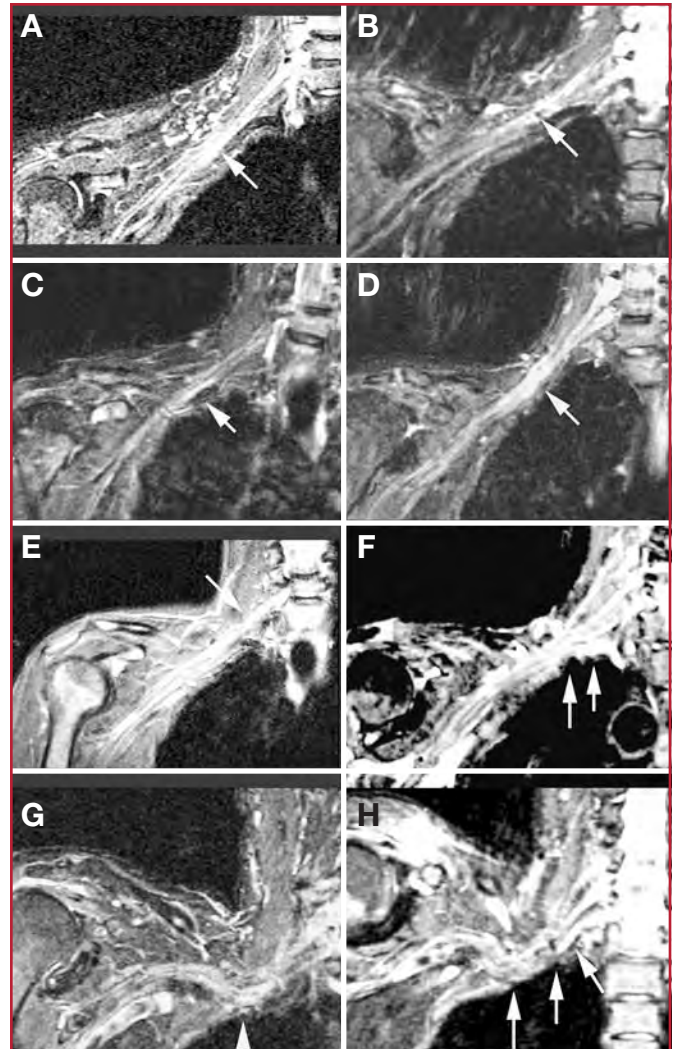


FIGURE 7. Varying degrees of severity of brachial plexus entrapment in thoracic outlet syndromes. **A**, linear plexus with short segment of mild hyperintensity consistent with nerve irritative changes near the later border of the scalene triangle. **B**, evidence of more restrictive fibrosis associated with narrowing and brightening of plexus elements near the scalene border (note linear plexus despite elevated shoulder). **C**, short segment of marked hyperintensity with slight swelling. **D**, severe multiple element abnormality with narrowed and swollen segments and marked hyperintensity. **E**, linear normal plexus with isolated focal impingement of C5 spinal nerve, just proximal to the scalene triangle. **F**, fibrous band causing sharp downward distortion of the mid and lower trunk proximal to the scalene triangle, with a second sharp upward distortion of the lower trunk near scalene insertion at the first rib. **G**, moderate restrictive impingement of plexus at the scalene triangle causing generalized distortion of the course of the plexus with a short segment of focal hyperintensity. **H**, patient presenting with severe pain, numbness, and weakness from progressive thoracic outlet syndrome: multiple points of sharp nerve course distortion with edema and hyperintensity affecting multiple brachial plexus elements.

image characteristics than nerve: there is no long T2 low-protein water component to deal with.

Conspicuity and Reconstructions

One important aspect of MRN is to use MRI pulse sequences and acquisition strategies that tend to make nerve image intensity brighter than that of immediately surrounding tissues. When this is achieved, it greatly aids the process of generating 3-D projection images as well as multiplanar reformatted images. This process often helps in the recognition of the overall nerve course and of variations in the types of other image findings along the length of a nerve. Among the 5000 patients evaluated, 3-D analysis could be used in more than 99%. Findings in the 3-D reports revealed additional information not recognized in 2-dimensional analysis in 28% of patients. The greatest amount of additional diagnostic information in these analyses occurred in the brachial plexus studies. Because of the significant incremental amount of clinical information provided by this type of analysis and the susceptibility of most studies, these were considered essential aspects of the diagnostic interpretation process in this group.

Multiplanar reformat and maximum intensity projection reconstructions were also important in limiting artifactual variations in nerve image intensity that can occur from partial volume averaging; this means that when a given sampled voxel is partially filled with nerve and partially filled with an adjacent low-intensity tissue, the resulting pixel on the image will appear to show low-intensity nerve. Reconstruction techniques such as multiplanar reformats in linear planes allow the reading clinicians to readily assess this sort of issue. Curved reformats made along a "nerve course plane" drawn along the main nerve axis by a technologist or radiologist reduce the accuracy of the spatial information but provide for optimal reduction of image intensity averaging effects.

Image Findings in Brachial Plexus Studies

MRN proved effective for identifying the presence of a variety of types of abnormalities in brachial plexus studies. These include distortions of the course of the proximal elements at the scalene triangle (Figs. 6 and 7, A–D), fibrous band entrapments affecting C8 and T1 spinal nerve and the lower trunk of the brachial plexus (Fig. 7F), gross distortions of the midplexus (Figs. 7, G and H), hyperintensity consistent with nerve irritation at the level of the first rib (Fig. 6), and distal plexus hyperintensity.

In most peripheral nerve studies it has proven useful for identifying areas of hyperintensity consistent with nerve irritation by a comparison of results from following serial nerve cross sections oriented to be perpendicular to the principal long axis of nerves to images taken to be more or less parallel to the long axis. In nerve perpendicular images, the fascicle pattern can generally be observed. This will demonstrate expansion of the fascicle compartment at the expense of the interfascicular compartment at areas of focal hyperintensity. The nerve parallel images can provide a linear overview. In general, effective interpretation of nerve parallel images depends on the ability of the MRN imaging sequence to make the nerve brighter than surrounding tissues. In this fashion the nerve image plane can be adjusted by multiplanar reformatting or the nerve can be assembled by maximum intensity projection. If this is not done, partial volume

effects at the edges of nerves can lead to the artifactual appearance of variation of image intensity within an image. In the brachial plexus, multiplanar reformatting is usually sufficient to generate a series of images that can reliably confirm the existence of a focal change in nerve image intensity. This is aided by positioning the patient in the scanner in a way that tends to straighten the plexus. When a change in the fascicle pattern shows increased intensity in the nerve perpendicular views that matches a change seen in nerve parallel views, there can be a very high level of confidence about the clinical reality of nerve edema at the location that appears abnormal in the image.

MRN in the Pelvis

The use of MRN has revolutionized neurological diagnosis in the pelvis (20, 21, 23). Although sciatic pathological conditions have been an important part of the progress, the ability of MRN to track other nerve elements in the pelvis has contributed greatly to resolving what had been a troublesome "black box."

Patients with face, neck, arm, and hand conditions tend to be very effective in identifying the location of pain, numbness, and dysfunction. The physical examination is straightforward and well understood by many clinicians. Electrodiagnostic studies are readily applied. In the pelvis, the situation is quite different. Although the sciatic nerve in the leg poses accessibility similar to what the clinician experiences in the upper body, there has been great difficulty in applying physical examination and imaging and electrodiagnostic studies in the pelvis. Furthermore, patients often have great difficulty explaining the location of pains. It is common for low buttock pain to be described as "back pain," whereas patients readily distinguish between shoulder and neck pain. "Groin" pain could refer to problems involving the femoral nerve, ilioinguinal nerve, genitofemoral nerve, pudendal nerve, obturator nerve, or nerve to the obturator internus, among others.

The ability to reliably locate all of these nerve elements in MRN images greatly aids in physical examination. The ability of open magnetic resonance-guided injections to distinguish the superior gluteal nerve, inferior gluteal nerve, posterior femoral cutaneous nerve, cluneal nerve (superior, middle, and inferior), nerve to the obturator internus, and nerve to the quadratus femoris has also supplemented the role of MRN for identifying pathological conditions in these nerves. Clarification of the nerve course anatomy has also greatly enhanced the efficacy of a physical examination and elucidated the meaning of a variety of new types of physical examination maneuvers.

With regard to lower extremity radiculopathy, MRN has made it convenient to determine distinctions by imaging that help locate impingements in spinal foramina, at the distal foramen, at the lateral marginal osteophytes several centimeters distal to the foramen (Fig. 8), in the lumbosacral plexus, on the medial aspect of the piriformis muscle (Fig. 9), in association with division of the nerve by the piriformis muscle (Fig. 10), at the ischial margin, at the tendon of the obturator internus, at the distal ischial tunnel on the lateral aspect of the ischial tuberosity, and at various locations in the thigh. Because MRN is a very sensitive test, a completely negative MRN result (Fig.

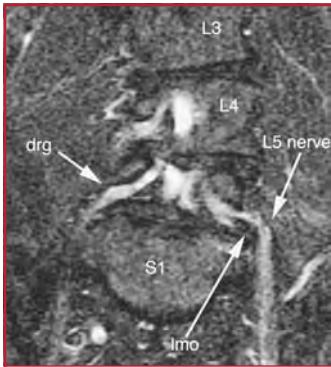


FIGURE 8. Extraforaminal impingement of descending L5 spinal nerve by lateral marginal osteophyte distal to the foramen. drg, dorsal root ganglion, lmo, lateral marginal osteophyte.

9) is often very useful, just as a completely normal lumbar MRI scan can be. In both cases, the definitively negative study results can substantively change the direction of further diagnostic efforts.

Reliable identification of anatomic variants of the sciatic nerve now plays a critical role in improving the safety of operations for the release of pelvic sciatic nerve entrapment. Isolated section of a single piriformis segment in patients with a split nerve passing through a split muscle can cause nerve compromise after surgery if this condition is not detected in advance (Fig. 11). Identification of the presence or absence of pudendal nerve hyperintensity consistent with nerve irritation in the Alcock canal (Fig. 12) along the medial aspect of the obturator internus muscle or at the rectal branch of the pudendal nerve proximal to its entrance to the Alcock canal (Fig. 13) has also been quite useful clinically (21).

Imaging of the complete course of the L4 spinal nerve as it progresses into the femoral nerve has made it possible to search for abnormalities along the intra-abdominal and intrapelvic course that were previously almost impossible to diagnose. Identification of abnormalities along the ilioinguinal and genitofemoral nerves is similarly greatly aided by MRN.

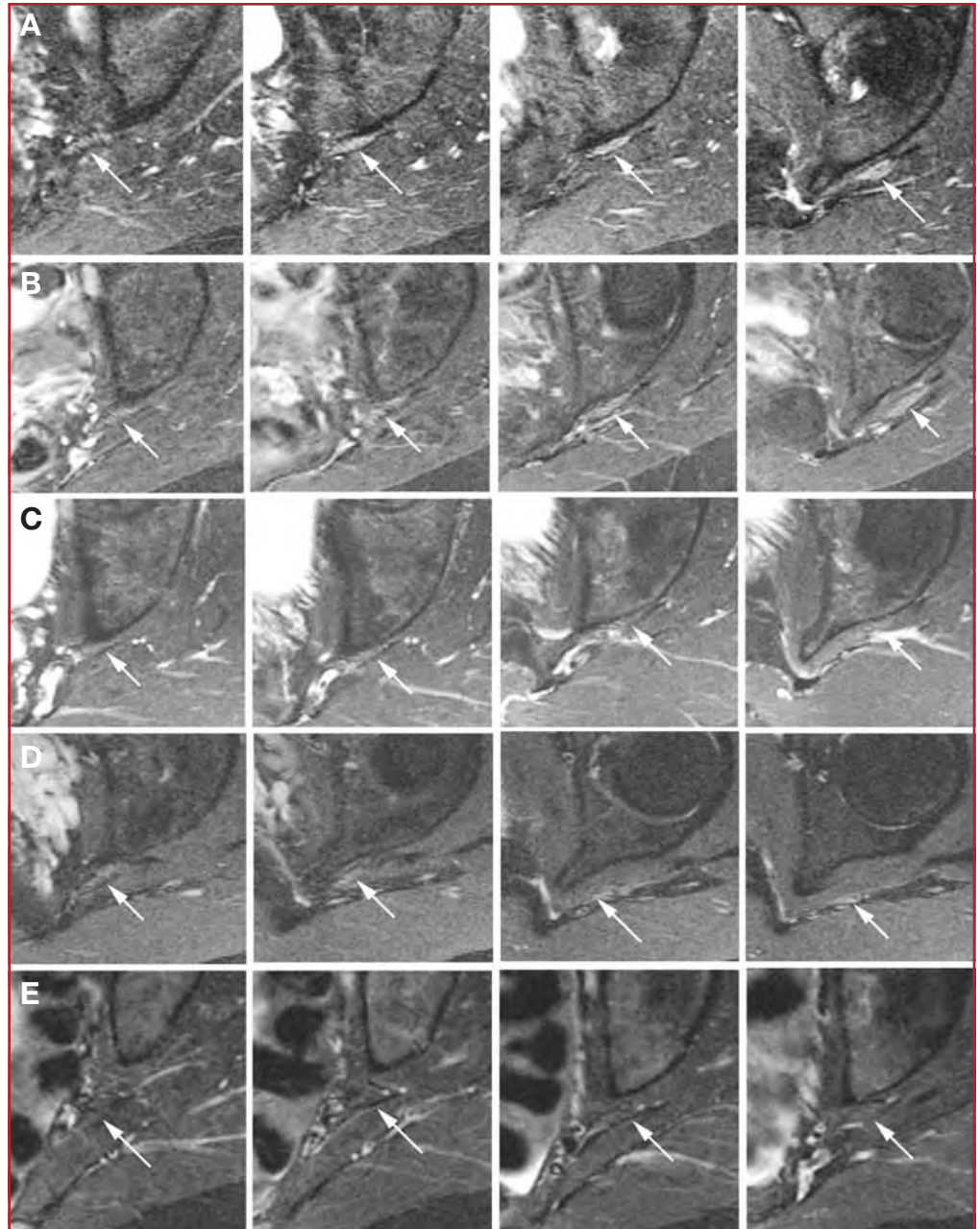


FIGURE 9. Comparison of sciatic nerve appearance at the sciatic notch in patients with hyperintensity and in normal patients. **A** and **B**, hyperintensity in the sciatic nerve in a series of images as the nerve exits the sciatic notch and descends below the level of the piriformis tendon. **C**, **D**, and **E**, sciatic nerve is nearly isointense with surrounding muscle tissue. Arrow indicates sciatic nerve in all images.

Nerve Imaging for Distal Entrapments

Patients with distal entrapments including less common problems such as posterior interosseous nerve entrapment of the distal radial nerve as well as common issues such as peroneal nerve entrapment at or above the fibular head, tarsal tunnel syndrome, cubital tunnel syndrome, and carpal tunnel syn-

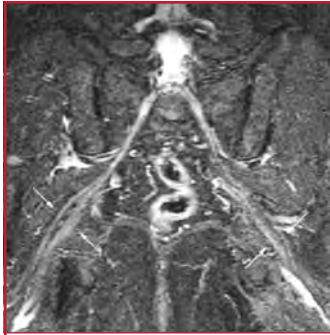


FIGURE 10. Bilateral split sciatic nerve at the piriformis muscle in patient with bilateral piriformis syndrome. Among the most important aspects of preoperative planning in management of sciatic nerve entrapments in the pelvis is the identification of patients with a split sciatic nerve partly passing through the piriformis muscle. This image demonstrated the S1 spinal roots, spinal nerves, lumbosacral plexus, and split peroneal and tibial components of the sciatic nerve (arrows) as they are deviated by segments of the piriformis muscle bilaterally.

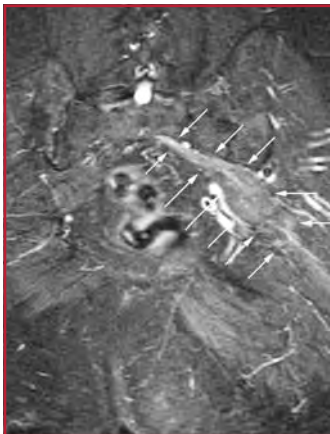


FIGURE 11. Severe focal compression of the sciatic nerve at the sciatic notch. The nerve is flattened, hyperintense, and expanded to more than twice its normal diameter. This is a postoperative result that occurred when only one of the 2 bipartite elements of the piriformis muscle was released in a patient with split nerve and split muscle. Differential retraction of the cut piriformis segment relative to the intact segment caused a severe mechanical impingement syndrome.

drome benefit from MRN imaging when a physical examination or electrodiagnostic studies show that locations other than the most routine sites may be involved. For instance, median nerve entrapment in the distal forearm can lead to failure of treatment if only the flexor retinaculum is addressed. Ulnar entrapment in the Guyon canal and proximal peroneal nerve entrapments along the tendon of the biceps femoris just distal to the sciatic bifurcation are other specialized issues that can be investigated best by imaging. Electrodiagnostic studies can be misleading if they are done with the assumption that abnormalities in certain regions (e.g., the median nerve in the distal forearm) will always be at the flexor retinaculum, particularly if uncomfortable and time-consuming “inching” studies are not done.

Clinical Outcomes and MRN

The evidence for clinical utility for MRN has been evaluated with 2 different types of outcome studies. First, it has been compared with electrodiagnostic studies in the well-defined environment of assessing median nerve compressions at the wrist (41, 42). In this setting, in the evaluation of 120 patients, MRN has proven to be as effective or slightly better than electrodiagnostic studies for predicting which patients will have good surgical outcome from carpal tunnel decompression. Second, a different paradigm has been applied using class A study methodology for evaluating the utility of MRN for positively affecting patient out-



FIGURE 12. Pudendal nerve entrapment between the ischial spine and the Alcock canal. In patients with unilateral pudendal entrapment in the Alcock canal, it is typical to see asymmetric swelling and hyperintensity affecting the pudendal neurovascular bundle. Note increased caliber and hyperintensity at the left pudendal nerve indicated by the left arrow. (From Filler AG: *Diagnosis and management of pudendal nerve entrapment syndromes: Impact of MR neurography and open MR-guided injections. Neurosurg Q 18:1-6, 2008 [21].*)

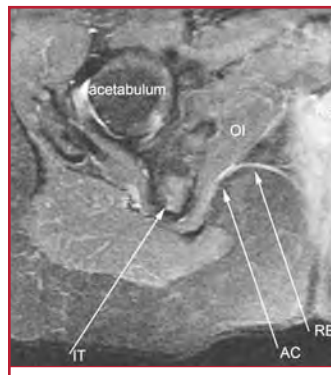


FIGURE 13. Distal pudendal nerve neurographic image anatomy. The pudendal nerve in the Alcock canal (AC) runs along the medial aspect of the obturator internus muscle (OI) medial to the ischial tuberosity (IT). The rectal branch of the nerve (RB) is well seen in most imaging studies. Re, rectum. (From Filler AG: *Diagnosis and management of pudendal nerve entrapment syndromes: Impact of MR neurography and open MR-guided injections. Neurosurg Q 18:1-6, 2008 [21].*)

comes in proximal sciatic entrapment, a condition for which there is no gold standard method (23, 44, 45). In this study evaluating 239 patients, use of MRN resulted in a strongly significant improvement in success for treating patients with sciatica who had either negative diagnostic study results or in whom treatment failed when managed by information from standard diagnostic studies alone. In these studies, image interpretation was performed by neuroradiologists blinded to outcome results.

Diffusion Tensor Imaging

From the earliest report on the use of DTI to visualize neural pathological conditions (59), it has been clear that this technique has great potential for use in detecting inflammatory brain conditions. It is also proving to be promising for evaluation of stroke, dementia, and diffuse axonal head injury and to aid in surgical navigation in brain tumor resections. It is also being explored for evaluation of myelopathy in the cervical spinal cord. It is very demanding from the point of view of motion suppression, but increasing clinician experience with the special requirements is leading to steady advances in establishing the utility of the technique.

Physical Basis

Nuclear magnetic resonance generally depends on using a radiofrequency stimulation to push energy into a group of nuclei and then using an antenna to detect the decay of the stimulated signal. For a given type of atomic nucleus, such as the single proton nucleus of

hydrogen atoms, there is a nuclear spin rate or frequency that is related to any magnetic field applied to the nucleus according to a physical relationship we call the gyromagnetic ratio. This means that, for instance, in a 4.7-T magnetic field, hydrogen nuclei will be aligned with the direction of the main magnetic field and have a natural spin rate (resonant frequency) of 200 MHz; in a 1.5-T magnet, the spin rate will be 64 MHz, and so on. Therefore, for a given magnet field strength, we know the resonant frequency for hydrogen nuclei and can pump in a pulse of radiofrequency energy at that resonant frequency, thus causing most of the protons in the volume to spin in phase with each other. They will then emit a radiosignal at that frequency that can be detected when the incoming stimulus pulse is turned off. With elapse of time over tens and hundreds of milliseconds, the protons will gradually lose their coherent behavior: Some will spin a little faster and some a little slower, and the return signal will gradually decay away.

When we measure the T1 and T2 decay rates, we are observing the effects of the spins interacting with their surroundings or “matrix.” For instance, a little bit of iron in the tissue will perturb the magnetic environment to a variable degree (T1 decay), and we will also see the effects of the protons interacting with each other (spin-spin or T2 decay). Because these decays occur at differing rates in different tissues, we can see contrast between tissues that can be expressed as gray or white in an image of a volume that we are measuring.

In MRI, we use magnetic gradients in 3 planes to assign a slightly different field strength to each location in the tissue volume. For instance, in the very center, the field strength could be 4.7 T, but a little to the right it would be 4.7001 T and a little to the left it would be 4.699 T. The protons on the right now spin at 200.001 MHz, and the protons on the left spin at 199.99 MHz. In this fashion, we can assign a unique field strength and therefore a unique frequency to each voxel (3-D pixel) in our imaging volume, and we can “listen” individually to the decay rate in each individual volume in the tissue. The entire process is done with a mixed complex of frequencies and a Fourier transform is used to sort them all out.

In diffusion imaging, we rely on a special property of axons to establish a source of information from an entirely different cause of spin decay. A pulsed “diffusion” magnetic gradient is applied so that as water molecules diffuse to different locations in a tissue, their spins dephase because a group of water molecules that started out next to each other in a single field strength now find themselves in different field strengths. Thus, they have different spin rates and the spins dephase from each other, resulting in signal decay. Water molecules in some tissues diffuse equally in all directions (isotropic diffusion), but in nerves and nerve tracts, diffusion takes place preferentially along the long axis of the nerve tract (anisotropic diffusion) (Fig. 14). If a magnetic gradient is directed perpendicular to the direction of a nerve or tract, the water diffusing in the nerve will tend to remain in the same strength region of the gradient and will show relatively little decay from diffusion, gradually

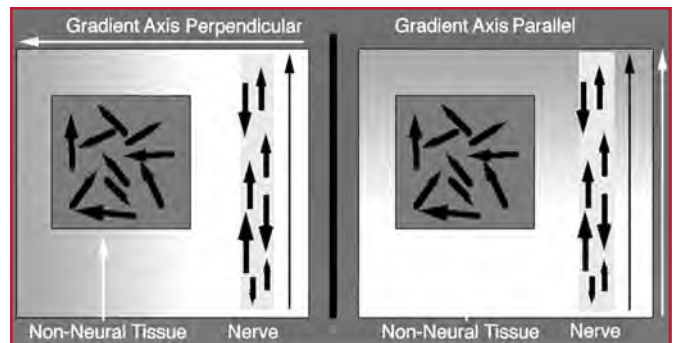


FIGURE 14. Isotropic and anisotropic diffusion of water molecules in diffusion magnetic resonance imaging. Shades of gray intensity indicate the intensity of the magnetic field, which varies across the image plane because of the imposed pulsed magnetic field gradient. Water diffuses in all directions in most nonneural tissues (isotropically) but diffuses preferentially along the long axis of nerves (anisotropically). When all of the water molecules in a tissue experience identical magnetic field strength despite diffusion movements, the magnetic resonance signal from that tissue remains bright relative to the signal decay in surrounding isotropically diffusing tissue water. This is the situation on the left where the magnetic gradient is oriented perpendicular to the nerve. In the situation on the right, the water molecules in nerve move preferentially to different positions in the gradients more rapidly than in the nonneural tissue so that the signal remains brighter from nonneural tissue.

becoming brighter relative to the tissue around it. However, if the gradient is then oriented parallel to the direction of the nerve, the anisotropically diffusing water molecules will tend to move up and down the gradient more rapidly compared with isotropically diffusing water molecules and so will actually experience a more rapid signal decay, making the nerve tend to go dark relative to other tissues around it.

However, what happens if the nerve or tract takes a curved course? How do we get the diffusion gradient to be perpendicular or parallel to it? This was the essence of the problem, but the solution comes from very simple mathematical geometry. In essence, if we can determine the degree of anisotropy in each voxel relative to the three principle directional axes, we can provide an estimate of the true dominant direction of anisotropy inside the 3-D space of that voxel. The direction, whether in 2- or 3-D is a vector, however—as will be explained below—we need a more elaborate data structure called a “tensor” in order to fully describe the anisotropy data. Isolated diffusion measurements provide an orientation but not a direction (e.g., the anisotropy goes up and down the z-axis)—it turns out that to fill out the 9 elements of the matrix that describes a tensor in 3-D space we need at least 6 measurements.

In standard DWI, we want to know the total amount of diffusion within a given voxel when viewed with no special attention to direction. For DTI, we want to know both the true magnitude and the true 3-D direction of the anisotropy in each voxel independent of the angle from which we view the voxel. This information is used in 2 different ways. One way is to make an image slice in which the relative amount of anisotropy

is described as the fractional anisotropy (FA), which more or less determines how bright a voxel will be, and uses a standard set of colors to depict some of the information about the orientation of the fiber tracts. This results in cross sections showing some of the information about bulk orientation of white matter tracts in regions of the brain. The other way is for tractography. Here, various mathematical algorithms are applied to generate linear tracts in 3 dimensions that represent the course of bundles of axons in the white matter of the brain or of nerve fibers in peripheral nerves (Fig. 15).

From one point of view, the development of DTI and tractography was hindered for many years by a mathematical model deriving from Basser et al. (6) due to the “elipsoid” formalism that takes a different approach to the analysis than in the original vector and tensor model from Filler (29) and Richards (59) that underlies modern tractography. The equations used for the first tractographic image are as follows:

$$(1) (\text{Vector length})^2 = BX^2 + BY^2 + BZ^2$$

$$(2a) \text{ Diffusion vector angle between } BX \text{ and } BY = \arctan (BY/BX)$$

$$(2b) \text{ Diffusion vector angle between } BX \text{ and } BZ = \arctan (BZ/BX)$$

$$(2c) \text{ Diffusion vector angle between } BY \text{ and } BZ = \arctan (BZ/BY)$$

The first of these basic equations establish a vector length analogous to what is now called the axial diffusivity (B is an image intensity measure related to the effects of different decay time measured in each of the three axes assessed in three separate measurements, X then Y then Z). This vector length calculation has the important effect of making the measurement of the amount of anisotropic diffusion in a given voxel independent of the orientation of the anisotropy relative to the orientation of the gradients applied. This made it possible to make, for the first time, a valid image showing the degree of anisotropy in all parts of each image slice. Previously—in a standard diffusion imaging model—a given tract would be bright or dark depend-

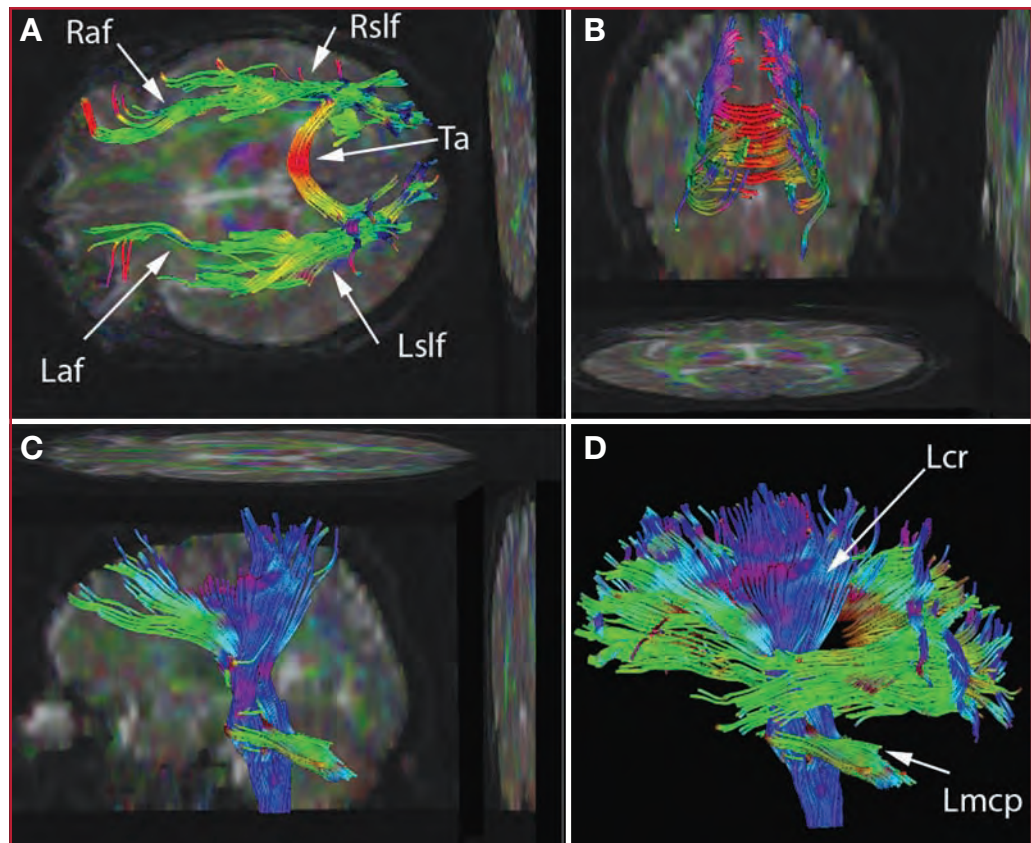


FIGURE 15. Diffusion tensor imaging data have been used to seed various tractographic assessments of this patient’s brain. These are seen in superior (A), posterior (B), and lateral views (C and D). The seeds have been used to develop arcuate and superior longitudinal fasciculi in A and B, for brainstem, and corona radiata in C and as combined data sets in D. Some of the 2-dimensional projections of the tractographic result are also shown. The data set may be rotated continuously into various planes to better appreciate the structure. Color has been assigned on the basis of the dominant direction of the fibers. There is asymmetry in the tractographic fiber volume between the right (Raf) and left arcuate fasciculus (Laf) (smaller on the left) and between the right (Rslf) and left superior longitudinal fasciculus (Lslf) (smaller on the right). Also seen are tapetum (Ta), left corona radiata (Lcr), and left middle cerebellar peduncle (Lmcp).

ing on its orientation in a given voxel even if it was highly anisotropic at that location.

The second set of equations allows us to take three looks at our voxel—each seeing it in 2 dimensions. It uses the arctangent function to measure the angle between the neural tract and the gradient axis direction that is in denominator of the equation. If BY is 0.1 and BX is nearly 1.0, then the arctangent of BY/BX will be about 5 degrees. When the measure is equal in two directions (Y = 0.5 and X = 0.5), the arctangent is 45 degrees.

Because of the vector length and the arctangent function, we can correctly interpret a voxel in which all three angles of measurement are equal. It does not describe a sphere nor does it describe an isotropic voxel. We know it has length and is oriented at 45 degrees to the reference frame—a line along the diagonal of the cube. We can also depict the arctangent value in successive voxels to see coherence in the angle of direction from voxel to voxel as we progress along a neural tract.

Basser and LeBihan (6, 7) proposed that each voxel be viewed as containing an ellipsoid that needed to be defined in shape from 6 different gradient measurements rather than just 3 (55). Although it is true that the thickness of the ellipsoid encodes relevant information about the fine structure inside each voxel, the practical finding has been that only the FA and the primary eigenvector (the length and direction of the long axis of each ellipsoid) has been required for tractography because the tensor model as originally described by Filler, Howe, and Richards models axons. In their fundamental anatomy, these are linear structures and any analysis that turns them into series of complexly shaped and directed ellipsoids can actually obscure the underlying biological and biophysical characteristics. Collecting images that accurately describe the ellipsoids is still a usable formalism but the measurements of the thickness and equatorial orientation of the "jellybean" have so far proven to have little use in tractography. The ellipsoid representation makes more sense in some areas of physics such as magnetic or electric field studies, but has no clear biological correlate in neural tract tracing. Most importantly, if 2 tracts are crossing in a single voxel, the ellipsoid fuses and obscures the axonal data.

As discussed below there is an equally usable formalism that is closer to the anatomy of the axons and neural tracts. In any case, the data processing will continue to advance in complexity as dozens or even hundreds of different gradient axes are sampled—posing significant technical challenge in MRI well into the foreseeable future.

Tensors and Vectors for MRI

At first glance, it might seem that if we measure diffusion in three directions that are the orthogonal x, y, and z axes in a Cartesian 3-D space, then we will be able to know the length and direction of a vector that we can use to support tractography and FA analyses (see Figure 16). The problem is that diffusion measurements in a given orientation do not distinguish which direction the water molecules are moving along the measured axis. In fact, the molecules do move both proximally and distally along the axon, but are only restricted in that they tend to move along the long axis of the axon rather than freely in any direction.

To understand the implications of this, you can consider a 3-D coordinate system such as we see in Figure 17-I. When we provide a measurement showing diffusivity with resulting intensity of 100 (out of 256) along the x-axis (axial orientation), we must draw this as a line running from +50 to -50. Now we can measure in the y-axis (coronal) and let's use the intensity of 100 again—that is it seems bright in the second axis as well. Returning to our drawing, we draw the line from +50 to -50 on the y-axis.

If we look for an axon line that would meet this description, we get 4 different options on the vectors that might tell us where the axon might be. When we take a third measure—this time in the z-axis (sagittal) and again get a result of a high intensity of 100, we have to draw a third line—this time from +50 to -50 on the z-axis. We now have eight different possible solutions—

8 different diagonal vector lines running through each of the 8 octants of 3-D space in our voxel.

We can now start to get some help in figuring out the real tract direction if we measure in a fourth axis and then a fifth axis, each oriented along one of the diagonals as shown in Figure 17-II. When this comes back as a low intensity of 3, we know we can throw out any of the vectors that had no significant apparent length in the 4 octants that our plane passes through. A sixth measurement is then made along one of the remaining diagonals which—in this example—comes back as a low intensity of 4 (see Figure 17-III). This eliminated 2 more octants and leaves only 1 possible solution.

If, instead, the sixth measurement had been along the diagonal with the actual neural tract, it would measure out around 140—which happens to follow the Pythagorean theorem relative to our other positive measurements [hypotenuse of a right triangle equals the square root of the sum of the squares of the 2 sides: $(100)^2 + (100)^2 = (140)^2$]. With this information, we can be confident that 1 pair of vectors represents the line across our voxel that is the correct source of the signal.

The fact that 6 measurements will always solve the problem seems puzzling, but we can gain confidence by understanding that there is a basis for this in mathematical geometry. The information comes from a special area called tensor analysis.

It is not true that a tensor is just a 3-D vector. Tensors are defined on complex mathematical grounds and do not necessarily have any simple geometric equivalent the physician or biologist can readily rely on to support an understanding of them. Einstein struggled with aspects of tensor theory for a few years before he was able to understand them well enough to use them as the basis for his theory of relativity. To make matters worse, there a number of different ways that tensors can be explained and defined—some deriving from formal modern mathematics, some from physics, some from engineering.

For the purpose of understanding diffusion tensor imaging, however, there is a reasonably accessible approach. A scalar is a simple number. A vector has a length and a direction. A scalar can also be described as a tensor of rank 0. A vector can also be described as a tensor of rank 1.

In the example above, we showed a number of vectors that were bound to the 0 point of a Cartesian coordinate system. It is readily apparent that these vectors were 3-D objects. Each

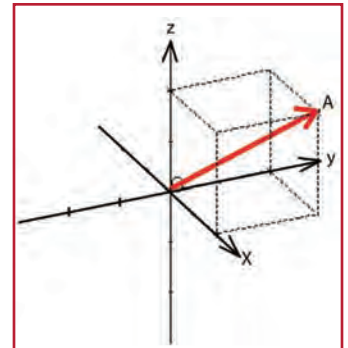


FIGURE 16. A Cartesian orthogonal frame of reference depicting Vector A. The measurement of the projection of this vector onto each of the three axes, X, Y, and Z is 2 units. Because all of the measurements are positive, the vector (A) points into the octant of space bound on each side by the positive half of each axis.

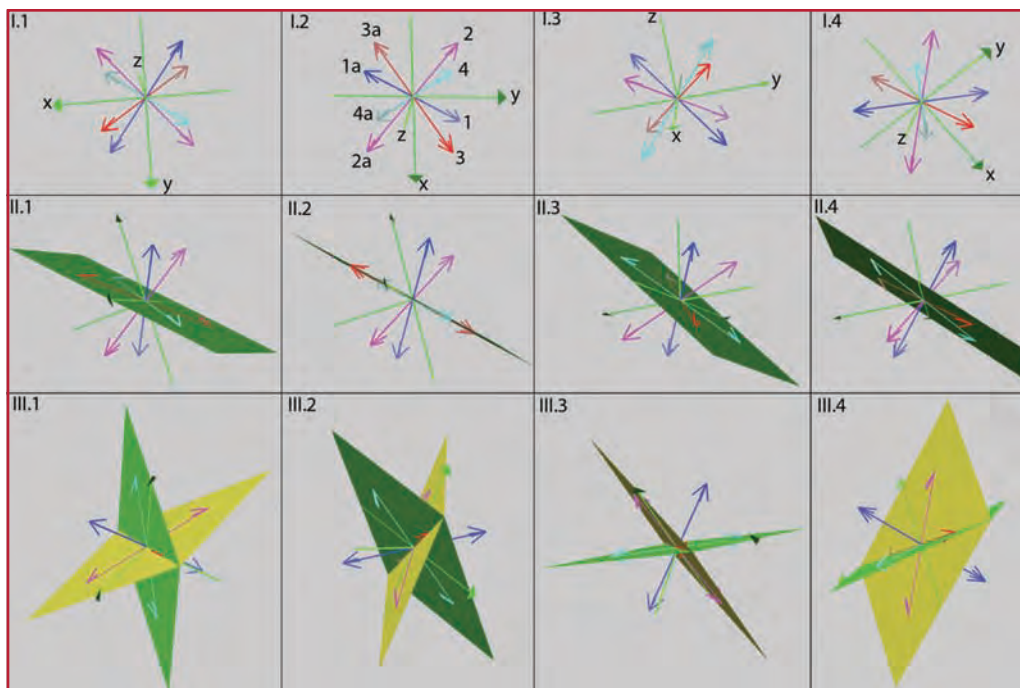


FIGURE 17. Explanation of antisymmetric dyadic tensor. For each of 3 graph series (I–III) there are 4 different rotations shown to help with visualization. (I) For diffusion measurements along each axis, the direction (sign) is not known. In this example the neural tract is running along the diagonal of the voxel so the measurements on X, Y, and Z are equal. As shown, the ambiguity leads to eight possible vectors (1 and 1a: blue; 2 and 2a: purple; 3 and 3a: red; 4 and 4a: turquoise) along the 4 diagonals of the space. This uncertainty arises when only 3 orthogonal diffusion directions are measured. Each vector runs along a diagonal in 1 of the 8 possible octants of this Cartesian space. We know that 6 of the vectors must be artifactual “ghosts” but we must use 3 more diffusion gradient acquisition directions to distinguish the ghosts from the dyad that actually represents the true neural tract orientation. (II) To clarify the situations, 2 more gradient axes have been measured, each of which was oriented along 1 of the diagonals of the space. A green plane determined by these 2 new measurement lines has been drawn. Notice that this plane incorporates the red (3 and 3a) and the turquoise (4 and 4a) vector pairs. Because our measurement was near 0 in these 2 directions, we can discard the 4 vectors in these 4 octants. (III) A sixth gradient measure has now been made. This also had a very low intensity (rapid decay) we know we can discard the 2 vectors in these 2 octants as well. A yellow plane that incorporates the red (3 and 3a) and the purple (2 and 2a) vectors is shown to demonstrate how the actual vector can have length along all 6 Cartesian axes but not be zeroed by the 2 diagonal planes. Notice that by observing the various rotations, we see that the dyad made up of the blue vectors (1 and 1a) runs in the octants that remain. This shows how 6 measurements can orient the dyad and determine which of 4 possibilities is the true tractographic course.

vector could be “expanded” for its description. Expansion is a mathematical term that means we could give a scalar on each of the 3 axes and use these 3 numbers to uniquely describe the vector (see figure 16). As we saw in our example, 3 measurements might be enough to describe a vector, but if we don't know the sign or direction on each axis, then this clearly is not enough information to describe the direction of an axon or neural tract as it traverses our MRI voxel.

For tractography, we need to use some kind of tensor of rank 2. There are a number of different mathematical constructs that are rank 2 tensors. One thing they all share in common is that they can be fully described by 9 measurements—often written out in a 3-by-3 matrix. However, since 6 measurements fully describe our neural tract you might expect that there is some special type of tensor we need to focus on.

However, the strain will differ from place to place in the solid depending on the material it is made of and the way that the force of the stress is being applied. A tensor field might be used to generate force vectors for each unit volume of the cube in a predictable mathematical progression.

However in the diffusion tensor data set in clinical MRI, the field of tensors in the brain (for instance) is determined by anatomy and really cannot be arrived at by any complex mathematical formula. We can generate tractographic atlas data to use in algorithms to help guide the tractographic process, however, for the most part, the preference has been to allow the tractographic process to proceed from the data collected for each voxel in the imaged area.

Tractography is done in a wide variety of ways, but there are 2 main classes of approaches to the problem. In 1 group of

The correct construct is called a dyad. This is a structure that has a scalar quantity and 2 directions. Fortunately for biologists and physicians, it is acceptable to conceive of a dyad as being made up of 2 vectors. Even more specifically, what we need for our neural tract is a type of dyad called an anti-symmetric dyad. This is a dyad in which the 2 vectors are identical in length (symmetric), but have exactly opposite directions.

One consequence of the anti-symmetry is that we don't need all 9 measurements to fully describe the dyad. Three of the measurements can be dispensed with because of the symmetric nature of the mathematical structure.

Because an antisymmetric dyad is a special case of a tensor of second rank, we can take advantage of a wide expanse of mathematical formulations for assembling and manipulating the data we collect. However, it is not true that our diffusion tensor measurements form a classical tensor field.

One of the original ideas behind tensor math was the problem in physics and engineering that arises when we have a stress applied to a surface of a cube. We consider that the cube is placed under strain and is deformed by the tension of the applied force.

methods, we more or less follow from 1 dyadic line to the next using various seeds as starting points. In the other group of methods we lay out the field of dyadic tensor lines and try to allow a line to find the lowest energy course (the path of least resistance) through the thicket of dyads.

Future Challenges

An additional challenge for tractography derives from the fact that diffusion imaging in general and diffusion tensor imaging especially, are extremely sensitive to motion. This is because we are trying to measure the motion of water molecules due to diffusion. At a very fine level, brain pulsations due to the arterial pulse and respiratory effects on the venous pressure—along with bulk movements from respiration, can only be suppressed by extraordinarily rapid imaging—images requiring a fraction of a second to acquire.

Even with complete suppression of motion, brain tractography is limited by the problem of fiber tracts in differing directions passing through each other. Many of these conflicts can be resolved with increasingly fine spatial resolution, so that a given voxel tends to contain fascicles mostly with a single direction. However, very fine spatial resolution requires very high signal to noise performance. This can be accomplished with long repetitive scans in high field magnets (3-T), but the very fast echo planar scans used to suppress motion and acquire multiple gradient axes tend to lose ground on signal strength and spatial resolution. Abandoning the ellipsoid, we can use multiple vectors or higher order tensors to allow multiple axonal directions in a single voxel.

There are a few situations in which a limited number of gradient orientations can be sufficient. This is the case if we use an Atlas or a non-diffusion nerve image in peripheral nerve tractography as a guide to make decisions about which axes to accept and which to ignore. Another simple method proposed by Kinosada (47, 48) is to use 1 or 2 gradient acquisitions to generate bright spots in cross sectional images. We then apply maximum intensity projection methods to look through a stack of these images in order to convert the 2-D data to 3-D tractographic images, much like the methodology is some forms of MR angiography. This is more likely to be effective with peripheral nerve since it has low resolving power for diverging tracts along complex courses such as we find more frequently in the brain.

In any case, the compromise of using the single primary eigenvector or the equivalent anti-symmetric dyad and dispensing with full use of the additional information in the ellipsoid, has made it possible to carry out good tractography in 1.5-T MRI scanners on most patients. The power of DTI is therefore now starting to be revealed.

Clinical Utility of DTI

A critical aspect to keep in mind is that in T2 MRN, the nerve anatomy becomes progressively more clear and detailed as the pathological condition becomes more severe. The opposite is true of DTI. Any significant irritative or ischemic abnormality tends to decrease the anisotropy and therefore to make the involved neural tracts disappear. Although this means that DTI tractography studies can be read for tract “drop out” as a sign

of a pathological condition, it also means that results must be assessed very carefully when they are relied on to demarcate tract borders near tumors or other irritative lesions.

Although simple DWI is very useful for identifying cerebral infarctions, DTI has greatly expanded the clinical utility of diffusion decay information. The key difference between DWI and DTI is reliance on the apparent diffusion coefficient (ADC) in DWI versus the FA in DTI. Simply put, the ADC provides a single “scalar” number that estimates the relative degree of anisotropy versus isotropy in a given voxel. The estimate is flawed because it eliminates the anisotropy signal arising from differences in orientation of the direction of diffusion that occur between the axons in the volume and the arbitrarily chosen imaging planes. Conversely, the FA measures the anisotropy in each voxel in a way that closely approximates the true length of the principal vector in each voxel, whatever direction it is pointing in.

The beneficial effect on the quality of diffusion data that results from use of FA as opposed to ADC is already clear from the first few formal outcome studies that evaluated the clinical utility of the FA measurement. In a study of 17 patients comparing ADC and FA measurements in white matter tracts adjacent to spontaneous intracerebral hemorrhage (63), the FA provided a statistically significant prediction of outcome, whereas ADC did not. In a longitudinal study with repeat imaging and FA analysis in 23 patients with traumatic brain injury (60), the increase in FA was highly correlated with an increase in Glasgow outcome score during recovery and most of this correlation derived from the principal eigenvalue parallel to the main direction of the axons in a given voxel.

The use of tractography in image segmentation for tumor resection planning has now also been formally evaluated in a randomized, controlled, prospective trial (62) involving 238 patients that compared success of gross total resection, Karnofsky performance at 6 months, and survival from high-grade gliomas using neuronavigation guidance from DTI tractography versus neuronavigation from standard MRI. This study showed statistically significant improvement in these measures when DTI tractography was used, resulting in a 43% reduction in risk of death in the hazard risk time period evaluated.

CONCLUSIONS

At this point, it is clear that when the precise location of a peripheral nerve lesion cannot be determined externally, nerve imaging should be performed. Because MRN demonstrates pathological lesions as well as anatomy because of its view into the intrinsic signal from the endoneurial fluid, it should be the method of choice unless there is some overwhelming reason to not want to know the available information.

DTI provides increased sensitivity for CNS pathological conditions relative to other magnetic resonance-based imaging techniques. Because FA encodes directional and functional information not captured by other techniques, its information content regarding pathological conditions affecting both structure and membrane stability is higher. It seems to be indicated

for diagnostic and prognostic information as well as for tracking recovery in the setting of ischemic, traumatic, inflammatory, infectious, and degenerative disease, particularly when an asymmetric pathological condition that will allow comparison between an ipsilateral affected side and contralateral unaffected side is suspected.

As with spine imaging, neurographic and tractographic imaging can provide false-positive findings. However, these are often very specific anatomically and can be considered and tested for clinical relevance.

The technical aspects of imaging hardware that will improve MRN in the future include larger areas of excellent magnetic field homogeneity, which will allow for large field-of-view studies with uniform fat suppression and image quality throughout the larger image volumes, and improvements in antenna coil technology, which will also tend to improve the signal-to-noise ratio. Use of black blood contrast agents such as ferrite agents could improve visualization of very small nerves for which the anatomic distinction from very small vessels is unreliable.

For diffusion-based methods such as DTI, even the vibration of the scanner caused by the interactions between the gradient coils and the main magnetic field have become a significant problem, limiting spatial resolution. This is the interaction that causes the typical knocking sound, which can rise to a deafening level when high fields, powerful, fast-rising gradients, and very rapid pulse sequences are deployed. The solutions here include design of magnets with inertially resistant gradient coils that provide physical dampening of vibration along with advances in the design of balancing gradients that cancel the physical and mechanical effects of the magnetic interaction. The resulting improvement in spatial resolution and signal strength will be necessary to help to resolve brain regions in which fiber bundles pass through each other in different directions or in which they diverge slowly.

The introduction of imaging techniques capable of demonstrating the intrinsic signal of nerves as well as of preserving and displaying structural linear properties of neural tissue in general is progressively transforming all neuroimaging as these techniques transform our approach to diagnosis, treatment planning, and surgical access. The next 10 years will be an extremely exciting period for the various forms of neural tractography. It is reasonable to expect that there will be a logarithmic expansion of the use of these techniques so that more than 5 million such imaging studies will probably be performed in the next 10 years. Many of the fundamental obstacles have been overcome and advances in the power of imaging equipment and postprocessing technology will similarly help drive these methods to the forefront of neurology and neurosurgery.

REFERENCES

- Aagaard BD, Maravilla KR, Kliot M: MR neurography. MR imaging of peripheral nerves. *Magn Res Imaging Clin N Am* 6:179–194, 1998.
- Aagaard BD, Maravilla KR, Kliot M: Magnetic resonance neurography: Magnetic resonance imaging of peripheral nerves. *Neuroimaging Clin N Am* 11:viii, 131–146, 2001.
- Ambrose J, Hounsfield G: Computerized transverse axial tomography. *Br J Radiol* 46:148–149, 1973.
- Atlas SW: *Magnetic Resonance Imaging of the Brain and Spine*. New York, Raven Press, 1996.
- Basser PJ, LeBihan D: Fiber orientation mapping in an anisotropic medium with NMR diffusion spectroscopy. Presented at the 11th Annual Meeting of the Society for Magnetic Resonance in Medicine, Berlin, Germany, August 8–14, 1992.
- Basser PJ, Mattiello J, LeBihan D: MR diffusion tensor spectroscopy and imaging. *Biophys J* 66:259–267, 1994.
- Basser PJ, Mattiello J, LeBihan D: Diagonal and off-diagonal components of the self-diffusion tensor: Their relation to and estimation from the NMR spin-echo signal. Presented at the 11th Annual Meeting of the Society for Magnetic Resonance in Medicine, Berlin, Germany, August 8–14, 1992.
- Bowen BC, Pattany PM, Saraf-Lavi E, Maravilla KR: The brachial plexus: Normal anatomy, pathology, and MR imaging. *Neuroimaging Clin N Am* 14:59–85, vii–viii, 2004.
- Chappell KE, Robson MD, Stonebridge-Foster A, Glover A, Allsop JM, Williams AD, Herlihy AH, Moss J, Gishen P, Bydder GM: Magic angle effects in MR neurography. *AJNR Am J Neuroradiol* 25:431–440, 2004.
- Chua TC, Wen W, Slavin MJ, Sachdev PS: Diffusion tensor imaging in mild cognitive impairment and Alzheimer's disease: A review. *Curr Opin Neurol* 21:83–92, 2008.
- Dailey AT, Tsuruda JS, Filler AG, Maravilla KR, Goodkin R, Kliot M: Magnetic resonance neurography of peripheral nerve degeneration and regeneration. *Lancet* 350:1221–1222, 1997.
- Deacon TW: Cortical connections of the inferior arcuate sulcus cortex in the macaque brain. *Brain Res* 573:8–26, 1992.
- Deacon TW: *The Symbolic Species: The Co-evolution of Language and the Brain*. New York, WW Norton, 1997.
- Diehl B, Busch RM, Duncan JS, Piao Z, Tkach J, Lders HO: Abnormalities in diffusion tensor imaging of the uncinate fasciculus relate to reduced memory in temporal lobe epilepsy. *Epilepsia* 49:1409–1418, 2008.
- Filler AG: Anatomical specializations in the hominoid lumbar region. *Am J Phys Anthropol* 54:218, 1981.
- Filler AG: Axonal transport and MR imaging: Prospects for contrast agent development. *J Magn Reson Imaging* 4:259–267, 1994.
- Filler AG: *Axial Character Seriation in Mammals: An Historical and Morphological Exploration of the Origin, Development, Use and Current Collapse of the Homology Paradigm*. Boca Raton, BrownWalker Press, 2007.
- Filler AG: Homeotic evolution in the mammalia: Diversification of thierian axial seriation and the morphogenetic basis of human origins. *PLoS ONE* 2:e1019, 2007.
- Filler AG: The emergence and optimization of upright posture among hominiform hominoids and the evolutionary pathophysiology of back pain. *Neurosurg Focus* 23:E4, 2007.
- Filler AG: Piriformis and related entrapment syndromes: Diagnosis & management. *Neurosurg Clin N Am* 19:609–622, vii; 2008.
- Filler AG: Diagnosis and management of pudendal nerve entrapment syndromes: Impact of MR neurography and open MR-guided injections. *Neurosurg Q* 18:1–6, 2008.
- Filler AG, Bell BA: Axonal transport, imaging, and the diagnosis of nerve compression. *Br J Neurosurg* 6:293–295, 1992.
- Filler AG, Haynes J, Jordan SE, Prager J, Villablanca JP, Farahani K, McBride DQ, Tsuruda JS, Morisoli B, Batzdorf U, Johnson JP: Sciatica of nondisc origin and piriformis syndrome: Diagnosis by magnetic resonance neurography and interventional magnetic resonance imaging with outcome study of resulting treatment. *J Neurosurg Spine* 2:99–115, 2005.
- Filler AG, Howe FA: Images, apparatus, algorithms, and methods. GB 9205541. UK Patent Office. 1992.
- Filler AG, Howe FA, Hayes CE, Kliot M, Winn HR, Bell BA, Griffiths JR, Tsuruda JS: Magnetic resonance neurography. *Lancet* 341:659–661, 1993.
- Filler AG, Howe FA, Richards TL, Tsuruda JS: Image neurography and diffusion anisotropy imaging. In: World Intellectual Property Organization IB (ed), 1993.
- Filler AG, Kliot M, Howe FA, Hayes CE, Saunders DE, Goodkin R, Bell BA, Winn HR, Griffiths JR, Tsuruda JS: Application of magnetic resonance neurography in the evaluation of patients with peripheral nerve pathology. *J Neurosurg* 85:299–309, 1996.
- Filler AG, Maravilla KR, Tsuruda JS: MR neurography and muscle MR imaging for image diagnosis of disorders affecting the peripheral nerves and musculature. *Neurol Clin* 22:643–682, vi–vii, 2004.

29. Filler AG, Tsuruda JS, Richards TL, Howe FA: Images, apparatus, algorithms, and methods. GB 9216383. UK Patent Office. 1992.
30. Filler AG, Tsuruda JS, Richards TL, Howe FA: Image neurography and diffusion anisotropy imaging. US patent 5,560,360. Filed March 8, 1993; granted October 1, 1996.
31. Filler AG, Whiteside G, Bacon M, Frederickson M, Howe FA, Rabinowitz MK, Sokoloff AJ, Deacon TW, Abell C, Munglani R, Griffiths JR, Bell BA, Lever AM: Successful use of axonal transport for drug delivery by synthetic molecular vehicles. *Nat Preced* 2008. <http://hdl.handle.net/10101/npre.2008.2164.1>. Accessed August 6, 2008.
32. Filler AG, Winn HR, Howe FA, Griffiths JR, Bell BA, Deacon TW: Axonal transport of superparamagnetic metal oxide particles: Potential for magnetic resonance assessments of axoplasmic flow in clinical neuroscience. Presented at 10th Annual Meeting of the Society for Magnetic Resonance in Medicine, San Francisco, California, 1991.
33. Filler AG, Winn HR, Westrum LE, Sirrotta P, Krohn K, Deacon TW: Intramuscular injection of WGA yields systemic distribution adequate for imaging of axonal transport in intact animals. *Soc Neurosci Abs* 17:1480, 1991.
34. Grant GA, Britz GW, Goodkin R, Jarvik JG, Maravilla K, Kliot M: The utility of magnetic resonance imaging in evaluating peripheral nerve disorders. *Muscle Nerve* 25:314–331, 2002.
35. Grant GA, Goodkin R, Maravilla KR, Kliot M: MR neurography: Diagnostic utility in the surgical treatment of peripheral nerve disorders. *Neuroimaging Clin N Am* 14:115–133, 2004.
36. Heide AC, Richards TL, Alvord EC Jr, Peterson J, Rose LM: Diffusion imaging of experimental allergic encephalomyelitis. *Magn Reson Med* 29:478–484, 1993.
37. Hounsfield GN: Computerized transverse axial scanning (tomography). 1. Description of the system. *Br J Radiol* 46:1016–1022, 1973.
38. Howe FA, Filler AG, Bell BA, Griffiths JR: Magnetic resonance neurography. *Magn Reson Med* 28:328–338, 1992.
39. Howe FA, Filler AG, Bell BA, Griffiths JR: Magnetic resonance neurography: Optimizing imaging techniques for peripheral nerve identification. Presented at the 11th Annual Meeting of the Society for Magnetic Resonance in Medicine, Berlin, Germany, August 8–14, 1992.
40. Igarashi T, Yabuki S, Kikuchi S, Myers RR: Effect of acute nerve root compression on endoneurial fluid pressure and blood flow in rat dorsal root ganglia. *J Orthop Res* 23:420–424, 2005.
41. Jarvik JG, Comstock BA, Heagerty PJ, Haynor DR, Fulton-Kehoe D, Kliot M, Franklin GM: Magnetic resonance imaging compared with electrodiagnostic studies in patients with suspected carpal tunnel syndrome: Predicting symptoms, function, and surgical benefit at 1 year. *J Neurosurg* 108:541–550, 2008.
42. Jarvik JG, Yuen E, Haynor DR, Bradley CM, Fulton-Kehoe D, Smith-Weller T, Wu R, Kliot M, Kraft G, Wang L, Erlich V, Heagerty PJ, Franklin GM: MR nerve imaging in a prospective cohort of patients with suspected carpal tunnel syndrome. *Neurology* 58:1597–1602, 2002.
43. Kakuda W, Lansberg MG, Thijs VN, Kemp SM, Bammer R, Wechsler LR, Moseley ME, Parks MP, Albers GW: Optimal definition for PWI/DWI mismatch in acute ischemic stroke patients. *J Cereb Blood Flow Metab* 28:887–891, 2008.
44. Kent DL, Haynor DR, Longstreth WT, Jr., Larson EB: American College of Physicians, Position paper: Magnetic resonance imaging of brain and spine: A revised statement. *Ann Intern Med* 120:872–875, 1994.
45. Kent DL, Haynor DR, Longstreth WT Jr, Larson EB: The clinical efficacy of magnetic resonance imaging in neuroimaging. *Ann Intern Med* 120:856–871, 1994.
46. Khalil C, Hancart C, Le Thuc V, Chantelot C, Chechin D, Cotten A: Diffusion tensor imaging and tractography of the median nerve in carpal tunnel syndrome: Preliminary results. *Eur Radiol* 18:2283–2291, 2008.
47. Kinoshita Y, Nakagawa T: New non-invasive technique to visualize three-dimensional anatomic structures of myelinated white matter tracts of human brain in vivo. *Front Med Biol Eng* 6:37–49, 1994.
48. Kinoshita Y, Ono M, Okuda Y, Seta H, Hada Y, Hattori T, Nomura Y, Sakuma H, Takeda K, Ishii Y: MR tractography—visualization of structure of nerve fiber system from diffusion weighted images with maximum intensity projection method (in Japanese). *Nippon Igaku Hoshasen Gakkai Zasshi* 53:171–179, 1993.
49. Kramer M, Deacon TW, Sokoloff A, Filler A: Organization of motoneurons innervating epaxial and hypaxial musculature in the frog, rat, and monkey. *Soc Neurosci Abstr* 13:526, 1987.
50. Kuntz CT, Blake L, Britz G, Filler A, Hayes CE, Goodkin R, Tsuruda J, Maravilla K, Kliot M: Magnetic resonance neurography of peripheral nerve lesions in the lower extremity. *Neurosurgery* 39:750–757, 1996.
51. Lansberg MG, Thijs VN, O'Brien MW, Ali JO, de Crespigny AJ, Tong DC, Moseley ME, Albers GW: Evolution of apparent diffusion coefficient, diffusion-weighted, and T2-weighted signal intensity of acute stroke. *AJNR Am J Neuroradiol* 22:637–644, 2001.
52. Le Bihan D: Molecular diffusion nuclear magnetic resonance imaging. *Magn Reson Q* 7:1–30, 1991.
53. LeBihan D: IVIM method measures diffusion and perfusion. *Diagn Imaging* 12:133, 136, 1990.
54. Mizisin AP, Kalichman MW, Myers RR, Powell HC: Role of the blood-nerve barrier in experimental nerve edema. *Toxicol Pathol* 18:170–185, 1990.
55. Mori S: *Introduction to Diffusion Tensor Imaging*. New York, Elsevier, 2007.
56. Moseley ME, Kucharczyk J, Mintorovitch J, Cohen Y, Kurhanewicz J, Derugin N, Asgari H, Norman D: Diffusion-weighted MR imaging of acute stroke: Correlation with T2-weighted and magnetic susceptibility-enhanced MR imaging in cats. *AJNR Am J Radiol* 11:423–429, 1990.
57. Myers RR, Rydevik BL, Heckman HM, Powell HC: Proximodistal gradient in endoneurial fluid pressure. *Exp Neurol* 102:368–370, 1988.
58. Paulose JF, Low PA, Nickander KK, Dyck PJ: Mammalian endoneurial fluid: Collection and protein analysis from normal and crushed nerves. *Brain Res* 332:91–102, 1985.
59. Richards TL, Heide AC, Tsuruda JS, Alvord EC: Vector analysis of diffusion images in experimental allergic encephalomyelitis. Presented at the 11th Annual Meeting of the Society for Magnetic Resonance in Medicine, Berlin, Germany, August 8–14, 1992.
60. Sidaros A, Engberg AW, Sidaros K, Liptrot MG, Herning M, Petersen P, Paulous OB, Jernigan TL, Rostrop E: Diffusion tensor imaging during recovery from severe traumatic brain injury and relation to clinical outcome: A longitudinal study. *Brain* 131:559–572, 2008.
61. Viallon M, Vargas MI, Jlassi H, Löfblad KO, Delavelle J: High-resolution and functional magnetic resonance imaging of the brachial plexus using an isotropic 3D T2 STIR (short term inversion recovery) SPACE sequence and diffusion tensor imaging. *Eur Radiol* 18:1018–1023, 2008.
62. Wu JS, Zhou LF, Tang WJ, Mao Y, Hu J, Song YY, Hong XN, Du GH: Clinical evaluation and follow-up outcome of diffusion tensor imaging-based functional neuronavigation: A prospective, controlled study in patients with gliomas involving pyramidal tracts. *Neurosurgery* 61:935–949, 2007.
63. Yoshioka H, Horikoshi T, Aoki S, Hori M, Ishigame K, Uchida M, Sugita M, Araki T, Kinouchi H: Diffusion tensor tractography predicts motor functional outcome in patients with spontaneous intracerebral hemorrhage. *Neurosurgery* 62:97–103, 2008.

Acknowledgments

I thank David Kline, M.D., H. Richard Winn, M.D., B. Anthony Bell, M.D., John Griffiths, D.Phil., Franklyn Howe, D.Phil., Todd Richards, Ph.D., Ken Maravilla, M.D., Terrence Deacon, Ph.D., Jodean Peterson, B.A., and Shirlee Jackson, B.A., for their assistance, contributions, and inspiration in the course of this effort.

Disclosures

Portions of this work were supported by National Institutes of Health Grant PHS 5 T32 GM07117-09 0011 (Harvard University), National Institutes of Health Grant NSTG 5T32 NS-07144-09 (University of Washington), The Wellcome Trust “MR Imaging of Neural Tracts,” the UK Cancer Research Campaign, and the Neurosciences Research Foundation of Atkinson Morley’s Hospital. Aaron G. Filler, M.D., Ph.D., is a coinventor on patents that cover the use of magnetic resonance neurography and diffusion tensor imaging. He has received funding from the National Institutes of Health, The Wellcome Trust, and the Atkinson Morley’s Research Foundation for scientific research related to the subject matter. His clinical neurosurgical practice uses these imaging techniques. He performs radiology interpretations on magnetic resonance neurography and diffusion tensor images. He is a shareholder in NeuroGrafix, a company that administers patent technology licenses under agreement from the University of Washington, which owns the patent and which also manages image data transport for neural tract imaging, although he has not received any funds from NeuroGrafix.

EXHIBIT 6

Perfusion CT imaging as a diagnostic and prognostic tool for dementia: prospective case–control study

Sanket Dash¹, Yatish Agarwal¹, Swarna Jain ^{1,*}, Anuradha Sharma¹, Neera Chaudhry²

¹Department of Radiology, Vardhman Mahavir Medical College and Safdarjung Hospital, New Delhi, India

²Department of Neurology, Vardhman Mahavir Medical College and Safdarjung Hospital, New Delhi, India

*Correspondence to: Dr Swarna Jain, Department of Radiology, Vardhman Mahavir Medical College and Safdarjung Hospital, New Delhi, Delhi, India; drswarna007@gmail.com

Abstract

Background: As functional changes precede structural changes in dementia, we aimed to elucidate changes on cerebral perfusion CT (PCT) for early diagnosis of dementia; and to differentiate Alzheimer's disease (AD) from vascular dementia (VaD). We also aimed to study correlation between Montreal Cognitive Assessment (MOCA) score and PCT parameters.

Methods: We conducted a prospective case–control study enrolling 25 dementia patients (15 cases of VaD, 10 cases of AD) and 25 age-matched controls. PCT was performed on a 256-slice CT scanner. Using perfusion software, colour maps were generated for cerebral blood flow (CBF), cerebral blood volume (CBV), mean transit time and time-to-peak. These colour maps were first visually inspected for any abnormalities. Subsequently, quantitative assessment of perfusion parameters was done using symmetrical freehand region of interests drawn in bilateral frontal, temporal, parietal regions, basal ganglia and hippocampi.

Results: Strategic infarcts were present in 93.3% cases and white matter ischaemic changes in 100% cases of VaD. A global reduction in CBF and CBV was also observed in cases of VaD; whereas these parameters were significantly lower mainly in temporoparietal regions and hippocampi of patients with AD. There was significant positive correlation between MOCA score and various perfusion parameters in both forms of dementia.

Conclusion: PCT is a reliable imaging modality for early diagnosis of dementia and in differentiating VaD from AD. As perfusion parameters show positive correlation with MOCA score, they could be used as a surrogate marker of cognitive status in the follow-up of patients with dementia.

Keywords: neuroradiology, diagnostic radiology, computed tomography, dementia, geriatric medicine

Introduction

Dementia is a major cause of morbidity and reduced quality of life in older individuals. It affects memory and other mental faculties; and leads to impairment of daily activities [1]. With increasing life expectancy, geriatric population is increasing with consequent global rise in prevalence of dementias. As per WHO, dementia contributes 4.1% of all disability-adjusted life-years [2]. Among senile dementias, Alzheimer's dementia (AD) is the most common followed by vascular dementia (VaD), frontotemporal dementia, dementia with Lewy bodies and mixed dementia [3].

Neuroimaging has become an indispensable adjunct to clinical examination in diagnosis of dementia [4]. Structural imaging like CT or MRI help in assessing degree and pattern of cerebral atrophy; and in excluding reversible causes of dementia like tumour, subdural haematoma or normal-pressure hydrocephalous. With advancement in therapeutic horizons, newer medications have been developed for treatment of mild to moderate dementias. To enable timely institution of therapy, it is imperative to focus on imaging techniques which facilitate early diagnosis of dementias before cortical atrophy sets in [4]. Several studies have demonstrated alterations in blood flow in different areas of the brain precede structural changes in dementia. These can be measured with functional techniques like positron emission tomography (PET), single-photon emission computed tomography (SPECT) and

arterial spin labelled (ASL) MRI [5–7]. However, these modalities have their own drawbacks including low specificity, high cost and poor availability. In addition, perfusion SPECT and PET involve use of radioisotopes; while ASL MRI suffers from low spatial resolution and only directly obtains an estimate of cerebral blood flow (CBF) [8].

First described by Heinz *et al*, perfusion CT (PCT) is another excellent functional neuroimaging technique which detects abnormalities of cerebral microcirculation; thereby reflecting areas with altered perfusion-metabolism status. In contrast to PET and SPECT, CT scanners and PCT software are more widely available and economical. PCT is performed by monitoring the first pass of iodinated contrast through intracranial vasculature. It enables quantification and display of various perfusion parameters like CBF, cerebral blood volume (CBV), mean transit time (MTT) and time-to-peak (TTP). It is based on the central volume principle which states that $CBF = CBV/MTT$ [9].

In several institutions, PCT is nowadays an integral component of stroke protocol for differentiating infarct core from ischaemic penumbra. PCT has also been applied to brain tumours in grading of gliomas and differentiating tumour recurrence from radiation necrosis. However, role of PCT in evaluation of dementias is still at a nascent stage. Few studies in this context have shown conflicting results regarding which areas of brain are affected; and which

Received: October 12, 2021. Accepted: December 31, 2021

© The Author(s) 2022. Published by Oxford University Press on behalf of Postgraduate Medical Journal. All rights reserved. For permissions, please e-mail: journals.permissions@oup.com

are the most reliable parameters. Most of these studies also had limited coverage of the brain as they used lower slice count CT scanners.

With increase in life expectancy, the geriatric population is increasing and it is imperative to focus on the technique which can detect the dementia process in advance for better patient management and care [10, 11]. Previous studies have shown that some drugs used in AD like acetylcholinesterase inhibitors donepezil have variable clinical response with greater increase in the CBF on SPECT in the patients who are responsive. PCT by virtue of its ability to measure the blood flow as SPECT can be used to evaluate the CBF and hence the response to treatment in these patients [12–14].

Hence, we conducted a study aimed at evaluating the changes on cerebral PCT in dementia; and to determine whether PCT parameters could differentiate the types of dementia. As a secondary objective, we also aimed to study the correlation between clinical severity score and PCT parameters.

Methods

This prospective case–control study was carried out in a tertiary care hospital over a time span of 18 months after obtaining clearance from institutional ethics committee.

Selection of participants

Taking CBF value in study by Yildirim *et al*, minimum required sample size with 95% power of study and 5% level of significance was 23 patients in each study group. Thus, 25 patients presenting with cognitive impairment and diagnosed as dementia as per the Diagnostic and Statistical Manual of Mental Disorders, fifth edition (DSM-V) criteria were included. They were assigned to either VaD or AD subgroup as per DSM-V criteria for each. An equal number of age-matched healthy subjects were included as controls. Patients having a major territorial infarct, intracranial space-occupying lesion (ICSOL), seizure disorder, acute traumatic brain injury, or contraindications to undergo contrast-enhanced CT scan due to deranged renal functions or prior documented severe contrast reaction were excluded. Detailed neuropsychiatric evaluation including Montreal Cognitive Assessment (MOCA) was undertaken in each patient [15]. Based on this, dementia cases were classified as having mild (score 19–23), moderate (score 11–18) or severe (score ≤ 10) cognitive impairment. Detailed informed consent was obtained from all study participants or their caregivers prior to their enrolment in the study. Risks of radiation exposure were clearly explained while obtaining consent. As most of the controls underwent PCT for unrelated indications such as part of stroke protocol which turned out to be negative, the risk-benefit ratio for radiation harm was very low.

PCT image acquisition

The study was performed using a 256-slice CT scanner (Somatom Definition Flash, Siemens Healthineers). Following a non-contrast CT (NCCT) to rule out infarction, haemorrhage or ICSOL, 50 mL iodinated contrast (370 mg iodine/mL) was injected intravenously via pressure injector at 5 mL/s, followed by saline chaser. PCT data were acquired in dynamic mode for z-axis coverage of 10 cm to include the whole brain (slice width 10 mm, FOV 200 mm, matrix 1024×1024). Scanning parameters were optimised to have lowest possible exposure during perfusion study (80 kV, 180 mAs).

PCT postprocessing and image analysis

This was done on an advanced multimodality workstation using Neuro VPCT package of Syngo.VIA VB20 software. Arterial input and venous outflow functions were defined manually taking anterior cerebral arteries and superior sagittal sinus as reference points to generate the time-density curve for the automated PCT variable calculations. Using automated threshold-based deconvolution algorithms, colour maps were generated for the PCT parameters CBF, CBV, MTT and TTP. The colour maps were first qualitatively evaluated by visual inspection for any abnormalities. Presence of chronic lacunar infarcts visualised as dark blue or black colour holes on CBF/CBV colour maps due to decreased perfusion with increased delay was recorded. Subsequently, quantitative assessment of perfusion parameters was done using bilateral symmetrical freehand region of interests drawn on the maximum intensity projection perfusion images in bilateral frontal, temporal, parietal regions, basal ganglia and hippocampi.

Statistical analysis

As all variables (CBF, CBV, MTT and TTP) were not normally distributed in the three subgroups of control, AD and VaD, non-parametric tests (Kruskal-Wallis test) were used to make group comparisons. Receiver operating characteristic (ROC) curve analysis was done to study the diagnostic performance and determine cut-off values of quantitative PCT parameters to differentiate cases from controls; as well as to differentiate the two subgroups of dementia. Spearman's correlation coefficient (r) was used to explore the strength of association between MOCA score and PCT parameters.

Results

Our study had 50 participants comprising equal number of dementia patients and controls. Among the dementia patients, 15 belonged to VaD subgroup and 10 belonged to AD subgroup (Figure 1). The mean age \pm SD of VaD patients, AD patients and controls was 62.0 \pm 6.9, 60.1 \pm 7.1, and 60.5 \pm 6.6 years, respectively. The male:female ratio was 2:1, 3:2 and 2.1:1 for VaD patients, AD patients and controls respectively. The difference in age ($p=0.680$) and gender ($p=0.901$) distribution of the three groups was statistically insignificant. The demographic and clinical details of the study participants is summarised in Table 1.

PCT picked up additional lacunar infarcts in all cases of dementia which were undetected on NCCT. Among dementia cases, 93.3% cases of VaD had strategic infarcts; whereas these were not seen in any case of AD ($p<0.001$). PCT could also reliably detect white matter ischaemic changes in VaD subgroup, whereas these were not that evident in AD or controls ($p<0.001$).

With respect to the quantitative PCT parameters (Tables 2 and 3), CBF and CBV were significantly lower in cases of VaD as compared with the controls in bilateral frontal, temporal, parietal regions, basal ganglia and hippocampi ($p<0.001$). These two parameters were found to be significantly lower in bilateral temporoparietal regions and hippocampi in AD subgroup compared with controls ($p<0.001$); whereas the difference in frontal regions and basal ganglia was not significant.

In pairwise comparison of the two dementia subgroups, VaD cases showed significantly lower CBF and CBV in bilateral frontal regions as compared with AD cases ($p<0.001$). VaD cases also had significantly lower CBV in bilateral basal ganglia as compared with AD cases ($p<0.001$); but the difference in CBF of basal ganglia was only significant on the right side ($p=0.004$). CBF and CBV of

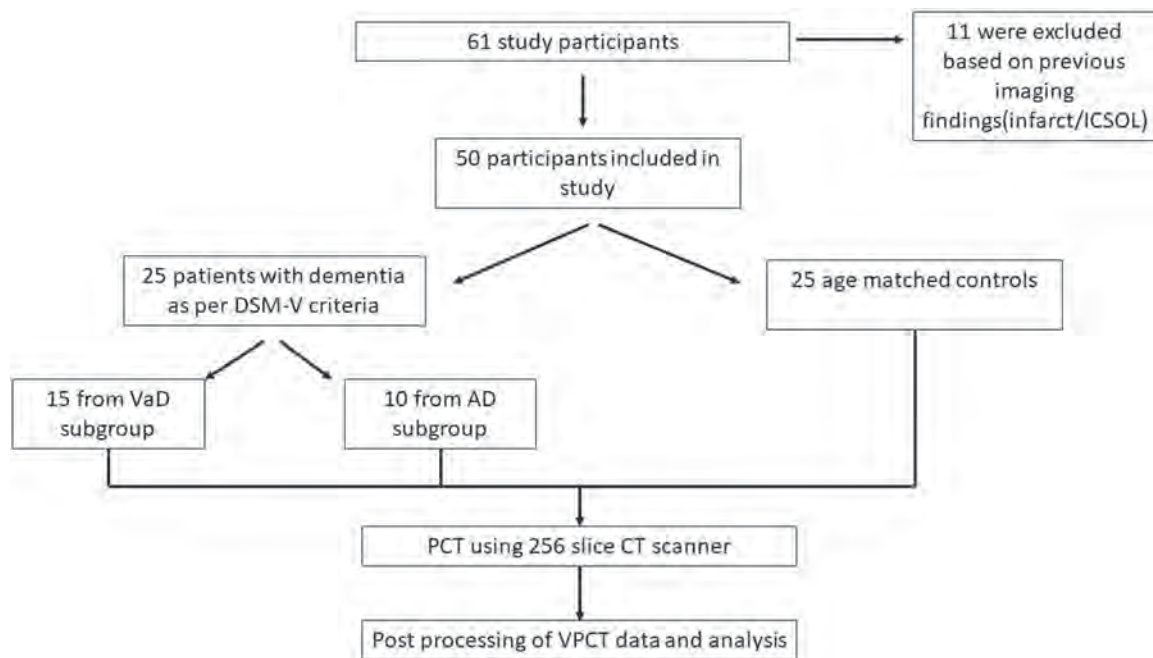


Figure 1. A flow diagram of participants through the study. AD, Alzheimer's disease; DSM-V, Diagnostic and Statistical Manual of Mental Disorders, fifth edition; ICSOL, intracranial space-occupying lesion; PCT, perfusion CT; VaD, vascular dementia; VPCT, volume PCT.

Table 1. Demographic and clinical profile of study participants

Study group	No of participants	Gender		Mean age (years)	MOCA score
		Male	Female		
Vascular dementia	15	10	5	62.0 + 6.9	11–21 (mean 16.67)
Alzheimer's disease	10	6	4	60.1 + 7.1	13–23 (mean 16.20)
Controls	25	17	8	60.5 + 6.6	–
Total	50	33	17		

MOCA, Montreal Cognitive Assessment.

Table 2. Comparison of the three subgroups of the variable clinical diagnosis in terms of CBF (n = 50)

Brain region	CBF (SD) (mL/100 g/min)	Kruskal-Wallis test			Pairwise comparison of subcategories of clinical diagnosis (adjusted p value)				
		AD (n = 10)	VaD (n = 15)	Control (n = 25)	X ²	P value	AD-control	AD-VaD	Control-VaD
Right frontal region	Mean (SD)	106.68 (12.93)	60.47 (16.30)	98.00 (2.36)	35.539	<0.001	0.070	<0.001	<0.001
Left frontal region	Mean (SD)	104.44 (19.55)	57.36 (15.37)	97.38 (2.81)	31.509	<0.001	0.818	<0.001	<0.001
Right basal ganglia	Mean (SD)	80.26 (25.04)	75.00 (15.73)	85.85 (2.17)	23.165	<0.001	0.907	0.004	<0.001
Left basal ganglia	Mean (SD)	75.83 (26.88)	75.52 (17.36)	85.39 (1.85)	13.099	0.001	0.349	0.345	<0.001
Right temporal region	Mean (SD)	60.97 (17.67)	59.91 (20.26)	92.92 (1.58)	25.995	<0.001	<0.001	0.994	<0.001
Left temporal region	Mean (SD)	51.85 (9.03)	53.32 (13.29)	91.65 (1.44)	37.260	<0.001	<0.001	0.862	<0.001
Right hippocampus	Mean (SD)	42.84 (13.48)	48.77 (14.35)	87.33 (1.31)	37.055	<0.001	<0.001	0.933	<0.001
Left hippocampus	Mean (SD)	37.91 (13.31)	50.02 (12.17)	86.47 (1.50)	38.577	<0.001	<0.001	0.446	<0.001
Right parietal region	Mean (SD)	63.18 (16.18)	62.85 (17.46)	99.12 (1.05)	26.046	<0.001	<0.001	0.986	<0.001
Left parietal region	Mean (SD)	59.84 (12.81)	56.75 (21.17)	97.59 (1.18)	36.954	<0.001	<0.001	0.965	<0.001

AD, Alzheimer's disease; CBF, cerebral blood volume; VaD, vascular dementia.

bilateral temporo-parietal regions and hippocampi did not differ significantly between the two dementia subgroups (Figure 2). CBF and CBV in different regions of brain are summarised in Tables 2 and 3, respectively.

In ROC analysis to differentiate between dementia cases from controls (Table 4), CBF and CBV of temporal regions, hippocampi, parietal regions followed by basal ganglia were the most important parameters with highest area under ROC curve (AUROC). Frontal region CBF and CBV were found to have the maximum

AUROC in differentiating between AD and VaD. No significant differences between these two subgroups were seen in CBF and CBV of other areas. MTT and TTP were not found to be significantly different between the three groups in any region.

Following neuropsychiatric examination, dementia cases were assigned a MOCA score. All cases in our study fell in the categories of mild and moderate cognitive impairment; with no case of severe cognitive impairment. The MOCA score of VaD patients ranged from 11 to 21 (mean 16.67); and that of AD patients

Table 3. Comparison of the three subgroups of the variable clinical diagnosis in terms of CBV (n = 50)

Brain region	CBV (SD) (mL/100 g/min)				Kruskal-Wallis test		Pairwise comparison of subcategories of clinical diagnosis (adjusted p value)		
		AD (n = 10)	VaD (n = 15)	Control (n = 25)	X ²	P value	AD-control	AD-VaD	Control-VaD
Right frontal region	Mean (SD)	6.75 (1.86)	3.27 (0.87)	5.99 (0.13)	31.174	<0.001	0.975	<0.001	<0.001
Left frontal region	Mean (SD)	6.47 (2.33)	3.15 (0.84)	5.89 (0.15)	31.127	<0.001	0.970	<0.001	<0.001
Right basal ganglia	Mean (SD)	5.62 (2.03)	3.97 (0.86)	5.80 (0.05)	27.777	<0.001	0.957	<0.001	<0.001
Left basal ganglia	Mean (SD)	5.48 (2.26)	4.01 (0.90)	5.77 (0.04)	27.802	<0.001	0.949	<0.001	<0.001
Right temporal region	Mean (SD)	4.25 (3.01)	3.49 (1.14)	5.18 (0.04)	20.526	<0.001	0.003	0.993	<0.001
Left temporal region	Mean (SD)	3.61 (2.33)	3.05 (0.76)	5.17 (0.03)	31.203	<0.001	<0.001	0.999	<0.001
Right hippocampus	Mean (SD)	2.94 (2.20)	2.71 (0.86)	5.16 (0.03)	31.175	<0.001	<0.001	1.000	<0.001
Left hippocampus	Mean (SD)	2.43 (1.27)	2.67 (0.70)	5.15 (0.03)	31.339	<0.001	<0.001	0.965	<0.001
Right parietal region	Mean (SD)	3.90 (2.31)	3.30 (0.85)	5.93 (0.09)	31.208	<0.001	<0.001	1.000	<0.001
Left parietal region	Mean (SD)	3.94 (2.74)	3.08 (1.02)	5.84 (0.09)	31.160	<0.001	<0.001	1.000	<0.001

AD, Alzheimer's disease; CBV, cerebral blood volume; VaD, vascular dementia.

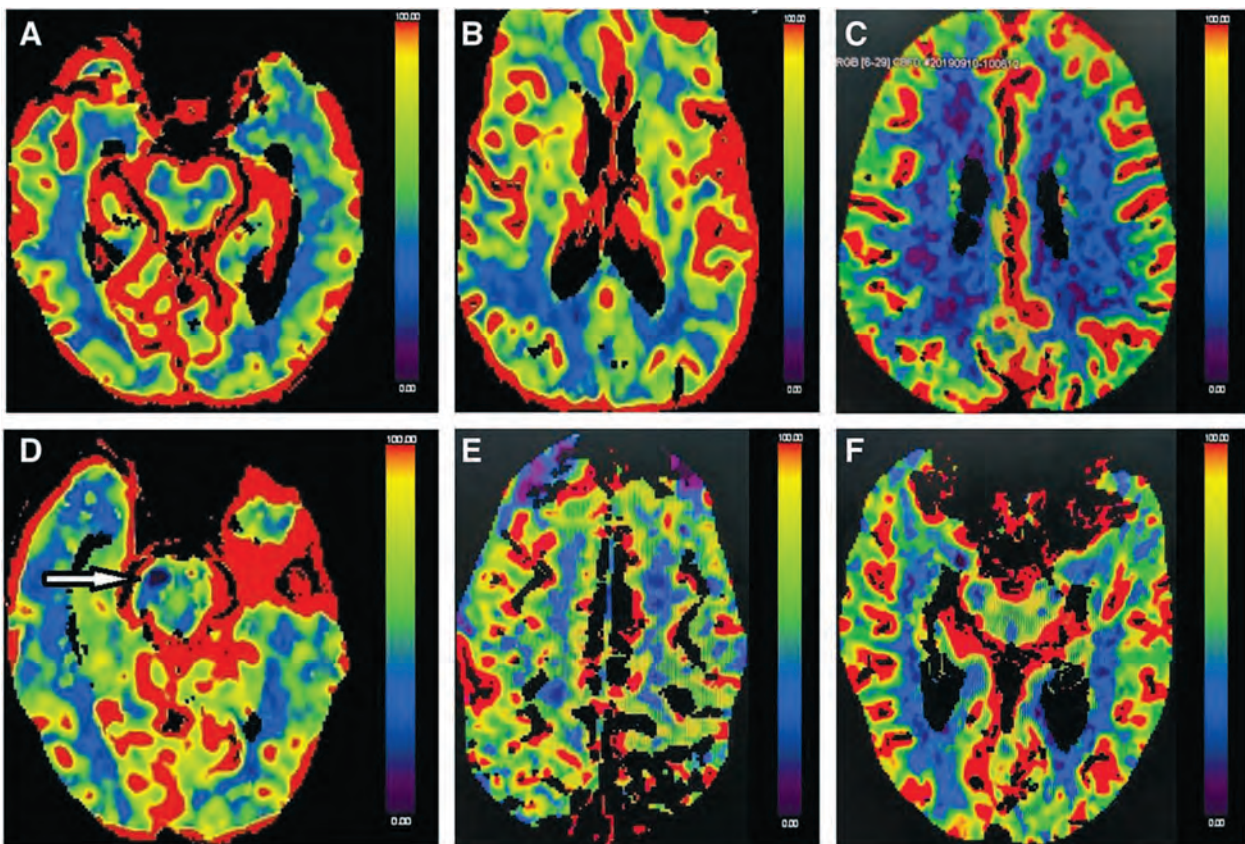


Figure 2. (A, B) CBF colour maps of a 55-year-old-man with transient focal motor deficit and no cognitive impairment (control) shows good perfusion seen as red-yellow colour in bilateral temporal regions and hippocampi (A) as well as in bilateral frontoparietal regions and basal ganglia (B). (C, D) CBF colour maps of a 67-year-old woman with VaD who had progressive decline in memory (MOCA score 18/30) show significant white matter hypoperfusion in bilateral frontoparietal white matter (C) with a focal perfusion deficit in right middle cerebral peduncle (white arrow) suggestive of lacunar infarct (D) which was not evident on NCCT of the patient (not shown). (E, F) CBF colour maps of a 67-year-old man with AD who had progressive cognitive impairment (MOCA score 11/30) show significantly reduced CBF in bilateral frontal regions (E) and right medial temporal region (F). AD, Alzheimer's disease; CBF, cerebral blood volume; MOCA, Montreal Cognitive Assessment; VaD, vascular dementia; NCCT - non-contrast CT.

ranged from 13 to 23 (mean 16.20). There was no significant difference between the two subgroups groups in terms of MOCA score ($p = 0.209$).

Association between cognitive status and PCT parameters is summarised in Table 5. As is evident, in AD subgroup, there was significant positive correlation between MOCA score and the following parameters: MTT of bilateral temporal regions and right hippocampus; CBF and CBV of bilateral hippocampi, left temporal and bilateral parietal regions. In VaD group, there was

significant positive correlation between MOCA score and the following parameters: CBF and CBV of bilateral frontal region, CBV of right basal ganglia and right temporal region, CBF of left basal ganglia, left temporal and bilateral parietal regions.

Discussion

Diagnosis and classification of dementia based on clinical criteria alone has been challenging [15]. Structural neuroimaging with

Table 4. ROC analysis: performance of study parameters for predicting group: case versus control and subtype versus control

PCT parameters	Region	Dementia versus control				VaD versus AD				P value
		Cut-off by ROC	Sensitivity	Specificity	AUROC	Cut-off by ROC	Sensitivity	Specificity	AUROC	
CBF (mL/100 g/min)	Rt frontal	78.48	56.0 (35–76)	100.0 (86–100)	0.657	95.67	100.0 (69–100)	100.0 (78–100)	1.00	<0.001
	Lt frontal	75.96	60.0 (39–79)	100.0 (86–100)	0.751	95.67	100.0 (69–100)	100.0 (78–100)	1.000	<0.001
CBF (mL/100 g/min)	Rt temporal	85.87	92.0 (74–99)	100.0 (86–100)	0.920	55.48	70.0 (35–93)	73.3 (45–92)	0.587	0.488
	Lt temporal	74.13	100.0 (86–100)	100.0 (86–100)	1.000	51.34	80.0 (44–97)	73.3 (45–92)	0.667	0.174
CBF (mL/100 g/min)	Rt basal ganglia	83.35	72.0 (51–88)	84.0 (64–95)	0.795	84.34	70.0 (35–93)	100.0 (78 to 100)	0.813	0.010
	Lt basal ganglia	83.74	72.0 (51–88)	80.0 (59–93)	0.771	82.91	70.0 (35–93)	80.0 (52–96)	0.687	0.127
CBF (mL/100 g/min)	RT parietal	69.88	92.0 (74–99)	100.0 (86–100)	0.920	57.45	50.0 (19–81)	80.0 (52–96)	0.607	0.389
	Lt parietal	89.74	100.0 (86–100)	100.0 (86–100)	1.000	60.71	80.0 (44–97)	66.7 (38–88)	0.600	0.421
CBF (mL/100 g/min)	Rt hippocampus	77.35	100.0 (86–100)	100.0 (86–100)	1.000	46.61	80.0 (44–97)	53.3 (27–79)	0.627	0.305
	Lt hippocampus	60.2	100.0 (86–100)	100.0 (86–100)	1.000	50.37	100.0 (69–100)	73.3 (45–92)	0.820	0.008
CBV (mL/100 g)	Rt frontal	4.98	60 (39–79)	100.0 (86–100)	0.777	5.79	100.0 (69–100)	100.0 (78 to 100)	1.000	<0.001
	Lt frontal	5.15	68.0 (46–85)	100.0 (86–100)	0.775	4.81	100.0 (78–100)	100.0 (69 to 100)	1.000	<0.001
CBV (mL/100 g)	Rt temporal	4.73	84.0 (64–95)	100.0 (86–100)	0.873	3.07	70.0 (35–93)	73.3 (45–92)	0.593	0.454
	Lt temporal	4.31	96.0 (80–100)	100.0 (86–100)	0.960	2.99	70.0 (35–93)	73.3 (45–92)	0.633	0.279
CBV (mL/100 g)	Basal ganglia right	4.67	64.0 (43–82)	100.0 (86–100)	0.811	5.68	90.0 (55–100)	100.0 (78–100)	0.900	0.001
	left	4.89	68.0 (46–85)	100.0 (86–100)	0.813	4.89	90.0 (55–100)	100.0 (78–100)	0.900	0.001
CBV (mL/100 g)	RT parietal	5.55	96.0 (80–100)	100.0 (86–100)	0.960	2.92	50.0 (19–81)	93.3 (68–100)	0.613	0.360
	Lt parietal	4.72	96.0 (80–100)	100.0 (86–100)	0.960	3.11	70.0 (35–93)	73.3 (45–92)	0.593	0.453
CBV (mL/100 g)	Rt hippocampus	4.36	96.0 (80–100)	100.0 (86–100)	0.960	2.58	80.0 (44–97)	60.0 (32–84)	0.593	0.454
	Lt hippocampus	3.25	96.0 (80–100)	100.0 (86–100)	0.960	2.54	80.0 (44–97)	73.3 (45–92)	0.700	0.101
MTT (s)	Rt frontal	3.43	76 (55–91)	56 (35–76)	0.685	3.12	90.0 (55–100)	33.3 (12–62)	0.573	0.560
	Lt frontal	3.24	56.0 (35–76)	68.0 (46–84)	0.630	3.22	70.0 (35–93)	86.7 (60–98)	0.700	0.101
MTT (s)	Rt temporal	3.62	56.0 (35–76)	68.0 (46–85)	0.584	3.45	90.0 (55–100)	53.3 (27–79)	0.600	0.421
	Lt temporal	3.62	56.0 (35–76)	72.0 (51–88)	0.544	3.52	80.0 (44–97)	60.0 (32–84)	0.640	0.255
MTT (s)	Rt basal ganglia	3.37	88.0 (69–97)	60.0 (39–79)	0.791	3.01	100.0 (69–100)	20.0 (4–48)	0.567	0.596
	Lt basal ganglia	3.58	68.0 (46–85)	68.0 (46–85)	0.767	3.16	80.0 (44–97)	33.3 (12–62)	0.510	0.956
MTT (s)	RT Parietal	3.59	56.0 (35–76)	64.0 (43–82)	0.518	3.8	40.0 (12–74)	100.0 (78 to 100)	0.723	0.066
	Lt parietal	3.58	68.0 (46–85)	68.0 (46–85)	0.648	3.72	70.0 (35–93)	73.3 (45–92)	0.650	0.222
MTT (S)	Rt hippocampus	3.29	80.0 (59–93)	36.0 (18–57)	0.521	3.43	70.0 (35–93)	53.3 (27–79)	0.567	0.598
	Lt hippocampus	3.41	52.0 (31–72)	60.0 (39–79)	0.514	3.67	50.0 (19–81)	100.0 (78–100)	0.787	0.018
TTP (s)	Rt frontal	11.06	20.0 (7–41)	100.0 (86–100)	0.558	11.57	70.0 (35–93)	60.0 (32–84)	0.590	0.470
	Lt frontal	11.58	68.0 (46–85)	48.0 (28–69)	0.550	11.58	60.0 (26–88)	80.0 (52–96)	0.643	0.244
TTP (s)	Rt temporal	11.68	80.0 (59–93)	56.0 (35–76)	0.686	11.78	90.0 (55–100)	33.3 (12–62)	0.517	0.912
	Lt temporal	11.56	80.0 (59–93)	40.0 (21–61)	0.598	12.44	100.0 (69–100)	26.7 (8–55)	0.590	0.471
TTP (S)	Rt basal ganglia	11.15	20.0 (7–41)	100.0 (86–100)	0.575	11.62	90.0 (55–100)	73.3 (45–92)	0.700	0.101
	Lt basal ganglia	11.28	44.0 (24–65)	84.0 (64–95)	0.665	11.64	100.0 (69–100)	40.0 (16–68)	0.593	0.454
TTP (s)	RT parietal	11.83	68.0 (46–85)	68.0 (46–85)	0.659	11.94	50.0 (19–81)	73.3 (45–92)	0.517	0.912
	Lt parietal	11.79	68.0 (46–85)	68.0 (46–85)	0.652	11.85	70.0 (35–93)	60.0 (32–84)	0.563	0.617
TTP (S)	RT hippocampus	11.76	76.0 (55–91)	60.0 (39–79)	0.649	11.88	80.0 (44–97)	60.0 (32–84)	0.580	0.523
	Lt hippocampus	11.85	52.0 (31–72)	76.0 (55–91)	0.595	11.95	60.0 (26–88)	80.0 (52–96)	0.670	0.165

AUROC, area under ROC curve; CBF, cerebral blood flow; CBV, cerebral blood volume; MTT, mean transit time; PCT, perfusion CT; ROC, receiver operating characteristic; TTP, time-to-peak.

Table 5. Significant PCT parameters and MOCA score correlation

Parameters	Correlation coefficient MOCA	P value
MTT (s) (right temporal region)	Correlation coefficient (r) = 0.68	0.0311
CBF (mL/100 g/min) (left temporal region)	Correlation coefficient (r) = 0.88	<0.0011
CBV (mL/100 g) (left temporal region)	Correlation coefficient (r) = 0.89	<0.0011
MTT (s) (left temporal region)	Correlation coefficient (r) = 0.63	0.0491
CBF (mL/100 g/min) (right hippocampus)	Correlation coefficient (r) = 0.96	<0.0011
CBV (mL/100 g) (right hippocampus)	Correlation coefficient (r) = 0.95	<0.0011
MTT (s) (right hippocampus)	Correlation coefficient (r) = 0.68	0.0311
CBF (mL/100 g/min) (left hippocampus)	Correlation coefficient (r) = 0.64	0.0461
CBV (mL/100 g) (left hippocampus)	Correlation coefficient (r) = 0.81	0.0041
CBF (mL/100 g/min) (right parietal region)	Correlation coefficient (r) = 0.89	<0.0011
CBV (mL/100 g) (right parietal region)	Correlation coefficient (r) = 0.88	<0.0011
CBV (mL/100 g) (left parietal region)	Correlation coefficient (r) = 0.77	0.0091
CBF (mL/100 g/min) (left parietal region)	Correlation coefficient (r) = 0.82	0.0031

CBF, cerebral blood flow; CBV, cerebral blood volume; MOCA, Montreal Cognitive Assessment; MTT, mean transit time; PCT, perfusion CT.

CT or MRI provides a clue for the diagnosis of dementia, and also help in identifying etiological subtype by recognising specific patterns of atrophy or vascular changes. However, they do so only in the later stages of the disease and without any prognostic benefit. Functional changes generally precede discernible changes in brain structure, as has been established by modalities such as PET, SPECT and ASL MRI [15, 16]. In particular, perfusion SPECT gives details of perfusion deficits and 18-fluorodeoxyglucose (FDG) PET gives information about reduced metabolic activity, both seen at early stages of disease [17, 18].

PCT also reflects changes in cerebral microcirculation that cannot be detected by conventional CT or MRI; and has proven to be an excellent functional neuroimaging technique. Functional imaging like FDG PET have shown that brain perfusion and metabolism are tightly coupled [19–21]. Hence, known patterns of hypometabolism in FDG PET in dementia can be transferred to patterns of hypoperfusion on PCT. In this study, we used a state-of-the-art 256-slice CT scan machine and were therefore, able to obtain a z-axis coverage of 10 cm covering the entire brain in a single acquisition. We found that CBF and CBV were the two parameters that were significantly different among the three study groups (Tables 2 and 3). VaD group showed statistically significant lower values of CBF and CBV in all regions of the brain evaluated in our study in comparison to controls. These two parameters were found to be significantly lower in bilateral temporoparietal regions and hippocampi in AD subgroup compared with controls.

AD is characterised by deposition of β -amyloid and neurofibrillary tangles; the latter is initially deposited in the entorhinal cortex of mesial temporal region, followed by the limbic system including the hippocampi, and eventually in the rest of the cortex. As our study had only mild to moderate cases of AD and no severe cases were included, this likely accounts for why AD subgroup had significantly lower values of CBF and CBV in bilateral hippocampi and temporal regions; whereas bilateral frontal regions and basal ganglia did not show any significant difference from the controls. A previous study by Yildirim *et al* showed a decrease in CBF in frontal, temporal cortex and lentiform nucleus in AD compared with healthy controls [22]. However, no difference in CBV was found between the groups in their study, which they attributed to vascular autoregulation. Though our results for temporal region CBF are similar, our study showed no difference in CBF in AD in frontal region and basal ganglia. Also, we found CBV values were significantly lower in AD compared with controls which is contradictory to their results [22].

VaD, on the other hand, occurs due to neuronal loss secondary to impaired circulation. This may be a result of small vessel disease with multiple lacunar infarcts including those in strategic locations such as medial thalamic nuclei. Alternately, this may also occur due to large vessel or watershed infarctions. Confluent T2W/FLAIR white matter hyperintensities and multiple infarcts are observed on MRI of these patients. In line with this underlying pathogenetic mechanism, strategic infarcts were detected in 93.3% cases and white matter ischaemic changes in 100% cases of VaD in our study. On quantitative assessment, VaD subgroup showed statistically significant lower values of CBF and CBV in all regions of the brain compared with controls. We could not find any literature on comparison of VaD with controls on PCT. However, comparison of senile dementia with controls was performed in the study by Tang *et al*, in which 55% cases were of AD and 45% cases were of VaD. They demonstrated that CBV and CBF of bilateral frontal and temporal cortices, basal ganglia and hippocampus were significantly higher; whereas MTT and TTP were significantly lower in the control group than in the dementia group [15]. Our results on VaD also show similar results in terms of CBF and CBV; though MTT and TTP showed no significant difference [15].

AD shows preferential involvement of temporo-parietal lobes and limbic system in early stages, with frontal hypoperfusion only in the later course of the disease. In contrast, there is generalised brain hypoperfusion in VaD from the initial stages itself. Therefore, on quantitative PCT evaluation, only the CBF and CBV of frontal regions and CBV of basal ganglia were found to be significantly lower in VaD compared with AD. The CBF and CBV of the two dementia subgroups did not differ significantly in temporo-parietal regions and hippocampi. On ROC analysis also, the cut-off of right frontal CBF ≥ 95.67 mL/min/100 g and left frontal CBF ≥ 91.99 mL/min/100 g had the maximum AUROC of 1 implying 100% sensitivity and specificity for differentiating AD and VaD (Table 4). Though Zimny *et al* also reported significant difference between AD and VaD on PCT, in stark contrast to our study results, they found CBF and CBV to be lower in frontal and temporal regions in AD compared with VaD [7]. However, due to limited brain sections acquired in their study, hippocampi and parietal regions were not evaluated separately. Tang *et al* did not find any significant difference between PCT parameters of AD and VaD cases in their study [15].

Out of the four perfusion parameters analysed, we found MTT and TTP were not significantly different in any of the regions between control group or either of the two dementia subgroups. This is in concordance with a previous study by Zimny *et al* who

Table 6. Comparison between significant findings in previous studies and our study

	Zimny et al [7] (2007)	Tang et al (2013) [15]	Yildirim et al (2015) [22]	Zhang et al (2017) [8]	Our study
Study groups	AD, VaD and mixed dementia	Control, AD and VaD	Control and AD	Control, MCI and AD	Control, AD and VaD
Significant brain regions	Frontal and temporal cortex	Frontal and temporal cortex, basal ganglia, hippocampus	Frontal, temporal and occipital cortex, basal ganglia	Frontal, temporal, parietal, occipital cortex, basal ganglia, hippocampus, internal capsule	Frontal, temporal, parietal region, basal ganglia, hippocampus
Significant perfusion parameters	CBF, CBV	CBF, CBV, MTT, TTP	CBF, TTP	CBF, CBV, MTT, TTP	CBF, CBV
Significant group comparison (CBF values)	AD <VaD AD<Mixed VaD, Mixed no difference	Dementia<control AD, VaD no difference	AD <control	AD <control	AD<control (parietotemporal region, hippocampus) VaD <control (all regions) VaD<AD (frontal region and basal ganglia)

AD, Alzheimer's disease; CBF, cerebral blood flow; CBV, cerebral blood volume; MCI, Mild Cognitive Impairment; MTT, mean transit time; TTP, time-to-peak; VaD, vascular dementia.

demonstrated no significant difference in MTT values between AD and VaD groups [7]. However, studies by Tang et al and Yildirim et al have demonstrated a significant difference in TTP and MTT between study groups [15, 22]. The former study showed higher values of both MTT and TTP in frontal lobe, temporal lobe, basal ganglia and hippocampus in senile dementia compared with healthy controls. The latter study established an increased TTP value in frontal, temporal, occipital cortex and lentiform nucleus in AD compared with controls. A comparison between findings of our study and other previous studies on PCT in dementia is summarised in Table 6.

In our study, we found positive correlation between MOCA score and PCT parameters in various regions of the brain (Table 5). These findings are in agreement with results obtained by Zimny et al and Streitparth et al, though they used the Mini-Mental State Examination score for cognitive assessment instead of the MOCA score [23, 24]. The positive correlation of MOCA scores and PCT parameters (CBF and CBV) can be explored to use them as surrogate markers of the cognitive status of patients with dementia. PCT can also serve as a potential tool for monitoring of disease progression and evaluating therapeutic responses during the course of treatment. Various studies have shown promising results in this regard [12–14].

Certain limitations of our study must be acknowledged. Due to time constraint, our study's sample size was small. Second, we only evaluated the two most common forms of dementia that is, AD and VaD. The less prevalent types of dementia such as frontotemporal dementia, mixed dementia or Lewy body dementia were not encountered in our study participants. Lastly, though we determined the correlation of MOCA scores and PCT parameters, we did this at only one time point. Therefore, we were unable to assess the changes in these parameters during the disease course, or their modification with therapy. Future research could be directed along these lines.

Conclusion

Our results demonstrate cerebral hypoperfusion evidenced by reduced CBF and CBV in cases of dementia. As functional changes precede structural alterations, PCT can be employed for the early diagnosis of dementia facilitating prompt initiation of treatment.

PCT may also reliably aid in the differentiation between AD and VaD. Preferential involvement of temporo-parietal regions and hippocampi with sparing of frontal regions and basal ganglia favours the diagnosis of AD. On the other hand, a more global reduction in CBF and CBV suggests the diagnosis of VaD. Detection of strategic infarcts and white matter ischaemic changes lend further support for the diagnosis of VaD. Moreover, since various perfusion parameters show positive correlation with MOCA score, PCT could potentially be utilised for differentiating varying severities of dementia, and in the follow-up of cases of dementia.

Main messages

- Cerebral hypoperfusion in the form of reduced CBF and CBV is seen on PCT in cases of dementia.
- Preferential involvement of temporoparietal regions and hippocampi favours AD; whereas global reduction in CBF and CBV suggests VaD.
- Strategic infarcts and white matter ischaemic changes are also additionally detected with PCT in VaD.
- As perfusion parameters show positive correlation with MOCA score, PCT could be useful in the follow-up of cases of dementia.

Current research questions

- Pattern of perfusion alterations in other rare varieties of dementia.
- Post-treatment follow-up of perfusion parameters in cases of dementia.
- Role of perfusion parameters in predicting the progression of dementia.

What is already known on the subject

- Modalities like PET and SPECT have demonstrated that functional changes in dementia precede cortical atrophy.
- Few studies which evaluated perfusion CT in this regard mostly had limited coverage of brain and showed heterogeneous results.

Acknowledgements

To all the technical staff.

Contributors

SD and SJ conceived the idea of this study. SD, YA and SJ did literature review. SD and SJ collected and analyzed data. SD and SJ prepared tables and wrote the first draft of manuscript. NC and AS helped with writing, reviewing and editing the manuscript. SJ is the guarantor for the work. YA was responsible for the supervision of this project. All authors approved the final version of this article.

Funding

The authors have not declared a specific grant for this research from any funding agency in the public, commercial or not-for-profit sectors.

Competing interests

None declared.

Provenance and peer review

Not commissioned; externally peer reviewed.

Data availability statement

All data relevant to the study are included in the article or uploaded as online supplemental information. Not applicable.

Ethics statements

Patient consent for publication

Consent obtained directly from patient(s)

Ethics approval

This study was approved by IEC/VMMC/SJH/THESIS/JUNE/2019.


References

- American Psychiatric Association. *Diagnostic and statistical manual of mental disorders*. 5th ed. Arlington, VA: American Psychiatric Publishing, 2013.
- Global burden of disease 2004 Update. *Disability weights for diseases and conditions [document on the internet]*. Geneva: World Health Organisation, 2004. http://www.who.int/healthinfo/global_burden_disease/GBD2004_DisabilityWeights.pdf.
- Shaji KS, Jotheeswaran AT, Girish N. *The dementia India report: prevalence, impact, costs and services for dementia: Executive summary*. Alzheimer's and Related Disorders Society of India, 2010: 1–38.
- Patel KP, Wymer DT, Bhatia VK, et al. Multimodality imaging of dementia: clinical importance and role of integrated anatomic and molecular imaging. *Radiographics* 2020;**40**:200–22.
- Matsuda H. The role of neuroimaging in mild cognitive impairment. *Neuropathology* 2007;**27**:570–7.
- Scheltens P, Korf ES. Contribution of neuroimaging in the diagnosis of Alzheimer's disease and other dementias. *Curr Opin Neurol* 2000;**13**:391–6.
- Zimny A, Sasiadek M, Leszek J, et al. Does perfusion CT enable differentiating Alzheimer's disease from vascular dementia and mixed dementia? A preliminary report. *J Neurol Sci* 2007;**257**:114–20.
- Zhang B, Gu G-J, Jiang H, et al. The value of whole-brain CT perfusion imaging and CT angiography using a 320-slice CT scanner in the diagnosis of MCI and AD patients. *Eur Radiol* 2017;**27**:4756–66.
- Aksoy FG, Lev MH. Dynamic contrast-enhanced brain perfusion imaging: technique and clinical applications. *Semin Ultrasound CT MR* 2000;**21**:462–77.
- Caroli A, Testa C, Geroldi C, et al. Cerebral perfusion correlates of conversion to Alzheimer's disease in amnesic mild cognitive impairment. *J Neurol* 2007;**254**:1698–707.
- WHO fact sheet dementia, 2020. Available: <http://www.who.int>.
- Nobili F, Koulibaly M, Vitali P, et al. Brain perfusion follow-up in Alzheimer's patients during treatment with acetylcholinesterase inhibitors. *J Nucl Med* 2002;**43**:983–90.
- Hanyu H, Shimizu T, Tanaka Y, et al. Regional cerebral blood flow patterns and response to donepezil treatment in patients with Alzheimer's disease. *Dement Geriatr Cogn Disord* 2003;**15**:177–82.
- Shimizu S, Hanyu H, Iwamoto T, et al. Spect follow-up study of cerebral blood flow changes during donepezil therapy in patients with Alzheimer's disease. *J Neuroimaging* 2006;**16**:16–23.
- Tang Z, Chen F, Huang J, et al. Low-Dose cerebral CT perfusion imaging (CTPI) of senile dementia: diagnostic performance. *Arch Gerontol Geriatr* 2013;**56**:61–7.
- Jagust W. Positron emission tomography and magnetic resonance imaging in the diagnosis and prediction of dementia. *Alzheimers Dement* 2006;**2**:36–42.
- Varma AR, Adams W, Lloyd JJ, et al. Diagnostic patterns of regional atrophy on MRI and regional cerebral blood flow change on SPECT in young onset patients with Alzheimer's disease, frontotemporal dementia and vascular dementia. *Acta Neurol Scand* 2002;**105**:261–9.
- Bohnen NI, Djang DSW, Herholz K, et al. Effectiveness and safety of 18F-FDG PET in the evaluation of dementia: a review of the recent literature. *J Nucl Med* 2012;**53**:59–71.
- Hoeffner EG, Case I, Jain R, et al. Cerebral perfusion CT: technique and clinical applications. *Radiology* 2004;**231**:632–44.
- Buxton RB, Frank LR. A model for the coupling between cerebral blood flow and oxygen metabolism during neural stimulation. *J Cereb Blood Flow Metab* 1997;**17**:64–72.
- Aubert A, Costalat R. A model of the coupling between brain electrical activity, metabolism, and hemodynamics: application to the interpretation of functional neuroimaging. *Neuroimage* 2002;**17**:1162–81.
- Yildirim T, Karakurum Göksel B, Demir Şenay, et al. Evaluation of brain perfusion in Alzheimer disease with perfusion computed tomography and comparison to elderly patient without dementia. *Turk J Med Sci* 2016;**46**:834–9.
- Zimny A, Leszek J, Kiejna A, et al. Analysis of correlation between the degree of cognitive impairment and the results of perfusion CT in patients with dementia. *Med Sci Monit* 2007;**13 Suppl 1**:23–30.
- Streitparth F, Wieners G, Kämena A, et al. [Diagnostic value of multislice perfusion CT in dementia patients]. *Radiologe* 2008;**48**:175–83.

EXHIBIT 7

RESEARCH ARTICLE

Longitudinal cerebral perfusion in presymptomatic genetic frontotemporal dementia: GENFI results

Maurice Pasternak^{1,2}  | Saira S. Mirza¹ | Nicholas Luciw^{1,3} | Henri J. M. M. Mutsaerts⁴ | Jan Petr⁵ | David Thomas⁶ | David Cash⁷ | Martina Bocchetta⁷ | Maria Carmela Tartaglia^{8,9,10} | Sara B. Mitchell¹⁰ | Sandra E. Black^{10,11,12} | Morris Freedman^{10,11} | David Tang-Wai^{10,11,13} | Ekaterina Rogaeva⁸ | Lucy L. Russell⁷ | Arabella Bouzigues⁶ | John C. van Swieten¹⁴ | Lize C. Jiskoot¹⁴ | Harro Seelaar¹⁴ | Robert Laforce Jr.¹⁵ | Pietro Tiraboschi¹⁶ | Barbara Borroni¹⁷ | Daniela Galimberti^{18,19} | James B. Rowe^{20,21,22} | Caroline Graff^{23,24} | Elizabeth Finger²⁵ | Sandro Sorbi^{26,27} | Alexandre de Mendonça²⁸ | Chris Butler^{29,30} | Alex Gerhard^{31,32,33} | Raquel Sanchez-Valle³⁴ | Fermin Moreno^{35,36} | Matthis Synofzik³⁷ | Rik Vandenberghe³⁸ | Simon Ducharme^{39,40} | Johannes Levin^{41,42} | Markus Otto⁴³ | Isabel Santana⁴⁴ | Antonio P. Strafella^{13,45,46} | Bradley J. MacIntosh^{1,3} | Jonathan D. Rohrer⁷ | Mario Masellis^{1,2,10,12,47} | on behalf of the GENetic Frontotemporal dementia Initiative (GENFI)

Correspondence

Mario Masellis, Cognitive and Movement Disorders Clinic, Sunnybrook Health Sciences Centre, 2075 Bayview Ave., Room A4 42, Toronto, Ontario M4N 3M5, Canada.
Email: mario.masellis@sunnybrook.ca

See Supporting Information for a list of GENFI consortium members.

Funding information

Canadian Institutes of Health Research, Grant/Award Numbers: MOP-327387, PJT-175242; Weston Brain Institute; Medical Research Council UK, Grant/Award Number: MR/M023664/1; JPND GENFI-PROX, Grant/Award Number: DLR/BMBF 2019-02248; Deutsche Forschungsgemeinschaft; Munich Cluster for Systems Neurology, Grant/Award Number: EXC 2145 SyNergy – ID 390857198; MRC Clinician Scientist Fellowship, Grant/Award Number: MR/M008525/1; NIHR Rare Disease

Abstract

INTRODUCTION: Effective longitudinal biomarkers that track disease progression are needed to characterize the presymptomatic phase of genetic frontotemporal dementia (FTD). We investigate the utility of cerebral perfusion as one such biomarker in presymptomatic FTD mutation carriers.

METHODS: We investigated longitudinal profiles of cerebral perfusion using arterial spin labeling magnetic resonance imaging in 42 *C9orf72*, 70 *GRN*, and 31 *MAPT* presymptomatic carriers and 158 non-carrier controls. Linear mixed effects models assessed perfusion up to 5 years after baseline assessment.

RESULTS: Perfusion decline was evident in all three presymptomatic groups in global gray matter. Each group also featured its own regional pattern of hypoperfusion over time, with the left thalamus common to all groups. Frontal lobe regions featured lower perfusion in those who symptomatically converted versus asymptomatic carriers past their expected age of disease onset.

DISCUSSION: Cerebral perfusion is a potential biomarker for assessing genetic FTD and its genetic subgroups prior to symptom onset.

This is an open access article under the terms of the [Creative Commons Attribution](https://creativecommons.org/licenses/by/4.0/) License, which permits use, distribution and reproduction in any medium, provided the original work is properly cited.

© 2024 The Authors. *Alzheimer's & Dementia* published by Wiley Periodicals LLC on behalf of Alzheimer's Association.

Translational Research Collaboration, Grant/Award Number: BRC149/NS/MH; ZonMW Memorabel, Grant/Award Number: 733 051 042; National Institute for Health Research Cambridge Biomedical Research Centre, Grant/Award Number: NIHR203312; Medical Research Council, Grant/Award Numbers: MC_UU_00030/14, MR/T033371/1; Saul A. Silverman Family Foundation; Canada International Scientific Exchange Program; Morris Kerzner Memorial Fund; Instituto de Salud Carlos III, Grant/Award Number: 20/0448; European Union; University of Toronto Medical Science Open; Joseph Bazylewicz Fellowships; Swedish FTD Initiative Schörling Foundation; EU Joint Programme Neurodegenerative Disease Research Prefrontals Vetenskapsrådet, Grant/Award Number: Dnr 529-2014-7504; EU Joint Programme Neurodegenerative Disease Research-GENFI-PROX; Vetenskapsrådet, Grant/Award Numbers: 2019-0224, 2015-02926, 2018-02754

KEYWORDS

arterial spin labeling, cerebral perfusion, frontotemporal dementia, presymptomatic biomarker

Highlights

- Gray matter perfusion declines in at-risk genetic frontotemporal dementia (FTD).
- Regional perfusion decline differs between at-risk genetic FTD subgroups.
- Hypoperfusion in the left thalamus is common across all presymptomatic groups.
- Converters exhibit greater right frontal hypoperfusion than non-converters past their expected conversion date.
- Cerebral hypoperfusion is a potential early biomarker of genetic FTD.

1 | BACKGROUND

Frontotemporal dementia (FTD) comprises a group of clinically and pathologically heterogeneous neurodegenerative disorders featuring regional neuron loss primarily in the frontal and temporal cerebral lobes.¹ It presents a significant burden on society and is a common cause of young onset dementia with an estimated prevalence being between 15 and 22 cases per 100,000 individuals, approaching that of Alzheimer's disease (AD) in this age group.² There is a strong genetic basis, with up to 20% of all cases stemming from autosomal dominant inheritance in three genes: hexanucleotide repeat expansions in chromosome 9 open reading frame 72 (*C9orf72*), as well as mutations in progranulin (*GRN*) and microtubule-associated protein tau (*MAPT*),^{3,4} with relative prevalence in that order.⁵

While there are currently no approved disease-modifying therapies for genetic FTD, several promising drug candidates are being evaluated in clinical trials.^{6,7} Such therapeutics would best be applied at prodromal stages of the disease when irrecoverable neuronal damage has not yet taken place. However, clinical trial design benefits from knowledge of the natural history of disease progression and heterogeneity, which highlights the importance of effective biomarker development to address these challenges. As evidenced in studies focusing on familial AD and Huntington's disease, there are crucial characteristics that effective biomarkers should possess.^{8,9} They should be acquired with relative ease for sustainable longitudinal assessment, reliably change at the presymptomatic stage in a manner that delineates not only individuals at risk of the disease versus those not at risk, but also disease variants. Furthermore, they should identify differences between individuals at risk who eventually develop symptoms versus those who remain asymptomatic, as this would be of particular interest to therapeutics that aim to impede disease progression.

Given the high penetrance of genetic FTD mutations, presymptomatic individuals are a particularly important population for inves-

tigating the early signatures of FTD progression and for the identification of disease-monitoring biomarkers.^{3,10} A variety of studies have provided robust neuroimaging findings on presymptomatic genetic FTD in terms of structural and functional brain changes.^{11–22} Assessment of these and other such studies also suggests that functional measures, such as neuronal connectivity, precede structural changes such as atrophy.⁵ There is a need to advance the body of evidence, notably: extending beyond cross-sectional design to study disease change over time, incorporating all three major mutation variants of genetic FTD, increasing sample size, using non-invasive imaging techniques that avoid ionizing radiation, and placing a greater focus on presymptomatic carriers as opposed to pooling presymptomatic and symptomatic carriers in comparisons.

We extend upon these previous observations by conducting the largest longitudinal analysis of cerebral perfusion across all three genetic FTD subgroups in presymptomatic individuals at risk for genetic FTD using arterial spin labeling (ASL) magnetic resonance imaging (MRI). ASL is a non-invasive imaging modality in which an individual's blood is magnetically labeled, thereby acting as an endogenous tracer to measure cerebral perfusion, which in turn is assumed to be tightly coupled to brain metabolism.²³ This study also highlights the image processing and quality-control steps necessary for robust cerebral perfusion quantification across multiple study sites and MRI scanners while accounting for partial volume effects stemming from gray matter atrophy.²⁴ We have previously demonstrated that regional perfusion delineates presymptomatic FTD carriers from non-carrier controls in a cross-sectional study of all three groups in genetic FTD using ASL.¹³

This study investigates regional and global cerebral perfusion changes over time in presymptomatic FTD mutation carriers stratified according to genetic subgroup. We hypothesized that cerebral perfusion would decline over time to a greater extent in one or more of the presymptomatic genetic subgroups relative to non-carrier controls.

Furthermore, the degree of this perfusion decline will differ among brain regions when comparing presymptomatic carrier groups. Finally, perfusion relative to baseline will have declined to a greater extent in presymptomatic carriers who eventually converted into symptomatic FTD versus unaffected carriers who surpassed the time at which they were expected to exhibit symptoms.

2 | METHODS

2.1 | Participants

Data were drawn from the fifth data freeze of the Genetic Frontotemporal Dementia Initiative (GENFI) database, with images acquired from 23 sites across Canada, the United Kingdom, Italy, the Netherlands, Sweden, and Portugal between January 30, 2012, and May 31, 2019. Participants were presymptomatic individuals at baseline who were carriers of a genetic mutation in one of the *C9orf72*, *GRN*, or *MAPT* genes, but who had no clinical symptoms of FTD present, as assessed by a trained clinician. Further details regarding the inclusion criteria are listed elsewhere.²⁰ Non-carrier controls were first-degree relatives of the presymptomatic carriers and who were confirmed to not carry mutations in *C9orf72*, *GRN*, or *MAPT*. Individuals who converted into symptomatic FTD during the study were included in a post hoc, secondary analysis after the primary study was complete (see details below).

2.2 | Ethics and patient consent

Ethical review boards from all sites approved the study protocol and all participating individuals provided written and informed consent in agreement with the Declaration of Helsinki.

2.3 | Genotype testing

Verification of *C9orf72*, *GRN*, or *MAPT* mutation being present/absent was done using a standardized protocol at each site. Mutations were detected either by DNA sequencing or allele-specific polymerase chain reaction (PCR)-based evaluation of *GRN* or *MAPT*. *C9orf72* hexanucleotide repeat expansions were evaluated using a previously described two-step genotyping procedure.²⁵ Genetic guardians at each site uploaded the mutation results directly to the centralized database. All research personnel and clinicians performing clinical and cognitive/behavioral evaluations, as well as the physical exam, were blinded to mutation status.

2.4 | MRI image acquisition

T1-weighted and ASL sequences were collected at the respective sites and image processing steps were taken to enable multi-site analysis.²⁰ Image processing accounted for five main ASL acquisition

RESEARCH IN CONTEXT

- 1. Systematic review:** The authors reviewed the literature using PubMed. Cerebral perfusion has shown promise in characterizing genetic frontotemporal dementia (FTD). However, most of the prior literature is cross-sectional and/or limited to one or two subsets of the major genetic groups (*C9orf72*, *GRN*, and *MAPT*).
- 2. Interpretation:** Our study provides evidence that cerebral perfusion may be an early biomarker for assessing at-risk genetic FTD. Decreases in cerebral perfusion delineate not only all major FTD genetic groups from controls, but also between-group differences as well. Cerebral perfusion decreases also distinguish converter individuals from older non-converters.
- 3. Future directions:** Measures of cerebral perfusion in early stages of FTD may improve prediction of symptom onset in those genetically at risk. Incorporating cerebral perfusion alongside other imaging measures, such as white matter tract integrity and gray matter atrophy, may significantly improve our understanding of disease mechanisms and can be incorporated into clinical trial design.

variants: pseudo-continuous ASL (PCASL) 2D gradient-echo echo-planar imaging (EPI) on 3T Philips Achieva scanners with and without accompanying proton-density (M0) scans; and pulsed ASL (PASL) 3D gradient- and spin-echo (GRaSE) on 3T Siemens Trio Tim or Prisma Fit machines with or without an accompanying M0 scan, and a PCASL 3D fast-spin-echo stack-of-spirals on 3T General Electric MR750 scanners with an M0 scan. Detailed ASL parameters are provided in the supporting information (Table S1).

2.5 | ASL image processing

As in our previous cross-sectional study,¹³ we used ExploreASL software (version 1.10.0),²⁶ which is based on the Statistical Parametric Mapping 12 (SPM12) MATLAB package to process ASL scans from the various sites, vendors, and sequences. Briefly, T1-weighted structural images were segmented into gray and white matter tissue partial volume maps and spatially normalized to a population template in Montreal Neurological Institute 152 standard space using geodesic shooting.²⁷ Structural volumes of whole brain gray matter tissues were collected at this time using SPM12 for ancillary structural MRI analysis. Transformation matrices were saved for subsequent application in bringing cerebral perfusion images into a common space for parcellation. ASL time series were corrected for motion outliers using rigid-body transformation coupled with the Enhancement of Automated Blood Flow Estimates (ENABLE) outlier exclusion algorithm,²⁸ followed by pairwise subtraction to produce perfusion-weighted images

(PWI). If M0 images were not acquired at scan time, substitute M0 images were constructed using the mean of the non-labeled ASL scans without background suppression. M0 volumes were smoothed with a 16 mm full-width half-maximum (FWHM) Gaussian kernel to create a bias field that avoided division artifacts during perfusion quantification and canceled out acquisition-specific B1-field inhomogeneities. Cerebral perfusion quantification itself followed a single-compartment model approach and recommendations outlined in the ASL consensus paper.²⁹

2.6 | Quality control and corrections

For cerebral perfusion image quality control, we used the same steps as previously described.¹³ Scans were independently and visually assessed by two authors (M.P., N.L.) with more than 3 years of experience handling ASL data. Scans which featured significant image acquisition or processing issues were discarded such as those with poor signal-to-noise, uneven labeling, arterial transit time artifacts, severe motion, distortions from improper coregistration, artifacts, and clipping (see examples in Figure S1 in supporting information). An intraclass correlation score of 0.83 was reached, which is considered "good."³⁰ Remaining inconsistencies were resolved by consensus. In total, 40 participants were excluded during this process. To account for arterial transit time artifacts not immediately evident by visual inspection, images were also assessed quantitatively by their gray matter spatial coefficient of variation,³¹ and excluded if this measure exceeded 0.8. This did not result in any further loss of participant scans.

To adjust for the effects of scans acquired at different sites, as well as differences arising from changes or upgrades to scanner models and software versions between time points within those sites, we performed a group-based voxel-wise bias field correction approach. Scans were placed into groupings according to their site, scanner model, and major software version. Groups that contained fewer than four scans were excluded, resulting in the removal of one participant. Scans acquired during visits in which a participant was confirmed by a trained clinician to convert into clinical FTD presentation ($n = 3$) were withheld from contributing to the generation of group-specific bias fields, as it is advised to estimate bias fields on the basis of individuals without potentially significant pathophysiological alterations.³² For each grouping, a mean perfusion image was calculated and smoothed with a 6.4 mm FWHM Gaussian kernel. A grand mean perfusion image for the entire population was then calculated from these individual group means. This grand-mean image was then rescaled such that the mean gray matter perfusion would be a physiologically reasonable 60 mL/min/100 g value,³³ which involved rescaling by a factor of 1.14. Bias fields for each grouping were then calculated by dividing its mean perfusion image by the rescaled grand-mean image. Finally, individual cerebral perfusion images were rescaled by being multiplied against their grouping's bias field image.¹³

To account for the effect of gray matter atrophy, which has been previously demonstrated to be detectable in presymptomatic FTD carriers,¹⁹ rescaled perfusion images were corrected for partial volume effects (PVE) using a voxel-wise local linear regression within a 3D

Gaussian kernel based on probability tissue maps.³⁴ For a secondary analysis (see below), converter scans which were initially withheld from bias field image generation were also rescaled by the appropriate group-based bias field that they would have otherwise belonged to, followed by PVE correction.

PVE-corrected images were parcellated using Automated Anatomical Labeling Atlas version 2 (AAL2) within voxels that had a gray matter partial volume $\geq 50\%$.³⁵ Mean perfusion values from parcellated regions were extracted for statistical analysis. Regions which were not covered in all ASL scans, such as the cerebellum, or those with fewer than 100 voxels of positive signal, were excluded from statistical analysis.

2.7 | Demographic, clinical, and behavioral data analysis

Participants underwent a standardized clinical assessment at each visit. Within this study, we report the Clinical Dementia Rating plus National Alzheimer's Coordinating Center Behavior and Language Domains Rating Scale Frontotemporal Lobar Degeneration (CDR plus NACC FTLD), the FTD Rating Scale score, the revised Cambridge Behavioral Inventory score, and the Mini-Mental State Examination (MMSE) score. These measures were statistically assessed between non-carrier controls and the three presymptomatic mutation carrier groups. To account for the effects of cardiovascular risk factors or other neurological/medical diseases on cerebral perfusion, clinical assessment also recorded the absence, recent occurrence, or remote occurrence of seizures, stroke, traumatic brain injury, hypertension, hypercholesterolemia, diabetes mellitus, smoking, excessive alcohol consumption, recreational drug use, and autoimmune disease. These data are presented in Table S2 in supporting information, and statistical comparisons were made across groups at baseline to ensure that they were balanced in terms of these potential perfusion-altering risk factors/diseases. To determine the impact of participant exclusion during the quality control and bias field correction steps, demographic and clinical variables were also compared between excluded participants and the retained participants.

Categorical variables were assessed either by Pearson chi square test or Fisher exact test depending on whether any given frequency was lower than a count of five. Continuous variables across groups were assessed with a type III analysis of variance and followed up with Tukey post hoc tests if the omnibus P value result was below an alpha of 0.05.

2.8 | Primary linear mixed effects analysis

A total of 158 non-carrier controls, 42 *C9orf72*, 70 *GRN*, and 31 *MAPT* presymptomatic carriers had useable scans for at least two time points (Table S3 in supporting information). For the primary analysis involving regional cerebral perfusion comparison between non-carrier controls and the three presymptomatic genetic subgroups, we used mixed effects linear models according to the following R-style

formula:

$$\text{Perfusion} \sim \text{Group} + \text{Time} + \text{Group} : \text{Time} + \text{Age}_{\text{baseline}} + \text{Sex} \\ + \text{CBF}_{\text{baseline}} + (1 | \text{SubjectID})$$

Perfusion is the cerebral perfusion at any given time point in a particular region of interest (ROI) from the AAL2 atlas or of the whole brain gray matter at a probability of at least 50%. Group is a factor variable with the following levels: non-carrier controls, presymptomatic *C9orf72* carriers, presymptomatic *GRN* carriers, or presymptomatic *MAPT* carriers. Time refers to the exact time from baseline scan measurement, reported in units of years (β). The interaction between these two effects is denoted above as Group:Time. Contrasts were encoded such that the control non-carrier group served as the reference group. Interaction coefficients are therefore reported as comparing a given presymptomatic genetic subgroup versus the control non-carrier group and are reported as β_{int} for a given group. To avoid collinearity issues with time from baseline, age at baseline was used as opposed to age at scan date as a covariate. Other covariates included biological sex and the perfusion measured at baseline for the same ROI. A random intercept clustered over participants was included due to the longitudinal nature of the study with repeat image acquisition and familial relatedness of the participants.

The above model was arrived at using a model-building approach from a more parsimonious model that did not include baseline perfusion as a covariate. Additional models that were initially tested included permitting a random slope across time for each participant, nesting participants within family membership, or a combination of the model alterations. However, these more complex models failed to properly converge regardless of optimization algorithm or otherwise failed to perform better based on Akaike information criterion, Bayesian information criterion, and a log-likelihood ratio test (Table S4 in supporting information) for model comparisons.

After confirmation of a significant result from the omnibus test mixed effects model, a post hoc analysis was conducted on the model to assess the profile of differences in whole brain gray matter perfusion between each presymptomatic genetic subgroup and non-carrier controls. This was achieved by estimating the marginal means at baseline assessment and 1-year intervals after, with contrasts selecting for the effect of perfusion difference between a given presymptomatic group versus non-carrier controls.

Linear mixed effects analyses were also conducted on structural MRI volumetric data using the following model:

$$\text{Volume} \sim \text{Group} + \text{Time} + \text{Group} : \text{Time} + \text{Age}_{\text{baseline}} + \text{Sex} \\ + \text{TIV}_{\text{baseline}} + (1 | \text{SubjectID})$$

where volume refers to global gray matter volumes extracted during image processing. $\text{TIV}_{\text{baseline}}$ refers to the total intracranial volume recorded during the baseline scan visit. All other terms and their meanings are akin to the previously described cerebral perfusion model.

Statistical analyses were carried out in R version 4.2.2 (R Foundation for Statistical Computing) and mixed effects models used the *lme4* package for model fitting, the *afex* package for model convergence assessment, and the *emmeans* package for post hoc testing of the whole-brain gray matter perfusion model.^{36–38} Resulting *P* values from multiple testing were adjusted using Bonferroni correction.

2.9 | Secondary analysis comparing converters to presymptomatic carriers beyond their expected age of disease onset

During participant recruitment, all presymptomatic carriers had a calculated years to expected disease onset (EYO), as covered in a previous GENFI study.²⁰ Briefly, the EYO for a given participant was defined as the difference between the age at baseline assessment versus mean age of disease onset within the family for that participant.

To better understand how cerebral perfusion may be related to clinical conversion, we compared mutation carriers who remained asymptomatic past their EYO ($n = 22$) versus mutation carriers who converted into symptomatic FTD during their follow-up period ($n = 19$). The definition of a converter within this study involved either a clinician's diagnosis and/or otherwise a change in CDR plus NACC FTLD into a score of one or greater. All control non-carriers or presymptomatic carriers who did not meet these criteria were excluded from this secondary analysis. This secondary analysis did not possess enough statistical power to stratify the converters across the three major genetic subgroups.

To reduce the influence of converter scans having more acquisitions at later time points, which may bias results in favor of demonstrating converter hypoperfusion, analysis was restricted to time point follow-up three, based on Fisher exact test confirming an equal proportion of visits between the two converter and non-converter groups (Table S5 in supporting information). This resulted in a removal of three converter scans that took place at follow-up visit four but with no loss of participants. An analysis of covariance was conducted to ascertain whether the perfusion difference at the final available time point relative to baseline was statistically different between the two groups. The change in perfusion between baseline and the last time point was the dependent variable. Covariates included the participant's age at baseline and their sex. As genetic subgroups had to be pooled together to achieve sufficient statistical power, this secondary analysis was only carried out for ROIs that passed Bonferroni correction in two or more genetic subgroups within the primary analysis. Additionally, as this was a post hoc analysis, correction across multiple tests was not conducted and only uncorrected *P* values are reported.

3 | RESULTS

3.1 | Demographic, clinical, and behavioral data

For demographic variables (Table 1), there were no significant differences between healthy controls and the three genetic FTD subgroups

TABLE 1 Demographic, structural imaging, and clinical characteristics (n = 301).

Characteristic	Group				P value
	Non-carrier controls, n = 158	C9orf72 presymptomatic carriers, n = 42	GRN presymptomatic carriers, n = 70	MAPT presymptomatic carriers, n = 31	
Demographics					
Age (years)	46.6 ± 13.0	41.7 ± 10.0	47.4 ± 11.9	38.4 ± 8.9	<0.001
Education (years)	14.7 ± 3.5	15.1 ± 2.5	15.2 ± 3.5	14.8 ± 3.1	0.70
Sex					0.71
Female	99 (63%)	30 (71%)	43 (61%)	19 (61%)	
Male	59 (37%)	12 (29%)	27 (39%)	12 (39%)	
Handedness					0.10
Left	8 (5.1%)	2 (4.8%)	10 (14%)	4 (13%)	
Right	149 (94%)	39 (93%)	59 (84%)	27 (87%)	
Other	1 (0.6%)	1 (2.4%)	1 (1.4%)	0 (0%)	
Clinical measures					
CDR plus NACC FTLD score (categories*)	0 (IQR 0–0)	0 (IQR 0–0)	0 (IQR 0–0)	0 (IQR 0–0)	–
FTD rating scale (/100)	96.4 ± 5.9	95.0 ± 8.0	95.5 ± 10.8	93.5 ± 10.3	0.37
Cambridge Behavioral Inventory (/180)	4.7 ± 6.1	6.4 ± 7.9	3.8 ± 6.7	7.4 ± 11.0	0.08
Mini-Mental State Examination (/30)	29.4 ± 1.0	29.7 ± 0.6	29.5 ± 1.0	29.7 ± 1.1	0.26
Structural imaging					
Gray matter (mm ³)	638 ± 2.4	618 ± 4.6	636 ± 3.6	638 ± 5.4	<0.001

Notes: For demographic and clinical measures, data are represented as either n (%), mean ± standard deviation, or median. P values stem from type III analysis of variance for continuous variables and χ^2 or Fisher exact tests for categorical variables, depending on whether all cells were > 5 or not, respectively. For structural measures, data are represented as group estimate ± standard error based on estimated marginal means extracted from the longitudinal linear mixed effects models. Bold emphasis has been placed on P values that are ≤ 0.05.

Abbreviations: C9orf72, chromosome 9 open reading frame 72; CDR, Clinical Dementia Rating; FTD, frontotemporal dementia; GRN, progranulin; IQR, interquartile range; MAPT, microtubule-associated protein tau; NACC FTLD, National Alzheimer's Coordinating Center Behavior and Language Domains Rating Scale.

*Clinical Dementia Rating plus National Alzheimer's Coordinating Center Behavior and Language Domains Rating Scale Frontotemporal Lobar Degeneration categories: 0 (normal); 0.5 (very mild); 1 (mild); 2 (moderate); 3 (severe).

across education, proportions of sex, or proportions of handedness. However, age was statistically different ($F[3, 297] = 9.98; P < 0.001$) among the groups and post hoc analysis for age demonstrated that presymptomatic MAPT mutation carriers were statistically younger than the non-carrier control population as well as the GRN presymptomatic carrier group. Clinical and behavioral measures (Table 1), including the CDR plus NACC FTLD, the FTD Rating Scale, the Cambridge Behavioral Inventory, and the MMSE were similar between presymptomatic genetic subgroups and non-carrier controls. Likewise, frequency analysis of cardiovascular risk factors and other neurological/medical diseases that could potentially influence cerebral perfusion (Table S2) found no differences between any participant groups at baseline.

The comparison between excluded participants and retained participants (Table S6 in supporting information) demonstrated that the two populations were statistically comparable for demographic and

clinical measures, apart from sex frequencies being significantly different ($\chi^2[1] = 8.02; P < 0.001$), with an increased proportion of male individuals featured in the excluded group.

3.2 | Global gray matter perfusion changes

Global gray matter longitudinal perfusion profiles (Figure 1) demonstrated an overall decreasing trend in all participant groups as a function of time from baseline (non-carriers = -0.76 ± 0.24 mL/min/100 g/year, $P = 0.002$; C9orf72 = -2.42 mL/min/100 g/year, $P < 0.001$; GRN = -3.42 ± 0.38 mL/min/100 g/year, $P < 0.001$; MAPT = -1.89 mL/min/100 g/year, $P = 0.003$), in agreement with the general observation that perfusion decreases with age.³⁹ All three presymptomatic genetic subgroups demonstrated a more pronounced rate of perfusion decline relative to non-carrier

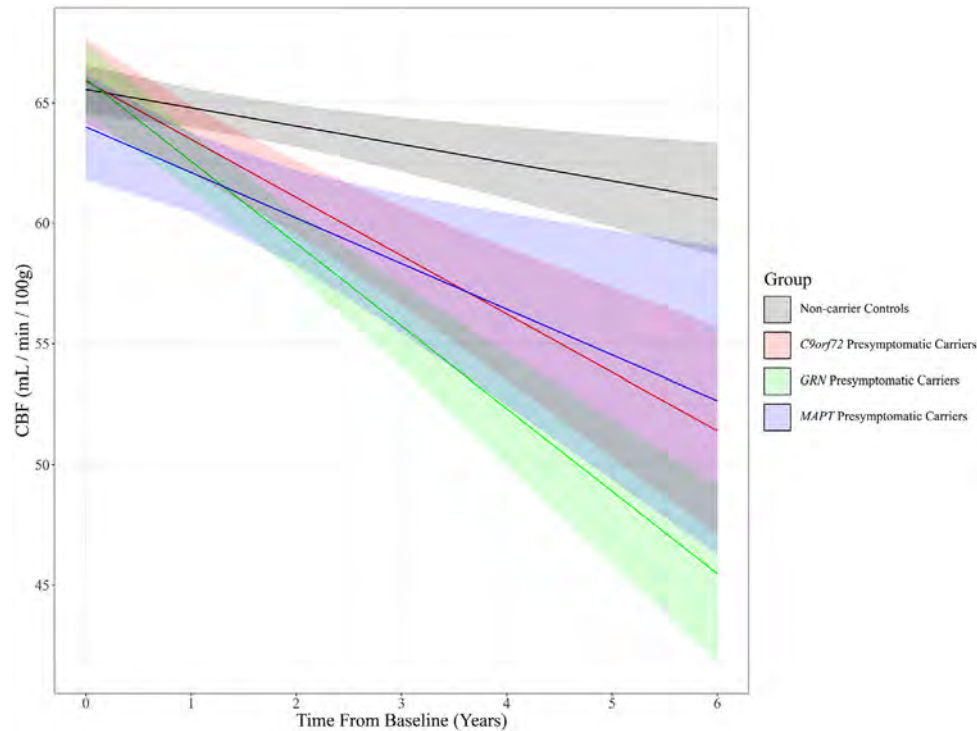


FIGURE 1 Mixed effects interaction plot of whole brain gray matter perfusion as a function of time from baseline assessment for non-carrier controls (black) versus presymptomatic carriers of mutations *C9orf72* (orange), *GRN* (green), and *MAPT* (cyan). Shaded areas represent 95% confidence intervals. *C9orf72*, chromosome 9 open reading frame 72; CBF, cerebral blood flow; *GRN*, progranulin; *MAPT*, microtubule-associated protein tau.

controls, albeit to varying degrees. The greatest rate of perfusion decline relative to non-carrier controls was demonstrated by the *GRN* group ($\beta_{int} = -2.4 \pm 0.5$ mL/min/100 g/year; $t[555] = -4.9$; $P < 0.001$), followed by *C9orf72* ($\beta_{int} = -1.5 \pm 0.6$ mL/min/100 g/year; $t[579] = -2.6$; $P = 0.009$) and finally the *MAPT* group ($\beta_{int} = -1.1 \pm 0.7$ mL/min/100 g/year; $t[542] = -1.4$; $P = 0.15$).

Post hoc analysis of the global perfusion model (Table 2) illustrated that lowered perfusion relative to non-carrier controls could be identified as early as 1 year after baseline assessment in both *GRN* (-2.22 ± 0.65 mL/min/100 g; $P = 0.002$) and *MAPT* (-2.69 ± 0.90 mL/min/100 g; $P = 0.009$) groups. Both groups also maintained significant lowered perfusion as late as 6 years post-baseline assessment. The *C9orf72* group also demonstrated significantly lowered global gray matter perfusion relative to controls by 2 years after baseline assessment (-2.96 ± 0.86 mL/min/100 g; $P = 0.002$) and maintained this significant difference onward.

3.3 | Global gray matter structural changes

Measures extracted from linear mixed effects models of global tissue volumes (Table 1) demonstrated that only the *C9orf72* group featured a measurable degree of gray matter atrophy as early as baseline relative to non-carrier controls (-19.3 ± 5.12 mm³; $P = 0.002$), with no significant differences in gray matter volume found for *GRN* (-1.1 ± 4.2

mm³; $P = 0.8$) or *MAPT* (0.7 ± 5.9 mm³; $P = 0.9$). However, no significant interaction was observed between the group effect and time (Figure S2 in supporting information), indicating no significant differences in the rates of global gray matter change within the approximate 5-year period for this population.

3.4 | Regional perfusion changes

Tables 3 and 4 show the coefficients for the main effect of time from baseline (β) as well as the interaction coefficients (β_{int}) for each of the three presymptomatic genetic subgroups relative to the reference non-carrier control group. Negative values indicate a more pronounced decline in perfusion over time relative to non-carrier controls. Figure 2 represents the regions that survived Bonferroni correction as t values overlaid upon axial brain slices.

The main effect of time from baseline was significant in certain ROIs and demonstrated a trend of hypoperfusion occurring in participants as a function of time. However, the interaction effects between time from baseline and presymptomatic genetic subgroups were generally far more pronounced in one or more of the presymptomatic genetic subgroups than this main effect alone. Additionally, the coefficients for the main effects of presymptomatic genetic subgroups within the interaction model were not significant ($P > 0.05$) in any region and therefore not presented in Table 3 or Table 4.

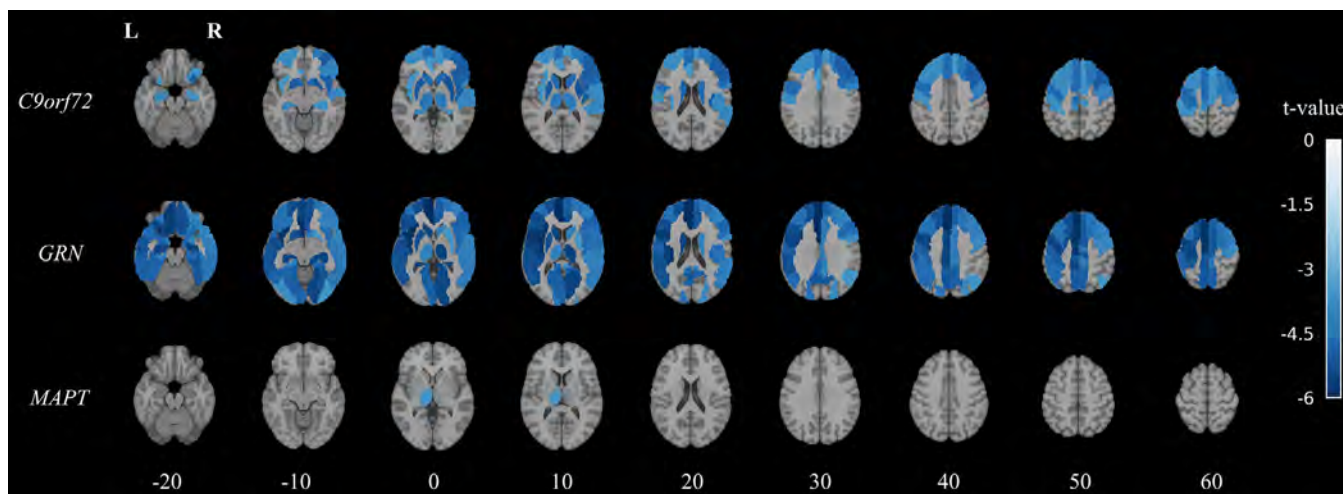


FIGURE 2 Statistical axial slice maps derived from the mixed effects region of interest analysis examining the interaction effect between mutation status (presymptomatic carrier versus non-carrier control) and time from baseline for each of the carrier groups. Colors represent Satterthwaite-approximated *t* values from regions which survived familywise error correction at *P* value < 0.05. Images are shown in neurological display convention, overlaid on top of the Montreal Neurological Institute 152 T1-weighted template image. *C9orf72*, chromosome 9 open reading frame 72; *GRN*, progranulin; L, left; *MAPT*, microtubule-associated protein tau; R, right.

Presymptomatic *C9orf72* carriers featured prominent changes in longitudinal perfusion in the frontal lobe; certain subcortical structures such as the caudate, putamen, and hippocampus; as well as the thalamus (Tables 3 and 4). Interestingly, while most significant regions were bilateral, a slight rightward asymmetry was observable across the inferior frontal lobe, with significant regions coming from the pars opercularis, pars orbitalis, pars triangularis, and orbitofrontal cortical regions, as well as the right superior temporal gyrus.

Coinciding with the global gray matter changes in perfusion, the presymptomatic *GRN* carriers featured more prominent decreases in perfusion over time relative to controls in a far more widespread manner, with nearly all regions demonstrating a significant effect. Notably, a leftward asymmetric effect is evident, as left hemispheric regions tended to demonstrate stronger effects based on *t* values and interaction coefficients than in similar right hemispheric regions (Tables 3 and 4).

MAPT presymptomatic carriers only showed significant decreases in perfusion over time in the left thalamus, an area that was also significant for *C9orf72* as well as *GRN* carriers, highlighting a region that is commonly affected in all genetic subgroups of FTD. No regions featured any significant increase in perfusion in any presymptomatic genetic subgroup relative to non-carrier controls.

3.5 | Perfusion in presymptomatic carriers beyond their expected year of symptom onset versus converters

Mutation-positive converters pooled across genetic subgroups ($n = 19$; *C9orf72* = 7, *GRN* = 8, *MAPT* = 4) demonstrated a significant decline in perfusion from baseline based on their last follow-up scan compared

to presymptomatic carriers who went beyond their expected age of symptom onset ($n = 22$; *C9orf72* = 6, *GRN* = 14, *MAPT* = 2) without showing symptoms or signs of FTD (Table 5). These regions included the right middle frontal gyrus, inferior frontal gyrus pars triangularis, dorsolateral superior frontal gyrus, and posterior orbitofrontal cortex.

4 | DISCUSSION

This longitudinal study has identified specific patterns of perfusion decline in the most prevalent genetic subsets of FTD (i.e., *C9orf72*, *GRN*, and *MAPT*) at the presymptomatic stage. We have found that all genetic subgroups feature a more significant degree of global gray matter perfusion decrease over time relative to healthy controls. This contrasted with a structural analysis examining global brain volumes, which only detected gray matter atrophy in the *C9orf72* group at baseline, in agreement with the prior literature,^{15,19} and which did not detect significant differences in rates of global gray matter volume change over time between any of the studied genetic subgroups. This observation highlights additional gains provided by cerebral perfusion measures longitudinally in the study of presymptomatic genetic FTD on top of volumetric analysis alone. Post hoc analysis further identified that significant hypoperfusion is detectable as early as year 1 follow-up in *GRN* and *MAPT* subsets, and in *C9orf72* by year 2 follow-up. Given that metrics typically used within FTD clinical practice could not differentiate presymptomatic groups from controls, these findings are strongly attributable to the effect of the disease mutation over nuisance factors such as age alone. Another key result was that the presymptomatic genetic subgroups featured their own regional patterns of perfusion decline, with *C9orf72* being focused around the frontal lobe with a slight right hemispheric bias, *GRN* featuring a more

TABLE 2 Post hoc marginal means estimation of whole brain gray matter perfusion differences between presymptomatic carriers versus non-carrier controls at fixed time points.

Time from baseline (years)	C9orf72 presymptomatic carriers minus non-carrier controls			GRN presymptomatic carriers minus non-carrier controls			MAPT presymptomatic carriers minus non-carrier controls		
	Estimate (mL/min/100 g)	df/T-ratio	P value	Estimate (mL/min/100 g)	df/T-ratio	P value	Estimate (mL/min/100 g)	df/T-ratio	P value
0	0.35 ± 1.01	631.2/0.35	1	0.44 ± 0.85	653.03/0.52	1	-1.55 ± 1.19	673.47/-1.3	0.580
1	-1.31 ± 0.79	301.59/-1.66	0.291	-2.22 ± 0.65	306.74/-3.42	0.002	-2.69 ± 0.90	303.33/-2.99	0.009
2	-2.96 ± 0.86	273.04/-3.46	0.002	-4.88 ± 0.72	337.04/-6.75	<0.001	-3.82 ± 1.07	432.75/-3.56	0.001
3	-4.62 ± 1.16	452.39/-3.97	<0.001	-7.54 ± 1.01	607.45/-7.45	<0.001	-4.95 ± 1.56	741.42/-3.17	0.005
4	-6.28 ± 1.58	627.34/-3.98	<0.001	-10.2 ± 1.39	762.33/-7.35	<0.001	-6.08 ± 2.17	798.69/-2.81	0.015
5	-7.93 ± 2.03	720.62/-3.91	<0.001	-12.86 ± 1.8	797.19/-7.16	<0.001	-7.21 ± 2.81	779.11/-2.57	0.031

Note: Data derived from the primary analysis linear mixed effects model for whole brain gray matter perfusion. Marginal mean estimates represented as mean ± standard error. P values were adjusted using Bonferroni correction. Bold emphasis has been placed on P values that are ≤ 0.05 after Bonferroni correction. Abbreviations: C9orf72, chromosome 9 open reading frame 72; df, degree of freedom; GRN, progranulin; MAPT, microtubule-associated protein tau.

global and left hemispheric bias, and MAPT restricted to the left thalamus. These observations suggest the utility of longitudinal cerebral perfusion as an imaging biomarker differentiating between the major genetic subgroups of FTD at this presymptomatic disease stage. We also identified that conversion into the symptomatic FTD stage was associated with hypoperfusion in several right hemispheric frontal lobe regions. Our study is therefore the first to indicate the potential protective effects of maintaining regional cerebral perfusion and suggest its possible utility as a measure of drug efficacy in terms of slowing down FTD disease progression. Altogether, the findings of this study indicate that cerebral perfusion, as measured by ASL, has the characteristics of a promising biomarker for assessing disease progression in genetic FTD prior to symptom onset.

This body of work adds to the growing evidence that the salience network, which is involved in guiding behavior and attention, is fundamentally tied to FTD disease progression.⁴⁰ Presymptomatic C9orf72 and GRN groups demonstrated declining perfusion in several key component areas of this network, including the insula and anterior cingulate cortex, as well as the posterior orbitofrontal cortex, which projects into the network.^{41,42} Both C9orf72 and GRN mutations most commonly present with the behavioral variant of FTD (bvFTD), which is functionally related to the salience network. Within the GENFI cohort, most symptomatic individuals had a bvFTD presentation.²⁰ Our perfusion findings are also consistent with observations of other genetic FTD neuroimaging studies that have identified connectivity reductions and gray matter atrophy in this network for presymptomatic and symptomatic individuals, respectively.^{18,19,21} Furthermore, it has been posited that von Economo neurons (VENs), cells that are concentrated within layer Vb of the of the cortex involved in salience network function, are particularly susceptible to pathology in the early stages of the FTD.⁴³ Indeed, TAR DNA-binding protein 43 (TDP-43) proteinopathy, which is the dominant inclusion in C9orf72 and GRN subsets of genetic FTD,⁵ has been detected within right fronto-insular VENs and is associated with salience network atrophy.⁴⁴ Within this study, the right hemispheric posterior orbitofrontal regions also showed significant hypoperfusion in converters compared to non-converters who went beyond their EYO, the bulk of which were C9orf72 and GRN individuals. In an earlier GENFI analysis of mutation carriers versus non-carriers, the insula featured neuroanatomical differences as early as 25 and 15 years prior to symptom onset for C9orf72 and GRN carriers, respectively.²⁰ From this collective evidence, we speculate that in C9orf72 and GRN genetic subgroups, there is a TDP-43-based neurodegenerative mechanism at play which targets the salience network at very early stages of the disease, with initial proteinopathy burden manifesting as local functional changes (hypoperfusion and connectivity loss) before translating into gross structural atrophy, and finally presenting as bvFTD in the clinic. We also speculate that certain genetic subgroups may exhibit either leftward or rightward frontal bias for the salience network, as the latter was evident in the C9orf72 subset of this study and is consistent with prior imaging and pathological case series.^{45,46} Future longitudinal neuroimaging studies will need to incorporate a complex multimodal approach on the same cohort to assess these conjectures.

TABLE 3 Longitudinal region of interest analysis comparing cerebral perfusion between presymptomatic carriers of each major FTD mutation and non-carrier controls modeled based on time from baseline and its interaction with carrier group within the left hemisphere.

Region	β	P	C9orf72		GRN		MAPT	
			β_{int}	P_{int}	β_{int}	P_{int}	β_{int}	P_{int}
Amygdala	-0.37 ± 0.3	1	-1.38 ± 0.62	1	-2.66 ± 0.55	<0.001	-0.86 ± 0.86	1
Angular gyrus	-0.82 ± 0.37	1	-1.62 ± 0.78	1	-3.26 ± 0.69	<0.001	-0.25 ± 1.07	1
Anterior cingulate cortex	-0.57 ± 0.35	1	-2.55 ± 0.73	0.045	-3.97 ± 0.65	<0.001	-0.8 ± 1.01	1
Anterior orbitofrontal cortex	-1.69 ± 0.34	<0.001	-1.1 ± 0.7	1	-2.77 ± 0.63	0.001	0.23 ± 0.97	1
Calcarine fissure	-1.08 ± 0.43	1	-1.18 ± 0.89	1	-3.87 ± 0.79	<0.001	-2.62 ± 1.22	1
Caudate nucleus	-0.45 ± 0.27	1	-2.61 ± 0.56	<0.001	-2.7 ± 0.49	<0.001	-0.79 ± 0.77	1
Dorsolateral superior frontal gyrus	-1.28 ± 0.33	0.012	-2.62 ± 0.7	0.016	-3.27 ± 0.62	<0.001	-0.71 ± 0.96	1
Fusiform gyrus	-0.54 ± 0.3	1	-1.0 ± 0.62	1	-2.68 ± 0.56	<0.001	-1.39 ± 0.87	1
Gyrus rectus	-0.17 ± 0.35	1	-1.52 ± 0.74	1	-3.72 ± 0.66	<0.001	-0.64 ± 1.03	1
Heschl's gyrus	-0.33 ± 0.38	1	-2.65 ± 0.79	0.072	-3.96 ± 0.7	<0.001	-1.32 ± 1.08	1
Hippocampus	-0.39 ± 0.28	1	-2.32 ± 0.59	0.009	-2.88 ± 0.53	<0.001	-1.55 ± 0.83	1
Inferior frontal gyrus pars opercularis	-0.56 ± 0.36	1	-2.54 ± 0.74	0.061	-3.81 ± 0.66	<0.001	-1.51 ± 1.02	1
Inferior frontal gyrus pars orbitalis	-1.11 ± 0.36	0.175	-1.45 ± 0.75	1	-3.01 ± 0.66	<0.001	-1.28 ± 1.03	1
Inferior frontal gyrus pars triangularis	-0.69 ± 0.35	1	-2.07 ± 0.74	0.454	-3.47 ± 0.65	<0.001	-1.31 ± 1.01	1
Inferior occipital gyrus	-0.95 ± 0.4	1	-0.68 ± 0.84	1	-2.84 ± 0.75	0.014	-0.59 ± 1.15	1
Inferior parietal gyrus	-1.06 ± 0.36	0.261	-1.34 ± 0.74	1	-3.01 ± 0.66	<0.001	-0.44 ± 1.02	1
Inferior temporal gyrus	-0.83 ± 0.27	0.167	0.18 ± 0.56	1	-2.41 ± 0.49	<0.001	-0.62 ± 0.76	1
Insular cortex	-0.46 ± 0.31	1	-2.34 ± 0.66	0.035	-3.4 ± 0.58	<0.001	-0.97 ± 0.9	1
Lateral orbitofrontal cortex	-1.4 ± 0.39	0.036	-0.67 ± 0.81	1	-2.52 ± 0.72	0.045	-0.81 ± 1.12	1
Lingual gyrus	-0.48 ± 0.36	1	-2.0 ± 0.75	0.729	-3.31 ± 0.67	<0.001	-2.37 ± 1.04	1
Medial orbitofrontal cortex	-0.66 ± 0.3	1	-1.01 ± 0.64	1	-3.24 ± 0.57	<0.001	-0.26 ± 0.88	1
Medial superior frontal gyrus	-0.63 ± 0.31	1	-3.03 ± 0.65	<0.001	-3.53 ± 0.58	<0.001	-0.9 ± 0.9	1
Medial-orbital superior frontal gyrus	-0.83 ± 0.36	1	-1.88 ± 0.76	1	-3.77 ± 0.68	<0.001	0.27 ± 1.05	1
Middle cingulate cortex	-0.97 ± 0.32	0.214	-1.94 ± 0.67	0.335	-3.26 ± 0.59	<0.001	-0.73 ± 0.91	1
Middle frontal gyrus	-1.23 ± 0.35	0.047	-2.79 ± 0.74	0.014	-2.96 ± 0.65	<0.001	-0.98 ± 1.02	1
Middle occipital gyrus	-1.3 ± 0.4	0.096	-0.76 ± 0.83	1	-2.41 ± 0.74	0.099	-0.23 ± 1.14	1
Middle temporal gyrus	-0.7 ± 0.3	1	-1.09 ± 0.62	1	-2.87 ± 0.55	<0.001	0.16 ± 0.86	1
Middle temporal pole	-0.52 ± 0.34	1	1.37 ± 0.7	1	-2.06 ± 0.63	0.095	-1.52 ± 0.97	1
Olfactory cortex	0.24 ± 0.35	1	-2.12 ± 0.74	0.369	-3.97 ± 0.66	<0.001	-0.73 ± 1.03	1
Paracentral lobule	-0.92 ± 0.33	0.478	-2.7 ± 0.69	0.009	-3.1 ± 0.61	<0.001	-0.51 ± 0.94	1
Parahippocampal gyrus	-0.37 ± 0.29	1	-0.75 ± 0.61	1	-2.28 ± 0.54	0.003	-1.04 ± 0.85	1
Postcentral gyrus	-0.71 ± 0.32	1	-2.47 ± 0.67	0.022	-2.92 ± 0.59	<0.001	-0.46 ± 0.92	1
Posterior cingulate cortex	-0.86 ± 0.4	1	-2.21 ± 0.84	0.768	-3.56 ± 0.74	<0.001	-2.45 ± 1.15	1
Posterior orbitofrontal cortex	-1.09 ± 0.31	0.040	-1.59 ± 0.64	1	-3.09 ± 0.57	<0.001	-0.93 ± 0.89	1
Precentral gyrus	-0.83 ± 0.34	1	-3.28 ± 0.71	<0.001	-3.43 ± 0.63	<0.001	-0.8 ± 0.98	1
Precuneus cortex	-0.94 ± 0.35	0.664	-1.97 ± 0.73	0.649	-3.3 ± 0.65	<0.001	-1.52 ± 1.0	1
Putamen	-0.13 ± 0.27	1	-2.82 ± 0.57	<0.001	-2.64 ± 0.5	<0.001	-1.31 ± 0.78	1
Rolandic operculum	-0.39 ± 0.34	1	-2.01 ± 0.7	0.395	-3.5 ± 0.63	<0.001	-0.63 ± 0.97	1
Superior occipital gyrus	-1.33 ± 0.43	0.163	-1.81 ± 0.89	1	-3.53 ± 0.79	<0.001	-1.95 ± 1.22	1
Superior parietal gyrus	-1.54 ± 0.37	0.003	-1.1 ± 0.78	1	-1.85 ± 0.69	0.661	0.26 ± 1.06	1

(Continues)

TABLE 3 (Continued)

Region	β	P	C9orf72		GRN		MAPT	
			β_{int}	P_{int}	β_{int}	P_{int}	β_{int}	P_{int}
Superior temporal gyrus	-0.67 ± 0.32	1	-1.83 ± 0.67	0.574	-3.16 ± 0.59	<0.001	-0.66 ± 0.92	1
Superior temporal pole	-0.71 ± 0.31	1	-0.01 ± 0.65	1	-2.75 ± 0.58	<0.001	-1.25 ± 0.89	1
Supplementary motor area	-0.6 ± 0.3	1	-2.86 ± 0.62	<0.001	-3.21 ± 0.55	<0.001	-0.99 ± 0.85	1
Supramarginal gyrus	-0.58 ± 0.33	1	-1.98 ± 0.69	0.373	-3.19 ± 0.61	<0.001	-1.37 ± 0.95	1
Thalamus	-0.67 ± 0.36	1	-3.19 ± 0.75	0.002	-2.69 ± 0.66	0.005	-3.58 ± 1.03	0.050

Note: β refers to the main effect of time from baseline. The interaction coefficients (β_{int}) represent the difference in perfusion change over time between a given presymptomatic carrier group relative to non-carrier controls. Coefficients reported as value ± standard error. P values for the main effect of time from baseline (P) and for the interaction effects (P_{int}) were adjusted using Bonferroni correction, presented here. Bold emphasis has been placed on P values that are ≤ 0.05 after Bonferroni correction.

Abbreviations: C9orf72, chromosome 9 open reading frame 72; FTD, frontotemporal dementia; GRN, progranulin; MAPT, microtubule-associated protein tau.

TABLE 4 Longitudinal region of interest analysis comparing cerebral perfusion between presymptomatic carriers of each major FTD mutation and non-carrier controls modeled based on time from baseline and its interaction with carrier group within the right hemisphere.

Region	β	P	C9orf72		GRN		MAPT	
			β_{int}	P_{int}	β_{int}	P_{int}	β_{int}	P_{int}
Amygdala	-0.62 ± 0.27	1	-1.35 ± 0.57	1	-2.05 ± 0.5	0.005	-0.44 ± 0.78	1
Angular gyrus	-0.95 ± 0.39	1	-0.99 ± 0.82	1	-2.57 ± 0.72	0.037	-1.54 ± 1.12	1
Anterior cingulate cortex	-0.69 ± 0.34	1	-1.85 ± 0.7	0.801	-3.24 ± 0.63	<0.001	-0.18 ± 0.97	1
Anterior orbitofrontal cortex	-1.66 ± 0.35	<0.001	-1.88 ± 0.73	0.904	-2.56 ± 0.65	0.007	-0.15 ± 1.0	1
Calcarine fissure	-0.88 ± 0.42	1	-1.43 ± 0.88	1	-4.29 ± 0.78	<0.001	-2.34 ± 1.21	1
Caudate nucleus	-0.78 ± 0.27	0.330	-2.62 ± 0.56	<0.001	-2.03 ± 0.49	0.004	-0.94 ± 0.76	1
Dorsolateral superior frontal gyrus	-1.38 ± 0.33	0.003	-2.98 ± 0.69	0.002	-2.76 ± 0.61	<0.001	-1.18 ± 0.95	1
Fusiform gyrus	-0.55 ± 0.28	1	-0.75 ± 0.59	1	-2.7 ± 0.53	<0.001	-0.83 ± 0.82	1
Gyrus rectus	-0.44 ± 0.32	1	-0.98 ± 0.68	1	-3.24 ± 0.61	<0.001	0.17 ± 0.94	1
Heschl's gyrus	-0.89 ± 0.39	1	-2.35 ± 0.82	0.384	-2.93 ± 0.73	0.006	-1.01 ± 1.13	1
Hippocampus	-0.38 ± 0.28	1	-2.16 ± 0.6	0.028	-2.92 ± 0.53	<0.001	-1.23 ± 0.82	1
Inferior frontal gyrus pars opercularis	-0.7 ± 0.35	1	-3.49 ± 0.74	<0.001	-3.0 ± 0.66	<0.001	-2.41 ± 1.01	1
Inferior frontal gyrus pars orbitalis	-1.23 ± 0.37	0.075	-3.09 ± 0.77	0.006	-2.76 ± 0.68	0.005	-1.03 ± 1.05	1
Inferior frontal gyrus pars triangularis	-0.6 ± 0.34	1	-3.57 ± 0.72	<0.001	-3.07 ± 0.64	<0.001	-1.57 ± 0.98	1
Inferior occipital gyrus	-0.86 ± 0.44	1	-0.03 ± 0.93	1	-2.94 ± 0.82	0.032	-0.29 ± 1.27	1
Inferior parietal gyrus	-1.04 ± 0.39	0.710	-1.51 ± 0.82	1	-2.44 ± 0.73	0.074	-1.77 ± 1.12	1
Inferior temporal gyrus	-0.7 ± 0.28	1	-0.87 ± 0.59	1	-2.28 ± 0.52	0.001	-0.6 ± 0.81	1
Insular cortex	-0.61 ± 0.34	1	-3.58 ± 0.72	<0.001	-3.01 ± 0.64	<0.001	-1.89 ± 0.99	1
Lateral orbitofrontal cortex	-1.4 ± 0.42	0.088	-1.87 ± 0.84	1	-2.28 ± 0.81	0.476	0.02 ± 1.14	1
Lingual gyrus	-0.29 ± 0.35	1	-1.92 ± 0.74	0.870	-3.58 ± 0.65	<0.001	-1.77 ± 1.01	1
Medial orbitofrontal cortex	-1.09 ± 0.31	0.036	-2.17 ± 0.64	0.063	-2.94 ± 0.57	<0.001	0.19 ± 0.88	1
Medial superior frontal gyrus	-0.78 ± 0.31	1	-2.36 ± 0.65	0.028	-2.91 ± 0.58	<0.001	-0.64 ± 0.9	1
Medial-orbital superior frontal gyrus	-1.05 ± 0.36	0.319	-1.45 ± 0.75	1	-3.52 ± 0.67	<0.001	0.52 ± 1.04	1
Middle cingulate cortex	-0.98 ± 0.32	0.204	-1.67 ± 0.67	1	-2.54 ± 0.6	0.002	-0.31 ± 0.92	1

(Continues)

TABLE 4 (Continued)

Region	β	P	C9orf72		GRN		MAPT	
			β_{int}	P_{int}	β_{int}	P_{int}	β_{int}	P_{int}
Middle frontal gyrus	-1.12 ± 0.35	0.123	-3.59 ± 0.73	<0.001	-2.7 ± 0.65	0.003	-1.95 ± 1.0	1
Middle occipital gyrus	-1.33 ± 0.43	0.187	-0.52 ± 0.9	1	-2.11 ± 0.79	0.731	-2.01 ± 1.22	1
Middle temporal gyrus	-0.78 ± 0.32	1	-1.47 ± 0.68	1	-2.54 ± 0.6	0.002	-1.14 ± 0.93	1
Middle temporal pole	-0.37 ± 0.32	1	-0.39 ± 0.68	1	-2.18 ± 0.6	0.029	-1.05 ± 0.93	1
Olfactory cortex	-0.41 ± 0.33	1	-1.95 ± 0.7	0.466	-3.02 ± 0.62	<0.001	0.19 ± 0.97	1
Paracentral lobule	-0.78 ± 0.32	1	-2.29 ± 0.67	0.063	-2.53 ± 0.59	0.002	0.16 ± 0.91	1
Parahippocampal gyrus	-0.34 ± 0.28	1	-0.95 ± 0.58	1	-2.4 ± 0.52	<0.001	-0.75 ± 0.8	1
Postcentral gyrus	-1.08 ± 0.31	0.053	-1.86 ± 0.65	0.399	-1.77 ± 0.58	0.205	-1.1 ± 0.89	1
Posterior cingulate cortex	-1.05 ± 0.41	0.924	-2.76 ± 0.86	0.121	-2.92 ± 0.76	0.012	-2.35 ± 1.18	1
Posterior orbitofrontal cortex	-1.26 ± 0.32	0.009	-2.5 ± 0.68	0.022	-2.54 ± 0.6	0.002	-0.34 ± 0.93	1
Precentral gyrus	-0.9 ± 0.36	1	-3.1 ± 0.75	0.003	-2.55 ± 0.66	0.011	-1.75 ± 1.02	1
Precuneus cortex	-0.88 ± 0.35	1	-1.65 ± 0.74	1	-3.21 ± 0.65	<0.001	-1.49 ± 1.01	1
Putamen	-0.42 ± 0.27	1	-2.9 ± 0.57	<0.001	-1.79 ± 0.5	0.038	-0.99 ± 0.78	1
Rolandic operculum	-0.54 ± 0.33	1	-2.69 ± 0.7	0.011	-2.76 ± 0.62	<0.001	-1.68 ± 0.95	1
Superior occipital gyrus	-1.47 ± 0.43	0.064	-0.17 ± 0.91	1	-3.09 ± 0.8	0.012	-1.98 ± 1.24	1
Superior parietal gyrus	-1.25 ± 0.36	0.055	-1.57 ± 0.76	1	-1.81 ± 0.67	0.654	-0.36 ± 1.04	1
Superior temporal gyrus	-0.48 ± 0.33	1	-2.7 ± 0.69	0.010	-2.54 ± 0.61	0.003	-1.7 ± 0.95	1
Superior temporal pole	-0.8 ± 0.31	0.918	-1.76 ± 0.65	0.645	-2.35 ± 0.58	0.005	-0.78 ± 0.9	1
Supplementary motor area	-0.51 ± 0.3	1	-2.35 ± 0.63	0.021	-2.86 ± 0.56	<0.001	-0.59 ± 0.87	1
Supramarginal gyrus	-0.69 ± 0.36	1	-1.62 ± 0.76	1	-2.3 ± 0.67	0.061	-1.99 ± 1.04	1
Thalamus	-0.34 ± 0.35	1	-3.09 ± 0.73	0.003	-3.58 ± 0.65	<0.001	-2.89 ± 1.01	0.381

Note: β refers to the main effect of time from baseline. The interaction coefficients (β_{int}) represent the difference in perfusion change over time between a given presymptomatic carrier group relative to non-carrier controls. Coefficients reported as value ± standard error. P values for the main effect of time from baseline (P) and for the interaction effects (P_{int}) were adjusted using Bonferroni correction, presented here. Bold emphasis has been placed on P values that are ≤ 0.05 after Bonferroni correction.

Abbreviations: C9orf72, chromosome 9 open reading frame 72; FTD, frontotemporal dementia; GRN, progranulin; MAPT, microtubule-associated protein tau.

The observation that the rate of global gray matter perfusion decline was most prominent in GRN and that it featured hypoperfusion relative to controls as early as 1 year after baseline measurement coincides with observed atrophy rates of this FTD genotype relative to others.⁴⁷ Indeed, there is some evidence for disease acceleration to be more prominent in non-tau variants, which would coincide with both GRN and C9orf72 genotype groups featuring steeper global gray matter perfusion declines compared to MAPT.⁴⁸ This widespread hypoperfusion seen in presymptomatic GRN carriers has been previously noted by Dopfer et al.¹² However, it is also important to note that this GRN group has the most statistical power within GENFI and had the largest number of follow-up visits, which increases the probability of Type 1 statistical errors, even considering stringent multiple-testing correction, such as Bonferroni's method. As in the Dopfer et al. study,¹² our results also demonstrate a left-hemisphere asymmetry in terms of hypoperfusion effect size, which is in line with previous literature observing an asymmetric impact on the brain for this genotype.^{17,20,49} This may link to prior findings that GRN carriers also present as non-fluent-variant primary progressive aphasia (nfvPPA),⁵⁰ which is associated with atrophy and metabolic/perfusion decline

involving the left frontal region.⁵¹ One of the most prominent regions of hypometabolism within the GRN subgroup was in the left inferior frontal lobe pars opercularis, a region considered to have the earliest involvement in nfvPPA.⁵⁰ This region constitutes the main portion of Broca's speech area, which is primarily associated with the motor aspects of language production.⁵² Our hypoperfusion results in the GRN subgroup are also consistent with nfvPPA presenting with executive dysfunction alongside hypometabolism seen in the orbitofrontal cortex, anterior cingulate cortex, insula, precentral and postcentral gyrus, and thalamus.⁵³

The single common area of hypoperfusion observed across all presymptomatic genetic FTD subgroups was the thalamus. The thalamus is a complex association of 50 to 60 subnuclei that serves as a central signal-integration hub interconnected with networks that pass motor, visual, auditory, and somatosensory information to various cortical destinations.⁵⁴ While initial reports demonstrated atrophy of this structure in C9orf72 carriers,¹⁹ there have since been updates in the literature showing that both GRN and MAPT also feature thalamic atrophy.^{55,56} Post mortem analyses confirm the thalamus is impacted in FTD,⁵⁶⁻⁵⁸ with one study finding that, compared to controls, patients

TABLE 5 Analysis of covariance results for converters versus presymptomatics past their expected year of disease onset.

Region of interest	Between-groups delta	F value	P value uncorrected	Partial eta squared
Right middle frontal gyrus	-11.73	12.02	0.001	0.25
Right inferior frontal gyrus pars triangularis	-9.73	4.99	0.032	0.12
Right dorsolateral superior frontal gyrus	-8.28	4.78	0.035	0.11
Right posterior orbitofrontal cortex	-7.43	4.51	0.040	0.11
Right thalamus	-9.95	3.88	0.056	0.09
Left postcentral gyrus	-6.82	3.78	0.060	0.09
Left paracentral lobule	-9.14	3.71	0.063	0.11
Left precentral gyrus	-7.19	3.62	0.065	0.09
Right medial superior frontal gyrus	-6.63	2.98	0.093	0.07
Left middle frontal gyrus	-5.88	2.47	0.124	0.06
Right insular cortex	-7.00	2.46	0.126	0.06
Right inferior frontal gyrus pars orbitalis	-7.37	2.28	0.140	0.06
Right inferior frontal gyrus Pars opercularis	-6.95	2.04	0.162	0.05
Right caudate nucleus	-5.50	1.80	0.188	0.05
Right precentral gyrus	-6.18	1.58	0.217	0.04
Left dorsolateral superior frontal gyrus	-3.96	1.15	0.291	0.03
Right hippocampus	-4.87	1.07	0.307	0.03
Right supplementary motor area	-4.82	0.98	0.328	0.03
Left thalamus	-4.81	0.75	0.392	0.02
Left medial superior frontal gyrus	-3.03	0.67	0.417	0.02
Right rolandic operculum	-4.24	0.63	0.433	0.02
Left insular cortex	-3.20	0.60	0.443	0.02
Right putamen	-2.92	0.33	0.568	0.01
Right superior temporal gyrus	-2.75	0.28	0.600	0.01
Left hippocampus	1.35	0.23	0.633	0.01
Left anterior cingulate cortex	-1.55	0.14	0.710	0.00
Left putamen	0.85	0.09	0.767	0.00
Left supplementary motor area	-1.73	0.02	0.877	0.00
Left caudate nucleus	-0.67	0.01	0.924	0.00

Note: F values correspond to the main effect between the two groups. Between-groups delta refers to the difference between the degree of perfusion decline in the converters vs. presymptomatics past their expected year of onset. Statistics for the covariates of age and sex have been omitted. Partial eta squared has been included as a measure of effect size.

with tau pathology showed similar degrees of thalamic volume reductions to those with TDP-43 pathology.⁵⁵ Within the GENFI cohort itself, a neuroanatomical study found that thalamic volume reduction was evident in *C9orf72* subjects at the presymptomatic stage, and in both *GRN* and *MAPT* subjects by the time they scored ≥ 1 on CDR plus NACC FTLD.⁵⁹ These findings support the proposition that FTD may progress along large-scale white matter networks,⁶⁰ occurring at different rates for each genotype. Under such a hypothesis, it would not be surprising that one of the most interconnected regions of the brain features some perfusion decline in all FTD genetic subgroups. There is some evidence to suggest that subregions of the thalamus are relevant neuroanatomical structures in delineating variants of FTD, as seen in a meta-analysis of studies reporting on vol-

ume reductions in thalamic subregions, with differing patterns across phenotypes, genotypes, and identified pathology.⁵⁶ However, given the currently limited spatial resolution of ASL, only the overall left and right hemisphere equivalents of the thalamus could be reliably investigated.

This multicenter study is the largest longitudinal cerebral perfusion analysis in genetic FTD to date and assesses perfusion changes over time within all major genetic subgroups of FTD. The ASL analysis pipeline used was selected due to its adherence to ASL processing standards and ability to adjust for multicenter scanner, sequence, and software sources of variability.^{26,29} Site and acquisition effects were also corrected for with the biasfield intensity normalization semi-automatic spatial coefficient of variation quality control.^{13,31} Gray

matter atrophy effects were accounted for through robust regression-based partial volume correction.³⁴ Sensitivity analyses confirmed that individuals who were excluded due to these corrective measures were not significantly different by demographic and clinical measures. The decline in perfusion was also detectable in non-carrier controls in global gray matter, albeit to a lesser extent than in mutation carriers, and this is in agreement with ASL studies of aging in healthy populations.^{39,61,62} This study is not without its limitations. We were unable to account for several variables that are known to contribute both to inter- and intra-individual perfusion variation over time, including diurnal effects, caffeine consumption, post-prandial status, among other factors.⁶³ Additionally, the fewer number of follow-up visits and participants in the *MAPT* subgroup may have contributed to the less steep rate of perfusion decline observed in whole brain gray matter analysis for that subset versus *C9orf72* or *GRN*. Finally, not all scanners were able to accommodate measuring perfusion within the cerebellum, a region that has been noted to feature some atrophy in *C9orf72* carriers.^{15,19}

To conclude, this study has demonstrated that cerebral perfusion carries the characteristics of a potential biomarker for FTD. It differentiated all presymptomatic carriers from non-carriers, delineated variants of the disease from one another in terms of the regional pattern of perfusion decline, and showed promise in highlighting regions that feature the greatest change for participants who converted into a FTD phenotype. Ultimately, we hope that these results will not only further elucidate mechanisms leading to FTD that take place at the presymptomatic stage, but also facilitate effective therapeutic trial design to slow or even prevent FTD-related neurodegeneration.⁷

AFFILIATIONS

¹Hurvitz Brain Sciences Program, Sunnybrook Research Institute, Toronto, Ontario, Canada

²Institute of Medical Science, Temerty Faculty of Medicine, University of Toronto, Toronto, Ontario, Canada

³Medical Biophysics, University of Toronto, Toronto, Ontario, Canada

⁴Department of Radiology and Nuclear Medicine, Amsterdam Neuroscience, Amsterdam University Medical Center, Amsterdam, the Netherlands

⁵Helmholtz-Zentrum Dresden-Rossendorf, Institute of Radiopharmaceutical Cancer Research, Dresden, Germany

⁶Department of Brain Repair and Rehabilitation, UCL Queen Square Institute of Neurology, Queen Square, London, UK

⁷Dementia Research Centre, Department of Neurodegenerative Disease, UCL Queen Square Institute of Neurology, Queen Square, London, UK

⁸Tanz Centre for Research in Neurodegenerative Diseases, University of Toronto, Toronto, Ontario, Canada

⁹Memory Clinic, University Health Network, Toronto, Ontario, Canada

¹⁰Division of Neurology, Department of Medicine, Sunnybrook Health Sciences Centre, Toronto, Ontario, Canada

¹¹Rotman Research Institute, Baycrest Health Sciences, Toronto, Ontario, Canada

¹²Cognitive Neurology Research Unit, Sunnybrook Health Sciences Centre, Toronto, Ontario, Canada

¹³Krembil Research Institute, University Health Network, Toronto, Ontario, Canada

¹⁴Department of Neurology, Erasmus Medical Center, Rotterdam, the Netherlands

¹⁵Clinique Interdisciplinaire de Mémoire, CHU de Québec, Département des Sciences Neurologiques, Université Laval, Québec, Québec, Canada

¹⁶Division of Neurology, Fondazione IRCCS Istituto Neurologico Carlo Besta, Milan, Italy

¹⁷Department of Clinical and Experimental Sciences, University of Brescia, Brescia, Italy

¹⁸Department of Biomedical, Surgical and Dental Sciences, University of Milan, Milan, Italy

¹⁹Neurodegenerative Diseases Unit, Fondazione IRCCS Ca' Granda Ospedale Maggiore Policlinico, Milan, Italy

²⁰Department of Clinical Neurosciences, University of Cambridge, Cambridge, UK

²¹Cambridge University Hospitals NHS Trust, University of Cambridge, Cambridge, UK

²²Medical Research Council Cognition and Brain Sciences Unit, University of Cambridge, Cambridge, UK

²³Department of Neurobiology, Care Sciences and Society, Karolinska Institutet, Huddinge, Sweden

²⁴Unit for Hereditary Dementias, Karolinska University Hospital, Solna, Sweden

²⁵Department of Clinical Neurological Sciences, Western University, London, Ontario, Canada

²⁶Department of Neurofarba, University of Florence, Florence, Italy

²⁷Fondazione Don Carlo Gnocchi, Istituto di Ricovero e Cura a Carattere Scientifico, Florence, Italy

²⁸Neurology Department, Faculty of Medicine, University of Lisbon, Lisbon, Portugal

²⁹Nuffield Department of Clinical Neurosciences, Medical Sciences Division, University of Oxford, Oxford, UK

³⁰Department of Brain Sciences, Imperial College London, London, UK

³¹Division of Psychology Communication and Human Neuroscience, Wolfson Molecular Imaging Centre, University of Manchester, Manchester, UK

³²Department of Geriatric Medicine, Klinikum Hochsauerland GmbH, Arnsberg, Germany

³³Department of Nuclear Medicine, Center for Translational Neuro- and Behavioral Sciences University Hospital Essen, Essen, Germany

³⁴Alzheimer's Disease and Other Cognitive Disorders Unit, Hospital Clinic de Barcelona, Barcelona, Spain

³⁵Cognitive Disorders Unit, Department of Neurology, Donostia University Hospital Gipuzkoa Building, Begiristain Dokorea Pasealekua, Donostia-San Sebastian, Gipuzkoa, Spain

³⁶Neuroscience Area, Biodonostia Health Research Institute, Donostia-San Sebastian, Gipuzkoa, Spain

³⁷Department of Neurodegenerative Diseases, Hertie-Institute for Clinical Brain Research and Center of Neurology, University of Tübingen, Tübingen, Germany

³⁸Laboratory for Cognitive Neurology, Department of Neurosciences, KU Leuven, Leuven, Belgium

³⁹Department of Psychiatry, Douglas Mental Health University Institute, McGill University, Montreal, Quebec, Canada

⁴⁰McConnell Brain Imaging Centre, Montreal Neurological Institute and Hospital, Montreal, Quebec, Canada

⁴¹Department of Neurology, Ludwig-Maximilians-University, Munich, Germany

⁴²Munich Cluster of Systems Neurology (SyNergy), Munich, Germany

⁴³Department of Neurology, University of Ulm, Ulm, Germany

⁴⁴Center for Neuroscience and Cell Biology, Faculty of Medicine, University of Coimbra, Coimbra, Portugal

⁴⁵Campbell Family Mental Health Research Institute, Centre for Addiction and Mental Health, Toronto, Ontario, Canada

⁴⁶Edmond J. Safra Parkinson Disease Program & Morton and Gloria Shulman Movement Disorder Unit, Toronto Western Hospital UHN, Toronto, Ontario, Canada

⁴⁷Department of Medicine, Division of Neurology, University of Toronto, Toronto, Ontario, Canada

ACKNOWLEDGMENTS

The authors wish to express their gratitude to the participants, their relatives, and their study partners for taking part in the GENFI study. We also wish to thank the broader neuroscience open-source developer community for their everyday contributions that make up neuroimaging analysis pipelines. M.M. has received funding from two [Canadian Institutes of Health Research](#) (CIHR) project grants (MOP-327387 and PJT-175242) and from the [Weston Brain Institute](#) for the conduct of this study. GENFI was funded by the Medical Research Council UK (MR/M023664/1), the Bluefield Project, the JPND GENFI-PROX grant (by DLR/BMBF 2019-02248), CIHR project grants (MOP-327387 and PJT-175242), and by the [Deutsche Forschungsgemeinschaft](#) (DFG, German Research Foundation) under Germany's Excellence Strategy within the framework of the Munich Cluster for Systems Neurology (EXC 2145 SyNergy – ID 390857198). J.D.R. is supported by an MRC Clinician Scientist Fellowship (MR/M008525/1) as well as funding from the NIHR Rare Disease Translational Research Collaboration (BRC149/NS/MH). J.C.vS, L.C.J., and H.S. have received funding from ZonMW Memorabel (Deltaplan Dementie, 733 051 042). J.B.R. was funded by the National Institute for Health Research Cambridge Biomedical Research Centre (NIHR203312) and the [Medical Research Council](#) (MC_UU_00030/14; MR/T033371/1). M.F. received support from the Saul A. Silverman Family Foundation as a Canada International Scientific Exchange Program, and the [Morris Kerzner Memorial Fund](#). R.S.V. has received funding from the [Instituto de Salud Carlos III](#) (20/0448), cofounded by the [European Union](#). R.V. was funded by the Mady Browaeys Fund for Research into Frontotemporal Degeneration. M.P. received support from the University of Toronto Medical Science Open and Joseph Bazylewicz Fellowships. C.G. received funding from the Swedish FTD Initiative Schörling Foundation, EU Joint Programme Neurodegenerative Disease Research Prefrontals Vetenskapsrådet (Dnr 529-2014-7504), EU Joint Programme Neurodegenerative Disease Research-GENFI-PROX, [Vetenskapsrådet](#) 2019-0224, [Vetenskapsrådet](#) 2015-02926, [Vetenskapsrådet](#) 2018-02754, Alzheimer Foundation, Brain Foundation, Dementia Foundation, and Region Stockholm ALF-project. Funding sources were not involved in the design, data collection, data analysis, decision to publish, nor preparation of the manuscript for this body of work.

CONFLICT OF INTEREST STATEMENT

M.M. holds additional grants unrelated to this work from the Ontario Brain Institute, Washington University, as well as the Women's Brain

Health Initiative and Brain Canada as part of the EU Joint Programme for Neurodegenerative Disease Research; has clinical trials contracts with Roche and Alector; has received consulting fees from Ionis, Alector, Biogen Canada, Wave Life Science, Eisai Canada, and Novo Nordisk Canada; received royalties from the Henry Stewart Talks; has received payments from MINT Memory Clinics and ECHO Dementia Series; and holds unpaid Scientific Advisory Board roles with Alzheimer's Society Canada and Parkinson Canada. A.P.S. is a member on the Board of Directors for Parkinson Canada and the Canadian Academy of Health Sciences. B.B. is waiting on a patent on therapeutic intervention in genetic frontotemporal dementia and has received personal fees from UCB, Lilly, AviadoBio, and Denali. C.G. has received payment from Demensdagarna Örebro 2023, Diakonia Ersta sjukhus, and Göteborgsregionen 2023 and is involved as a leader of the Swedish FTD Initiative. D.C. received support from Alzheimer's Research UK (ARUK-PG2017-1946), the UCL/UCLH NIHR Biomedical Research Centre, and the UK Dementia Research Institute, which receives its funding from DRI Ltd; and holds a chair position in the Alzheimer's Association Neuroimaging Professional Interest Area. D.T.W. holds an unpaid medical advisory board member position for Hydrocephalus Canada. F.M. holds grants from the Tau Consortium (#A1133749), and the Carlos III Health Institute (PI19/01637). I.S. has participated on the board of Novo Nordisk. J.L. has received support from the DFG German Research Foundation under Germany's Excellence Strategy within the framework of the Munich Cluster for Systems Neurology (EXC 2145 SyNergy – ID 390857198); has received personal fees from EISAI and Biogen; has received payments from Abbvie, Bayer Vital, Biogen, EISAI, TEVA, Roche, and Zambon; and is on an advisory board for Axon Neuroscience. J.P. holds grants with the Eurostars-2 joint programme with co-funding from the European Union Horizon 2020 research and innovation program (ASPIRE E!113701), the Dutch Heart Foundation (2020T049), the EU Joint Programme for Neurodegenerative Disease Research, provided by the Netherlands Organisation for Health Research and Development and Alzheimer Nederland DEBBIE (JPND2020-568-106), and the Czech Health Research Council (NU23-08-00460). J.B.R. has received consulting fees from Astex, Curasen, UCB, WAVE, Prevail, and SVHealth; and is a participant on the board of Asceneuron, an Associate Director at the Dementias Platform UK, and a Medical Advisor to both Cumulus Neuro and Astronautx. L.L.R. received support from the Guarantors of Brain and Alzheimer's Research UK. M.S. has received payments from UCB, Prevail, Ionis, Orphazyme, Servier, Reata, AviadoBio, GenOrph, Biohaven, Zavra, and Lilly. M.C.T. has received support from NIH and the Weston Brain Foundation; holds positions as a scientific advisor in the Women's Brain Project, Brain Injury Canada, and PSP Canada; and is involved in clinical trials conducted by Janssen, Biogen, Avanex, Green Valley, and Roche. M.F. is listed on a patent related to methods and kits for differential diagnosis of Alzheimer's disease versus frontotemporal dementia using blood biomarkers. J.D.R. participated on advisory boards for Aviado Bio, Arkuda Therapeutics, Prevail Therapeutics, Denali, and Wave Life Sciences. R.S.V. has received additional support from Sage Pharmaceuticals, outside the present study; has received consulting fees

from Ionis, AviadoBio, Novo Nordisk, Pfizer, and Lilly; has received payments from Neuraxpharma and Roche Diagnostics; has received travel support from Esteve; and participates on the board of Wave Pharmaceuticals. R.V. is in contract with Alector, Denali, Eli Lilly, J&J, UCB, and Biogen; and participates on the boards of AC Immune, and Novartis. S.E.B. has received contracts from Genentech, Optina, Roche, Eli Lilly, Eisai/Biogen Idec, Novo Nordisk, Lilly Avid, and ICON; has received consulting fees from Roche, Biogen, Novo Nordisk, Eisai, and Eli Lilly; has received payments from Biogen, Roche New England Journal Manuscript, Roche Models of Care Analysis in Canada, and Eisai; and has participated on the boards of the Conference Board of Canada, World Dementia Council, University of Rochester Contribution to the Mission and Scientific Leadership of the Small Vessel VCID Biomarker Validation Consortium, and the National Institute of Neurological Disorders and Stroke. S.D. has been sponsored by Biogen, Novo Nordisk, Janssen, Alnylam, Wave Life Sciences, and Passage Bio; has received consulting fees from Eisai, QuRALIS, AI Therapeutics, and Eli Lilly; has received payments from Eisai; and has participated in the boards of IntelGenX and AVIADO Bio. M.O. reports receiving funding from BMBF – FTLD Consortium, the ALS Association, and EU-MIRAIDE; has received consulting fees from Biogen, Axon, Roche, and Grifols; has patents with Foundation state Baden-Wuerttemberg for beta-Syn as a biomarker for neurodegenerative diseases; and participates on the Biogen ATLAS trail board; is a speaker for the FTLD consortium, is involved in an unpaid role with the German Society for CSF Diagnostics and Neurochemistry, and is involved without pay with the Society for CSF Diagnostics and Neurochemistry. M.P., S.M., N.L., H.J.J.M.M., D.T., M.B., S.B.M., E.R., A.B., J.C.v.S., L.C.J., H.S., R.L., P.T., D.G., E.F., S.S., A.d.M., C.B., A.G., and B.J.M. report no conflicts. Author disclosures are available in the [supporting information](#).

CONSENT STATEMENT

Ethical review boards from all sites approved the study protocol and all participating individuals provided written and informed consent in agreement with the Declaration of Helsinki.

ORCID

Maurice Pasternak  <https://orcid.org/0000-0003-0647-172X>

REFERENCES

- Seelaar H, Rohrer JD, Pijnenburg YAL, Fox NC, van Swieten JC. Clinical, genetic, and pathological heterogeneity of frontotemporal dementia: a review. *J Neurology Neurosurg Psychiatry*. 2011;82:476. doi:10.1136/jnnp.2010.212225
- Onyike CU, Diehl-Schmid J. The epidemiology of frontotemporal dementia. *Int Rev Psychiatr*. 2013;25:130-137. doi:10.3109/09540261.2013.776523
- Warren JD, Rohrer JD, Rossor MN. Clinical review. Frontotemporal dementia. *Bmj Clin Res Ed*. 2013;347:f4827. doi:10.1136/bmj.f4827
- Mahoney CJ, Beck J, Rohrer JD, et al. Frontotemporal dementia with the C9ORF72 hexanucleotide repeat expansion: clinical, neuroanatomical and neuropathological features. *Brain*. 2012;135:736-750. doi:10.1093/brain/awr361
- Greaves CV, Rohrer JD. An update on genetic frontotemporal dementia. *J Neurol*. 2019;266:2075-2086. doi:10.1007/s00415-019-09363-4
- Genik B, Sephton CF, Dewey CM, et al. Suberoylanilide hydroxamic acid (vorinostat) up-regulates progranulin transcription. *J Biol Chem*. 2011;286:16101-16108. doi:10.1074/jbc.M110.193433
- Desmarais P, Rohrer JD, Nguyen QD, et al. Therapeutic trial design for frontotemporal dementia and related disorders. *J Neurology Neurosurg Psychiatry*. 2018;90:412-423. doi:10.1136/jnnp-2018-318603
- Bateman RJ, Xiong C, Benzinger TLS, et al. Clinical and biomarker changes in dominantly inherited Alzheimer's disease. *New Engl J Med*. 2012;367:795-804. doi:10.1056/nejmoa1202753
- Zeun P, Scahill R, Osborne-Crowley K, et al. Biological and clinical manifestations of Huntington's disease in gene carriers very far from predicted onset. *J Neurology Neurosurg Psychiatry*. 2022;93:A14.1-A14.2. doi:10.1136/jnnp-2022-abn.40
- Rohrer JD. Structural brain imaging in frontotemporal dementia. *Biochimica Et Biophysica Acta Bba-Mol Basis Dis*. 2012;1822:325-332. doi:10.1016/j.bbadis.2011.07.014
- Walhout R, Schmidt R, Westeneng H-J, et al. Brain morphologic changes in asymptomatic C9orf72 repeat expansion carriers. *Neurology*. 2015;85:1780-1788. doi:10.1212/wnl.0000000000002135
- Dopper EGP, Chalos V, Ghariq E, et al. Cerebral blood flow in presymptomatic MAPT and GRN mutation carriers: a longitudinal arterial spin labeling study. *Neuroimage Clin*. 2016;12:460-465. doi:10.1016/j.nicl.2016.08.001
- Mutsaerts HJMM, Mirza SS, Petr J, et al. Cerebral perfusion changes in presymptomatic genetic frontotemporal dementia: a GENFI study. *Brain*. 2019;142:awz039. doi:10.1093/brain/awz039
- Bertrand A, Wen J, Rinaldi D, et al. early cognitive, structural, and microstructural changes in presymptomatic C9orf72 carriers younger than 40 years. *Jama Neurol*. 2018;75:236-245. doi:10.1001/jamaneurol.2017.4266
- Popuri K, Dowds E, Beg MF, et al. Gray matter changes in asymptomatic C9orf72 and GRN mutation carriers. *Neuroimage Clin*. 2018;18:591-598. doi:10.1016/j.nicl.2018.02.017
- Popuri K, Beg MF, Lee H, et al. FDG-PET in presymptomatic C9orf72 mutation carriers. *Neuroimage Clin*. 2021;31:102687. doi:10.1016/j.nicl.2021.102687
- Jiskoot LC, Panman JL, Meeter LH, et al. Longitudinal multimodal MRI as prognostic and diagnostic biomarker in presymptomatic familial frontotemporal dementia. *Brain*. 2019;142:193-208. doi:10.1093/brain/awy288
- Lee SE, Sias AC, Mandelli ML, et al. Network degeneration and dysfunction in presymptomatic C9ORF72 expansion carriers. *Neuroimage Clin*. 2017;14:286-297. doi:10.1016/j.nicl.2016.12.006
- Cash DM, Bocchetta M, Thomas DL, et al. Patterns of gray matter atrophy in genetic frontotemporal dementia: results from the GENFI study. *Neurobiol Aging*. 2017;62:191-196. doi:10.1016/j.neurobiolaging.2017.10.008
- Rohrer JD, Nicholas JM, Cash DM, et al. Presymptomatic cognitive and neuroanatomical changes in genetic frontotemporal dementia in the Genetic Frontotemporal dementia Initiative (GENFI) study: a cross-sectional analysis. *Lancet Neurology*. 2015;14:253-262. doi:10.1016/s1474-4422(14)70324-2
- Dopper EGP, Rombouts SARB, Jiskoot LC, et al. Structural and functional brain connectivity in presymptomatic familial frontotemporal dementia. *Neurology*. 2014;83:e19-e26. doi:10.1212/wnl.0000000000000583
- Tavares TP, Mitchell DGV, Coleman K, et al. Ventricular volume expansion in presymptomatic genetic frontotemporal dementia. *Neurology*. 2019;93. doi:10.1212/wnl.0000000000008386
- Wolk DA, Detre JA. Arterial spin labeling MRI: an emerging biomarker for Alzheimer's disease and other neurodegenerative conditions. *Curr Opin Neurol*. 2012;25:421-428. doi:10.1097/wco.0b013e328354ff0a
- Petr J, Mutsaerts HJMM, Vita ED, et al. Effects of systematic partial volume errors on the estimation of gray matter cerebral blood flow with arterial spin labeling MRI. *Magnetic Reson Mater*

- Phys Biology Medicine*. 2018;31:725-734. doi:10.1007/s10334-018-0691-y
25. DeJesus-Hernandez M, Mackenzie IR, Boeve BF, et al. Expanded GGGGCC hexanucleotide repeat in noncoding region of C9ORF72 causes chromosome 9p-Linked FTD and ALS. *Neuron*. 2011;72:245-256. doi:10.1016/j.neuron.2011.09.011
 26. Mutsaerts HJMM, Petr J, Groot P, et al. ExploreASL: an image processing pipeline for multi-center ASL perfusion MRI studies. *Neuroimage*. 2020;219:117031. doi:10.1016/j.neuroimage.2020.117031
 27. Ashburner J, Friston KJ. Diffeomorphic registration using geodesic shooting and Gauss-Newton optimisation. *Neuroimage*. 2011;55:954-967. doi:10.1016/j.neuroimage.2010.12.049
 28. Shirzadi Z, Crane DE, Robertson AD, et al. Automated removal of spurious intermediate cerebral blood flow volumes improves image quality among older patients: a clinical arterial spin labeling investigation. *J Magn Reson Imaging*. 2015;42:1377-1385. doi:10.1002/jmri.24918
 29. Alsop DC, Detre JA, Golay X, et al. Recommended implementation of arterial spin-labeled perfusion MRI for clinical applications: a consensus of the ISMRM perfusion study group and the European consortium for ASL in dementia. *Magnet Reson Med*. 2015;73:102-116. doi:10.1002/mrm.25197
 30. Koo TK, Li MY. A guideline of selecting and reporting intraclass correlation coefficients for reliability research. *J Chiropr Medicine*. 2016;15:155-163. doi:10.1016/j.jcm.2016.02.012
 31. Mutsaerts HJ, Petr J, Václavů L, et al. The spatial coefficient of variation in arterial spin labeling cerebral blood flow images. *J Cereb Blood Flow Metab*. 2016;37:3184-3192. doi:10.1177/0271678X16683690
 32. Mutsaerts HJMM, Petr J, Thomas DL, et al. Comparison of arterial spin labeling registration strategies in the multi-center Genetic Frontotemporal Dementia Initiative (GENFI): comparison of ASL registration strategies. *J Magn Reson Imaging*. 2017;47:131-140. doi:10.1002/jmri.25751
 33. Jezzard P, Chappell MA, Okell TW. Arterial spin labeling for the measurement of cerebral perfusion and angiography. *J Cereb Blood Flow Metabolism*. 2017;38:603-626. doi:10.1177/0271678X17743240
 34. Asllani I, Borogovac A, Brown TR. Regression algorithm correcting for partial volume effects in arterial spin labeling MRI. *Magnet Reson Med*. 2008;60:1362-1371. doi:10.1002/mrm.21670
 35. Rolls ET, Joliot M, Tzourio-Mazoyer N. Implementation of a new parcellation of the orbitofrontal cortex in the automated anatomical labeling atlas. *Neuroimage*. 2015;122:1-5. doi:10.1016/j.neuroimage.2015.07.075
 36. Bates D, Mächler M, Bolker B, Walker S. Fitting linear mixed-effects models using lme4. *J Stat Softw*. 2015;67:1. doi:10.18637/jss.v067.i01
 37. Barr DJ, Levy R, Scheepers C, Tily HJ. Random effects structure for confirmatory hypothesis testing: keep it maximal. *J Mem Lang*. 2013;68:255-278. doi:10.1016/j.jml.2012.11.001
 38. Lenth RV. *emmeans: Estimated Marginal Means, aka Least-Squares Means*. 2023
 39. Zhang N, Gordon ML, Ma Y, et al. The age-related perfusion pattern measured with arterial spin labeling MRI in healthy subjects. *Front Aging Neurosci*. 2018;10:214. doi:10.3389/fnagi.2018.00214
 40. Menon V. *Brain Mapping*. Syst. 2015;2:597-611. doi:10.1016/b978-0-12-397025-1.00052-x
 41. Seeley WW. The Salience Network: a Neural System for Perceiving and Responding to Homeostatic Demands. *J Neurosci*. 2019;39:9878-9882. doi:10.1523/jneurosci.1138-17.2019
 42. Viskontas IV, Possin KL, Miller BL. Symptoms of Frontotemporal Dementia Provide Insights into Orbitofrontal Cortex Function and Social Behavior. *Ann Ny Acad Sci*. 2007;1121:528-545. doi:10.1196/annals.1401.025
 43. Seeley WW. Anterior insula degeneration in frontotemporal dementia. *Brain Struct Funct*. 2010;214:465-475. doi:10.1007/s00429-010-0263-z
 44. Pasquini L, Nana AL, Toller G, et al. Salience network atrophy links neuron type-specific pathobiology to loss of empathy in frontotemporal dementia. *Biorxiv*. 2020:691212. doi:10.1101/691212. bioRxiv.
 45. Gordon E, Rohrer JD, Fox NC. Advances in neuroimaging in frontotemporal dementia. *J Neurochem*. 2016;138:193-210. doi:10.1111/jnc.13656
 46. Irwin DJ, McMillan CT, Xie SX, et al. Asymmetry of post-mortem neuropathology in behavioural-variant frontotemporal dementia. *Brain J Neurology*. 2017;141:288-301. doi:10.1093/brain/awx319
 47. Whitwell JL, Weigand SD, Gunter JL, et al. Trajectories of brain and hippocampal atrophy in FTD with mutations in MAPT or GRN. *Neurology*. 2011;77:393-398. doi:10.1212/WNL.0b013e318227047f
 48. Whitwell JL, Jack CR, Pankratz VS, et al. Rates of brain atrophy over time in autopsy-proven frontotemporal dementia and Alzheimer disease. *Neuroimage*. 2008;39:1034-1040. doi:10.1016/j.neuroimage.2007.10.001
 49. Whitwell JL, Weigand SD, Boeve BF, et al. Neuroimaging signatures of frontotemporal dementia genetics: c9orf72, tau, progranulin and sporadics. *Brain*. 2012;135:794-806. doi:10.1093/brain/aws001
 50. Peet BT, Spina S, Mundada N, Joie RL. Neuroimaging in frontotemporal dementia: heterogeneity and relationships with underlying neuropathology. *Neurotherapeutics*. 2021;18:728-752. doi:10.1007/s13311-021-01101-x
 51. Spinelli EG, Mandelli ML, Miller ZA, et al. Typical and atypical pathology in primary progressive aphasia variants. *Ann Neurol*. 2017;81:430-443. doi:10.1002/ana.24885
 52. Petrides M, Pandya DN. *The Human Nervous System*. 3rd ed. V Cortex; 2012:988-1011. doi:10.1016/b978-0-12-374236-0.10026-4
 53. Routier A, Habert M-O, Bertrand A, et al. Structural, microstructural, and metabolic alterations in primary progressive aphasia variants. *Front Neurol*. 2018;9:766. doi:10.3389/fneur.2018.00766
 54. Herrero M-T, Barcia C, Navarro J. Functional anatomy of thalamus and basal ganglia. *Child S Nerv Syst*. 2002;18:386-404. doi:10.1007/s00381-002-0604-1
 55. Bocchetta M, Gordon E, Cardoso MJ, et al. Thalamic atrophy in frontotemporal dementia – Not just a C9orf72 problem. *Neuroimage Clin*. 2018;18:675-681. doi:10.1016/j.nicl.2018.02.019
 56. McKenna MC, Lope J, Bede P, Tan EL. Thalamic pathology in frontotemporal dementia: predilection for specific nuclei, phenotype-specific signatures, clinical correlates, and practical relevance. *Brain Behav*. 2023;13:e2881. doi:10.1002/brb3.2881
 57. Tan RH, Wong S, Kril JJ, et al. Beyond the temporal pole: limbic memory circuit in the semantic variant of primary progressive aphasia. *Brain*. 2014;137:2065-2076. doi:10.1093/brain/awu118
 58. Broe M, Hodges JR, Schofield E, Shepherd CE, Kril JJ, Halliday GM. Staging disease severity in pathologically confirmed cases of frontotemporal dementia. *Neurology*. 2003;60:1005-1011. doi:10.1212/01.wnl.0000052685.09194.39
 59. Bocchetta M, Todd EG, Peakman G, et al. Differential early subcortical involvement in genetic FTD within the GENFI cohort. *Neuroimage Clin*. 2021;30:102646. doi:10.1016/j.nicl.2021.102646
 60. Seeley WW, Crawford RK, Zhou J, Miller BL, Greicius MD. Neurodegenerative Diseases Target Large-Scale Human Brain Networks. *Neuron*. 2009;62:42-52. doi:10.1016/j.neuron.2009.03.024
 61. Vis JB, Peng S, Chen X, et al. Arterial-spin-labeling (ASL) perfusion MRI predicts cognitive function in elderly individuals: a 4-year longitudinal study. *J Magn Reson Imaging*. 2018;48:449-458. doi:10.1002/jmri.25938

62. Staffaroni AM, Cobigo Y, Elahi FM, et al. A longitudinal characterization of perfusion in the aging brain and associations with cognition and neural structure. *Hum Brain Mapp.* 2019;40:3522-3533. doi:[10.1002/hbm.24613](https://doi.org/10.1002/hbm.24613)
63. Clement P, Mutsaerts H-J, Václavů L, et al. Variability of physiological brain perfusion in healthy subjects - A systematic review of modifiers. Considerations for multi-center ASL studies. *J Cereb Blood Flow Metabolism.* 2018;38:1418-1437. doi:[10.1177/0271678X17702156](https://doi.org/10.1177/0271678X17702156)

SUPPORTING INFORMATION

Additional supporting information can be found online in the Supporting Information section at the end of this article.

How to cite this article: Pasternak M, Mirza SS, Luciw N, et al. Longitudinal cerebral perfusion in presymptomatic genetic frontotemporal dementia: GENFI results. *Alzheimer's Dement.* 2024;20:3525-3542. <https://doi.org/10.1002/alz.13750>

EXHIBIT 8

787 Fed.Appx. 710

This case was not selected for publication in West's Federal Reporter. See Fed. Rule of Appellate Procedure 32.1 generally governing citation of judicial decisions issued on or after Jan. 1, 2007. See also U.S.Ct. of App. Fed. Cir. Rule 32.1. United States Court of Appeals, Federal Circuit.

NEUROGRAFIX, [Neurography Institute Medical Associates, Inc.](#), Image-Based Surgicenter Corporation, Aaron Gershon Filler, Plaintiffs-Appellants
v.
BRAINLAB, INC., [Brainlab AG](#), Brainlab Medizinische Computersysteme GmbH, Defendants-Appellees

2018-2363

|

Decided: October 7, 2019

Synopsis

Background: Owner of patent for particular methods of generating images of nerves and other bodily structures by use of magnetic resonance imaging (MRI) technology brought infringement action. The case was consolidated with cases filed against other defendants and assigned to multidistrict litigation court. The United States District Court for the Northern District of Illinois, [Matthew F. Kennelly, J.](#), [2018 WL 2392000](#), granted summary judgment of noninfringement to alleged infringers, and denied owner's motion for reconsideration. Owner appealed.

[Holding:] The Court of Appeals, [Taranto](#), Circuit Judge, held that patent owner was not required to produce evidence of actual infringement on motion for summary judgment of noninfringement.

Reversed and remanded.

Procedural Posture(s): On Appeal; Motion for Summary Judgment.

West Headnotes (4)

[1] Patents

🔑 [Methods or processes](#)

Owner of patent describing and claiming particular methods of generating images of nerves and other bodily structures by use of magnetic resonance imaging (MRI) technology was not required to produce evidence of actual infringement on motion for summary judgment of noninfringement, where accused infringer argued only that, under its construction of “selected structure,” the accused software was not capable of infringement, not that, under the construction adopted by the court, there was no evidence of actual infringement.

[2] Patents

🔑 [Methods or processes](#)

Genuine issue of material fact existed regarding whether accused software product was capable of infringing uses, precluding summary judgment on claims that accused product infringed patent describing and claiming particular methods of generating images of nerves and other bodily structures by use of magnetic resonance imaging (MRI) technology.

[3] Patents

🔑 [Medical devices and appliances](#)

To “select a structure” as claimed in patent describing and claiming particular methods of generating images of nerves and other bodily structures by use of magnetic resonance imaging (MRI) technology, was to choose it as a subject for placement into the claimed process that started with exposing a region to a magnetic field, proceeded to sensing a resonant response, and continued as claimed.

[4] Patents

🔑 [In general; utility](#)

US Patent  5,560,360. Cited.

*711 Appeal from the United States District Court for the Northern District of Illinois in No. 1:12-cv-06075, Judge [Matthew F. Kennelly](#).

Attorneys and Law Firms



[Aaron Gershon Filler](#), Tensor Law, P.C., Santa Monica, CA, argued for plaintiffs-appellants.

[Jay Campbell](#), Tucker Ellis LLP, Cleveland, OH, argued for defendants-appellees. Also represented by [David Aaron Bernstein](#).

Before [Newman](#), [O'Malley](#), and [Taranto](#), Circuit Judges.


Opinion


[Taranto](#), Circuit Judge.

 U.S. Patent No. 5,560,360, which names Dr. Aaron Filler as a co-inventor, describes and claims particular methods of generating images of nerves and other bodily structures by use of [magnetic resonance imaging](#) (MRI) technology. Dr. Filler and the three appellants named in the caption (collectively, NeuroGrafix) sued the appellees named in the caption (collectively, Brainlab), asserting infringement of the  '360 patent. The case was consolidated with cases filed against other defendants and assigned for pretrial purposes to a multidistrict litigation (MDL) court. The MDL court granted summary judgment of non-infringement to Brainlab, and it denied reconsideration, as did the original district court when the case returned from the MDL court. NeuroGrafix appeals. We conclude that the grant of summary judgment was procedurally improper, and we resolve the parties' key disputes about claim construction. We reverse and remand.

I


A

The  '360 patent describes methods and systems for creating detailed images of neural tissues by using diffusion tensor imaging (DTI), an application of MRI technology.

 '360 patent, Abstract; *see also id.*, col. 21, lines 35–45. DTI exploits certain facts about water diffusion in, *e.g.*, brain structures. Notably, diffusion along white matter nerve tracts is anisotropic: substances such as water diffuse freely along the main, long axis of the nerve tract, but diffusion is very limited in a direction perpendicular to (across) that axis. *Id.*, col. 5, lines 5–11. By contrast, the surrounding gray matter is relatively isotropic: substances *712 diffuse at similar rates in all directions. *Id.*, col. 5, lines 11–12.

In the patented method, pulsed magnetic field gradients are applied in two orthogonal (perpendicular) directions in a region containing the nerve tissues for which a precise image is sought. *Id.*, col. 5, lines 17–21; *see also id.*, col. 15, lines 40–57. “[I]f the axis of the nerve is generally known to the operator,” the specification explains, “the direction of the desired orthogonal diffusional weighting gradients can be readily determined.” *Id.*, col. 15, lines 58–62; *see also id.*, col. 16, lines 34–47. “On the other hand, if the axis of the peripheral nerve is not known, or if many[] nerves having different axes are being imaged,” the initial directions for the magnetic field gradients are “arbitrarily selected,” and then a number of alternative directions are used. *Id.*, col. 15, lines 63–67; *id.*, col. 16, lines 48–53.

The result of this process of applying magnetic field gradients depends on the types of tissue in the subject region. In isotropic tissue, the signal reduction will be the same regardless of how the magnetic field gradients are oriented relative to the tissue, whereas in anisotropic tissue, the signal reduction will be greatest when the magnetic field gradients are parallel and perpendicular, respectively, to the direction of the anisotropy, *i.e.*, along the major, long axis of the neural tract. *Id.*, col. 5, lines 21–39. Accordingly, neural tissue can be identified and visually differentiated from the surrounding structures by determining the areas of greater relative anisotropy. *Id.*, col. 6, lines 46–55; *see also id.*, col. 15, lines 52–57 (“[W]ith gradients approximately perpendicular and parallel to the axis of the peripheral nerve at the particular point being imaged, the parallel gradient image can be subtracted from the perpendicular gradient image to produce the desired ‘nerve only’ image.”).

Claim 36 of the  '360 patent is the only independent claim at issue in this appeal, and the parties have generally treated that claim as representative. That claim recites:

36. A method of utilizing magnetic resonance to determine the shape and position of a structure, said method including the steps of:

(a) exposing a region to a magnetic polarizing field including a predetermined arrangement of diffusion-weighted gradients, the region including a selected structure that exhibits diffusion anisotropy and other structures that do not exhibit diffusion anisotropy;

(b) exposing the region to an electromagnetic excitation field;


(c) for each of said diffusion-weighted gradients, sensing a resonant response of the region to the excitation field and the polarizing field including the diffusion-weighted gradient and producing an output indicative of the resonant response; and


(d) vector processing said outputs to generate data representative of anisotropic diffusion exhibited by said selected structure in the region, regardless of the alignment of said diffusion-weighted gradients with respect to the orientation of said selected structure; and

(e) processing said data representative of anisotropic diffusion to generate a data set describing the shape and position of said selected structure in the region, said data set distinguishing said selected structure from other structures in the region that do not exhibit diffusion anisotropy.

Id., col. 42, line 43, through col. 43, line 2. The central dispute in this appeal involves the “selected structure” limitation in steps (a), (d), and (e).

*713 B


In August 2012, NeuroGrafix, Neurography Institute Medical Associates, Inc., and Image-Based Surgicenter Corporation sued Brainlab, Inc., Brainlab AG, and Brainlab Medizinische Computersysteme GmbH in the Northern District of Illinois, and in August 2014, Dr. Filler became a co-plaintiff by the filing of an amended complaint. The plaintiffs (NeuroGrafix) alleged that users of Brainlab’s FiberTracking software directly infringed the ’360 patent and that Brainlab induced the direct infringement by those users through statements in its manual and advertisements directing users to use the software in an infringing manner.¹ In particular,

NeuroGrafix asserted claims 36–37, 39–42, 44, 46–47, and 49, all of which are method claims. Brainlab counterclaimed for a declaratory judgment that the asserted claims of the ’360 patent are invalid.

In April 2013, the Judicial Panel on Multidistrict Litigation transferred the case to the District of Massachusetts, where it was consolidated, for pretrial proceedings, with several cases that NeuroGrafix brought against various MRI equipment manufacturers and university and hospital end-users.

In May 2016, Brainlab filed the first of its two motions for summary judgment of non-infringement. Brainlab relied on customer-protection provisions of settlement agreements NeuroGrafix had entered into with MRI-equipment makers Siemens, GE, and Philips. Brainlab argued that its FiberTracking software is used to process the output from MRI systems made by those manufacturers and that FiberTracking users do not infringe under the terms of the settlement agreements. In its response, NeuroGrafix argued, among other things, that Brainlab could still be liable for infringement by “unauthorized independent medical practitioners” who use Brainlab’s software but are not customers of Siemens, GE, or Philips.

The MDL court granted the motion, but only in part, in August 2016. It held that summary judgment of non-infringement was proper with respect to Brainlab’s customers using Siemens MRI systems but not as to Brainlab’s customers using GE and Philips MRI systems, reasoning that only the Siemens settlement agreement, not the GE or Philips agreements, extended to Brainlab’s software. The court also held summary judgment of non-infringement proper as to the alleged independent medical practitioners, concluding that NeuroGrafix had produced “no evidence that any of the handful of such practitioners identified by [NeuroGrafix] used Brainlab products in their alleged infringement.” J.A. 51.

Brainlab eventually filed a second motion for summary judgment, but before that occurred, NeuroGrafix, in September 2017, sought leave to file a second amended complaint that, if allowed, would add allegations that Brainlab itself directly infringed the ’360 patent because the steps performed by Brainlab’s customers were attributable to Brainlab under an agency theory. In conjunction with its proposed second amended complaint, NeuroGrafix filed a declaration from Dr. Filler and attached several articles and other exhibits allegedly demonstrating infringement

by several of Brainlab's customers, such as Memorial Sloan Kettering Cancer Center *714 and Akron General Hospital. The MDL court denied NeuroGrafix permission to file a second amended complaint, characterizing the new allegations as a "last-ditch attempt to repackage the inducement claim," which it had "long alleged but neglected until the close of fact discovery," as a direct-infringement claim under an agency theory. J.A. 6986.

In February 2018, Brainlab filed its second motion for summary judgment of non-infringement. Brainlab's entire argument was that users of the software do not commit direct infringement and therefore Brainlab could not be liable for induced infringement; it made no argument against inducement liability except for the absence of direct infringement. J.A. 7309 ("without direct infringement there can be no induced infringement"), 7327 ("Absent direct infringement, there can be no induced infringement."). On direct infringement, Brainlab argued that users of the FiberTracking software do not satisfy two limitations of claim 36—the "selected structure" limitation and the "do not exhibit the diffusion anisotropy" limitation. In support of that assertion, Brainlab set forth essentially three arguments in its motion.

First, and most significantly for present purposes, Brainlab argued that "selected structure" requires that a user know the "existence and location" of the structure of interest before performing the claimed steps of exposing a region to a magnetic field, sensing a resonant response, and so forth. J.A. 7308. Brainlab asserted that it was impossible for users of the FiberTracking software to "select[] [a] structure" because "Brainlab's FiberTracking module does not permit a user to isolate or select a specific structure for tractography" before scanning; instead, the accused software "automatically generates all tracts that intersect a certain volume, like a tumor, if they meet certain criteria," and those tracts "are not visible until after the FiberTracking software has been run." J.A. 7322; see J.A. 7308 ("users of Brainlab's FiberTracking module cannot infringe claim 36" because they cannot select a structure as required), 7309 (same), 7312 (same), 7322 (same), 7324 (same), 7325 (same), 7327 (same). Second, Brainlab contended that "selected structure" was limited to peripheral nerves, whereas the FiberTracking software was used to image only nerves in the brain, which are not considered peripheral nerves. J.A. 7317–18. Third, Brainlab argued that "do not exhibit diffusion anisotropy" should be construed as requiring zero diffusion anisotropy. J.A. 7321. Under that construction, Brainlab asserted, the limitation was

not satisfied because the gray matter distinguished by the FiberTracking software has a small but nonzero anisotropy, J.A. 7325–27, and the FiberTracking software does not permit users to choose zero as the anisotropy threshold above which structures will be displayed, J.A. 7322.

In its opposition, NeuroGrafix responded to Brainlab's arguments. It argued that "selected structure" does not require that the precise location and orientation of the chosen structure be known in advance. J.A. 8011–12. According to NeuroGrafix, users *could* satisfy the claim by, for instance, obtaining a preliminary MRI image, choosing a structure that would be "distinctive and visibly apparent" from the preliminary image (such as the pyramidal tract), and then performing the steps of the claimed method with the chosen structure as the subject. J.A. 8012; see J.A. 8011–13, 8025–26. NeuroGrafix also asserted that the FiberTracking software was capable of being used in such a manner, pointing to Brainlab's advertisements, which state that users can use the software to image the pyramidal tract, J.A. 8013, 8015, and the FiberTracking manual, which instructs that users can select fiber *715 bundles to include or exclude in the region of interest, J.A. 8020.

The MDL court granted Brainlab's second summary-judgment motion in May 2018. [In re NeuroGrafix \('360\) Patent Litig.](#), MDL No. 13-2432, 2018 WL 2392000, at *5 (D. Mass. May 25, 2018) ([Summary Judgment Op.](#)). It rejected Brainlab's claim-construction arguments limiting "selected structure" to peripheral nerves and limiting "do not exhibit diffusion anisotropy" to zero anisotropy. See [id.](#) at *3. As to Brainlab's argument that some aspects of the "selected structure" must be known in advance, the court rejected Brainlab's position that it was not possible to use the FiberTracking software in a manner that satisfies the claim limitation. See [id.](#) "[D]epending on the physician's purpose and objective," the court held, "FiberTracking is capable of both infringing uses and non-infringing uses," though it did not identify precisely what those infringing and non-infringing uses would be. [Id.](#)

Nevertheless, the court concluded, summary judgment was warranted because NeuroGrafix had pointed to no evidence that any FiberTracking users actually used the software in an infringing manner, *i.e.*, there was "nothing in the record showing that either Brainlab or any of its customers actually uses FiberTracking in the manner hypothesized

by Neuro[G]rafix.” [Id.](#) at *4; *see also* [id.](#) at *4 n.5 (concluding that there was “no evidence in the record” that neurosurgeons used FiberTracking to “ascertain the precise location of the pyramidal tract” to avoid injuring it during surgery). The court also determined that instances of direct infringement could not be inferred from statements in Brainlab’s advertisements that it was “possible” to use the FiberTracking software to delineate the pyramidal tract, noting that those materials “do[] not teach a means of selecting a particular ROI and FA Threshold and Minimum Length values to accomplish this, nor does it recommend this as a superior or even commensurate mode of use.” [Id.](#) at *4. In a footnote, the court added a conclusion seemingly about the absence of inducement even apart from the absence of direct infringement, even though Brainlab’s motion had not so argued. It stated that, as a matter of law, Brainlab did not induce infringement “for the same reason that a reasonable factfinder cannot infer instances of direct infringement,” namely, the FiberTracking advertisements and manual “[do not] teach an infringing use of the device *such that* we are willing to infer from those instructions an affirmative intent to infringe the patent.” [Id.](#) at *4 n.6 (quoting [Takeda Pharm. U.S.A., Inc. v. W.-Ward Pharm. Corp.](#), 785 F.3d 625, 631 (Fed. Cir. 2015)).

In June 2018, NeuroGrafix moved for reconsideration of the MDL court’s grant of summary judgment, primarily arguing that several articles attached to NeuroGrafix’s motion for leave to file a second amended complaint had provided evidence of actual infringing uses of the FiberTracking software. The MDL court denied NeuroGrafix’s motion for reconsideration, noting that NeuroGrafix had not included or relied on the relevant articles in its opposition to Brainlab’s summary-judgment motion.

The case was then remanded to the Northern District of Illinois for proceedings on Brainlab’s invalidity counterclaim. [A191] In July 2018, NeuroGrafix asked the Illinois court to reconsider the MDL court’s summary-judgment order, contending, as relevant here, that the MDL court had granted summary judgment on a basis not asserted in Brainlab’s summary-judgment motion. J.A. 8775–76, 8781–83. The district court denied NeuroGrafix’s motion for reconsideration and dismissed Brainlab’s *716 invalidity counterclaim without prejudice, producing a final judgment.

NeuroGrafix appeals. We have jurisdiction under 28 U.S.C. § 1295(a)(1).

II

A

[1] We begin by addressing NeuroGrafix’s procedural challenge to the MDL court’s grant of summary judgment. NeuroGrafix argues that it was improper for the MDL court to fault it for failing to produce evidence of actual infringement because Brainlab argued only that, under its construction of “selected structure,” the accused software was not capable of infringement, not that, under the construction adopted by the MDL court, there was no evidence of actual infringement. We review the MDL court’s grant of summary judgment *de novo*. [Momenta Pharm., Inc. v. Teva Pharm. USA Inc.](#), 809 F.3d 610, 614 (Fed. Cir. 2015) (following First Circuit law); *see also* [In re Cygnus Telecomms. Tech., LLC, Patent Litig.](#), 536 F.3d 1343, 1352 (Fed. Cir. 2008) (following law of MDL court’s regional circuit in deciding issues involving summary-judgment procedures). We agree with NeuroGrafix and accordingly reverse the grant of summary judgment.

As Brainlab’s motion for summary judgment repeatedly made clear, its non-infringement position depended on the premise that “select[ing] [a] structure” requires knowing in advance the location of the chosen structure. Under that construction, Brainlab argued, the FiberTracking software is not capable of infringement, since the software is used to detect structures whose location is not already known. *See, e.g.*, J.A. 7311 (“Claim 36 is focused on determining the location and shape of an anisotropic structure that is already known and ‘selected’ for imaging in advance of scanning.... Conversely, Brainlab’s Fiber[T]racking module is focused on *finding* patient specific anisotropic structures that are *not* previously known.”); J.A. 7322 (“The user certainly cannot select a structure in advance of scanning. The reason is simple: Brainlab’s FiberTracking module is used to find white matter tracts that are not visible until after the FiberTracking software has been run....”).

Moreover, the expert reports cited in Brainlab’s summary-judgment motion were also premised on this understanding of “selected structure.” Dr. James Leach declared that “the neuroradiologist cannot select certain white matter structures or tracts in advance for imaging” because “the position or orientation of white matter tracts is not known in advance of imaging” in cranial DTI. J.A. 7921. Dr. Andrew Tsung

stated that “I do not select certain white matter structures for imaging by the MRI,” as “[t]he location of white matter tracts are not identifiable prior to imaging.” J.A. 7912. And Dr. Michael Moseley asserted that “a ‘selected’ structure is one where the axis of the structure, such as a nerve, ... would be known in advance of the imaging,” J.A. 7946, and using that understanding, he added that “there is no ‘selected structure’ when DTI imaging is performed” using Brainlab’s FiberTracking software because “the axes of the white matter fiber tracts are not known in advance,” J.A. 7947. Neither Brainlab nor its experts argued in the alternative that, even if “selected structure” did not include a requirement of knowing the position, orientation, location, or axes of a structure in advance, the record was devoid of evidence that Brainlab’s customers used the FiberTracking software to image particular chosen structures.

In its summary-judgment opposition, NeuroGrafix disputed this claim construction, essentially arguing that “selected *717 structure” simply requires choosing a particular structure as a subject for the claimed process. That is possible in the FiberTracking software, NeuroGrafix asserted, because at least the pyramidal tract is visible after taking a preliminary image and can then be chosen for imaging according to the claimed method. *See* J.A. 8012 (“[E]ither visually after opening the skull or from preliminary routine MRI scout images, the technologist can select[] a brain structure called the pyramidal tract.”); J.A. 8014–15 (“With tractography and DTI, it is possible to select this structure of the brain ... and then to provide this selected structure as an ROI for the FiberTracking software.”). And NeuroGrafix pointed to Brainlab’s advertisements as evidence that such a use was possible and even encouraged by Brainlab. *See* J.A. 8015 (showing Brainlab advertisement that says: “It is possible to delineate major white matter tracts, such as the pyramidal tract, by applying fiber tracking algorithms.”); *see also* J.A. 8013 (showing Brainlab advertisement that says: “Waves of DTI data on exotic eloquent white matter specimens, like pyramidal tracts, now flow easily to your BrainLAB IGS.”). In other words, NeuroGrafix argued, and the MDL court eventually agreed, that the FiberTracking software is capable of infringing uses as well as non-infringing uses.

[2] That showing was sufficient for NeuroGrafix to defeat summary judgment, and the MDL court erred in concluding otherwise. NeuroGrafix demonstrated that there was a genuine dispute of material fact on the only issue raised by Brainlab, namely, whether the FiberTracking software was capable of infringing uses. Evidence of actual infringing uses

of the FiberTracking software was unnecessary to answer the only grounds for summary judgment asserted by Brainlab.²

A court cannot grant summary judgment on a ground that was neither asserted by the movant nor made the subject of judicial action under Rule 56(f) that gave the non-movant proper notice of the ground and of the obligation “to come forward with all of her evidence.” *Celotex Corp. v. Catrett*, 477 U.S. 317, 326, 106 S.Ct. 2548, 91 L.Ed.2d 265 (1986); *see Glaverbel Societe Anonyme v. Northlake Mktg. & Supply, Inc.*, 45 F.3d 1550, 1562 (Fed. Cir. 1995) (following Seventh Circuit law); *see also, e.g., Lusson v. Carter*, 704 F.2d 646, 647 (1st Cir. 1983). And in the specific context of patent infringement, we have held that summary judgment of non-infringement requires the accused infringer to “point[] to the specific ways in which accused systems did not meet the claim limitations.” *Exigent Technology, Inc. v. Atrana Solutions, Inc.*, 442 F.3d 1301, 1309 (Fed. Cir. 2006). The MDL court’s ruling was contrary to those basic principles in that it granted summary judgment against NeuroGrafix for its failure to come forward with evidence to answer a non-infringement ground that had not been asserted and of which it had not been given proper notice.

To be sure, our law is clear that, in this case, NeuroGrafix could not sustain a claim of direct infringement of the method claims by merely showing that the accused software is “capable of” operating in an infringing manner. *See, e.g., Fujitsu Ltd. v. Netgear Inc.*, 620 F.3d 1321, 1329 (Fed. Cir. 2010). We assume, without questioning, *718 that in this case NeuroGrafix must ultimately make a showing that the accused software was *actually* used in an infringing manner by Brainlab (for direct infringement) or by one or more of Brainlab’s customers (for indirect infringement). Moreover, it is understandable that the district court might be surprised that NeuroGrafix made no such showing after the years of litigation and discovery this MDL spanned. Nevertheless, the motion being considered by the district court in this case was one structured and limited by the movant. The court was not free to look down the road and consider what the non-movant might need to establish to survive a differently structured, well-supported motion. The motion before it necessarily limited the court’s inquiry.

For the same reason, the MDL court’s apparent holding that Brainlab’s advertisements and manual do not induce infringement as a matter of law also was procedurally

improper. See [Summary Judgment Op.](#) at *4 n.6. Brainlab’s summary-judgment motion argued only that “Brainlab cannot induce infringement of the asserted claims of the [’360 patent](#)” because “[a]bsent direct infringement, there can be no induced infringement.” J.A. 7327. It did not argue, as the MDL court seemed to conclude, that the relevant Brainlab materials merely suggested that an infringing use was possible rather than instructing how to use the software in an infringing manner. To the extent that this conclusion was an independent basis for the MDL court’s grant of summary judgment, we reverse the court’s decision on that ground as well.³

B

[3] The MDL court’s procedural error is an adequate ground for reversal and does not depend on whether its claim construction of “selected structure” was correct. But we address the disputes about the proper construction of that term so that the district court can apply the correct construction on remand. We review the MDL court’s claim construction de novo and any underlying factual findings based on extrinsic evidence for clear error. [Teva Pharm. USA, Inc. v. Sandoz, Inc.](#), 574 U.S. 318, 135 S. Ct. 831, 841, 190 L.Ed.2d 719 (2015).

We conclude that to “select[] [a] structure” is simply to choose it as a subject for placement into the claimed process that starts with exposing a region to a magnetic field, proceeds to sensing a resonant response, and continues as claimed. That meaning follows from the language of claim 36 itself: in step (a), the region exposed to a magnetic polarizing field includes the “selected structure,” and in step (e), the resulting data set distinguishes the “selected structure” from other structures in the region. [’360 patent](#), col. 42, lines 46–50; *id.*, col. 42, line 64, through col. 43, line 2. The specification does not use the language of “selected structure,” but it uses “select” simply to describe choosing something before taking some action. See, e.g., *id.*, col. 14, lines 53–62 (discussing “select[ing]” a region of interest before determining the average intensity within that region of interest); *id.*, col. 28, lines 23–26 (discussing “select[ing] a volume of interest” before rendering that volume of interest into a projection neurogram).

The MDL court did not set forth a precise claim construction of “selected structure” in its summary-judgment opinion.⁴ In one key respect, though, the [*719](#) court’s understanding of the phrase fits the simple construction that we think is mandated. The court correctly rejected the construction that seemingly underlies Brainlab’s contention that infringing use of the FiberTracking software is impossible, namely, that a “selected structure” is one whose location, orientation, axis, or the like is known in advance of the claimed mapping process to the same degree it will become known upon completion of that process. And the court indicated that “delineat[ing] the pyramidal tract,” [Summary Judgment Op.](#) at *4, and “ascertain[ing] the precise location of the pyramidal tract,” [id.](#) at *4 n.5, would satisfy the “selected structure” limitation. Those observations fit the specification’s express contemplation of performing the patented method even when, for example, “the axis of the peripheral nerve is not known.” *Id.*, col. 15, lines 63–64.

Two further points about claim construction contentions advanced by the parties—one by Brainlab, one by NeuroGrafix—are warranted. Brainlab has suggested that software that tracks all fibers in an area cannot perform the method, because the tracking is not limited to a particular selected structure. That view is not supported by claim 36’s language. As long as a chosen structure is among those put into the process for distinguishing the data or images in the way the claim specifies, the claim is satisfied, even if the process used to do that results in comparable data and images for other structures as well. Both claim 36’s preamble and the claim phrase “region including a selected structure” use the word “including.” [’360 patent](#), col. 42, lines 45, 48. We have “consistently interpreted ‘including’ and ‘comprising’ to have the same meaning, namely, that the listed elements ... are essential but other elements may be added.” [Lucent Techs., Inc. v. Gateway, Inc.](#), 525 F.3d 1200, 1214 (Fed. Cir. 2008). And nothing in the language following either of the “including” terms implies that no other structure may be mapped in the claimed way when a particular chosen structure is placed into the claimed mapping process.

For its part, NeuroGrafix argues on appeal that “selected structure” should be construed as equivalent to “region” and that all uses of the FiberTracking software are therefore infringing because Brainlab’s customers necessarily choose a region to be the subject of the claimed method before performing the steps of the method. That always-

infringes contention is the polar opposite of Brainlab’s never-infringes contention, and it is equally wrong. The argument was likely forfeited by not being adequately presented; indeed, in its motion for reconsideration before the MDL court, NeuroGrafix specifically agreed with the MDL court’s conclusion that “FiberTracking is capable of both infringing uses and non-infringing uses.” J.A. 8449 (quoting [Summary Judgment Op. at *3](#)). In any event, NeuroGrafix’s construction contradicts the claim language. Claim 36 refers to “selected structure” and “region” as separate concepts, with “selected structure” being something merely located in the “region.” See [’360 patent](#), col. 42, lines 48–50 (“the region including a selected structure that exhibits diffusion anisotropy and other structures that do not exhibit diffusion anisotropy”).

III

For the foregoing reasons, we reverse the MDL court’s grant of summary judgment [*720](#) and remand for further proceedings consistent with this opinion.

Each party shall bear its own costs.

REVERSED AND REMANDED**All Citations**

787 Fed.Appx. 710

Footnotes

- 1 There is evidence in the record before us that a user of the FiberTracking software selects a region of interest from an anatomical image fused with DTI data and chooses a minimum diffusion value and a minimum length, and the software then displays all fibers that intersect the chosen region of interest and exceed the minimum diffusion and length parameters.
- 2 Thus, we need not and do not decide whether, even if NeuroGrafix did not produce direct evidence of actual infringement, instances of infringement can be inferred from the statements and figures in Brainlab’s advertisements and manual. See [Summary Judgment Op. at *4](#) (citing [Toshiba Corp. v. Imation Corp.](#), 681 F.3d 1358, 1364 (Fed. Cir. 2012); [Fujitsu Ltd. v. Netgear Inc.](#), 620 F.3d 1321, 1329 (Fed. Cir. 2010)).
- 3 The MDL court’s rejection of NeuroGrafix’s inducement claim may also have been based on a construction of “selected structure” that, as we discuss below, was incorrect.
- 4 The MDL court did not construe “selected structure” in its August 2016 claim-construction order; nor did the parties agree to a construction of the phrase. See [In re NeuroGrafix \(’360\) Patent Litig.](#), 201 F. Supp. 3d 206, 212 & n.4 (D. Mass. 2016).

EXHIBIT 9

Oral Argument

1
2
3
4
5
6
7
8
9
10
11
12
13
14
15
16
17
18
19
20
21
22
23
24
25

UNITED STATES COURT OF APPEALS
FOR THE FEDERAL CIRCUIT

<hr/>)
NEUROGRAFIX, NEUROGRAPHY))
INSTITUTE MEDICAL ASSOCIATES,))
INC., IMAGE-BASED SURGICENTER))
CORPORATION, AARON GERSHON))
FILLER,))
))
Plaintiffs-Appellants,))
))
vs.)	Case No. 18-2363
))
BRAINLAB, INC., BRAINLAB AG,))
BRAINLAB MEDIZINISCHE))
COMPUTERSYSTEM, GMBH,))
))
Defendants-Appellees.))
<hr/>)

REPORTER'S TRANSCRIPT OF RECORDED ORAL ARGUMENT
BEFORE THE HONORABLE PAULINE NEWMAN
AND HONORABLE RICHARD G. TARANTO

AARON G. FILLER, ESQ. FOR PLAINTIFFS-APPELLANTS
JAY R. CAMPBELL, ESQ. FOR DEFENDANTS-APPELLEES

Transcribed by Kelly Paulson, CSR No. 8295

Page 2

ORAL ARGUMENT
* * *

JUDGE NEWMAN: Okay. The next argued case is No. 18-2363, NeuroGrafix against Brainlab. Mr. Filler.

MR. FILLER: Good morning, your honor. Pleased to be here and honored and also with my good friend Jay Campbell, (inaudible) many times over the years, including wrote up a section in my book. I wrote about patents some time ago about his arguments and attorney's fees in Medtronics versus Brainlab. We were opposite in Sarif v. Brainlab.

So what I wanted to do is to make three points here. Firstly, I'd like to show that absolutely this patent was infringed by Brainlab and induced, direct infringement by Memorial Sloan-Kettering and inducement to that. I'd like to show that the way that the Court disposed of the motion for summary judgment by finding that the patent did not apply to unknown tracts is a complete misunderstanding of the patent, and because of this, there is no non-infringing -- substantial non-infringing use.

JUDGE TARANTO: Okay. Can I, just to hope that you will focus on what's in my mind, tell you a little bit about what's in my mind? And maybe it will

Page 3

fit with what you're trying to say or not.

I was focused on kind of two arguments that I take you to be making. One of them is a claim construction argument about selected structure, and that all that means is that it is a brain structure that the user of this method chooses to subject to the process of scanning, etc., and that it plainly does not require that one knows either the specific location or the orientation of the selected structure. Just it means identifying the structure that you are subjecting this -- was it diffusion tensor imaging process to?

Because after all, the whole point of this process is to produce an accurate map of the orientation and location. You don't have to know it in advance. So that's -- and that the District Court was simply wrong about the claim construction to the extent it went beyond that.

And the second is a procedural point, which is that you could not be faulted for not putting on, in response to the summary judgment motion, a whole lot of evidence about what users of the -- what's the software that you called --

MR. FILLER: FiberTracking.

JUDGE TARANTO: What's it --

MR. FILLER: FiberTracking.

Page 4

JUDGE TARANTO: FiberTracking. Because that was not actually the argument that they made a summary judgment motion on. They never said if all you need is identifying the structure that you are going to subject -- you know put through this process, that nobody does that. And, therefore, it completely doesn't matter whether you didn't submit a whole lot of evidence.

MR. FILLER: Yes. Those are two arguments at the core of what I have to say.

So to fill that in, this court in Intelligent Biosystems versus Alumina, 2016, and before that Abbott Laboratories versus Sandoz, 2009, address this conundrum that, well, we certainly couldn't have claimed something unknown in the claims without making the claim indefinite.

But what's happening in Abbott is you have a product by process, and the product's unknown, but you say, well, okay, we have a process. And if you look at this Intelligent Biosystems, very similar. We're sequencing DNA. The DNA sequence is unknown. It's not that we don't know that it's DNA.

So yes, the Court finds that since there are some areas that are unknown that must be a substantial non-infringing use, and so this is completely wrong because the whole purpose of the patent, as you just

Page 5

stated, is to map -- find the direction of unknown tissues. In fact, Claim 36 --

JUDGE TARANTO: That's what it says in the Preamble, in fact. This is a process for the purpose of determining the shape and position of a structure. It would be very odd to interpret claim language in here that says you have to know that in advance before you run the process.

MR. FILLER: Absolutely, because the -- and, in fact, even Claim 36 is general. We have a picture of celery it's used on. Claim 37 attaches to mammals and neural tissues, but 36 is very broad because this is the solution, is that we had a way with MRI when the direction is known to the peripheral nerve in the arm because we could see the direction of diffusion, which is anisotropic, primarily down a nerve, not isotropic, diffusion in all directions.

So and the consequence of that is if you have an anisotropic flow in a nerve, if you turn the gradient so first it's parallel and then it's perpendicular, in one image the nerve will be bright. The other would be dark. But if you have isotropic or uniformly diffusing water, then it's the same image intensity no matter how you point the gradient.

But when we have complex curving nerve

Page 6

1 structures, how do we know which way to point our
 2 gradient? And my solution was, the solution of this
 3 invention, is take the image from multiple directions
 4 and carry out mathematics, that's the tensor bit, to
 5 determine the vector orientation on a voxel-by-voxel
 6 basis.

7 So it's a single voxel which is a -- which is
 8 the unit in which we measure the direction and do a
 9 calculation. We fill each little voxel with a vector,
 10 and that is discovering the direction of the tissue or
 11 structure, and after Claim 37, neural tissue in a
 12 mammal and then we go on in settlement claims, 39, to
 13 do it over multiple sections and run an arrow between
 14 them, follow onto the next. We have these tracts.

15 And the Appendix 06050, Figure 9,
 16 there they tell us Memorial Sloan Kettering, you're
 17 using Brainlab FiberTracking. It's a great, great
 18 image because it sweeps across all of neuroscience and
 19 right into this patent because they tell us that they
 20 have used functional MRI, fMRI, a different method.

21 JUDGE TARANTO: I'm sorry. And these are
 22 materials that were, in fact, attached to your
 23 opposition to summary judgment or no? You have a real
 24 problem --

25 MR. FILLER: Yes.

Page 7

1 JUDGE TARANTO: -- if you are relying on the
 2 proposition, as much of your brief does but not all of
 3 it, that the District Court, the MDL District Court,
 4 erred in declining to consider a lot of articles, a lot
 5 of evidence, that you attach to your proposed amended
 6 complaint but did not cite in the summary judgment
 7 motion.

8 MR. FILLER: Right, and I want to --

9 JUDGE TARANTO: That's -- that's a tough thing
 10 to fight.

11 MR. FILLER: But I want to -- but I think that
 12 in order for the Court to think about reaching across
 13 that and listening to argument, you have to know that
 14 if you did reach across it, there is a piece -- there
 15 is solid evidence of what --

16 (Talking simultaneously)

17 JUDGE TARANTO: Well, let's assume that, but I
 18 mean you've --

19 MR. FILLER: Okay.

20 JUDGE TARANTO: -- got to make legal arguments
 21 about why Judge Stearns was wrong in what he did, and
 22 one is he agreed with you on like two and a half of the
 23 claim constructions. Right? You don't have to have
 24 zero anisotropic. Right? It doesn't have to be zero
 25 anisotropic.

Page 8

1 The second one about only peripheral nerves
 2 recovered, he agreed with you about that, and then what
 3 it then came down to was some notion of what exactly a
 4 selected structure is. And it seems to me the opinion
 5 is not all that clear about that, but the argument that
 6 they made on that point was that you actually needed to
 7 know, in one of their declarations, the location and
 8 then the other was I think the orien- -- there were
 9 three declarations. I forget what the names were,
 10 Moseley, Tsung, and somebody else, and they all talked
 11 about assuming that you knew the location, the
 12 position, and/or orientation.

13 And if you're fighting the claim construction
 14 saying no, no, you don't need to know that, that's a
 15 legal argument that's available to you which has a
 16 certain appeal.

17 MR. FILLER: Yeah, and that is very key
 18 because in the -- in the patent, this is at Appendix
 19 0217, there's a series of paragraphs that discuss when
 20 measuring unknown orientation, the word "unknown" again
 21 and again. We're measuring unknown orientations and --

22 JUDGE TARANTO: Right. The spec repeatedly
 23 says this is a lot easier if you actually know the
 24 orientation because then you know what's perpendicular,
 25 what's orthogonal, et cetera.

Page 9

1 MR. FILLER: You don't have to --
 2 (Talking simultaneously)

3 JUDGE TARANTO: But if you don't know it, pick
 4 a random one and start and you'll find it.

5 MR. FILLER: Yes, so exactly. So it's
 6 completely wrong. He's just erred completely because
 7 he goes through it all and then -- then Judge Stearns
 8 comes through and says, ah, but there must be
 9 something unknown here.

10 And this is very much like saying, well, we
 11 don't know the exact margins of someone's femur but,
 12 therefore, we can't measure it because it's unknown.
 13 No, we know exactly where the femur is. We know
 14 exactly how to take a picture of it. We just don't
 15 know the exact shape, and this is what this does is it
 16 solves exact shape. It's like sequencing DNA. We're
 17 finding the orientation of tissue.

18 So because the Court finds that there is a
 19 substantial non-infringing use incorrectly, they say,
 20 well, since there's something unknown. And they look
 21 at unknown. You look at known. Therefore, there's a
 22 substantial non-infringing use.

23 We look to the Toshiba case which says that,
 24 well, if there is a substantial non-infringing use, and
 25 that was one where they were making DVDs --

Page 10

1 JUDGE TARANTO: I'm sorry. Why are we talking
 2 about substantial non-infringing use? There was an
 3 inducement claim and a direct infringement claim.
 4 There was no contributory infringement claim for which
 5 substantial non-infringing use is relevant.
 6 MR. FILLER: Well, it's because he uses that
 7 argument to say that it's a -- that you need to have --
 8 you need to pull direct evidence into the opposition.
 9 JUDGE TARANTO: Right, but I thought your -- I
 10 guess the -- you say a bunch of different things in
 11 your brief in response to that. The one that I guess
 12 I'm focusing on which doesn't depend on that -- right,
 13 that doesn't depend -- is simply when you look at the
 14 arguments that the other side made in its summary
 15 judgment argument, you had no argument to answer that
 16 required you to show the downstream users, the
 17 technology -- the technicians or the neurosurgeons or
 18 the interventional radiologists or whoever, had to be
 19 actually doing this.
 20 Their argument was it is impossible to use the
 21 BrainTracking -- BrainTracking? FiberTracking. The
 22 FiberTracking software to do this, not that you don't
 23 have evidence that anybody does.
 24 MR. FILLER: Exactly. So we --
 25 JUDGE TARANTO: So you didn't have to answer

Page 11

1 that because there wasn't a "that" to answer.
 2 MR. FILLER: Yeah, because he would have had
 3 to attack the evidence that we have to require us.
 4 That's why I claim it's a -- I'd argue it's a deficient
 5 motion for summary judgment because he doesn't attack
 6 the substantive evidence. He tries to do the attack by
 7 knocking the whole thing out by saying it's impossible
 8 to infringe because we only select -- we only select
 9 unknown tissue, and the patent calls for known tissue.
 10 And if you accept that the Court got this
 11 completely wrong, because this is about identifying
 12 unknown tissue, then we are only obligated to answer
 13 the issues raised in the motion for summary judgment by
 14 the movant and we did that so . . .
 15 JUDGE TARANTO: You know, there's kind of a
 16 finding the signal in the noise here problem in the
 17 briefing that's -- that's presented some challenges.
 18 MR. FILLER: I appreciate that, but that's --
 19 you know, certainly the key piece of it is -- because
 20 then I would then go on to say in argument that if the
 21 Court found, no, there is a -- either because the
 22 Court's right on that or because there is a substantial
 23 non-infringing use and we were required, he argues
 24 that, therefore, we were required to bring in
 25 the specific event -- specific bits of evidence even

Page 12

1 though the movant hadn't raised them, and that's where
 2 we objected in the motion for reconsideration.
 3 This was like a sua sponte after-the-fact
 4 decision. He's telling us only at the time of issuing
 5 the order that we're going to have to respond to
 6 something that the moving party hasn't -- hasn't
 7 asserted.
 8 JUDGE TARANTO: Do you happen to remember,
 9 does the joint appendix contain the actual motion for
 10 reconsideration? If you don't remember, don't --
 11 MR. FILLER: Yes, it does.
 12 JUDGE TARANTO: Okay. I'll look at it.
 13 MR. FILLER: Okay.
 14 JUDGE TARANTO: I see it. Thanks.
 15 MR. FILLER: So, and I -- and I appreciate
 16 that you've saved a lot of time by focusing on these --
 17 on these key issues, but I identified where to look in
 18 the patent for this fact that we're addressing, unknown
 19 orientations. That's why you have to take the multiple
 20 directions and do the calculation is to -- is to find
 21 the directions.
 22 It's just like sequencing a DNA, find where
 23 the actual sequence is, find what the actual
 24 orientations are, because once we figure out the
 25 orientations of each little voxel on the brain, we can

Page 13

1 then march from point to point and map out these
 2 connections, transform neuroscience and, you know, save
 3 thousands of lives, which is what this has done. So
 4 I'll hold over my, if I may, additional time to my
 5 rebuttal and allow Brainlab to proceed.
 6 JUDGE NEWMAN: Yes. Thank you. Mr. Filler.
 7 Mr. Campbell.
 8 MR. CAMPBELL: May it please the Court, your
 9 Honor, I want to address a couple questions from
 10 Judge Taranto first.
 11 He asked about claim construction and the
 12 Court's claim construction. The Court adopted
 13 completely NeuroGrafix's claim construction. There was
 14 an issue as to what selected structure meant, but it
 15 wasn't really a claim construction issue on selected
 16 structure. It was whether, according to NeuroGrafix,
 17 you could interpret the word ROI, region of interest,
 18 or region to be the same thing as a selected structure.
 19 The specification does talk about selecting a
 20 structure. There are many indications as to how you
 21 can select a structure. Those structures can be known
 22 in advance. Peripheral nerves are known in advance.
 23 The optic nerve position is known in advance. Other
 24 nerves, peripheral nerves around the brain, are known
 25 in advance. They selected that language to use. The

Page 14

1 specification may be broader and may talk about
 2 choosing regions, but that's not what they claimed.
 3 JUDGE TARANTO: All right, but put -- but put
 4 aside that. So a selected structure is just a brain
 5 structure that somebody choosing to adopt -- to
 6 implement this method chooses to subject to the method.
 7 MR. CAMPBELL: An anisotropic structure first.
 8 JUDGE TARANTO: Yeah, yeah, the other, but
 9 you --
 10 MR. CAMPBELL: It just can't be a region.
 11 JUDGE TARANTO: Right, but you lost on --
 12 MR. CAMPBELL: Peripheral.
 13 JUDGE TARANTO: Right. You lost on
 14 peripheral. You've lost on zero anisotropic.
 15 MR. CAMPBELL: Correct.
 16 JUDGE TARANTO: Right? So . . .
 17 MR. CAMPBELL: Right.
 18 JUDGE TARANTO: And then you said our software
 19 cannot do what this says because it actually maps
 20 everything and not just one thing, and the claim is not
 21 a pick out one and do only one.
 22 MR. CAMPBELL: Um-hmm.
 23 JUDGE TARANTO: As long as you've got one, you
 24 can be mapping everything under the sun as long as
 25 you've got one. It's within the claim.

Page 15

1 MR. CAMPBELL: Well, that's not true. In our
 2 motion for summary judgment, specifically Appendix 7322
 3 and on, we talk about the fact that none of our
 4 customers use it the way they claim. None of our
 5 customers use it to select a structure, whether it be
 6 in advance, no matter what kind of structure it is,
 7 whether it be a peripheral nerve or a nerve in the
 8 brain or white matter that you don't see in advance.
 9 Because the way Brainlab uses it is we've got
 10 a neurosurgeon, and he wants to perform some kind of
 11 surgery around gray matter, typically matter that
 12 doesn't have anisotropy. And he wants to see, or she,
 13 if there is a fiber, a white matter fiber, near that.
 14 So he doesn't know or she doesn't know in advance. The
 15 whole purpose of doing FiberTracking is Brainlab
 16 markets --
 17 JUDGE TARANTO: Everybody knows that there's
 18 this pyramidal structure in the brain. Right?
 19 MR. CAMPBELL: Um-hmm.
 20 JUDGE TARANTO: What more do you need? Say I
 21 want to do this to find the damn thing.
 22 MR. CAMPBELL: Well, if you wanted to do --
 23 define the pyramidal structure you could.
 24 JUDGE TARANTO: Or maybe you want to find
 25 something else. You want to find a tumor.

Page 16

1 MR. CAMPBELL: Right. You may want to find
 2 something else, but the key to Brainlab's use of it is
 3 we don't select anything in advance. We just run it.
 4 And, in fact, as NeuroGrafix argues in Section 3 of
 5 their brief, Brainlab runs FiberTracking in advance of
 6 anything, before a user selects any structure,
 7 whether -- or any region of interest. It's only after
 8 the region of interest that you see these fibers, and
 9 as we showed --
 10 JUDGE TARANTO: I'm sorry. A tech- -- you
 11 know, the neurologist --
 12 MR. CAMPBELL: Um-hmm.
 13 JUDGE TARANTO: -- or the neurosurgeon says
 14 I'm about to do some surgery in the following area of
 15 the brain. I really want a precise map of a bunch of
 16 things that I would like to stay away from.
 17 MR. CAMPBELL: Um-hmm.
 18 JUDGE TARANTO: Why isn't that selecting a
 19 structure? And so we're going to use FiberTracking
 20 tomorrow.
 21 MR. CAMPBELL: I'm going to use FiberTracking,
 22 and I'm going to use FiberTracking to select a region
 23 around --
 24 JUDGE TARANTO: No, no, no, no. You're not
 25 using it to select it. You selected it. I want to

Page 17

1 know where the pyramidal track is (sic) -- tract is,
 2 and so now I'm going to run FiberTracking.
 3 MR. CAMPBELL: Um-hmm.
 4 JUDGE TARANTO: Selected is just this is one
 5 of the things I am looking for when I do this process.
 6 MR. CAMPBELL: That's not as the parties
 7 interpreted it. The parties interpreted looking for
 8 a structure that you know is there, looking for --
 9 JUDGE TARANTO: Right.
 10 MR. CAMPBELL: -- a nerve that may be --
 11 JUDGE TARANTO: I'm sorry. Why -- why is that
 12 different from what I'm at least trying to show?
 13 MR. CAMPBELL: Because we're looking for some
 14 known structure.
 15 JUDGE TARANTO: You know that there's a
 16 pyramidal tract in there.
 17 MR. CAMPBELL: You know that there's a
 18 pyramidal but --
 19 JUDGE TARANTO: Pyramidal? Is that how you
 20 say it? Sorry about that.
 21 MR. CAMPBELL: I'm sorry?
 22 JUDGE TARANTO: Pyramidal? I'm sorry. I'm
 23 not --
 24 MR. FILLER: Pyramidal.
 25 JUDGE TARANTO: -- familiar with the --

Page 18

1 MR. CAMPBELL: Dr. Filler --

2 JUDGE TARANTO: Okay. Pyram- -- we'll say

3 pyramidal. Good.

4 MR. CAMPBELL: -- corrected me several times,

5 and now I think I say it at least the way he says it.

6 But, you know, you're getting back to the

7 point, never did NeuroGrafix introduce any evidence

8 that Brainlab's customers use it to find the pyramidal

9 structure.

10 JUDGE TARANTO: I don't --

11 MR. CAMPBELL: Introduce any evidence that

12 they use it in any fashion. There was no evidence that

13 Brainlab customers even use it.

14 JUDGE TARANTO: Your advertisements and manual

15 were in their opposition to summary judgment and

16 it --

17 MR. CAMPBELL: That you could use it to find

18 the pyramidal structure.

19 JUDGE TARANTO: Right, and -- really? It's

20 a -- it's a contestable proposition that people were

21 using this without having in their mind any idea of

22 a -- of a structure that they were hoping to map?

23 Really?

24 MR. CAMPBELL: Yes. Yes, we had testimony

25 from --

Page 19

1 JUDGE NEWMAN: No, but how can that be?

2 MR. CAMPBELL: We have testi- --

3 JUDGE NEWMAN: These are very serious

4 procedures.

5 MR. CAMPBELL: True.

6 JUDGE NEWMAN: It certainly has to be -- the

7 supposition for the entire structure is that these are

8 administered by experts. Claims are very broad.

9 Claims don't include the limitations you're telling us

10 about.

11 MR. CAMPBELL: Well, the claim does require

12 you --

13 JUDGE NEWMAN: 36 doesn't talk about --

14 MR. CAMPBELL: -- to select --

15 JUDGE NEWMAN: -- white matter.

16 MR. CAMPBELL: I'm sorry.

17 JUDGE NEWMAN: It says we're looking for the

18 shape and position of structure.

19 MR. CAMPBELL: Of a --

20 JUDGE NEWMAN: And, of course, there are the

21 suspicions based on all of the peripheral evidence that

22 there may very well be structure in the brain.

23 MR. CAMPBELL: We are looking for the position

24 of a selected anisotropic structure, a selected nerve.

25 Many of these nerves --

Page 20

1 JUDGE NEWMAN: It's not in the claim.

2 MR. CAMPBELL: I'm sorry?

3 JUDGE NEWMAN: It's not in the claim.

4 MR. CAMPBELL: Yes, it is. The selected

5 structure isn't any structure. It's a selected

6 structure that exhibits diffusional anisotropy, in

7 other words, it's white matter structure. Now, much of

8 this light --

9 JUDGE NEWMAN: And the diffuse -- diffusion

10 gradients.

11 MR. CAMPBELL: Um-hmm.

12 JUDGE NEWMAN: Where --

13 MR. CAMPBELL: (Inaudible).

14 JUDGE NEWMAN: I'm trying to put it together.

15 The claims are quite broad.

16 MR. CAMPBELL: In some fashions they --

17 JUDGE NEWMAN: Are they not?

18 MR. CAMPBELL: In some fashion it is, but it's

19 not because it does say selected structure, and it says

20 that throughout. As NeuroGrafix would do, they just

21 eliminate that completely. They say you can select any

22 area of the brain in any areas of structure, but that's

23 not true. You have to have a selected anisotropic

24 structure, which basically is a white matter.

25 JUDGE TARANTO: So did you -- did you say in

Page 21

1 your summary judgment motion, and if so where,

2 no user -- there is no evidence that any user of

3 FiberTracking undertakes to use FiberTracking with the

4 idea in mind of trying to map an anisotropic structure?

5 MR. CAMPBELL: No. We say that we don't do it

6 trying to find any known isotropic structure and

7 that's -- that was the testimony of the experts and the

8 users.

9 JUDGE TARANTO: But, but, but -- I'm sorry,

10 but I know and it seemed to me you did a most

11 interest- -- you had Tsung, Leach, and Moseley. Right?

12 MR. CAMPBELL: Yeah.

13 JUDGE TARANTO: And Moseley expressly has a

14 paragraph that says, "I interpret the claim language of

15 selected to require" -- I forget whether his is

16 orientation or location.

17 MR. CAMPBELL: Um-hmm.

18 JUDGE TARANTO: Now, he -- there's

19 orientation, location, and position between Tsung,

20 Leach and --

21 MR. CAMPBELL: Yeah.

22 JUDGE TARANTO: And they all assume something

23 that the term "selected structure" does not properly

24 construed assume.

25 MR. CAMPBELL: Well, no. They all assume that

Page 22

1 that means you're selecting something, and you're going
 2 to try then to track it.

3 JUDGE TARANTO: But Moseley, for example, does
 4 not say no user of this system has in mind a structure
 5 that any neurologist would know is anisotropic and is
 6 using this software to get a precise map of it.

7 On its face it sounds preposterous to me. I'm
 8 not an expert, but what else are they using this for?

9 MR. CAMPBELL: They use it to see if there is
 10 a structure. It doesn't have to be pyramidal
 11 structure. It can be any structure, any white matter
 12 anisotropic structure that is passing through --

13 JUDGE TARANTO: And that there's -- and that
 14 there's no user of the FiberTracking system that has in
 15 mind such a structure that they're looking to map
 16 precisely?

17 MR. CAMPBELL: In advance?

18 JUDGE TARANTO: In advance.

19 MR. CAMPBELL: There's no testimony from
 20 anybody.

21 JUDGE TARANTO: Where did you --

22 MR. CAMPBELL: No evidence from anybody.

23 JUDGE TARANTO: Where did you say in the
 24 summary judgment motion that if you assume that
 25 selected structure simply means a structure that a user

Page 23

1 wants to subject to this process and get a precise map
 2 of, that there is no evidence that any user of the
 3 system does that?

4 MR. CAMPBELL: Yes. In 7322 and the couple
 5 pages that follow they respond -- they incorporate
 6 statements from Dr. Leach and Dr. Tsung, both of which
 7 say they do not look to --

8 JUDGE TARANTO: Right, but all -- all of those
 9 three statements, Leach, Tsung, and Moseley, they all
 10 come in that very paragraph at the bottom of 22 and
 11 23 --

12 MR. CAMPBELL: Right.

13 JUDGE TARANTO: -- all building the assumption
 14 that you already know the location.

15 MR. CAMPBELL: They are building on the
 16 assumption that if you -- that the way they use
 17 Brainlab's system is you don't look for anything in
 18 specific. You're not looking for, for example,
 19 pyramidal structure, not -- you're not looking for any
 20 known structure, any pre-selected structure.

21 You just want to find out what is around that
 22 tumor. That's what they're concerned about, because
 23 there may be fibers that go from that tumor to another
 24 part in the brain, and they don't want to intersect
 25 them.

Page 24

1 JUDGE NEWMAN: Well, they're standard
 2 diagnostic procedures that you're talking about, and I
 3 can't find such a distinction being drawn as to whether
 4 you know or don't know in advance what you're going to
 5 find.

6 MR. CAMPBELL: Well, isn't that the whole use
 7 of the word "selected"? And in fact --

8 JUDGE TARANTO: But you just -- you just said,
 9 right, you're scanning this area because there are
 10 structures you know you don't want to -- I forget what
 11 your verb was.

12 MR. CAMPBELL: Well, you don't know. No, you
 13 don't know. You don't know what's there. That's
 14 why -- that's the difference between --

15 JUDGE TARANTO: Really? The people -- the
 16 people who are running this don't know that there's a
 17 pyramidal structure in the brain?

18 MR. CAMPBELL: No. They know there's a
 19 pyramidal --

20 JUDGE TARANTO: And they would really like --

21 MR. CAMPBELL: They know --

22 JUDGE TARANTO: -- not to touch it?

23 MR. CAMPBELL: -- there's a pyramidal
 24 structure, but they don't know the pyramidal structures
 25 anywhere near the tumor, and in many cases it's not.

Page 25

1 It's nowhere near it. They have a tumor and they want
 2 to know what's around it, and that's why they run it.

3 They don't know there's a pyramidal structure
 4 right next to it and they're trying to see how close.
 5 They don't know that there's any white matter
 6 structures, significant ones, next to it. All they do
 7 is -- and this is what the experts said.

8 You know, there was no testimony from any
 9 expert whatsoever or any testimony that NeuroGrafix
 10 admitted saying as to how anybody uses this. The only
 11 testimony was from Leach --

12 JUDGE TARANTO: No testa- --

13 MR. CAMPBELL: -- and Tsung.

14 JUDGE TARANTO: I'm sorry. No testimony
 15 but --

16 MR. CAMPBELL: Right.

17 JUDGE TARANTO: -- there were, what, two pages
 18 from advertisements, your advertisements --

19 MR. CAMPBELL: That you could select the
 20 pyramidal --

21 JUDGE TARANTO: Can I finish my --

22 MR. CAMPBELL: You could do that.

23 JUDGE TARANTO: No, no. I'd like to ask you
 24 to let me finish my question.

25 MR. CAMPBELL: I'm sorry.

Page 26

1 JUDGE TARANTO: Thank you.

2 MR. CAMPBELL: I apologize, your Honor.

3 JUDGE TARANTO: They were, I think, two

4 advertising pictures and one in the manual which

5 referred to, hey, a terrific benefit of this is that

6 you can identify the location of the pyramidal tract.

7 MR. CAMPBELL: Um-hmm.

8 JUDGE TARANTO: Why is that not sufficient

9 evidence that it's done? If you were advertising it

10 and telling people you could use it that way, I bet

11 there were doctors out there that were using it for

12 that purpose saying, "I'd like to know where this tract

13 is so that I don't do harm when I intervene."

14 MR. CAMPBELL: Well, there may be doctors who

15 do that, but that's not sufficient to prove

16 infringement. They have to do that. Now, it's

17 just the claim wasn't this capable.

18 JUDGE TARANTO: Why is that not -- I'm sorry.

19 Why is that not sufficient to prove -- and we're

20 getting beyond what I think is probably --

21 MR. CAMPBELL: I think we're getting to

22 inducement maybe.

23 JUDGE TARANTO: No, no. You said that the

24 prin- -- the principal ground of the District Court's

25 decision -- the inducement is just in a footnote.

Page 27

1 Right? I mean, the principal ground of the District

2 Court's decision is there was no proof that anybody

3 was directly infringing.

4 MR. CAMPBELL: True.

5 JUDGE TARANTO: Right.

6 MR. CAMPBELL: There is no proof that anybody

7 was directly infringing, and that's where it ends.

8 There was no proof and, in fact, NeuroGrafix admits

9 that there was no proof. They admit that they

10 introduced absolutely no proof and no argument of

11 direct infringement. That should end it there.

12 And, in fact, there is no evidence. There are

13 two advertisements which mention pyramidal structure,

14 but it doesn't say that you have to do that. You could

15 do FiberTracking to find any of the other structures

16 that aren't the pyramidal structure and, in fact, the

17 testimony of our experts is that's how they do it.

18 They're not looking specifically for the pyramidal

19 structure.

20 JUDGE TARANTO: Right, but why if--

21 some of your summary judgment brief and I guess some of

22 your brief here suggests that for there to be a

23 selected structure, the result of the process has to be

24 limited to mapping that one and not mapping anything

25 else.

Page 28

1 MR. CAMPBELL: Yes, we argue that as well.

2 JUDGE TARANTO: Right, but that --

3 MR. CAMPBELL: Because you're not --

4 JUDGE TARANTO: There's nothing in the claim

5 about that. Right? This is --

6 MR. CAMPBELL: Well . . .

7 JUDGE TARANTO: This is all -- the fact that

8 you select a structure doesn't mean that you're not

9 interested in or even getting the information about

10 everything else surrounding it. All this says is that

11 you have to scan -- I'm using "scan" as a way to

12 expose -- yes, exposing a region that contains a

13 selected structure.

14 MR. CAMPBELL: Right.

15 JUDGE TARANTO: It doesn't say that you are

16 exposing a region that contains -- which would be

17 silly, but contains that structure and no other

18 structure.

19 MR. CAMPBELL: Well, it doesn't say that

20 structure and no other structure.

21 JUDGE TARANTO: Right.

22 MR. CAMPBELL: I agree with you. It says a

23 selected structure. So you're scanning it --

24 JUDGE NEWMAN: It says selected structure and

25 other structures.

Page 29

1 MR. CAMPBELL: Right, the region.

2 The region you scan must -- or is supposed to include

3 the selected structures and other structures, but still

4 it says just not anis- -- it doesn't say the region

5 includes anisotropic structures and isotropic

6 structures. It says a selected anisotropic structure.

7 That's Step A, Claim 36.

8 JUDGE NEWMAN: It says selected but exhibits

9 diffusion anisotropy and other structures that do not

10 exhibit diffusion anisotropy.

11 MR. CAMPBELL: True, but it says a selected

12 structure that does. So what does "selected" mean?

13 "Selected" must mean that you're looking for something

14 in specific. Right?

15 JUDGE NEWMAN: So you --

16 MR. CAMPBELL: And in fact --

17 JUDGE NEWMAN: -- run your first scan and you

18 select the structure, and then you run another one for

19 precision and so on and there it is, the --

20 MR. CAMPBELL: You only run it once. You

21 don't run it first to look for a structure and then run

22 it again? In Brainlab --

23 JUDGE NEWMAN: Well, but that really is --

24 that is the whole issue, that you run it. You don't

25 run it just for fun just to see what different colors

Page 30

1 are going to turn up in your brain scan.
 2 MR. CAMPBELL: True, your Honor.
 3 JUDGE NEWMAN: So you have --
 4 MR. CAMPBELL: But you run it to --
 5 JUDGE NEWMAN: -- significant information to
 6 start with before you do all of this, I would think or
 7 hope.
 8 MR. CAMPBELL: Well, no, and that's the key
 9 between, I think, the patent and what Brainlab does.
 10 Brainlab doesn't care what's there in advance. They're
 11 not looking for something --
 12 JUDGE NEWMAN: Any diagnostic procedure then
 13 would -- would not meet any kind of definition of
 14 diagnostic procedure because you're looking for
 15 something whose presence you then verify when you
 16 conduct the procedure.
 17 And why doesn't that apply to the way this
 18 brain (sic) -- this claim is written as a selected
 19 structure?
 20 MR. CAMPBELL: Well, because it requires, I
 21 guess, selected structure. It doesn't say any
 22 structure that exhibits diffusional anisotropy and
 23 isotropic structures. It says a selected structure.
 24 So you have to have some structure that you
 25 know something of in advance. You believe it's there.

Page 31

1 Maybe the pyramidal tract. You believe that there's a
 2 structure here, and that's what you're selecting and
 3 that's what you're looking for in advance. When
 4 Brainlab uses its device, it just draws a region of
 5 interest around a tumor.
 6 JUDGE NEWMAN: But was the summary judgment
 7 based on that or was it based on absence of evidence,
 8 of actual as opposed to contributory infringement?
 9 MR. CAMPBELL: Well, it was based on the fact
 10 that plaintiff produced no evidence of anybody using
 11 FiberTracking in any manner, in any manner whatsoever,
 12 and especially not in the manner in which they argue,
 13 their hypothetical use, which is essentially to always
 14 find the pyramidal structure.
 15 JUDGE NEWMAN: So your brochure with
 16 instructions say --
 17 MR. CAMPBELL: Hmm?
 18 JUDGE NEWMAN: You're saying that the
 19 instructions in the -- in the brochure as to what the
 20 system can do are insufficient.
 21 MR. CAMPBELL: Yes. It doesn't say you must
 22 select a pyramidal structure. It doesn't say you must
 23 select anything. In fact, the manual for FiberTracking
 24 doesn't use the word "pyramidal." It doesn't say you
 25 have to use it in a certain way. The patent doesn't --

Page 32

1 JUDGE TARANTO: The manual doesn't? That's
 2 just the advertisement? Is that right? I thought
 3 there was one reference in the manual. Am I
 4 misremembering that?
 5 MR. CAMPBELL: The manual never talks about
 6 it.
 7 JUDGE TARANTO: No, no, no. Don't.
 8 MR. CAMPBELL: Hmm?
 9 JUDGE NEWMAN: Mr. Filler is pointing out that
 10 we're running over time.
 11 MR. CAMPBELL: I understand we've run over
 12 time.
 13 JUDGE NEWMAN: But that's --
 14 MR. CAMPBELL: I'm just trying to finish the
 15 answer to the questions.
 16 JUDGE NEWMAN: Is there anything else you need
 17 to tell us?
 18 MR. CAMPBELL: I think I just want to conclude
 19 by saying that never did NeuroGrafix introduce any
 20 evidence that anybody uses Brainlab's device in any
 21 way, in any fashion, whether it be the -- you know,
 22 some infringing method that finds a pyramidal structure
 23 or does anything else, all the non-infringing methods,
 24 and the Court found there were both infringing possibly
 25 methods and non-infringing methods.

Page 33

1 And mention just briefly sua sponte. Never
 2 did NeuroGrafix argue sua sponte in any of the briefs,
 3 and it was not in their motion for reconsideration. So
 4 we believe the judge's opinion below should be
 5 affirmed. Thank you very much.
 6 JUDGE NEWMAN: Thank you, Mr. Campbell, and we
 7 will add --
 8 MR. CAMPBELL: And, your Honor, I appreciate
 9 if I talked over you a couple times. I was just
 10 getting excited.
 11 JUDGE NEWMAN: We will add to Mr. Filler's
 12 time the amount we've run over, Mr. Campbell.
 13 MR. FILLER: Thanks very much. So I did want
 14 to address this issue of their -- that you should know
 15 that in the event that you reverse and remand that the
 16 record does contain exactly what Mr. Campbell says it
 17 does not, and that's why I was pointing to that
 18 particular page beginning 06050.
 19 Because neurosurgeons know there's areas of
 20 the brain you could take out a large amount and have
 21 not much trouble for the patient and other parts where
 22 you'd have a devastating injury from a tiny amount, and
 23 the pyramidal tract is one of these. And, yes,
 24 pyramidal tract is named specifically in the manual.
 25 That is correct, Judge Taranto.

Page 34

1 So what happens in Figure 9 is they tell us
 2 that they use this fMRI to locate Broca's and
 3 Wernicke's area. What are these? These are -- I talk
 4 about that there is -- there are no unknown structures.
 5 It's the unknown detail.
 6 Broca's is speech generation discovered in
 7 1861. People had a series of -- he had a series of
 8 patients who lost speech and then they died, and he
 9 sectioned the brain and found the injury. That was
 10 motor speech. And Wernicke's, around the same year,
 11 1861, Carl Wernicke in Germany found receptive speech
 12 area. If it was injured, people could no longer
 13 understand speech.
 14 Now, ten years later they found that
 15 connecting the two, motor speech and receptive speech,
 16 was a tract which they called the arcuate fasciculus,
 17 and that's what this image is about. Because this
 18 patient has a tumor between the motor speech area and
 19 the receptive speech area pushing the arcuate
 20 fasciculus out of place, and they want to know can we
 21 get the tumor out without injuring the arcuate
 22 fasciculus. And they used Brainlab to find out exactly
 23 where the arcuate fasciculus has been pushed to by the
 24 tumor and where the edges are.
 25 This is exactly, exactly laid out. They're

Page 35

1 doing something that appears in the patent,
 2 specifically talks about exactly this issue of the
 3 parts of the brain that the tracts are immersed in the
 4 speech areas. So, in the use of MRI, fMRI, which is
 5 for something called B-O-L-D or BOLD imaging to
 6 identify a functional area, that also appears in the
 7 manual which I'm sure Mr. Campbell will have to agree
 8 to.
 9 So on remand, yes, absolutely, evidence before
 10 the jury will include this user of Brainlab wanting to
 11 avoid injury to this tract exactly as you have just
 12 been disputing. They've set out to do this. They know
 13 the tumor is near the arcuate fasciculus, and if they
 14 hit the fasciculus, they're going to severely impair
 15 the patient's speech.
 16 They want to know exactly where it is. They
 17 pick the two structures using Brainlab, it's totally
 18 capable of this, with this intention and, in fact, the
 19 manual tells them to use BOLD imaging for this and for
 20 a pyramidal tract. And they advertise for it, and
 21 that's what neurosurgeons want.
 22 And so Mr. Campbell -- which you may have
 23 noticed about all of his experts is they all say just
 24 about the same thing, and that didn't happen by chance.
 25 So I think that you're looking at a legal argument and

Page 36

1 not true medical opinion.
 2 The other issue that he raises about selecting
 3 a structure is to suggest that somehow it means that
 4 you have to select the entire structure, but the method
 5 in the patent, the Claim 36, is really at a single
 6 voxel. You just have to select a structure because
 7 that's a level at which it determines the orientation.
 8 It does it voxel by voxel.
 9 So again, I won't use up all my time, but I
 10 believe that the judge, Honorable Judge Stearns, was
 11 wrong when he found there was a substantial
 12 non-infringing use. He uses that. He points to
 13 Toshiba to say, therefore, you did have to bring
 14 extra -- specific evidence in even though they didn't
 15 cite -- even though they didn't attack the other
 16 evidence.
 17 We don't. We don't say there's no evidence of
 18 infringement. What we do -- we don't admit that. We
 19 just say you always infringe. Whenever you do these
 20 things you're infringing because there's no
 21 non-infringing use. That's why -- that's our response.
 22 They're saying we don't have to attack the evidence
 23 because we never infringe. We come back and say you
 24 always infringe.
 25 The Court decides it by saying, ahh, there's

Page 37

1 unknown tissue and we don't -- I don't think the patent
 2 covers unknown tissue. 100 percent wrong. That needs
 3 to change. It reverses the whole thing. They have
 4 a -- it's a deficient motion in that it didn't cite
 5 individual infringement, but if we take it as a valid
 6 motion, it is sufficient.
 7 It argues one thing. You can't infringe. The
 8 answer is the judge got it wrong. They always
 9 infringe, and that's why the motion for summary
 10 judgment must fail, because there is substantial
 11 evidence of infringement which a jury could readily
 12 find. This is not a position of a judge to prevent
 13 this from getting in front of a jury. Thank you very
 14 much.
 15 JUDGE NEWMAN: Thank you. Thank you both.
 16 The case is taken under submission. That concludes our
 17 argued cases for this morning and afternoon.
 18 THE BAILIFF: All rise. The Honorable Court
 19 is adjourned until tomorrow morning.
 20 (End of oral argument)
 21
 22 * * *
 23
 24
 25

CERTIFICATION

1
2
3
4
5
6
7
8
9
10
11
12
13
14
15
16
17
18
19
20
21
22
23
24
25

I, Kelly Paulson, CSR No. 8295, certified shorthand reporter for the State of California, do hereby certify:

That said audio recorded material was transcribed into typewriting under my direction and supervision to the best of my ability, except in the instances where the transcript indicates "inaudible." And I hereby certify that said material is a full, true, and correct transcript of the audio recorded material.

I further certify that I am neither counsel for nor related to any party to said action, nor in any way interested in the outcome thereof.

IN WITNESS WHEREOF, I hereunto subscribe my name this 14th day of November, 2019.



Kelly Paulson, CSR No. 8295

<p>0</p> <p>0217 8:19</p> <p>06050 6:15</p>	<p>23:22 24:2</p> <p>28:5,9 32:5</p> <p>absence 31:7</p> <p>absolutely</p> <p>2:14 5:9</p> <p>27:10</p>	<p>after-the-fact</p> <p>12:3</p> <p>again 8:20,21</p> <p>29:22</p> <p>against 2:5</p> <p>ago 2:10</p>	<p>11,13,19,20,</p> <p>22 22:1,5,13</p> <p>23:1,4,6,9,</p> <p>10,24 24:2,7,</p> <p>20,25 25:1,2,</p> <p>4,7,13 26:4,</p>
<p>1</p> <p>18-2363 2:5</p>	<p>accept 11:10</p> <p>according</p> <p>13:16</p> <p>accurate 3:13</p>	<p>agree 28:22</p> <p>agreed 7:22</p> <p>8:2</p> <p>ahh 9:8</p>	<p>10,19 27:7,8,</p> <p>10,12,16,21,</p> <p>24 28:17,20,</p> <p>24 29:3,5,9,</p>
<p>2</p> <p>2009 4:12</p> <p>2016 4:11</p> <p>22 23:10</p> <p>23 23:11</p>	<p>across 6:18</p> <p>7:12,14</p> <p>actual 12:9,</p> <p>23 31:8</p> <p>actually 4:2</p> <p>8:6,23 10:19</p> <p>14:19</p>	<p>all 3:5,12</p> <p>4:3 5:17 6:18</p> <p>7:2 8:5,10</p> <p>9:7 14:3</p> <p>19:21 21:22,</p> <p>25 23:8,9,13</p> <p>25:6 28:7,10</p> <p>30:6 32:23</p>	<p>21 30:8,9,17,</p> <p>22 31:2,12</p> <p>32:24,25</p> <p>and/or 8:12</p> <p>anis- 29:4</p>
<p>3</p> <p>3 16:4</p> <p>36 5:2,10,12</p> <p>19:13 29:7</p> <p>37 5:11 6:11</p> <p>39 6:12</p>	<p>additional</p> <p>13:4</p> <p>address 4:12</p> <p>13:9</p> <p>addressing</p> <p>12:18</p> <p>administered</p> <p>19:8</p> <p>admit 27:9</p> <p>admits 27:8</p>	<p>allow 13:5</p> <p>already 23:14</p> <p>also 2:7</p> <p>Alumina 4:11</p> <p>always 31:13</p> <p>am 17:5 32:3</p> <p>amended 7:5</p> <p>and 2:7,11,</p>	<p>5:16,19 7:24,</p> <p>25 14:7,14</p> <p>19:24 20:23</p> <p>21:4 22:5,12</p> <p>29:5,6</p> <p>anisotropy</p> <p>15:12 20:6</p> <p>29:9,10 30:22</p>
<p>7</p> <p>7322 15:2</p> <p>23:4</p>	<p>admission</p> <p>25:10</p> <p>adopt 14:5</p> <p>adopted 13:12</p> <p>advance 3:15</p>	<p>15,16,20,25</p> <p>3:5,7,14,15,</p> <p>18 4:6,11,17,</p> <p>18,24 5:5,9,</p> <p>12,18,20 6:2,</p> <p>4,8,10,11,12,</p>	<p>29:18</p> <p>another 23:23</p> <p>29:18</p> <p>answer 10:15,</p> <p>25 11:1,12</p> <p>32:15</p> <p>any 16:6,7</p>
<p>9</p> <p>9 6:15</p>	<p>5:7 13:22,23,</p> <p>25 15:6,8,14</p> <p>16:3,5 22:17,</p> <p>18 24:4</p> <p>30:10,25 31:3</p>	<p>13,15,18,21</p> <p>7:8,13,21,22</p> <p>8:2,4,7,10,</p> <p>13,17,21 9:4,</p> <p>7,8,10,15,20,</p> <p>24 10:3 11:9,</p>	<p>18:7,11,12,21</p> <p>20:5,21,22</p> <p>21:2,6 22:5,</p> <p>11 23:2,19,20</p> <p>25:5,8,9</p> <p>27:15 30:12,</p> <p>13,21 31:11</p> <p>32:19,20,21</p>
<p>A</p> <p>Abbott 4:11,</p> <p>16</p> <p>about 2:10,25</p> <p>3:4,16,21</p> <p>7:12,21 8:1,</p> <p>2,5,11 10:2</p> <p>11:11 13:11,</p> <p>19 14:1 15:3</p> <p>16:14 17:20</p> <p>19:10,13</p>	<p>advertisement</p> <p>32:2</p> <p>advertisements</p> <p>18:14 25:18</p> <p>27:13</p> <p>advertising</p> <p>26:4,9</p> <p>after 3:12</p> <p>6:11 16:7</p>	<p>10,14,23</p> <p>12:1,15,20</p> <p>13:1,2,5,11</p> <p>14:1,18,20,21</p> <p>15:3,10,12</p> <p>16:4,8,19,22</p> <p>17:2 18:5,14,</p> <p>15,19 19:18,</p> <p>20 20:9,19</p> <p>21:1,6,7,10,</p>	<p>25:5,8,9</p> <p>27:15 30:12,</p> <p>13,21 31:11</p> <p>32:19,20,21</p> <p>anybody 10:23</p> <p>22:20,22</p> <p>25:10 27:2,6</p> <p>31:10 32:20</p> <p>anything</p> <p>16:3,6 23:17</p> <p>27:24 31:23</p> <p>32:16,23</p>

anywhere 24:25	articles 7:4	10:6 11:1,2, 5,8,11,19,21, 22 12:24	briefing 11:17
apologize 26:2	as 4:25 7:2 13:14,18,20 14:23,24	14:19 15:9 17:13 20:19 23:22 24:9 28:3 30:14,20	bright 5:21 bring 11:24 broad 5:12 19:8 20:15
appeal 8:16	20:20 24:3 25:10 28:1,11 30:18 31:8,19	before 4:11 5:7 16:6 30:6	broader 14:1 brochure 31:15,19
appendix 6:15 8:18 12:9 15:2	aside 14:4	being 24:3	building 23:13,15
apply 2:19 30:17	ask 25:23	believe 30:25 31:1	bunch 10:10 16:15
appreciate 11:18 12:15	asked 13:11	benefit 26:5	but 4:16,17 5:12,22,25 7:2,6,11,17 8:5 9:3,8,11 10:9 11:18 12:17 13:14 14:2,3,8,11 16:2 17:18 18:6 19:1 20:18,22 21:9,10 22:3, 8 23:8 24:8, 24 25:15 26:15 27:14, 20 28:2,17 29:3,8,11,23 30:4 31:6 32:13
are 3:10 4:4, 8,22,23 6:21 7:1 10:1 11:12 12:24 13:20,22,24 19:3,7,8,20, 23 20:15,17 22:8 23:15 24:9,16 27:12 28:15 30:1 31:20	asserted 12:7	bet 26:10	by 2:15,16,18 4:17 11:6,7, 13 12:16 19:8 32:19
area 16:14 20:22 24:9	assume 7:17 21:22,24,25 22:24	between 6:13 21:19 24:14 30:9	
areas 4:23 20:22	assuming 8:11	beyond 3:17 26:20	
aren't 27:16	assumption 23:13,16	Biosystems 4:11,19	
argue 11:4 28:1 31:12	at 4:8,18 8:18 9:21 10:13 12:4,12 17:12 18:5 23:10	bit 2:25 6:4	
argued 2:4	attach 7:5	bits 11:25	
argues 11:23 16:4	attached 6:22	book 2:9	
argument 2:1 3:4 4:2 7:13 8:5,15 10:7, 15,20 11:20 27:10	attaches 5:11	both 23:6 32:24	
arguments 2:10 3:2 4:8 7:20 10:14	attack 11:3, 5,6	bottom 23:10	
arm 5:14	attorney's 2:11	brain 3:5 12:25 13:24 14:4 15:8,18 16:15 19:22 20:22 23:24 24:17 30:1,18	
around 13:24 15:11 16:23 23:21 25:2 31:5	available 8:15	Brainlab 2:5, 11,12,15 6:17 13:5 15:9,15 16:5 18:13 29:22 30:9,10 31:4	
arrow 6:13	away 16:16	Brainlab's 16:2 18:8 23:17 32:20	
		Braintracking 10:21	
		brief 7:2 10:11 16:5 27:21,22	
	B		C
	back 18:6		calculation 6:9 12:20
	based 19:21 31:7,9		called 3:22
	basically 20:24		calls 11:9
	basis 6:6		came 8:3
	because 2:20 3:12 4:1,25 5:9,12,15 6:18,19 8:18, 24 9:6,12,18		Campbell 2:8 13:7,8 14:7, 10,12,15,17, 22 15:1,19,22 16:1,12,17,21

<p>17:3,6,10,13, 17,21 18:1,4, 11,17,24 19:2,5,11,14, 16,19,23 20:2,4,11,13, 16,18 21:5, 12,17,21,25 22:9,17,19,22 23:4,12,15 24:6,12,18, 21,23 25:13, 16,19,22,25 26:2,7,14,21 27:4,6 28:1, 3,6,14,19,22 29:1,11,16,20 30:2,4,8,20 31:9,17,21 32:5,8,11,14, 18</p> <p>can 2:23 12:25 13:21 14:24 19:1 20:21 22:11 25:21 26:6 31:20</p> <p>can't 9:12 14:10 24:3</p> <p>cannot 14:19</p> <p>capable 26:17</p> <p>care 30:10</p> <p>carry 6:4</p> <p>case 2:4 9:23</p> <p>cases 24:25</p> <p>celery 5:11</p> <p>certain 8:16 31:25</p> <p>certainly 4:13 11:19 19:6</p> <p>cetera 8:25</p> <p>challenges 11:17</p> <p>chooses 3:6 14:6</p> <p>choosing 14:2,5</p>	<p>cite 7:6</p> <p>claim 3:3,16 4:15 5:2,6, 10,11 6:11 7:23 8:13 10:3,4 11:4 13:11,12,13, 15 14:20,25 15:4 19:11 20:1,3 21:14 26:17 28:4 29:7 30:18</p> <p>claimed 4:14 14:2</p> <p>claims 4:14 6:12 19:8,9 20:15</p> <p>clear 8:5</p> <p>close 25:4</p> <p>colors 29:25</p> <p>come 23:10</p> <p>comes 9:8</p> <p>complaint 7:6</p> <p>complete 2:20</p> <p>completely 4:6,24 9:6 11:11 13:13 20:21</p> <p>complex 5:25</p> <p>concerned 23:22</p> <p>conclude 32:18</p> <p>conduct 30:16</p> <p>connections 13:2</p> <p>consequence 5:18</p> <p>consider 7:4</p> <p>construction 3:4,16 8:13 13:11,12,13, 15</p> <p>constructions 7:23</p> <p>construed 21:24</p>	<p>contain 12:9</p> <p>contains 28:12,16,17</p> <p>contestable 18:20</p> <p>contributory 10:4 31:8</p> <p>conundrum 4:13</p> <p>core 4:9</p> <p>Correct 14:15</p> <p>corrected 18:4</p> <p>could 3:19 5:15 13:17 15:23 18:17 25:19,22 26:10 27:14</p> <p>couldn't 4:13</p> <p>couple 13:9 23:4</p> <p>course 19:20</p> <p>court 2:17 3:15 4:10,22 7:3,12 9:18 11:10,21 13:8,12 32:24</p> <p>Court's 11:22 13:12 26:24 27:2</p> <p>curving 5:25</p> <p>customers 15:4,5 18:8, 13</p> <hr/> <p style="text-align: center;">D</p> <hr/> <p>damn 15:21</p> <p>dark 5:22</p> <p>decision 12:4 26:25 27:2</p> <p>declarations 8:7,9</p> <p>declining 7:4</p> <p>deficient 11:4</p>	<p>define 15:23</p> <p>definition 30:13</p> <p>depend 10:12, 13</p> <p>determine 6:5</p> <p>determining 5:5</p> <p>device 31:4 32:20</p> <p>diagnostic 24:2 30:12,14</p> <p>did 2:19 7:6, 14,21 11:14 18:7 20:25 21:10 22:21, 23 32:19</p> <p>didn't 4:7 10:25</p> <p>difference 24:14</p> <p>different 6:20 10:10 17:12 29:25</p> <p>diffuse 20:9</p> <p>diffusing 5:23</p> <p>diffusion 3:11 5:15,17 20:9 29:9,10</p> <p>diffusional 20:6 30:22</p> <p>direct 2:15 10:3,8 27:11</p> <p>direction 5:1,14,15 6:8,10</p> <p>directions 5:17 6:3 12:20,21</p> <p>directly 27:3,7</p> <p>discovering 6:10</p> <p>discuss 8:19</p> <p>disposed 2:18</p>
--	---	--	---

distinction 24:3	13,16,24 25:3,5 26:13 29:21,24 32:7	10:8,23 11:3, 6,25 18:7,11, 12 19:21 21:2 22:22 23:2 26:9 27:12 31:7,10 32:20	fiber 15:13 fibers 16:8 23:23
District 3:15 7:3 26:24 27:1	done 13:3 26:9	exact 9:11, 15,16	Fibertracking 3:23,25 4:1 6:17 10:21,22 15:15 16:5, 19,21,22 17:2 21:3 22:14 27:15 31:11, 23
DNA 4:20,21 9:16 12:22	down 5:16 8:3	example 22:3 23:18	fight 7:10 fighting 8:13 figure 6:15 12:24
do 2:13 6:1, 8,13 10:22 11:6 12:8,20 14:19,21 15:20,21,22 16:14 17:5 20:20 21:5 23:7 25:6,22 26:13,15,16 27:14,15,17 29:9 30:6 31:20	downstream 10:16	exactly 8:3 9:5,13,14 10:24	fill 4:10 6:9 Filler 2:5,6 3:23,25 4:8 5:9 6:25 7:8, 11,19 8:17 9:1,5 10:6,24 11:2,18 12:11,13,15 13:6 17:24 18:1 32:9
doctors 26:11,14	Dr 18:1 23:6	exhibit 29:10 exhibits 20:6 29:8 30:22	find 5:1 9:4 12:20,22,23 15:21,24,25 16:1 18:8,17 21:6 23:21 24:3,5 27:15 31:14
does 3:7 4:5 7:2 9:15 10:23 12:9,11 13:19 19:11 20:19 21:23 22:3 23:3 29:12 30:9 32:23	drawn 24:3 draws 31:4 DVDS 9:25	expert 22:8 25:9 experts 19:8 21:7 25:7 27:17	finding 2:18 9:17 11:16 finds 4:22 9:18 32:22 finish 25:21, 24 32:14
doesn't 4:6 7:24 10:12,13 11:5 15:12,14 19:13 22:10 27:14 28:8, 15,19 29:4 30:10,17,21 31:21,22,24, 25 32:1	DVDS 9:25	expose 28:12 exposing 28:12,16 expressly 21:13 extent 3:16	first 5:20 13:10 14:7 29:17,21 Firstly 2:14 fit 3:1 flow 5:19 fmri 6:20 focus 2:24 focused 3:2
doing 10:19 15:15	each 6:9 12:25	face 22:7 fact 5:2,4,10 6:22 12:18 15:3 16:4 24:7 27:8,12, 16 28:7 29:16 31:9,23	
don't 3:14 4:21 7:23 8:14 9:1,3, 11,14 10:22 12:10 15:8 16:3 18:10 19:9 21:5 23:17,24 24:4,10,12,	easier 8:23 either 3:8 11:21	familiar 17:25 fashion 18:12 20:18 32:21 fashions 20:16 faulted 3:19 fees 2:11 femur 9:11,13	
	eliminate 20:21		
	else 8:10 15:25 16:2 22:8 27:25 28:10 32:16, 23		
	end 27:11 ends 27:7 entire 19:7 erred 7:4 9:6 especially 31:12 essentially 31:13 etc 3:7 even 5:10 11:25 18:13 28:9 event 11:25 Everybody 15:17 everything 14:20,24 28:10 evidence 3:21 4:7 7:5,15		
	E	F	

focusing 10:12 12:16	22:1 24:4 30:1	having 18:21	32:14
follow 6:14 23:5	good 2:6,7 18:3	he 7:21,22 8:2 9:7 10:6 11:2,5,6,23 13:11 15:10, 12,14 18:5 21:18	idea 18:21 21:4
following 16:14	got 7:20 11:10 14:23, 25 15:9	He's 9:6 12:4	identified 12:17
footnote 26:25	gradient 5:20,24 6:2	here 2:7,14 5:7 9:9 11:16 27:22 31:2	identify 26:6
for 2:18 3:19 5:4 7:12 10:4 11:5,9,13 12:2,9,18 15:2 17:5,7, 8,13 19:7,17, 23 22:3,8 23:17,18,19 26:11 27:18, 22 29:13,18, 21,25 30:11, 14 31:3,23	gradients 20:10	hold 13:4	identifying 3:10 4:4 11:11
forget 8:9 21:15 24:10	gray 15:11	honor 2:6 13:9 26:2 30:2	if 4:3,18 5:18,19,22 7:1,14 8:13, 23 9:3,24 11:10,20 12:10 13:4 15:13,22 21:1 22:9,24 23:16 26:9
found 11:21 32:24	great 6:17	honored 2:7	if-- 27:20
friend 2:8	ground 26:24 27:1	hope 2:23 30:7	image 5:21,23 6:3,18
from 6:3 13:1,9 16:16 17:12 18:25 22:19,22 23:6,23 25:8, 11,18	guess 10:10, 11 27:21 30:21	hoping 18:22	imaging 3:11
fun 29:25	<hr/>	how 5:24 6:1 9:14 13:20 17:19 19:1 25:4,10 27:17	implement 14:6
functional 6:20	<hr/> H <hr/>	hypothetical 31:13	impossible 10:20 11:7
<hr/> G <hr/>	had 5:13 10:15,18 11:2 18:24 21:11	<hr/> I <hr/>	in 2:9,11,12, 24,25 3:14,19 4:10,14,16 5:2,3,4,6,7, 10,14,17,19, 21 6:8,11,12, 22 7:4,6,12, 21 8:7,18 10:10,11,14 11:13,16,20, 24 12:2,17 13:22,23,25 15:1,6,7,8, 14,18 16:3,4, 5,14 17:16 18:12,15,21 19:22 20:1,3, 6,16,18,22,25 21:4 22:4,14, 17,18,23 23:4,10,17,24 24:4,7,17,25
general 5:10	hadn't 12:1	I'D 2:14,17 11:4 25:23 26:12	
get 22:6 23:1	half 7:22	I'LL 12:12 13:4	
getting 18:6 26:20,21 28:9	happen 12:8	I'M 6:21 10:1,12 16:10,14,21, 22 17:2,11, 12,21,22 19:16 20:2,14 21:9 22:7 25:14,25 26:18 28:11	
go 6:12 11:20 23:23	happening 4:16		
goes 9:7	harm 26:13		
going 4:4 12:5 16:19, 21,22 17:2	has 8:15 13:3 19:6 21:13 22:4,14 27:23		
	hasn't 12:6		
	have 3:14 4:9,13,16,18 5:7,10,18,22, 25 6:14,20,23 7:13,23,24 9:1 10:7,23, 25 11:2,3 12:5,19 15:12 19:2 20:23 22:10 25:1 26:16 27:14 28:11 30:3,24 31:25		

<p>26:4,25 27:8, 12,16 28:4,9 29:14,16,22 30:1,10,25 31:3,11,12, 19,23,25 32:3,20,21 inaudible 2:8 20:13 include 19:9 29:2 includes 29:5 including 2:9 incorporate 23:5 incorrectly 9:19 indefinite 4:15 indications 13:20 induced 2:15 inducement 2:16 10:3 26:22,25 information 28:9 30:5 infringe 11:8 infringed 2:15 infringement 2:16 10:3,4 26:16 27:11 31:8 infringing 27:3,7 32:22, 24 instructions 31:16,19 insufficient 31:20 Intelligent 4:10,19 intensity 5:24 interest 13:17 16:7,8</p>	<p>31:5 interest- 21:11 interested 28:9 interpret 5:6 13:17 21:14 interpreted 17:7 intersect 23:24 intervene 26:13 interventional 10:18 into 6:19 10:8 introduce 18:7,11 32:19 introduced 27:10 invention 6:3 is 2:4,13,19, 21 3:3,5,13, 18 4:3,16,20, 24 5:1,4,10, 12,13,14,16, 18 6:3,7,10 7:14,15,22 8:4,5,17,18, 23 9:10,13, 15,18,24 10:5,13,20 11:11,19,21, 22 12:20,23 13:3,23 14:4, 20 15:6,9,13, 15 16:2 17:1, 4,8,11,19 19:7 20:4,18, 24 21:2,15 22:5,9,12 23:2,17,21 25:7 26:5,8, 13,18,19,20, 25 27:2,6,12, 17 28:5,7,10 29:2,19,23,24</p>	<p>30:18 31:13 32:2,9,16 isn't 16:18 20:5 24:6 isotropic 5:16,22 21:6 29:5 30:23 issue 13:14, 15 29:24 issues 11:13 12:17 issuing 12:4 it 2:25 3:5, 7,9,11,14,17, 24 4:6 5:3,6 6:13,18 7:3, 14,24 8:3,4 9:3,4,7,12, 14,15 10:20 11:19 12:11, 12,14 13:8, 14,16 14:10, 19 15:4,5,6, 7,9 16:2,3,25 17:7,20 18:5, 8,12,13,16,17 19:6,17 20:4, 14,18,19 21:5,10 22:2, 6,7,9,10,11 24:22 25:1,2, 4,6 26:9,10, 11 27:7,11, 14,17 28:10, 15,19,22,23, 24 29:4,6,8, 11,19,20,21, 22,24,25 30:4,20,21,23 31:4,7,9,21, 22,24,25 32:6,21 it's 4:20,21 5:11,20,23 6:7,17 9:5, 12,16 10:6,7 11:4,7 12:22 14:25 16:7 18:19,20</p>	<p>20:1,3,5,7,18 24:25 25:1 26:9,16 30:25 its 10:14 22:7 31:4</p> <hr/> <p>J</p> <hr/> <p>Jay 2:8 joint 12:9 Judge 2:4,23 3:24 4:1 5:3 6:21 7:1,9, 17,20,21 8:22 9:3,7 10:1,9, 25 11:15 12:8,12,14 13:6,10 14:3, 8,11,13,16, 18,23 15:17, 20,24 16:10, 13,18,24 17:4,9,11,15, 19,22,25 18:2,10,14,19 19:1,3,6,13, 15,17,20 20:1,3,9,12, 14,17,25 21:9,13,18,22 22:3,13,18, 21,23 23:8,13 24:1,8,15,20, 22 25:12,14, 17,21,23 26:1,3,8,18, 23 27:5,20 28:2,4,7,15, 21,24 29:8, 15,17,23 30:3,5,12 31:6,15,18 32:1,7,9,13, 16 judgment 2:18 3:20 4:3 6:23 7:6 10:15 11:5,13 15:2 18:15 21:1</p>
--	--	---	---

<p>22:24 27:21 31:6 just 2:23 3:9 4:25 9:6,14 12:22 14:4, 10,20 16:3 17:4 20:20 23:21 24:8 26:17,25 29:4,25 31:4 32:2,14,18</p> <hr/> <p style="text-align: center;">K</p> <hr/> <p>Kettering 6:16 key 8:17 11:19 12:17 16:2 30:8 kind 3:2 11:15 15:6,10 30:13 knew 8:11 knocking 11:7 know 3:14 4:5,21 5:7 6:1 7:13 8:7, 14,23,24 9:3, 11,13,15 11:15,19 13:2 15:14 16:11 17:1,8,15,17 18:6 21:10 22:5 23:14 24:4,10,12, 13,16,18,21, 24 25:2,3,5,8 26:12 30:25 32:21 known 5:14 9:21 11:9 13:21,22,23, 24 17:14 21:6 23:20 knows 3:8 15:17</p>	<hr/> <p style="text-align: center;">L</p> <hr/> <p>Laboratories 4:12 language 5:6 13:25 21:14 Leach 21:11, 20 23:6,9 25:11 least 17:12 18:5 legal 7:20 8:15 let 25:24 let's 7:17 light 20:8 like 2:14,17 7:22 9:10,16 12:3,22 16:16 24:20 25:23 26:12 limitations 19:9 limited 27:24 listening 7:13 little 2:25 6:9 12:25 lives 13:3 location 3:8, 14 8:7,11 21:16,19 23:14 26:6 long 14:23,24 look 4:18 9:20,21,23 10:13 12:12, 17 23:7,17 29:21 looking 17:5, 7,8,13 19:17, 23 22:15 23:18,19 27:18 29:13 30:11,14 31:3</p>	<p>lost 14:11, 13,14 lot 3:20 4:7 7:4 8:23 12:16</p> <hr/> <p style="text-align: center;">M</p> <hr/> <p>made 4:2 8:6 10:14 make 2:13 7:20 making 3:3 4:14 9:25 mammal 6:12 mammals 5:11 manner 31:11, 12 manual 18:14 26:4 31:23 32:1,3,5 many 2:8 13:20 19:25 24:25 map 3:13 5:1 13:1 16:15 18:22 21:4 22:6,15 23:1 mapping 14:24 27:24 maps 14:19 march 13:1 margins 9:11 markets 15:16 materials 6:22 mathematics 6:4 matter 4:6 5:24 15:6,8, 11,13 19:15 20:7,24 22:11 25:5 may 13:4,8 14:1 16:1 17:10 19:22 23:23 26:14</p>	<p>maybe 2:25 15:24 26:22 31:1 MDL 7:3 me 8:4 18:4 21:10 22:7 25:24 mean 7:18 27:1 28:8 29:12,13 means 3:5,10 22:1,25 meant 13:14 measure 6:8 9:12 measuring 8:20,21 Medtronics 2:11 meet 30:13 Memorial 2:16 6:16 mention 27:13 method 3:6 6:20 14:6 32:22 methods 32:23,25 mind 2:24,25 18:21 21:4 22:4,15 misremembering 32:4 misunderstandi ng 2:20 more 15:20 morning 2:6 Moseley 8:10 21:11,13 22:3 23:9 most 21:10 motion 2:18 3:20 4:3 7:7 11:5,13 12:2, 9 15:2 21:1 22:24</p>
--	--	---	--

<p>movant 11:14 12:1</p> <p>moving 12:6</p> <p>Mr 2:5,6 3:23,25 4:8 5:9 6:25 7:8, 11,19 8:17 9:1,5 10:6,24 11:2,18 12:11,13,15 13:6,7,8 14:7,10,12, 15,17,22 15:1,19,22 16:1,12,17,21 17:3,6,10,13, 17,21,24 18:1,4,11,17, 24 19:2,5,11, 14,16,19,23 20:2,4,11,13, 16,18 21:5, 12,17,21,25 22:9,17,19,22 23:4,12,15 24:6,12,18, 21,23 25:13, 16,19,22,25 26:2,7,14,21 27:4,6 28:1, 3,6,14,19,22 29:1,11,16,20 30:2,4,8,20 31:9,17,21 32:5,8,9,11, 14,18</p> <p>MRI 5:13 6:20</p> <p>much 7:2 9:10 20:7</p> <p>multiple 6:3, 13 12:19</p> <p>must 4:23 9:8 29:2,13 31:21,22</p> <p>my 2:7,9,24, 25 6:2 13:4 25:21,24</p>	<p style="text-align: center;">N</p> <hr/> <p>names 8:9</p> <p>near 15:13 24:25 25:1</p> <p>need 4:3 8:14 10:7,8 15:20 32:16</p> <p>needed 8:6</p> <p>nerve 5:14, 16,19,21,25 13:23 15:7 17:10 19:24</p> <p>nerves 8:1 13:22,24 19:25</p> <p>neural 5:12 6:11</p> <p>Neurografix 2:5 13:16 16:4 18:7 20:20 25:9 27:8 32:19</p> <p>Neurografix's 13:13</p> <p>neurologist 16:11 22:5</p> <p>neuroscience 6:18 13:2</p> <p>neurosurgeon 15:10 16:13</p> <p>neurosurgeons 10:17</p> <p>never 4:3 18:7 32:5,19</p> <p>NEWMAN 2:4 13:6 19:1,3, 6,13,15,17,20 20:1,3,9,12, 14,17 24:1 28:24 29:8, 15,17,23 30:3,5,12 31:6,15,18 32:9,13,16</p> <p>next 2:4 6:14 25:4,6</p>	<p>no 2:5,21 5:24 6:23 8:14 9:13 10:4,15 11:21 15:6 16:24 18:12 19:1 21:2,5,25 22:4,14,19,22 23:2 24:12,18 25:8,12,14,23 26:23 27:2,6, 8,9,10,12 28:17,20 30:8 31:10 32:7</p> <p>nobody 4:5</p> <p>noise 11:16</p> <p>non-infringing 2:21,22 4:24 9:19,22,24 10:2,5 11:23 32:23,25</p> <p>none 15:3,4</p> <p>not 2:19 3:1, 7,19 4:2,20 5:16 7:2,6 8:5 10:22 14:2,20 15:1 16:24 17:6,23 20:1,3,17,19, 23 21:23 22:4,8 23:7, 18,19 24:22, 25 26:8,15, 18,19 27:18, 24 28:3,8 29:4,9 30:11, 13 31:12</p> <p>nothing 28:4</p> <p>notion 8:3</p> <p>now 17:2 18:5 20:7 21:18 26:16</p> <p>nowhere 25:1</p> <hr/> <p style="text-align: center;">O</p> <hr/> <p>objected 12:2</p>	<p>obligated 11:12</p> <p>odd 5:6</p> <p>of 2:18,20 3:2,3,6,7,9, 12,13,20,21 4:7,9,25 5:1, 5,11,15,18 6:2,10,18 7:2,4,5,15,22 8:3,7,19 9:11,14,17 10:10 11:15, 19,25 12:4, 16,25 13:3,17 15:3,4,6,10, 15 16:2,4,5, 7,8,14,15 17:5 18:21,22 19:18,19,20, 21,24,25 20:7,22 21:2, 4,7,14 22:4, 6,14 23:2,6, 8,10 24:7 26:5,6,24 27:1,10,15, 17,21,23 30:6,13,25 31:4,7,8,10</p> <p>okay 2:4,23 4:18 7:19 12:12,13 18:2</p> <p>on 2:24 3:2, 19 4:3 5:11 6:5,12 7:1,22 8:6 10:12 11:20,22 12:16,17,25 13:15 14:11, 13,14 15:3 19:21 22:7 23:15 29:19 31:7,9</p> <p>once 12:24 29:20</p> <p>one 3:3,8 5:21 7:22 8:1,7 9:4,25</p>
---	--	---	--

<p>10:11 14:20, 21,23,25 17:4 26:4 27:24 29:18 32:3 ones 25:6 only 8:1 11:8,12 12:4 14:21 16:7 25:10 29:20 onto 6:14 opinion 8:4 opposed 31:8 opposite 2:12 opposition 6:23 10:8 18:15 optic 13:23 or 3:1,8 5:22 6:10,23 10:17,18 11:22 13:18 15:7,8,12,14, 24 16:7,13 21:16 24:4 25:9 28:9 29:2 30:6 31:7 32:23 ORAL 2:1 order 7:12 12:5 orien- 8:8 orientation 3:9,14 6:5 8:12,20,24 9:17 21:16,19 orientations 8:21 12:19, 24,25 orthogonal 8:25 other 5:22 8:8 10:14 13:23 14:8 20:7 27:15 28:17,20,25 29:3,9 our 6:1 14:18 15:1,3,4</p>	<p>27:17 out 6:4 11:7 12:24 13:1 14:21 23:21 26:11 32:9 over 2:8 6:13 13:4 32:10,11</p> <hr/> <p>P</p> <hr/> <p>pages 23:5 25:17 paragraph 21:14 23:10 paragraphs 8:19 parallel 5:20 part 23:24 parties 17:6, 7 party 12:6 passing 22:12 patent 2:15, 19,20 4:25 6:19 8:18 11:9 12:18 30:9 31:25 patents 2:10 people 18:20 24:15,16 26:10 perform 15:10 peripheral 5:14 8:1 13:22,24 14:12,14 15:7 19:21 perpendicular 5:21 8:24 pick 9:3 14:21 picture 5:10 9:14 pictures 26:4 piece 7:14 11:19</p>	<p>plainly 3:7 plaintiff 31:10 please 13:8 Pleased 2:7 point 3:12,18 5:24 6:1 8:6 13:1 18:7 pointing 32:9 points 2:13 position 5:5 8:12 13:23 19:18,23 21:19 possibly 32:24 pre-selected 23:20 Preamble 5:4 precise 16:15 22:6 23:1 precisely 22:16 precision 29:19 preposterous 22:7 presence 30:15 presented 11:17 primarily 5:16 prin- 26:24 principal 26:24 27:1 probably 26:20 problem 6:24 11:16 procedural 3:18 procedure 30:12,14,16 procedures 19:4 24:2</p>	<p>proceed 13:5 process 3:7, 11,13 4:5,17, 18 5:4,8 17:5 23:1 27:23 produce 3:13 produced 31:10 product 4:17 product's 4:17 proof 27:2,6, 8,9,10 properly 21:23 proposed 7:5 proposition 7:2 18:20 prove 26:15, 19 pull 10:8 purpose 4:25 5:4 15:15 26:12 put 4:5 14:3 20:14 putting 3:19 Pyram- 18:2 pyramidal 15:18,23 17:1,16,18, 19,22,24 18:3,8,18 22:10 23:19 24:17,19,23, 24 25:3,20 26:6 27:13, 16,18 31:1, 14,22,24 32:22</p> <hr/> <p>Q</p> <hr/> <p>question 25:24 questions 13:9 32:15</p>
--	--	---	--


software 3:21 10:22 14:18 22:6	stay 16:16	such 22:15 24:3	16,18,23 15:17,20,24
solid 7:15	Stearns 7:21 9:7	sufficient 26:8,15,19	16:10,13,18, 24 17:4,9,11, 15,19,22,25
solution 5:13 6:2	step 29:7	suggests 27:22	18:2,10,14,19 20:25 21:9, 13,18,22
solves 9:16	still 29:3	summary 2:18 3:20 4:2 6:23 7:6 10:14 11:5,13 15:2 18:15 21:1 22:24 27:21 31:6	22:3,13,18, 21,23 23:8,13 24:8,15,20,22 25:12,14,17, 21,23 26:1,3, 8,18,23 27:5, 20 28:2,4,7, 15,21 32:1,7
some 2:10 4:23 8:3 11:17 15:10 16:14 17:13 20:16,18 27:21 30:24 32:22	structure 3:4,5,9,10 4:4 5:5 6:11 8:4 13:14,16, 18,20,21 14:4,5,7 15:5,6,18,23 16:6,19 17:8, 14 18:9,18,22 19:7,18,22,24 20:5,6,7,19, 22,24 21:4,6, 23 22:4,10, 11,12,15,25 23:19,20 24:17,24 25:3 27:13,16,19, 23 28:8,13, 17,18,20,23, 24 29:6,12, 18,21 30:19, 21,22,23,24 31:2,14,22 32:22	sun 14:24	tech- 16:10
somebody 8:10 14:5	structures 6:1 13:21 24:10,24 25:6 27:15 28:25 29:3,5,6,9 30:23	supposed 29:2	technicians 10:17
someone's 9:11	sua 12:3	supposition 19:7	technology 10:17
something 4:14 9:9,20 12:6 15:25 16:2 21:22 22:1 29:13 30:11,15,25	subject 3:6 4:4 14:6 23:1	surgery 15:11 16:14	tell 2:24 6:16,19 32:17
sorry 6:21 10:1 16:10 17:11,20,21, 22 19:16 20:2 21:9 25:14,25 26:18	subjecting 3:10	surrounding 28:10	telling 12:4 19:9 26:10
sounds 22:7	submit 4:7	suspicious 19:21	tensor 3:11 6:4
spec 8:22	substantial 2:21 4:23 9:19,22,24 10:2,5 11:22	sweeps 6:18	term 21:23
specific 3:8 11:25 23:18 29:14	substantive 11:6	system 22:4, 14 23:3,17 31:20	terrific 26:5
specifically 15:2 27:18			testa- 25:12
specification 13:19 14:1			testi- 19:2
sponte 12:3			testimony 18:24 21:7 22:19 25:8,9, 11,14 27:17
standard 24:1			Thank 13:6 26:1
start 9:4 30:6			Thanks 12:14
stated 5:1			that 2:14,17, 19,24 3:2,5, 6,7,8,10,15, 17,19,22 4:1, 2,4,5,6,10, 11,13,21,22, 23 5:7,13,18 6:10,19,22 7:3,5,11,13, 17 8:2,5,6,
statements 23:6,9			
		T	
		take 3:3 6:3 9:14 12:19	
		talk 13:19 14:1 15:3 19:13	
		talked 8:10	
		talking 7:16 9:2 10:1 24:2	
		talks 32:5	
		Taranto 2:23 3:24 4:1 5:3 6:21 7:1,9, 17,20 8:22 9:3 10:1,9,25 11:15 12:8, 12,14 13:10 14:3,8,11,13,	

<p>11,14,17,19 9:18,23,25 10:6,7,11,12, 13,14,15,22, 23 11:1,3,10, 14,18,20,22, 24 12:5,6,16, 18 13:25 14:4,5 15:3, 8,11,13,17 16:8,16,18 17:8,10,11, 15,17,19,20 18:8,11,12, 17,20,22 19:1,7,21 20:6,20,21 21:2,5,7,14, 23,25 22:1,5, 12,13,14,15, 24,25 23:2,3, 5,10,14,16, 21,23 24:2,6, 16 25:5,9,19, 22 26:5,8,9, 10,11,12,13, 15,16,18,19, 23 27:2,6,9, 11,14,16,22, 24 28:1,2,5, 7,8,10,12,15, 16,17,19 29:9,12,13, 23,24 30:17, 22,24 31:1,7, 10,18 32:2,4, 9,19,20,22</p> <p>that's 3:15 5:3 6:4 7:9 8:14,15 11:4, 17,18 12:1,19 14:2 15:1 17:6 20:22 21:7 23:22 24:13,14 25:2 26:15 27:7,17 29:7 30:8 31:2,3 32:1, 13</p>	<p>their 8:7 10:20 16:5 18:15,21 31:13</p> <p>them 3:3 6:14 12:1 23:25</p> <p>then 5:20,23 6:12 8:2,3,8, 24 9:7 11:12, 20 13:1 14:18 22:2 29:18,21 30:12,15</p> <p>there 2:21 4:22 6:16 7:14 8:8 9:8, 18,24 10:2,4 11:1,21,22 13:13,20 15:13 17:8,16 18:12 19:20, 22 21:2 22:9 23:2,23 24:9, 13 25:8,17 26:11,14 27:2,6,8,9, 11,12,22 29:19 30:10, 25 32:3,16,24</p> <p>there's 8:19 9:20,21 11:15 15:17 17:15, 17 21:18 22:13,14,19 24:16,18,23 25:3,5 28:4 31:1</p> <p>therefore 4:6 9:12,21 11:24</p> <p>these 6:14,21 12:16,17 13:1 16:8 19:3,7, 25</p> <p>they 4:2,3 6:16,19 8:6, 10 9:19,20,25 13:25 14:2 15:4 18:12,22 20:16,17,20, 21 21:22,25</p>	<p>22:8,9 23:5, 7,9,15,16,24 24:18,20,21, 24 25:1,2,3, 5,6 26:3,16 27:9,17 31:12</p> <p>they're 22:15 23:22 24:1 25:4 27:18 30:10</p> <p>thing 7:9 11:7 13:18 14:20 15:21</p> <p>things 10:10 16:16 17:5</p> <p>think 7:11,12 8:8 18:5 26:3,20,21 30:6,9 32:18</p> <p>this 2:14,21 3:6,11,12 4:5,10,12,19, 24 5:4,12 6:2,19 8:18, 23 9:10,15 10:19,22 11:10,11 12:3,18 13:3 14:6,19 15:18,21 17:4,5 18:21 20:8 22:4,6,8 23:1 24:9,16 25:7,10 26:5, 12,17 28:5,7, 10 30:6,17,18</p> <p>those 4:8 13:21 23:8</p> <p>though 12:1</p> <p>thought 10:9 32:2</p> <p>thousands 13:3</p> <p>three 2:13 8:9 23:9</p> <p>through 4:5 9:7,8 22:12</p>	<p>throughout 20:20</p> <p>time 2:10 12:4,16 13:4 32:10,12</p> <p>times 2:8 18:4</p> <p>tissue 6:10, 11 9:17 11:9, 12</p> <p>tissues 5:2, 12</p> <p>to 2:7,13,14, 17,19,23 3:1, 3,6,11,13,14, 16,20 4:4,9, 10 5:1,6,7, 11,14 6:1,4, 12,22,23 7:4, 5,8,10,11,12, 13,20,23,24 8:3,4,6,14,15 9:1,14,23 10:7,8,11,15, 16,18,20,22, 25 11:1,3,6, 8,12,20,24 12:5,8,17,19, 20 13:1,4,5, 9,14,16,18, 20,25 14:5,6 15:5,10,12, 21,22,24,25 16:1,2,14,16, 19,21,22,25 17:2,12 18:6, 8,15,17,22 19:6,14 20:14,23 21:3,4,6,10, 15 22:2,6,7, 9,10,15 23:1, 7,21,23,24 24:3,4,10,22 25:2,4,6,10, 23,24 26:5, 12,15,16,19, 21 27:14,15, 22,23,24</p>
---	---	--	---

<p>28:11 29:2, 21,25 30:1,4, 5,17,24 31:8, 13,19,25 32:14,15,17, 18 together 20:14 tomorrow 16:20 Toshiba 9:23 touch 24:22 tough 7:9 track 17:1 22:2 tract 17:1,16 26:6,12 31:1 tracts 2:19 6:14 transform 13:2 tries 11:6 true 15:1 19:5 20:23 27:4 29:11 30:2 try 22:2 trying 3:1 17:12 20:14 21:4,6 25:4 32:14 Tsung 8:10 21:11,19 23:6,9 25:13 tumor 15:25 23:22,23 24:25 25:1 31:5 turn 5:19 30:1 two 3:2 4:8 7:22 25:17 26:3 27:13 typically 15:11</p>	<p style="text-align: center;">u</p> <p>Um-hmm 14:22 15:19 16:12, 17 17:3 20:11 21:17 26:7 under 14:24 understand 32:11 undertakes 21:3 uniformly 5:23 unit 6:8 unknown 2:19 4:14,17,20,23 5:1 8:20,21 9:9,12,20,21 11:9,12 12:18 up 2:9 30:1 us 6:16,19 11:3 12:4 19:9 32:17 use 2:22 4:24 9:19,22,24 10:2,5,20 11:23 13:25 15:4,5 16:2, 19,21,22 18:8,12,13,17 21:3 22:9 23:16 24:6 26:10 31:13, 24,25 used 5:11 6:20 user 3:6 16:6 21:2 22:4,14, 25 23:2 users 3:21 10:16 21:8 uses 10:6 15:9 25:10 31:4 32:20 using 6:17 16:25 18:21 22:6,8 26:11</p>	<p>28:11 31:10</p> <p style="text-align: center;">v</p> <p>vector 6:5,9 verb 24:11 verify 30:15 versus 2:11 4:11,12 very 4:19 5:6,12 8:17 9:10 19:3,8, 22 23:10 voxel 6:7,9 12:25 voxel-by-voxel 6:5</p> <p style="text-align: center;">w</p> <p>want 7:8,11 13:9 15:21, 24,25 16:1, 15,25 23:21, 24 24:10 25:1 32:18 wanted 2:13 15:22 wants 15:10, 12 23:1 was 2:15 3:2, 11,15 4:2 6:2 7:21 8:3,6,8 9:25 10:2,4, 20 12:3 13:13,16 18:12 21:7 24:11 25:8,11 27:2,3,7,8,9 31:6,7,9 32:3 wasn't 11:1 13:15 26:17 water 5:23 way 2:17 5:13 6:1 15:4,9 18:5 23:16 26:10 28:11</p>	<p>30:17 31:25 32:21 we 2:11 4:13, 18,21 5:10, 13,15,25 6:1, 8,9,12,14 9:10,12,13, 14,23 10:1,24 11:3,8,12,14, 23,24 12:2, 24,25 15:3 16:3,9 18:24 19:2,23 21:5 28:1 we'll 18:2 we're 4:19 8:21 9:16 12:5,18 16:19 17:13 19:17 26:19,21 32:10 we've 15:9 32:11 well 4:13,18 7:17 9:10,20, 24 10:6 15:1, 22 19:11,22 21:25 24:1,6, 12 26:14 28:1,6,19 29:23 30:8,20 31:9 went 3:17 were 2:12 6:22 8:8,9 9:25 11:23,24 18:15,20,22 25:17 26:3,9, 11 32:24 what 2:13 3:1,21 4:9 5:3 7:15,21 8:2,3,9 9:15 12:23 13:3,14 14:2,19 15:6, 20 17:12 22:8 23:21,22 24:4,10 25:7, 17 26:20</p>
--	---	--	---

<p>29:12,25 30:9 31:2,3,19 what's 2:24, 25 3:21,24 4:16 8:24,25 24:13 25:2 30:10 whatsoever 25:9 31:11 when 5:13,25 8:19 10:13 17:5 26:13 30:15 31:3 where 9:13,25 12:1,17,22 17:1 20:12 21:1 22:21,23 26:12 27:7 whether 4:7 13:16 15:5,7 16:7 21:15 24:3 32:21 which 3:18 5:15 6:1,7,8 8:15 9:23 10:4,12 13:3 20:24 23:6 26:4 27:13 28:16 31:12, 13 white 15:8,13 19:15 20:7,24 22:11 25:5 who 24:16 26:14 whoever 10:18 whole 3:12,20 4:7,25 11:7 15:15 24:6 29:24 whose 30:15 why 7:21 10:1 11:4 12:19 16:18 17:11 24:14 25:2 26:8,18,19 27:20 30:17</p>	<p>will 2:24,25 5:21 with 2:7 3:1 5:13 6:9 7:22 8:2 17:25 21:3 28:22 30:6 31:15 within 14:25 without 4:14 18:21 word 8:20 13:17 24:7 31:24 words 20:7 would 5:6,22 11:2,20 16:16 20:20 22:5 24:20 28:16 30:6,13 written 30:18 wrong 3:16 4:24 7:21 9:6 11:11 wrote 2:9,10</p> <hr/> <p style="text-align: center;">y</p> <hr/> <p>yeah 8:17 11:2 14:8 21:12,21 years 2:9 yes 4:8,22 6:25 9:5 12:11 13:6 18:24 20:4 23:4 28:1,12 31:21 you 2:24 3:3, 10,14,19,22 4:3,4,5,7,16, 17,18,25 5:7, 8,18,19,22,24 6:23 7:1,5, 13,14,22,23 8:2,6,11,14, 15,23,24 9:1, 3,21 10:7,8, 10,13,15,16,</p>	<p>22,25 11:10, 15,19 12:8, 10,19 13:2,6, 17,20 14:9, 11,13,18,23 15:8,20,22, 23,24,25 16:1,8,10,25 17:8,15,17,19 18:6,17 19:12 20:21,23,25 21:10,11 22:21,23,24 23:14,16,17, 21 24:4,8,10, 12,13 25:8, 19,22,23 26:1,6,9,10, 23 27:14 28:8,11,15,22 29:2,15,17, 18,20,24 30:3,4,6,15, 24,25 31:1, 21,22,24 32:16,21 you'll 9:4 you're 3:1 6:16 8:13 16:24 18:6 19:9 22:1 23:18,19 24:2,4,9 28:3,8,23 29:13 30:14 31:2,3,18 you've 7:18 12:16 14:14, 23,25 your 2:6 6:22 7:2,5 10:9,11 13:8 18:14 21:1 24:11 25:18 26:2 27:21,22 29:17 30:1,2 31:15</p>	<hr/> <p style="text-align: center;">z</p> <hr/> <p>zero 7:24 14:14</p>
--	--	---	---

EXHIBIT 10

 KeyCite Red Flag - Severe Negative Treatment
Overruled by [Perry v. Bakewell Hawthorne, LLC](#), Cal., February 23, 2017

38 Cal.3d 18
Supreme Court of California,
In Bank.

Zelvern W. MANN, as Administrator,
etc., et al., Plaintiffs and Appellants,

v.

Andrea CRACCHIOLO III, et al.,
Defendants and Respondents.

L.A. 31837.
|
Feb. 19, 1985.

Synopsis

Wrongful death action was brought against medical center and officials thereof and practitioners thereat claiming negligence in failing to diagnose fracture of the odontoid process. The Superior Court, Los Angeles County, Peter S. Smith and Eli Chernow, JJ., rendered summary judgment for defendants, and plaintiff survivors appealed. The Supreme Court, Broussard, J., held that: (1) by appearing and participating plaintiffs have waived issue of whether stay of “all proceedings” issued by Court of Appeal precluded filing of summary judgment motions; (2) trial court erred in ruling that late-filed opposition to motion should not be considered; (3) it was error to reject declarations of plaintiff’s medical expert on ground that it was conclusory; (4) **diplomate of American Boards of Surgery and Neurological Surgery was competent to render opinion as to standard of care in reading X rays, in submitting X ray reports and in diagnosing**; (5) trier of fact could infer negligence from factual statements of plaintiff’s expert; and (6) certain defendants could not be found negligent.

Affirmed in part and reversed in part.

Bird, C.J., filed concurring opinion.

West Headnotes (17)

[1] Judgment

Defects and objections

By appearing and arguing merits of summary judgment motions and failing to challenge filing of motions in face of Court of Appeal's stay of “all proceedings” the plaintiff opponents had waived any defects or irregularities in notice of the motion.

12 Cases that cite this headnote

[2] Courts

Power to regulate procedure

Courts

Operation and Effect of Rules

Absent legislative direction to the contrary, courts may adopt local rules with the force of law.

17 Cases that cite this headnote

[3] Judgment

Affidavits, Form, Requisites and Execution of

Reasonable local rules limiting the time to file opposition to summary judgment motion were not precluded by statute, as existed in fall, 1981, which was silent as to time to file counter-affidavits. [West's Ann.Cal. C.C.P. § 437c](#).

9 Cases that cite this headnote

[4] Judgment

Affidavits, Form, Requisites and Execution of

Trial court abused its discretion in enforcing then applicable three-day limitation for filing summary judgment opposition material by refusing to consider opposition rather than shortening the time or continuing the hearing where although the opposition papers, as filed two days before scheduled hearing, were voluminous such late filing did not preclude full consideration of the opposition and judge was fully prepared to consider the opposition, which had been filed by the clerk.

[14 Cases that cite this headnote](#)

[5] Judgment

🔑 [Nature of summary judgment](#)

Summary judgment procedure, inasmuch as it denies the right of the adverse party to a trial, is drastic and should be used with caution.

[46 Cases that cite this headnote](#)

[6] Judgment

🔑 [Existence or non-existence of fact issue](#)

Summary judgment is properly granted only when the evidence in support of the moving party establishes that there is no issue of fact to be tried.

[88 Cases that cite this headnote](#)

[7] Health

🔑 [Requisite skill, training, qualifications](#)

Health

🔑 [Surgery in general](#)

It is required only that physicians and surgeons exercise in diagnosis and treatment that reasonable degree of skill, knowledge, and care ordinarily possessed and exercised by members of the medical profession under similar circumstances.

[38 Cases that cite this headnote](#)

[8] Health

🔑 [Gross or obvious negligence and matters of common knowledge](#)

In deciding whether physicians and surgeons have met applicable standard of care, the trier of fact may infer failure of the practitioner to have done so in cases in which the happening of the accident does not normally occur in the absence of negligence, but other cases may require expert testimony to establish the standard of care.

[7 Cases that cite this headnote](#)

[9] Evidence

🔑 [Matters of opinion or facts](#)

Health

🔑 [Presumptions](#)

In wrongful death action, trier of fact could infer negligence on part of radiologist in view of declaration of plaintiffs' medical expert that the subject X ray showed fracture of the odontoid process and that radiology report failed to show the fracture, and it was error to reject the declaration on ground that it was conclusory.

[10 Cases that cite this headnote](#)

[10] Health

🔑 [Presumptions](#)

Trier of fact in medical malpractice action could infer that in common X-ray procedure the patients do not fall in absence of negligence and that when patients do fall the person positioning the patient is probable the person responsible.

[Cases that cite this headnote](#)

[11] Evidence

🔑 [Due care and proper conduct in general](#)

Diplomate in surgery and neurosurgery was competent to testify as to standard of care exercised by other specialists, such as radiologists and internists, treating respiratory problems and was competent to opinion as to whether such other practitioners failed to meet applicable standard of care in allegedly failing to diagnose broken neck from subject X rays.

[8 Cases that cite this headnote](#)

[12] Appeal and Error

🔑 [Competency and qualifications](#)

Although trial court's ruling on qualification of an expert ordinarily will not be disturbed absent clear abuse of discretion, the court will be deemed to have abused its discretion if the witness has disclosed sufficient knowledge of

the subject to entitle his opinion to go to the jury.

[68 Cases that cite this headnote](#)

[13] Judgment

🔑 Admissibility

Fact that medical expert, whose services were recently obtained, was not listed by plaintiffs as one of their experts for trial did not preclude consideration of his opinion in opposing defendants' summary judgment motions. *West's Ann.Cal.C.C.P. §§ 2037.4, 2037.6.*

[2 Cases that cite this headnote](#)

[14] Death

🔑 Exemplary damages

Punitive damages were not recoverable in wrongful death action brought against medical practitioners absent evidence of conspiracy to conceal, of intentional performance of useless operations or of an attempt to kill, with asserted deficiencies being failure to observe, report or diagnose fracture of the odontoid process.

[Cases that cite this headnote](#)

[15] Health

🔑 Radiology, ultrasound, and other medical imaging

Anesthesiologist who did not order any X rays or interpret or consult any previous X rays and who was not shown to have been responsible to study X rays, to diagnose decedent's ailments or to have treated decedent, was not negligent as regards asserted failure to observe from X rays, report or diagnose fracture of the odontoid process.

[1 Cases that cite this headnote](#)

[16] Health

🔑 Radiology, ultrasound, and other medical imaging

Intern in orthopedic department who consigned order for administration of drug and prescribed sleeping pill and whose examination of decedent was limited to that necessary to verify orders of prescribing physician and who did not order X rays, consult or interpret X rays could not be found negligent as regards asserted failure to observe X rays, report or diagnose fracture of the odontoid process.

[1 Cases that cite this headnote](#)

[17] Appeal and Error

🔑 Nature of question or defect

Appeal from postjudgment orders which were not specifically attacked in opening brief, would not be separately considered.

[4 Cases that cite this headnote](#)

Attorneys and Law Firms

***763 **1135 *24 Kenneth Crews Mann Sherman Oaks, and Bruce Ogden Mann, San Juan Capistrano, in pro. per. and for plaintiffs and appellants.

Rushfeldt, Shelley & McCurdy, Hollywood, Horvitz & Greines, Horvitz & Levy, Ellis J. Horvitz, S. Thomas Todd, Encino, Harrington, Foxx, Dubrow & Canter, Dale *25 B. Goldfarb, Mark W. Flory and Patty Mortl, Los Angeles, for defendants and respondents.

Opinion

***764 BROUSSARD, Justice.

Plaintiffs, the surviving husband and three sons of Ada Crews Mann,¹ deceased, appeal from summary judgments in favor of defendants in this wrongful death action and from denial of postjudgment orders. Plaintiffs' complaint charged the UCLA Medical Center, 54 individual doctors, a radiology technician, the associate director of the hospital, and the hospital's data processing manager and finance director with breaking the decedent's neck, conspiring to conceal the existence of the broken neck, refusing to treat it, intentionally performing useless operations upon decedent to obtain Medicare and

MediCal funds, and then attempting to kill her to conceal their complicity in causing and concealing the existence of the broken neck.

As might be expected when there are allegations such as these, the instant case has generated a great amount of hostility, personal clashes, side issues, and related litigation.² From July until October 1981, there were filings or hearings almost daily. The briefs filed herein continue to delve into side issues without always specifying their relevancy. We will set forth the facts relevant to the major issues in a brief manner, omitting facts bearing on side issues, numerous discovery motions, and motions to disqualify.

We review the court's order granting the motions for summary judgment.³ In granting the summary judgment motions, Judge Peter S. Smith concluded that plaintiffs' opposition was not timely filed and therefor was not considered. *26 He also determined that even if plaintiffs' opposition had been considered, it was insufficient to raise a triable issue of fact because the doctor's declaration offered in opposition to the motion lacked the requisite foundational facts to qualify him to testify as to the standard of care and tended to "shotgun his opinions in a conclusionary way." The court also concluded that at most plaintiffs' declaration would make out a claim for medical negligence and would not justify the claim for punitive damages. The summary judgment was filed October 26, 1981.

THE COURT OF APPEAL STAY AND THE TIMELINESS OF PLAINTIFFS' OPPOSITION TO THE SUMMARY JUDGMENT MOTIONS

In January 1981, the trial court granted plaintiffs' motion for trial preference on the ground that one of them was over age 70 and set trial for August 31, 1981. On May 1, the case was assigned to Judge Smith for all pretrial proceedings. On June 4, defendants filed a demand for a list of plaintiffs' expert witnesses to be served no later than July 12. On the latter date, plaintiffs furnished the list, and defendants in mid-July noticed the depositions of the experts. On August 11, defendants' motion to continue the trial date was granted, and trial was set for October 26.

On August 26, plaintiffs filed an affidavit of bias against Judge Smith. On September 2, Judge Smith filed an

answer and transferred the case to another department. ***765 **1137 Judge Rickles of Orange County ruled on September 18 that Judge Smith was not disqualified. After Judge Smith rejected another attempt to disqualify him, plaintiffs, on September 24, filed a petition for extraordinary relief in the Court of Appeal challenging Judge Rickles' ruling and Judge Smith's order striking the second motion to disqualify him.

On the same day the Court of Appeal issued the following temporary stay: "In order that this court may have an opportunity to consider [the] within petition, IT IS HEREBY ORDERED that all proceedings ... are stayed pending determination of the within petition or until further order of this court."⁴

On October 5, defendants served and filed 11 motions for summary judgment or for orders specifying issues as without substantial controversy. The motions were noticed for hearing on October 15.

*27 On October 6, plaintiffs filed a petition in the Court of Appeal for writ of prohibition to prevent hearing on the summary judgment motions claiming that the motions were in violation of the stay. On October 8, the Court of Appeal denied the petitions of September 28 and October 6, and terminated the temporary stay forthwith. On the same day plaintiffs were notified by telephone that the stay had been lifted. On October 13, Judge Smith issued a minute order that all pending motions in the case, including summary judgment motions, would be heard as scheduled on October 15.

Plaintiffs filed their opposition on October 13, relying upon the October 7 declaration of J. DeWitt Fox, M.D., whose name had not been included in the list of experts furnished to defendants in July. Defense counsel had not received copies of the opposition at the time of hearing on October 15. Although two defense counsel went to court to read its copy on the 14th, a third did not, and the hearing was recessed to permit him to read the opposition papers.

After the recess, the hearing continued involving numerous motions, as well as the summary judgment motions. Plaintiffs did not claim that the summary judgment motions filed while the stay was in force were invalid. After defense counsel claimed that the opposition was untimely and Judge Smith had expressed concern that

defense counsel had not received the opposition papers, plaintiffs suggested a continuance to permit defense counsel to further review the papers, but the trial court stated it would not continue the proceedings. Aside from the above statement by plaintiffs they did not suggest a continuance.

[1] At the outset the parties dispute whether the stay of “all proceedings” issued by the Court of Appeal precluded the filing of the summary judgment motions and whether further proceedings were defective. Whether “all proceedings” should be read as referring to all court actions only or as including actions by the parties presents an interesting question, but we need not reach it. Plaintiffs chose to appear and argue the merits of the summary judgment motions and did not challenge the filing of the motions at the hearing of the motions. “It is well settled that the appearance of a party at the hearing of a motion and his or her opposition to the motion on its merits is a waiver of any defects or irregularities in the notice of the motion. [Citations.]” (*Tate v. Superior Court* (1975) 45 Cal.App.3d 925, 930, 119 Cal.Rptr. 835; *Lacey v. Bertone* (1949) 33 Cal.2d 649, 651–652, 203 P.2d 755.)

Plaintiffs urge that the trial court erred in refusing to consider the opposition papers on grounds that they were not timely filed. Rule 16, subdivision B of the Law and Motion Rules of the Los Angeles County Superior Court provides: “B. All papers, other than those initiating the proceedings, whether in opposition or support, shall be filed directly with the court clerk in the law and discovery department in which the matter is pending at least five calendar days but in no event later than 4:30 p.m. of the third court day preceding the scheduled hearing or they will not be considered, unless time is shortened by order of the court.”

Monday, October 12, 1981, was a holiday; therefore, the third court day preceding the scheduled hearing was Friday, October 9, 1981. As pointed out above, plaintiffs mailed their papers to defense counsel on October 12 and filed with the court on October 13.⁵

Pointing out that [Code of Civil Procedure section 437c](#) provides that summary judgment motions may be made on 10 days' notice but is silent as to the time to file counteraffidavits, the court in *Albermont Petroleum Ltd. v. Cunningham* (1960) 186 Cal.App.2d 84, 93, 9 Cal.Rptr. 405, concluded as an alternate ground of decision that

a local rule like rule 16 which restricts the time for opposing affidavits is void and unenforceable. The court also pointed out that the summary judgment remedy is “unusual and drastic” and for this reason should be used with caution to safeguard the right to trial with any doubt as to the granting of the motion resolved in favor of the opposing party. (186 Cal.App.2d at p. 92, 9 Cal.Rptr. 405.)

The holding of *Albermont* was rejected in *Shadle v. City of Corona* (1979) 96 Cal.App.3d 173, 178–179, 157 Cal.Rptr. 624, where the court reasoned that, had the Legislature intended to grant parties opposing summary judgment the right to file opposition to the summary judgment motion up to and including the hearing, it would have said so and that in the absence of legislative direction the time for filing opposition is subject to court rule. The court points out that last minute filings will often interrupt and delay hearings while the parties and the court study the documents.

A third view was expressed recently in *Kapitanski v. Von's Grocery Co.* (1983) 146 Cal.App.3d 29, 32–33, 193 Cal.Rptr. 839: “ ‘Local court rules and policies have the force of procedural statutes, so long as they are not contrary to legislative enactments. [Citations.]’ (*Shadle v. City of Corona* (1979) 96 Cal.App.3d 173, 177 [157 Cal.Rptr. 624].) ... Judges ... generally prefer to avoid acting as automatons and routinely reject requests by counsel to function solely in a ministerial capacity. Rigid rule following is not always consistent with a court's function to see that justice is done. *29 Cognizant of the strong policy favoring the disposition of cases on their merits (*Weitz v. Yankosky* (1966) 63 Cal.2d 849, 854–855 [48 Cal.Rptr. 620, 409 P.2d 700]; *Slusher v. Durrer* (1977) 69 Cal.App.3d 747, 753–754 [138 Cal.Rptr. 265]), judges usually consider whether to exercise their discretion in applying local court rules and frequently consider documents which have been untimely filed. Judges are well aware of the unnecessary burdens placed on courts and counsel when strict compliance with local procedural rules results in the expenditure of unnecessary time and money for the preparation of later section 473 motions....

“In applying the statutory grounds for relief under section 473 trial courts must consider the specific contexts in which such motions arise and should employ a flexible rather than rigid or formalistic approach to decisionmaking. Even without an empirical study it is

apparent that appellate courts are more inclined to affirm orders resulting in trials on the merits than orders denying relief from defaults. (*Weitz v. Yankosky*, *supra*, 63 Cal.2d at p. 854 [48 Cal.Rptr. 620, 409 P.2d 700]; *Slusher v. Durrer*, *supra*, 69 Cal.App.3d at p. 753 [138 Cal.Rptr. 265].) An attorney's neglect in untimely filing opposing papers must be evaluated in light of the reasonableness of ***767 **1139 the attorney's conduct. (*Robinson v. Varela* (1977) 67 Cal.App.3d 611, 615–616 [136 Cal.Rptr. 783].) In circumstances such as those present here trial courts must also consider the propriety of strictly enforcing local procedural rules. The salutary purpose of such rules regulating the filing of opposing papers is to ‘... ensure that the court and the parties will be familiar with the facts and the issues so that meaningful argument can take place and an informed decision rendered at the earliest convenient time.’ (*Shadle v. City of Corona*, *supra*, 96 Cal.App.3d at pp. 178–179 [157 Cal.Rptr. 624].) Also pertinent are the effects of strict enforcement on the rights of the parties and the furtherance of justice. (*Slusher v. Durrer*, *supra*, 69 Cal.App.3d at pp. 754–755 [138 Cal.Rptr. 265]; see also *Albermont Petroleum, Ltd. v. Cunningham* (1969) 186 Cal.App.2d 84, 90 [9 Cal.Rptr. 405].)”

[2] [3] We agree with the view expressed in *Shadle* and *Kapitanski* that in the absence of legislative direction to the contrary courts may adopt local rules with the force of law and that reasonable local rules limiting the time to file opposition to the summary judgment motion were not precluded by former *Code of Civil Procedure* section 437c.⁶ Interruption and delay of hearings which such rules are designed to prevent justify court management of its procedures. However, weighing the potential for interruption and delay against the policy in favor of disposition of cases on their merits, the drastic nature of the summary judgment remedy, and the potentially *30 short time available to respond to the summary judgment motion, we are satisfied that courts were required to exercise their discretion and relieve the attorney from tardy opposition filings when his conduct was reasonable, as pointed out in *Kapitanski*. If the court concluded that the tardy filing of opposition papers would prejudice the moving party or other parties, it could continue the hearing requiring the tardy party to pay reasonable costs. (See *Code Civ.Proc.*, §§ 473, 594a, 1024.) Rule 16, subdivision B of the Law and Motion Rules contemplates that the trial court may exercise its discretion in enforcing it by providing that the court may shorten the three-day

period before hearing during which opposition may not be filed.

[4] In the circumstances of the instant case, the trial court abused its discretion in enforcing the three-day limitation by refusing to consider the opposition rather than shortening the time or continuing the hearing. The motions were made on 10 days' notice. The motions and their supporting materials comprise over 800 pages. There were several other motions in the case set for the same day for which counsel was required to prepare. Plaintiffs' points and authorities in opposition to the motion comprise 30 pages, and Dr. Fox's declaration with its attached report is 15 pages in length. As we have seen, the summary judgment motions were made on October 5, and under the rule—because of the weekend and the holiday under the superior court's approach—compliance with the local rule would have required filings on October 9, four days later. A stay was in effect until October 8. Compliance with the local rule obviously would have required Herculean efforts.

The clerk filed the untimely opposition. While it is true that plaintiffs did not make a formal motion for continuance at the hearing, it was apparent from the trial court's statement—in response to plaintiffs' suggestion of a continuance—that it would not grant a continuance. It was also apparent that the court was prepared to consider the merits of the motion and the showing made in favor and in opposition and that the tardiness of the filing of the opposition had not interfered with its ability to fully consider the motion. At the hearing the trial court proceeded to permit ***768 **1140 argument on the merits of the summary judgment motion and the showing in opposition both before and after the violation of rule 16 was called to its attention. The trial court subsequently ruled on the showing in opposition, and its determination that tardy filing precluded consideration contradicts the record.

Thus, it is clear that the fact that the showing in opposition was filed two rather than three days prior to the hearing did not preclude full consideration of the opposition. In view of time burdens created by the stay, the lengthy motions and supporting documents, and the fact that the judge was fully prepared to, and did, consider the opposition to the motion, we conclude *31 that the trial court erred in ruling that the opposition to the motion could not be considered.

THE CONTENTS OF DR. FOX' DECLARATION

The trial court also rejected Dr. Fox' declaration on the grounds that it lacked the requisite foundational facts to qualify him to testify about the standard of care and tended to "shotgun his opinions in a conclusionary way." While we agree that Dr. Fox' declaration was conclusionary in a number of respects, the declaration contains several factual assertions establishing triable issues of fact and precluding its rejection. We also conclude that Dr. Fox was qualified to testify about the standard of care.

Dr. Fox' summary of decedent's medical records outlining the treatment administered is not challenged but is reinforced by the defense showing. On November 1, 1977, decedent went to the UCLA radiology department as an out-patient for X-rays of her toes preparatory to surgery for rheumatoid arthritis of the joints of her toes. She fell and struck her head. A skull series was taken. She returned to the hospital in December, and the surgery was performed. On January 10, she was rehospitalized because of some infections in the incisional sites of the foot. The next day X-rays were taken including X-rays of the cervical spine. In September and October 1978, she was again in the hospital because of infection in her foot, and during this period she was treated for rheumatoid arthritis, dislocated hip, respiratory difficulties, and apparently she was given a pacemaker. She was removed to St. Joseph Hospital at the request of her family on November 9 where she was discharged on November 17. She returned to St. Joseph Hospital a week later, and she died March 26, 1979. An autopsy revealed that the cause of death was a fracture of the odontoid process with spinal cord damage.

The motions for summary judgment of the defendant physicians, including the radiologists, and of Holly Hoberg, a radiology technician, were supported by the declarations of the moving parties, the declaration of D.M. Forrester, M.D., and portions of the deposition of George Campion, M.D.

In addition, the motion of defendant Richard D. Ferkel, M.D., a general surgeon, was also supported by the declaration of Ronald W. Busuttill, M.D., board certified in general surgery; the motions of defendants Baldwin,

Bernstein, Cooman, Cracchiolo, Galleno, Levensen, Purcell and Tibone, all orthopedic surgeons, were also supported by the declaration of Leonard Marmor, M.D., a board certified orthopedic surgeon; and the motions of defendants Barnett, Carlson, Cassan, Croft, Levy, Kovick, *32 MacAlpin, Simmons, and Van Herle, whose specialties were rheumatology, internal medicine, respiratory care, cardiology, pulmonary diseases, and endocrinology, were also supported by the declaration of Matthew O. Locks, M.D., who is board certified in internal medicine.

The declarations of the doctor defendants categorically denied the charging allegations of the complaint and declared, inter alia, their specific involvements in the case of Ada Crews Mann, that they were not in the room when she fell on November 1, 1977; that they had not at any time concealed, attempted, or conspired to conceal, any information from anyone regarding the health, care, and/or treatment of her; that services they provided for decedent were ***769 **1141 not provided for the purpose of artificially inflating her bill or obtaining Medicare or MediCal funds; that they never attempted or conspired to kill Ada Crews Mann, and that, in their opinion, their conduct at all times conformed to the standard of practice in the community relating to the practice of their named specialty.

The declaration of Holly Hoberg declares that her only involvement with the decedent occurred when she and decedent were in an X-ray room on November 1, 1977; that she had never concealed or attempted or conspired to conceal any information from anyone regarding the health, care, and/or treatment of decedent; that the services she had provided to decedent were not for the purpose of inflating her bill or obtaining funds, and that she never attempted or conspired to kill decedent.

An earlier affidavit of Hoberg had been filed in the court's records. It declared that her function at UCLA was to position patients so that X-rays could be taken and then to take X-rays; that she had been positioning Ada Crews Mann's feet for X-rays when she fell on November 1, 1977; and that the allegations of the complaint that Hoberg was a party to a conspiracy to conceal medical facts and that she kept decedent in a drugged state and attempted to kill her were sham, spurious, and scandalous.

The declaration of D.M. Forrester, M.D., a board certified radiologist dated August 28, 1981, declared that she had reviewed copies of the X-rays of decedent taken after her fall on November 1, 1977, and copies of many other listed X-rays and of radiology reports, all of which had the name of Ada Crews Mann on them and were from UCLA. In her opinion, all of “those reports were prepared in conformity with the standard of practice for radiologists in this community.” She further states: “To a reasonable degree of medical certainty the November 1, 1977 x-rays do not show any fracture or dislocation. To a reasonable degree of medical certainty I do not believe the patient sustained a fracture of the odontoid process on November 1, 1977 at any time that day prior to the taking of those x-rays. Some of *33 the reasons for my opinion are: (1) The alignment of C-1 and C-2 is normal; (2) There is no evidence of prevertebral soft tissue swelling, which normally would be present if the patient sustained a fracture of the odontoid process; (3) If the patient had recently sustained a fracture of the odontoid process she would have been in too much pain to rotate her head to the positions required for that series of x-rays.”

George Campion, M.D., is director of radiology at St. Joseph Medical Center, Burbank, California. In his deposition, he stated in reference to the November 1 [skull X-ray](#) pictures of decedent Ada Crews Mann that “... you cannot anatomically rule it out [a fracture of the odontoid process] on radiographic method, although the fact that she can turn her neck for the positioning of the skull X/ rays, it is unlikely that she does have a fracture at this time,” and that, if her odontoid had been fractured on that date, “... I don't think the patient would have been able to turn her neck in order to position her head for these lateral views.” Campion also stated that he had not formulated an opinion as to whether any of defendant Doctors Arndt, Bassett, Bein, Bennett, Bernstein, Bohman, Drake, Feigenbaum, Friedman, Gold, Levine, Manger, Morton, Russell, Scanlon, Schmidt and Weiner had failed to comply with the standard practice relating to radiology in relation to decedent Ada Crews Mann and that he had never told anyone that any of those doctors had failed to comply with the standard of practice.

The declaration of Dr. Busuttil, supporting the motion of defendant Ferkel, declared that he had reviewed ***770 the UCLA Hospital and Clinic's chart pertaining to Ada Crews Mann. In his opinion, the care rendered to her by Richard Ferkel, M.D., conformed to the standard of

practice relating to general surgeons in the community in the light of her history and symptoms.

The declaration of Leonard Marmor, M.D., supporting the motions of the orthopedic surgeons declared that he had reviewed **1142 the UCLA Hospital and Clinic's chart relating to Ada Crews Mann and copies of numerous listed X-rays pertaining to her, including those of November 1. In his opinion the care rendered to decedent by the eight orthopedic surgeons conformed to the standard of practice for orthopedic surgeons in the community in the light of her history and symptoms.

The declaration of Matthew O. Locks, M.D., supporting the motions of the remaining treating doctors, declared that he had reviewed a copy of the UCLA Hospital and Clinic report pertaining to Ada Crews Mann. Based upon his education, professional background, and review of the above-mentioned records, it was his opinion that the care rendered to Ada Crews Mann by each of those doctors, naming each of them, was appropriate and reasonable, in light of Ada Crews Mann's history and symptoms. The records *34 reflected that she had a multitude of serious medical problems, including severe [rheumatoid arthritis](#), and that the care and treatment rendered to decedent by those doctors conformed to the standard of practice in the community of internists.

The declaration of defendant Bernard Strohm established that he was the associate director/administrator at UCLA Hospital and Clinics; that he had no contact with Ada Crews Mann and was not aware that she was a patient at UCLA until after the instant lawsuit was filed; and that he never concealed or attempted or conspired to conceal any information from anyone regarding the health, care, and/or treatment of Ada Crews Mann and had never attempted or conspired to kill her.

The declaration of defendant William S. Russell established that he was the data processing manager at UCLA Hospital and Clinics during the relevant period of time. He had no contact with Ada Crews Mann and was not aware that she was a patient at UCLA until after the lawsuit was filed. He had never concealed or attempted or conspired to conceal any information concerning her health or care or medical treatment from anyone and had never attempted or conspired to kill her.

Dr. Fox, plaintiff's expert, a diplomate of the American Boards of Surgery and of Neurological Surgery, filed a declaration which incorporates his report and may be summarized as follows: A December 21, 1976, X-ray shows no fracture, dislocation, or subluxation of the odontoid. The lateral skull film of November 1, 1977, reveals fracture of the odontoid just below the skull line, and there is no open-mouth view to confirm it. There were no cervical spine films to compare. The X-ray report of November 1 is very sketchy and incomplete and states that the tape was broken.⁷ The January 11, 1978, films confirm a [fracture-dislocation](#) of the odontoid process. The radiologist, Richard H. Gold, M.D., interpreted this as erosion of the dens secondary to [rheumatoid disease](#). He recommended an open-mouth view, which was never taken, and [tomography](#), which was never obtained. The medical records show repeated complaints of head and neck pain in 1977 and 1978. The September 4, 1978, films confirm the subluxation of C-1 and C-2 with [posterior displacement](#), and this is confirmed by the radiology reports of the UCLA radiology department. Decedent was never treated for the fracture at the UCLA Medical Center.

In Dr. Fox' opinion, after reviewing the medical records and X-rays, the treatment at the medical center was below the standard of practice. It was ***35** below the standard of practice not to discover the fracture and to fail to take cervical spine films on November 1, 1977. Because the earlier films showed no injury, it is reasonable to assume that the fracture occurred when decedent fell on November 1.

Dr. Fox was critical of Dr. Forrester's declaration. Pointing to her statement that *****771 **1143** the alignment of C-1 and C-2 is normal, he points out that no films of the cervical spine were taken on November 1 and that the January 11 and September 4 films which were of the cervical spine show a [fracture dislocation](#) and subluxation of C-1 and C-2. Dr. Fox criticizes Dr. Forrester's reliance on the absence of prevertebral soft tissue swelling, stating that the patient did not have time to develop swelling because the films were taken immediately after the fall. Dr. Fox also criticizes the third reason offered by Dr. Forrester for concluding there was no fracture on November 1—if decedent had sustained a fracture the patient would have been in too much pain to rotate her head to the positions required for the [skull X-rays](#). Dr. Fox states that decedent “obviously did have the

films and did not have to rotate her head to obtain laterals or AP's or Towne views, no rotation was needed!”

Dr. Fox also challenges the other nondefendant doctors who filed declarations that the defendant doctors conformed to the standard of practice. He asserts that in view of the history of [head injury](#), the symptoms of neck pain reported in the nurse's notes, and respiratory distress, the orthopedic surgeons should have evaluated the patient's neck. Dr. Fox also asserts internal medicine specialists and other respiratory specialists, in view of the symptoms, should have been alert to cervical damage. Finally, he challenges the general surgeon's declaration, asserting that it is inappropriate for a general surgeon to determine the standard of care for arthritic specialists and a cardiologist.

[5] [6] The summary judgment procedure, inasmuch as it denies the right of the adverse party to a trial, is drastic and should be used with caution. (*Eagle Oil & Ref. Co. v. Prentice* (1942) 19 Cal.2d 553, 556, 122 P.2d 264.) Summary judgment is properly granted only when the evidence in support of the moving party establishes that there is no issue of fact to be tried. (*Code Civ.Proc.*, § 437c; *Lipson v. Superior Court* (1982) 31 Cal.3d 362, 374, 182 Cal.Rptr. 629, 644 P.2d 822.)

“The moving party bears the burden of furnishing supporting documents that establish that the claims of the adverse party are entirely without merit on any legal theory.” (*Lipson v. Superior Court, supra*, 31 Cal.3d at p. 374, 182 Cal.Rptr. 629, 644 P.2d 822.) “The affidavits of the moving party are strictly construed and those of his opponent liberally construed, and doubts as to the ***36** propriety of summary judgment should be resolved against granting the motion.” (*Slobojan v. Western Travelers Life Ins. Co.* (1969) 70 Cal.2d 432, 436–439, 74 Cal.Rptr. 895, 450 P.2d 271.) “... [I]ssue finding rather than issue determination is the pivot upon which the summary judgment law turns.” (*Walsh v. Walsh* (1941) 18 Cal.2d 439, 441, 116 P.2d 62.)

[7] [8] The courts require only that physicians and surgeons exercise in diagnosis and treatment that reasonable degree of skill, knowledge, and care ordinarily possessed and exercised by members of the medical profession under similar circumstances. (*Bardessono v. Michels* (1970) 3 Cal.3d 780, 788, 91 Cal.Rptr. 760, 478 P.2d 480.) In deciding whether physicians and surgeons

have met this standard, the trier of fact may infer failure of the practitioner to have done so in cases in which the happening of the accident does not normally occur in the absence of negligence. While other cases may require expert testimony to establish the standard of care, such cases do not. (*Id.*, at pp. 788–793, 91 Cal.Rptr. 760, 478 P.2d 480.)

[9] [10] The trier of fact may infer negligence from the factual statements of Dr. Fox. His declaration that the November 1 X-ray shows the fracture and the radiology report fails to show the fracture would warrant the trier of fact upon reviewing the X-rays to conclude that the radiologists were negligent in not observing what was apparent from the X-rays and taking appropriate action.⁸ Moreover, Dr. Fox's declaration ***772 **1144 clearly undermines the factual basis for Dr. Forrester's declaration which forms the basis of the radiologists' motions for summary judgment.

The trier of fact could also infer that in common X-ray procedures the patients do not fall in the absence of negligence and that when patients do fall, the person positioning the patient is probably the person responsible.

In addition, according to Dr. Fox, the radiologist reports of January 11 and September 4 reflect a problem as to C-1 and C-2 and recommend further procedures. The recommended procedures were not done. A trier of fact without expert testimony as to the standard of care could infer that failure to follow the recommendations constituted negligence. An excuse for failure to follow the recommendations might require testimony as to the standard of care, but no excuse has been offered. Without expert testimony as to the standard of care, the trier of fact upon viewing the January 11 and September 4 X-rays in the light of Dr. Fox' declaration that they show the fracture *37 could infer, depending upon their viewing of the X-rays, that the radiologists should have identified a fracture and were negligent in not observing it. Accordingly, entirely apart from his statements as to the standard of care, Dr. Fox' declaration contained factual assertions which if accepted would permit a finding of negligence and it was error for the trial court to reject his declaration on the grounds that it was conclusory.

[11] In any event, Dr. Fox was competent to testify as to the standard of care. In *Brown v. Colm* (1974) 11 Cal.3d 639, 644, 114 Cal.Rptr. 128, 522 P.2d 688,

we rejected “an invariable rule which would require in all cases that an expert must have acquired a personal, working knowledge of the standard of care at the precise time when the alleged malpractice occurred.” The court reasoned in part: “While a layman may not testify to a fact which he has learned only by reading a medical book, there is no question that a professional physician may rely upon medical texts as the basis for his testimony. (*Healy v. Visalia etc. R.R. Co.* (1894) 101 Cal. 585, 591–592 [36 P. 125]; *Hope v. Arrowhead & Puritas Waters, Inc.* (1959) 174 Cal.App.2d 222, 230 [344 P.2d 428]; *Brown v. Los Angeles Transit Lines* (1955) 135 Cal.App.2d 709, 716 et seq. [287 P.2d 810]; *Forrest v. Fink* (1925) 71 Cal.App. 34, 39–40 [234 P. 860].) Wigmore justifies the foregoing distinction by pointing out that a medical doctor possesses a professional experience which gives him a knowledge of the trustworthy authorities and the proper sources of information, as well as a degree of personal observation of the general subject enabling him to estimate the plausibility of the views expressed. Furthermore, he opines, it may be impossible to obtain information on the particular matter except through the reported data. (2 Wigmore on Evidence (1940) § 665b, pp. 784–785.) ...

“The unmistakable general trend in recent years has been toward liberalizing the rules relating to the testimonial qualifications of medical experts. Thus, whereas a number of earlier cases held that a physician of necessity must possess the skill ordinarily practiced only in the *same* locality (see, e.g., *Trindle v. Wheeler* (1943) 23 Cal.2d 330, 333 [143 P.2d 932]), only six years later this requirement was relaxed so that a physician was deemed qualified as an expert if he could testify to the practice in a *similar* community. (*Sinz v. Owens, supra*, 33 Cal.2d 749, 756 [205 P.2d 3].) Some early cases were unbending in requiring expertise as to the precise injury involved in the litigation, as, e.g., not permitting an autopsy surgeon to testify on urology (*Moore v. Belt* (1949) 34 Cal.2d 525 [212 P.2d 509]). Other authorities, however, have permitted variations, as, e.g., a pathologist was qualified to testify as to causes of *aseptic necrosis* (*Agnew v. City of Los Angeles* ***773 **1145 (1950) 97 Cal.App.2d 557, 566 [218 P.2d 66]); an expert in otolaryngology to testify regarding *plastic surgery* (*Mirich v. Balsinger* (1942) 53 Cal.App.2d 103 [127 P.2d 639]); a homeopathic physician and surgeon to testify on the degree of care required of a physician educated in the allopathic school of medicine (*Hutter v. Hommel* (1931) 213 Cal. 677, 681

[3 P.2d 554]); a pathologist and professor of pathology to testify on the subject of gynecology (*Cline v. Lund* [(1973)], *supra*, 31 Cal.App.3d [755] at p. 766 [107 Cal.Rptr. 629]).

“There are sound and persuasive reasons supporting this trend toward permitting admissibility more readily, rather than rigidly compelling rejection of expert testimony. It is obvious that an overly strict standard of qualification would make it difficult and in some instances virtually impossible to secure a qualified expert witness.” (11 Cal.3d at pp. 644–646, fn. omitted, 114 Cal.Rptr. 128, 522 P.2d 688.)

The court concluded the determinative issue in each case must be whether the witness has sufficient skill or experience in the field so that his testimony would be likely to assist the jury in the search for the truth, and “no hard and fast rule can be laid down which would be applicable in every circumstance.” (11 Cal.3d at p. 645, 114 Cal.Rptr. 128, 522 P.2d 688.) Where a witness has disclosed sufficient knowledge, the question of the degree of knowledge goes more to the weight of the evidence than its admissibility. (*Chadock v. Cohn* (1979) 96 Cal.App.3d 205, 209, 157 Cal.Rptr. 640.)

Dr. Fox is a diplomate in surgery and [neurosurgery](#), and it would be unreasonable to assume that he does not regularly read X-rays and radiologists' reports and is unfamiliar with the standard of care exercised by radiologists in reading X-rays and preparing reports. In considering the claim that Dr. Fox is not shown competent to testify to the standard of care exercised by the various other specialists, it must be remembered that his challenge is they failed to diagnose the broken neck. The fact that the patient exhibits symptomatology coming within a particular specialty does not mean that there is not disease or injury coming within another specialty. A specialist must be alert to such possibilities and the need to consult other specialists. The specialist treating respiratory problems, in other words, must be alert to the possibility that the respiratory problems are caused in whole or in part by spinal dislocations and be prepared to call in neurosurgeons when proper diagnostic procedures so require.

Defendants argue that as a surgeon and neurosurgeon Dr. Fox has qualifications not possessed by the other specialists, that a higher standard of care would be

applicable to a neurosurgeon than to doctors engaged in other specialties, and that his declaration as to the standard of care could be rejected on the basis that he is in a sense overqualified. However, a neurosurgeon is obviously aware not only of the practice of his speciality but *39 also the symptomology which leads other specialists to treat patients coming within his speciality and to refer patients to neurosurgeons.

[12] Defendants rely on authorities that hold that the qualification of an expert is ordinarily a matter addressed to the sound discretion of the court and its ruling will not be disturbed unless a clear abuse is shown. (*Chadock v. Cohn, supra*, 96 Cal.App.3d 205, 208, 157 Cal.Rptr. 640.) However, the court will be deemed to have abused its discretion if the witness has disclosed sufficient knowledge of the subject to entitle his opinion to go to the jury. (*Brown v. Colm, supra*, 11 Cal.3d 639, 647, 114 Cal.Rptr. 128, 522 P.2d 688.) As a diplomate of surgery and [neurosurgery](#), Dr. Fox is qualified to testify as to the standard of care in reading X-rays, in submitting X-ray reports, and in diagnosing, and the court abused its discretion in concluding that there was no proper foundation.

[13] Defendants also urge that because Dr. Fox was not listed by plaintiffs as one of their experts for trial, he could not be called as a witness at trial (**1146 ***774 Code Civ.Proc., § 2037 et seq.) and that because the purpose of a summary judgment motion is to determine whether there are any triable issues of fact, the court in ruling on the summary judgment motions was required to disregard Dr. Fox' declaration. At the argument on the summary judgment motions, plaintiffs asserted that they had recently obtained the services of Dr. Fox.⁹

[Code of Civil Procedure section 2037.6](#) provides that the court upon such terms as may be just may permit a party to call an expert witness not included in the list of expert witnesses so long as the court finds that the party made a good faith attempt to list expert witnesses, that the party has given notice to the opposing party in accordance with [section 2037.4](#), and that as of the date of the exchange of lists the party would “not in the exercise of reasonable diligence have determined to call such witness.”¹⁰ *40 Because the trial court might choose to grant relief, the court ruling on the motions for summary judgment could not assume that it would not.

For the foregoing reasons, we conclude that the court could not properly reject Dr. Fox's declaration on the grounds it stated. This does not mean that the summary judgment motions must be denied as to all defendants. Because the judge rejected Dr. Fox' declaration for all purposes, he had no occasion to reach the further issue that the declaration was sufficient to give rise to issues of fact as to some defendants but not others. Although Dr. Fox states generally that the physicians should have been alerted to the fracture on the basis of certain X-rays and the patient's complaints and symptoms, it is apparent that many of the defendants were not involved in the reading of the X-rays reflecting the fracture, and the declaration does not specify the particular complaints or symptoms or indicate when they occurred. The statements that the doctors generally should have been alerted to the fracture are obviously conclusionary and do not furnish a basis for denial of the summary judgment motions made by individual doctors. Upon remand, the judge should consider as to each defendant whether there is a factual basis for liability shown by Dr. Fox' declaration or any additional declaration that may be filed.

PUNITIVE DAMAGES

[14] The summary judgment on the punitive damages issues must be sustained. Dr. Fox' declaration at most makes out a case for medical malpractice and does not justify the claim for punitive damages. There is no evidence of a conspiracy to conceal, of intentional performance of useless operations or of attempt to kill. At most all that was shown in opposition to the motions was a failure to observe, report or diagnose. Such failure does not establish intentional misconduct.

***775 **1147 DR. NACHMAN

[15] Summary judgment was properly entered in favor of Dr. Nachman on March 4, 1981. His declaration may be summarized: Dr. Nachman specializes in the field of anesthesiology and examined decedent once for the purpose of determining her suitability for anesthesia for an operation. The operation was postponed, and he did not administer anesthesia. He did not order any X-rays or interpret or consult any previous X-rays. He did not *41 enter into any agreement to conceal facts regarding her treatment. In opposition plaintiffs did not offer any

expert declarations. There being nothing to indicate that Dr. Nachman should have studied the X-rays, that he was to diagnose decedent's ailments, or that he treated decedent, the summary judgment was properly granted.

DR. DAVIDSON

[16] Dr. Davidson's motion for summary judgment was granted on July 15, 1981. ¹¹ His declaration states that he was an intern in the orthopedic department. On October 23, 1978, he cosigned an order made by a Dr. Gausewitz for administration of the drug Lasix, and on October 28, at the decedent's request, he prescribed a sleeping pill, Dalmane. His examination of decedent was limited to that necessary to verify the order of Dr. Gausewitz and to safely prescribe Dalmane. He did not order X-rays or consult or interpret X-rays. He did not conceal any facts and did not take any actions to speed decedent's death. Again, plaintiffs did not offer any expert declarations. The motion was properly granted.

MOTION TO TAKE JUDICIAL NOTICE

Plaintiffs request this court to take judicial notice of 20 matters. As to a code section and a rule of court, no motion is necessary. Similarly, the issue table in a Court of Appeal brief is also properly before us. The remaining matters all appear to be factual matters which were not called to the court's attention when it ruled on the motions for summary judgment and may not be used to vacate the orders.

APPEAL FROM POSTJUDGMENT ORDERS

[17] Although plaintiffs appealed from postjudgment orders, they did not in their opening brief specifically attack any of those orders. Accordingly, the appeal from those orders need not be separately considered. (See *Johnston v. Board of Supervisors* (1947) 31 Cal.2d 66, 70, 187 P.2d 686; *Henderson v. Security Nat. Bank* (1977) 72 Cal.App.3d 764, 769, 140 Cal.Rptr. 388; *42 6 Witkin, Cal.Procedure (2d ed. 1971) Appeal, § 425, pp. 4391–4393, § 442, pp. 4405–4406.)

The summary judgment of March 4, 1981, in favor of Dr. Nachman is affirmed. The summary judgment filed October 26, 1981, is amended to include a provision denying recovery against Dr. Davidson. That summary judgment as amended is affirmed insofar as it denies recovery for punitive damages and any recovery against Dr. Davidson. In all other respects, the summary judgment filed October 26, 1981, is reversed. Because of our reversal of the latter summary judgment, the postjudgment orders incident to the summary judgment are nullified (6 Witkin, *Cal.Procedure*, *supra*, Appeal, § 542, pp. 4483–4484), except insofar as one of them relates to punitive damages. To the extent that the postjudgment order relates to the punitive-damages claim, it is affirmed. Drs. Nachman and Davidson shall recover their costs on appeal from plaintiffs and plaintiffs shall recover their costs, other than that portion relating to their appeals from the summary judgment in favor of Drs. Nachman and Davidson, from the remaining respondents.

MOSK, KAUS, REYNOSO, GRODIN and LUCAS, JJ., concur.

***776 BIRD, Chief Justice, concurring.

I write separately because I believe it is important to clarify the effect of a stay of “all proceedings” for future litigants. (See maj. opn., *ante*, at pp. 765–766.) In cases where a stay is in effect when a motion is noticed, the stay should “stop the clock” from running either toward a hearing date or toward a date on which opposition papers are due. Any other rule permits the clock to run toward conditional, uncertain dates, leaving the nonmoving party unclear as to when opposition must be filed and when an appearance must be made. It is unfair to allow the moving party to profit from such uncertainty.

Here, hearing on a motion for summary judgment was noticed for October 15th. Both parties agree that the stay order would have prevented the trial court from hearing the motion on that date unless it was lifted. The law and motion judge clearly informed all parties that while moving papers could be *filed* in his department, no *hearing* could be held unless the stay order were dissolved.

Under the terms of the local rule,¹ the filing of defendants' motions made plaintiffs' opposition due three to five days before the noticed hearing date. *43 Yet the stay rendered both the hearing date and, a fortiori, the deadline

for filing an opposition entirely speculative at the time notice was given. The hearing could not go forward on the 15th unless an intervening event—the dissolution of the stay—occurred.

Plaintiffs argue that a stay of “all proceedings” not only bars a court from hearing a motion, but also the parties from filing any notice of motion. Alternatively, they argue that if a filing were allowed, a stay order would toll any period which would otherwise begin to run when the motion was filed. If a stay is in effect, a party may not file a motion and thereby create a deadline for an opponent which carries adverse consequences.

Judicial definitions of the term “proceeding” might well have led plaintiffs to believe that either interpretation of the stay order was correct. “The term ‘proceeding’ may refer not only to a complete remedy (see [Code Civ.Proc.] § 23) but also to a mere procedural step that is part of a larger action or special proceeding. [Citations.]” (*Rooney v. Vermont Investment Corp.* (1973) 10 Cal.3d 351, 367, 110 Cal.Rptr. 353, 515 P.2d 297.) Arguably, the term includes steps taken by the parties as well as by a court. In *Lukes v. Logan* (1884) 66 Cal. 33, 4 P. 883, the term was held to encompass the settlement of a bill of exceptions between two parties in preparation for a motion for a new trial. Citing *Lukes* with approval in *Stonesifer v. Kilburn* (1892) 94 Cal. 33, 43, 29 P. 332, this court observed that “[t]he word [proceeding] is generally applicable to *any step taken by a suitor* to obtain the interposition or action of a court.” (Italics added, citation omitted.)

In *Burns v. Superior Court* (1903) 140 Cal. 1, 73 P. 597, the term “proceedings” was held to include the issuance of a subpoena by a notary at the request of one party seeking to depose another. (*Id.*, at p. 9, 73 P. 597.) Though a trial court does not act directly in deposition proceedings, *Burns* viewed a deposition as “a means furnished by law for the use of the court for the purpose of enabling it to obtain the evidence....” (*Ibid.*) Thus, “[t]he taking of a deposition is as clearly one of the ‘proceedings’ of the court as was the taking of testimony before the master or examiner in a suit in equity.” (*Ibid.*)

As *Burns* noted, “[t]he word ‘proceeding’ necessarily has different meanings, according to the context and the subject to which it relates.... In section 473 of the Code of Civil Procedure, and in similar statutory provisions of other states, it has a broader signification, and includes

any step taken in a case, whether by the court or by one of the parties thereto. [Citations.] ‘*In its more general sense, in law, it means all the steps or* *44 *measures adopted in the* ***777 *prosecution or defense of an action.*’ [Citation.]” **1149 (*Burns, supra*, 140 Cal. at pp. 5–6, italics added, 73 P. 597.)

In light of these holdings, a nonmoving party could reasonably have concluded that a stay of “all proceedings” prohibited his opponent from noticing a hearing date or creating a deadline for the filing of opposition. Such notice is a prerequisite to having the motion heard. (Code Civ.Proc., § 1010.) Like the subpoena in *Burns*, the notice is the means by which the parties are brought before the court. Like the settlement of a bill of exceptions, the notice is a “ ‘step taken by a suitor to obtain the interposition or action of a court.’ ” (*Stonesifer v. Kilburn, supra*, 94 Cal. at p. 43, 29 P. 332.) Logically, it is a “proceeding” which is stayed by a stay of “all proceedings.”

The case law is not the only source which could lead a nonmoving party to believe that a hearing or opposition due date is inoperative if a stay is in effect. Conditional dates are by their very nature inadequate notice. Here, the October 15th hearing date was a conditional one. The hearing could not proceed as noticed unless the stay were dissolved. A fortiori, the deadline for plaintiffs to file their opposition was conditional and uncertain when the notice was given.

This ambiguity as to the deadline for filing an opposition should not be construed against the nonmoving party. This is particularly true with summary judgment, which is so final a remedy. The moving party should not be

able to take advantage of his opponent's uncertainty as to the date on which his opposition papers must be filed. Furthermore, given the short time available to prepare an opposition even when the noticed deadline is an operative one, any uncertainty about the deadline could be critically unfair to the responding party.

“It is academic that the burden is on the party moving for summary judgment; because of the drastic nature of the remedy sought, he is held to strict compliance with the procedural requisites.” (*Department of General Services v. Superior Court* (1978) 85 Cal.App.3d 273, 284, 147 Cal.Rptr. 422.) One “procedural requisite” for any motion is that the notice of motion specify the date on which the motion will be heard. (Code Civ.Proc., § 1010.) A notice which specifies only a conditional hearing date and, therefore, fixes a conditional date for filing opposition papers, does not constitute “strict compliance with the procedural requisites.”

To prevent such problems in the future, this court should make it clear that a stay of “all proceedings” tolls *any* deadlines which come into existence while a stay is in effect. A stay does not necessarily bar a party from filing a motion, but a moving party should be required to renounce any *45 hearing date which was conditional at the time of the original notice. Such a rule would prevent a moving party from profiting from an ambiguity created by his own action and would ensure that the rules of fair notice to an opponent are respected.

All Citations

38 Cal.3d 18, 694 P.2d 1134, 210 Cal.Rptr. 762

Footnotes

- 1 Two of the sons are attorneys, and they represent themselves and the other two plaintiffs.
- 2 During the course of the pretrial proceedings, plaintiffs attempted to disqualify a total of six superior court judges, Judges Choate, Rittenband, Cole, Chernow, Smith and Sumner. Eight petitions for extraordinary relief have been filed with the Court of Appeal. Several petitions for hearing have been denied by this court. Plaintiffs filed an action in the federal court naming three defense counsel, their firm, four judges and a special master as defendants charging that the defendants were conspiring to deprive plaintiffs of their rights under the federal Constitution. Judgment of dismissal was affirmed with sanctions. While this appeal was pending, plaintiff filed another federal court action—this time against five of the doctor defendants and the administrator of the UCLA Medical Center. The action was dismissed with an award of attorney fees to the defendants, and the dismissal was affirmed with the award upheld on the ground that the action was frivolous.
- 3 One of the defendant doctors' motions for summary judgment was granted in March and another in July 1981. Those motions will be discussed later in this opinion. The discussion in the first portion relates to the motions of the remaining defendants heard on October 15, 1981. Unless otherwise indicated the term defendants refers only to the latter defendants.

- 4 On October 1, plaintiffs filed another petition for extraordinary relief in the Court of Appeal, which like an earlier petition, sought to disqualify the special master appointed to preside at depositions, retired Judge Joseph Wapner, and to vacate Judge Eagleson's order that depositions be held in the courthouse in the presence of a bailiff. The petition was denied, and we denied a petition for hearing.
- 5 Plaintiffs have not argued that the filing was timely under [Code of Civil Procedure sections 12 and 12a](#) extending time for performance of an act when the last day for performance is a holiday.
- 6 In 1983, [Code of Civil Procedure section 437c](#) was amended to provide that the motion for summary judgment must be made at least on 28 days' notice rather than 10 and that opposition papers must be filed 14 days before the hearing unless the court for good cause orders otherwise. (Stats.1983, ch. 490, § 1.)
- 7 The radiologist's final report of the November 1 X-rays incorporated in several of defendants' declarations states that decedent fell and the contemplated X-rays could not be completed. It continues [typewriting]: "Skull films were done, however, and there is a ... [something is written in handwriting but it could not be deciphered]."
- 8 Alternatively, if the radiologists did observe the fracture but failed to report it because they ran out of tape, the trier of fact without expert testimony on the standard of care could infer that the failure to report constituted negligence.
- 9 In their brief, plaintiffs state that they were unable to obtain the neurologist they listed as an expert witness.
- 10 [Code of Civil Procedure section 2037.4](#) provides: "A party who is required to exchange lists of witnesses shall diligently give notice to the parties upon whom his or her list was served if, after notice of it, he or she determines to call an expert witness not included in it, and a party shall make available for deposition such expert witnesses as he or she has determined to call and shall immediately make available for inspection and copying all of such expert witness's discoverable reports and writings."
[Code of Civil Procedure section 2037.6](#) provides: "(a) The court may, upon such terms as may be just (including but not limited to continuing the trial for a reasonable period of time and awarding costs and litigation expenses), permit a party to call a witness, or permit a witness called by a party to testify to an opinion or data on direct examination, during the party's case in chief where such witness, is required to be, but is not, included in such party's list of expert witnesses so long as the court finds that such party has made a good faith effort to comply with [Sections 2037](#) through [2037.3](#), inclusive, that he has complied with [Section 2037.4](#), and that as of the date of exchange he: [¶] (1) Would not in the exercise of reasonable diligence have determined to call such witness; or [¶] (2) Failed to determine to call such witness through mistake, inadvertence, surprise, or excusable neglect.

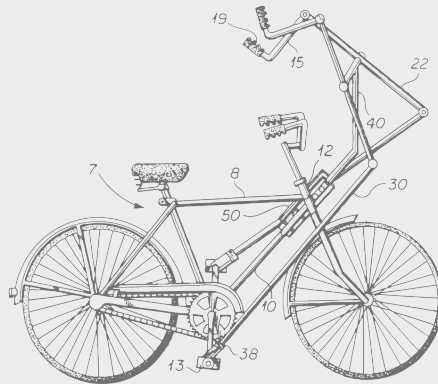
"(b) In making a determination under this section, the court shall take into account the extent to which the opposing party has relied upon the list of expert witnesses and will be prejudiced if the witness is called."

- 11 The summary judgment was not formally entered. It is appropriate to preserve the appeal by amending the summary judgment filed October 26, 1981, to include a judgment for Dr. Davidson in order to establish an appealable judgment, and we so order. (See [Varjabedian v. City of Madera \(1977\) 20 Cal.3d 285, 289, fn. 1, 142 Cal.Rptr. 429, 572 P.2d 43.](#))
- 1 See majority opinion, *ante*, at page 765 of 210 Cal.Rptr., p. 1137, of 694 P.2d.

EXHIBIT 11

THE SMART GUIDE TO

Patents



BY AARON G. FILLER

The Smart Guide To Patents

Published by

Smart Guide Publications, Inc.

2517 Deer Chase Drive

Norman, OK 73071

www.smartguidepublications.com

Copyright © 2012 by Aaron G. Filler. All rights reserved. No part of this book, including interior design, cover design, illustrations and icons may be reproduced or transmitted in any form or stored in a retrieval system, or transmitted by any means, electronic, mechanical, photocopying, recording, or otherwise, without written permission from the publisher. Although every precaution has been taken in the preparation of this book, the publisher and author assume no responsibility for errors or omissions. The author and publisher specifically disclaim any responsibility for any liability, loss, or risk, personal or otherwise, which is incurred as a consequence, directly or indirectly, of the use and application of any of the contents of this book.

For information, address: Smart Guide Publications, Inc. 2517 Deer Creek Drive, Norman, OK 73071

SMART GUIDE and Design are registered trademarks licensed to Smart Guide Publications, Inc.

International Standard Book Number: 978-0-9834421-0-3

Library of Congress Catalog Card Number:

11 12 13 14 15 10 9 8 7 6 5 4 3 2 1

Printed in the United States of America

Cover design: Lorna Llewellyn

Copy Editor: Ruth Strother

Back cover design: Joel Friedlander, Eric Gelb, Deon Seifert

Back cover copy: Eric Gelb, Deon Seifert

Illustrations: James Balkovek

Production: Zoë Lonergan

Indexer: Cory Emberson

V.P./Business Manager: Cathy Barker

In 1474, Venice established a formal statutory patent system (a system of laws) granting a ten-year monopoly for innovations.

In England, the use of “letters patent” was caught up politically in controversies of the use of royal monopolies in general. James I of England was forced to cancel all monopolies that had been granted, but he prevailed in convincing Parliament that those monopolies granted to inventors for new advances should not be cancelled. It was widely accepted at the time that the favorable treatment of new technology had been extremely beneficial to England over the course of the previous three centuries.



Patent Vocab

A monopoly is a restriction enforced by a government that allows only one entity to do business in that area. In a patent system, monopolies are given to the one true original inventor of something that can be sold or made, or of a method that can be used to make a commercial item.

The resolution of the monopolies problem led to the Statute of Monopolies of 1623 just before King James I’s reign drew to a close, and it is the first formal English legal patent system and is the basis from which all subsequent English and US patent laws eventually grew. It took the position that in the future no monopolies could be granted unless they are for completely novel inventions. It created a grant of monopoly lasting fourteen years that was available only to “the true and first inventor.”

Elements of the 1623 statute were still in force in England despite major revisions and expansions of patent law in 1843, 1863, 1883, and 1948. Only with the Patents Act of 1977 did the UK formally abandon the 1623 statute completely to harmonize with the patent law of other European countries. Most importantly, this shifted the system to a “first to file” instead of the “first to invent” system that was in force in the United States until it was partially abandoned by legislation in 2011 (see Chapter 6).

The Lessons of Johannes Gutenberg

One of the greatest inventions of all time is the printing press, which led to the wide availability of books. It is hard for us to even imagine a world without books, but until 1455, every book or scroll had to be copied by hand, letter by letter, making books extremely

expensive and rare. The story of the invention illustrates a number of aspects of the inventing process as well as pointing out the role of patents.

Making Coins and Souvenirs

Johannes Gutenberg was trained in the craft of making coins. To do this, the gold or silver would be heated to a liquid, and then poured into a disklike mold. The craftsman would engrave the markings of the coin onto a punch. The punch would then be hammered onto the face of the coin, and the soft metal would flow a bit so that the coin surface would have the reverse image of the engraving on the punch.

This method of manufacturing coins was quite ancient even then. Craftsmen learned the method just as their ancestors had before them for thousands of years.

Gutenberg wanted to make a private business based on mass producing something like a coin. He hit on the idea of making souvenirs for an annual religious pilgrimage that was drawing over 100,000 people each year to the town of Aachen in Germany. He made numerous copies of the punch engraving for this souvenir with a plan to line up scores of these punches on a board. He would then use the workings of a wine press to drive all of the punches into a sheet of soft metal at the same time, making dozens of souvenirs in one stroke. Soon he had thousands to sell.

The plan was foiled by a plague, which caused the pilgrimage to be cancelled. Gutenberg was left with the now-useless wine press and metal, which had cost him a great deal.

The Printing Press

Gutenberg's disappointment was followed by a flash of genius: he could engrave a different letter on each punch, then use the press to make them all apply ink to a page of paper, which would lead to the mass production of books. But he had a series of technical challenges to solve.

One challenge he faced was how to extend the letters from each punch after the fine lines were cut. His solution was to engrave molds of each letter and pour the metal so that each letter would be like a punch, but raised rather than indented. He had to experiment with metals to find a mixture that would pour well into the fine lines of the letters, yet hold up when pressed against paper many times. He had to find a paper that could rapidly absorb the ink, and he had to find an ink that would adhere to the letter blocks—the movable type—without running.

The type blocks were movable so that a small number of blocks could be rearranged to make the words on a given page, print numerous copies, and then make up the words of a new page.

The whole development process lasted two decades, consuming money from his family and from various partners, all along keeping the nature of the project secret—even from some of the investors. Eventually, the cost of investment became extremely large, yet he had no product to sell and no proof that the whole thing would ever work.

He finally began to experiment by printing simple schoolbooks referred to as the *Donatus*, but they had many flaws. Gradually, however, the technical problems were solved and a reliable working process was developed.

When the process was finally honed, Gutenberg printed his first commercial product: a mass-produced Bible. Just as the Bible was ready to be released, his partner Johann Fust called in all the loans and took just about everything Gutenberg had—a judge allowed Gutenberg to keep his home and one older press. Fust and a partner then printed the Bibles, listing themselves as the publishers, not even allowing Gutenberg's name to appear anywhere on the Bible. Others immediately understood what had been done; the secret was out and others immediately began to print books.

Because Gutenberg had no intellectual property rights, because there were no patents, all of the investment, all of the genius and passion, all of the wondrous benefits the world would see in the 450 years between the first Bible and the first e-book were of no monetary value at all for the inventor.

The story highlights some of the important ways that inventions are identified. There was clearly an enormous unmet need for books. The fundamental elements of the technology were there for anyone to use. The printing press could have been built in ancient Greece or by anyone over a 2,000-year spread of time, but it was one person, Gutenberg, who had made it happen. His work demonstrates a key feature of inventions called nonobviousness.



Patent Vocab

Most patent laws require that an invention be “nonobvious.” It must significantly advance what is currently known in a way that would not occur to a knowledgeable but noncreative person.

Gutenberg brought together a wine-making machine, a new twist on engraving and coin making, and the ancient tradition of copying texts—three separate areas of technology—to make something that was greater than the sum of its parts.

Simply putting a wine press, a coin punch, and a copied biblical scroll next to each other would not accomplish the synthetic development of a new technology—the printing press of movable type. One can safely say that nearly no one else in the world who saw those three objects next to each other would think to put them together to mass-produce books; it's not an obvious use of those objects.